



รายงานวิจัยฉบับสมบูรณ์

โครงการ เฟร์โรอิเล็กทริกทวิภาคซับซ้อนใกล้ขอบเขตเฟสมอร์โฟโทรปิกที่มี
สมรรถนะสูง
(High performance complex binary ferroelectrics near morphotropic
phase boundary)

โดย รองศาสตราจารย์ ดร. สุกานดา เจียรศิริสมบูรณ์ และคณะ

มิถุนายน 2560

รายงานวิจัยฉบับสมบูรณ์

โครงการ เฟอร์โรอิเล็กทริกทวิภาคซับซ้อนใกล้ขอบเขตเฟสมอร์โฟโทรปิกที่มี
สมรรถนะสูง
(High performance complex binary ferroelectrics near morphotropic
phase boundary)

รองศาสตราจารย์ ดร. สุกานดา เจียรศิริสมบูรณ์
มหาวิทยาลัยเทคโนโลยีสุรนารี

สนับสนุนโดยสำนักงานกองทุนสนับสนุนการวิจัย
และมหาวิทยาลัยเทคโนโลยีสุรนารี

(ความเห็นในรายงานนี้เป็นของผู้วิจัย สกว. และมหาวิทยาลัยเทคโนโลยีสุรนารี
ไม่จำเป็นต้องเห็นด้วยเสมอไป)

บทคัดย่อ

รหัสโครงการ : RSA5780032
ชื่อโครงการ : เฟอร์ไรต์อิเล็กทริกทวิภาคซับซ้อนใกล้ขอบเขตเฟสเฟอร์ไรต์ที่มีสมรรถนะสูง
ชื่อนักวิจัย : รองศาสตราจารย์ ดร. สุกานดา เจียรศิริสมบุรณ์
E-mail Address : sukanda.jian@sut.ac.th
ระยะเวลาโครงการ : 3 ปี

โครงการวิจัยนี้มีจุดประสงค์จะทำการปรับปรุงสมบัติของวัสดุเฟอร์ไรต์อิเล็กทริกด้วยวัสดุทั้งที่มีโครงสร้างนาโนและสารประกอบโครงสร้างแบบชั้นเชิงซ้อน โดยวัสดุเฟอร์ไรต์อิเล็กทริกที่สนใจมีทั้งชนิดที่มีสารตะกั่วเป็นองค์ประกอบ เช่น เลดเซอร์โคเนตไทเทเนต (PZT) และเลดแมงกานีสเตียมไนโอเบตไทเทเนต (PMNT) และชนิดที่ไร้สารตะกั่วที่มีโครงสร้างแบบชั้นเชิงซ้อน เช่น สตรอนเทียมบิสมาทไนโอเบต (SBN) และ สตรอนเทียมบิสมาทแทนทาล (SBT) วัสดุเฟอร์ไรต์อิเล็กทริกแบบใหม่ๆ จึงได้ถูกผลิตขึ้น ซึ่งบางระบบจะอยู่ในรูปของฟิล์มบาง แต่ส่วนใหญ่จะอยู่ในรูปของเซรามิก ดังนั้น กระบวนการผลิตเพื่อให้ได้วัสดุคุณภาพสูง โครงสร้างจุลภาค องค์ประกอบทางเคมี และสมบัติทางไฟฟ้าจึงถูกศึกษาอย่างละเอียด ในรายงานผลการวิจัยฉบับสมบูรณ์ของโครงการฉบับนี้ได้เลือกผลการวิจัยที่น่าสนใจและแล้วเสร็จมานำเสนอไว้เพียง 2 ส่วน ดังนี้

งานวิจัยส่วนที่ 1 ศึกษาการเตรียมและการหาลักษณะเฉพาะของเซรามิกเฟอร์ไรต์อิเล็กทริก PZT ที่ถูกเติมด้วยสารประกอบเฟอร์ไรต์อิเล็กทริกประเภทเพอโรฟสไกต์ที่มีโครงสร้างเชิงซ้อนของ SBT โดยงานวิจัยนี้ทำการเตรียมเซรามิก $(1-x)\text{PZT}-x\text{SBT}$ (เมื่อ $x = 0, 0.1, 0.3, 0.5, 0.7, 0.9$ และ 1.0 เศษส่วนโดยน้ำหนัก) เมื่อตรวจสอบค่าคงที่ไดอิเล็กทริก พบว่า มีค่าสูงที่สุดที่อัตราส่วน $0.9\text{PZT}-0.1\text{SBT}$ แต่จะมีค่าลดลงเมื่อปริมาณ SBT เพิ่มขึ้น สำหรับสมบัติเฟอร์ไรต์อิเล็กทริก พบว่า การเพิ่มปริมาณ SBT เข้าไปใน PZT เพียงเล็กน้อย ($x = 0.1$ เศษส่วนโดยน้ำหนัก) สามารถปรับปรุงค่าสนามลบล้าง ค่าโพลาริเซชันคงค้าง และความเป็นเหลี่ยมของวงวนฮิสเทอรีซิส อย่างไรก็ตามเมื่อปริมาณ SBT เพิ่มขึ้นจะทำให้สมบัติเฟอร์ไรต์อิเล็กทริกของเซรามิกลดลง ในส่วนของสมบัติพีโซอิเล็กทริก พบว่า การเติมปริมาณ SBT ในปริมาณ $x = 0.1$ เศษส่วนโดยน้ำหนัก จะช่วยปรับปรุงค่าสัมประสิทธิ์พีโซอิเล็กทริกให้แก่เซรามิก PZT ได้

งานวิจัยส่วนที่ 2 งานวิจัยนี้ศึกษาพฤติกรรมความล้าทางไฟฟ้าของเซรามิกเฟอร์ไรต์อิเล็กทริก PMNT สำหรับประยุกต์เป็นตัวขับเคลื่อน เซรามิกเลด PMNT ถูกเตรียมด้วยวิธีผสมออกไซด์และซินเทอร์ที่อุณหภูมิ 1240 องศาเซลเซียส เป็นเวลา 2 ชั่วโมง เซรามิกที่เตรียมได้มีความหนาแน่นสัมพัทธ์มากกว่า 98 เปอร์เซ็นต์ ขนาดเกรนของเซรามิกมีค่าเท่ากับ 3 ไมโครเมตร พฤติกรรมความล้าทางไฟฟ้าของเซรามิกจะถูกวัดภายใต้การให้สนามไฟฟ้ากระแสสลับที่มีแอมพลิจูด 2 เท่าของสนามไฟฟ้าลบล้างของเซรามิก และมีความถี่เท่ากับ 5 10 50 และ 100 เฮิร์ตซ์ ความล้าทางไฟฟ้าของเซรามิกหาได้จากการเปลี่ยนแปลงของโครงสร้างจุลภาค วงวนฮิสเทอรีซิส และเส้นโค้งความเครียด-สนามไฟฟ้า ที่จำนวนรอบ

สนามไฟฟ้าต่าง ๆ จนถึง 10^6 รอบ โดยการใช้กล้องจุลทรรศน์อิเล็กตรอนแบบส่องกราด เครื่องวัดสมบัติเพอร์โรอิเล็กทริก และเครื่องวัดความเครียดที่เชื่อมต่อกับเครื่องจ่ายไฟฟ้าความต่างศักย์สูง ตามลำดับจากการทดลองพบว่าเกิดความเสียหายของชั้นผิวหน้าในเซรามิกที่ผ่านการทดสอบความล้าทางไฟฟ้า โดยที่ความหนาของชั้นที่เสียหายดังกล่าวลดลงเมื่อความถี่ไฟฟ้าเพิ่มขึ้น นอกจากนี้ โพลาริเซชันคงค้างและความเครียดสูงสุดของเซรามิกมีค่าลดลงเมื่อจำนวนรอบของสนามไฟฟ้าเพิ่มขึ้น ความล้าทางไฟฟ้าของเซรามิกลดลงเมื่อความถี่เพิ่มขึ้น พฤติกรรมความล้าทางไฟฟ้าของเซรามิกเลดแมกนีเซียมในโอเบตไทเทเนตสามารถอธิบายได้โดยปรากฏการณ์การป้องกันสนามไฟฟ้าและการเป็นหมุดยึดขอบโดเมนของตำหนิ

งานวิจัยในโครงการนี้โดยสรุปถือว่าประสบความสำเร็จในการเตรียม ศึกษาความสัมพันธ์ระหว่างกระบวนการผลิต โครงสร้าง และสมบัติต่าง ๆ ของวัสดุเพอร์โรอิเล็กทริกแบบใหม่ๆ หลายระบบ ซึ่งผลการทดลองที่ได้นี้ทำให้เข้าใจพฤติกรรมและการเปลี่ยนแปลงสมบัติของวัสดุเหล่านี้ ตามสภาวะการเตรียมและปริมาณเฟสที่ใช้ในการเติม ซึ่งให้ข้อมูลที่เป็นประโยชน์ และช่วยชี้แนะแนวทางในการทำวิจัยต่อและพัฒนาวัสดุเพอร์โรอิเล็กทริกเหล่านี้ให้ดียิ่งขึ้น เพื่อการประยุกต์ใช้งานในอุตสาหกรรมอิเล็กทรอนิกส์ได้ต่อไปในอนาคต

คำหลัก : เซรามิกเพอร์โรอิเล็กทริก โครงสร้างนาโน โครงสร้างแบบชั้นเชิงซ้อน เฟส สมบัติทางไฟฟ้า

Abstract

Project Code : RSA5780032
Project Title : High performance complex binary ferroelectrics near morphotropic phase boundary
Investigator : Assoc. Prof. Dr. Sukanda Jiansirisomboon
E-mail Address : sukanda.jian@sut.ac.th
Project Period : 3 years

This research project aims to improve ferroelectric materials using nanostructures and complex layered-structured compounds. The interested ferroelectric materials include Pb-base compounds, i.e. lead zirconate titanate (PZT) and lead magnesium niobate titanate (PMNT), and lead free compounds, i.e. strontium bismuth niobate (SBN) and strontium bismuth tantalate (SBT). Several new ferroelectric systems were fabricated in this project. Some systems were in a form of thin film, while most of them were in a ceramic form. Therefore, fabrication process for high quality materials, microstructure, chemical composition and electrical properties were carefully studied in details. In this final research project will present 2 interested research parts that were completely done which are shown below.

The first part of this research studied the fabrication and characterization of ferroelectric PZT added with complex layer-structured perovskite compounds of SBT. This research prepared (1-x)PZT-xSBT (when $x = 0, 0.1, 0.3, 0.5, 0.7, 0.9$ and 1.0 weight fraction). The maximum value of dielectric constant was found in 0.9PZT-0.1SBT ceramics. The values were decreased with further increase in the amount of SBT. Ferroelectric property measurements showed that an addition of a small amount of SBT ($x = 0.1$) into PZT improved coercive field, remanent polarization and loop squareness. Further increasing the amount of SBN or SBT degraded the ferroelectric properties. For piezoelectric properties, the addition of small amounts of SBT with $x = 0.1$ could improve the piezoelectric coefficient of PZT ceramic.

The second part of this work studies bipolar electrical fatigue behaviour of lead magnesium niobate titanate (PMNT) ferroelectric ceramics for actuator applications. The PMNT ceramics were prepared by using conventional mixed-oxide and sintered at 1240°C for 2 hrs. Ceramics with $> 98\%$ relative density and $\sim 3\ \mu\text{m}$ were obtained. Fatigue behaviour of ceramics was measured under an application of AC electric field with an amplitude 2 times of

the ceramic's coercive field. The frequency of the applied electric field was also varied as 5, 10, 50 and 100 Hz. The fatigue behaviour was determined from the change of microstructures, polarization-electric field hysteresis loops and strain-electric field curves measured at different cycle numbers up to 10^6 cycles by using a scanning electron microscope (SEM), ferroelectric measurement system and a strain in conjunction with a high voltage supplier, respectively. The damage of the surfaces underneath the electrode layers was observed in all fatigued samples. The thickness of the damaged layers decreased with increasing fatigue frequency. Moreover, remanent polarization and maximum strain tended to decrease with increasing cycle number. The degradation of properties due to fatigue of the ceramics decreased with an increase in frequency. The observed fatigue behaviour of the ceramics was explained based on domain pinning and electric field screening effects.

To conclude, this research was successful in fabrication, study of relations between fabrication, structure and properties of new ferroelectric systems. The results provided insight understanding of property changes upon processing condition and number of additional phases. This research suggested further research direction and development of these materials for actual applications in electronic industries.

Keywords: Ferroelectric ceramics, nanocomposite, processing, structure, mechanical properties, electrical properties,

หน้าสรุปโครงการ (Executive Summary)

หน้าสรุปโครงการ (Executive Summary)

สารประกอบเฟอร์โรอิเล็กทริก (ferroelectric) ซึ่งจัดอยู่ในกลุ่มสารที่มีสมบัติเพียโซอิเล็กทริก (piezoelectric property) มีความสำคัญต่อมนุษย์ในหลากหลายด้าน ซึ่งจัดว่าเป็นวัสดุฉลาด (smart materials) กล่าวคือ สามารถรับรู้การเปลี่ยนแปลงของสภาพแวดล้อมที่วัสดุทำงานอยู่ และสามารถตอบสนองต่อการเปลี่ยนแปลงนั้นตามรูปแบบที่มีการกำหนดไว้ก่อนแล้วล่วงหน้า วัสดุเหล่านี้มีสมบัติพิเศษ คือ เมื่อได้รับแรงกลจะสามารถให้แรงดันไฟฟ้า และในทางกลับกันเมื่อวัสดุได้รับแรงดันไฟฟ้า จะเกิดการเปลี่ยนแปลงรูปร่างและเกิดแรงทางกลขึ้น การเปลี่ยนกลับไปกลับมาระหว่างพลังงานกลและพลังงานไฟฟ้านี้ได้ถูกนำมาประยุกต์ใช้งานอย่างแพร่หลายและอย่างมีประสิทธิภาพ โดยสารเหล่านี้ได้ถูกนำไปใช้เป็นส่วนหนึ่งในการสร้างอุปกรณ์/เครื่องมืออิเล็กทรอนิกส์หลายประเภท ขึ้นกับสมบัติเด่นของสารแต่ละชนิด สำหรับสารเซรามิกเฟอร์โรอิเล็กทริกที่มีความไวต่อสนามไฟฟ้าและมีสมบัติเพียโซอิเล็กทริกนั้น ถูกนำไปประยุกต์ใช้งานมากที่สุด โดยสามารถแบ่งการใช้งานออกได้เป็น 4 ประเภท คือ เครื่องกำเนิดไฟฟ้า (generators) มอเตอร์ (motors) อุปกรณ์ที่ใช้ทั้งสองหลักการร่วมกัน (generator/motor) และอุปกรณ์เรโซแนนซ์ (resonant devices) ซึ่งอุปกรณ์อิเล็กทรอนิกส์ที่ใช้กันมาก ได้แก่ ตัวขับเคลื่อน (actuators) ตัวแปลง (transducers) และตัวเก็บประจุ (capacitors) สารจำพวกนี้ยังถูกนำไปใช้ในการสร้างเครื่องมือทางการแพทย์หลายชนิด เช่น มอเตอร์อัลตราโซนิก (ultrasonic motors) และเครื่องตรวจวัดอัลตราซาวด์ (ultrasound) เป็นต้น นอกจากนี้อุปกรณ์/เครื่องมือที่กล่าวมาข้างต้นแล้ว พบว่า ในปัจจุบันสารเฟอร์โรอิเล็กทริกได้มีบทบาทในชีวิตประจำวันของมนุษย์มากยิ่งขึ้น

อย่างไรก็ตาม ปัญหาหลักที่ทำให้การพัฒนาการประยุกต์ใช้งานของวัสดุกลุ่มเซรามิกเฟอร์โรอิเล็กทริกยังไม่ประสบความสำเร็จสูงสุดเกิดขึ้นจากธรรมชาติที่เปราะของวัสดุนั่นเอง โดยเฉพาะการใช้งานของเซรามิกเฟอร์โรอิเล็กทริกทางด้านตัวขับเคลื่อนหรือตัวแปลงที่มักเกิดขึ้นภายใต้สภาวะที่มีความเค้น ดังนั้นความเข้าใจเกี่ยวกับการเสื่อมสภาพหรือการเสียหายเชิงกลจึงมีความสำคัญไม่ยิ่งหย่อนไปกว่าสมบัติทางไฟฟ้า เช่น สมบัติไดอิเล็กทริก เฟอร์โรอิเล็กทริก และเพียโซอิเล็กทริกที่มีการศึกษากันอย่างแพร่หลาย แต่เนื่องด้วยสารเฟอร์โรอิเล็กทริกเหล่านี้ไม่ได้ถูกออกแบบมาเพื่อประยุกต์ในเชิงโครงสร้างที่เกี่ยวข้องกับสมบัติเชิงกลโดยตรง ดังนั้นการใช้งานส่วนใหญ่ของสารเหล่านี้จึงมีได้คำนึงถึงความแข็งแรงและความทนทานสูงเป็นสำคัญ ส่งผลให้งานวิจัยทางด้านสมบัติเชิงกลของสารเหล่านี้จึงไม่แพร่หลายเท่าที่ควรเมื่อเทียบกับสมบัติทางไฟฟ้า จากเหตุดังกล่าวข้างต้นผู้วิจัยจึงมีแนวคิดจะพัฒนาเซรามิกเฟอร์โรอิเล็กทริกชนิดใหม่ๆ ที่มีความต้านทานการเสื่อมสภาพเชิงกลที่ดีรวมทั้งสามารถคงไว้ซึ่งสมบัติทางไฟฟ้าที่ดี และ/หรือ มีสมบัติทางไฟฟ้าที่ดีขึ้น

โครงการวิจัยนี้มีจุดประสงค์จะทำการปรับปรุงสมบัติของวัสดุเฟอร์โรอิเล็กทริกด้วยวัสดุโครงสร้างนาโนและสารประกอบโครงสร้างแบบชั้นเชิงซ้อน โดยวัสดุเฟอร์โรอิเล็กทริกที่สนใจมีทั้งชนิดที่มีสารตะกั่วเป็นองค์ประกอบ เช่น เลดเซอร์โคเนตไทเทเนต (PZT) และเลดแมกนีเซียมไนโอเบตไทเทเนต (PMNT) และชนิดที่ไร้สารตะกั่วที่มีโครงสร้างแบบชั้นเชิงซ้อน เช่น สตรอนเทียมบิสมาทไนโอ

เบต (SBN) และ สตรอนเทียมบิสมาทแทนทาเลต (SBT) วัสดุเฟอร์โรอิเล็กทริกแบบใหม่ ๆ จึงได้ถูกผลิตขึ้น ซึ่งบางระบบจะอยู่ในรูปของฟิล์มบาง แต่ส่วนใหญ่จะอยู่ในรูปของเซรามิก ดังนั้นกระบวนการผลิตเพื่อให้ได้วัสดุคุณภาพสูง โครงสร้างจุลภาค องค์ประกอบทางเคมี และสมบัติทางไฟฟ้าจึงถูกศึกษาอย่างละเอียด ในรายงานผลการวิจัยฉบับสมบูรณ์ของโครงการฉบับนี้จะเลือกนำเสนอผลการวิจัยที่น่าสนใจและแล้วเสร็จไว้ 2 ส่วน คือ

งานวิจัยส่วนที่ 1 เพื่อศึกษาการเตรียม และสมบัติของเซรามิกแบบใหม่อย่างเลดเซอร์โคเนตไทเทเนต ($\text{Pb}(\text{Zr}_{0.52}\text{Ti}_{0.48})\text{O}_3$)-สตรอนเทียมบิสมาทแทนทาเลต ($\text{SrBi}_2\text{Ta}_2\text{O}_9$) ซึ่งมีสูตรทั่วไปคือ $(1-x)\text{PZT}-x\text{SBT}$ เมื่อ x เท่ากับ 0, 0.1, 0.3, 0.5, 0.7, 0.9 และ 1.0 เศษส่วนโดยน้ำหนัก ในขั้นตอนแรกนั้น ผง PZT และ SBT จะถูกเตรียมด้วยวิธีผสมออกไซด์ จากนั้นทำการเผาแคลไซน์ผง PZT ที่อุณหภูมิ 800 องศาเซลเซียส เป็นเวลา 2 ชั่วโมง ในขณะที่ผง SBT ทำการแคลไซน์ที่อุณหภูมิ 950 องศาเซลเซียส เป็นเวลา 3 ชั่วโมง หลังจากนั้นนำผงทั้งสองมาผสมรวมกันในอัตราส่วนต่างๆ ด้วยอาศัยการบดย่อย และทำการอบแห้งเพื่อให้ได้ผง $(1-x)\text{PZT}-x\text{SBT}$ ขั้นตอนต่อมาคือ การนำผงผสมที่ได้ไปอัดขึ้นรูปแล้วทำการเผาซินเตอร์ที่อุณหภูมิ 1000-1250 องศาเซลเซียส เป็นเวลา 3 ชั่วโมง จากนั้นตรวจสอบสมบัติของเซรามิกแบบ PZT-SBT พบว่า ปริมาตรของหน่วยเซลล์ (unit cell volume) ของเฟส PZT ลดลงหลังการเติมสารประกอบ SBT ในปริมาณน้อยๆ ($0.1 \leq x \leq 0.3$) ลงไปในเซรามิก PZT แต่เมื่อปริมาณการเติม SBT เพิ่มขึ้นจนถึง x เท่ากับ 0.9 พบว่าโครงสร้างออร์โธโรมบิกของ SBT เกิดการบิดเบี้ยว นอกจากนี้แล้ว ยังพบว่า มีการเกิดเฟสใหม่อย่างเฟสคิวบิก $\text{Pb}_{1.2}\text{Ti}_{0.4}\text{Ta}_{1.6}\text{O}_6$ หรือ PTT ในเซรามิกที่มีการเติม SBT ทุกอัตราส่วน ($0.1 \leq x \leq 0.9$) ซึ่งให้เห็นว่ามีการเกิดปฏิกิริยาทางเคมีระหว่าง PZT และ SBT ขึ้นระหว่างกระบวนการเผาซินเตอร์นั่นเอง ผลการตรวจสอบพฤติกรรมการแนบตัว แสดงให้เห็นว่าที่อุณหภูมิการเผา 1200 องศาเซลเซียส คืออุณหภูมิซินเตอร์ที่เหมาะสมสำหรับเซรามิกแบบ PZT-SBT เนื่องจากเซรามิกที่เผา ณ อุณหภูมิดังกล่าวนี้นี้มีความหนาแน่นที่ใกล้เคียงกัน การตรวจสอบทางโครงสร้างจุลภาค พบว่าการเติมปริมาณ SBT เพียงเล็กน้อย (x เท่ากับ 0.1) ส่งผลทำให้ขนาดเกรนของ PZT ลดลง และยังช่วยปรับปรุงความเป็นเนื้อเดียวกันให้แก่โครงสร้างจุลภาค ในขณะเดียวกัน การเติม PZT ในปริมาณน้อยๆ ($0.1\text{PZT}-0.9\text{SBT}$) ก็ส่งผลทำให้ขนาดเกรนแบบแผ่นของเฟส SBT ลดลง และช่วยพัฒนาความเป็นเนื้อเดียวกันให้แก่พื้นผิวของเซรามิก SBT ด้วยเช่นกัน สำหรับการวัดสมบัติทางไฟฟ้า พบว่าการเติม 0.1SBT ลงไปใน PZT ส่งผลทำให้ค่าคงที่ไดอิเล็กทริกและค่าโพลาริเซชันคงค้างเพิ่มสูงขึ้น เนื่องจากกระบวนการรวมตัวกันของตัวเจืออย่างไอออนของบิสมาท (Bi^{3+}) และแทนทาเลต (Ta^{5+}) (จาก SBT) ที่เข้าไปในแลตทิซเพอโรฟสไกต์ของเซรามิก PZT ในส่วนของการทดสอบความล้าชี้ให้เห็นว่า เซรามิก PZT บริสุทธิ์ แสดงการลดลงของค่าโพลาริเซชันคงค้างเป็นอย่างมาก แต่ที่เป็นที่น่าสนใจว่า ความต้านทานต่อความล้าของ PZT ได้ถูกปรับปรุงเพิ่มขึ้นเป็นอย่างมากหลังจากทำการเติม SBT ซึ่งเป็นผลมาจากการหมุดผนังโดเมนที่อ่อนแรงนั่นเอง

งานวิจัยส่วนที่ 2 งานวิจัยนี้ศึกษาพฤติกรรมความล้าทางไฟฟ้าของเซรามิกเฟอร์โรอิเล็กทริกเลดแมกนีเซียมไนโอเบตไทเทเนตสำหรับประยุกต์เป็นตัวขับเคลื่อน เซรามิกเลดแมกนีเซียมไนโอเบตถูก

เตรียมด้วยวิธีผสมออกไซด์แบบดั้งเดิมและซินเทอร์ที่อุณหภูมิ 1240 องศาเซลเซียส เป็นเวลา 2 ชั่วโมง เซรามิกที่เตรียมได้มีความหนาแน่นสัมพัทธ์มากกว่า 98 เปอร์เซ็นต์ ขนาดเกรนของเซรามิกมีค่าเท่ากับ 3 ไมโครเมตร พฤติกรรมความล้าทางไฟฟ้าของเซรามิกจะถูกวัดภายใต้การให้สนามไฟฟ้า กระแสลับที่มีแอมพลิจูด 2 เท่าของสนามไฟฟ้าลบล้างของเซรามิก และมีความถี่เท่ากับ 5 10 50 และ 100 เฮิร์ตซ์ ความล้าทางไฟฟ้าของเซรามิกหาได้จากการเปลี่ยนแปลงของโครงสร้างจุลภาค วงวนฮีสเทอรีซิส และเส้นโค้งความเครียด-สนามไฟฟ้า ที่จำนวนรอบสนามไฟฟ้าต่างๆ จนถึง 10^6 รอบ โดยการใช้กล้องจุลทรรศน์อิเล็กตรอนแบบส่องกราด เครื่องวัดสมบัติเพอร์โรอิเล็กทริก และเครื่องวัดความเครียดที่เชื่อมต่อกับเครื่องจ่ายไฟฟ้าความต่างศักย์สูง ตามลำดับ จากการทดลองพบว่า เกิดความเสียหายของชั้นผิวหน้าในเซรามิกที่ผ่านการทดสอบความล้าทางไฟฟ้า ความหนาของชั้นที่เสียหายดังกล่าวลดลงเมื่อความถี่ไฟฟ้าเพิ่มขึ้น นอกจากนี้ โพลาริเซชันคงค้างและความเครียดสูงสุดของเซรามิกมีค่าลดลงเมื่อจำนวนรอบของสนามไฟฟ้าเพิ่มขึ้น ความล้าทางไฟฟ้าของเซรามิกลดลงเมื่อความถี่เพิ่มขึ้น พฤติกรรมความล้าทางไฟฟ้าของเซรามิกเลดแมงกานีสในโอเบดไทเทเนตถูกอธิบายโดยปรากฏการณ์การป้องกันสนามไฟฟ้าและการเป็นหมุดยึดขอบโดเมนของตำหนิ

งานวิจัยนี้โดยสรุปประสบความสำเร็จในการเตรียม ศึกษาความสัมพันธ์ระหว่างกระบวนการผลิต โครงสร้าง และสมบัติต่างๆ ของวัสดุเพอร์โรอิเล็กทริกแบบใหม่ ๆ ซึ่งผลการทดลองที่ได้นี้ทำให้เข้าใจพฤติกรรมการเปลี่ยนแปลงสมบัติของวัสดุเหล่านี้ ตามสภาวะการเตรียมและปริมาณเฟสที่ใช้ในการเติม ซึ่งให้ข้อมูลที่เป็นประโยชน์และช่วยชี้แนะแนวทางในการทำวิจัยต่อและพัฒนาวัสดุเพอร์โรอิเล็กทริกเหล่านี้ให้ดียิ่งขึ้น เพื่อการประยุกต์ใช้งานในอุตสาหกรรมอิเล็กทรอนิกส์ได้จริงในอนาคต ผลพลอยได้ที่สำคัญอีกประการหนึ่ง คือ บทความตีพิมพ์ในวารสารวิชาการระดับนานาชาติจำนวน 16 เรื่อง ผลงานนำเสนอในที่ประชุมสัมมนาวิชาการระดับชาติจำนวน 7 เรื่อง และผลงานนำเสนอในที่ประชุมสัมมนาวิชาการระดับนานาชาติจำนวน 10 เรื่อง รวมทั้งสิ้น 17 เรื่อง และตลอดช่วงเวลา 3 ปีในการทำวิจัย โครงการนี้ได้สร้างเครือข่ายความร่วมมือทางการวิจัยทั้งกับนักวิจัยระดับประเทศและต่างประเทศอย่างเป็นรูปธรรม อีกทั้งยังสามารถผลิตบัณฑิตได้ทั้งในระดับปริญญาตรี จำนวน 1 คน ระดับปริญญาโท จำนวน 2 คน ระดับปริญญาเอก จำนวน 5 คน โดยนักศึกษาระดับปริญญาเอกได้รับทุนจากโครงการปริญญาเอกกาญจนาภิเษก (คปก.) ภายใต้สำนักงานกองทุนสนับสนุนการวิจัย (สกว.) และโครงการเครือข่ายเชิงกลยุทธ์เพื่อการผลิตและพัฒนาอาจารย์ในสถาบันอุดมศึกษาจากคณะกรรมการการอุดมศึกษา (สกอ.)

เนื้อหางานวิจัย

เนื้อหางานวิจัยตอนที่ 1

เรื่อง

เซรามิกเฟอร์โรอิเล็กทริกที่มีเลดเซอร์โคเนตไทเทเนต
เป็นหลักกับโครงสร้างซับซ้อนของสตรอนเทียม
บิสมาทแทนทาเลต

ตอนที่ 1 – เซรามิกเพอร์โรอิเล็กทริกที่มีเลดเซอร์โคเนตไทเทเนตเป็นหลักกับโครงสร้าง ซับซ้อนของสตรอนเทียมบิสมาทแทนทาเลด

1. บทคัดย่อ

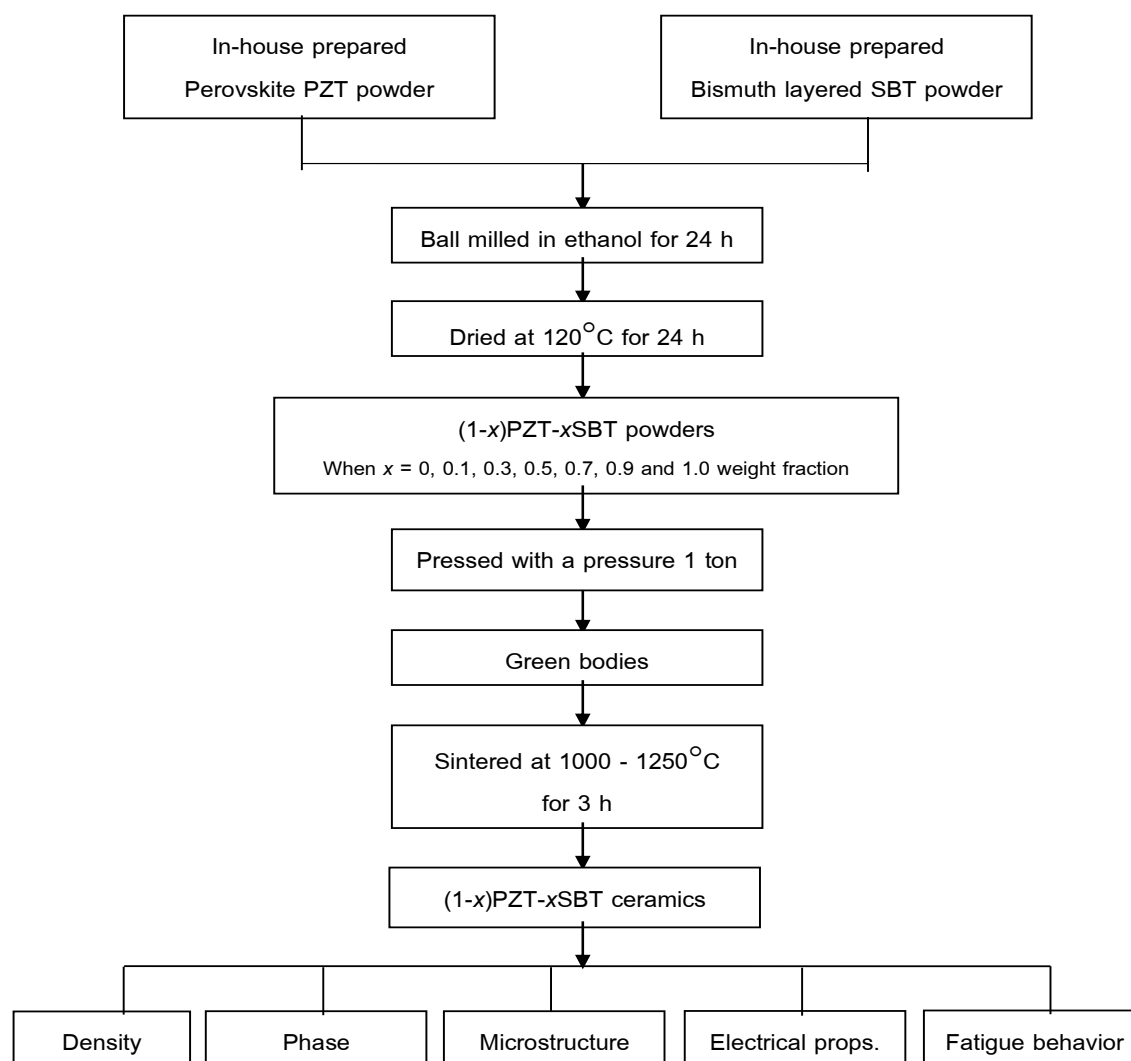
โครงการวิจัยนี้ได้ดำเนินการเพื่อศึกษาการเตรียม และสมบัติของเซรามิกระบบใหม่อย่าง เลดเซอร์โคเนตไทเทเนต ($\text{Pb}(\text{Zr}_{0.52}\text{Ti}_{0.48})\text{O}_3$)-สตรอนเทียมบิสมาทแทนทาเลด ($\text{SrBi}_2\text{Ta}_2\text{O}_9$) ซึ่งมี สูตรทั่วไปคือ $(1-x)\text{PZT}-x\text{SBT}$ เมื่อ x เท่ากับ 0, 0.1, 0.3, 0.5, 0.7, 0.9 และ 1.0 เศษส่วนโดย น้ำหนัก ในขั้นตอนแรกนั้น ผง PZT และ SBT จะถูกเตรียมด้วยวิธีผสมออกไซด์ จากนั้นทำการเผา แคลไซน์ผง PZT ที่อุณหภูมิ 800 องศาเซลเซียส เป็นเวลา 2 ชั่วโมง ในขณะที่ผง SBT ทำการแคล ไชน์ที่อุณหภูมิ 950 องศาเซลเซียส เป็นเวลา 3 ชั่วโมง หลังจากนั้นนำผงทั้งสองมาผสมรวมกันใน อัตราส่วนต่างๆ ด้วยอาศัยการบดย่อย และทำการอบแห้งเพื่อให้ได้ผง $(1-x)\text{PZT}-x\text{SBT}$ ขั้นตอน ต่อมาคือ การนำผงผสมที่ได้ไปอัดขึ้นรูปแล้วทำการเผาซินเตอร์ที่อุณหภูมิ 1000-1250 องศา เซลเซียส เป็นเวลา 3 ชั่วโมง จากนั้นทำการวิเคราะห์สมบัติต่างๆ ของเซรามิก PZT-SBT ได้แก่ ความหนาแน่น การเปลี่ยนแปลงของเฟส โครงสร้างจุลภาค สมบัติไดอิเล็กทริก สมบัติเพอร์โรอิเล็กทริก และความต้านทานต่อความล้า

จากผลการทดลองในการตรวจสอบสมบัติของเซรามิกระบบ PZT-SBT พบว่า ปริมาตรของ หน่วยเซลล์ (unit cell volume) ของเฟส PZT ลดลงหลังการเติมสารประกอบ SBT ในปริมาณน้อยๆ ($0.1 \leq x \leq 0.3$) ลงไปในเซรามิก PZT แต่เมื่อปริมาณการเติม SBT เพิ่มขึ้นจนถึง x เท่ากับ 0.9 พบว่า โครงสร้างออร์โธโรมบิกของ SBT เกิดการบิดเบี้ยว นอกจากนี้แล้ว ยังพบว่า มีการเกิดเฟสใหม่ อย่างเฟสคิวบิก $\text{Pb}_{1.2}\text{Ti}_{0.4}\text{Ta}_{1.6}\text{O}_6$ หรือ PTT ในเซรามิกที่มีการเติม SBT ทุกอัตราส่วน ($0.1 \leq x \leq 0.9$) ซึ่งให้เห็นว่ามีการเกิดปฏิกิริยาทางเคมีระหว่าง PZT และ SBT ขึ้นระหว่างกระบวนการเผา ซินเตอร์นั่นเอง ผลการตรวจสอบพฤติกรรมการณ์ตัว แสดงให้เห็นว่าที่อุณหภูมิการเผา 1200 องศาเซลเซียส คืออุณหภูมิซินเตอร์ที่เหมาะสมสำหรับเซรามิกระบบ PZT-SBT เนื่องจากเซรามิกที่ เผา ณ อุณหภูมิดังกล่าวนี้มีค่าความหนาแน่นที่ใกล้เคียงกัน การตรวจสอบทางโครงสร้างจุลภาค พบว่าการเติมปริมาณ SBT เพียงเล็กน้อย (x เท่ากับ 0.1) ส่งผลทำให้ขนาดเกรนของ PZT ลดลง และยังช่วยปรับปรุงความเป็นเนื้อเดียวกันให้แก่โครงสร้างจุลภาค ในขณะเดียวกัน การเติม PZT ใน ปริมาณน้อยๆ ($0.1\text{PZT}-0.9\text{SBT}$) ก็ส่งผลทำให้ขนาดเกรนแบบแผ่นของเฟส SBT ลดลง และช่วย พัฒนาความเป็นเนื้อเดียวกันให้แก่พื้นผิวของเซรามิก SBT ด้วยเช่นกัน สำหรับการวัดสมบัติทาง ไฟฟ้า พบว่าการเติม 0.1SBT ลงไปใน PZT ส่งผลทำให้ค่าคงที่ไดอิเล็กทริกและค่าโพลาริเซชันคง ค้างเพิ่มสูงขึ้น เนื่องจากกระบวนการรวมตัวกันของตัวเจืออย่างไอออนของบิสมาท (Bi^{3+}) และแทนทา เลด (Ta^{5+}) (จาก SBT) ที่เข้าไปในแลตทิซเพอโรฟสไกต์ของเซรามิก PZT ในส่วนของการทดสอบ ความล้าชี้ให้เห็นว่า เซรามิก PZT บริสุทธิ์ แสดงการลดลงของค่าโพลาริเซชันคงค้างเป็นอย่างมาก แต่ที่เป็นที่น่าสนใจว่า ความต้านทานต่อความล้าของ PZT ได้ถูกปรับปรุงเพิ่มขึ้นเป็นอย่างมาก หลังจากทำการเติม SBT ซึ่งเป็นผลมาจากการหมุดผนังโดเมนที่อ่อนแรงแน้นเอง

จากงานวิจัยดังกล่าวนี้ สามารถสรุปได้ว่าเซรามิกระบบใหม่ออย่าง PZT-SBT สามารถที่จะรวมข้อดีของทั้งเซรามิก PZT และ SBT เข้าไว้ด้วยกัน โดยเฉพาะอย่างยิ่งที่อัตราส่วน x เท่ากับ 0.1 (0.9PZT-0.1SBT) โดยเซรามิกดังกล่าวนี้มีสมบัติที่ไดอิเล็กทริกที่ดีเยี่ยม ค่าโพลาไรเซชันคงค้างที่สูง ค่าลบلاث์สนามไฟฟ้าที่ต่ำ และค่าความต้านทานต่อความล้าที่โดดเด่น ซึ่งเซรามิกนี้สามารถที่จะนำไปพัฒนาและประยุกต์ใช้ในอุปกรณ์อิเล็กทรอนิกส์ได้จริง โดยเฉพาะอย่างยิ่งในอุปกรณ์หน่วยความจำ

2. วิธีการทดลอง

รายละเอียดขั้นตอนการทดลองแสดงดังรูป 2.1



รูป 2.1 แผนผังขั้นตอนการเตรียมเซรามิกระบบ (1-x)PZT-xSBT

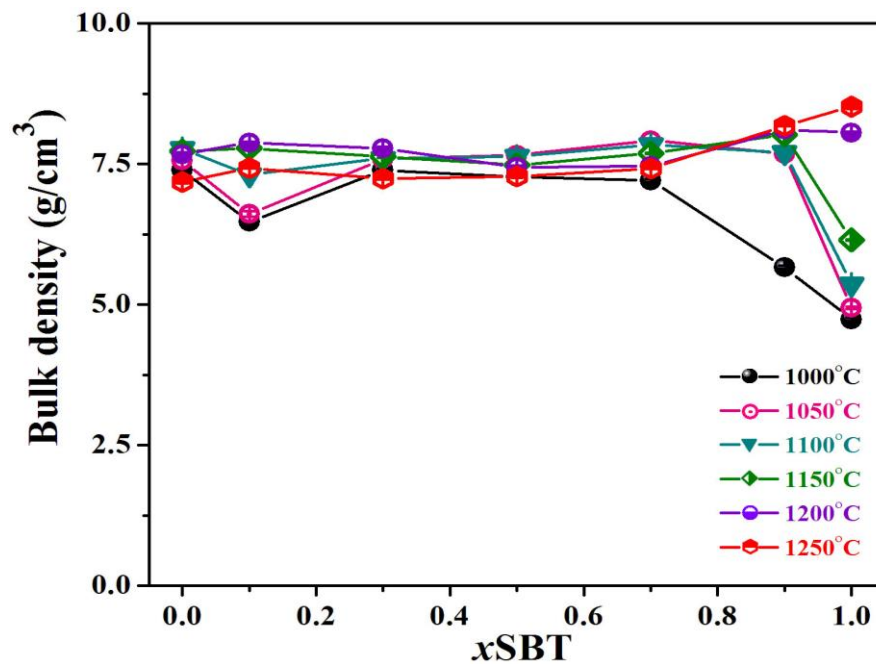
3. ผลการวิเคราะห์ PZT-SBT

ในหัวข้อนี้จะนำเสนอเกี่ยวกับผลการทดลองของการเตรียม (1-x)PZT-xSBT เมื่อ x เท่ากับ 0, 0.1, 0.3, 0.5, 0.7, 0.9 และ 1.0 เศษส่วนโดยน้ำหนัก พร้อมผลการวิเคราะห์ห้องค์ประกอบทางเคมี

การเปลี่ยนเฟส โครงสร้างทางจุลภาค สมบัติทางไฟฟ้าของ $(1-x)\text{PZT}-x\text{SBT}$ พร้อมทั้งอภิปรายผล การทดลองตามลำดับดังนี้

3.1 ผลการตรวจสอบความหนาแน่นของเซรามิก PZT-SBT

หลังจากนำผง $(1-x)\text{PZT}-x\text{SBT}$ เมื่อ x เท่ากับ 0, 0.1, 0.3, 0.5, 0.7, 0.9 และ 1.0 เศษส่วน โดยน้ำหนัก ไปอัดเม็ดและเผาซินเทอร์ที่อุณหภูมิ 1000-1250 องศาเซลเซียสเพื่อให้ได้เม็ดเซรามิก ที่มีคุณภาพแล้ว จากนั้นเซรามิก PZT-SBT ที่ผ่านการเผาซินเทอร์เหล่านี้จะถูกนำไปตรวจสอบ ความหนาแน่นด้วยหลักการของอาร์คิมิดีส ซึ่งได้ผลดังแสดงในรูป 3.1 ผลการทดลองแสดงให้เห็นว่า ความหนาแน่นของเซรามิก PZT บริสุทธิ์มีค่าเพิ่มขึ้นเมื่อเพิ่มอุณหภูมิซินเทอร์ และมีค่าสูงสุดที่ อุณหภูมิการเผา 1150 องศาเซลเซียส แต่อย่างไรก็ตามเมื่ออุณหภูมิซินเทอร์มากกว่า 1200 องศา เซลเซียส ปรากฏว่าค่าความหนาแน่นกลับค่อยๆ ลดลง ซึ่งเป็นผลเนื่องมาจากการระเหยของเลดออกไซด์ (PbO) ในระบบของ PZT [8-9] ในส่วนของเซรามิก SBT บริสุทธิ์ พบว่า ค่าความหนาแน่น ของเซรามิกจะเพิ่มขึ้นตามอุณหภูมิซินเทอร์ที่เพิ่มสูงขึ้น โดยจะมีค่าสูงสุดที่อุณหภูมิ 1200 องศา เซลเซียส เมื่อทำการเติม SBT ในปริมาณ x เท่ากับ 0.1 และ 0.3 พบว่าค่าความหนาแน่นของเซรา มิกเหล่านี้มีแนวโน้มเพิ่มขึ้นตามอุณหภูมิที่เพิ่มสูงขึ้น แต่อย่างไรก็ตามเมื่อทำการเผามากกว่า 1200 องศาเซลเซียส กลับพบว่าค่าความหนาแน่นของเซรามิกกลับลดลง การลดลงดังกล่าวนี้อาจเป็นผล เนื่องมาจากการระเหยของส่วนประกอบภายในเซรามิก เช่น เลดออกไซด์และบิสฟัทออกไซด์ เป็น ต้น สำหรับเซรามิกที่มีปริมาณการเติม SBT เท่ากับ 0.5 ถึง 0.7 ร้อยละโดยน้ำหนัก พบว่าอุณหภูมิ ซินเทอร์ที่ทำให้เซรามิกเหล่านี้มีค่าความหนาแน่นสูงสุดคือ 1050 องศาเซลเซียส ซึ่งชี้ให้เห็นว่าการ เติม SBT ในปริมาณมาก สามารถที่จะลดอุณหภูมิซินเทอร์ของทั้งเซรามิก PZT และ SBT บริสุทธิ์ ได้ แต่อย่างไรก็ตามเมื่อทำการเพิ่มปริมาณการเติม SBT จนถึง 0.9 เศษส่วนโดยน้ำหนัก พบว่าค่า ความหนาแน่นของเซรามิกนี้จะเพิ่มสูงขึ้นตามอุณหภูมิซินเทอร์ที่เพิ่มขึ้น และจะมีค่าคงที่ในช่วง อุณหภูมิ 1200-1250 องศาเซลเซียส จากผลความหนาแน่นตัวของเซรามิกระบบ PZT-SBT จะเห็นได้ว่า ที่อุณหภูมิซินเทอร์ 1200 องศาเซลเซียส ชิ้นงานเซรามิกทุกอัตราส่วนจะมีความหนาแน่นตัวที่ค่อนข้าง สูงและมีค่าที่ใกล้เคียงกันมากกว่าอุณหภูมิซินเทอร์อื่นๆ ดังนั้นในงานวิจัยนี้จึงทำการเลือกอุณหภูมิ การเผาที่ 1200 องศาเซลเซียส เพื่อศึกษาผลของการเติมปริมาณ SBT ต่อเฟส โครงสร้างจุลภาค ความหนาแน่น และสมบัติทางไฟฟ้า รวมทั้งความต้านทานต่อความล้าของเซรามิก PZT โดยค่า ความหนาแน่นของเซรามิกที่เผา ณ อุณหภูมิดังกล่าวนี้ได้แสดงในตาราง 3.1 ซึ่งแสดงให้เห็นว่าเมื่อ ทำการเติมปริมาณ SBT ในปริมาณ 0.1 ถึง 0.3 เศษส่วนโดยน้ำหนัก ลงไปใน PZT พบว่า ค่าความ หนาแน่นของเซรามิกมีค่าเพิ่มสูงขึ้น และจะมีค่าลดลงจนถึงค่าต่ำสุด เมื่อปริมาณการเติม SBT เพิ่ม สูงขึ้นถึง x เท่ากับ 0.7 และจะกลับมาเพิ่มอีกครั้งเมื่อปริมาณการเติม SBT เพิ่มขึ้นถึง x เท่ากับ 0.9 โดยการเปลี่ยนแปลงของค่าความหนาแน่นในเซรามิกระบบ PZT-SBT นี้จะทำการอภิปรายใน รายละเอียดเชิงลึกต่อไปในส่วนของผลโครงสร้างจุลภาค



รูป 3.1 ความหนาแน่นของเซรามิก (1-x)PZT-xSBT ที่ทำการเผา ณ อุณหภูมิซินเทอร์ต่างๆ

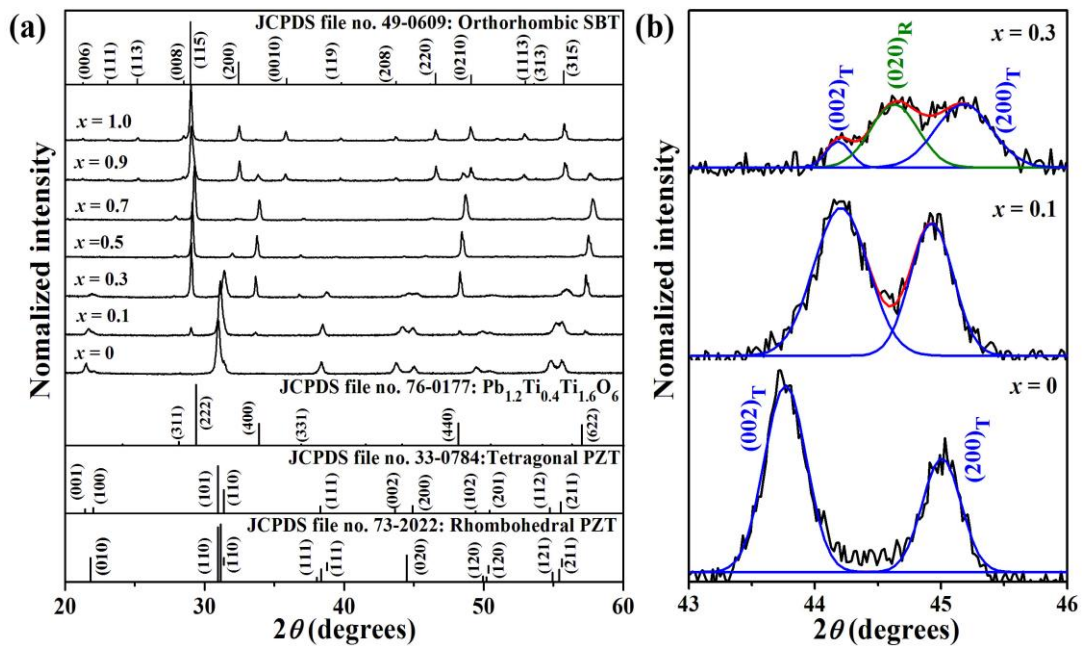
ตาราง 3.1 ความหนาแน่นของเซรามิก (1-x)PZT-xSBT ที่เผาซินเทอร์ที่อุณหภูมิ 1200 องศาเซลเซียส

ปริมาณการเติม SBT (x)	ความหนาแน่น (กรัมต่อลูกบาศก์เซนติเมตร)
0	7.67 ± 0.04
0.1	7.88 ± 0.02
0.3	7.78 ± 0.07
0.5	7.44 ± 0.07
0.7	7.46 ± 0.09
0.9	8.11 ± 0.03
1.0	8.06 ± 0.01

3.2 ผลการตรวจสอบเฟสของเซรามิก PZT-SBT

เซรามิก PZT-SBT ที่ทำการเผาซินเทอร์ที่อุณหภูมิ 1200 องศาเซลเซียส จะถูกนำมาวิเคราะห์เฟส โดยอาศัยเทคนิคการเลี้ยวเบนของรังสีเอกซ์ ซึ่งรูปแบบการเลี้ยวเบนของรังสีเอกซ์ของเซรามิกได้แสดงดังรูป 3.2 จากผลการทดลองพบว่า รูปแบบการเลี้ยวเบนของรังสีเอกซ์ของเซรามิก PZT บริสุทธิ์ มีความสอดคล้องกับไฟล์มาตรฐาน JCPDS หมายเลข 330784 ซึ่งมีโครงสร้างเตตระโกนอลของแลตทิซเพอร์รอฟสไกท์ ในขณะที่เซรามิก SBT แสดงโครงสร้างออร์โธโรมบิกของชั้นบิสปัท โดยสอดคล้องกับ JCPDS หมายเลข 49-0609 เมื่อทำการเติม SBT ในปริมาณ x เท่ากับ 0.1 ส่งผลทำให้พีคของเฟส PZT เลื่อนไปทางมุม 2θ ที่สูงขึ้น ซึ่งส่งผลทำให้

ค่าพารามิเตอร์แลตทิซและค่าความเป็นเตตระโกนอล (c/a) ลดลง แสดงดังตาราง 3.2 โดยการลดลงของพารามิเตอร์แลตทิซและค่าความเป็นเตตระโกนอลนี้ มีผลเนื่องมาจากไอออนจาก SBT ละลายเข้าไปในโครงสร้างของ PZT ซึ่ง Sr^{2+} (1.18 อังสตรอม) และ Bi^{3+} (1.03 อังสตรอม) จะเข้าไปแทนที่ในตำแหน่ง Pb^{2+} (1.19 อังสตรอม) ส่วน Ta^{5+} (0.64 อังสตรอม) จะเข้าไปแทนที่ในตำแหน่ง Zr^{4+} (0.72 อังสตรอม) หรือ Ti^{4+} (0.605 อังสตรอม) [11] จึงส่งผลทำให้พารามิเตอร์แลตทิซและค่าความเป็นเตตระโกนอลลดลง ที่สำคัญที่สุดยังพบว่าพีคของเฟส PZT ยังมีความกว้างเพิ่มขึ้น ซึ่งสามารถระบุได้ว่าเฟส PZT ที่ปรากฏขึ้นในเซรามิกเหล่านี้ เป็น PZT-based solid solution เมื่อปริมาณการเติม SBT เพิ่มขึ้นถึง 0.3 เศษส่วนโดยน้ำหนัก พบว่า เฟส PZT-based solid solution และ PTT-based solid solution ยังคงปรากฏในรูปแบบการเลี้ยวเบนของรังสีเอ็กซ์ แต่ความสูงของพีคของเฟส PZT มีค่าลดลงเป็นอย่างมาก ในขณะที่พีคของ PTT เพิ่มขึ้นอย่างรวดเร็ว ผลดังกล่าวนี้สามารถระบุได้ว่าปริมาณของเฟส PTT เพิ่มขึ้น แต่เฟสของ PZT กลับลดลง แสดงให้เห็นว่า PZT เข้าไปเกิดปฏิกิริยากับ SBT ในอัตราส่วนที่มากขึ้นนั่นเอง ทั้งนี้เมื่อทำการเพิ่มปริมาณ SBT ไปจนถึง 0.7 เศษส่วนโดยน้ำหนัก พบว่าปรากฏพีคของเฟส PTT เป็นเฟสหลัก และมีพีคของ SBT ปรากฏเพียงเล็กน้อย โดยพีคของ SBT ที่เกิดขึ้นได้แก่พีคของระนาบ (115) และ (200) ซึ่งแสดงว่าปริมาณ SBT ในเซรามิกเหล่านี้มีค่าน้อยมาก แต่เมื่อปริมาณการเติม SBT เพิ่มสูงถึง 0.9 กลับพบว่าความสูงของพีคและจำนวนพีค SBT เพิ่มสูงขึ้น ในขณะที่พีคของ PTT กลับมีความสูงและจำนวนพีคลดลง ทั้งนี้ยังพบว่าพีคของ SBT 2θ ที่สูงขึ้นเมื่อทำการเปรียบเทียบกับรูปแบบการเลี้ยวเบนของเซรามิก SBT บริสุทธิ์ การเลื่อนของพีคในเฟสของ SBT ส่งผลทำให้ค่าพารามิเตอร์แลตทิซ (ทั้งแกน a , b , c) และปริมาตรของหน่วยเซลล์ลดลง เมื่อพิจารณาพีค PTT พบว่ารูปแบบการเลี้ยวเบนเกิดการเลื่อนไปในมุม 2θ ที่ต่ำลงเมื่อเปรียบเทียบกับรูปแบบการเลี้ยวเบนของรังสีเอ็กซ์ของเฟส PTT ในเซรามิก 0.3PZT-0.7SBT ซึ่งส่งผลทำให้ค่าพารามิเตอร์แลตทิซ (ทั้งแกน a , b , c) และปริมาตรของหน่วยเซลล์เพิ่มขึ้น การเลื่อนตัวของทั้งเฟส SBT และ PTT สามารถระบุได้ว่าทั้งเฟส SBT และ PTT ที่ปรากฏในชิ้นงาน 0.1PZT-0.9SBT คือ เฟส SBT-based solid solution และ PTT-based solid solution ตามลำดับ จากการศึกษาเฟสในเซรามิกระบบ PZT-SBT พบว่า เฟสมีการเปลี่ยนแปลงเป็นอย่างมาก โดยเปลี่ยนจากโครงสร้างเพอรอฟสไกต์ของแลตทิซเตตระโกนอลไปสู่โครงสร้างแบบชั้นบิสปัทของแลตทิซออร์โธโรมบิก ซึ่งคาดว่า การเปลี่ยนแปลงที่เกิดขึ้นนี้จะส่งผลโดยตรงต่อสมบัติต่างๆ ไม่ว่าจะเป็นสมบัติไดอิเล็กทริก เฟอร์โรอิเล็กทริก รวมทั้งพฤติกรรมเชิงความล้าของเซรามิกระบบ PZT-SBT



รูป 3.2 (a) รูปแบบการเลี้ยวเบนของรังสีเอกซ์ของเซรามิก $(1-x)\text{PZT}-x\text{SBT}$ ที่เผาขึ้นเทอร์ที่อุณหภูมิ 1200 องศาเซลเซียส (b) แสดงพีค (002) และ (200) ของโครงสร้างเตตระโกนอล ในขณะที่พีคของ (020) เป็นพีคของโครงสร้างรอมโบอีตรอล (020) ที่มุม $2\theta \approx 43-46$ องศา ของเซรามิกที่มี x เท่ากับ 0 ถึง 0.3

ตาราง 3.2 พารามิเตอร์แลตทิซของเซรามิก $(1-x)\text{PZT}-x\text{SBT}$

ปริมาณการเติม SBT (x)	เฟส PZT				เฟส PTT		เฟส SBT			
	a (Å)	c (Å)	c/a	V (Å ³)	a (Å)	V (Å ³)	a (Å)	b (Å)	c (Å)	V (Å ³)
0	4.024	4.131	1.027	66.901	-	-	-	-	-	-
0.1	4.031	4.093	1.015	66.497	10.654	1209.506	-	-	-	-
0.3	4.009	4.095	1.021	65.820	10.639	1204.305	-	-	-	-
0.5	-	-	-		10.621	1197.991	-*	-*	-*	-*
0.7	-	-	-		10.562	1178.216	-*	-*	-*	-*
0.9	-	-	-		10.582	1184.943	5.519	5.524	25.125	765.877
1.0	-	-	-		-	-	5.523	5.528	25.110	766.662

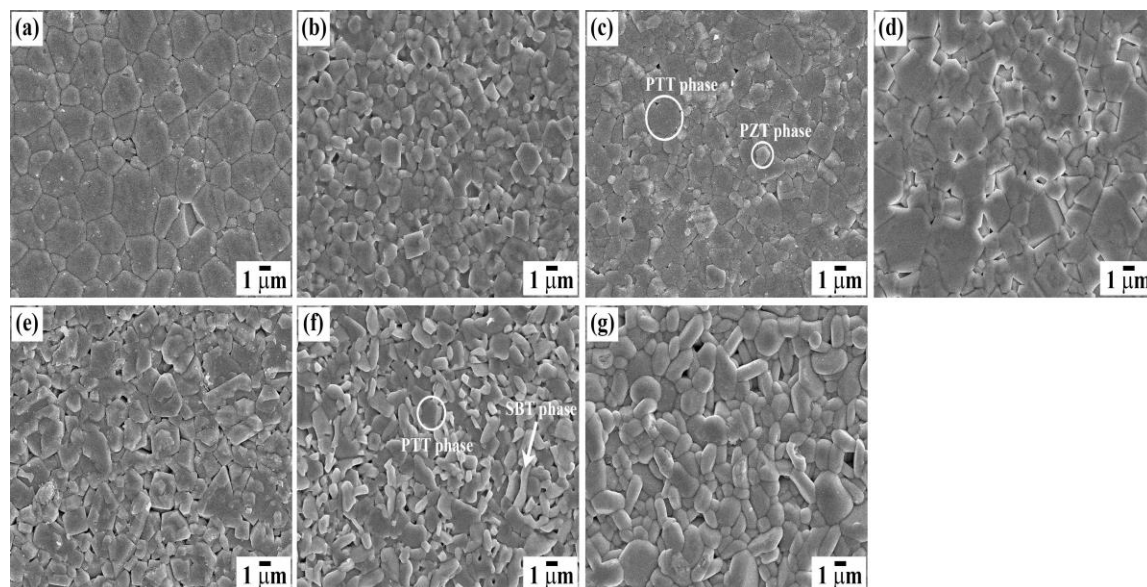
หมายเหตุ a = พารามิเตอร์แลตทิซ a, b = พารามิเตอร์แลตทิซ b, V = ปริมาณของหน่วยเซลล์, Å คือ อังสตรอม, c/a คือค่าความเป็นเตตระโกนอล * ระบุว่าชิ้นงานดังกล่าวไม่สามารถหาค่าพารามิเตอร์แลตทิซของเฟส SBT ได้ เนื่องจากชิ้นงานเหล่านี้ปรากฏพีคของ SBT เพียงสองพีคหลักเท่านั้น

3.3 ผลการตรวจสอบโครงสร้างจุลภาคของเซรามิก PZT-SBT

เนื่องจากโครงสร้างจุลภาคของเซรามิกเพอร์โรอิเล็กทริกมีผลโดยตรงต่อสมบัติทางไฟฟ้า ดังนั้นจึงได้ทำการศึกษาพื้นผิวของเซรามิก $(1-x)\text{PZT}-x\text{SBT}$ โดยตรวจสอบโดยกล้องจุลทรรศน์อิเล็กตรอนแบบส่องกราด ซึ่งผลการตรวจสอบได้แสดงดังรูป 3.3 จากรูปจะเห็นได้ว่าเซรามิก PZT บริสุทธิ์จะมีเกรนทรงหลายเหลี่ยม ในขณะที่เกรนรูปร่างแผ่นจะปรากฏในเซรามิก SBT บริสุทธิ์ แสดงดังรูป 3.3(a) และ (g) ตามลำดับ เมื่อทำการเติม SBT ในปริมาณ 0.1 ถึง 0.3 เศษส่วนโดยน้ำหนัก พบว่าเซรามิกมีความสม่ำเสมอของโครงสร้างจุลภาคมากขึ้น ทั้งนี้ยังปรากฏเกรนทรงหลายหน้าของ PTT อยู่ในพื้นผิวของเซรามิกอีกด้วย ซึ่งสอดคล้องกับผลการวิเคราะห์เฟสที่ได้อภิปรายในหัวข้อ 3.1.2 แต่เมื่อปริมาณการเติม SBT เพิ่มขึ้นถึง 0.7 พบว่าพื้นผิวของเซรามิกจะปรากฏเฉพาะเกรนของ PTT ทั้งนี้อาจเนื่องมาจากชิ้นงานเหล่านี้มีปริมาณ SBT ที่น้อยเกินไปนั่นเอง แต่เมื่อปริมาณการเติม SBT เพิ่มขึ้นจนถึง 0.9 ปรากฏว่าพื้นผิวมีทั้งเกรนรูปร่างแผ่นของ SBT และเกรนทรงหลายหน้าของ PTT อย่างไรก็ตามเมื่อทำการวิเคราะห์ขนาดเกรนของแต่ละเฟส ดังแสดงในตาราง 3.3 พบว่าการเติม SBT ในช่วง 0.1 ถึง 0.3 จะช่วยลดขนาดเกรนของเฟส PZT ซึ่งเป็นผลเนื่องมาจากการแทนที่ของไอออนแบบตัวเกิน (donor-like substitutions) ในโครงสร้างของ PZT จากผล XRD ซึ่งให้เห็นว่า PZT ที่ปรากฏในเซรามิกเหล่านี้ เป็น PZT ที่มีไอออนของเฟส SBT เข้าไปละลายในโครงสร้างเพอโรฟสไกต์ของ PZT ซึ่งมีตำแหน่ง SBT-doped PZT-based solid solution โดยการแทนที่ของไอออนเหล่านี้ไม่ว่าจะเป็นไอออน Bi^{3+} และ Ta^{5+} จะทำให้ปริมาณช่องว่างของเลด (Lead vacancy) เพิ่มขึ้น ในขณะที่ปริมาณของช่องว่างของออกซิเจนกลับลดลง เพื่อสร้างสมดุลประจุตนเอง ปกติแล้วค่าความหนาแน่นของเซรามิกระบบ PZT จะถูกควบคุมด้วยปริมาณของตำแหน่งช่องว่างของเลด [12] ตำแหน่งดังกล่าวนี้จะเข้าไปช่วยปรับปรุงปริมาตรการแพร่ในระบบ เนื่องจากในเซรามิกเหล่านี้มีการเหนี่ยวนำทำให้เกิดปริมาณของช่องว่างของเลดที่สูงขึ้นเนื่องจากผลของการเข้าไปแทนที่ของไอออน Bi^{3+} และ Ta^{5+} (จากเฟสของ SBT) ส่งผลทำให้อัตราการแพร่ของอะตอมในระบบเพิ่มสูงขึ้น จนในที่สุดชิ้นงานมีความหนาแน่น นอกจากปริมาณของช่องว่างของเลดจะช่วยควบคุมความหนาแน่นของเซรามิกเพอร์โรอิเล็กทริกแบบ PZT แล้ว ตำแหน่งดังกล่าวนี้ยังสามารถควบคุมขนาดของเกรนได้อีกด้วย [13] โดยช่องว่างของเลดจะเข้าไปหมุดที่บริเวณขอบเกรน (grain boundary) ทำให้การเคลื่อนตัวของอะตอมบริเวณขอบเกรนทำได้ยากขึ้นระหว่างกระบวนการซินเทอร์ เมื่ออะตอมเกิดการแพร่ได้ยากขึ้น ก็จะส่งผลทำให้การเติบโตของเกรนลดลง ดังนั้นเซรามิกที่มีปริมาณการเติม SBT ที่ x เท่ากับ 0.1 ถึง 0.3 จึงมีขนาดเกรนของเฟส PZT ที่เล็กกว่าเซรามิก PZT บริสุทธิ์

เมื่อปริมาณการเติม SBT เพิ่มขึ้น จนถึง x เท่ากับ 0.7 พบว่าพื้นผิวของเซรามิกมีเฉพาะเกรนรูปทรงหลายหน้าของเฟส PTT โดยที่ไม่ปรากฏเกรนแบบแผ่นของ SBT อาจเนื่องมาจากปริมาณของเฟส SBT ในชิ้นงานเหล่านี้มีค่าน้อยมากนั่นเอง ทั้งนี้ยังพบว่าการสร้างพันธะระหว่างเกรนต่อเกรนยังมีค่าต่ำ สังเกตได้จากการมีรูพรุนในพื้นผิวของชิ้นงาน ส่งผลทำให้ค่าความหนาแน่นมีค่าต่ำ ซึ่งสอดคล้องกับค่าความหนาแน่นที่ได้อภิปรายในหัวข้อ 3.1.1 ในกรณีของเซรามิกที่มีการเติม x เท่ากับ 0.9 พบว่าพื้นผิวของเซรามิกมีทั้งเกรนแบบแผ่นของ SBT และเกรนทรงหลายหน้า

ของ PTT ทั้งนี้ชั้นงานนี้ยังมีความสม่ำเสมอของโครงสร้างจุลภาค ทั้งนี้อาจเนื่องดำหนึ่ในระบบที่เกิดจาก PZT-doped SBT-based solid solution เข้าไปช่วยปรับปรุงความแน่นตัวของเซรามิกนี้ เมื่อทำการพิจารณาขนาดเกรนของเฟส SBT-based solid solution ในตาราง 3.3 พบว่าขนาดเกรนมีขนาดลดลงเมื่อทำการเปรียบเทียบกับเซรามิก SBT บริสุทธิ์ ทั้งนี้เนื่องจากการเกิดเฟสที่สองอย่าง PTT โดยเฟส PTT นี้อาจจะเข้าไปขัดขวางกระบวนการแพร่ของอะตอม ณ บริเวณขอบเกรนภายในเฟสของ SBT ระหว่างกระบวนการซินเทอร์ ส่งผลทำให้ขนาดเกรนแบบแผ่นของ SBT ลดลง นั่นเอง



รูป 3.3 โครงสร้างจุลภาคของพื้นผิวของเซรามิก (1-x)PZT-xSBT เมื่อ (a) $x = 0$ (b) $x = 0.1$ (c) $x = 0.3$ (d) $x = 0.5$ (e) $x = 0.7$ (f) $x = 0.9$ และ (g) $x = 1.0$ ตามลำดับ

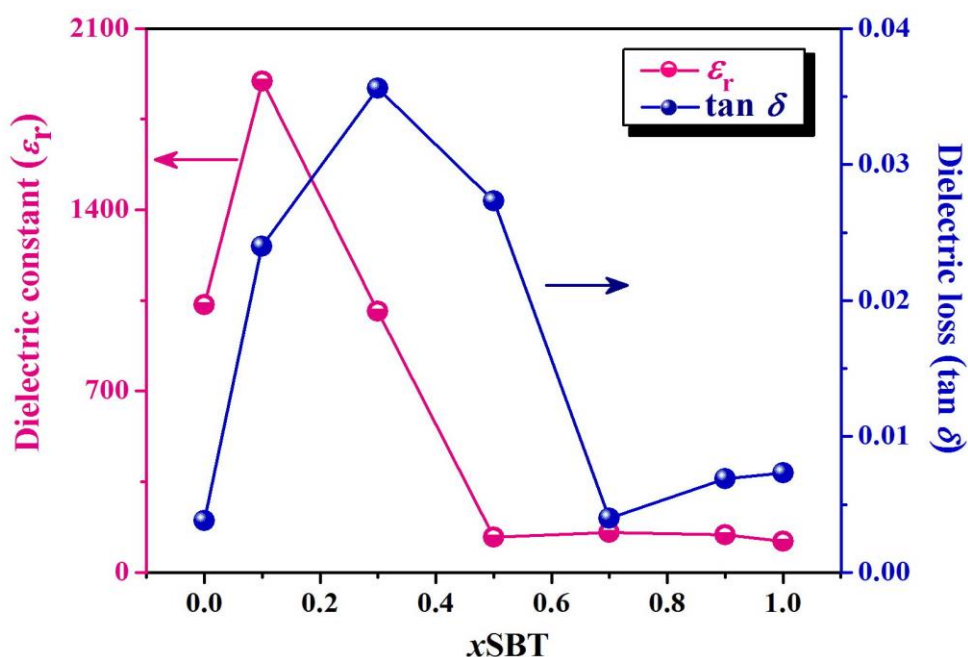
ตาราง 3.3 ขนาดเกรนของเซรามิก (1-x)PZT-xSBT

ปริมาณการเติม SBT (x)	ขนาดเกรนโดยเฉลี่ย (ไมโครเมตร)			
	เกรนรูปทรง เหลี่ยมมุม	เกรนรูปทรง หลายหน้า	เกรนแบบแผ่น	
			ความยาว	ความหนา
0	2.72 ± 0.13	-	-	-
0.1	1.21 ± 0.05	1.50 ± 0.09	-	-
0.3	1.28 ± 0.08	2.40 ± 0.12	-	-
0.5	-	2.93 ± 0.28	-	-
0.7	-	1.98 ± 0.13	-	-
0.9	-	1.29 ± 0.09	0.54 ± 0.04	1.69 ± 0.08
1.0	-	-	0.76 ± 0.05	2.15 ± 0.11

3.4 ผลการตรวจสอบสมบัติไดอิเล็กทริกของเซรามิก PZT-SBT

เมื่อนำเซรามิกระบบ (1-x)PZT-xSBT ที่ผ่านการเผาซินเทอร์อุณหภูมิ 1200 องศาเซลเซียส มาศึกษาค่าคงที่ไดอิเล็กทริก (dielectric constant) และค่าการสูญเสียทางไดอิเล็กทริก (dielectric loss) โดยวัดที่อุณหภูมิห้องและความถี่ 1 กิโลเฮิร์ตซ์ ดังรูป 3.4 และตาราง 3.4 พบว่า ค่าคงที่ไดอิเล็กทริกและค่าการสูญเสียทางไดอิเล็กทริกของเซรามิก PZT บริสุทธิ์ มีค่ามากกว่าเซรามิก SBT บริสุทธิ์เป็นอย่างมาก ซึ่งสอดคล้องกับผลงานวิจัยที่ของ Zhang และคณะ [6] ที่ระบุว่าสาร SBT มี

ค่าคงที่ไดอิเล็กทริกที่ต่ำถ้าเทียบกับ PZT เมื่อทำการเติมปริมาณ SBT เพียงเล็กน้อย (x เท่ากับ 0.1 เศษส่วนโดยน้ำหนัก) พบว่า ค่าคงที่ไดอิเล็กทริกของเซรามิกสูงขึ้นเป็นอย่างมาก ซึ่งอาจกล่าวได้ว่าเป็นค่าที่สูงที่สุดของเซรามิกระบบ PZT-SBT นี้ก็ว่าได้ การปรับปรุงค่าคงที่ไดอิเล็กทริกในอัตราส่วนนี้มีผลเนื่องจากแทนที่ของไอออนแบบตัวเกิน (donor-like substitutions) โดยการที่ไอออน Bi^{3+} เข้าไปแทนที่ตำแหน่ง Pb^{2+} และ Ta^{5+} เข้าไปแทนที่ในตำแหน่ง Ti^{4+} หรือ Zr^{4+} ทำให้ปริมาณช่องว่างของออกซิเจนลดลงเป็นอย่างมาก โดยช่องว่างของออกซิเจนนี้จะชอบเข้าไปหมุดที่ผนังโดเมนของสารเฟอร์โรอิเล็กทริกเนื่องจากบริเวณดังกล่าวมีค่าพลังงานที่ต่ำ ดังนั้นเมื่อปริมาณช่องว่างของออกซิเจนลดต่ำลงส่งผลทำให้ปริมาณการหมุดโดเมนลดลง กล่าวอีกแง่คือโดเมนสามารถสวิตช์ได้ง่ายขึ้น เมื่อโดเมนสวิตช์ได้ง่ายค่าคงที่ไดอิเล็กทริกและค่าการสูญเสียทางไดอิเล็กทริกจึงเพิ่มขึ้น เมื่อทำการเติมปริมาณการเติม SBT จนถึง x เท่ากับ 0.7 ส่งผลทำให้ค่าคงที่ไดอิเล็กทริกและค่าการสูญเสียทางไดอิเล็กทริกของเซรามิกลดลงอย่างรวดเร็ว ผลดังกล่าวนี้เกิดจากการปรากฏของเฟสที่ไม่มีสมบัติเฟอร์โรอิเล็กทริกอย่าง PTT นั่นเอง ในกรณีของเซรามิกที่ทำการเติม SBT เท่ากับ 0.9 ร้อยละโดยน้ำหนัก พบว่า ค่าคงที่ไดอิเล็กทริกเพิ่มขึ้นเพียงเล็กน้อยเมื่อทำการเปรียบเทียบกับเซรามิก SBT บริสุทธิ์ ในขณะที่ค่าการสูญเสียทางไดอิเล็กทริกมีค่าใกล้เคียงกับเซรามิก SBT บริสุทธิ์ ถึงแม้ว่าชั้นงานดังกล่าวนี้เป็น ลักษณะตำหนิแบบ PZT-doped SBT-based solid solution แต่ทั้งนี้การเกิดเฟสใหม่อย่าง PTT ในชั้นงานดังกล่าวนี้ส่งผลทำให้ตำหนิในระบบเกิดขึ้นได้ยาก ดังนั้นสมบัติไดอิเล็กทริกจึงไม่ค่อยมีการเปลี่ยนแปลงมากเท่าใดเมื่อเทียบกับเซรามิก SBT บริสุทธิ์



รูป 3.4 กราฟความสัมพันธ์ระหว่างค่าคงที่ไดอิเล็กทริกและค่าการสูญเสียทางไดอิเล็กทริกกับอัตราส่วน การเติม SBT ในเซรามิก $(1-x)\text{PZT}-x\text{SBT}$ ที่ความถี่การวัด 1 กิโลเฮิร์ตซ์

ตาราง 3.4 สมบัติไดอิเล็กทริกของเซรามิก (1-x)PZT-xSBT ที่ความถี่ 1 กิโลเฮิร์ตซ์

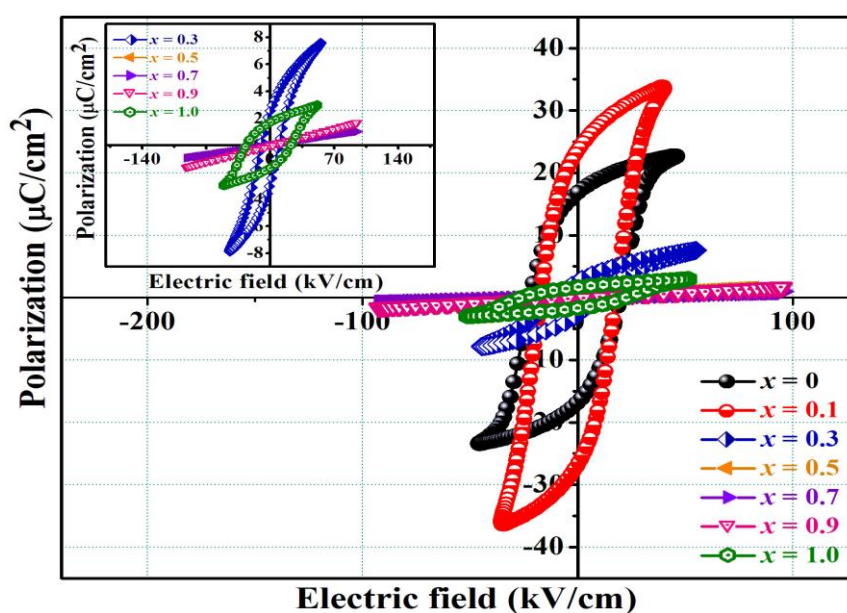
ปริมาณการเติม SBT (เศษส่วนโดยน้ำหนัก)	ค่าคงที่ไดอิเล็กทริก	ค่าการสูญเสียทางไดอิเล็กทริก
0	1032.48	0.0038
0.1	1895.81	0.024
0.3	1008.46	0.0356
0.5	136.76	0.0273
0.7	154.56	0.004
0.9	145.42	0.0069
1.0	119.28	0.0073

3.5 ผลการตรวจสอบสมบัติเฟอร์โรอิเล็กทริกของเซรามิก PZT-SBT

เนื่องจากสมบัติเฟอร์โรอิเล็กทริกเป็นอีกหนึ่งสมบัติที่มีความสำคัญเป็นอย่างมากในหน่วยความจำ ดังนั้นจึงทำการวัดความสัมพันธ์ระหว่างโพลาริเซชันกับสนามไฟฟ้า ($P-E$) ที่อุณหภูมิห้องด้วยความถี่ 50 เฮิร์ตซ์ ซึ่งผลการทดลองได้แสดงดังรูป 3.5 ทั้งนี้ค่าโพลาริเซชันคงค้าง ($2P_r$) และสนามลบกลับ ($2E_c$) ของเซรามิก (1-x)PZT-xSBT แสดงดังตาราง 3.5 จากผลการทดลองพบว่า กราฟ $P-E$ ของเซรามิก PZT บริสุทธิ์มีลักษณะวงวนที่ผอม โดยมีค่าโพลาริเซชันคงค้างที่สูง ขณะที่สนามลบกลับมีค่าต่ำ แต่ในกรณีของเซรามิก SBT บริสุทธิ์ พบว่าลักษณะวงวนจะมีค่าโพลาริเซชันคงค้างที่ต่ำและมีค่าสนามลบกลับที่สูง โดยชี้ให้เห็นว่าพฤติกรรมทางเฟอร์โรอิเล็กทริกของ PZT มีความแตกต่างจาก SBT เป็นอย่างมาก ซึ่งใน PZT นั้น เมื่อทำการจ่ายสนามไฟฟ้าให้แก่ PZT โดเมนภายในจะเกิดการสวิตช์ได้อย่างง่าย ในขณะที่ SBT จะเกิดการสวิตช์ที่ยาก เนื่องจากผลของโครงสร้างที่มีชั้นของ Bi_2O_3 ครอบคลุมทั่วทั้งของชั้นเพอโรฟสไกต์อยู่ ดังนั้นเมื่อทำการจ่ายสนามไฟฟ้า โดเมนจึงขยับหรือหมุนตัวได้ยาก ส่งผลทำให้ค่าโพลาริเซชันคงค้างมีค่าต่ำ และต้องใช้สนามปริมาณมากในการเหนี่ยวนำทำให้เกิดการสวิตช์ของโดเมนภายใน SBT จึงทำให้ค่าสนามลบกลับมีค่าสูงนั่นเอง [25]

เมื่อทำการเติม SBT ในปริมาณ 0.1 เศษส่วนโดยน้ำหนัก ส่งผลทำให้ค่าโพลาริเซชันคงค้างเพิ่มสูงขึ้น ในขณะที่ค่าสนามลบกลับลดลง ซึ่งเป็นคุณสมบัติที่เหมาะสมเป็นอย่างยิ่งต่ออุปกรณ์หน่วยความจำ การเพิ่มขึ้นของค่าโพลาริเซชันคงค้างและการลดลงของสนามลบกลับเนื่องจากผลของการแทนที่ของไอออนจาก SBT เข้าไปในโครงสร้างของ PZT โดยในเซรามิกนี้ ไอออนของ Bi^{3+} และ Ta^{5+} จะเหนี่ยวนำทำให้เกิดช่องว่างของเลต ในขณะเดียวกันปริมาณของช่องว่างของออกซิเจนก็จะลดลงอย่างรวดเร็ว เนื่องจากผลสมดุลประจุ [16-17] ตำแหน่งที่เกิดขึ้นเหล่านี้จะช่วยเพิ่มความสามารถในการเคลื่อนที่ของโดเมนภายในเฟส PZT จึงส่งผลทำให้ค่าโพลาริเซชันคงค้างเพิ่มขึ้น ทั้งนี้สนามไฟฟ้าที่ใช้ในการสวิตช์โดเมนภายในชั้นงานจึงมีค่าลดลง ทำให้ค่าสนามลบกลับลดลงนั่นเอง เมื่อทำการเพิ่มปริมาณ SBT เท่ากับ 0.3 เศษส่วนโดยน้ำหนัก พบว่ารูปร่างของวงวนฮิสทีรีซิสจะมีลักษณะเล็กและแคบ โดยมีค่าโพลาริเซชันคงค้างและค่าสนามลบกลับที่ต่ำ ซึ่งชี้ให้เห็นว่าสมบัติเฟอร์โรอิเล็กทริกลดลง อันเป็นผลเนื่องมาจากเฟสของ PTT เข้าไปขัดขวางการสวิตช์ของเฟอร์

โรอีเล็กทริกโดเมนของ PZT ทำให้โดเมนเกิดการเคลื่อนที่ได้ยาก ส่งผลให้ค่าโพลาริเซชันคงค้างลดลงเป็นอย่างมาก ทั้งนี้เมื่อทำการเพิ่มปริมาณการเติม SBT จนถึง 0.9 เศษส่วนโดยน้ำหนัก กลับพบว่าลักษณะฮิสทีรีซิสเป็นเส้นตรงไม่ปรากฏทั้งค่าโพลาริเซชันคงค้างและค่าสนามลบล่าง โดยลักษณะดังกล่าวนี้เป็นพฤติกรรมของพาราอีเล็กทริก [18] การเปลี่ยนแปลงจากสมบัติเฟอร์โรอีเล็กทริกจาก PZT สู่สมบัติพาราอีเล็กทริกใน PZT-SBT เป็นผลเนื่องมาจากการปรากฏของเฟส PTT จากพฤติกรรมเฟอร์โรอีเล็กทริกของเซรามิกระบบ PZT-SBT พบว่ามีเพียง 4 อัตราส่วนที่เกิดลักษณะวงวนของวัสดุเฟอร์โรอีเล็กทริกคือ PZT, 0.9PZT-0.1SBT, 0.7PZT-0.3SBT และ SBT ดังนั้นเซรามิกทั้ง 4 อัตราส่วนนี้จึงน่าสนใจที่จะทำการศึกษาผลของความล่าต่อความสามารถในการโพลาริเซชันต่อไป ซึ่งจะอภิปรายในหัวข้อถัดไป



รูป 3.5 กราฟความสัมพันธ์ระหว่างโพลาริเซชันกับสนามไฟฟ้าของเซรามิก (1-x)PZT-xSBT ที่ทำการวัด ณ อุณหภูมิห้องด้วยความถี่ 50 เฮิร์ตซ์

ตาราง 3.5 โพลาริเซชันคงค้างและสนามลบล่างของเซรามิก (1-x)PZT-xSBT

ปริมาณการเติม SBT (x)	โพลาริเซชันคงค้าง; $2P_r$ (ไมโครคูลอมป์ต่อตารางเซนติเมตร)	สนามลบล่าง; $2E_c$ (กิโลโวลต์ต่อเซนติเมตร)
0	34.96	68.10
0.1	51.37	34.78
0.3	4.46	22.28
0.5	-	-
0.7	-	-
0.9	-	-
1.0	3.49	52.02

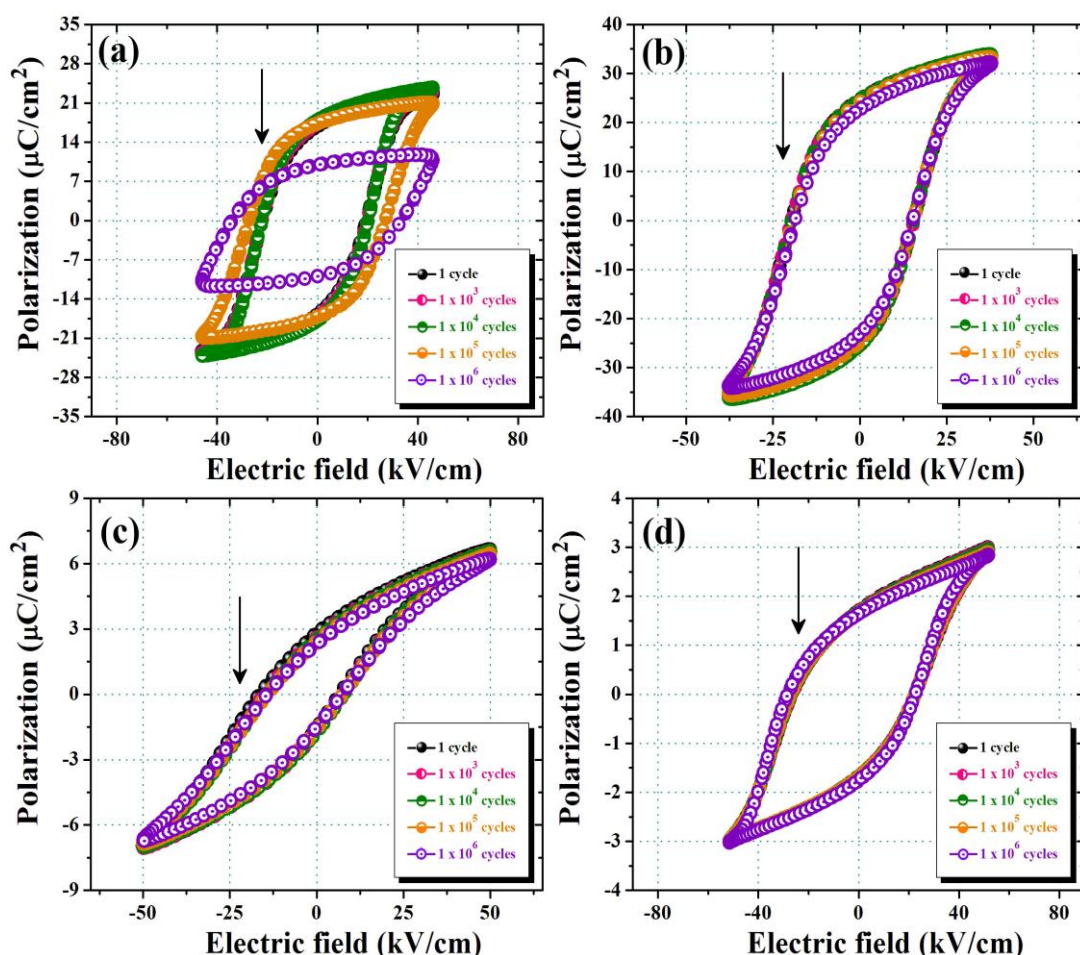
3.6 ผลการตรวจสอบสมบัติเฟอร์โรอิเล็กทริกของเซรามิก PZT-SBT

หลังจากทำการวัดสมบัติเฟอร์โรอิเล็กทริกของเซรามิกระบบ PZT-SBT แล้ว หลังจากนั้นได้ทำการจ่ายสนามไฟฟ้าต่อเนื่องให้แก่ชิ้นงาน PZT, 0.9PZT-0.1SBT, 0.7PZT-0.3SBT และ SBT เพื่อศึกษาผลของความล้าที่มีต่อสมบัติเฟอร์โรอิเล็กทริก โดยจะทำการวัดกราฟ $P-E$ ที่แต่ละจำนวนสวิตช์ ได้แก่ 1, 1000, 10000, 100000 และ 1000000 รอบ แสดงดังรูป 3.6 จากผลการทดลองชี้ให้เห็นการกราฟ $P-E$ ของเซรามิกเกิดการเปลี่ยนแปลงรูปร่างเป็นอย่างมากเมื่อเทียบกับเซรามิก SBT บริสุทธิ์ ซึ่งพบว่าค่าโพลาริเซชันคงค้างลดลงอย่างรวดเร็วขณะที่ค่าสนามลบกลับกลับเพิ่มสูงขึ้น แต่ในกรณีของเซรามิก $(1-x)\text{PZT}-x\text{SBT}$ เมื่อ x เท่ากับ 0.1 ถึง 0.3 กลับพบว่าลักษณะกราฟของ $P-E$ แทบไม่มีการเปลี่ยนแปลงเลย เมื่อเทียบกับเซรามิก PZT บริสุทธิ์ แต่อย่างไรก็ตามการวัดผลเพียงแค่การเปลี่ยนแปลงของกราฟ $P-E$ ยังไม่สามารถระบุถึงอัตราของความล้าได้อย่างชัดเจน ดังนั้นจึงได้ทำการศึกษาการลดลงของค่าโพลาริเซชันคงค้าง (normalized remanent polarization) เทียบกับจำนวนรอบการสวิตช์โดเมน แสดงดังรูป 3.7 จากผลการศึกษา พบว่าค่าโพลาริเซชันคงค้างของ PZT ลดลงเป็นอย่างมากเมื่อเทียบกับเซรามิกที่อัตราส่วนอื่นๆ โดยเปอร์เซ็นต์การลดลงของค่าคงค้างโพลาริเซชันมีค่าสูงถึง 49% (ตาราง 3.6) ทั้งนี้เป็นผลเนื่องมาจาก PZT มีปริมาณช่องว่างออกซิเจนที่มากจากผลของการระเหยของเลดออกไซด์ โดยตำหนินี้จะเข้าไปหมุดโดเมนของ PZT และเมื่อทำการจ่ายจำนวนรอบของสนามไฟฟ้าเพิ่มขึ้นเรื่อยๆ ก็จะทำให้เกิดการสะสมของความเครียดเนื่องจากการหมุดนี้ ส่งผลทำให้โดเมนภายในชิ้นงานเกิดการสวิตช์ได้ยากมากขึ้น ทำให้ค่าโพลาริเซชันคงค้างลดลง [20-21] ในขณะเดียวกันโดเมนบางส่วนที่ไม่ถูกหมุดก็ยังคงต้องการที่จะสวิตช์ แต่โดเมนเหล่านี้จะต้องอาศัยค่าสนามไฟฟ้าที่สูงกว่าค่าเริ่มต้นจึงทำให้ค่าสนามไฟฟ้าลบกลับมีค่าเพิ่มสูงขึ้นด้วยนั่นเอง เมื่อพิจารณาในเซรามิก SBT บริสุทธิ์พบว่าค่าโพลาริเซชันคงค้างแทบไม่มีการลดลง ผลดังกล่าวนี้เกิดจากความมีเสถียรภาพสูงของโครงสร้างแบบชั้นบิสัทของ SBT นั่นเอง โดยที่ชั้น Bi_2O_3 จะเข้าไปช่วยลดประสิทธิภาพในการหมุดของโดเมนภายใน SBT [26] ดังนั้นเมื่อทำการจ่ายสนามไฟฟ้าไปในจำนวนรอบที่มากขึ้น ผลของการหมุดโดเมนก็แทบจะไม่เกิดขึ้น หรืออาจเกิดได้น้อยมาก ส่งผลทำให้ค่าโพลาริเซชันคงค้างไม่ลดลง

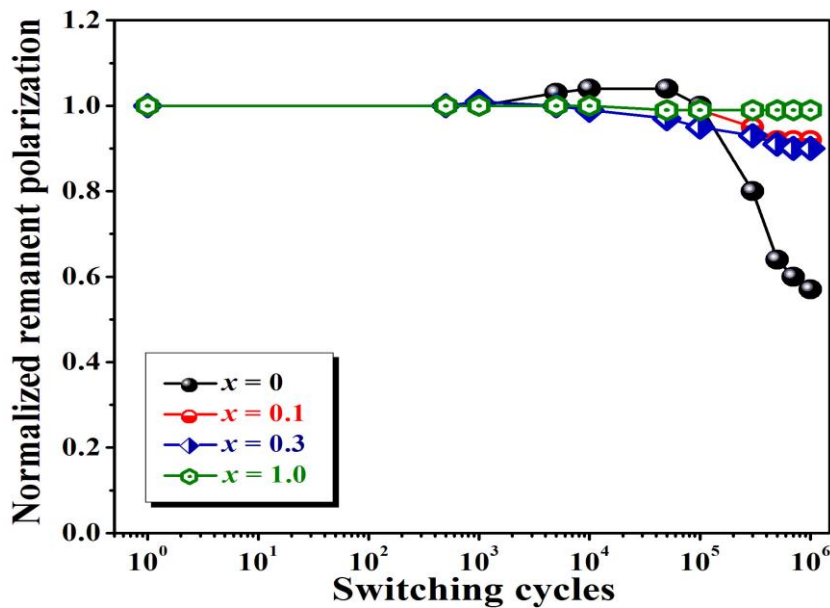
เมื่อพิจารณาในเซรามิกที่มีปริมาณการเติม SBT เท่ากับ 0.1 และ 0.3 พบว่าอัตราการลดลงของค่าโพลาริเซชันคงค้างมีค่าต่ำกว่า PZT เป็นอย่างมาก ซึ่งมีค่าการลดลงเพียง 9-10% ของค่าเริ่มต้น ดังนั้นจึงกล่าวได้ว่าเซรามิก ณ อัตราเหล่านี้สามารถปรับปรุงค่าความต้านทานของ PZT ได้อย่างดีเยี่ยม โดยผลของการแทนที่ของไอออนจาก SBT เข้าไปใน PZT ถือเป็นเหตุผลหลักในการปรับปรุงสมบัติเชิงความล้า เนื่องจากไอออนที่เข้าไปในระบบของ PZT จะเข้าไปลดจำนวนของช่องว่างออกซิเจน เมื่อปริมาณของช่องว่างออกซิเจนลดลง การหมุดของโดเมนก็จะลดลง ส่งผลทำให้โดเมนสามารถสวิตช์ได้อย่างต่อเนื่องโดยที่เกิดการสูญเสียการโพลาริเซชันเพียงเล็กน้อยเมื่อสิ้นสุดกระบวนการจ่ายสนามไฟฟ้าแบบต่อเนื่อง ทั้งนี้การลดลงของค่าความเป็นเตตระโกนอลของเซรามิกเหล่านี้ ดังได้อธิบายไว้แล้วในหัวข้อ 3.1.2 โดยทั่วไปแล้วความเค้นภายใน (internal stress) อันเนื่องมาจากการเปลี่ยนเฟสของสารเฟอร์โรอิเล็กทริกจะสามารถระบุได้ค่าความเป็นเตตระ

โกนอล ซึ่งถ้าชิ้นงานใดมีความเค้นสะสมที่มากก็จะส่งผลต่อการสวิตช์ของโดเมน กล่าวคือ ถ้าปริมาณของความเค้นภายในมีค่ามากเพียงพอ จะทำให้โดเมนไม่สามารถทำการสวิตช์ได้ต่อไป [22] โดยปกติแล้วค่าความเค้นภายในจะแปรผันตรงกับค่าความเป็นเตตระโกนอล [23-24] ซึ่งเมื่อพิจารณาจากตาราง 3.2 จะพบว่าค่า c/a ของเซรามิก 0.9PZT-0.1SBT และ 0.7PZT-0.3SBT มีค่าน้อยกว่า PZT ดังนั้นปริมาณความเค้นภายในของเซรามิกนี้จึงมีค่าน้อยกว่าเซรามิก PZT บริสุทธิ์ เมื่อความเค้นมีปริมาณน้อยกว่า จึงส่งผลทำให้โดเมนสามารถสวิตช์ได้ตามปกติเมื่อทำการจ่ายสนามไฟฟ้าต่อเนื่อง ดังนั้นอัตราการลดลงของค่าโพลาไรเซชันคงค้างจึงมีต่ำกว่าเซรามิก PZT บริสุทธิ์ นั่นเอง

จากผลการศึกษาพฤติกรรมความล้าของเซรามิกระบบ $(1-x)\text{PZT}-x\text{SBT}$ เปรียบเทียบกับเซรามิก PZT และ SBT บริสุทธิ์ พบว่าการเติม SBT เข้าไปใน PZT สามารถที่จะช่วยปรับปรุงค่าความต้านทานความล้าให้แก่ PZT ได้อย่างดีเยี่ยม ซึ่งสามารถชี้ให้เห็นว่าอายุการใช้งานของวัสดุ PZT-SBT มีค่าสูงกว่าเซรามิก PZT บริสุทธิ์ ทำให้มีแนวโน้มว่าสามารถใช้วัสดุระบบใหม่นี้ทดแทน



รูป 3.6 กราฟความสัมพันธ์ระหว่างสนามไฟฟ้าและโพลาไรเซชันของเซรามิก $(1-x)\text{PZT}-x\text{SBT}$ ที่จำนวนรอบการสวิตช์ต่างๆ โดย (a) $x = 0$ (b) $x = 0.1$ (c) $x = 0.3$ และ (d) $x = 1.0$



รูป 3.7 การเปลี่ยนแปลงค่าโพลาไรเซชันคงค้างเทียบกับจำนวนรอบการสวิตช์ที่เพิ่มขึ้นของเซรามิก กระจกแบบ (1-x)PZT-xSBT

ตาราง 3.6 ค่าโพลาไรเซชันคงค้างของเซรามิก (1-x)PZT-xSBT ที่ทำการวัดก่อนและหลังวัดความ ล้า

ปริมาณการเติม SBT (x)	ก่อนวัด	หลังวัด	เปอร์เซ็นต์การลดลงของ ค่าโพลาไรเซชันคงค้าง
0	34.96	20.05	43
0.1	51.37	46.96	9
0.3	4.46	4	10
1.0	3.49	3.47	0.6

4. สรุปผลการทดลอง

จากผลการตรวจสอบความหนาแน่น เฟส โครงสร้างจุลภาค สมบัติไดอิเล็กทริก สมบัติเพอร์โรวีเอตริก และสมบัติไดอิเล็กโตรสตริกทีฟของเซรามิก PZT-SBT สามารถสรุปผลได้ ดังนี้

- อุณหภูมิซินเทอร์ที่เหมาะสมสำหรับเซรามิกแบบ PZT-SBT คือ 1200 องศาเซลเซียส ซึ่งเป็นอุณหภูมิที่ทำให้เซรามิกทุกอัตราส่วนมีค่าความหนาแน่นที่ใกล้เคียงกัน
- ค่าความหนาแน่นของเซรามิก PZT เพิ่มขึ้นเมื่อทำการเติม SBT โดยปัจจัยหลักของการเพิ่มขึ้นคือการเพิ่มขึ้นของตำหนิในโครงสร้าง ช่วยให้อัตราการแพร่สูงขึ้น และส่งผลทำให้เซรามิกที่ความแน่นตัว
- ค่าพารามิเตอร์แลตทิซและปริมาตรของหน่วยเซลล์ของเซรามิก PZT บริสุทธิ์ มีแนวโน้มลดลงเมื่อเติม SBT ในอัตราส่วน 0.1 ถึง 0.3 ร้อยละโดยน้ำหนัก

- โครงสร้างจุลภาค PZT-SBT แสดงถึงการเปลี่ยนอย่างชัดเจน โดยจะพบเกรนรูปทรงเหลี่ยมมุมในเซรามิกที่มีอัตราส่วนการเติม SBT น้อยๆ ไปสู่เกรนแบบแผ่นในเซรามิกที่มีการเติม SBT เพิ่มมากขึ้น
- การเติม SBT ในปริมาณ 0.1 เศษส่วนโดยน้ำหนัก ช่วยเพิ่มค่าคงที่ไดอิเล็กทริกของเซรามิก PZT บริสุทธิ์ ประมาณ 1.5 เท่าตัว
- สมบัติเฟอร์โรอิเล็กทริกของ PZT ถูกปรับปรุงหลังจากเติม SBT ในปริมาณ 0.1 เศษส่วนโดยน้ำหนัก โดยมีค่าโพลาริเซชันคงค้างที่เพิ่มขึ้น และค่าสนามลบลงที่ลดลง ซึ่งเป็นผลดีแก่อุปกรณ์หน่วยความจำเป็นอย่างยิ่ง
- การเติม SBT ในปริมาณ 0.1 ถึง 0.3 เศษส่วนโดยน้ำหนัก เข้าไปใน PZT สามารถที่จะลดความล้าของเซรามิกได้ เมื่อเปรียบเทียบกับเซรามิก PZT บริสุทธิ์
- จากการศึกษาและทดลองชี้ให้เห็นว่าเซรามิกระบบใหม่อย่าง PZT-SBT มีสมบัติเฟอร์โรอิเล็กทริกที่ดีเยี่ยม โดยมีค่าโพลาริเซชันคงค้างที่สูงและค่าสนามไฟฟ้าที่ต่ำ ทั้งยังมีสมบัติความล้าที่ดีเยี่ยม ดังนั้นจึงเป็นการเหมาะสมที่จะนำเซรามิกระบบนี้ไปพัฒนาเพื่อใช้ในอุปกรณ์หน่วยความจำแทนที่ PZT

5. เอกสารอ้างอิง

- [1] G.H. Haertling, Ferroelectric ceramics: History and technology, J. Am. Ceram. Soc. 82(4) (1999) 797-818.
- [2] B. Jaffe, W.R. Cook and H. Jaffe, Piezoelectric Ceramics, Academic Press, London, 1971.
- [3] D.H. Bao, N. Wakiya, K. Shinozaki and N. Mizutani, Ferroelectric properties of sandwich structured $(\text{Bi, La})_4\text{T}_3\text{O}_{12}/\text{Pb}(\text{Zr, Ti})\text{O}_3/(\text{Bi, La})_4\text{Ti}_3\text{O}_{12}$ thin films on Pt/Ti/SiO₂/Si substrates, J. Phys. D: Appl. Phys. A 35 (2002) L1-L5.
- [4] N. Balke, H. Kungl, T. Granzow, D. C. Lupascu, M. J. Hoffmann and J. Rödel, Bipolar fatigue caused by field screening in $\text{Pb}(\text{Zr,Ti})\text{O}_3$ ceramics, J. Am. Ceram. Soc. 90(12) (2007) 3869-3874.
- [5] C.A. Paz de Arujo, J.D. Cuchiaro, L.D. McMillan, M.C. Scott and J.F. Scott, Fatigue-free ferroelectric capacitors with platinum electrodes, Nature. 374 (1995) 627-629.
- [6] W.Q. Zhang, A.D. Li, Q.Y. Shao, Y.D. Xia, D. Wu, Z.G. Liu and N.B. Ming, Ferroelectric properties of bilayer structured $\text{Pb}(\text{Zr}_{0.52}\text{Ti}_{0.48})\text{O}_3/\text{SrBi}_2\text{Ta}_2\text{O}_9$ (PZT/SBT) thin films on Pt/TiO₂/SiO₂/Si substrates, Appl. Surf. Sci. 254 (2008) 1583-2586
- [7] H.H. Park, H.H. Park, T.S. Kim and R.H. Hill, Electric and ferroelectric properties of PZT/SBT multilayer films prepared by photochemical metal-organic deposition, Sensors and Actuat. B130 (2008) 696-700.

- [8] A.I. Kingon, and J.B. Clark, Sintering of PZT ceramics: I, Atmosphere control, J. Am. Ceram. Soc. 66(4) (1983) 253-256.
- [9] A.I. Kingon, and J.B. Clark, Sintering of PZT Ceramics: II, Effect of PbO content on densification kinetics, J. Am. Ceram. Soc. 66(4) (1983) 256-260.
- [10] M. Hu, C. Luo, H. Tian and H. Gu, Phase evolution, crystal structure and dielectric behavior of $(1-x)\text{Nd}(\text{Zn}_{0.5}\text{Ti}_{0.5})\text{O}_3+x\text{Bi}(\text{Zn}_{0.5}\text{Ti}_{0.5})\text{O}_3$ compound ceramics, J. Alloys Compd. 509 (2011) 2993–2999.
- [11] R.D. Shannon, Revised effective ionic radii and systematic studies of interatomic distances in halides and chalcogenides, Acta Cryst. A32 (1976) 751-767.
- [12] M. Hammer and M. J. Hoffmann, Sintering model for mixed-oxide-derived. Lead zirconate titanate ceramics, J. Am. Ceram. Soc. 81 (1998) 3277-3284.
- [13] J.Y. Yi, J.K. Lee, and K.S. Hong, Dependence of the microstructure and the electrical properties of lanthanum-substituted $(\text{Na}_{1/2}\text{Bi}_{1/2})\text{TiO}_3$ on cation vacancies, J. Am. Ceram. Soc. 85 (2002) 3004-3010.
- [14] Y. Wu, C. Nguyen, S. Seraji, M. J. Forbess, S. J. Limmer, T. Chou and G. Cao, Processing and properties of strontium bismuth vanadate niobate ferroelectric ceramics, J. Am. Ceram. Soc. 84(12) (2001) 2882-2888.
- [15] C.A. Randall, N. Kim, J. P. Kucera, W. Cao and T. R. Shrout, Intrinsic and extrinsic size effects in fine-grained morphotropic-phase-boundary lead zirconate titanate ceramics, Am. Ceram. Soc. 81(3) (1998) 677-688.
- [16] K.B. Lee, H.S. Lee and S.K. Cho, Characterization of a bismuth-doped lead zirconate titanate thin film capacitor, J. Korean Phys. Soc. 31(3) (1997) 532-536
- [17] M. Pereira, A. G. Peixoto and M. J. M. Gomes, Effect of Nb doping on the microstructural and electrical properties of the PZT ceramics, J. Eur. Ceram. Soc. 21 (2001) 1353-1356.
- [18] W. Jo, R. Dittmer, M. Acosta, J. Zang, C. Groh, E. Sapper, K. Wang and J. Rödel, Giant electric-field-induced strains in lead-free ceramics for actuator applications – status and perspective, J. Electroceram. 29 (2012) 71-93.
- [19] I.K. Yoo and S.B. Desu, Mechanism of fatigue in ferroelectric thin films, Mater. Sci. Eng. B 13 (1992) 319-322.
- [20] W.L. Warren, D. Dimos, B.A. Tuttle, R.D. Nasby and G.E. Pike, Electronic domain pinning in $\text{Pb}(\text{Zr,Ti})\text{O}_3$ thin films and its role in fatigue, Appl. Phys. Lett. 65 (1994) 1018-1020.

- [21] H.N. Al-Shareef, D. imos, T.J. Boyle, W.L. Warren and B.A. Tuttle, Qualitative model for the fatigue-free behavior of $\text{SrBi}_2\text{Ta}_2\text{O}_9$, Appl. Phys. Lett. 68 (1996) 690-692.
- [22] C.S. Lynch, The effect of uniaxial stress on the electro-mechanical response of 8/65/35 PLZT, Acta. Mater. 44 (1996) 4137-4148.
- [23] D.A. Hall, T. Mori, T.P. Comyn, E. Ringgaard and J. P. Wright, Residual stress relief due to fatigue in tetragonal lead zirconate titanate ceramics, J. Appl. Phys. 114 (2013) 024103-6.
- [24] K. Okazaki, Mechanical behavior of ferroelectric ceramics, Bull. Am. Ceram. Soc. 63, (1983) 1150-1152.
- [25] R.R. Das, S.B. Majumder and R.S. Katiyar, Comparison of the electrical characteristics of PZT and SBT thin films, Integr. Ferroelectr. 42 (2002) 323-334.
- [26] B.H. Park, B.S. Kang, S.D. Bu, T.W. Noh, J. Lee, H.-D. Kim and T.H. Kim, Origins for fatigue-free properties of Bi-layered perovskite materials, J. Korean Phys. Soc. 35 (1999) S1306-S1309.

เนื้อหางานวิจัยตอนที่ 2

เรื่อง

ศึกษาพฤติกรรมความล้าทางไฟฟ้าของเซรามิกเพอร์
โรอีเล็กทริกเลดแมกนีเซียมไนโอเบตไทเทเนตเป็น
หลักสำหรับประยุกต์เป็นตัวขั้วรับ

ตอนที่ 2 – ศึกษาพฤติกรรมความล้าทางไฟฟ้าของเซรามิกเพอร์โรอิเล็กทริกเลดแมกนีเซียมไนโอเบตไทเทเนตเป็นหลักสำหรับประยุกต์เป็นตัวขับเคลื่อน

1. บทคัดย่อ

งานวิจัยนี้ศึกษาพฤติกรรมความล้าทางไฟฟ้าของเซรามิกเพอร์โรอิเล็กทริกเลดแมกนีเซียมไนโอเบตไทเทเนตสำหรับประยุกต์เป็นตัวขับเคลื่อน เซรามิกเลดแมกนีเซียมไนโอเบตถูกเตรียมด้วยวิธีผสมออกไซด์แบบดั้งเดิมและซินเทอร์ที่อุณหภูมิ 1240 องศาเซลเซียส เป็นเวลา 2 ชั่วโมง เซรามิกที่เตรียมได้มีความหนาแน่นสัมพัทธ์มากกว่า 98 เปอร์เซ็นต์ ขนาดเกรนของเซรามิกมีค่าเท่ากับ 3 ไมโครเมตร พฤติกรรมความล้าทางไฟฟ้าของเซรามิกจะถูกวัดภายใต้การให้สนามไฟฟ้ากระแสสลับที่มีแอมพลิจูด 2 เท่าของสนามไฟฟ้าสลับของเซรามิก และมีความถี่เท่ากับ 5, 10, 50 และ 100 เฮิรตซ์ ความล้าทางไฟฟ้าของเซรามิกหาได้จากการเปลี่ยนแปลงของโครงสร้างจุลภาค วงวนฮิสเทอรีซิส และเส้นโค้งความเครียด-สนามไฟฟ้า ที่จำนวนรอบสนามไฟฟ้าต่างๆ จนถึง 10^6 รอบ โดยการใช้กล้องจุลทรรศน์อิเล็กตรอนแบบส่องกราด เครื่องวัดสมบัติเพอร์โรอิเล็กทริก และเครื่องวัดความเครียดที่เชื่อมต่อกับเครื่องจ่ายไฟฟ้าความต่างศักย์สูง ตามลำดับ จากการทดลองพบว่า เกิดความเสียหายของชั้นผิวหน้าในเซรามิกที่ผ่านการทดสอบความล้าทางไฟฟ้า ความหนาของชั้นที่เสียหายดังกล่าวลดลงเมื่อความถี่ไฟฟ้าเพิ่มขึ้น นอกจากนี้ โพลาริเซชันคงค้างและความเครียดสูงสุดของเซรามิกมีค่าลดลงเมื่อจำนวนรอบของสนามไฟฟ้าเพิ่มขึ้น ความล้าทางไฟฟ้าของเซรามิกลดลงเมื่อความถี่เพิ่มขึ้น พฤติกรรมความล้าทางไฟฟ้าของเซรามิกเลดแมกนีเซียมไนโอเบตไทเทเนตถูกอธิบายโดยปรากฏการณ์การป้องกันสนามไฟฟ้าและการเป็นหมุดยึดขอบโดเมนของตำหนิ

2. วิธีการทดลอง

2.1 แหล่งที่มาของข้อมูล

เฟสของผงเลดแมกนีเซียมไนโอเบตไทเทเนต (PMNT) ถูกตรวจสอบด้วยเทคนิคการเลี้ยวเบนของรังสีเอกซ์ (XRD, Model X-pert, Panalytical B.V.) การทดสอบความล้าทางไฟฟ้าของเซรามิกเลดแมกนีเซียมไนโอเบตไทเทเนต (PMNT) ถูกตรวจสอบโดยการให้สนามไฟฟ้าจากเครื่องกำเนิดไฟฟ้าความต่างศักย์สูง (Trek, 20/20C, USA) และบันทึกค่าโพลาริเซชันด้วยวงจรรีเลย์-ทาวเวอร์ (Sawyer-Tower circuit) ความเครียดถูกวัดโดยเซนเซอร์วัดความเครียด (ZX-TDS01T, OMRON, Japan) ค่าที่ได้จะถูกบันทึกไว้ในคอมพิวเตอร์ ซึ่งทำการทดสอบ ณ มหาวิทยาลัยเทคโนโลยีสุรนารี โครงสร้างจุลภาคของชิ้นงานเซรามิกที่ผ่านการทดสอบความล้าทางไฟฟ้าถูกตรวจสอบด้วยกล้องจุลทรรศน์อิเล็กตรอนแบบส่องกราด (SEM, JSM-6335F, JEOL, Japan) ซึ่งทำการทดสอบ ณ มหาวิทยาลัยเชียงใหม่

2.2 วิธีการเก็บรวบรวมข้อมูล

2.2.1 การเตรียมเซรามิกเลดแมกนีเซียมไนโอเบตไทเทเนต

เซรามิกเลดแมกนีเซียมไนโอเบตไทเทเนต (PMNT) ถูกเตรียมจากผง PMNT ที่เตรียมจากสารตั้งต้นเลดออกไซด์ (PbO) แมกนีเซียมออกไซด์ (MgO) ไนโอเบียมออกไซด์ (Nb₂O₅) และ

ไทเทเนียมออกไซด์ (TiO_2) สารตั้งต้นถูกชั่งน้ำหนักตามสูตร $\text{Pb}(\text{Mg}_{1/3}\text{Nb}_{2/3})_{0.65}\text{Ti}_{0.35}\text{O}_3$ แล้วนำมาผสมด้วยการผสมแบบเม็ดบอลลในตัวกลางเอทานอลเป็นเวลา 24 ชั่วโมง นำสารผสมที่ได้มาอบแห้งในเตาอบที่อุณหภูมิ 120 องศาเซลเซียส เป็นเวลา 24 ชั่วโมง จากนั้นนำผงผสมไปเผาแคลไซน์ที่เงื่อนไขที่เหมาะสม นำผง PMNT ไปอัดขึ้นรูปแบบแกนเดี่ยว ภายใต้ความดัน 1 ตัน เป็นเวลา 10 วินาที จากนั้นนำเม็ดที่อัดขึ้นรูปไปเผาซินเทอร์ที่อุณหภูมิ 1240 องศาเซลเซียส เป็นเวลา 2 ชั่วโมง ภายใต้บรรยากาศ PMNT นำเซรามิกที่เตรียมได้ไปตรวจสอบความหนาแน่นด้วยหลักการอาร์คิมิดีส นำเซรามิกที่เตรียมได้มาตัดและขัดด้วยกระดาษทรายเบอร์ 1200 เพื่อให้ได้ชิ้นงานที่มีขนาด $1.5 \times 3.5 \times 3.0 \text{ mm}^3$ ผิวหน้าที่มีขนาด $3.5 \times 3.0 \text{ mm}^2$ ถูกขัดผองอะลูมินาขนาด 5.0 1.0 และ 0.05 ไมโครเมตร ตามลำดับ เพื่อให้ได้ชิ้นงานที่มีผิวหน้าที่เรียบคล้ายกระจก ชิ้นงานที่ถูกขัดทั้งหมดจะถูกนำไปอบอ่อนที่อุณหภูมิ 500 องศาเซลเซียส เป็นเวลา 5 ชั่วโมง เพื่อไล่ความเค้นที่ตกค้างเนื่องจากกระบวนการขัด ทำการทากาวเงินลงบนผิวหน้า $3.5 \times 1.5 \text{ mm}^2$ ทั้งสองเพื่อทำเป็นขั้วไฟฟ้า แล้วนำไปเผาที่อุณหภูมิ 650 องศาเซลเซียสเป็นเวลา 15 นาที เพื่อไล่สารอินทรีย์และทำให้กาวเงินยึดกับชิ้นงานได้ดี

2.2.2 การตรวจสอบความล้าทางไฟฟ้าของเซรามิกเลดแมกนีเซียมไนโอเบตไทเทเนต

นำเซรามิกที่ทำขั้วไฟฟ้าไปทดสอบความล้าทางไฟฟ้าโดยการให้สนามไฟฟ้ากระแสสลับที่มีแอมพลิจูด 2 เท่าของสนามไฟฟ้าลบล่างของเซรามิก PMNT ซึ่งมีค่าเท่ากับ 7 กิโลโวลต์ต่อเซนติเมตร โดยชิ้นงานจะถูกแช่ในน้ำมันซิลิโคนที่ทำหน้าที่เป็นฉนวนไฟฟ้าเพื่อป้องกันการรสปาร์คของไฟฟ้าความต่างศักย์สูง ความถี่ไฟฟ้าที่ใช้ทดสอบความล้าทางไฟฟ้าของเซรามิก PMNT คือ 5, 10, 50 และ 100 เฮิร์ตซ์ ในการทดสอบแต่ละความถี่ จะมีการจ่ายสนามไฟฟ้าไปจนถึง 10^6 รอบ โดยมีการบันทึกข้อมูลในรูปของวงวนฮิสเทอรีซิสของโพลาริเซชันและสนามไฟฟ้า (P-E hysteresis loops) ในช่วงจำนวนรอบ 1 ถึง 10^3 รอบ จะทำการบันทึกวงวนฮิสเทอรีซิสทุกๆ 100 รอบ ช่วง 10^3 - 10^4 รอบ บันทึกทุกๆ 10^3 รอบ ช่วง 10^4 - 10^5 รอบ บันทึกทุกๆ 10^4 รอบ ช่วง 10^5 - 10^6 รอบ บันทึกทุกๆ 10^5 รอบ นำข้อมูลที่ได้มาพล็อตกราฟ จากนั้นทำการหาค่าโพลาริเซชันคงค้างและสนามไฟฟ้าลบล่างจากวงวนฮิสเทอรีซิส นำค่าโพลาริเซชันและสนามไฟฟ้าลบล่างของแต่ละความถี่มาพล็อตเทียบกับจำนวนรอบสนามไฟฟ้า

ทำการวัดวงวนฮิสเทอรีซิสที่สถานะต่างๆ คือ ก่อนการทดสอบความล้า หลังจากการให้สนามไฟฟ้าเป็นจำนวน 10^6 รอบ หลังจากการเอาผิวหน้าที่เสียหายออก และหลังจากการอบอ่อนที่อุณหภูมิ 500 องศาเซลเซียส เป็นเวลา 2 ชั่วโมง นำวงวนฮิสเทอรีซิสที่ถูกวัดที่สถานะต่างๆ ที่แต่ละความถี่มาพล็อตร่วมกันเพื่อเปรียบเทียบ

ทำการวัดความเครียดที่ถูกเหนี่ยวนำเนื่องจากไฟฟ้าที่จำนวนรอบสนามไฟฟ้า 10^1 , 10^2 , 10^3 , 10^4 และ 10^5 รอบ นำข้อมูลของแต่ละความถี่มาพล็อตกราฟเทียบกับสนามไฟฟ้า

2.2.3 การตรวจสอบโครงสร้างจุลภาคของเซรามิกเลดแมกนีเซียมไนโอเบตไทเทเนต

ผิวหน้าของเซรามิกที่ถูกขัดให้เรียบคล้ายกระจกถูกนำไปตรวจสอบโครงสร้างจุลภาคโดยผิวหน้าดังกล่าวจะถูกเคลือบด้วยทองด้วยเครื่องสเป็คเตอร์ หลังจากนั้นนำไปตรวจสอบ

โครงสร้างจุลภาคด้วยกล้องจุลทรรศน์อิเล็กตรอนแบบส่องกราด โดยจะทำการตรวจสอบบริเวณตรงกลางชิ้นงานและบริเวณใกล้กับขั้วไฟฟ้า จากนั้นทำการบันทึกภาพ ทำการวัดความหนาของผิวชิ้นงานที่เสียหาย และความกว้างของรอยแตกที่อยู่บริเวณกลางชิ้นงาน แล้วนำข้อมูลที่ได้มาหาค่าเฉลี่ย

2.3 วิธีวิเคราะห์ข้อมูล

2.3.1 การวิเคราะห์โครงสร้างจุลภาคของเซรามิกเลดแมงกานีสในโอเบตไทเทเนต

จากภาพโครงสร้างจุลภาคที่ได้จากกล้องจุลทรรศน์อิเล็กตรอนแบบส่องกราด จะทำการพิจารณาความเสียหายทางโครงสร้างจุลภาคที่เกิดขึ้นในชิ้นงานที่ผ่านการทดสอบความล้า พร้อมกับตรวจสอบลักษณะการแตกของเกรนภายในโครงสร้างของเซรามิก จากนั้นทำการวิเคราะห์ว่าความกว้างของความเสียหายของชั้นที่อยู่ใกล้กับขั้วไฟฟ้ามีการเปลี่ยนแปลงอย่างไรเมื่อทำการปรับเปลี่ยนความถี่ในการทดสอบความล้า นอกจากนี้จะพิจารณาความเสียหาย เช่น รอยแตกบริเวณกลางชิ้นงาน และพิจารณาความกว้างและจำนวนของรอยแตกว่าขึ้นอยู่กับความถี่ที่ใช้ในการทดสอบความล้าหรือไม่

2.3.2 การวิเคราะห์พฤติกรรมความล้าทางไฟฟ้าจากสมบัติเฟอร์โรอิเล็กทริก

จากกราฟที่พล็อตระหว่างสมบัติเฟอร์โรอิเล็กทริก (โพลาริเซชันคงค้างและสนามไฟฟ้าลบล้าง) และจำนวนรอบของสนามไฟฟ้า จะทำการพิจารณาว่าค่าโพลาริเซชันและสนามไฟฟ้าลบล้างเริ่มมีการเปลี่ยนแปลง (เพิ่มขึ้น/ลดลง) ที่จำนวนรอบของสนามไฟฟ้าเท่าใด พร้อมทั้งเปรียบเทียบว่าจำนวนรอบของสนามไฟฟ้าที่สมบัติเฟอร์โรอิเล็กทริกเริ่มมีการเปลี่ยนแปลงของชิ้นงานที่ทดสอบความล้าที่ความถี่ต่างๆ มีค่าต่างกันอย่างไร ทำการเปรียบเทียบว่าที่จำนวนรอบสนามไฟฟ้าเท่ากับ 10^5 รอบ การลดลงของโพลาริเซชันคงค้างและการเพิ่มขึ้นของสนามไฟฟ้าลบล้างของชิ้นงานที่ความถี่ต่างๆ มีค่าต่างกันอย่างไร และเมื่อจำนวนรอบเพิ่มขึ้นเป็น 10^6 รอบ ค่าดังกล่าวจะต่างกันหรือไม่ อย่างไร

2.3.3 การวิเคราะห์สมบัติเฟอร์โรอิเล็กทริกที่ถูกวัดที่สถานะต่าง ๆ

จากกราฟวงวนฮิสเทอรีซิสที่ทำการวัดที่สถานะต่างๆ ของชิ้นงานที่ถูกทดสอบความล้าทางไฟฟ้าที่ความถี่ต่างๆ จะทำการวิเคราะห์ว่าที่แต่ละความถี่ วงวนฮิสเทอรีซิสที่วัดที่สถานะต่างๆ มีความแตกต่างกันหรือไม่ อย่างไร และที่แต่ละสถานะ วงวนฮิสเทอรีซิสที่ความถี่ต่างๆ มีความแตกต่างกันหรือไม่ อย่างไร นอกจากนี้ จากกราฟความหนาของชั้นที่เสียหาย โพลาริเซชันคงค้างและสนามไฟฟ้าลบล้างที่พล็อตเทียบกับจำนวนรอบของสนามไฟฟ้า จะทำการวิเคราะห์ว่าการเปลี่ยนแปลงของค่าต่างๆ กับจำนวนรอบของสนามไฟฟ้า มีแนวโน้มไปทางเดียวกันหรือไม่ อย่างไร ถ้าหากการเปลี่ยนแปลงของความหนาของชั้นที่เสียหายมีแนวโน้มไปในทิศทางเดียวกันกับการเปลี่ยนแปลงของสมบัติเฟอร์โรอิเล็กทริก ก็อาจเป็นไปได้ว่า ความเสียหายทางโครงสร้างจุลภาคส่งผลให้เกิดความล้าทางไฟฟ้าในชิ้นงานเซรามิก แต่ถ้าหากการเปลี่ยนแปลงไม่เป็นไปในทิศทางเดียวกัน ก็อาจจะมีสาเหตุอื่นที่มีผลต่อความล้าของเซรามิกดังกล่าว

2.3.4 การวิเคราะห์พฤติกรรมความล้าทางไฟฟ้าจากความเครียดที่ถูกเหนี่ยวนำด้วยไฟฟ้า

จากกราฟระหว่างความเครียดและสนามไฟฟ้าที่วัดที่จำนวนรอบของสนามไฟฟ้าต่างๆ ของเซรามิกที่ถูกทดสอบความล้าที่ความถี่ต่างๆ จะทำการวิเคราะห์ว่า ที่แต่ละความถี่ เมื่อจำนวนรอบของสนามไฟฟ้าเพิ่มขึ้น ลักษณะของกราฟ เช่น ความสมมาตร ค่าความเครียดสูงสุด และค่าสนามไฟฟ้าที่ใช้ในการกลับทิศของโดเมน มีการเปลี่ยนแปลงไปอย่างไร ที่จำนวนรอบเท่ากัน การเปลี่ยนแปลงดังกล่าวของชิ้นงานที่ทำการทดสอบความล้าที่ความถี่ต่างๆ มีความแตกต่างกันอย่างไร นอกจากนี้ จากกราฟความสัมพันธ์ระหว่างความเครียดและสนามไฟฟ้าสามารถหาสัมประสิทธิ์เพียโซอิเล็กทริกของเซรามิกได้ โดยหาจากความชันของเส้นตรงที่สัมพันธ์กราฟที่ตำแหน่งสนามไฟฟ้าเท่ากับศูนย์ จากนั้นทำการวิเคราะห์ว่าสัมประสิทธิ์เพียโซอิเล็กทริกหลังจากให้สนามไฟฟ้าจำนวน 10^6 รอบ เมื่อเทียบกับเมื่อเริ่มทำการวัด มีการเปลี่ยนแปลงไปอย่างไร และที่ความถี่ต่างๆ การเปลี่ยนแปลงดังกล่าวมีความแตกต่างกันอย่างไร

การเปลี่ยนแปลงของสมบัติทางไฟฟ้าของเซรามิกเนื่องจากความล้าจะพิจารณาจากเปอร์เซ็นต์การเปลี่ยนแปลงของสมบัติดังสมการ

$$\% \text{change in property} = \frac{P_A - P_B}{P_B} \times 100 \quad (1)$$

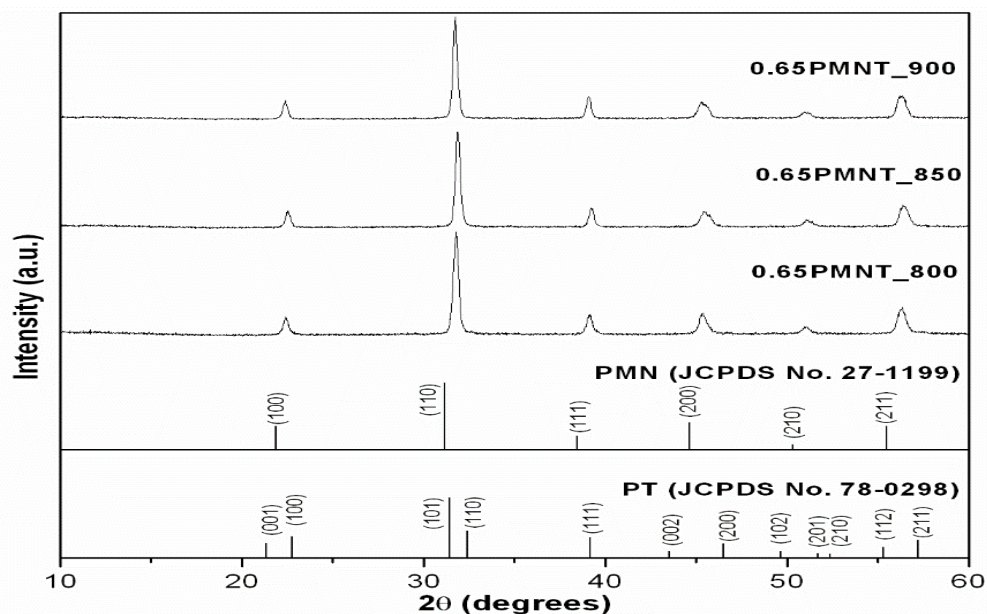
เมื่อ P_A คือ ค่าสมบัติที่ถูกวัดหลังจากการทดสอบความล้า

P_B คือ ค่าสมบัติที่ถูกวัดในช่วงเริ่มทดสอบความล้า

3. ผลการวิเคราะห์ข้อมูลและการอภิปรายผล

3.1 ผลการตรวจสอบเฟสของผงเลดแมกนีเซียมไนโอเบตไทเทเนต

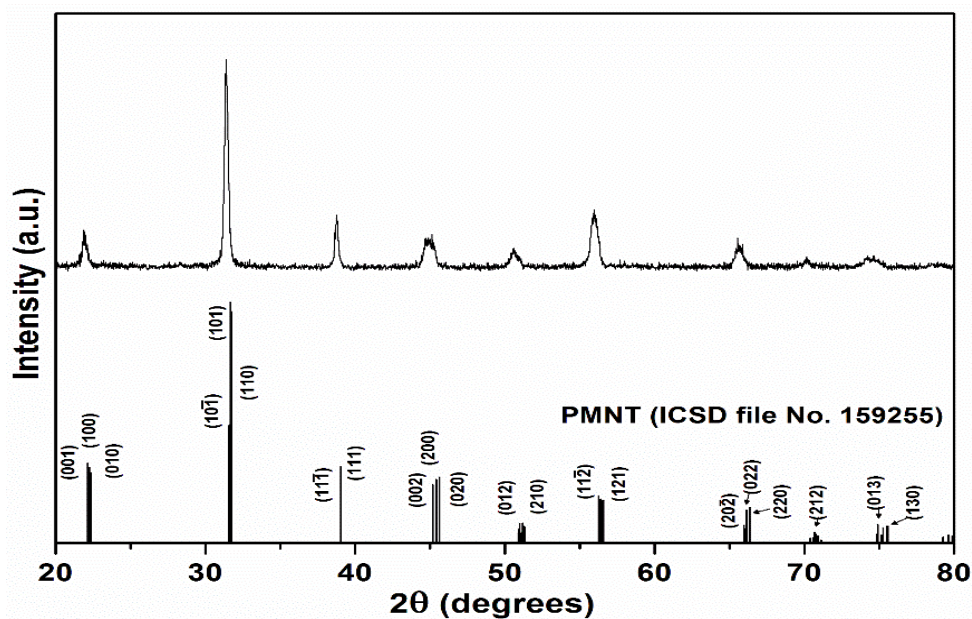
เฟสของผงเลดแมกนีเซียมไนโอเบตไทเทเนต (PMNT) ที่ผ่านการเผาแคลไซน์ที่อุณหภูมิ 800, 850 และ 900 องศาเซลเซียส เป็นเวลา 2 ชั่วโมง ถูกตรวจสอบด้วยเทคนิคการเลี้ยวเบนของรังสีเอกซ์ (XRD) ผลการทดลองแสดงดังรูป 3.1 รูปแบบ XRD ของผงถูกเปรียบเทียบกับรูปแบบมาตรฐานของสาร $\text{Pb}(\text{Mg}_{1/3}\text{Nb}_{2/3})\text{O}_3$ ไฟล์ JCPDS หมายเลข 27-1199 และสาร PbTiO_3 ไฟล์ JCPDS หมายเลข 78-0298 ผลการทดลองแสดงให้เห็นว่าผง PMNT ที่ผ่านการเผาทุกอุณหภูมิ แสดงเฟสบริสุทธิ์ของเฟสเพอรอฟสไกต์โดยไม่มีการปรากฏของเฟสที่สองหรือเฟสที่ไม่ต้องการ ซึ่งให้เห็นว่า ทุกเงื่อนไขการแคลไซน์สามารถทำให้สารตั้งต้น (PbO , MgO , Nb_2O_5 และ TiO_2) สามารถทำปฏิกิริยาเคมีกันและฟอร์มตัวเป็นสาร PMNT ที่ต้องการได้อย่างสมบูรณ์ ดังนั้น เงื่อนไขการเผาแคลไซน์ทุกสภาวะจึงมีความเหมาะสมที่จะนำไปใช้เตรียมผง PMNT ที่มีเฟสบริสุทธิ์ได้ อย่างไรก็ตาม เมื่อพิจารณาเรื่องของพลังงานที่ใช้ในการเผาแคลไซน์ อุณหภูมิ 800 องศาเซลเซียส จึงมีความเหมาะสมในการเผาแคลไซน์ผง PMNT มากที่สุด เนื่องจากใช้พลังงานน้อยที่สุด ดังนั้น ในงานวิจัยนี้ จึงเลือกใช้เงื่อนไขการเผาแคลไซน์ที่อุณหภูมิ 800 องศาเซลเซียส เป็นเวลา 2 ชั่วโมง



รูป 3.1 รูปแบบการเลี้ยวเบนของรังสีเอกซ์ของผงด PMNT ที่เผาแคลไซน์ที่อุณหภูมิ 800 850 และ 900 องศาเซลเซียส เป็นเวลา 2 ชั่วโมง

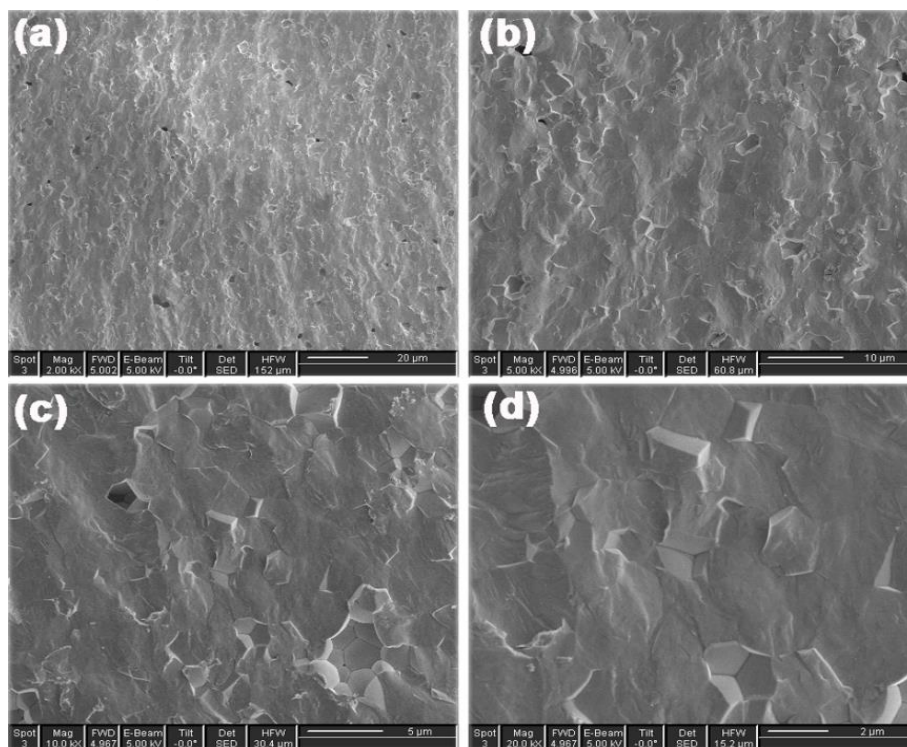
3.2 ผลการตรวจสอบเฟส ความหนาแน่น และโครงสร้างจุลภาคของเซรามิกเลดแมกนีเซียมไนโอเบตไทเทเนต

เฟสของเซรามิก PMNT ที่ผ่านการเผาซินเทอร์ที่อุณหภูมิ 1240 องศาเซลเซียส เป็นเวลา 2 ชั่วโมง ถูกตรวจสอบด้วยเทคนิค XRD ผลการทดลองแสดงดังรูป 3.2 รูปแบบ XRD ของเซรามิก PMNT สอดคล้องกับไฟล์มาตรฐาน ICSD หมายเลข 159255 ซึ่งเป็นของสารประกอบ $\text{Pb}(\text{Mg}_{1/3}\text{Nb}_{2/3})_{0.65}\text{Ti}_{0.35}\text{O}_3$ ที่มีโครงสร้างผลึกแบบโมโนคลินิก ดังนั้นเซรามิก PMNT ที่เตรียมได้จึงมีเฟสเพอรอฟสไกต์ที่มีโครงสร้างผลึกแบบโมโนคลินิก



รูป 3.2 รูปแบบการเลี้ยวเบนของรังสีเอกซ์ของเซรามิก PMNT ที่เผาซินเทอร์ที่อุณหภูมิ 1240 องศาเซลเซียส เป็นเวลา 2 ชั่วโมง

ความหนาแน่นของเซรามิกถูกตรวจสอบด้วยหลักการของอาร์คิมิดีส ซึ่งพบว่าความหนาแน่นของเซรามิก PMNT ที่เตรียมได้มีค่าเท่ากับ 7.7 g/cm^3 หรือคิดเป็นความหนาแน่นสัมพัทธ์เท่ากับ 95 % โครงสร้างจุลภาคของผิวหักของเซรามิก PMNT ถูกตรวจสอบด้วยกล้องจุลทรรศน์อิเล็กตรอนแบบส่องกราด ซึ่งได้ผลการทดลองดังรูป 3.3 จากรูปจะเห็นได้ว่า เซรามิกมีการแตกแบบผสม คือมีทั้งการแตกแบบผ่าเกรน (transgranular fracture) และแตกแบบระหว่างเกรน (intergranular fracture) ขนาดเกรนโดยเฉลี่ยของเซรามิกมีค่าเท่ากับ 3 ไมโครเมตร

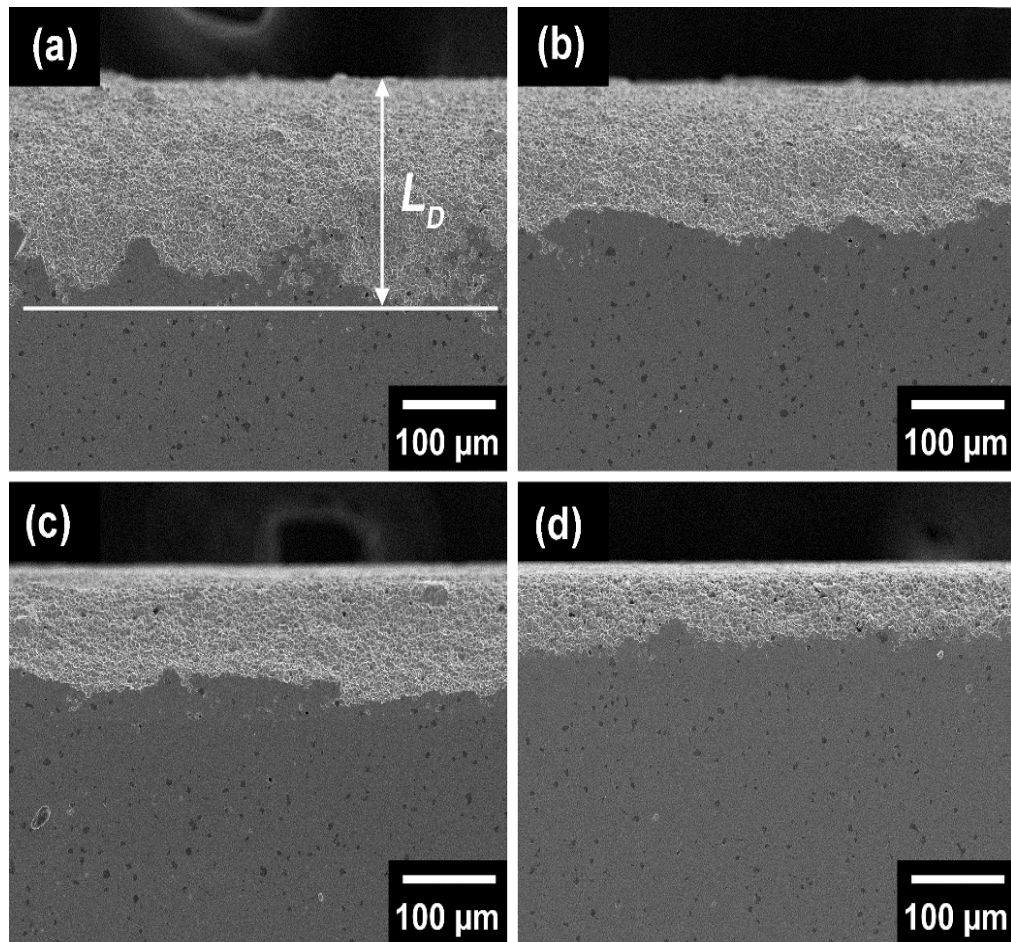


รูป 3.3 โครงสร้างจุลภาคของผิวแตกที่กำลังขยาย (a) 2000 (b) 5000 (c) 10000 และ (d) 20000 ของเซรามิก PMNT

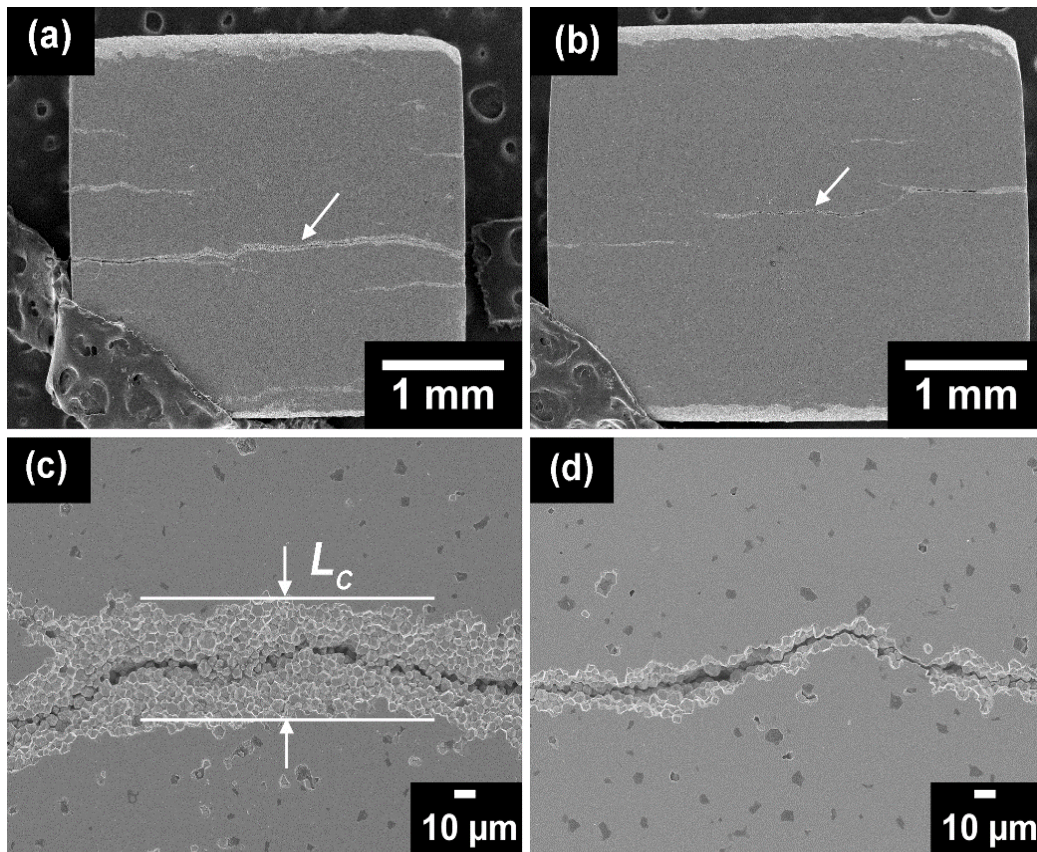
3.3 ผลการตรวจสอบโครงสร้างจุลภาคของเซรามิก PMNT หลังการทดสอบความล้าทางไฟฟ้า

ภาพถ่ายจากกล้องจุลทรรศน์อิเล็กตรอนแบบส่องกราดของโครงสร้างจุลภาคของผิวหน้าเซรามิกที่ผ่านการทดสอบความล้าทางไฟฟ้าเป็นจำนวน 10^6 รอบ ที่ความถี่ต่างๆ แสดงดังรูป 3.4 ความเสียหายทางโครงสร้างจุลภาคของผิวหน้าที่เกิดจากความล้าทางไฟฟ้าถูกพบในชิ้นงานทุกความถี่ ความเสียหายของผิวหน้าที่พบมีความสอดคล้องกับผลการทดลองก่อนหน้าของ Balke และคณะ และยังพบว่า ความล้าทางไฟฟ้ามีผลอย่างเด่นชัดต่อความเสียหายของผิวหน้าที่ตั้งฉากกับทิศทางของสนามไฟฟ้าที่ให้ ซึ่งสอดคล้องกับผลการทดลองก่อนหน้าของ Fang และคณะ นอกจากนี้ความเสียหายของผิวหน้าที่อยู่ใต้ขั้วไฟฟ้าแล้ว ยังพบรอยแตกที่เกิดจากการทดสอบความล้าในส่วนเนื้อชิ้นงานในเซรามิกที่ผ่านการทดสอบความล้าที่ความถี่ 5 และ 10 เฮิร์ตซ์ ดังแสดงในรูป 3.5 ภาพขยายของรอยแตกของชิ้นงานทั้งสอง (ดังแสดงในรูป 3.5(a) และ (b)) แสดงถึงการแตกแบบระหว่างเกรน และยังพบว่าจำนวนและขนาดของรอยแตกในชิ้นงานที่ทำการทดสอบความล้าที่ความถี่ต่ำกว่า

มีค่าสูงกว่าค่าที่พบในชิ้นงานที่ความถี่สูงกว่า ความหนาของชั้นเสียหายและขนาดของรอยแตก (ซึ่งแทนด้วยสัญลักษณ์ L_D และ L_C ตามลำดับ) ของเซรามิกพบว่า มีค่าลดลงเมื่อความถี่เพิ่มขึ้น ค่า L_D ของชิ้นงานที่ทำการทดสอบความล้าที่ความถี่ 5 10 50 และ 100 เฮิร์ตซ์ มีค่าเท่ากับ 165 ± 7 , 121 ± 5 , 98 ± 4 และ 66 ± 4 ไมโครเมตร ตามลำดับ ค่า L_C ของชิ้นงานที่ทดสอบความล้าที่ความถี่ 5 และ 10 เฮิร์ตซ์ มีค่าเท่ากับ 45 ± 2 และ 19 ± 1 ไมโครเมตร ตามลำดับ เชื่อว่าการเกิดการขยายตัวของรอยแตกคือสาเหตุของการเกิดความล้าในสมบัติเฟรโรอิเล็กทริกและเพียโซอิเล็กทริกของเซรามิก PMNT ซึ่งจะถูกอภิปรายในหัวข้อต่อไป



รูป 3.4 ภาพถ่ายจากกล้องจุลทรรศน์อิเล็กตรอนแบบส่องกราดของโครงสร้างจุลภาคของผิวหน้าเซรามิก PMNT ที่ผ่านการทดสอบความล้าทางไฟฟ้าเป็นจำนวน 10^6 รอบ ที่ความถี่ (a) 5 (b) 10 (c) 50 และ (d) 100 เฮิร์ตซ์



รูป 3.5 ภาพถ่ายจากกล้องจุลทรรศน์อิเล็กตรอนแบบส่องกราดแสดงความเสียหายที่เกิดขึ้นในเนื้อเซรามิก PMNT ทดสอบความล้าที่ความถี่ (a) 5 (b) 10 (c) 50 และ (d) 100 เฮิร์ตซ์

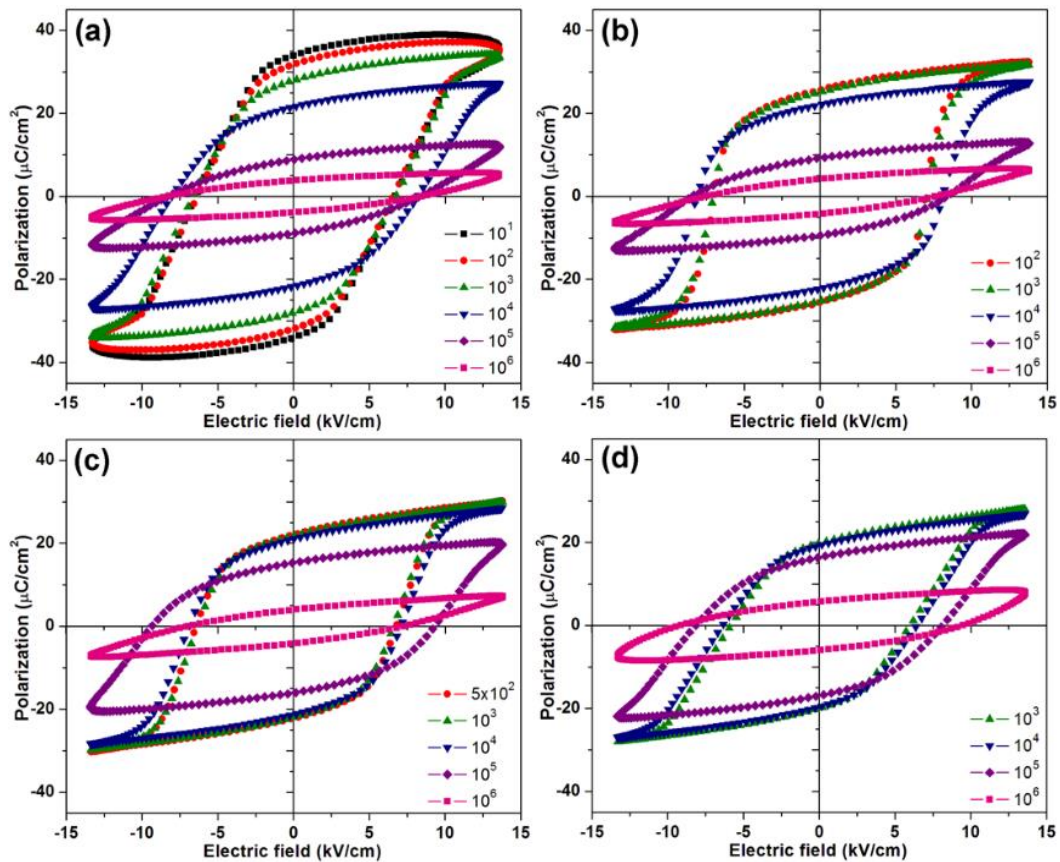
3.4 ผลการตรวจสอบความล้าทางไฟฟ้าของเซรามิก PMNT

3.4.1 ความล้าทางไฟฟ้าของสมบัติเพอร์โรอิเล็กทริก

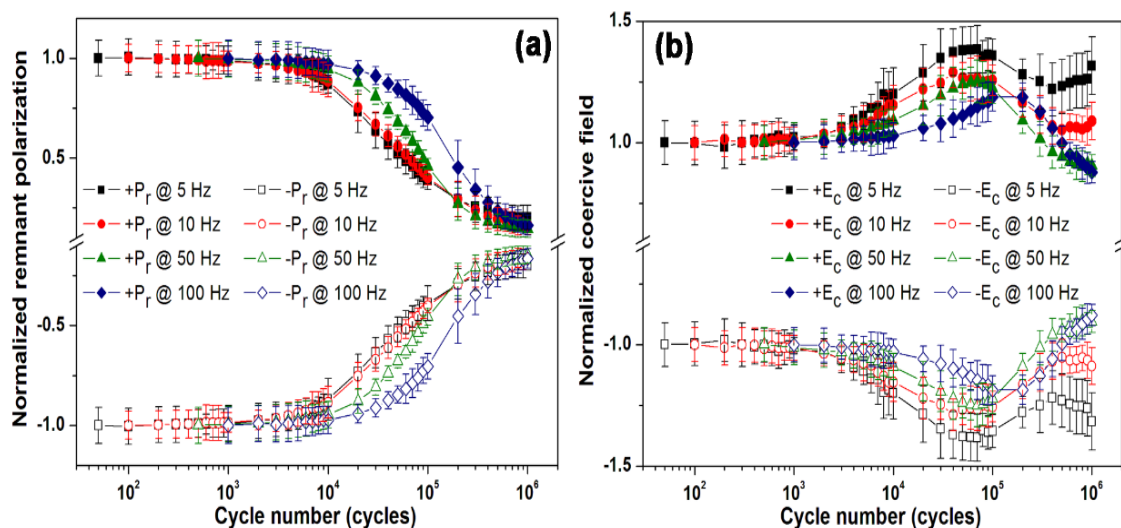
เพื่อทำการตรวจสอบความล้าของเซรามิก PMNT จึงทำการวัดวงวนฮีสเทอรีซิสของโพลาริเซชันและสนามไฟฟ้าที่จำนวนรอบสนามไฟฟ้าต่างๆ จนถึง 10^6 รอบ กราฟวงวนฮีสเทอรีซิสที่จำนวนรอบสนามไฟฟ้า รอบ ที่ความถี่ 5 10 50 และ 100 เฮิร์ตซ์ ของเซรามิก PMNT แสดงดังรูป 3.6

ที่ช่วงเริ่มต้นของการทดสอบความล้า วงวนฮีสเทอรีซิสที่วัดที่ความถี่ต่ำจะแสดงค่าโพลาริเซชันคงค้างและสนามไฟฟ้าลบกลับที่สูงกว่าที่วัดที่ความถี่สูง การให้สนามไฟฟ้าจำนวน 1 รอบ ที่ความถี่ต่ำจะทำให้ผนังโดเมนสามารถเคลื่อนที่ได้ระยะที่ไกลกว่าและปริมาตรของโดเมนที่จัดเรียงตัวในทิศทางของสนามไฟฟ้าที่ให้กับจะมีขนาดใหญ่กว่า ดังนั้น จึงมีความต้องการปริมาณสนามไฟฟ้าที่สูงกว่าเพื่อใช้ในการกลับทิศของโดเมนไปยังทิศทางตรงข้าม ซึ่งส่งผลให้โพลาริเซชันคงค้างและสนามไฟฟ้าลบกลับมีค่ามากขึ้น นอกจากนี้ยังมีสาเหตุอื่นที่เป็นไปได้ที่ทำให้เกิดผลการทดลองดังที่พบ คือ การมีอยู่ของโพลาริเซชันของประจุอวกาศ (space charge polarization) ซึ่งอาจเกิดจากตำหนิที่มีประจุ เช่น ช่องว่างของออกซิเจน ที่อยู่บริเวณขอบเกรนของเซรามิก โพลาริเซชันนี้สามารถหมุนตัวเมื่อมีการให้สนามไฟฟ้าความถี่ต่ำ ส่งผลให้ค่าโพลาริเซชันคงค้างและสนามไฟฟ้าลบกลับสูงขึ้น อย่างไรก็ตาม โพลาริเซชันของประจุอวกาศถูกจำกัดที่ความถี่สูงขึ้น

เนื่องจากความถี่ดังกล่าวส่งผลต่อการกลับทิศของโดเมน ส่งผลให้โพลาริเซชันคงค้างและสนามไฟฟ้าลบมีค่าลดลง



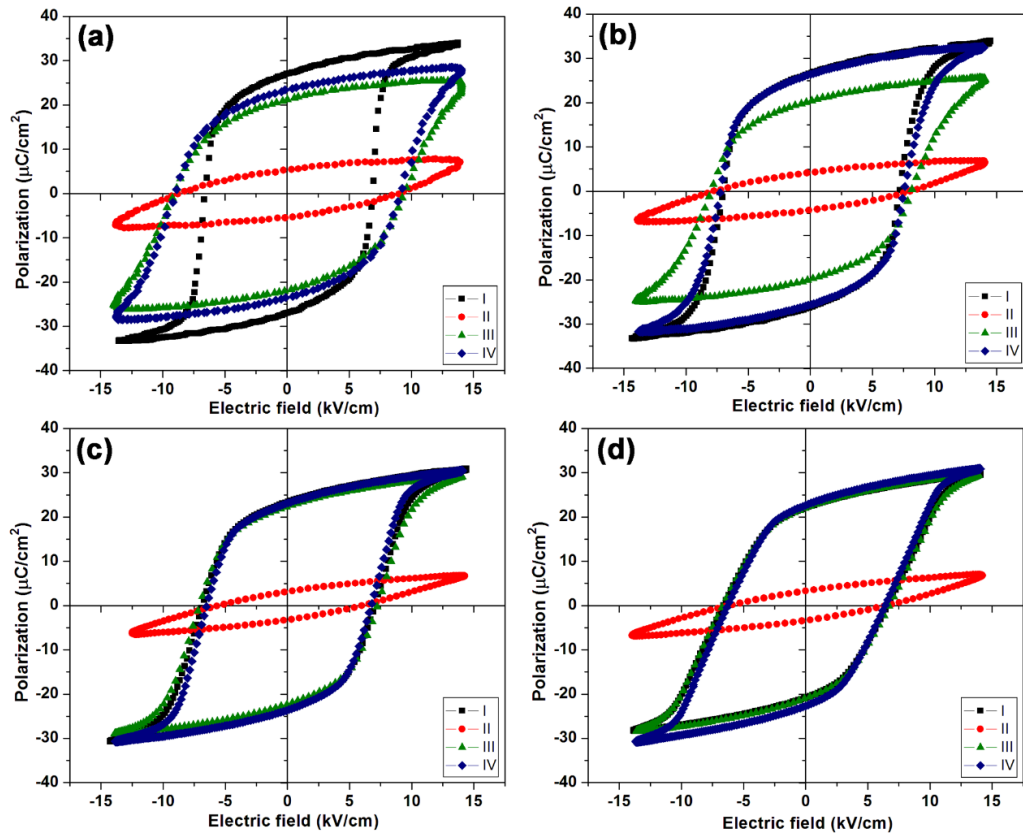
รูป 3.6 วงวนฮิสเทอรีซิสที่จำนวนรอบสนามไฟฟ้าต่างๆ ของเซรามิก PMNT ที่ถูกทดสอบความถี่ทางไฟฟ้าที่ความถี่ (a) 5 (b) 10 (c) 50 และ (d) 100 เฮิรตซ์



รูป 3.7 กราฟแสดงความสัมพันธ์ระหว่าง (a) โพลาริเซชันคงค้าง และ (b) สนามไฟฟ้าลบกับจำนวนรอบของสนามไฟฟ้าของเซรามิก PMNT

เพื่อเปรียบเทียบผลของความถี่ต่อความล้าทางไฟฟ้าของชิ้นงาน ค่าโพลาริเซชันคงค้างและสนามไฟฟ้าลบข้างของแต่ละชิ้นงานถูกหารด้วยค่าโพลาริเซชันคงค้างและสนามไฟฟ้าลบข้างที่วัดในช่วงเริ่มต้นของการทดสอบความล้า ผลการทดลองแสดงดังรูป 3.7 จากรูปจะเห็นได้ว่า ที่จำนวนรอบ $\leq 10^3$ รอบ ค่าโพลาริเซชันคงค้างและสนามไฟฟ้าลบข้างของชิ้นงานทั้งหมดไม่มีการเปลี่ยนแปลงกับจำนวนรอบสนามไฟฟ้า อย่างไรก็ตาม เมื่อจำนวนรอบสนามไฟฟ้าเพิ่มขึ้น โพลาริเซชันคงค้างมีแนวโน้มลดลงจนถึง 10^6 รอบ และสนามไฟฟ้าลบข้างมีการเพิ่มขึ้นจนถึง 10^5 รอบ และลดลงเมื่อจำนวนรอบเพิ่มขึ้นจนถึง 10^6 รอบ อย่างไรก็ตาม สำหรับชิ้นงานที่ทดสอบความล้าที่ความถี่ 5 และ 10 เฮิร์ตซ์ สนามไฟฟ้าลบข้างไม่ลดลงต่อไปเมื่อจำนวนรอบ $\geq 4 \times 10^5$ รอบ ดังที่พบในงานวิจัยก่อนหน้านี้ การลดลงของสมบัติเนื่องจากการความล้าเกิดจากการป้องกันสนามที่เกิดจากการเสียหายของผิวหน้าและการเป็นหมุดยึดขอบโดเมนซึ่งจะอธิบายในหัวข้อถัดไป

เพื่อทำการหาสาเหตุของการเกิดความล้าของเซรามิก จึงทำการวัดวงวนฮิสเทอรีซิสที่สถานะต่างๆ คือ (I) ช่วงเริ่มต้นของการทดสอบความล้า (II) หลังจากการทดสอบความล้าเป็นจำนวน 10^6 รอบ (III) หลังจากการเอาชิ้นที่เสียหายออก และ (IV) หลังจากการอบอ่อนที่อุณหภูมิ 500 องศาเซลเซียส เป็นเวลา 2 ชั่วโมง ผลการทดลองแสดงดังรูป 3.8 สำหรับชิ้นงานที่ทดสอบความล้าทุกความถี่ วงวนฮิสเทอรีซิสที่วัดที่สถานะ II ถูกจำกัดอย่างมาก โดยมีค่าโพลาริเซชันคงค้างน้อยกว่าค่าที่วัดที่สถานะ I มาก ที่สถานะ III วงวนฮิสเทอรีซิสของชิ้นงานที่ทดสอบความล้าที่ความถี่ 50 และ 100 เฮิร์ตซ์ มีการฟื้นฟูอย่างสมบูรณ์การเอาชิ้นที่เสียหายออก อย่างไรก็ตาม วงวนฮิสเทอรีซิสของชิ้นงานที่ทดสอบความล้าที่ความถี่ 5 และ 10 เฮิร์ตซ์ ไม่กลับเป็นอย่างเดิมเมื่อเอาชิ้นที่เสียหายออก ที่สถานะ IV หลังจากการทำอบอ่อน วงวนฮิสเทอรีซิสของชิ้นงานที่ความถี่ 10 เฮิร์ตซ์ มีการกลับเป็นอย่างเดิมอย่างสมบูรณ์ในขณะที่ชิ้นงานที่ความถี่ 5 เฮิร์ตซ์ มีการกลับเป็นอย่างเดิมบางส่วน การฟื้นฟูที่ไม่สมบูรณ์ของวงวนฮิสเทอรีซิสของชิ้นงานที่ความถี่ 5 เฮิร์ตซ์ เนื่องมาจากการเกิดรอยแตกเนื่องจากการทดสอบความล้า แม้ว่าชิ้นงานที่ทำการทดสอบความล้าที่ความถี่ 10 เฮิร์ตซ์ จะมีรอยแตก อย่างไรก็ตาม รอยแตกมีจำนวนน้อยกว่าและเล็กกว่า จึงทำให้การฟื้นฟูของวงวนฮิสเทอรีซิสด้วยการเอาชิ้นที่เสียหายออกและการอบอ่อนที่ง่ายกว่า นอกจากนี้ เพื่อหาความสัมพันธ์ระหว่างชั้นผิวหน้าที่เสียหายและการเปลี่ยนแปลงของสมบัติเฟอร์โรอิเล็กทริก จึงได้พล็อตกราฟของความหนาของชั้นผิวที่เสียหาย โพลาริเซชันคงค้าง และสนามไฟฟ้าลบข้างที่ขึ้นอยู่กับจำนวนรอบสนามไฟฟ้าของชิ้นงานที่ทดสอบความล้าที่ความถี่ 50 เฮิร์ตซ์ ดังแสดงในรูป 3.9 จากรูปแสดงให้เห็นว่า ที่จำนวนรอบ $\leq 10^5$ รอบ ความหนาของชั้นที่เสียหายที่เพิ่มขึ้นส่งผลให้มีการลดลงของโพลาริเซชันคงค้างและการเพิ่มขึ้นของสนามไฟฟ้าลบข้าง ที่จำนวนรอบ $> 10^5$ รอบ ความหนาของชั้นที่เสียหายมีการเพิ่มขึ้นเพียงเล็กน้อย และที่จำนวนรอบสนามไฟฟ้าช่วงนี้ โพลาริเซชันคงค้างมีการลดลงอย่างต่อเนื่องในขณะที่สนามไฟฟ้าลบข้างเริ่มมีการลดลงเมื่อจำนวนรอบเพิ่มขึ้นสู่ 10^6 รอบ

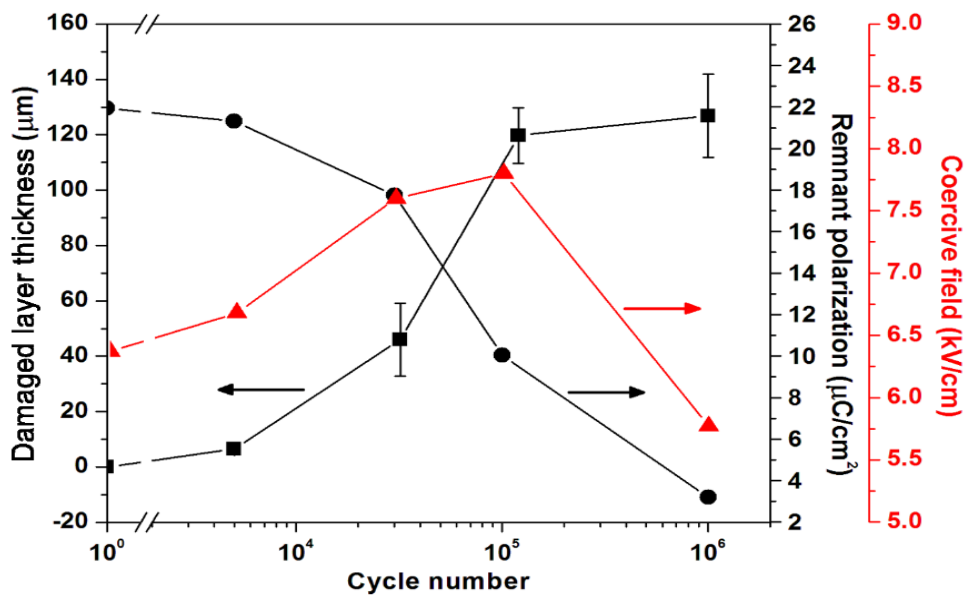


รูป 3.8 วงวนฮีสเทรีซิสที่อุณหภูมิที่สถานะต่างๆ (I) ช่วงเริ่มต้นของการทดสอบความล้า (II) หลังจากการทดสอบความล้าเป็นจำนวน 10^6 รอบ (III) หลังจากการเอาชิ้นที่เสียหายออก และ (IV) หลังจากการอบอ่อนที่อุณหภูมิ 500 องศาเซลเซียส เป็นเวลา 2 ชั่วโมง ของเซรามิกที่ทดสอบความล้าที่ความถี่ (a) 5 (b) 10 (c) 50 และ (d) 100 เฮิร์ตซ์

จำนวนรอบที่มีการลดลงของสมบัติเนื่องจากความล้า กล่าวคือ จำนวนรอบที่อัตราการลดลงของโพลาริเซชันคงค้างมีค่าสูงสุด ถูกแสดงไว้ในตาราง 3.1 จะเห็นได้ว่า จำนวนรอบดังกล่าวมีค่าเพิ่มขึ้นเมื่อความถี่เพิ่มขึ้น ซึ่งบ่งบอกถึงความถี่ที่เกิดขึ้นในชิ้นงานที่ทำการทดสอบความล้าที่ความถี่ต่ำกว่าจะเกิดขึ้นเร็วกว่า ร้อยละการเปลี่ยนแปลงของสมบัติหลังจากทดสอบความล้าจำนวนรอบ 10^5 รอบ ที่เทียบกับค่าที่วัดขณะเริ่มทำการทดสอบถูกแสดงไว้ในตาราง 3.1 พบว่าปริมาณการลดลงของสมบัติเฟอร์โรอิเล็กทริกมีแนวโน้มลดลงเมื่อความถี่เพิ่มขึ้น ซึ่งชี้ให้เห็นว่าความรุนแรงของการเกิดความล้าของสมบัติเฟอร์โรอิเล็กทริกในเซรามิกมีค่าลดลงเมื่อความถี่เพิ่มขึ้น

ตาราง 3.1 พฤติกรรมความล้าทางไฟฟ้าของสมบัติเฟอร์โรอิเล็กทริกหลังจากการทดสอบความล้าเป็นจำนวน 10^5 รอบ ที่ความถี่ต่างๆ ของเซรามิก PMNT

ความถี่ (เฮิร์ตซ์)	จำนวนรอบ (รอบ)	ร้อยละการเปลี่ยนแปลงของ โพลาริเซชันคงค้าง	ร้อยละการเปลี่ยนแปลงของ สนามไฟฟ้าลบ
5	30000	-61	+36
10	63000	-60	+26
50	86000	-54	+22
100	140000	-29	+19

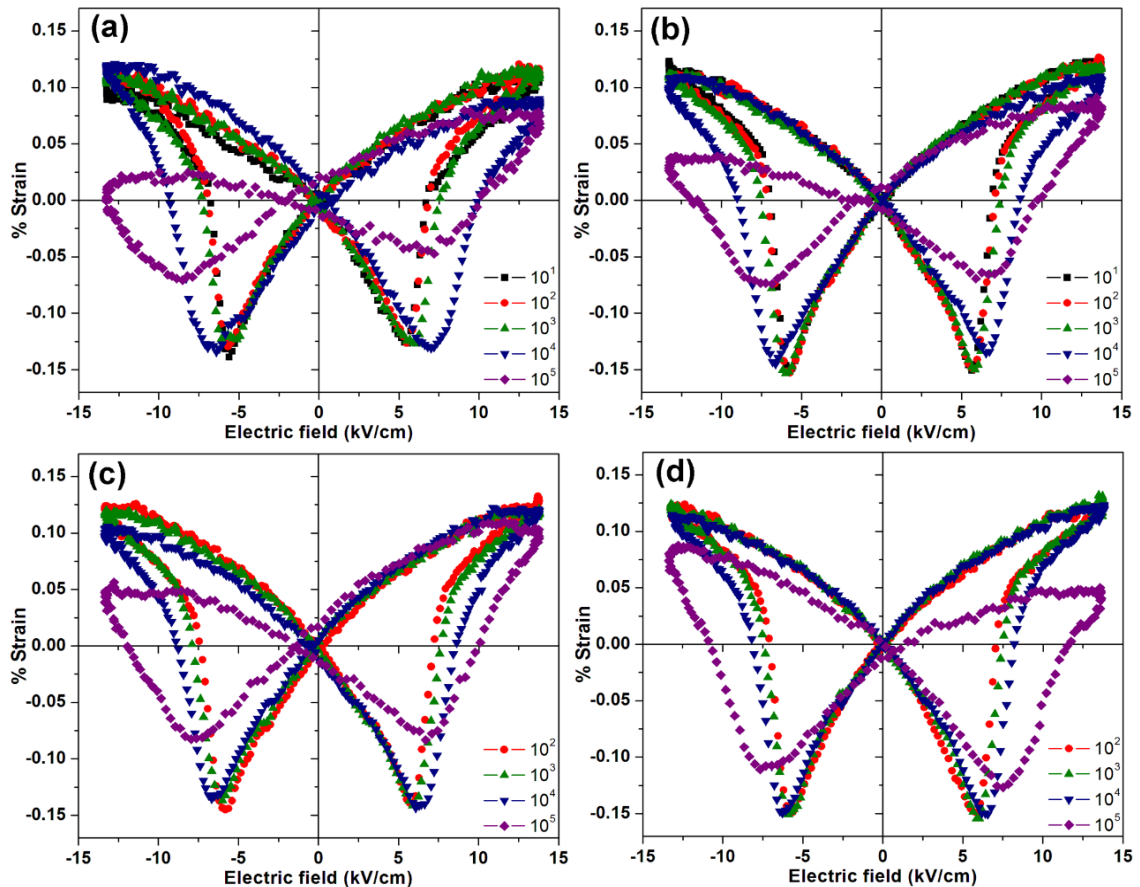


รูป 3.9 ความหนาของชั้นผิวหน้าที่เสียหาย โพลาริเซชันคงค้าง และสนามไฟฟ้าลบค้างที่เป็นฟังก์ชันกับจำนวนรอบสนามไฟฟ้า

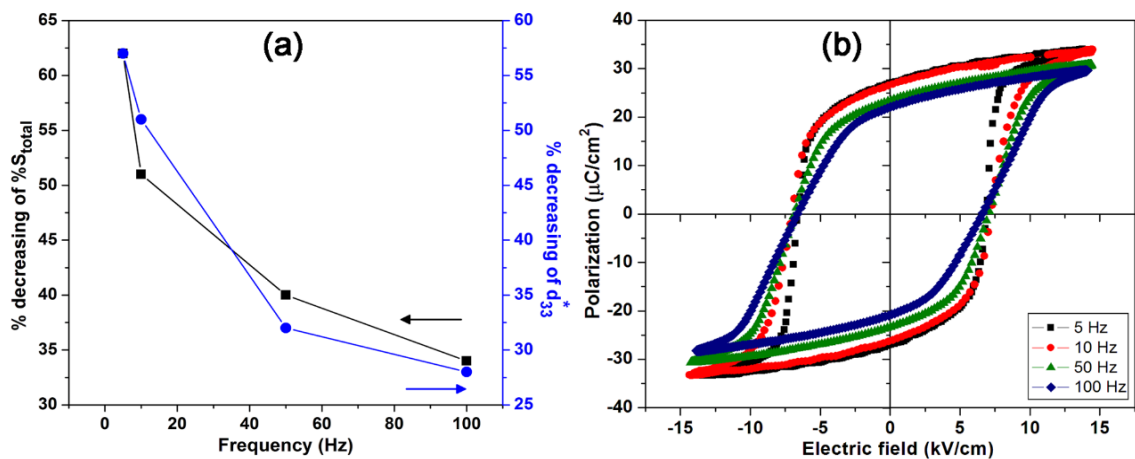
3.4.2 ความล้าทางไฟฟ้าของความเครียดที่ถูกเหนี่ยวนำด้วยไฟฟ้า

กราฟความสัมพันธ์ระหว่างความเครียดและสนามไฟฟ้าที่มีลักษณะคล้ายผิเสื้อของชิ้นงานที่ถูกทดสอบความล้าที่ความถี่ต่างๆ ถูกวัดที่จำนวนรอบสนามไฟฟ้าต่างๆ จนถึง 10⁵ รอบ ดังแสดงในรูป 3.10 ในชิ้นงานที่ทุกๆ ความถี่ วงวนความเครียดและสนามไฟฟ้าที่ถูกทดสอบความล้าจำนวน 10⁵ รอบ มีลักษณะไม่สมมาตร ซึ่งแสดงถึงการกลับทิศของโดเมนที่ไม่สมบูรณ์ สำหรับแต่ละความถี่ ความเครียดรวมหาได้จากผลต่างระหว่างความเครียดสูงสุดและความเครียดต่ำสุด

นอกจากนี้ สัมประสิทธิ์เพียโซอิเล็กทริกหาได้จากความชันของเส้นสัมผัสกราฟที่สนามไฟฟ้าเป็นศูนย์ ค่าสัมประสิทธิ์เพียโซอิเล็กทริกของเซรามิกที่วัดก่อนการทดสอบความล้ามีค่าเท่ากับ 1700 พิโกเมตร/โวลต์ สำหรับแต่ละความถี่ ค่าความเครียดรวมและสัมประสิทธิ์เพียโซอิเล็กทริกที่ถูกวัดหลังจากทดสอบความล้าจำนวน 10⁵ รอบ ถูกนำมาเปรียบเทียบกับค่าที่วัดขณะเริ่มการทดสอบความล้า กราฟแสดงการเปลี่ยนแปลงของความเครียดรวมและสัมประสิทธิ์เพียโซอิเล็กทริกที่เป็นฟังก์ชันกับความถี่แสดงดังรูป 3.11 (a) เมื่อความถี่เพิ่มขึ้น การเปลี่ยนแปลงของสมบัติจะลดลง



รูป 3.10 กราฟความสัมพันธ์ระหว่างความเครียดและสนามไฟฟ้าที่ถูกวัดที่จำนวนรอบสนามไฟฟ้าต่างๆ ของเซรามิก PMNT ที่ถูกทดสอบความล้าที่ความถี่ (a) 5 (b) 10 (c) 50 และ (d) 100 เฮิรตซ์



รูป 3.11 (a) กราฟแสดงความสัมพันธ์ระหว่างร้อยละการลดลงของความเครียดรวมและสัมประสิทธิ์เพียโซอิเล็กทริกที่เป็นฟังก์ชันกับความถี่ และ (b) วงวนฮิสเทอรีซิสที่ถูกวัดที่ความถี่ต่างๆ ของเซรามิก PMNT ที่ไม่ผ่านการทดสอบความล้า

ร้อยละการเปลี่ยนแปลงของโพลาริเซชันคงค้างและสนามไฟฟ้าลบหลังจากการทดสอบความล้าจำนวน 10^6 รอบ ของชิ้นงาน PMNT ที่ทดสอบความล้าที่ความถี่ 10 เฮิรตซ์ ถูกนำไปเปรียบเทียบกับสารเฟอร์โรอิเล็กทริกที่มีตะกั่วและไม่มีตะกั่วเป็นองค์ประกอบ ดังแสดงในตาราง

3.2 การเปลี่ยนแปลงของสมบัติเฟอร์โรอิเล็กทริกของเซรามิก PMNT ในงานวิจัยนี้ มีค่ามากกว่าค่าที่พบในเซรามิก PMN ที่เจือด้วย La อย่างไรก็ตาม การเปลี่ยนแปลงของโพลาริเซชันคงค้างของเซรามิก PMNT ไม่ต่างจากเซรามิก $0.675\text{Pb}(\text{Mg}_{1/3}\text{Nb}_{2/3})\text{O}_3$ - 0.325PbTiO_3 (0.675PMN-0.325PT) อย่างมีนัยสำคัญ แต่การเปลี่ยนแปลงของสนามไฟฟ้าลบกลับมีค่าต่ำกว่ามาก นอกจากนี้ ความต้านทานความล้าของเซรามิก PMNT มีค่ามากกว่าเซรามิก PZT ทางการค้า ในทางกลับกัน เมื่อเปรียบเทียบกับวัสดุที่ไม่มีตะกั่วเป็นองค์ประกอบ เช่น $0.025\text{Bi}(\text{Mg}_{1/2}\text{Ti}_{1/2})\text{O}_3$ - $0.40(\text{Bi}_{1/2}\text{K}_{1/2})\text{TiO}_3$ - $0.575(\text{Bi}_{1/2}\text{Na}_{1/2})\text{TiO}_3$ (2.5BMT-40BKT-57.5BNT), SrTiO_3 -modified $\text{Bi}_{0.5}\text{Na}_{0.5}\text{TiO}_3$ - BaTiO_3 (ST-modified BNT-BT) และ CaZrO_3 -modified $(\text{K}_{0.49}\text{Na}_{0.49}\text{Li}_{0.02})(\text{Ta}_{0.2}\text{Nb}_{0.8})\text{O}_3$ (CZr-modified KNN) เซรามิก PMNT จะมีความต้านทานความล้าที่น้อยกว่า

ตาราง 3.2 ร้อยละการเปลี่ยนแปลงของโพลาริเซชันคงค้างและสนามไฟฟ้าลบกลับของเซรามิก PMNT เมื่อเทียบกับเซรามิกเฟอร์โรอิเล็กทริกที่มีและไม่มีตะกั่วเป็นองค์ประกอบ

วัสดุ	ความถี่	จำนวนรอบ	ร้อยละการเปลี่ยนแปลงของโพลาริเซชันคงค้าง	ร้อยละการเปลี่ยนแปลงของสนามไฟฟ้าลบกลับ
PMNT*	10 Hz, $2E_c$	10^6	-83	+9
1%La-doped PMN	-	10^6	-1	0
0.675PMN-0.325PT	10 Hz, $3E_c$	10^6	-72	+82
PZT	10 Hz, $2E_c$	5×10^5	-63	+49
2.5BMT-40BKT-57.5BNT	10 Hz, $3.3E_c$	10^6	-1	-2
ST-modified BNT-BT	10 Hz, $2E_c$	10^6	-1	-23
CZr-modified KNN	50 Hz, $2E_c$	10^6	-6	-4

* เซรามิก PMNT ที่ใช้ในงานวิจัยนี้

4. การอภิปรายผล

ในระหว่างการให้สนามไฟฟ้ากระแสสลับ ผนังโดเมนบางอันไม่เคลื่อนที่ตามการเปลี่ยนแปลงของทิศทางของสนามไฟฟ้า ซึ่งอาจเนื่องมาจากการขัดขวางของตำหนิที่มีขนาดระดับไมโครเมตรภายในเกรนที่ลดความสามารถในการเคลื่อนที่ของผนังโดเมน ซึ่งทำให้มีการฟอร์มตัวของความเค้นภายใน ความเสียหายของผิวอาจเกิดขึ้นที่ตำแหน่งเหล่านี้เมื่อความเข้มของความเค้นมีค่าเพิ่มขึ้นสู่ความต้านทานการแตกหักของวัสดุ ในกรณีสนามไฟฟ้าความถี่ต่ำ โดเมนได้รับสนามไฟฟ้าเป็นเวลานาน ซึ่งส่งเสริมการเคลื่อนที่ของผนังโดเมน ส่งผลให้ความเค้นที่มีค่าสูงเกิดขึ้นและเกิดความเสียหายที่มาก ดังจะถูกยืนยันโดยค่าโพลาริเซชันคงค้างที่สูงเมื่อทำการวัดที่ความถี่ที่ต่ำกว่า ซึ่งแสดงถึงการเคลื่อนที่ของผนังโดเมนที่มากกว่า ดังแสดงในรูป 3.11 (b) สำหรับชิ้นงานที่ทดสอบความล้าที่ความถี่ 5 และ 10 เฮิร์ตซ์ เนื่องจากความเค้นเฉพาะตำแหน่งที่มาก จึงทำให้เกิดรอยแตกขึ้นในเซรามิกดังกล่าว

จากรูป 3.8 ความล้าที่พบในชิ้นงานที่ทดสอบความล้าที่ความถี่ 50 และ 100 เฮิร์ตซ์ อาจเกิดจากผลของความเสียหายของผิวเป็นหลัก (กระบวนการย้อนกลับไม่ได้) เนื่องจากวงวนฮีสเทอรีซิสสามารถฟื้นฟูได้หลังจากการเอาพื้นผิวที่เสียหายออก การฟื้นฟูของวงวนฮีสเทอรีซิสโดยการเอาพื้นผิวที่เสียหายออกไม่สมบูรณ์สำหรับชิ้นงานที่ความถี่ 5 และ 10 เฮิร์ตซ์ ซึ่งบ่งบอกว่าความล้าทางไฟฟ้าของเซรามิกเกิดจากผลการยึดโดเมน (กระบวนการย้อนกลับได้) ด้วยเช่นกัน ภายใต้การให้สนามไฟฟ้าความถี่ต่ำ ตำแหน่งที่มีประจุ เช่น ช่องว่างออกซิเจน สามารถเคลื่อนที่ไปยังรอยต่อเฉพาะตำแหน่ง เช่น ผงโดเมน ซึ่งขัดขวางการกลับทิศของโดเมน ซึ่งส่งผลต่อการลดลงของสมบัติเฟอร์โรอิเล็กทริก เมื่อทำการอบด้วยความร้อน วงวนฮีสเทอรีซิสของชิ้นงานที่ความถี่ 10 เฮิร์ตซ์สามารถฟื้นฟูได้อย่างสมบูรณ์ อย่างไรก็ตาม วงวนฮีสเทอรีซิสของชิ้นงานที่ความถี่ 5 เฮิร์ตซ์ มีการฟื้นฟูเพียงเล็กน้อยหลังจากการอบด้วยความร้อน ผลดังกล่าวอาจเกิดจากการเกิดรอยแตกที่มีขนาดใหญ่ที่เกิดจากการทดสอบความล้า

จากการอภิปรายข้างต้น ความเสียหายทางโครงสร้าง เช่น ความเสียหายของผิวที่อยู่ใกล้กับขั้วไฟฟ้า และรอยแตกเนื่องจากความล้า ที่มากกว่าจะเกิดที่ความถี่ต่ำกว่า ส่งผลต่อการลดลงของสมบัติเฟอร์โรอิเล็กทริกและเพียโซอิเล็กทริกที่มากกว่า เช่น การลดลงของโพลาริเซชันคงค้าง ความเครียดรวม และสัมประสิทธิ์เพียโซอิเล็กทริก และการเพิ่มของสนามไฟฟ้าลบถาวรของวัสดุ

ดังแสดงในรูป 3.9 ที่จำนวนรอบ $\leq 10^5$ รอบ การลดลงของโพลาริเซชันคงค้างและการลดลงของสนามไฟฟ้าลบถาวรอาจเกิดจากการฟอร์มตัวของชั้นที่เสียหายที่มีสมบัติเฟอร์โรอิเล็กทริกและเพียโซอิเล็กทริกที่ต่ำ ที่จำนวนรอบสนามไฟฟ้า $> 10^5$ รอบ แม้ว่าความหนาของชั้นที่เสียหายเพิ่มขึ้นเล็กน้อยเท่านั้น เชื่อว่ารอยแตกขนาดไมโครเมตรอาจเกิดขึ้นโดยการทดสอบความล้าที่จำนวนรอบสนามไฟฟ้าที่มากขึ้น ดังนั้น ที่จำนวนรอบสนามไฟฟ้า $> 10^5$ รอบ สนามไฟฟ้าที่ให้กับป้องกันโดยชั้นที่เสียหายและรอยแตกที่มีขนาดไมโครเมตรดังกล่าว สิ่งนี้ทำให้เกิดการลดลงของปริมาณของสนามไฟฟ้าที่กระทำต่อบริเวณที่ไม่มีการเสียหาย ปริมาณของสนามไฟฟ้าอาจต่ำกว่าสนามไฟฟ้าลบถาวรของวัสดุ ทำให้การกลับตัวของโดเมนในเซรามิกไม่สมบูรณ์ นำไปสู่ค่าโพลาริเซชันคงค้างที่ต่ำลง มากกว่านั้น การกลับทิศของโดเมนที่ไม่สมบูรณ์ยังส่งผลต่อการลดลงของความแข็งแรงอันตรกิริยาระหว่างโดเมน ทำให้วัสดุต้องการปริมาณสนามไฟฟ้าที่ใช้ในการกลับทิศของโดเมนต่ำลง ส่งผลให้ค่าสนามไฟฟ้าลบถาวรของเซรามิกลดลง

ได้มีการนำเสนอโดย Lou ว่า ปัจจัยที่ส่งผลต่อพฤติกรรมความล้าของเซรามิกเฟอร์โรอิเล็กทริกประกอบด้วย (i) ชนิดของวัสดุที่นำมาทำเป็นขั้วไฟฟ้า (ii) คุณภาพของรอยต่อระหว่างวัสดุกับขั้วไฟฟ้า (iii) โครงสร้างผลึกของวัสดุ (iv) โครงสร้างจุลภาคประกอบด้วยองค์ประกอบทางเคมีขนาดเกรน และรูพรุน (v) การเจือด้วยธาตุอื่นๆ (vi) เงื่อนไขการเตรียมวัสดุ และ (vii) ทิศทางของการวัดสมบัติเมื่อเทียบกับทิศทางของสนามไฟฟ้าในการทดสอบความล้า จากการเปรียบเทียบในตาราง 2 พฤติกรรมความล้าที่ต่างกันของเซรามิก PMNT และเซรามิก PZT อาจเกิดจากโครงสร้างผลึกที่แตกต่างกัน เซรามิก PZT มีเฟสเตตระโกนอล ในขณะที่เซรามิก PMNT มีโครงสร้างผสมระหว่างโมโนคลินิกและเตตระโกนอล สำหรับวัสดุ PMN การลดลงเนื่องจากความล้าที่มากกว่าอาจ

เกิดจากการที่มีความเป็นเตตระโกนอลที่สูงกว่า ซึ่งยืนยันโดยผลการทดลองที่พบในการศึกษาของ Jiang และคณะ ที่การลดลงเนื่องจากความล้าของวัสดุที่มีสมมาตรแบบบรอไมอีตรอลจะมีค่าน้อยกว่าวัสดุที่มีโครงสร้างเตตระโกนอลหรือออโรธอมบิก ความต้านทานความล้าที่ยืดเยื้อของเซรามิกที่ไม่มีตะกั่วเป็นองค์ประกอบอาจเกิดจากปริมาณตำหนิภายใน เช่น ช่องว่างของประจุบวกและลบ ที่น้อยกว่า การเพิ่มขึ้นของความมีอัตลักษณ์ และการไม่มีการเหนี่ยวนำความเป็นเตตระโกนอลในระหว่างการทดสอบความล้า จากการเปรียบเทียบ ความต้านทานความล้าของเซรามิก PMNT มีค่ามากกว่าเซรามิก PZT เล็กน้อย แต่ต่ำกว่าเซรามิกเพียโซอิเล็กทริกที่ไม่มีตะกั่วเป็นองค์ประกอบ ดังนั้น สำหรับการประยุกต์ใช้งาน เช่น ตัวขับเคลื่อน และหน่วยความจำสำรอง ความต้านทานความล้าของเซรามิก PMNT ยังคงต้องการการพัฒนาต่อไป

5. สรุปผลการทดลอง

งานวิจัยนี้ได้ทำการทดสอบความล้าทางไฟฟ้าของเซรามิก PMNT ที่ความถี่ 5 10 50 และ 100 เฮิร์ตซ์ ความเสียหายของพื้นผิวที่อยู่ใต้ขั้วไฟฟ้าถูกพบในชิ้นงานทั้งหมด ในขณะที่รอยแตกที่เกิดจากการทดสอบความล้าพบในชิ้นงานที่ทดสอบความล้าที่ความถี่ 5 และ 10 เฮิร์ตซ์ ความหนาของชั้นที่เสียหายและขนาดของรอยแตกลดลงเมื่อความถี่เพิ่มขึ้น การลดลงเนื่องจากความล้าของสมบัติทางไฟฟ้าในชิ้นงานที่ความถี่ต่ำกว่าจะเกิดขึ้นเร็วกว่าที่ความถี่สูง การเปลี่ยนแปลงของโพลาริเซชันคงค้าง สนามไฟฟ้าลบล้าง ความเครียด และสัมประสิทธิ์เพียโซอิเล็กทริกลดลงเมื่อความถี่เพิ่มขึ้น ความเครียดเฉพาะตำแหน่งที่ถูกเหนี่ยวนำขึ้นโดยการให้สนามไฟฟ้ามีค่าลดลงเมื่อความถี่เพิ่มขึ้น ซึ่งส่งผลต่อการลดลงของระดับของความเสียหายของพื้นผิวและระดับการลดลงของสมบัติทางไฟฟ้า พฤติกรรมความล้าของชิ้นงานที่ความถี่ต่ำอาจเกิดจากทั้งผลของการยืดขอบโดเมนและการเสียหายของพื้นผิว ที่ความถี่สูง ผลของพื้นผิวที่เสียหายมีผลเด่นชัดต่อพฤติกรรมความล้า ความต้านทานความล้าของเซรามิก PMNT มีค่าสูงกว่าเซรามิก PZT แต่ต่ำกว่าเซรามิก PMN และเซรามิกเพียโซอิเล็กทริกที่ไม่มีตะกั่วเป็นองค์ประกอบ ดังนั้น โครงสร้างผลึกและโครงสร้างจุลภาคของเซรามิก PMNT จึงต้องการการพัฒนาต่อไปเพื่อนำไปใช้งานเป็นตัวขับเคลื่อนและหน่วยความจำสำรอง

6. เอกสารอ้างอิง

- [1] M. Alguero, A. Moure, J. Pardo, J. Holc, M. Kosec, Processing by mechano synthesis and properties of piezoelectric $\text{Pb}(\text{Mg}_{1/3}\text{Nb}_{2/3})\text{O}_3\text{-PbTiO}_3$ with different compositions, *Acta Mater.* 54 (2006) 501–511.
- [2] Z.-G. Ye, High-performance piezoelectric single crystals of complex perovskite solid solutions, *Mater. Res. Bull.* 34 (2009) 277–283.
- [3] Y. Chen, K. H. Lam, D. Zhou, W. F. Cheng, J. Y. Dai, H. S. Luo, H. L. W. Chan, High frequency PMN-PT single crystal focusing transducer fabricated by a mechanical dimpling technique, *Ultrasonics* 53 (2013) 345–349.

- [4] G.-T. Hwang, H. Park, J.-H. Lee, S. Oh, K.-I. Park, M. Byun, H. Park, G. Ahn, C. K. Jeong, K. No, H.-S. Kwon, S.-G. Lee, B. Joung, K. J. Lee, Self-powered cardiac pacemaker enabled by flexible single crystalline PMN-PT piezoelectric energy harvester, *Adv. Mater.* 26 (2014) 4880–4887.
- [5] N. Balke, H. Kungl, T. Granzow, D. C. Lupascu, M. J. Hoffmann, J. Rödel, Bipolar fatigue caused by field screening in $\text{Pb}(\text{Zr,Ti})\text{O}_3$ ceramics, *J. Am. Ceram. Soc.* 90 (2007) 3869–3874.
- [6] J. Glaum, T. Granzow, J. Rödel, Evaluation of domain wall motion in bipolar fatigued lead-zirconate-titanate: A study on reversible and irreversible contributions, *J. Appl. Phys.* 107 (2010) 104119/1–6.
- [7] F. W. Zeng, H. Wang, H. Lin, Fatigue and failure response of lead zirconate titanate multilayer actuator under unipolar high-field electric cycling fatigue, *J. Appl. Phys.* 114 (2013) 024101/1–9.
- [8] D.A. Hall, T. Mori, T.P. Comyn, E. Ringgaard, J.P. Wright, Residual stress relief due to fatigue in tetragonal lead zirconate titanate ceramics, *J. Appl. Phys.* 114 (2013) 024101/1–9.
- [9] Q.Y. Jiang, E.C. Subbarao, L.E. Cross, Effect of composition and temperature on electric fatigue of La-doped lead zirconate titanate ceramics, *J. Appl. Phys.* 75 (1994) 7433–7443.
- [10] L. Jin, F. Li, S. Zhang, Decoding the fingerprint of ferroelectric loops: comprehension of the material properties and structures, *J. Am. Ceram. Soc.* 97 (2014) 1–27.
- [11] J. Nuffer, D.C. Lupascu, J. Rödel, Microcrack clouds in fatigued electrostrictive 9.5/65/35 PLZT, *J. Eur. Ceram. Soc.* 21 (2001) 1421–1423.
- [12] J. Nuffer, D.C. Lupascu, A. Glazounov, H.J. Kleebe, J. Rödel, Microstructural modifications of ferroelectric lead zirconate titanate ceramics due to bipolar electric fatigue, *J. Eur. Ceram. Soc.* 22 (2002) 2133–2142.
- [13] J. Glaum, M. Hoffman, Electric fatigue of lead-free piezoelectric materials, *J. Am. Ceram. Soc.* 97 (2014) 665–680.
- [14] D. Lin, Z. Li, Z.-Y. Cheng, Z. Xu, X. Yao, Electric-field-induced polarization fatigue of [001]-oriented $\text{Pb}(\text{Mg}_{1/3}\text{Nb}_{2/3})\text{O}_3$ -0.32 PbTiO_3 single crystals, *Solid State Commun.* 151 (2011) 1188–1191.
- [15] Y. Yan, Y. Zhou, S. Gupta, S. Priya, Fatigue mechanism of textured $\text{Pb}(\text{Mg}_{1/3}\text{Nb}_{2/3})\text{O}_3$ - PbTiO_3 ceramics, *Appl. Phys. Lett.* 103 (2013) 082906/1–5.

- [16] E.A. McLaughlin, T. Liu, C.S. Lynch, Relaxor ferroelectric PMN-32%PT crystals under stress and electric field loading: I-32 mode measurements, *Acta Mater.* 52 (2004) 3849–3857.
- [17] K. Lee, B. R. Rhee, C. Lee, Characteristics of ferroelectric $\text{Pb}(\text{Zr,Ti})\text{O}_3$ thin films having Pt/PtO_x electrode barriers, *Appl. Phys. Lett.* 79 (2001) 821–823.
- [18] S.B. Majumder, Y.N. Mohapatra, D.C. Agrawal, Fatigue resistance in lead zirconate titanate thin ferroelectric films: effect of cerium doping and frequency dependence, *Appl. Phys. Lett.* 70 (1997) 138–140.
- [19] M. Grossmann, D. Bolten, O. Lohse, U. Boettger, R. Waser, S. Tiedke, Correlation between switching and fatigue in $\text{PbZr}_{0.3}\text{Ti}_{0.7}\text{O}_3$ thin films, *Appl. Phys. Lett.* 77 (2000) 1894–1896.
- [20] M. Promsawat, A. Watcharapasorn, Z.-G. Ye, S. Jiansirisomboon, Enhanced dielectric and ferroelectric properties of $\text{Pb}(\text{Mg}_{1/3}\text{Nb}_{2/3})_{0.65}\text{Ti}_{0.35}\text{O}_3$ ceramics by ZnO modification, *J. Am. Ceram. Soc.* 98 (2015) 848–854.
- [21] S. Pojprapai, J. Russell, H. Man, J.L. Jones, J.E. Daniels, M. Hoffman, Frequency effects on fatigue crack growth and crack tip domain-switching behavior in a lead zirconate titanate ceramic, *Acta Mater.* 57 (2009) 3932–3940.
- [22] Z. Luo, J. Glaum, T. Granzow, W. Jo, R. Dittmer, M. Hoffman, J. Rödel, Bipolar and unipolar fatigue of ferroelectric BNT-based lead-free piezoceramics, *J. Am. Ceram. Soc.* 94 (2011) 529–535.
- [23] E.A. Patterson, D.P. Cann, Bipolar piezoelectric fatigue of $\text{Bi}(\text{Zn}_{0.5}\text{Ti}_{0.5})\text{O}_3$ - $(\text{Bi}_{0.5}\text{K}_{0.5})\text{TiO}_3$ - $(\text{Bi}_{0.5}\text{Na}_{0.5})\text{TiO}_3$ Pb-free ceramics, *Appl. Phys. Lett.* 101 (2012) 042905/1–6.
- [24] N. Kumar, D.P. Cann, Electromechanical strain and bipolar fatigue in $\text{Bi}(\text{Mg}_{1/2}\text{Ti}_{1/2})\text{O}_3$ - $(\text{Bi}_{1/2}\text{K}_{1/2})\text{TiO}_3$ - $(\text{Bi}_{1/2}\text{Na}_{1/2})\text{TiO}_3$ ceramics, *J. Appl. Phys.* 114 (2013) 054102/1–6.
- [25] D.N. Fang, Y.H. Zhang, G.Z. Mao, Electric-field-induced fatigue crack growth in ferroelectric ceramics, *Theor. Appl. Fract. Mech.* 54 (2010) 98–104.
- [26] C. Brennan, Model of ferroelectric fatigue due to defect/domain interactions, *Ferroelectrics* 150 (1993) 199–208.
- [27] J. Glaum, T. Granzow, L.A. Schmitt, H.J. Kleebe, J. Rödel, Temperature and driving field dependence of fatigue processes in PZT bulk ceramics, *Acta Mater.* 59 (2011) 6083–6092.

- [28] Z. Luo, S. Pojprapai, J. Glaum, M. Hoffman, Electrical fatigue-induced cracking in lead zirconate titanate piezoelectric ceramic and its influence quantitatively analyzed by refatigue method, *J. Am. Ceram. Soc.* 95 (2012) 2593–2600.
- [29] C. Tian, F. Wang, X. Ye, Y. Xie, T. Wang, Y. Tang, D. Sun, W. Shi, Bipolar fatigue-resistant behavior in ternary $\text{Bi}_{0.5}\text{Na}_{0.5}\text{TiO}_3\text{-BaTiO}_3\text{-SrTiO}_3$ solid solutions, *Scr. Mater.* 83 (2014) 25–28.
- [30] F.-Z. Yao, E.A. Patterson, K. Wang, W. Jo, J. Rödel, J.-F. Li, Enhanced bipolar fatigue resistance in CaZrO_3 -modified $(\text{K},\text{Na})\text{NbO}_3$ lead-free piezoceramics, *Appl. Phys. Lett.* 104 (2014) 242912/1–5.
- [31] D. Lupascu, J. Rödel, Fatigue in bulk lead zirconate titanate actuator materials, *Adv. Eng. Mater.* 7 (2005) 882–898.
- [32] Q.Y. Jiang, E.C. Subbarao, L.E. Cross, Grain size dependence of electric fatigue behavior of hot pressed PLZT ferroelectric ceramics, *Acta. Metall. Mater.* 42 (1994) 3687–3694.
- [33] J. Shieh, J.E. Huber, N.A. Fleck, Fatigue crack growth in ferroelectrics under electrical loading, *J. Euro. Ceram. Soc.* 26 (2006) 95–109.
- [34] Y.A. Genenko, J. Glaum, M.J. Hoffmann, K. Albe, Mechanisms of aging and fatigue in ferroelectrics, *Mater. Sci. Eng. B* 192 (2015) 52–82.
- [35] W. Li, R.M. McMeeking, C.M. Landis, On the crack face boundary conditions in electromechanical fracture and an experimental protocol for determining energy release rates, *Eur. J. Mech. A. Solids* 27 (2008) 285–301.
- [36] X.J. Lou, Polarization fatigue in ferroelectric thin films and related materials, *J. Appl. Phys.* 105 (2009) 024101/1–24.
- [37] N. Kumar, T.Y. Ansell, D.P. Cann, Role of point defects in bipolar fatigue behavior of $\text{Bi}(\text{Mg}_{1/2}\text{Ti}_{1/2})\text{O}_3$ modified $(\text{Bi}_{1/2}\text{K}_{1/2})\text{TiO}_3\text{-(Bi}_{1/2}\text{Na}_{1/2})\text{TiO}_3$ relaxor ceramics, *J. Appl. Phys.* 115 (2014) 154104/1–9.

OUTPUT ที่ได้จากโครงการ

Output ที่ได้จากโครงการ

1. ผลงานที่ได้รับการตีพิมพ์ในวารสารวิชาการระดับนานาชาติ (ภาคผนวก 1)

- 1.1 O. Namsar, S. Pojprapai, A. Watcharapasorn and **S. Jiansirisomboon**, Enhancement of Fatigue Endurance in Ferroelectric PZT Ceramic by the Addition of Bismuth Layered SBT, *J. Appl. Phys.* 116 (2014) 164105. (เอกสารแนบ 1.1)
- 1.2 M. Promsawat, A. Watcharapasorn, Z-G. Ye and **S. Jiansirisomboon**, Enhanced Ferroelectric Order of $\text{Pb}(\text{Mg}_{1/3}\text{Nb}_{2/3})_{0.9}\text{Ti}_{0.1}\text{O}_3$ Ceramics by ZnO Modification, *J. Electroceram.* 33 (2014) 96-104. (เอกสารแนบ 1.2)
- 1.3 N. Thongmee, A. Watcharapasorn and **S. Jiansirisomboon**, Effects of Dy Substitution for Bi on Phase, Microstructure and Dielectric Properties of Layered-structured $\text{Bi}_{4-x}\text{Dy}_x\text{Ti}_3\text{O}_{12}$ Ceramics, *Ferroelectrics* 458 (2014) 76-82. (เอกสารแนบ 1.3)
- 1.4 P. Jaita, A. Watcharapasorn and **S. Jiansirisomboon**, Compositional Range and Electrical Properties of Lead-free $\text{Bi}_{0.5}(\text{Na}_{0.8}\text{K}_{0.2})_{0.5}\text{TiO}_3$ - $(\text{Ba}_{0.98}\text{Nd}_{0.02})\text{TiO}_3$ System, *Ferroelectrics* 458 (2014) 49-55. (เอกสารแนบ 1.4)
- 1.5 M. Promsawat, J.Y.Y. Wong, Z. Ren, H.N. Tailor, A. Watcharapasorn, Z-G. Ye and **S. Jiansirisomboon**, Enhancements in Dielectric, Ferroelectric, and Electrostrictive Properties of $\text{Pb}(\text{Mg}_{1/3}\text{Nb}_{2/3})_{0.9}\text{Ti}_{0.1}\text{O}_3$ Ceramics by CuO Addition, *J. Alloy Compd.* 587 (2014) 618-624. (เอกสารแนบ 1.5)
- 1.6 P. Jaita, A. Watcharapasorn, D.P. Cann and **S. Jiansirisomboon**, Dielectric, Ferroelectric and Electrical Field-induced Strain Behavior of $\text{Ba}(\text{Ti}_{0.90}\text{Sn}_{0.10})\text{O}_3$ -modified $\text{Bi}_{0.5}(\text{Na}_{0.80}\text{K}_{0.20})_{0.5}\text{TiO}_3$ Lead-free Piezoelectrics, *J. Alloy Compd.* 596 (2014) 98-106. (เอกสารแนบ 1.6)
- 1.7 O. Namsar, S. Pojprapai, A. Watcharapasorn and **S. Jiansirisomboon**, Polarization Fatigue in Ferroelectric $\text{Pb}(\text{Zr}_{0.52}\text{Ti}_{0.48})\text{O}_3$ - $\text{SrBi}_2\text{Nb}_2\text{O}_9$ Ceramics, *Electron. Mater. Lett.* 11 [5] (2015) 881-889. (เอกสารแนบ 1.7)
- 1.8 P. Jaita, A. Watcharapasorn, N. Kumar, D.P. Cann and **S. Jiansirisomboon**, Large Electric Field-Induced Strain and Piezoelectric Responses of Lead-Free $\text{Bi}_{0.5}(\text{Na}_{0.80}\text{K}_{0.20})_{0.5}\text{TiO}_3$ - $\text{Ba}(\text{Ti}_{0.90}\text{Sn}_{0.10})\text{O}_3$ Ceramics Near Morphotropic Phase Boundary, *Electron. Mater. Lett.*, 11 (2015) 828-835. (เอกสารแนบ 1.8)
- 1.9 O. Namsar, A. Watcharapasorn, M. Hoffman, J. Glaum and **S. Jiansirisomboon**, Dielectric, Polarization and Strain Response of Enhanced Complex Ceramics: The

Study through $\text{Pb}(\text{Zr}_{0.52}\text{Ti}_{0.48})\text{O}_3\text{-SrBi}_2\text{Ta}_2\text{O}_9$, *Ferroelectrics*. 488 (2015) 79–88.
(เอกสารแนบ 1.9)

- 1.10 M. Promsawat, M. Sriyod, Z. Liu, W. Ren, A. Watcharapasorn, Z.-G. Ye and **S. Jiansirisomboon**, Phase Development and Dielectric, Ferroelectric and Piezoelectric Properties of $\text{Pb}(\text{Mg}_{1/3}\text{Nb}_{2/3})_{0.9}\text{Ti}_{0.1}\text{O}_3\text{-Bi}_{0.5}(\text{Na}_{0.74}\text{K}_{0.26})_{0.5}\text{TiO}_3$ Ceramics, *Ferroelectrics*. 487 (2015) 1-8. (เอกสารแนบ 1.10)
- 1.11 P. Wannasut, P. Jaita, A. Watcharapasorn and **S. Jiansirisomboon**, X-ray Photoelectron Spectroscopy Analysis and Electrical Properties of $\text{Bi}_{0.5}(\text{Na}_{0.80}\text{K}_{0.20})_{0.5}\text{TiO}_3\text{-LiNbO}_3$ Lead-Free Piezoelectrics, *Ferroelectrics*. 489[1] (2015) 118-128. (เอกสารแนบ 1.11)
- 1.12 M. Promsawat, A. Watcharapasorn, Z-G. Ye and **S. Jiansirisomboon**, Enhanced Dielectric and Ferroelectric Properties of $\text{Pb}(\text{Mg}_{1/3}\text{Nb}_{2/3})_{0.65}\text{Ti}_{0.35}\text{O}_3$ Ceramics by ZnO Modification, *J. Am. Ceram. Soc.* 98 (2015) 848-854. (เอกสารแนบ 1.12)
- 1.13 P. Wannasut, P. Jaita, A. Watcharapasorn and **S. Jiansirisomboon**, Electrical Properties of Ternary System $\text{Bi}_{0.5}(\text{Na}_{0.80}\text{K}_{0.20})_{0.5}\text{TiO}_3\text{-0.005LiNbO}_3\text{-BaTiO}_3$ Lead-free Piezoelectric Ceramics, *Integrated Ferro*. 175 (2016) 1-8. (เอกสารแนบ 1.13)
- 1.14 O. Namsar, A. Watcharapasorn, M. Hoffman, J. Glaum and **S. Jiansirisomboon**, Dielectric Properties, Electric-field-induced Polarization and Strain Behavior of Lead Zirconate Titanate-Strontium Bismuth Niobate Ceramics, *J. Electroceramics*. 36 (2016) 70-75. (เอกสารแนบ 1.14)
- 1.15 P. Jaimeewong, M. Promsawat, A. Watcharapasorn and **S. Jiansirisomboon**, Comparative Study of Properties of BCZT Ceramics Prepared from Conventional and Sol–Gel Auto Combustion Powders, *Intergrated Ferro*. 175 (2016) 25-32. (เอกสารแนบ 1.15)
- 1.16 M. Promsawat, N. Promsawat, J.W. Wong, Z. Luo, S. Pojprapai, **S. Jiansirisomboon**, Effects of Frequency on Electrical Fatigue Behavior of ZnO-modified $\text{Pb}(\text{Mg}_{1/3}\text{Nb}_{2/3})_{0.65}\text{Ti}_{0.35}\text{O}_3$ Ceramics, *Ceram. Int.* 43 (2017) 13475-13482. (เอกสารแนบ 1.16)

2. ผลงานที่นำเสนอในการประชุมวิชาการระดับชาติ (ภาคผนวก 2)

- 2.1 M. Promsawat, A. Watcharapasorn, S. Pojprapai, Z.-G. Ye and **S. Jiansirisomboon**, Improvement of ferroelectric and piezoelectric properties of $\text{Pb}(\text{Mg}_{1/3}\text{Nb}_{2/3})_{0.65}\text{Ti}_{0.35}\text{O}_3$ ceramics by ZnO modification, The 41st Congress on

- Science and Technology of Thailand (STT41), Suranaree University of Technology, Nakhon Ratchasima, Thailand, November 6-8, 2015. (เอกสารแนบ 2.1)
- 2.2 P. Wannasut, P. Jaita, A. Watcharapasorn and **S. Jiansirisomboon**, Piezoelectric Performance of Lead-free $(1-x-y)\text{Bi}_{0.5}(\text{Na}_{0.80}\text{K}_{0.20})_{0.5}\text{TiO}_3-x\text{LiNO}_3-y\text{BaTiO}_3$ Ternary System, The 41st Congress on Science and Technology of Thailand (STT41), Suranaree University of Technology, Nakhon Ratchasima, Thailand, November 6-8, 2015. (เอกสารแนบ 2.2)
- 2.3 S. Faichaekhammun, P. Wannasut, P. Jaita, A. Watcharapasorn and **S. Jiansirisomboon**, Preparation and Characterization of Lead-free $\text{Bi}_5(\text{Na}_{0.8}\text{K}_{0.2})_{0.5}\text{TiO}_3-(\text{Ba}_{0.7}\text{Sr}_{0.3})\text{TiO}_3$ Piezoelectric Ceramics, The 41st Congress on Science and Technology of Thailand (STT41), Suranaree University of Technology, Nakhon Ratchasima, Thailand, November 6-8, 2015. (เอกสารแนบ 2.3)
- 2.4 P. Wannasut, P. Jaita, A. Watcharapasorn and **S. Jiansirisomboon**, Influence of LiSbO_3 on Microstructure and Electrical Properties of $\text{Bi}_{0.5}(\text{Na}_{0.80}\text{K}_{0.20})_{0.5}\text{TiO}_3$ Ceramics, Siam Physics Congress 2015 (SPC2015), Sofitel Krabi Phokeethra Golf and Spa Resort, Krabi, Thailand, May 20-22, 2015. (เอกสารแนบ 2.4)
- 2.5 M. Promsawat, N. Petnoi, A. Watcharapasorn and **S. Jiansirisomboon**, Comparative Study of Effects of Metal Oxides Modifications on Properties of $\text{Pb}(\text{Mg}_{1/3}\text{Nb}_{2/3})_{0.9}\text{Ti}_{0.1}\text{O}_3$ Ceramics, Siam Physics Congress 2015 (SPC2015), Sofitel Krabi Phokeethra Golf and Spa Resort, Krabi, Thailand, May 20-22, 2015. (เอกสารแนบ 2.5)
- 2.6 P. Wannasut, P. Jaita, A. Watcharapasorn and **S. Jiansirisomboon**, Microstructure and Electrical Properties of Lead-free $\text{Bi}_{0.5}(\text{Na}_{0.80}\text{K}_{0.20})_{0.5}\text{TiO}_3-\text{LiNbO}_3$ Ceramics, The 31st Annual Conference of the Microscopy Society of Thailand (MST31), Nakhonratchasima, Thailand, 29-31 January 2014. (เอกสารแนบ 2.6)
- 2.7 M. Sriyod, M. Promsawat, A. Watcharapasorn and **S. Jiansirisomboon**, Microstructure and Dielectric Properties of $(1-x)\text{Pb}(\text{Mg}_{1/3}\text{Nb}_{2/3})_{0.9}\text{Ti}_{0.1}\text{O}_3-x\text{Bi}_{0.5}(\text{Na}_{0.74}\text{K}_{0.26})_{0.5}\text{TiO}_3$ Ferroelectric Ceramics, The 31st Annual Conference of the Microscopy Society of Thailand (MST31), Nakhonratchasima, Thailand, 29-31 January 2014. (เอกสารแนบ 2.7)
- 3. ผลงานที่นำเสนอในประชุมวิชาการระดับนานาชาติ (ภาคผนวก 3)**
- 3.1 P. Jaita, A. Watcharapasorn, David P. Cann and S. Jiansirisomboon, Large Electric Field-Induced Strain and Piezoelectric Responses of Lead-Free

- $\text{Bi}_{0.5}(\text{Na}_{0.80}\text{K}_{0.20})_{0.5}\text{TiO}_3\text{-Ba}(\text{Ti}_{0.90}\text{Sn}_{0.10})\text{O}_3$ Ceramics near Morphotropic Phase Boundary, International Conference on Electronic Materials and Nanotechnology for Green Environment (ENGE2014), Ramada Plaza Jeju Hotel, Jeju, Korea, November 16 - 19, 2014. (เอกสารแนบ 3.1)
- 3.2 O. Namsar, A. Watcharapasorn, S. Pojprapai and S. Jiansirisomboon, Polarization Fatigue in Ferroelectric PZT-SBN Ceramics, International Conference on Electronic Materials and Nanotechnology for Green Environment (ENGE2014), Ramada Plaza Jeju Hotel, Jeju, Korea, November 16 - 19, 2014. (เอกสารแนบ 3.2)
- 3.3 M. Promsawat, M. Sriyod, Z. Liu, A. Watcharapasorn, W. Ren, Z.-G. Ye and **S. Jiansirisomboon**, Phase Development, and Dielectric, Ferroelectric and Piezoelectric Responses in $\text{Pb}(\text{Mg}_{1/3}\text{Nb}_{2/3})_{0.9}\text{Ti}_{0.1}\text{O}_3\text{-Bi}_{0.5}(\text{Na}_{0.74}\text{K}_{0.26})_{0.5}\text{TiO}_3$ Ceramics, The 9th Asian Meeting on Ferroelectricity (AMF-9) and the 9th Asian Meeting on Electroceramics (AMEC-9), Ceramics, International Convention Center Shanghai, Shanghai, China, October 26 – 30, 2014. (เอกสารแนบ 3.3)
- 3.4 O. Namsar, A. Watcharapasorn, M. Hoffman, J. Glaum and **S. Jiansirisomboon**, Dielectric, Polarization and Strain Response of Enhanced Complex Ceramics: The Study Through $\text{Pb}(\text{Zr}_{0.52}\text{Ti}_{0.48})\text{O}_3\text{-SrBi}_2\text{Ta}_2\text{O}_9$, The 9th Asian Meeting on Ferroelectricity (AMF-9) and the 9th Asian Meeting on Electroceramics (AMEC-9), Ceramics, International Convention Center Shanghai, Shanghai, China, October 26 – 30, 2014. (เอกสารแนบ 3.4)
- 3.5 P. Wannasut, P. Jaita, A. Watcharapasorn and **S. Jiansirisomboon**, X-ray Photoelectron Spectroscopy Analysis and Electrical Properties of $\text{Bi}_{0.5}(\text{Na}_{0.80}\text{K}_{0.20})_{0.5}\text{TiO}_3\text{-LiNbO}_3$ Lead-free Piezoelectrics, The 9th Asian Meeting on Ferroelectricity (AMF-9) and the 9th Asian Meeting on Electroceramics (AMEC-9), Ceramics, International Convention Center Shanghai, Shanghai, China, October 26 – 30, 2014. (เอกสารแนบ3.5)
- 3.6 M. Promsawat, N. Petnoi, S. Pojprapai and **S. Jiansirisomboon**, Effect of Frequency on Bipolar Electrical Fatigue Behavior of ZnO-Modified Lead Magnesium Niobate Titanate Ceramics, The 2015 Joint IEEE International Symposium on Applications of Ferroelectric (ISAF), International Symposium on Integrated Functionalities (ISIF), Piezoresponse Force Microscopy Workshop (PFM), the Matrix building, the Biopolis, Singapore, May 24-27, 2015. (เอกสารแนบ 3.6)

- 3.7 P. Wannasut, P. Jaita, A. Watcharapasorn and **S. Jiansirisomboon**, Microstructure and Electrical Properties of Ternary Lead-free $\text{Bi}_{0.5}(\text{Na}_{0.80}\text{K}_{0.20})_{0.5}\text{TiO}_3\text{-}0.005\text{LiNaO}_3\text{-BaTiO}_3$ Piezoelectric Ceramics, The 2015 Joint IEEE International Symposium on Applications of Ferroelectric (ISAF), International Symposium on Integrated Functionalities (ISIF), Piezoresponse Force Microscopy Workshop (PFM), the Matrix building, the Biopolis, Singapore, May 24-27, 2015. (เอกสารแนบ 3.7)
- 3.8 P. Wannasut, P. Jaita, A. Watcharapasorn and **S. Jiansirisomboon**, Electrical Properties of Ternary System $\text{Bi}_{0.5}(\text{Na}_{0.80}\text{K}_{0.20})_{0.5}\text{TiO}_3\text{-}0.005\text{LiNO}_3\text{-BaTiO}_3$ Lead-free Piezoelectric Ceramics, The 2015 Join 10th International Conference on the Physical Properties and Application of Advanced Materials (ICPMAT2015), Chiang Mai, Thailand, November 17-21, 2015. (เอกสารแนบ 3.8)
- 3.9 P. Jaimeewong, M. Promsawat, A. Watcharapasorn and **S. Jiansirisomboon**, Comparative Study of Properties of BCZT Ceramics Prepared from Conventional and Sol-Gel Auto Combustion Methods, The 2015 Join 10th International Conference on the Physical Properties and Application of Advanced Materials (ICPMAT2015), Chiang Mai, Thailand, November 17-21, 2015. (เอกสารแนบ 3.9)
- 3.10 P. Jaimeewong, M. Promsawat, A. Watcharapasorn and **S. Jiansirisomboon**, Influence of pH Values on Properties of BCZT Nanopowders Synthesized via Sol-Gel Auto Combustion Method, The 2015 Joint The 19th International Conference on Surface Modification of Materials by Ion Beams (SMMIB-19), Chiang Mai, Thailand, November 22-27, 2015. (เอกสารแนบ 3.10)

4. การนำผลงานไปใช้ประโยชน์

- 4.1 สามารถสร้างงานวิจัยใหม่หลากหลายหัวข้อที่ช่วยให้เกิดการพัฒนาการวิจัยทางด้านวัสดุศาสตร์ นาโนวิทยาและนาโนเทคโนโลยีในประเทศได้
- 4.2 สามารถใช้งานวิจัยนี้เป็นส่วนหนึ่งในการเรียนการสอนในสาขาวิชาวัสดุศาสตร์ ภาควิชาฟิสิกส์และวัสดุศาสตร์ คณะวิทยาศาสตร์ มหาวิทยาลัยเชียงใหม่ได้
- 4.3 สามารถผลิตผลงานวิจัยเพื่อตีพิมพ์ และนำเสนอในที่ประชุมวิชาการทั้งระดับชาติและนานาชาติได้
- 4.4 สามารถสร้างเครือข่ายและความร่วมมือในการทำวิจัยกับคณาจารย์และนักวิจัยภายในและภายนอกสถาบันทั้งในและต่างประเทศได้
- 4.5 สามารถสร้างงานวิจัยเพื่อรองรับนักศึกษาทุนต่าง ๆ ได้แก่
 - โครงการปริญญาเอกกาญจนาภิเษก (คปก.) รุ่นที่ 9 - 12 จาก สกว. จำนวน 3 คน
 - โครงการพัฒนาอาจารย์ในสถาบันอุดมศึกษา จาก สกอ. จำนวน 1 คน

- โครงการเครือข่ายเชิงกลยุทธ์ เพื่อการผลิตและพัฒนาอาจารย์ในสถาบันอุดมศึกษาจาก สกอ. จำนวน 1 คน
- 4.6 สามารถผลิตบัณฑิตสาขาวิชาวัสดุศาสตร์ของภาควิชาฟิสิกส์และวัสดุศาสตร์ คณะวิทยาศาสตร์ มหาวิทยาลัยเชียงใหม่ในระดับปริญญาตรีจำนวน 1 คน นักศึกษาระดับปริญญาโทจำนวน 2 คน และปริญญาเอกจำนวน 5 คน
- 4.7 มีเครือข่ายร่วมกับนักวิจัยต่างประเทศทั้งด้านการวิจัย และรับนักศึกษาปริญญาเอกเพื่อไป ทำวิจัยในต่างประเทศ เช่น
 - Prof. Mark Hoffman, The University of New South Wales ประเทศออสเตรเลีย
 - Prof. David P. Cann, Oregon State University ประเทศสหรัฐอเมริกา
 - Prof. Brady J. Gibbons, Oregon State University ประเทศสหรัฐอเมริกา
 - Prof. Zuo-Guang Ye, Simon Fraser University ประเทศแคนาดา

ภาคผนวก 1
ผลงานที่ได้รับการตีพิมพ์ในวารสารวิชาการ
ระดับนานาชาติ



Enhancement of fatigue endurance in ferroelectric PZT ceramic by the addition of bismuth layered SBT

O. Namsar,¹ S. Pojprapai,^{2,3} A. Watcharapasorn,^{1,4} and S. Jiansirisomboon^{1,4,a)}

¹Department of Physics and Materials Science, Chiang Mai University, Chiang Mai 50200, Thailand

²School of Ceramic Engineering, Suranaree University of Technology, Nakhon Ratchasima 30000, Thailand

³Smart and Innovative Energy Research Unit, Suranaree University of Technology, Nakhon Ratchasima 30000, Thailand

⁴Materials Science Research Center, Faculty of Science, Chiang Mai University, Chiang Mai 50200, Thailand

(Received 14 August 2014; accepted 12 October 2014; published online 27 October 2014)

Electrical fatigue properties of $(1-x)\text{PZT}-x\text{SBT}$ ceramics ($x=0-1.0$ weight fraction) were characterized. It was found that pure PZT ceramic had severe polarization fatigue. This was mainly attributed to an occurrence of the macroscopic cracks at near-electrode regions. On the contrary, pure SBT ceramic exhibited excellent fatigue resistance, which was attributed primarily to weak domain wall pinning. As small amount of SBT ($0.1 \leq x \leq 0.3$) was added into PZT, a small reduction of remanent polarization after fatigue process was observed. This demonstrated that these ceramics had high stability during the repeated domain switching due to their low oxygen vacancy concentration. Therefore, these results suggested that this new ceramic PZT-SBT system seemed to be an alternative material for replacing pure PZT in ferroelectric memory applications. © 2014 AIP Publishing LLC. [<http://dx.doi.org/10.1063/1.4899237>]

I. INTRODUCTION

Ferroelectric materials are used in several electronic devices including actuators, sensors, and non-volatile random access memories.¹ These electronic devices utilize the polarization switching during their operations. High remanent polarization (P_r), low coercive field (E_c), high fatigue resistance, and long lifetime are therefore required. One of the most popular ferroelectric materials for these applications is perovskite $\text{Pb}(\text{Zr}_{0.52}\text{Ti}_{0.48})\text{O}_3$ (PZT) due to its large remanent polarization and small coercive field.² Nevertheless, a critical problem that limits the performance of PZT is fatigue phenomenon caused by an alternating electric field.³ The bismuth layered structure like $\text{SrBi}_2\text{Ta}_2\text{O}_9$ (SBT) has become an attractive candidate for these ferroelectric applications because of its high fatigue endurance.⁴ However, the main drawbacks of SBT are low remanent polarization and high coercive field.⁵ Many research groups have attempted to combine the fatigue-free properties of SBT and superior ferroelectric properties of PZT together in the form of multilayer films.^{6,7} Their results suggested that the combination of two different crystal structures, i.e., perovskite and bismuth layered structure in a form of film, showed an improvement in fatigue endurance.

However, fundamental research on the combination of the perovskite and bismuth layered perovskite structures in a form of ceramic is quite scarce. Therefore, the aim of this present study is to determine the electrical fatigue properties of $(1-x)\text{PZT}-x\text{SBT}$ ceramics ($x=0, 0.1, 0.3, 0.5, 0.7, 0.9$, and 1.0 weight fraction). It is expected that this research

would bring new understanding of this ceramic system for further use especially in memory applications.

II. EXPERIMENTAL DETAILS

The conventional solid-state mixed-oxide method was employed to prepare $(1-x)\text{Pb}(\text{Zr}_{0.52}\text{Ti}_{0.48})\text{O}_3-x\text{SrBi}_2\text{Ta}_2\text{O}_9$ or $(1-x)\text{PZT}-x\text{SBT}$ samples. First, PZT and SBT were synthesized separately from raw materials of PbO (99%, Riedel-de Haën), ZrO_2 (99%, Riedel-de Haën), TiO_2 (99%, Riedel-de Haën), SrCO_3 (98%, Aldrich), Bi_2O_3 (99.9%, Aldrich), and Ta_2O_5 (99%, Aldrich). The starting powders were weighed, ball-milled in ethanol for 24 h and dried at 120°C . The mixed powders were calcined at 800°C for 2 h for PZT and at 950°C for 3 h for SBT powders. The calcined PZT and SBT powders were then weighed, mixed by ball-milling and dried to produce a powder mixture of $(1-x)\text{PZT}-x\text{SBT}$, where $x=0, 0.1, 0.3, 0.5, 0.7, 0.9$, and 1.0 weight fraction. Each mixture was pressed into pellets with 3 wt. % polyvinyl alcohol added as a binder. The pellets were covered with their own powders and sintered at 1200°C in air for 3 h with a heating/cooling rate of $5^\circ\text{C}/\text{min}$. The firing profile also included 1 h dwell time at 500°C for binder burn-out.

X-ray diffraction analysis (Phillips Model X-pert) was used for phase identification. For fatigue characterization, the ceramic samples were lapped to obtain parallel faces which were subsequently coated with silver paint as electrodes. The densities of the ceramics were determined by the Archimedes method. A sawyer-tower circuit was used for the electrical cycling and to measure the polarization hysteresis loop. The samples were fatigued under bipolar electric field of about twice the coercive field magnitude (i.e., $\sim 2E_c$) with the frequency fixed at 50 Hz up to 10^6 switching cycles. During the bipolar cyclic loading, the polarization hysteresis loops of the sample were measured at different decades of

^{a)}Author to whom correspondence should be addressed. Electronic mail: sukanda.jian@cmu.ac.th. Tel.: +66 53 94 1921 ext. 631. Fax: +66 53 94 3445.

cycle numbers. The remanent polarization ($2P_r$) and coercive field ($2E_c$) were computed from the recorded polarization hysteresis loops during cyclic loading. Fatigue rate is defined as the change in the remanent polarization as a function of the switching cycle numbers. For the microstructural observation, the fracture surfaces of unfatigued and fatigued samples were observed by a scanning electron microscope (SEM, JEOL JSM-5910LV). The grain sizes determined from the as-sintered surfaces of the ceramics.

III. RESULTS AND DISCUSSION

Phase characteristics as mixed $(1-x)\text{PZT}-x\text{SBT}$ powders at different x values are depicted in Fig. 1. The phase of pure PZT powder showed a composition near the morphotropic phase boundary (MPB), which consisted of two crystallographic (i.e., tetragonal and rhombohedral) phases. Pure SBT powder was identified as a bismuth layered perovskite material with orthorhombic symmetry. For the compositions with $0.1 \leq x \leq 0.9$, two component phases co-existed with relative intensities corresponding to the relative amount of each phase. The XRD patterns of $(1-x)\text{PZT}-x\text{SBT}$ ceramics sintered at 1200°C are shown in Fig. 2. The pattern for PZT ceramic contained the tetragonal symmetry as a major phase and small amount of rhombohedral phase. The reduction of the rhombohedral symmetry in this ceramic was believed to be caused by the change in compositional stoichiometry due to high sintering temperature.⁸ On the contrary, the pattern of SBT ceramic was nearly identical to its powder but slightly sharper due to larger crystallite size. When small addition of SBT ($0.1 \leq x \leq 0.3$) was added into PZT, the two phases of PZT and a new phase coexisted in the samples. A new phase can be matched with a standard data of the cubic structure $\text{Pb}_{1.2}\text{Ti}_{0.4}\text{Ta}_{1.6}\text{O}_6$ or PTT (JCPDS file no. 76-0177) having a centrosymmetric $\text{Fd}\bar{3}\text{m}$ space group. Furthermore, it should be noted that the PZT peaks shifted slightly to the right, implying that the slight amount of

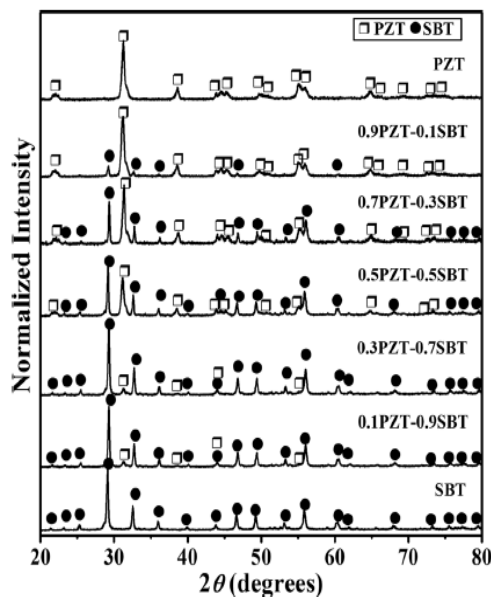


FIG. 1. XRD patterns of $(1-x)\text{PZT}-x\text{SBT}$ powders.

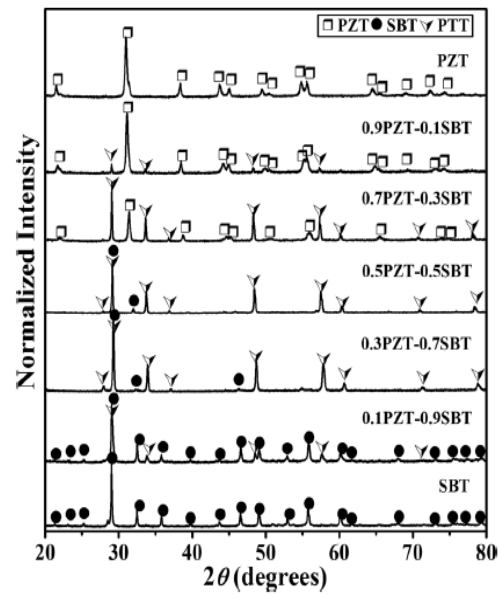


FIG. 2. XRD patterns of $(1-x)\text{PZT}-x\text{SBT}$ ceramics sintered at 1200°C .

substituted ions such as Sr^{2+} , Bi^{3+} , Ta^{5+} from SBT dissolved into the PZT structure to form PZT-based solid solutions, PZT (s.s.). Further increasing the SBT concentration from $x=0.5$ to 0.9 weight fraction, the orthorhombic SBT-based solid solution (SBT(s.s.)) and cubic PTT phases were both present in the samples. Fig. 3 illustrates a relationship between (approximated) various phase fields SBT content in PZT ceramic. The relative phase content in the sample was calculated from the ratio between the integrated peak intensities of each phase (I_p) and the integrated peak intensities of all phases (I_{total})⁹ which can be defined as: %Phase content = $(I_p/I_{\text{total}}) \times 100\%$. The boundaries between phase fields though approximate represented the changing point of phase evolution. Phase field A and E represented PZT-based and SBT-based solid solutions. Three composite regions (B, C, and D) were also present. The region B indicated composite ceramics between PZT(s.s.) + PTT phases ($0.1 \leq x \leq 0.3$).

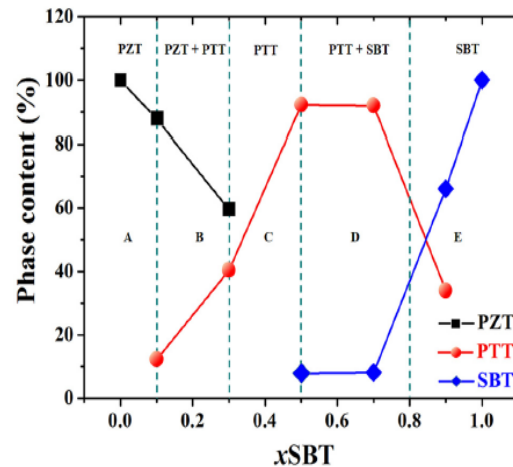


FIG. 3. The relationship between phase field and SBT content in PZT ceramic.

It was found that the amount of PZT(s.s.) decreased while that of PTT increased with increasing of SBT up to $x=0.3$. The region C was the dominant PTT phase ($0.3 \leq x \leq 0.5$) and the region D was composed of SBT(s.s.) + PTT phases ($0.5 \leq x \leq 0.9$). This phase field vs. SBT content shown roughly represented the room temperature stable phase diagram of PZT-SBT system. It should be noted that PTT phase whose existence covered a very wide range of composition ($0.1 \leq x \leq 0.9$) actually had varying composition inside PTT phase field (region C). For example, as analyzed by EDS, the trend showed that the ratio of Pb/(Sr+Bi) in PTT phase decreased with increasing added SBT. This indicated that the cubic structure of PTT could tolerate such compositional variation and was therefore a very stable phase in the phase diagram. This also implied that PZT had a very limited solid solubility in SBT and vice versa.

Due to the ferroelectric fatigue properties of ferroelectric materials were known to be effected by the density and grain size,^{10–12} these parameters of $(1-x)\text{PZT}-x\text{SBT}$ ceramics were first investigated as listed in Table I. It was found that the addition of small amount of SBT ($0.1 \leq x \leq 0.3$) can increase density and reduce grain size of PZT ceramic. The reduction of grain size and increase in density for these ceramics was caused by donor-like substitution. In these ceramics, the donor dopants, i.e., Bi^{3+} and Ta^{5+} (in SBT) was believed to substitute into Pb^{2+} and $(\text{Zr}^{4+}/\text{Ti}^{4+})$ sites, respectively. These substitutions would lead to increase the Pb-vacancies or to decrease the oxygen vacancies. As well known, the main densification mechanism was volume diffusion which was controlled by the concentration of vacancies.¹³ Therefore, the formation of Pb-vacancies in these ceramics helped to enhance volume diffusion, thereby promoting high density for the ceramics. Furthermore, the creation of Pb-vacancies can be considered as a main caused for the reduction of grain size. It was reported that Pb-vacancies were preferably existed along grain boundaries rather than inner grains.¹⁴ Grain boundaries were then pinned by these vacancies, leading to obstruct grain boundary migration and inhibit grain growth.^{15–17} This in turn resulted in small-grained microstructure for these ceramics. The addition of SBT in the range of $0.5 \leq x \leq 0.7$ exhibited low density which was mainly due to the presence of cubic PTT phase in the samples. For high SBT-rich composition (0.1PZT-0.9SBT), it was found that this ceramic showed nearly the

same value of density compared to pure SBT ceramic. On the contrary, the plate size (both length and thickness) of this ceramic was lower than that pure SBT ceramic. The reduction of plate size in this ceramics can be explained by the secondary PTT phase. This secondary phase could interrupt grain boundary migration of SBT phase during sintering and thus retard the grain growth. Therefore, small plate size of SBT phases was observed in 0.1PZT-0.9SBT ceramic. This result was in accordance with previous studies^{18,19} that grain growth in isotropic perovskite ferroelectrics can be inhibited by second phase particles. As the results, the variation of both density and grain size was expected to influence on fatigue endurance of $(1-x)\text{PZT}-x\text{SBT}$ ceramics.

The normalized remanent polarization of $(1-x)\text{PZT}-x\text{SBT}$ ceramics as a function of the number of switching cycles is shown in Fig. 4(a). For the samples with $0.5 \leq x \leq 0.9$, the linear electric-field induced polarization curves were observed. The linear hysteresis loops of these compositions did not possess remanent polarization and coercive field. This behavior indicated that these ceramics exhibited a paraelectric nature. Therefore, these samples were excluded from further fatigue investigation. The disappearance of hysteresis loop for these ceramics were apparently dominated by the occurrence of non-ferroelectric cubic PTT phase, as observed in X-ray diffraction patterns (Fig. 1(b)). For pure PZT ceramic, the normalized remanent polarization increased slightly at 5×10^3 cycles and then began to decrease after 10^5 cycles. Finally, it dropped to 43% of the initial values after 10^6 switching cycles. The increase in polarization at 5×10^3 to 10^5 cycles was possibly due to the “wake-up” process.^{20–22} This wake up process was believed to occur as a result of locked localized space charges present at the interfaces between the ferroelectric bulks and electrodes. It is well known that the volatilization of PbO during fabrication process of PZT ceramic results in the formation of defect charges such as lead and oxygen vacancies.²³ Due to the lower mobility of lead vacancies when compared to that of oxygen vacancies, the latter can move more easily under an external electric field during fatigue test. The positively-charged oxygen vacancies were driven towards to domain walls or grain boundaries where they were captured by space charge. These defect charges obstructed the reversal of domains and hence limited the reversible domain numbers. Since they are easily be removed by the repeated

TABLE I. Density and grain size behavior of $(1-x)\text{PZT}-x\text{SBT}$ ceramics.

$(1-x)\text{PZT}-x\text{SBT}$	Density (g cm^{-3})	Average grain size (μm)			
		PZT phase Diameter	PTT phase Diameter	SBT phase	
				Thickness	Diameter
PZT	7.67 ± 0.04	2.85 ± 0.14
0.9PZT-0.1SBT	7.88 ± 0.02	1.28 ± 0.07	2.08 ± 0.09
0.7PZT-0.3SBT	7.78 ± 0.07	1.75 ± 0.09	2.70 ± 0.15
0.5PZT-0.5SBT	7.44 ± 0.07	...	3.19 ± 0.19
0.3PZT-0.7SBT	7.46 ± 0.09	...	2.54 ± 0.17
0.1PZT-0.9SBT	8.11 ± 0.03	...	2.66 ± 0.18	0.74 ± 0.04	2.03 ± 0.12
SBT	8.06 ± 0.01	1.14 ± 0.07	4.17 ± 0.20

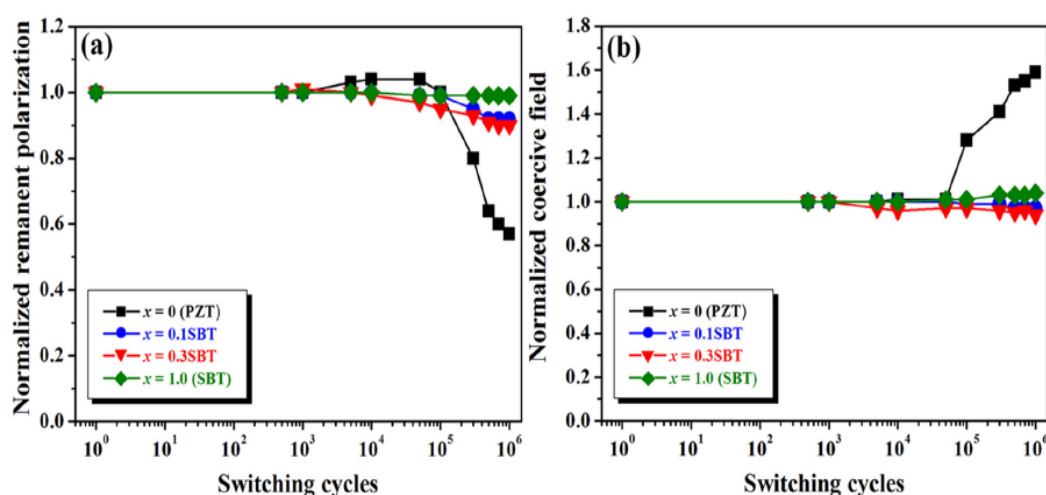


FIG. 4. (a) The normalized polarization as a function of switching cycles and (b) the normalized coercive field as a function of switching cycles of $(1-x)\text{PZT}-x\text{SBT}$ ceramics.

polarization reversals, the normalized remanent polarization increased at this stage.^{20–22} However, after 10^5 cycles, a strong loss of polarization was caused by the field screening effect.²⁴ The field screening effect involves the effective field that reaches the undamaged regions of the sample significantly being decreased because of the voltage drop across the cracks in damaged regions. In some regions this causes the field to be too small to switch domains resulting in loss of polarization but other regions are unaffected, increasing the coercive field. A more detailed explanation for the increase of the coercive field will be discussed in the next paragraph.

For the variation of the normalized coercive field as a function of switching cycle numbers of PZT ceramic shown in Fig. 4(b), it can be seen that the normalized coercive field was stable up to approximately 5×10^4 cycles and then it increased sharply after 10^5 switching cycles. Such results agreed well with other studies^{25–27} in the trend of coercive field under bipolar cycling. Jiang *et al.*¹¹ proposed that such variation in the coercive field could be used to qualitatively determine the electrical fatigue mechanism. They suggested that if the coercive field remained nearly constant, the electrical fatigue was dominated by the interaction between domains and defects. When the coercive field increased sharply with increasing switching cycles, the crack formation became dominant in the fatigue mechanism. From our experiments, it was found that the electrical fatigue process was occurred by both domain pinning (at $1\text{--}5 \times 10^4$ switching cycles) and crack formation (approximately after 10^5 switching cycles). However, the normalized coercive field at higher cycles (after 10^5 switching cycles) showed much higher change (with a 59% increase) than the value at lower cycles (for less than 5×10^4 switching cycles). This significant difference in the variation between these two stages suggested that the crack formation was the major mechanism for the bipolar fatigue of PZT ceramic. The presence of cracks was apparent as shown in SEM images (Fig. 5). The unfatigued sample in Fig. 5(a) showed a typical fracture surface of PZT with mainly transgranular fracture mode. Whereas in fatigued PZT sample, a damaged layer (i.e., crack) could be

seen on the fractured cross section Fig. 5(b). This cracking layer was formed in regions underneath the electrode. The showing results were in agreement with the previous observations on several PZT-related systems.^{24,28–30} The crack that forms under bipolar fatigue loading was due to the strain incompatibility between the near electrode regions and the bulk materials.^{31,32} These strain mismatches occurred because of heterogeneous switching of domains or from the incompatible deformation of grains.¹¹ The repeated domain switching caused a large strain incompatibility, resulting in a high stress intensity. When the stress intensity exceeded the elastic limit of the material, the cracks were initiated.^{33–35} The relationship between the damaged near electrode regions (i.e., cracks) and the electrical fatigue behavior can be explained by the field screening theory.²⁴ By this field screening effect, the appearance of crack resulted in a drop of the applied electric field across the cracks. This caused the effective field acting on the grains adjacent to cracks to be reduced to a level less than the coercive field (E_c), thereby limiting the orientation of domains in the grains. The lack of switching led to the reduction of the remanent polarization of PZT ceramic as shown in Fig. 4(a). In addition, these domains required the higher external field for polarization switching which was reflected by the observed increase the coercive field in fatigue measurement as shown in Fig. 4(b). As the small amount of 0.1SBT was added to PZT, the fatigue started after 10^5 cycles and the normalized remanent polarization dropped to 9% of the initial values after 10^6 cycles with no apparent change in the normalized coercive field. When the amount of SBT was increased to $x = 0.3$, the normalized remanent polarization started to decrease after 10^3 cycles and reduced by about 10% at 10^6 cycles, while a slight reduction in the normalized coercive field was also observed. Compared to pure PZT and $(1-x)\text{PZT}-x\text{SBT}$, pure SBT ceramic showed excellent fatigue endurance up to 10^6 switching cycles with no significant change in the normalized coercive field. As the results, PZT-SBT and SBT ceramics showed high fatigue resistance characteristic and a small change in the normalized coercive field. It was

suspected to be caused by weaker domain wall pinning in these samples. To confirm this hypothesis, the fracture surfaces near electrode/ceramic regions of the fatigued and unfatigued samples were compared to pure PZT ceramic, as displayed in Figs. 5(c)–5(h). For the composition with $x = 0.1$ SBT, the fracture mode of both unfatigued (Fig. 5(c)) and fatigued samples (Fig. 5(d)) was mainly transgranular. The intergranular fracture mode was also partially observed. When the concentration of SBT increased to $x = 0.3$, the fracture surface became a mixture between intergranular and transgranular modes (Figs. 5(e)–5(f)). From these observations, the addition of SBT caused the transformation of the fracture mode from mainly transgranular in pure PZT ceramic to the mixed-mode between intergranular and transgranular in the PZT-SBT ceramics. This phenomenon might be due to the heterogeneous microstructure and different orientation between the PZT and PTT grains. In the case of pure SBT ceramic, both unfatigued and fatigued samples exhibited the plate-shaped grains with the mixed-mode of intergranular and transgranular fracture. When compared to pure

PZT ceramic, the PZT-SBT and SBT ceramics showed no significant difference between the fracture surfaces of the unfatigued and fatigued samples. In addition, in fatigue samples, there were no cracking layer at the electrode/ceramic interface. This indicated that high fatigue endurance in these ceramics was mainly due to the unpinning domain walls whereas the cracking mechanism did not influence to the fatigue performance of these ceramics.

The strong fatigue effect in PZT ceramic after 10^6 switching cycles was also illustrated by the distorted hysteresis loops (i.e., the remanent polarization decreased while the coercive field increased) as represented in Fig. 6(a). The remanent polarization and coercive field values before and after fatigue test are also listed in Table II. The reduction in the remanent polarization and increase in the coercive field was mainly due to the field screening effect as explained above. Only small change in the shape of the hysteresis loops before and after fatigue test was observed in 0.9PZT-0.1SBT and 0.7PZT-0.3SBT ceramics (Figs. 6(b) and 6(c)). In the case of 0.9PZT-0.1SBT, it could be said that the decrease in domain wall pinning mechanism played an important role for controlling the fatigue process in the sample. The improvement in fatigue resistance was mainly owing to the donor-like substitution. It has been widely accepted that the polarization degradation of normal perovskite PZT mainly originates from oxygen vacancy accumulation near-electrode regions³⁶ and domain wall pinning by oxygen vacancy planes.^{37,38} In this sample, the donor dopants like Bi^{3+} and Ta^{5+} ions (from SBT) induced Pb-vacancies in PZT lattice for charge compensation and the oxygen vacancies concentration was greatly reduced. Reduction in oxygen vacancies helped to reduce the possibility of their accumulation at the ceramic bulk-electrode interface or the pinning of the domain walls or grain boundaries during the repeated switching cycles. This could result in the high stability of domain switching process, and thereby less fatigue was observed. Another important factor that influences the fatigue rate for this sample was the small grain size. The influence of grain size on the fatigue behavior has also been studied.^{11,12} As the agglomeration of defects (i.e., oxygen vacancies) predominantly underneath the electrodes was a primary cause for fatigue behavior, the fraction of grain touching the electrode can be used to determine the mechanism of the electrical fatigue.¹² In small grain size, the fraction of grains touched the electrodes would reduce. During electric cycling, the positive space charge and charged point defects near the ceramic/electrode interfaces would move to the electrodes and then accumulate at those sites. Therefore, low fraction of grains touched the electrodes led to reduce the possibility of oxygen vacancy accumulation at the ceramic/electrode interfaces and then increase fatigue resistance.

For the 0.7PZT-0.3SBT ceramic, the smaller magnitude of the remanent polarization was the main cause of the improvement in fatigue endurance. Since the remanent polarization magnitude can be used to determine the trapped charges density at a domain wall (or domain wall pinning rate),³⁹ the relatively low remanent polarization for this ceramic ($2P_r \sim 4.46 \mu\text{C}/\text{cm}^2$, see Table II) led to relatively small trapped charge concentration at domain wall sites of ferroelectric PZT phase, which resulted in a weaker domain

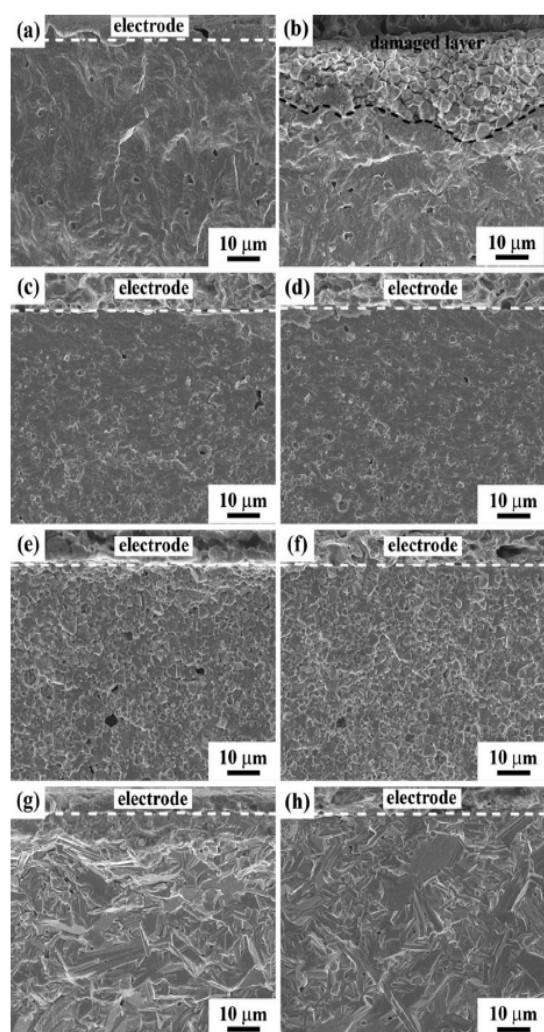


FIG. 5. Fracture surfaces of unfatigued (left) and fatigued samples (right) for $(1-x)\text{PZT}-x\text{SBT}$ ceramics, where (a-b) $x=0$, (c-d) $x=0.1$, (e-f) $x=0.3$, and (g-h) $x=1.0$, respectively.

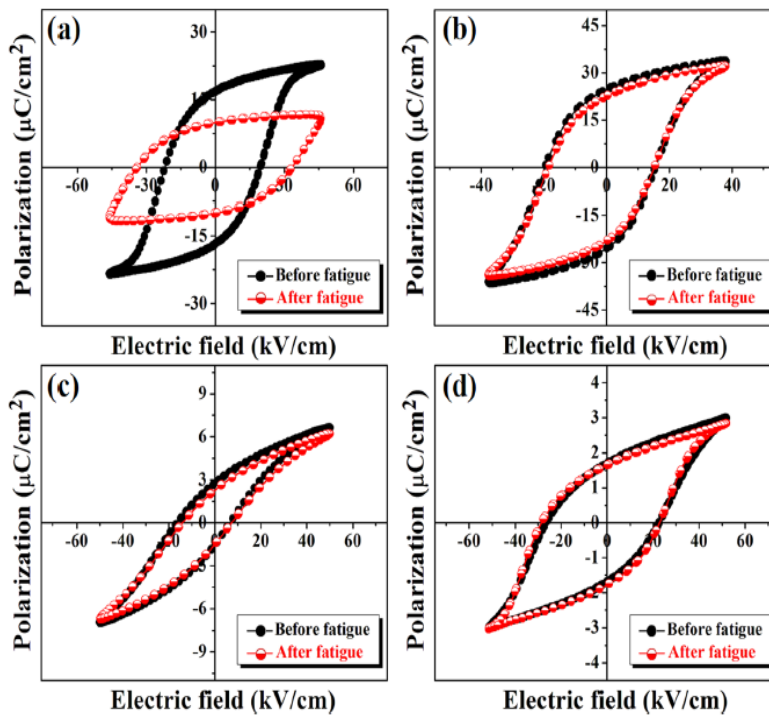


FIG. 6. P - E hysteresis loops of $(1-x)$ PZT- x SBT ceramics before and after electric fatigue 10^6 switching cycles when (a) pure PZT (b) 0.9PZT-0.1SBT (c) 0.7PZT-0.3SBT, and (d) pure SBT.

wall pinning strength. Thus, a small loss in the normalized remanent polarization after fatigue test was observed, implying that the sample was more stable under a conditions cyclic driving electric field than pure PZT ceramic. In addition, it should be observed that this ceramic had higher density than that of PZT ceramic as listed in Table I. Therefore, this reason was also contributed to high fatigue endurance for this ceramic. It has been reported that pores inside the ceramics can be considered as reservoirs of space charge due to they can create a large area of internal free surface.¹⁰ In this case, the density of this ceramic was higher than that of pure PZT ceramic which suggested that this ceramics exhibited lower pore concentration. With a lower pore concentration, there was a reduction in the number of trap sites by space charge at domain walls, allowing domains to orientate continuously by the cyclic applied field. This in turn resulted in a small reduction of polarization.

Fig. 6(d) displays the hysteresis loops before and after the fatigue test for SBT ceramic. Clearly, the P - E loop showed a little change in the shape and became squareness. This result implied that this ceramic had a high switching stability through the fatigue process due to their low number of pinned domains. The fatigue free behavior of the layered perovskite SBT was predominantly related to the weak

domain wall pinning.³⁹ For bismuth layered perovskite like SBT, the absence of a volatile cation on A-site (Sr-site) resulted in lower oxygen vacancy concentration in the $(\text{SrTa}_2\text{O}_7)^{2-}$ perovskite blocks while higher oxygen vacancy concentration appeared in the $(\text{Bi}_2\text{O}_2)^{2+}$ layers due to the volatilization of Bi_2O_3 . However, the ability to pin the domain walls of oxygen vacancies at the $(\text{Bi}_2\text{O}_2)^{2+}$ layers was less effective than oxygen vacancies in $(\text{SrTa}_2\text{O}_7)^{2-}$ perovskite blocks.⁴⁰ Therefore, the pinning of the oxygen vacancies at domain walls became much less pronounced in SBT ceramic, which resulted in no net loss of the switchable polarization. This research therefore demonstrated that improved fatigue properties of PZT ceramic could be achieved by small addition of SBT compound.

IV. CONCLUSIONS

Ferroelectric fatigue endurance under bipolar electric field cycling was investigated for the $(1-x)$ PZT- x SBT ceramics. The perovskite PZT showed a strong degradation of the remanent polarization and increase the coercive field. Fatigue macrocracking was a major contribution to electrical fatigue in PZT. Whereas, the bismuth layered perovskite SBT ceramic exhibited no obvious reduction of switchable

TABLE II. Remanent polarization ($2P_r$) and coercive field ($2E_c$) of $(1-x)$ PZT- x SBT ceramics measured before and after fatigued tests.

(1-x)PZT-xSBT	$2P_r$			$2E_c$		
	Before	After	% of decrease	Before	After	% of change
PZT	34.96	20.05	43	42.79	68.10	Increased by 59%
0.9PZT-0.1SBT	51.37	46.96	9	36.07	34.78	Decreased by 4%
0.7PZT-0.3SBT	4.46	4	10	23.70	22.28	Decreased by 6%
SBT	3.49	3.47	0.6	50.17	52.02	Increased by 4%

polarization at 10^6 cycles. The fatigue-free behavior of SBT was mainly attributed to the unpinned domain walls. The fatigue behavior of PZT ceramic was improved after small amount of SBT ($0.1 \leq x \leq 0.3$) incorporation. The improvement in fatigue endurance of these ceramics was mainly attributed to unpinned domain walls. The unpinned domain walls caused less residual ferroelastic stress, resulting in the reduction of the probability of crack propagation. Less cracks led to less field screening effect and greater fatigue resistance for these ceramics. Based on our results, the ferroelectric properties of 0.9PZT-0.1SBT ceramic with fatigue free characteristics could be further improved for being employed particularly in ferroelectric memory applications.

ACKNOWLEDGMENTS

This work was financially supported by the Thailand Research Fund (TRF) and the National Research University Project under Thailand's Office of the Higher Education Commission (OHEC). The Faculty of Science and the Graduate School, Chiang Mai University is also acknowledged. O.N. would like to acknowledge financial support from the TRF through the Royal Golden Jubilee Ph.D. Program.

- ¹G. H. Haertling, *J. Am. Ceram. Soc.* **82**, 797 (1999).
- ²R. Dat, D. J. Lichtenwalner, O. Auciello, and A. I. Kingon, *Appl. Phys. Lett.* **64**, 2673 (1994).
- ³D. H. Bao, N. Wakiya, K. Shinozaki, and N. Mizutani, *J. Phys. D: Appl. Phys.* **35**, L1 (2002).
- ⁴C. A. Paz De Araujo, J. D. Cuchiaro, L. D. McMillan, M. C. Scott, and J. F. Scott, *Nature* **374**, 627 (1995).
- ⁵K. Kato, *Jpn. J. Appl. Phys. Part 1* **37**, 5178 (1998).
- ⁶W. Q. Zhang, A. D. Li, Q. Y. Shao, Y. D. Xia, D. Wu, Z. G. Liu, and N. B. Ming, *Appl. Surf. Sci.* **254**, 1583 (2008).
- ⁷H. H. Park, H. H. Park, T. S. Kim, and R. H. Hill, *Sens. Actuators B* **130**, 696 (2008).
- ⁸A. I. Kingon and J. B. Clark, *J. Am. Ceram. Soc.* **66**, 253 (1983).
- ⁹B. D. Cullity, *Elements of X-Ray Diffraction* (Addison-Wesley Publishing, Massachusetts, 1956) p. 388.
- ¹⁰Q. Y. Jiang and L. E. Cross, *J. Mater. Sci.* **28**, 4536 (1993).
- ¹¹Q. Y. Jiang, E. C. Subbarao, and L. E. Cross, *Acta. Metall. Mater.* **42**, 3687 (1994).
- ¹²F. Yan, P. Bao, H. L. W. Chan, C. L. Choy, and Y. N. Wang, *Thin Solid Films* **406**, 282 (2002).
- ¹³M. Hammer and M. J. Hoffmann, *J. Am. Ceram. Soc.* **81**, 3277 (1998).
- ¹⁴J. Y. Yi, J. K. Lee, and K. S. Hong, *J. Am. Ceram. Soc.* **85**, 3004 (2002).
- ¹⁵F. Kulcsar, *J. Am. Ceram. Soc.* **42**, 343 (1959).
- ¹⁶R. B. Atkin and R. M. Fulrath, *J. Am. Ceram. Soc.* **54**, 265 (1971).
- ¹⁷G. H. Haertling, *Am. Ceram. Soc. Bull.* **43**, 875 (1964).
- ¹⁸S.-J. Yoon, J.-W. Choi, and J.-Y. Choi, *J. Korean Phys. Soc.* **57**, 863 (2010).
- ¹⁹D. W. Yuan, S. F. Wang, W. Huebner, and G. Simkovich, *J. Mater. Res.* **8**, 1675 (1993).
- ²⁰S. Okamura, S. Miyata, Y. Mizutani, T. Nishida, and T. Shiosaki, *Jpn. J. Appl. Phys. Part 1* **38**, 5364 (1999).
- ²¹S. Okamura, M. Takaoka, T. Nishida, and T. Shiosaki, *Jpn. J. Appl. Phys.* **39**, Part 1 5481 (2000).
- ²²S. Okamura, N. Abe, Y. Otani, and T. Shiosaki, *Integr. Ferroelectr.* **52**, 127 (2003).
- ²³J. Chen, M. P. Harmerand, and M. Smyth, *J. Appl. Phys.* **76**, 5394 (1994).
- ²⁴N. Balke, H. Kungl, T. Granzow, D. C. Lupascu, M. J. Hoffmann, and J. Rödel, *J. Am. Ceram. Soc.* **90**, 3869 (2007).
- ²⁵Q. Y. Jiang, W. Cao, and L. E. Cross, *J. Am. Ceram. Soc.* **77**, 211 (1994).
- ²⁶D. B. Fraser and J. R. Maldonado, *J. Appl. Phys.* **41**, 2172 (1970).
- ²⁷W. R. Salaneck, *Ferroelectrics* **4**, 97 (1972).
- ²⁸D. Fang, B. Liu, and C. T. Sun, *J. Am. Ceram. Soc.* **87**, 840 (2004).
- ²⁹A. Furuta and K. Uchino, *J. Am. Ceram. Soc.* **76**, 1615 (1993).
- ³⁰J. Nuffer, D. C. Lupascu, and J. Rödel, *J. Eur. Ceram. Soc.* **21**, 1421 (2001).
- ³¹S. Winzer, N. Shankar, and A. P. Ritter, *J. Am. Ceram. Soc.* **72**, 2246 (1989).
- ³²J. Shieh, J. E. Huber, and N. A. Fleck, *J. Euro. Ceram. Soc.* **26**, 95 (2006).
- ³³J. Nuffer, D. C. Lupascu, A. Glazounov, H. J. Kleebe, and J. Rödel, *J. Eur. Ceram. Soc.* **22**, 2133 (2002).
- ³⁴E. C. Subbarao, V. Srikanth, W. Cao, and L. E. Cross, *Ferroelectrics* **145**, 271 (1993).
- ³⁵S. Pojprapai, J. L. Jones, T. Vodenitcharova, J. V. Bernier, and M. Hoffman, *Scr. Mater.* **64**, 1 (2011).
- ³⁶J. F. Scott, C. A. Araujo, B. M. Melnick, I. D. McMillan, and R. Zuleeg, *J. Appl. Phys.* **70**, 382 (1991).
- ³⁷E. L. Colla, S. Hong, D. V. Taylor, A. K. Tagantsev, N. Setter, and K. No, *Appl. Phys. Lett.* **72**, 2763 (1998).
- ³⁸C. H. Park and D. J. Chadi, *Phys. Rev. B* **57**, R13961 (1998).
- ³⁹H. N. Al-Shareef, D. Dimos, T. J. Boyle, W. L. Warren, and B. A. Tuttle, *Appl. Phys. Lett.* **68**, 690 (1996).
- ⁴⁰B. H. Park, B. S. Kang, S. D. Bu, T. W. Noh, J. Lee, H.-D. Kim, and T. H. Kim, *J. Korean Phys. Soc.* **35**, S1306 (1999).

Enhanced ferroelectric order in $\text{Pb}(\text{Mg}_{1/3}\text{Nb}_{2/3})_{0.9}\text{Ti}_{0.1}\text{O}_3$ ceramics by ZnO modification

M. Promsawat · A. Watcharaporn · Z.-G. Ye ·
S. Jiansirisomboon

Received: 21 November 2013 / Accepted: 23 May 2014 / Published online: 31 May 2014
© Springer Science+Business Media New York 2014

Abstract In this research, the effects of ZnO modification on ferroelectric order of $\text{Pb}(\text{Mg}_{1/3}\text{Nb}_{2/3})_{0.9}\text{Ti}_{0.1}\text{O}_3$ (PMNT) ceramics were studied through characterizations of dielectric and ferroelectric properties. The PMNT/ x ZnO (where $x=0, 0.4, 2.0, 4.0$ and 11.0 mol.%) ceramics were prepared by solid state reaction and sintering process. The lattice parameter a and unit cell volume of pure PMNT ceramic were increased with ZnO modification. The temperature of maximum dielectric constant (T_{max}), the freezing temperature (T_f), the depolarization temperature (T_d) and the polar ordering temperature (T_p) increased while the diffuseness parameter (δ) decreased with the increase in ZnO content, indicating an enhancement of ferroelectric ordering and a decrease in a degree of relaxor behavior of PMNT ceramics by ZnO modification. Polarization-electric field hysteresis loop and butterfly-like strain-electric field curve were displayed around room temperature in the 11.0 mol.% ZnO-modified PMNT sample, which indicated an establishment of polar macro domains. Electrostrictive coefficient (M) reached a highest value of $22.22 \times 10^{-16} \text{ m}^2/\text{V}^2$ for the PMNT/ 4.0 mol.%ZnO ceramic, which made it a promising material for applications as electrostrictive actuators.

Keywords $\text{Pb}(\text{Mg}_{1/3}\text{Nb}_{2/3})_{0.9}\text{Ti}_{0.1}\text{O}_3$ (PMNT) · ZnO-doping · Dielectric properties · Ferroelectric properties · Electrostrictive properties

1 Introduction

Complex perovskite solid solution compound of $\text{Pb}(\text{Mg}_{1/3}\text{Nb}_{2/3})_{0.9}\text{Ti}_{0.1}\text{O}_3$ (PMNT) is a well known relaxor ferroelectric material that shows good electrostrictive properties around room temperature which make it suitable to use as electrostrictive actuators [1, 2]. Because of the excellent properties of this family of materials, their structure and physical properties have been widely and continuously studied [3–5]. The origin of their excellent properties has often been explained in term of polar nano-regions (PNRs) which nucleated as the material is cooled down below the Burns temperature (T_B) [6, 7]. The size and volume of PNRs increase as the temperature decreased further, leading to an increase in dielectric permittivity. However, the dynamic of PNRs slows down with further decreasing the temperature, resulting in a decrease in dielectric permittivity and thereby creating the maximum dielectric permittivity at the temperature T_{max} . The dynamic of PNRs is frozen when the temperature is decreased below the freezing temperature (T_f) [8]. Below T_f , polar macro domains can be established by an application of electric field. The induced polar macro domains persist until the material is heated above the depolarization temperature (T_d) [9]. It is interesting to note that a large longitudinal induced strain and high electrostrictive coefficient (M) are observed above and near T_d due to the coexistence of micro- and induced macro domains [10, 11]. Therefore, it is expected that a high electric field-induced strain and electrostrictive coefficient around room temperature of PMNT ceramics can be achieved by shifting its T_d ($\sim 0^\circ\text{C}$ [12]) toward room temperature.

M. Promsawat · A. Watcharaporn · S. Jiansirisomboon
Department of Physics and Materials Science, Faculty of Science,
Chiang Mai University, Chiang Mai 50200, Thailand

M. Promsawat · A. Watcharaporn · S. Jiansirisomboon (✉)
Materials Science Research Center, Faculty of Science, Chiang Mai
University, Chiang Mai 50200, Thailand
e-mail: sukanda.jian@cmu.ac.th

M. Promsawat · Z.-G. Ye
Department of Chemistry and 4D LABS, Simon Fraser University,
British Columbia V5A 1S6, Canada

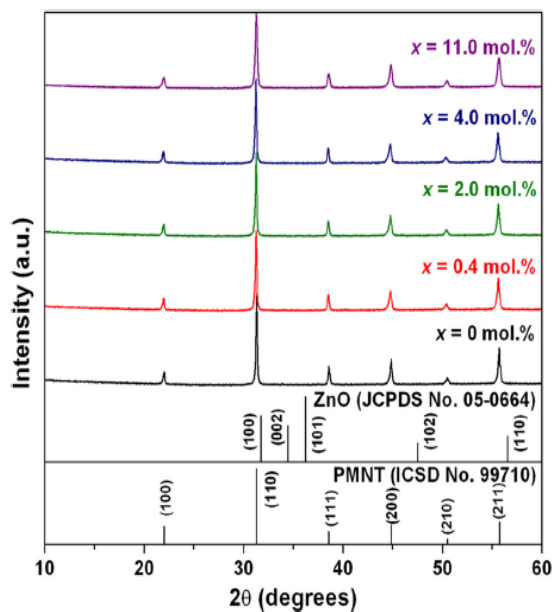


Fig. 1 XRD patterns of the PMNT/*x*ZnO ceramics

ZnO is known to be an effective sintering aid for dielectric and ferroelectric materials. From previous results, ZnO addition could promote the formation of a liquid phase which expedited mass transfer of ceramics during a sintering process, resulting in an enhancement of density and grain size, and an improvement in the dielectric, ferroelectric and piezoelectric properties of ceramics [13, 14]. Moreover, ZnO was also used as a substituent for ferroelectric ceramics such as PMW-PNN-PT-PZ [15], PZN-PZT [16], BNT [17, 18], PMnN-PZT [19] and NKN ceramics [20]. These results suggested that Zn^{2+} ion could enter the lattices of the ceramics, which led to the unit cell distortion. The distortion of unit cell could in turn affect

the phase transition temperature and electrical properties of the ceramics. For example, ZnO doping resulted in an increase in the phase transition temperature, an enhancement of the piezoelectric properties, and a decrease in the degree of relaxor behavior of ceramics [21]. It can be seen that ZnO acts as an effective sintering aid and a substituent, which causes an improvement in the electrical properties of dielectric and ferroelectric ceramics. These advantages make ZnO an interesting compound to be used as both an additive and a substituent for the PMNT ceramics. In this study, the PMNT ceramics modified with ZnO were fabricated. Ferroelectric ordering of the PMNT/ZnO ceramics was studied through characterizations of the dielectric and ferroelectric properties. Effects of ZnO modification on ferroelectric ordering and electrical properties of PMNT ceramics were also discussed.

2 Experiment

$\text{Pb}(\text{Mg}_{1/3}\text{Nb}_{2/3})_{0.9}\text{Ti}_{0.1}\text{O}_3$ (PMNT) powder was prepared by a columbite precursor method [22]. Different amounts ($x=0, 0.4, 2.0, 4.0$ and 11.0 mol.%) of ZnO were added into the PMNT powder. The mixed and ground powders were uniaxially pressed into pellets and then sintered at 1150°C for 2 hrs. Phase formation of the PMNT/*x*ZnO ceramics was characterized by an X-ray diffractometer (XRD, Model Xpert, Panalytical B.V.). The temperature dependences of dielectric constant (ϵ_r) and loss tangent ($\tan\delta$) of the unpoled samples were measured at frequencies of $1\text{--}10^6$ Hz using a computer-controlled alpha dielectric analyzer (Novocontrol). In this study, a soft polar nano-region model proposed by Bokov and Ye [6, 7] was adopted to describe the dielectric behavior of the samples. In this model, the dispersion of the

Fig. 2 Plots of lattice parameter *a* and unit cell volume as a function of ZnO content of the PMNT/*x*ZnO ceramics

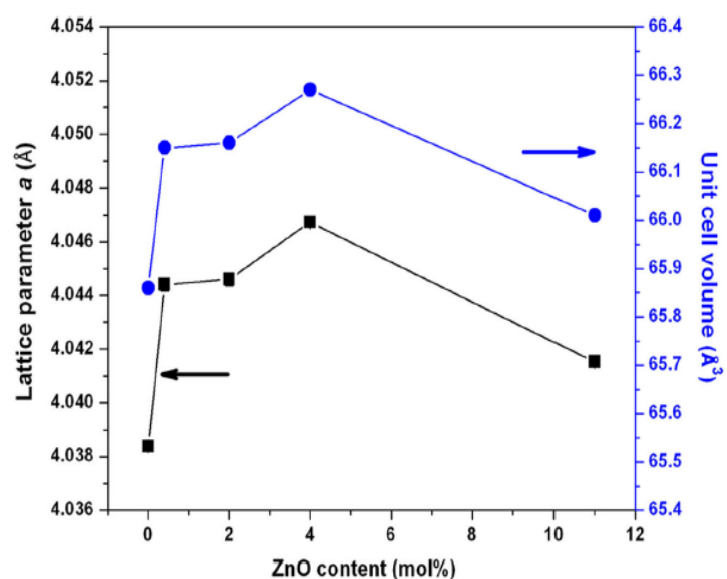


Table 1 Dielectric properties and the quadratic fitting parameters of the PMNT/xZnO ceramics

ZnO content <i>x</i> (mol.%)	ϵ'_{\max}	$\tan\delta$	T_{\max} (°C)	ϵ_A	T_A (°C)	δ (°C)
0	12,106	0.066	43	11,569	31±1	57±1
0.4	10,499	0.056	48	10,203	39±1	56±1
2.0	10,499	0.060	52	10,294	41±2	55±1
4.0	9,958	0.057	58	9,750	49±1	53±1
11.0	15,395	0.050	68	15,214	59±3	45±2

ϵ'_{\max} and $\tan\delta$ represent dielectric constant and dielectric loss tangent values measured at the temperature of the dielectric peak (T_{\max}). The measurements were carried out at the frequency of 1 kHz. δ and T_A represent the diffuseness parameter and the temperature of the static conventional permittivity maximum, respectively, extrapolated from the quadratic law

temperature of maximum dielectric permittivity (T_{\max}) in term of the frequency of alternating field (f) was described by a Vogel-Fulcher ($V-F$) relationship [8]. Moreover, a quadratic law was introduced to describe the temperature dependence of dielectric permittivity in the temperature range above T_{\max} [23]. Therefore, in this study, the experimental data was fitted to the $V-F$ relationship and the quadratic law in order to determine the fitting parameters such as the freezing temperature (T_f) and the diffuseness parameter (δ). In order to determine the depolarization temperature (T_d), above which induced polar macro domains are eliminated by thermal activation, the sample was firstly poled at room temperature with an electric field of 20 kV/cm. While the sample was being poled, it was cooled down to −50 °C. At −50 °C, the applied electric field was removed. Then the temperature dependence of the dielectric properties was measured upon heating. The polarization–electric field ($P-E$) curves were displayed using a ferroelectric testing instrument (Radiant Technologies RT66A). In order to determine the polar ordering temperature (T_p), at which the polarization is abruptly increased upon cooling, the temperature dependence of the remnant polarization ($P_r(T)$) was established. The strain versus electric field ($S-E$) curves were measured using a Fotonics sensor (MTI 2000, MTI Instruments) in conjunction with a computer controlled electrometer/voltage source (Keithley 2517A).

3 Results and discussion

3.1 Phase formation

X-ray diffraction patterns of the PMNT/xZnO ceramics were shown in Fig. 1, which were found to match the standard inorganic crystal structure database (ICSD) file No. 99710 of $\text{Pb}(\text{Mg}_{0.3}\text{Nb}_{0.6}\text{Ti}_{0.1})\text{O}_3$ in $Pm\bar{3}m$ cubic space group [24]. No secondary phase was found in the patterns. From the patterns, the lattice parameter a and unit cell volume were determined and plotted as a function of ZnO content, as shown in Fig. 2.

The lattice parameter a and unit cell volume of pure PMNT ceramic were about 4.038 Å and 65.85 Å³, respectively, which increased to 4.044 Å and 66.15 Å³, respectively, with an addition of 0.4–2.0 mol.% ZnO. They slightly increased to 4.052 Å and 66.25 Å³, respectively, as the ZnO content was increased to 4.0 mol.%. The increases in the lattice parameter a and unit cell volume were attributed to the substitution of Zn^{2+} ion for the smaller ions on the crystal lattice of PMNT. From the crystal chemistry requirements (the tolerance factor), for the stability of the perovskite structure, A-site has to be a large cation (i.e. Pb^{2+}) while B-site requires a relative smaller cation (i.e. Mg^{2+} , Nb^{5+} and Ti^{4+}). Based on ionic radius of Zn^{2+} ion ($r_{\text{Zn}^{2+}}=0.74$ Å), it was clear that Zn^{2+} could only substitute for the smaller cations on the B-site, i.e. Mg^{2+} , Nb^{5+} and Ti^{4+} ions ($r_{\text{Mg}^{2+}}=0.72$ Å, $r_{\text{Nb}^{5+}}=0.64$ Å and $r_{\text{Ti}^{4+}}=0.605$ Å [25]) in the lattice of PMNT. This was consistent with previous results obtained in PNN-PFN-PZT [26], PZNT [27], PZT-PMnN [28], PZT-PFW-PMN [29], BNCT [30], PZN-PZT [16], PZT-PMS-PZN [13], PT [31] and PZN-PT-BT [32] ceramics modified with ZnO. These suggested that the Zn^{2+} ion could substitute the ions located on the B-site lattice of the ceramics, which led to the structural change and unit cell distortion. It was proposed that this substitution was mainly due to the ionic radius of Zn^{2+} that was similar to that of the B-site ions. Therefore, it was reasonable to deduce that added Zn^{2+} ions entered the B-site lattice of the PMNT ceramics.

3.2 Dielectric properties

The selected values of dielectric properties, i.e. the maximum dielectric permittivity (ϵ'_{\max}), the temperature of maximum dielectric permittivity (T_{\max}) and the loss tangent at T_{\max} ($\tan\delta$), of the ceramics were given in Table 1. The ϵ'_{\max} of pure PMNT ceramic was found to be 12,000, which was decreased to 10,000 with an addition of 0.4–4.0 mol.% ZnO. However, the ϵ'_{\max} significantly increased to 15,000 with further increasing the ZnO content to 11.0 mol.%. The loss tangent of pure PMNT ceramic was 0.06, which did not

significantly change with the ZnO modification. The improvement in dielectric properties, i.e. the increase in ϵ'_{\max} and the decrease in $\tan\delta$, was believed to be arisen from an increase in grain size of the ceramics [33, 34]. Apart from this, the result showed that T_{\max} tended to increase with increasing the ZnO content.

In order to investigate the effects of ZnO on the diffuseness of the dielectric permittivity peak, the high temperature ($T > T_{\max}$) slope of dielectric peak measured at 10^5 Hz was fitted to the quadratic law introduced by

Bokov and Ye to describe the dielectric permittivity peak of relaxors in general [23]:

$$\frac{\epsilon_A}{\epsilon} = 1 + \frac{(T - T_A)^2}{2\delta^2} \quad (1)$$

where T_A and ϵ_A represent the temperature and value at the peak of static conventional permittivity of relaxors, respectively, which are extrapolated from the quadratic law, and δ (to be distinguished from the δ in $\tan\delta$) represents

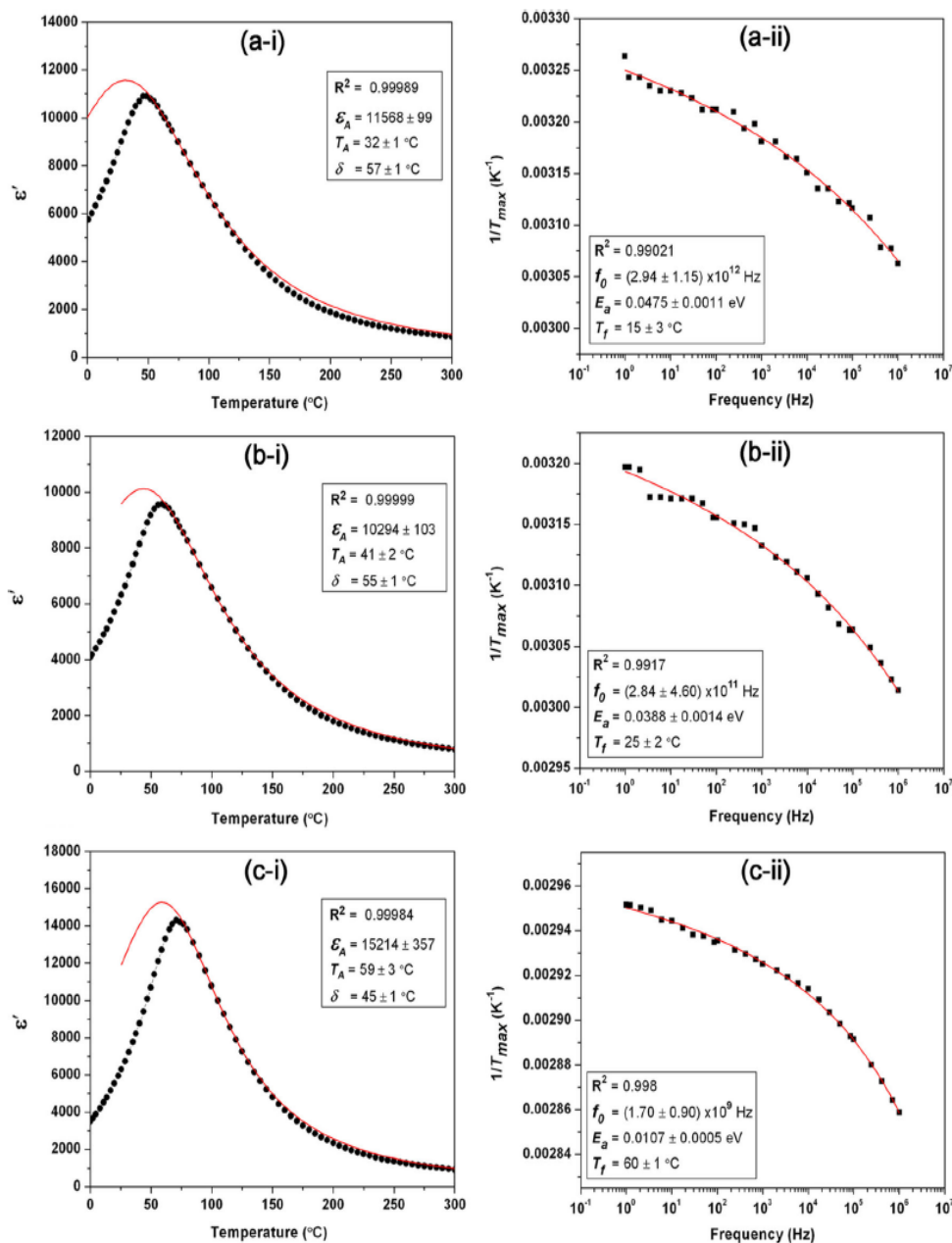


Fig. 3 (i) Quadratic fitting and (ii) Vogel-Fulcher fitting curves of (a) pure PMNT ceramic and the ceramics modified with (b) 2.0 and (c) 11.0 mol.% ZnO. The red lines are the curves plotted accordingly the obtained parameters

the diffuseness of the dielectric peak. The quadratic fitting curves of the selected compositions, $x=0$, 2.0 and 11.0 mol.%, were shown in Fig. 3(a-i), (b-i) and (c-i), respectively. It could be seen that the experimental data was fitted well to the quadratic law. The fitting parameters were listed in Table 1. It was found that the variations of the ε_A and T_A values with ZnO content had the similar trends with those of the ε'_{max} and T_{max} values, respectively. The diffuseness parameter (δ) tended to decrease with increasing ZnO content. This suggested that the degree of relaxor behavior of PMNT ceramics was attenuated by ZnO modification.

In order to study the effects of ZnO on the dynamics of dielectric relaxation in relaxors, the frequency dependence of T_{max} was fitted to the Vogel-Fulcher ($V-F$) relationship to describe the dispersion of T_{max} [8]:

$$f = f_o \exp \left[\frac{-E_a}{T_{max} - T_f} \right] \quad (2)$$

where f_o is the Debye frequency, E_a is the activation energy and T_f is the freezing temperature below which the dynamic of polar nanoregions (PNRs) is frozen. The $V-F$ fitting curves of the selected compositions, $x=0$, 2.0 and 11.0 mol.% ZnO, were shown in Fig. 3(a-ii), (b-ii) and (c-ii), respectively, and the fitting parameters were listed in Table 2. The f_o , E_a and T_f of pure PMNT ceramic were found to be 2.94×10^{12} Hz, 0.0475 eV and 15 °C, respectively, which were consistent with the previous results obtained by Viehland *et al.* [8]. The f_o and E_a tended to decrease while T_f increased with an increase in ZnO content. The increases in T_{max} , T_A and T_f and the decrease in δ were indicative of the increases in size and interaction strength of polar clusters. It was believed to be arisen from the substitution of Zn^{2+} ion for the ions located on B-site lattice of PMNT. This was consistent with previous results obtained in PZT-PMS-PZN [13], PZN-PZT [16], PNN-PFN-PZT [26], PZT-PMnN [28] and PZN-PT-BT [32] ceramics modified with ZnO. In these studies, in addition to the structural change and unit cell distortion, the observed change in

the phase transition temperature and decrease in the diffuseness parameter were also attributed to the effects of the substitution of Zn^{2+} ion for the ions located on the B-site lattice of the perovskite structure.

The temperature dependences of the dielectric properties of poled PMNT/ x ZnO samples were measured at the frequencies of 10^2 – 10^5 Hz. The results of the selected compositions, $x=0$, 0.4, 11.0 mol.%, were shown in Fig. 4(a-i), (b-i) and (c-i), respectively. At temperature range above T_{max} , the frequency dispersion of dielectric properties was observed at low frequencies, i.e. 10^2 and 10^3 Hz. This was believed to be the response of charge defects which could be moved by thermal activation [35]. The depolarization temperature (T_d), at which the field-induced polar macro domains decay abruptly upon zero-field heating, was indicated by a sharp increase in the temperature variation of the dielectric properties [9], as shown in Fig. 4(i). The transition at T_d corresponds to the transformation of the induced polar macro domains into micro-/nanodomains [26]. The T_d values were given in Table 3; T_d value of –4 °C for pure PMNT increased to 6, 11, 15 and 34 °C with the additions of 0.4, 2.0, 4.0 and 11.0 mol.% ZnO, respectively. The increase in T_d was also attributed to the effects of Zn^{2+} substitution, as described above.

3.3 Ferroelectric properties

The polarization-electric field ($P-E$) curves of PMNT/ x ZnO samples were displayed at various temperatures at the frequency of 1 Hz. The remanent polarization (P_r) read from the $P-E$ curve was plotted as a function of temperature (T). The $P_r(T)$ curves of the pure PMNT ceramic and the samples added with 2.0 and 11.0 mol.% ZnO were shown in Fig. 4(a-ii), (b-ii) and (c-ii), respectively. The polar ordering temperature (T_p) was defined as the temperature at which P_r increased suddenly upon cooling, i.e. the temperature of the maximum first derivative of the $P_r(T)$ curve. The T_p values were listed in Table 3. The T_p value of –3 °C for the pure PMNT ceramic increased to 4, 11, 16 and 28 °C with the additions of 0.4, 2.0, 4.0 and 11.0 mol.% ZnO, respectively. It could be seen that the T_p values were close to those of T_d for every sample. The $P-E$ curves of the pure PMNT ceramic and the PMNT/11.0 mol.%ZnO ceramic measured around room temperature were displayed, as shown in Fig. 5(a) and (b), respectively. The $P-E$ curve of the pure PMNT sample appeared to be slim loop with a low P_r and a small coercive field (E_c). However, the $P-E$ loop of the PMNT/11.0 mol.%ZnO sample was opened up, which revealed a characteristic of normal ferroelectric behavior [36]. The P_r and E_c values were given in Table 3. The P_r and E_c values for the pure PMNT sample were found to be 1.8 $\mu\text{C}/\text{cm}^2$ and 0.6 kV/cm, respectively. They slightly increased to 2.5 $\mu\text{C}/\text{cm}^2$ and 0.7 kV/cm, respectively, with an addition of 0.4 mol.% ZnO. The P_r value tended to increase to 3.8 $\mu\text{C}/\text{cm}^2$ with increasing ZnO content

Table 2 The $V-F$ fitting parameters of the PMNT/ x ZnO ceramics

ZnO content x (mol.%)	f_o (Hz)	E_a (eV)	T_f (°C)
0	$(2.94 \pm 1.15) \times 10^{12}$	0.0475 ± 0.0011	15 ± 3
0.4	$(2.49 \pm 1.14) \times 10^{12}$	0.0455 ± 0.0008	20 ± 2
2.0	$(2.84 \pm 4.60) \times 10^{11}$	0.0388 ± 0.0014	25 ± 2
4.0	$(1.02 \pm 1.31) \times 10^{10}$	0.0222 ± 0.0011	41 ± 2
11.0	$(1.70 \pm 0.90) \times 10^9$	0.0107 ± 0.0005	60 ± 1

f_o and E_a represent the Debye frequency and the activation energy, respectively. T_f represents the freezing temperature below which the dynamic of polar nanoregions (PNRs) is frozen

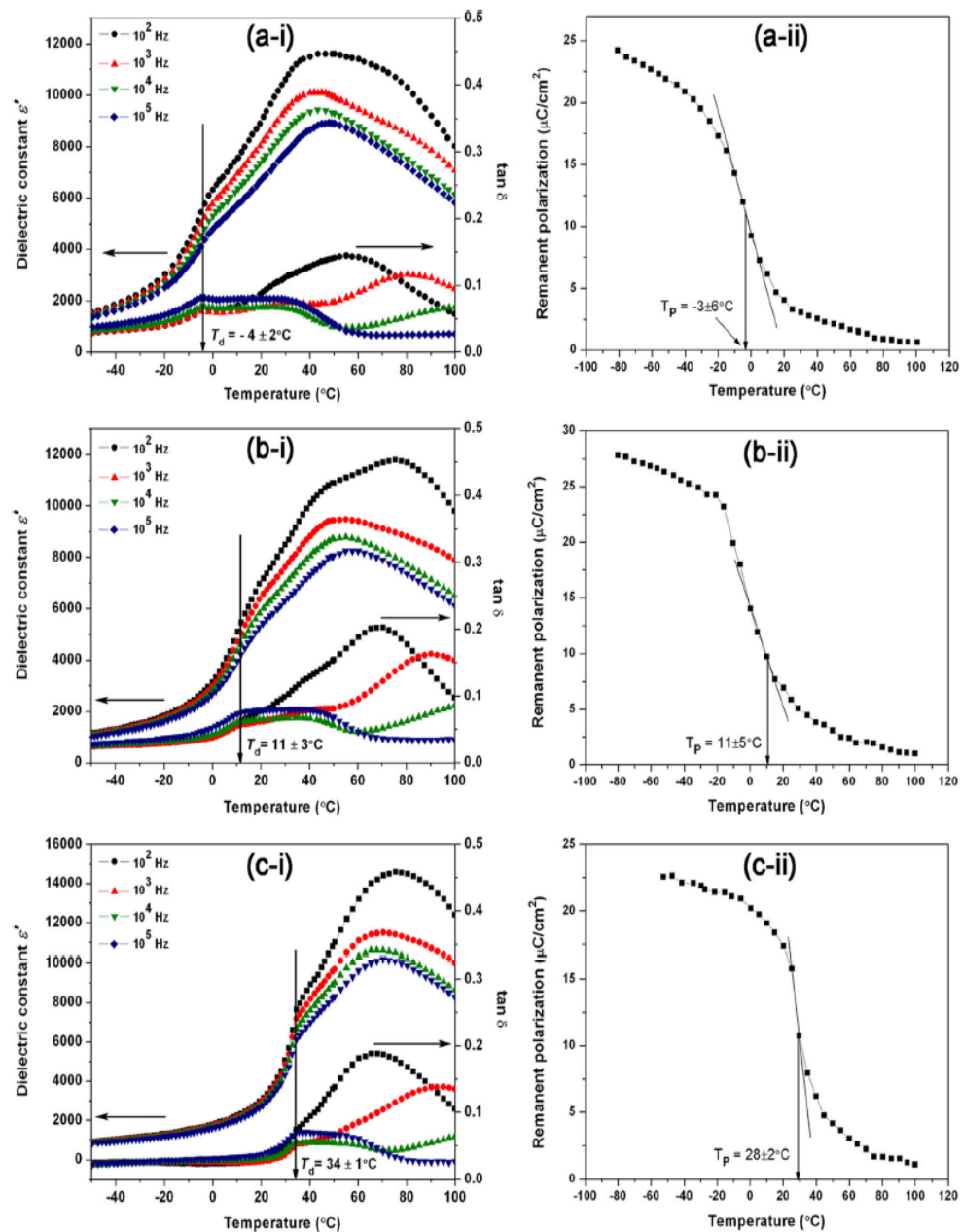


Fig. 4 Temperature dependences of (i) dielectric properties and (ii) remanent polarization of (a) pure PMNT ceramic and the ceramics modified with (b) 2.0 and (c) 11.0 mol.% ZnO

to 4.0 mol.% ZnO, while the E_c value did not significantly change. The P_r and E_c values remarkably increased to $17.6 \mu\text{C}/\text{cm}^2$ and $2.0 \text{ kV}/\text{cm}$, respectively, with further increasing ZnO content to 11.0 mol.%. The increases in P_r and E_c were attributed to the increase in the ferroelectric order, which was believed to be resulted from the effects of the substitution of the Zn^{2+} ion for the Mg^{2+} ion on the B-site lattice of PMNT. Compared with Mg^{2+} ion, the Zn^{2+} ion possesses a $3d^{10}$ electronic configuration, which favours covalent bonding with the $2p^6$ electrons of oxygen ion when it occupies the

octahedral site of perovskite structure. This makes the Zn^{2+} ion more ferroelectrically active than the Mg^{2+} ion. This can be attested by the fact that $\text{Pb}(\text{Zn}_{1/3}\text{Nb}_{2/3})\text{O}_3$ (PZN) based solid solution with PT (PZN-PT) exhibits a higher degree of ferroelectric ordering and a lower degree of relaxor behavior than PMN-PT solid solution system at a relatively low PT concentration [37, 38]. The chemical analysis by energy dispersive X-ray spectroscopy (EDX) showed that Zn^{2+} was presented in the grains of the PMNT/ $x\text{ZnO}$ ceramics (the EDS result is not shown here). It was believed that the ionic

Table 3 Depolarization temperature, polar-ordering temperature, ferroelectric and electrostrictive properties of the PMNT/*x*ZnO ceramics

ZnO content <i>x</i> (mol.%)	T_d (°C)	T_P (°C)	P_r (μC/cm ²)	E_c (kV/cm)	Strain (%)	M ($\times 10^{-16}$ m ² /V ²)
0	-4±2	-3±6	1.8	0.6	0.06	7.29±0.03
0.4	6±2	4±3	2.5	0.7	0.08	10.93±0.11
2.0	11±3	11±5	3.3	0.7	0.10	19.62±0.26
4.0	15±6	16±10	3.8	0.7	0.10	22.22±0.48
11.0	34±1	28±2	17.6	2.0	0.08	-

T_d and T_P represent the depolarization temperature and the polar ordering temperature, respectively. P_r and E_c represent a remanent polarization and a coercive field, respectively. M stands for electrostrictive coefficient. Ferroelectric and electrostrictive properties were measured at a frequency of 1 Hz

substitution could contribute to the formation of (PZN-PT)-type solid solution which had a higher degree of ferroelectric order and a lower degree of relaxor behavior [39, 40].

3.4 Electrostrictive properties

The strain-electric field (*S-E*) curves measured at room temperature at 1 Hz of the pure PMNT ceramic and the ceramic modified with 11.0 mol.% ZnO were shown in Fig. 5(a) and (b), respectively. The *S-E* curve of the pure PMNT ceramic showed a parabolic-like shape which was a characteristic of electrostrictive response [36]. However, a butterfly-like curve, typical of piezoelectric response [41], was observed in the PMNT/11.0 mol.%ZnO sample. From the *S-E* curves, the maximum induced strain and the electrostrictive coefficient (M) determined from the slope of the linear $S-E^2$ curve as shown in Fig. 6, were given in Table 3. The maximum strain and M values for the pure PMNT ceramic were found to be 0.06 % and 7.29×10^{-16} m²/V², respectively. They slightly increased to 0.08 % and 10.93×10^{-16} m²/V², respectively, with an addition of 0.4 mol.% ZnO and tended to increase to 0.10 % and 19.62×10^{-16} m²/V², respectively, when the ZnO content was increased to 2.0 mol.%. The coefficient M increased to 22.22×10^{-16} m²/V² with further increasing ZnO content to 4.0 mol.%, while the strain level remained the same.

The enhancement in the electrostrictive properties was attributed to the increase in the size of polar clusters, which was consistent with previous results obtained by Wang et al. [10] and Hao et al. [11]. From the slope of the strain-unipolar electric field curve of the PMNT/11.0 mol.%ZnO ceramic (the result is not shown here), the piezoelectric coefficient (d_{33}) of the ceramic could be determined and was found to be 310 pm/V. Together with the dielectric, ferroelectric and electrostrictive properties, it could be concluded that the ferroelectric ordering of PMNT ceramics was enhanced while the degree of relaxor behavior was attenuated with ZnO modification. Moreover, the characteristics of normal ferroelectrics, i.e. the ferroelectric *P-E* hysteresis loop and the butterfly-like *S-E* curve, were observed around room temperature in the PMNT/11.0 mol.%ZnO ceramic.

4 Conclusions

ZnO-modified Pb (Mg_{1/3}Nb_{2/3})_{0.9}Ti_{0.1}O₃ (PMNT) ceramics were prepared by solid state reaction and sintering process. Lattice parameter *a* and unit cell volume of pure PMNT ceramic were increased by ZnO modification. The characteristic temperatures T_{max} , T_A , T_f , T_d and T_P tended to increase

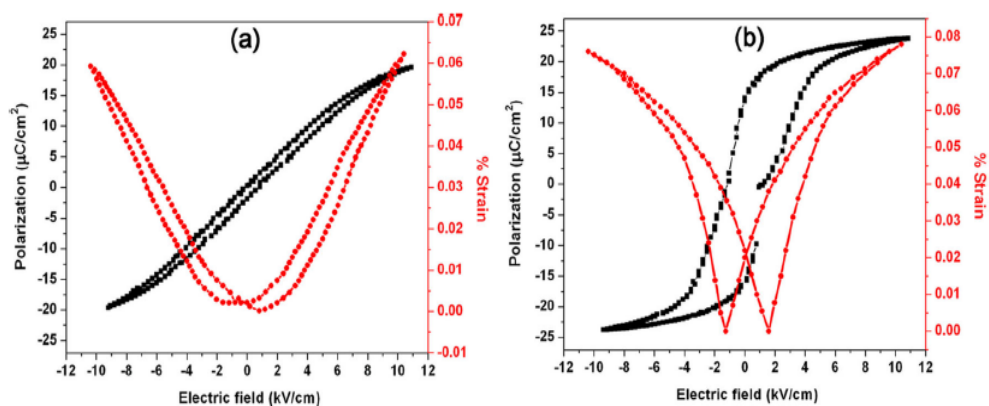


Fig. 5 *P-E* (black line) and *S-E* (red line) curves measured at room temperature at a frequency of 1 Hz of (a) pure PMNT ceramic and (b) the ceramic modified with 11.0 mol.% ZnO

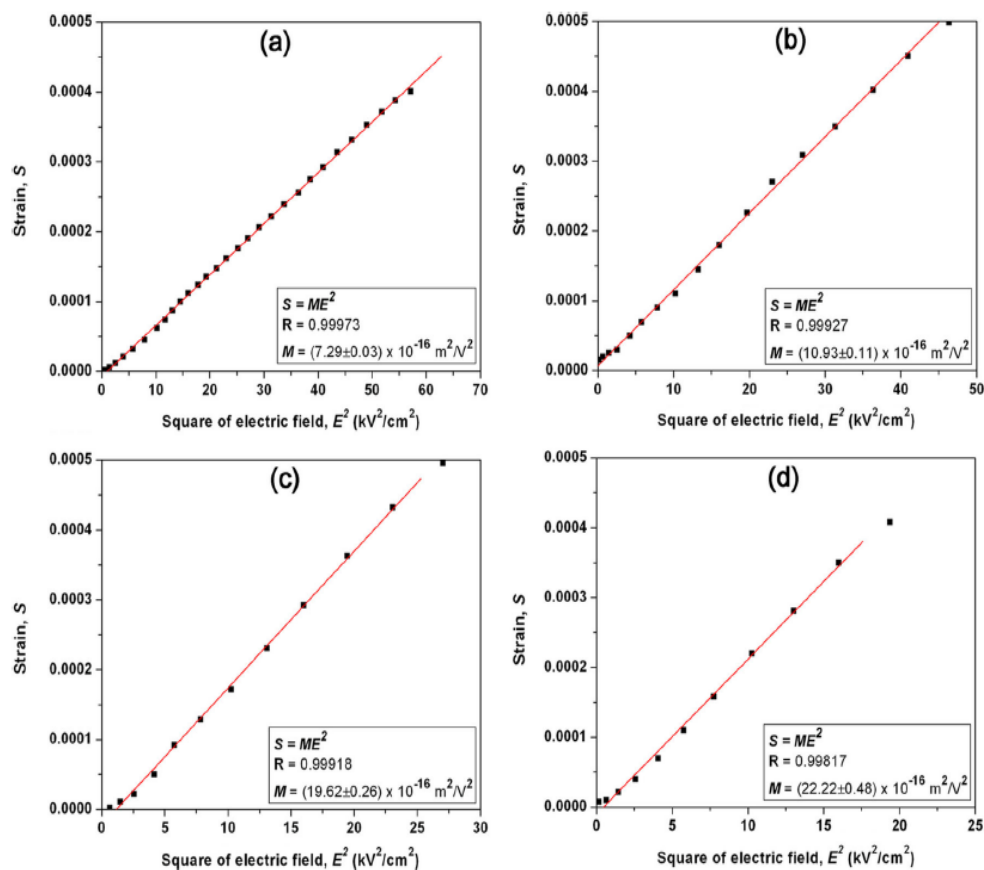


Fig. 6 Plots of strain (S) as a function of square of electric field (E^2) of (a) pure PMNT ceramic and the ceramics modified with (b) 0.4, (c) 2.0 and (d) 4.0 mol.% ZnO. The slope of a linear fitting line (a red line) is equal to an electrostrictive coefficient (M)

with increasing ZnO content while the diffuseness of the dielectric peak δ decreased. These were indicative of the enhancement of ferroelectric order and the decrease in the degree of relaxor behavior of the PMNT ceramics by ZnO modification. The improvements in ferroelectric and electrostrictive properties, e.g. the increases in a remanent polarization, a maximum induced strain and an electrostrictive coefficient, were observed as ZnO was incorporated into PMNT ceramics. The polar macro domains were established around room temperature, as the observed characteristics of normal ferroelectrics, i.e. a P - E hysteresis loop and a butterfly-like S - E curve, with an addition of 11.0 mol.% ZnO. The PMNT ceramic modified with 4.0 mol.% ZnO showed the high values of an electric field induced strain and an electrostrictive coefficient (0.10 % and $22.22 \times 10^{-16} \text{ m}^2/\text{V}^2$, respectively), which made it a promising material for applications as electrostrictive actuators in various technological applications.

Acknowledgments This work was supported by the Thailand Research Fund (TRF) and the National Research University Project under Thailand's Office of the Higher Education Commission (OHEC), the Faculty of Science and the Graduate School, Chiang Mai University. M.P. would also like to thank the financial support from the TRF through

the Royal Golden Jubilee Ph.D. Program. The work at Simon Fraser University was supported by the U.S. Office of Naval Research (Grants #N00014-11-1-0552 and #N00014-12-1-1045) and the Natural Science and Engineering Research Council of Canada (NSERC).

References

1. K. Babooram, H. Tailor, Z.-G. Ye, *Ceram. Int.* **30**, 1411 (2004)
2. A.S. Mischenko, Q. Zhang, R.W. Whatmore, J.F. Scott, N.D. Mathur, *Appl. Phys. Lett.* **89**, 242912 (2006)
3. X. Wen, C. Feng, L. Chen, S. Huang, *Ceram. Int.* **33**, 815 (2007)
4. J.D.L.S. Guerra, M.H. Lente, J.A. Eiras, *J. Eur. Ceram. Soc.* **27**, 4033 (2007)
5. R. Wongmaneeung, R. Yimnirun, S. Ananta, *Curr. Appl. Phys.* **9**, 268 (2009)
6. A.A. Bokov, Z.-G. Ye, *Appl. Phys. Lett.* **77**, 1888 (2000)
7. A.A. Bokov, Z.-G. Ye, *Phys. Rev. B* **66**, 064103 (2002)
8. D. Viehland, S.J. Jang, L.E. Cross, M. Wuttig, *J. Appl. Phys.* **68**, 2916 (1990)
9. Z.-G. Ye, H. Schmid, *Ferroelectrics* **145**, 83 (1993)
10. F. Wang, C. Jin, Q. Yao, W. Shi, *J. Appl. Phys.* **114**, 027004 (2013)
11. J. Hao, W. Bai, W. Li, B. Shen, J. Zhai, *J. Appl. Phys.* **114**, 044103 (2013)
12. O. Bidault, M. Licheron, E. Husson, G. Calvarin, A. Morell, *Solid State Commun.* **98**, 765 (1996)
13. H. Li, Z. Yang, L. Wei, Y. Chang, *Mat. Res. Bull.* **44**, 638 (2009)

14. H.-T. Li, B.-P. Zhang, M. Cui, W.-G. Yang, N. Ma, J.-F. Curr, Appl. Phys. **11**, 184 (2011)
15. J.-Y. Ha, J.-W. Choi, C.-Y. Kang, D.J. Choi, H.-J. Kim, S.-J. Mater, Chem. Phys. **90**, 396 (2005)
16. X. Zeng, A. Ding, X.-S. Zheng, T. Liu, Ceram. Int. **33**, 883 (2007)
17. Y.-C. Lee, T.-K. Lee, J.-H. Jan, J. Eur. Ceram. Soc. **31**, 3145 (2011)
18. K. Kumari, A. Prasad, K. Prasad, J. Mater. Sci. Technol. **27**, 213 (2011)
19. C.-C. Tsai, S.-Y. Chu, C.-S. Hong, S.-F. Chen, J. Eur. Ceram. Soc. **31**, 2013 (2011)
20. I.-Y. Kang, I.-T. Seo, Y.-J. Cha, J.-H. Choi, S. Nahm, T.-H. Sung, J.-H. Paik, J. Eur. Ceram. Soc. **32**, 2381 (2012)
21. H. Cheng, W. Zhou, H. Du, F. Luo, D. Zhu, D. Jiang, B. Xu, J. Alloys Compd. **579**, 192 (2013)
22. S.L. Swartz, T.R. Shrout, Mater. Res. Bull. **17**, 1245 (1982)
23. A.A. Bokov, Y.H. Bing, W. Chen, Z.-G. Ye, S.A. Bogatina, I.P. Raevski, S.I. Raevskaya, E.V. Sahkar, Phys. Rev. B **68**, 1 (2003)
24. J.C. Bruno, A.A. Cavaleiro, M.A. Zaghet, M. Cilense, J.A. Varela, Mater. Chem. Phys. **84**, 120 (2004)
25. R. D. Shannon, Acta Crystallogr., **751** (1976)
26. G. Du, R. Liang, J. Wang, L. Wang, W. Zhang, G. Wang, X. Dong, Ceram. Int. **39**, 9299 (2013)
27. K. Harada, S. Shimanuki, T. Kobayashi, Y. Yamashita, S. Saitoh, J. Am. Ceram. Soc. **85**, 145 (2002)
28. C.-C. Tsai, C.-S. Hong, C.-C. Shih, S.-Y. Chu, J. Alloys Compd. **511**, 54 (2012)
29. X. Chao, Z. Yang, X. Huang, D. Ma, J. Zeng, Curr. Appl. Phys. **9**, 1283 (2009)
30. Y. Yuan, E. Li, B. Tang, L. Bo, X. Zhou, J. Mater. Sci. Mater. Electron. **23**, 309 (2012)
31. R. Wongmaneeerung, S. Choopan, R. Yimnirun, S. Ananta, J. Alloys Compd. **509**, 3547 (2011)
32. M. Bonyani, A. Mirzaee, A. Barzegar, M.-R. Saeni, Micro Nano Lett. **7**, 762 (2012)
33. X.-G. Tang, H.L.-W. Chan, J. Appl. Phys. **97**, 034109 (2005)
34. M. Promsawat, A. Watcharapasorn, H.N. Taylor, S. Jiansirisomboon, Z.-G. Ye, J. Appl. Phys. **113**, 204101 (2013)
35. S.B. Majumder, D.C. Agrawal, Y.N. Mohapatra, R.S. Katiyar, Integr. Ferroelectr. **29**, 63 (2000)
36. A. Hall, M. Allahverdi, E.K. Akdogan, A. Safari, J. Electroceram. **15**, 143 (2005)
37. D. La-Orauttapong, B. Noheda, Z.-G. Ye, P.M. Gehring, J. Toulouse, D.E. Cox, G. Shirane, Phys. Rev. B **65**, 144101 (2002)
38. A.A. Bokov, Z.-G. Ye, J. Mater. Sci. **41**, 31 (2006)
39. B. Noheda, D.E. Cox, G. Shirane, J. Gao, Z.-G. Ye, Phys. Rev. B **66**, 054104 (2002)
40. S. Kamba, E. Buixaderas, J. Petzelt, J. Fousek, J. Nosek, P. Bridenbaugh, J. Appl. Phys. **93**, 933 (2003)
41. G.H. Haertling, J. Am. Ceram. Soc. **82**, 797 (1999)

Effects of Dy Substitution for Bi on Phase, Microstructure and Dielectric Properties of Layer-structured $\text{Bi}_{4-x}\text{Dy}_x\text{Ti}_3\text{O}_{12}$ Ceramics

NAVAVAN THONGMEE,^{1,*} ANUCHA WATCHARAPASORN,^{2,3}
AND SUKANDA JIANSIRISOMBOON^{2,3}

¹Program of Physics, Faculty of Science and Technology, Pibulsongkram
Rajabhat University, Phitsanulok, 65000, Thailand

²Department of Physics and Materials Science, Faculty of Science, Chiang Mai
University, Chiang Mai 50200, Thailand

³Materials Science Research Center, Faculty of Science, Chiang Mai University,
Chiang Mai 50200, Thailand

$\text{Bi}_{4-x}\text{Dy}_x\text{Ti}_3\text{O}_{12}$ (when $x = 0, 0.25, 0.5, 0.75$ and 1.0) powders and ceramics were prepared by solid-state mixed oxide method. The calcination was carried out at 900°C for 4 h with heating/cooling rate $5^\circ\text{C}/\text{min}$. The ceramics were then sintered at a temperature between $950\text{--}1100^\circ\text{C}$ for 4 hrs. The optimum sintering temperature was found to be 1000°C . X-ray diffraction indicated the existence of orthorhombic phase for all sintering temperatures. Scanning electron micrographs of ceramic surfaces showed a plate-like structure with different grain size. The results of room temperature dielectric constant revealed that Dy dopant could dielectric constant of $\text{Bi}_4\text{Ti}_3\text{O}_{12}$ ceramic where it was optimized at $x = 0.25$.

Keywords Solid-state mixed oxide; calcination; sintering; dielectric properties

Introduction

Ferroelectric materials have attracted considerable attention because of their possible uses in device applications such as sensors, micro-electromechanical system, nonvolatile random access memories, etc. [1]. Bismuth layer-structured ferroelectric (BLSF) materials have attracted great interest in the last few years because of their lead-free compositions with excellent piezoelectricity and ferroelectricity [2, 3]. The crystal structure of BLSFs consists of the interleaved bismuth oxide (Bi_2O_2)²⁺ layers and pseudo-perovskite blocks containing BO_6 octahedra. The BLSF chemical formula is generally expressed as $(\text{Bi}_2\text{O}_2)^{2+}(\text{A}_{m-1}\text{B}_m\text{O}_{3m+1})^{2-}$ where A represents a mono-, bi- or tri-valent ion, B denotes a tetra-, penta- or hexa-valent ion, m is the number of BO_6 octahedra in each pseudo-perovskite block ($m = 1, 2, 3, \dots$) [4]. Among BLSFs, bismuth titanate ($\text{Bi}_4\text{Ti}_3\text{O}_{12}$: BIT) has attracted much attention for potential utilization due to its large spontaneous polarization (P_s), low processing temperature, high Curie temperature (675°C) and high fatigue endurance [5]. This material has domain pinning due to defects such as Bi vacancies accompanied

Received December 11, 2012; in final form March 15, 2013.

*Corresponding author. E-mail: navavan_new@hotmail.com

[1254]/76

by oxygen vacancies. It is well known that oxygen-vacancy migration in BIT produces significant degradation problems associated with the dielectric and ferroelectric properties such as low dielectric constant (ϵ_r), high leakage current low remanent polarization (P_r) and high coercive field (E_c) [6, 7]. In order to minimize these defects, Bi-site substitution by replacement of the volatile Bi ion with less volatile ions is required. Recent studies revealed that substitution of Bi^{3+} ions in BIT structure using trivalent lanthanide ions, e.g. La [8], Sm [9], Nd [10] or Pr [11] have been explored for the improvement of dielectric and ferroelectric properties of BIT. However, fundamental study on phase formation, structure and properties of Dy-doped BIT powder and ceramic system has not yet been fully investigated.

Therefore, in this present study $\text{Bi}_{4-x}\text{Dy}_x\text{Ti}_3\text{O}_{12}$ with $x = 0, 0.25, 0.50, 0.75$ and 1.0 powders were prepared by a solid state mixed-oxide method and characterized in terms of densification, phase formation, dielectric properties and ferroelectric properties. The optimum composition of $\text{Bi}_{4-x}\text{Dy}_x\text{Ti}_3\text{O}_{12}$ (BDT) ceramic will also be reported and discussed in detail. It is expected that this research will bring more understanding and give useful information on these ceramics which can be further employed in actual applications; particularly in multi-functional device such as sensors and actuators.

Experimental Procedure

$\text{Bi}_{4-x}\text{Dy}_x\text{Ti}_3\text{O}_{12}$ (BDT) powders (when $x = 0, 0.25, 0.50, 0.75$ and 1.0) were prepared using the solid state mixed-oxide method. The starting chemical used were Bi_2O_3 (98%, Fluka), Dy_2O_3 (99%, Cerac) and TiO_2 (99%, Riedel-de Haën). The powders were weighted in stoichiometric ratios, mixed and ball-milled for 24 hrs and dried. The mixed powders were calcined at various temperatures between $500\text{--}900^\circ\text{C}$ for 4 hrs with a heating/cooling rate of $5^\circ\text{C}/\text{min}$. The calcined BDT powders were pressed into pellets to form disc-shape pellets 10 mm in diameter and 1 mm thickness with 3 wt% PVA (polyvinyl alcohol) added as a binder. The pellets were covered with their own powders and sintered at temperatures ranging from 950 to 1150°C for 4 hrs. with a heating/cooling rate $5^\circ\text{C}/\text{min}$. The firing profile also included 1 hr dwell time at 500°C for binder burn-out.

Phase analysis of mixed powders and sintered ceramics were carried out using an X-ray diffractometer (XRD, Phillips Model X-pert). Densities of the ceramics were measured by Archimedes' method. The samples were polished and thermally etched at 1050°C for 10 min prior to microstructural investigation using a scanning electron microscope (SEM, JEOL JSM-6335F). For electrical property characterization, the sintered samples were lapped to obtain parallel faces, which were subsequently coated with silver paint as electrodes. The dielectric properties were studied with an automated dielectric measurement system, LCZ-meter (Hewlett-Packard 4194A). The capacitance and the dielectric loss tangent were determined at room temperature at a frequency of 1 kHz. The dielectric constant was then calculated from $\epsilon_r = Cd/\epsilon_0 A$, where C is the capacitance of the sample, d and A are the thickness and the area of the electrode, respectively, and ϵ_0 is the dielectric permittivity of vacuum (8.854×10^{-12} F/m).

Results and Discussion

X-ray diffraction patterns of calcined $\text{Bi}_{4-x}\text{Dy}_x\text{Ti}_3\text{O}_{12}$ powders at 600°C are shown in Fig. 1. The patterns for all samples with different concentrations of Dy_2O_3 dopant were matched with ICSD file number 87810 of $\text{Bi}_4\text{Ti}_3\text{O}_{12}$ (BIT) database. The patterns showed that powders were identified as a single-phase material having an orthorhombic structure

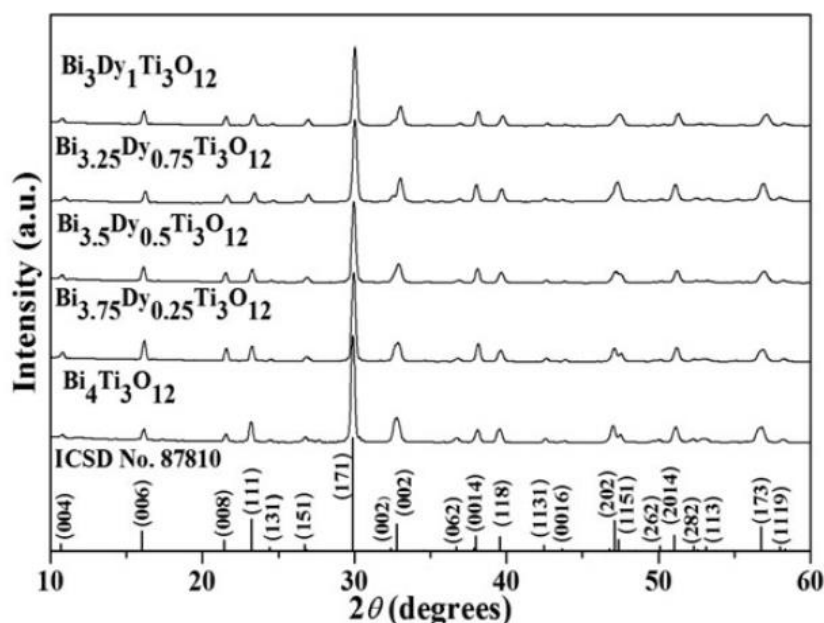


Figure 1. X-ray diffraction patterns of $\text{Bi}_{4-x}\text{Dy}_x\text{Ti}_3\text{O}_{12}$ calcined powders for $x = 0, 0.25, 0.5, 0.75$ and 1.0 .

without a detectable second phase. Diffraction data did not show any evidence of Dy_2O_3 or associated compounds that contained bismuth or titanium. Therefore, the fabricated powders were expected to maintain the layered structure similar to the bismuth layer structure of BIT even under extensive modifications by Dy^{3+} . However, as the amount of Dy increased, the X-ray diffraction patterns shift to higher 2θ angles, indicating a decrease in the lattice parameters in the crystal structure. The distortion of unit cell could be partly due to a substitution of Dy^{3+} into Bi^{3+} position. Based on the ionic radius of Dy^{3+} ($r_{\text{Dy}^{3+}} = 0.912 \text{ \AA}$)

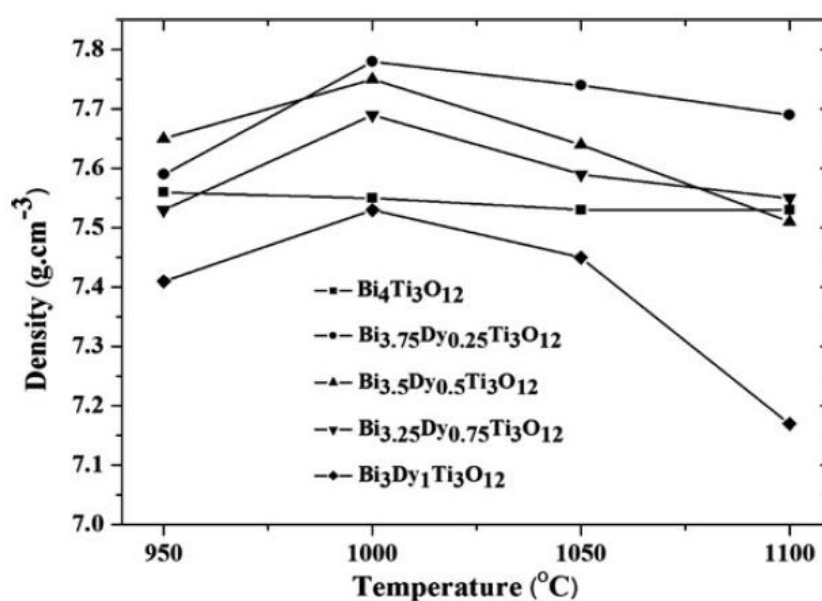


Figure 2. Density of $\text{Bi}_{4-x}\text{Dy}_x\text{Ti}_3\text{O}_{12}$ ceramics sintered at several different temperatures.

Table 1
Physical and dielectric properties of $\text{Bi}_{4-x}\text{Dy}_x\text{Ti}_3\text{O}_{12}$ ceramics

Materials	Density (g/cm^3)	Grain size (μm)		Dielectric properties*	
		Diameter (ϕ)	Thickness (t)	ϵ_r	$\tan \delta$
$\text{Bi}_4\text{Ti}_3\text{O}_{12}$	7.55 ± 0.02	1.88 ± 0.63	0.44 ± 0.09	110	0.0036
$\text{Bi}_{3.75}\text{Dy}_{0.25}\text{Ti}_3\text{O}_{12}$	7.78 ± 0.01	3.33 ± 0.99	0.87 ± 0.22	137	0.0038
$\text{Bi}_{3.5}\text{Dy}_{0.5}\text{Ti}_3\text{O}_{12}$	7.75 ± 0.01	3.16 ± 0.92	0.77 ± 0.18	123	0.0042
$\text{Bi}_{3.25}\text{Dy}_{0.75}\text{Ti}_3\text{O}_{12}$	7.69 ± 0.01	3.03 ± 1.05	0.86 ± 0.22	125	0.0034
$\text{Bi}_3\text{Dy}_1\text{Ti}_3\text{O}_{12}$	7.53 ± 0.01	3.33 ± 1.09	0.81 ± 0.19	130	0.0037

*Dielectric properties of 10 kHz at room temperature.

and Bi^{3+} ions ($r_{\text{Bi}^{3+}} = 1.03 \text{ \AA}$) [12], this ionic size difference appears to dominate this cell distortion.

Densification behavior of $\text{Bi}_{4-x}\text{Dy}_x\text{Ti}_3\text{O}_{12}$ ceramics sintered at temperature ranging from 950–1150°C are shown in Fig. 2. Variation of density for each composition of $\text{Bi}_{4-x}\text{Dy}_x\text{Ti}_3\text{O}_{12}$ for $x = 0, 0.25, 0.5, 0.75$ and 1.0 different sintering temperatures indicates similar tendencies. The results for that the optimum sintering temperature to be 1000°C indicate for maximum sample densification (Table 1). Therefore, the samples sintered at this temperature were selected for further characterization. Moreover, in $\text{Bi}_{4-x}\text{Dy}_x\text{Ti}_3\text{O}_{12}$ increasing Dy content consistently decreased the densification of the ceramics. The highest density of $\text{Bi}_{4-x}\text{Dy}_x\text{Ti}_3\text{O}_{12}$ was achieved at $x = 0.25$ ceramic (7.78 g/cm^3). Figure 3 shows XRD patterns of $\text{Bi}_{4-x}\text{Dy}_x\text{Ti}_3\text{O}_{12}$ ceramics sintered at 1000°C for 4 h. The pattern of all ceramics indicates single phase orthorhombic structures nearly identical to their powders but with sharper peaks indicative of larger crystallite size.

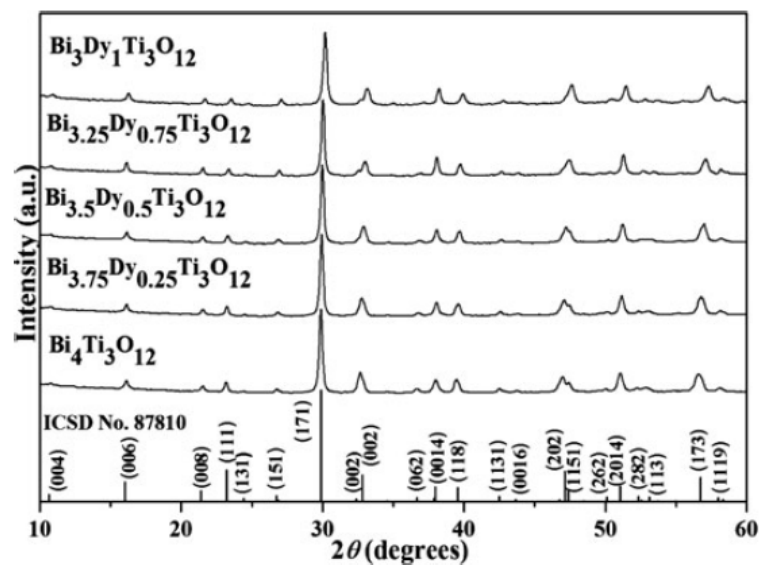


Figure 3. X-ray diffraction patterns of $\text{Bi}_{4-x}\text{Dy}_x\text{Ti}_3\text{O}_{12}$ ceramics sintered at 1000°C.

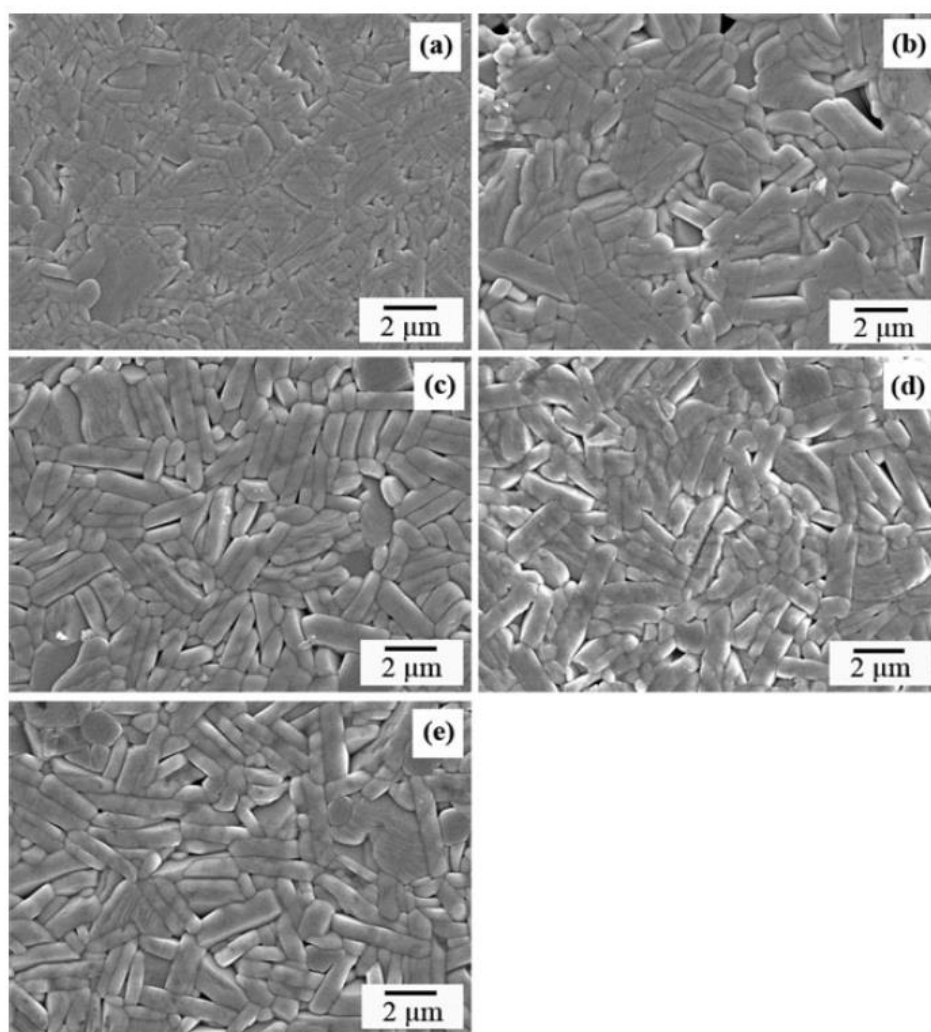


Figure 4. SEM micrographs of $\text{Bi}_{4-x}\text{Dy}_x\text{Ti}_3\text{O}_{12}$ ceramics; (a)–(e) for $x = 0, 0.25, 0.50, 0.75$ and 1.0 , respectively.

Typical surface morphology of polished and thermally etched surfaces of $\text{Bi}_{4-x}\text{Dy}_x\text{Ti}_3\text{O}_{12}$ ceramics are shown in Fig. 4. All compositions show plate-like morphology with different grain size and orientation. The grain sizes of all ceramic samples were measured in terms of diameter and thickness as listed in Table 1. With increasing addition of Dy^{3+} the grain diameter and thickness of the crystallites increase. The size of plate-like grains increases from 0.437 to $0.87 \mu\text{m}$ in diameter and from 1.88 to $3.33 \mu\text{m}$ in thickness. Dy_2O_3 appears to play an important role in increasing surface anisotropies through an increase in grain boundary energies and mobilities as suggested by Horn and Messing [13].

Dielectric properties of $\text{Bi}_{4-x}\text{Dy}_x\text{Ti}_3\text{O}_{12}$ ceramics sintered at 1000°C were investigated. The room temperature dielectric constant (ϵ_r) and dielectric loss tangent ($\tan\delta$) were measured at frequency of 10 kHz with values reported in Table 1. It is experimentally observed that an increase of Dy^{3+} substitutional content consistently increases the dielectric constant of the ceramic. The maximum of dielectric constant was found in $\text{Bi}_{3.75}\text{Dy}_{0.25}\text{Ti}_3\text{O}_{12}$ ceramic ($\epsilon_r = 137$). The dielectric constant appears to be dependent upon grain size and density. Namely, increasing Dy substitution for Bi content causes the grain size of $\text{Bi}_{4-x}\text{Dy}_x\text{Ti}_3\text{O}_{12}$ ceramics to increase gradually. It is generally accepted that for such conditions space

charges decrease which result in the enhanced dielectric constant. Moreover, the higher density of $\text{Bi}_{4-x}\text{Dy}_x\text{Ti}_3\text{O}_{12}$ yields higher dielectric constant ceramics.

Conclusions

$\text{Bi}_{4-x}\text{Dy}_x\text{Ti}_3\text{O}_{12}$ or BDT (where $x = 0, 0.25, 0.50, 0.75$ and 1.0) ceramics were successfully prepared using the solid-state mixed oxide method. The optimum sintering temperature for $\text{Bi}_{4-x}\text{Dy}_x\text{Ti}_3\text{O}_{12}$ (BDT) ceramic was found to be 1000°C for 4 hrs with a heating/cooling rate $5^\circ\text{C}/\text{min}$ for highest sample densification. All prepared ceramics were identified by X-ray diffraction method as single-phase with orthorhombic structure. The pattern peaks in the diffraction shift to higher angles of 2θ with increasing Dy^{3+} substitution for Bi^{3+} and indicates in a decreasing lattice parameter which is consistent of the smaller ionic radii of Dy^{3+} as compared with Bi^{3+} . Microstructure of ceramics show plate-like grains with grain size increasing with increasing substitution of Dy^{3+} for Bi^{3+} . Dielectric properties of ceramics in terms of dielectric constant and dielectric loss were investigated. The results indicate that an increase of substitution of Dy^{3+} for Bi^{3+} causes the dielectric constant of ceramic to increase. An increase in grain size leading to space charge decrease is believed to be responsible for the increased dielectric constant of ceramic. This study clearly indicates a correlation between the crystal structure, microstructure and dielectric properties of $\text{Bi}_{4-x}\text{Dy}_x\text{Ti}_3\text{O}_{12}$ (BDT) ceramics.

Acknowledgments

This work is financially supported by the Thailand Research Fund (TRF) and the National Research University Project under Thailand's Office of the Higher Education Commission (OHEC), and Faculty of Science and Technology, Pibulsongkram Rajabhat University.

References

1. G. H. Haertling, Ferroelectric ceramics: history and technology. *J Am Ceram Soc.* **82**, 797–818 (1999).
2. S. D. Bu, B. S. Kang, B. H. Park, and T. W. Noh, Composition dependence of the ferroelectric properties of lanthanum-modified bismuth titanate thin films grown by using pulsed-laser deposition. *J Korean Phys Soc.* **36**, L9–L12 (2000).
3. J. S. Kim, S. S. Kim, and T. K. Song, Ferroelectric properties of bismuth lanthanum titanate (BLT) thin films processed at low temperature. *J. Korean Phys. Soc.* **43**, 548–552 (2003).
4. H. Irie, M. Miyayama, and T. Kudo, Structure dependence of ferroelectric properties of bismuth layer-structured ferroelectric single crystals. *J. Appl. Phys.* **90** (8), 4089–4094 (2001).
5. S. E. Cummins, and L. E. Cross, Electrical and optical properties of ferroelectric $\text{Bi}_4\text{Ti}_3\text{O}_{12}$ single crystals. *J. Appl. Phys.* **9**, 2268–2274 (1968).
6. Y. Y. Yao, C. H. Song, P. Bao, D. Su, X. M. Lu, J. S. Zhu, and Y. N. Wang, Doping effect on the dielectric property in bismuth titanate. *J. Appl. Phys.* **95** (6), 3126–3130 (2004).
7. Y. Noguchi, and M. Miyayama, Large remanent polarization of vanadium-doped $\text{Bi}_4\text{Ti}_3\text{O}_{12}$. *Appl. Phys. Lett.* **78**, 1903–1905 (2001).
8. B. H. Park, B. S. Kang, S. D. Bu, T. W. Noh, J. Lee, and W. Jo, Lanthanum-substituted bismuth titanate for use in non-volatile memories. *Nature.* **401**, 682–684 (1999).
9. U. Chon, K. B. Kim, H. M. Jang, and G. C. Yi, Fatigue-free samarium-modified bismuth titanate ($\text{Bi}_{4-x}\text{Sm}_x\text{Ti}_3\text{O}_{12}$) film capacitors having large spontaneous polarizations. *Appl. Phys. Lett.* **79**, 3137–3140 (2001).
10. R. E. Melgarejo, M. S. Tomar, S. Bhaskar, P. S. Dobal, and R. S. Katiyar, Large ferroelectric response in $\text{Bi}_{4-x}\text{Nd}_x\text{Ti}_3\text{O}_{12}$ films prepared by sol-gel process. *Appl. Phys. Lett.* **81**, 2611–2614.

11. U. Chon, J. S. Shim, and H. M. Jang, Ferroelectric properties and crystal structure of praseodymium-modified bismuth titanate. *J. Appl. Phys.* **93**, 4769–4775 (2003).
12. R. D. Shannon, Revised effective ionic radii and systematic studies of interatomic distances in halides and chalcogenides. *Acta Crystallogr A*. **32**, 751–767 (1976).
13. D. S. Horn, and G. L. Messing, Anisotropic grain growth in TiO₂-doped alumina. *Mater. Sci. Eng. A*. **195**, 196–205 (1995).

Compositional Range and Electrical Properties of Lead-Free $\text{Bi}_{0.5}(\text{Na}_{0.8}\text{K}_{0.2})_{0.5}\text{TiO}_3$ -($\text{Ba}_{0.98}\text{Nd}_{0.02}$) TiO_3 System

P. JAITA,¹ A. WATCHARAPASORN,^{1,2}
AND S. JIANSIRISOMBOON^{1,2,*}

¹Department of Physics and Materials Science, Faculty of Science, Chiang Mai University, Chiang Mai 50200, Thailand

²Materials Science Research Center, Faculty of Science, Chiang Mai University, Chiang Mai 50200, Thailand

Lead-free piezoelectric ceramics $(1-x)\text{Bi}_{0.5}(\text{Na}_{0.8}\text{K}_{0.2})_{0.5}\text{TiO}_3$ - $x(\text{Ba}_{0.98}\text{Nd}_{0.02})\text{TiO}_3$ or $(1-x)\text{BNKT}$ - $x\text{BNdT}$ ($x = 0.05$ – 0.15 mol fraction) were synthesized by conventional mixed-oxide method. All samples had relative densities more than 98% of theoretical values. All compositions had pure perovskite structure and BNdT effectively diffused into BNKT lattice during sintering to form solid solutions. Grain size and shape were slightly affected by BNdT addition. The addition of BNdT into BNKT was also found to affect dielectric, ferroelectric and piezoelectric performances with the maximum values ($T_m = 328^\circ\text{C}$, $\epsilon_r = 1736$, $\tan\delta = 0.0714$, $P_r = 21.91 \mu\text{C}/\text{cm}^2$, $d_{33} = 228 \text{ pC}/\text{N}$) observed in 0.89BNKT - 0.11BNdT composition.

Keywords Lead-free piezoelectric; phase; microstructure; electrical properties

1. Introduction

It has been well accepted that the most widely used piezoelectric materials are PZT-based ceramics [1]. However, the toxicity of PbO when it is at high vapor pressure during sintering process causes a serious ecological problem [1]. A promising way to solve this problem is to develop environmentally friendly lead-free piezoelectric ceramics to replace PZT-based ceramics. This has become one of the main trends in the present development of piezoelectric materials.

Among recently investigated piezoelectric materials, BNKT has considerably attracted many researchers as they have no lead pollutant. $\text{Bi}_{0.5}(\text{Na}_{1-x}\text{K}_x)\text{TiO}_3$ is one of the most interesting compounds owing to an existence of a rhombohedral-tetragonal MPB in a range of $x = 0.16$ – 0.20 with relative high remanent polarization ($P_r = 38 \mu\text{C}/\text{cm}^2$), piezoelectric coefficient ($d_{33} = 167 \text{ pC}/\text{N}$) and electromechanical coupling coefficient ($k_{33} = 0.56$) [2–3]. In order to further enhance the properties of BNKT to meet requirements for practical uses, it is necessary to develop new BNKT-based ceramics. It has been proved that it is relatively easy to form solid solutions of BNKT with other perovskites such as BaTiO_3 [4–5] and $\text{Ba}(\text{Zr}_{0.04}\text{Ti}_{0.96})\text{O}_3$ [6]. These newly formed solid solutions had better piezoelectric

Received December 11, 2012; in final form March 5, 2013.

*Corresponding author. E-mail: sukanda.jian@cmu.ac.th

[1227]/49

properties and were easily poled when compared with pure BNKT ceramic. It is well known that barium neodymium titanate or BNdT as well as modified BaTiO₃. In 2008, Yao *et al.* [7] investigated phase and dielectric behavior of Ba_{1-x}Nd_xTiO₃ ceramics. XRD indicated that Ba_{1-x}Nd_xTiO₃ ceramic had tetragonal phase when $x < 0.05$, while it had cubic phase at $x \geq 0.05$. The Curie temperature (T_c) was shifted to lower value when Nd³⁺ was added. (Ba_{0.98}Nd_{0.02})TiO₃ ceramic had a maximum room temperature dielectric constant (~ 8000) in tetragonal phase region with T_c around 76°C.

In this work, (Ba_{0.98}Nd_{0.02})TiO₃ was added into Bi_{0.5}(Na_{0.8}K_{0.2})_{0.5}TiO₃ ceramic according to a formula of (1-x)Bi_{0.5}(Na_{0.8}K_{0.2})_{0.5}TiO₃-x(Ba_{0.98}Nd_{0.02})TiO₃, herein $x = 0.05$ – 0.15 mol fraction. The focus on the search for new lead-free piezoelectric ceramic at MPB composition where it is considered to show superior electrical properties.

2. Experimental

Bi_{0.5}(Na_{0.8}K_{0.2})_{0.5}TiO₃ and (Ba_{0.98}Nd_{0.02})TiO₃ powders were prepared by a conventional mixed-oxide method. The dried BNKT and BNdT powders were separately calcined at 900°C for 2 h and 1100°C for 2 h, respectively. Both calcined powders were then weighed and mixed to produce the mixed powders of (1-x)Bi_{0.5}(Na_{0.8}K_{0.2})_{0.5}TiO₃-x(Ba_{0.98}Nd_{0.02})TiO₃ or (1-x)BNKT-xBNdT ($x = 0.05, 0.07, 0.09, 0.10, 0.11, 0.13$ and 0.15 mol fraction). After drying, the powders were granulated by adding a few drops of 3 wt% PVA and then pressed into disks with 10 mm in diameter. The green disks were preheated in air at 500°C for 1 h to remove organic binders and then sintered at 1125°C for 2 h with a heating/cooling rate of 5°C/min.

X-ray diffractometer was used to identify phase of the ceramics. Bulk density of all ceramics was measured with Archimedes' method. The theoretical density was calculated based on the theoretical densities of BNKT (5.84 g/cm³) [8] and BaTiO₃ (6.01 g/cm³) [9]. Scanning electron microscope was used to determine microstructure of the samples. Grain size was determined by a mean linear interception method. For electrical characterizations, dielectric constant as function of temperature was measured in a range of 25–500°C at 10 kHz using 4284A LCR-meter connected to a high temperature furnace. A standard Sawyer-Tower circuit was used to measure ferroelectric hysteresis loop. The samples in a disk shape with 10 mm in diameter and 1 mm in thickness were poled in silicone oil at 60°C under 5 kV/mm for 15 min. The piezoelectric coefficient (d_{33}) was recorded from 1-day aged samples using d_{33} -meter (KCF technologies, Model S5865) at a frequency of 50 Hz.

3. Results and Discussion

After sintering the pellet-shaped samples at 1125°C for 2 h, it was found that the addition of BNdT into BNKT ceramic caused a slight decrease in sample density (see Table 1). However, their relative densities were more than 98% of the theoretical values for all compositions.

X-ray diffraction patterns of all ceramics scanned with wide and narrow 2θ range are shown in Fig. 1. All compositions exhibited a single phase of perovskite structure. No secondary phases could be detected, confirming that BNdT diffused into BNKT lattice to form homogeneous solid solutions of end compounds. With increasing BNdT content, the diffraction peaks gradually shifted to lower angle. This was attributed to the differences in the ionic radii between Bi³⁺ (1.17 Å), Na⁺ (1.18 Å), K⁺ (1.33 Å), Ba²⁺ (1.42 Å) and

Table 1
Physical and electrical properties of (1-x)BNKT-xBNDT ceramics

x	Density (g/cm ³)	c/a	Grain size (μm)	T_m ($^{\circ}\text{C}$)	T_d ($^{\circ}\text{C}$)	ε_r^a	$\tan\delta^a$	P_r ($\mu\text{C}/\text{cm}^2$)	E_c (kV/cm)	R_{sq}	d_{33} (pC/N)
0.05	5.82 ± 0.01	1.0136	0.40 ± 0.04	320	136	1602	0.0620	16.30	11.87	0.57	174
0.07	5.80 ± 0.01	1.0137	0.39 ± 0.03	325	141	1700	0.0677	19.27	18.00	0.79	179
0.09	5.78 ± 0.01	1.0139	0.40 ± 0.09	326	142	1710	0.0698	19.55	19.13	0.80	189
0.10	5.78 ± 0.01	1.0139	0.41 ± 0.05	327	148	1716	0.0701	20.15	22.95	0.93	211
0.11	5.78 ± 0.02	1.0143	0.46 ± 0.06	328	148	1736	0.0714	21.91	25.19	0.99	228
0.13	5.78 ± 0.03	1.0145	0.47 ± 0.06	327	149	1623	0.0708	21.03	26.27	0.98	190
0.15	5.77 ± 0.01	1.0187	0.52 ± 0.10	326	163	1284	0.0593	21.45	30.10	0.99	123

^aDielectric data obtained at room temperature and at a frequency of 1 kHz.

[1229]/51

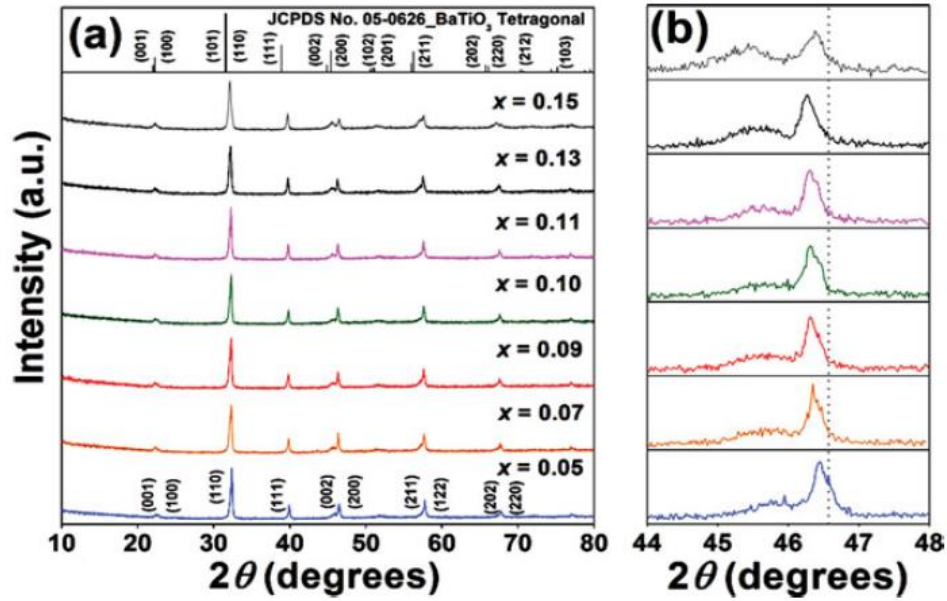


Figure 1. X-ray diffraction patterns of BNKT-BNdT ceramics where (a) $2\theta = 10\text{--}80^\circ$ and (b) $2\theta = 44\text{--}48^\circ$. (Color figure available online.)

Nd^{3+} (1.109 \AA) in A-site [10] which induced structural distortion and resulted in an enlargement of unit cell size. Similar peak shifting behavior by partial substitution of Ba^{2+} for $[\text{Bi}_{0.5}(\text{Na}_{0.80}\text{K}_{0.20})]^{2+}$ and Zr^{4+} for Ti^{4+} was also observed in BZT-modified BNKT ceramics [6]. The results of more detailed XRD analysis performed in $2\theta = 44\text{--}48^\circ$ are shown in Fig. 1(b). BNKT-0.05BNdT ceramic presented features of mixed rhombohedral-tetragonal symmetry but showed a domination of rhombohedral over tetragonal structure. This mixture of phases was maintained even when up to 11 mol% of BNdT was added into BNKT. It seemed that the sample at $x = 0.11$ became close to the morphotropic phase boundary (MPB) composition of BNKT-BNdT system. Further BNdT addition over 11 mol% intensified the separation of the (200) and (002) peaks which suggested a tetragonal-rich phase. This behavior became clearer after the analysis of calculated lattice parameters (a and c) indicated an increase in tetragonality (c/a) as shown in Table 1.

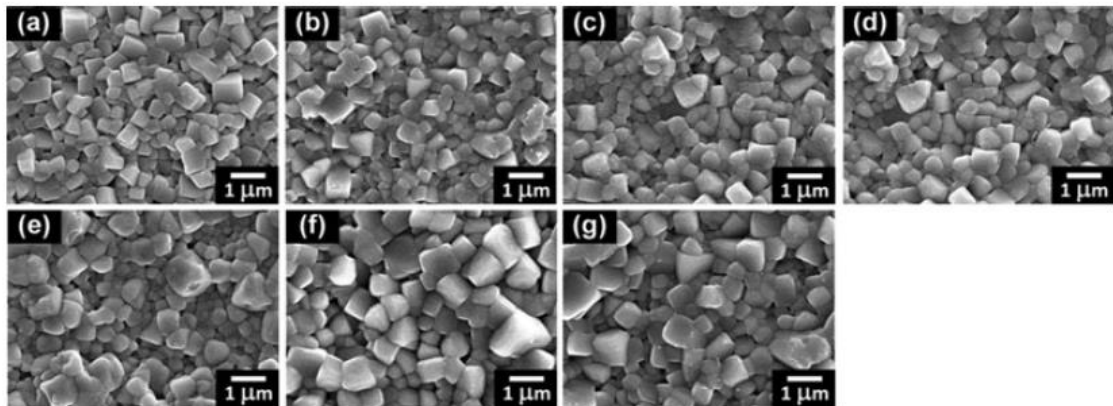


Figure 2. SEM micrographs of $(1-x)\text{BNKT}-x\text{BNdT}$ ceramics where (a) $x = 0.05$, (b) $x = 0.07$, (c) $x = 0.09$, (d) $x = 0.10$, (e) $x = 0.11$, (f) $x = 0.13$ and (g) $x = 0.15$.

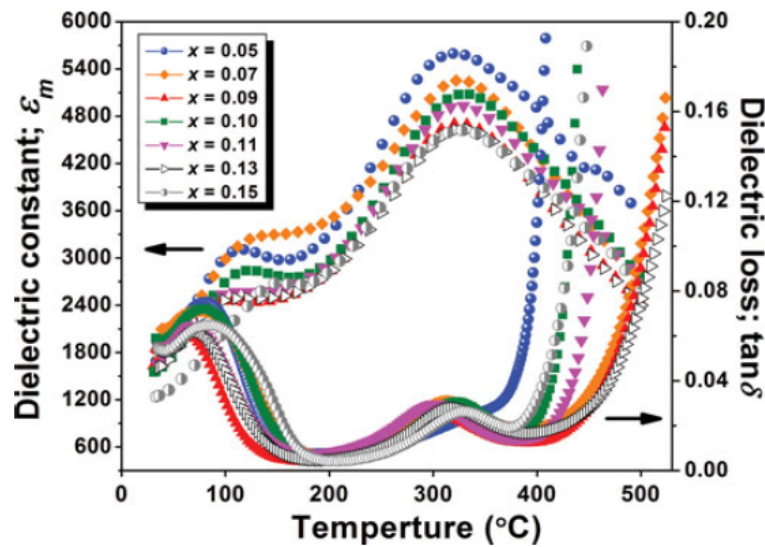


Figure 3. Plots of temperature dependence on dielectric constant and dielectric loss of BNKT-BNdT ceramics measured at a frequency of 10 kHz. (Color figure available online.)

From SEM images shown in Fig. 2, it could be seen that the grains had regular shape and crystalline boundaries were clearly observed in all samples. Almost no pores were found on the surface, suggesting well densified specimens. BNKT-0.05BNdT contained cubic-like shape with average side length $\sim 0.4 \mu\text{m}$. A small addition of BNdT (7–10 mol%) into BNKT had no significant influence on grain size and the values were rather similar (0.39–0.41 μm). At higher content of BNdT (11–15 mol%), the grain size slightly increased and rather coarse grains were formed.

Room temperature dielectric constant (ϵ_r) and dielectric loss ($\tan\delta$) of BNKT-BNdT ceramics measured at a frequency of 1 kHz are listed in Table 1. The ϵ_r initially increased with increasing BNdT content and reached a maximum value of 1736 at $x = 0.11$, then decreased with further increasing BNdT content to a minimum value of 1284 at $x = 0.15$. Variation of dielectric loss with increasing BNdT content followed that of ϵ_r . The variation of piezoelectric behavior with increasing BNdT also showed similar trend to that of dielectric responses. Based on the data listed in Table 1, the piezoelectric constant (d_{33}) increased with increasing of BNdT fraction up to $x = 11$ (0.89BNKT-0.11BNdT) near the MPB-like composition, possessing the highest value of 228 pC/N. As the free energy of rhombohedral phase was close to that of tetragonal phase, these two phases easily changed to each other when an electric field was applied. This helped promote the movement and polarization of ferroelectric active ion, leading to the increase of both ϵ_r and d_{33} in this particular composition [6]. With further increasing BNdT at $x > 0.11$, a slight decrease in d_{33} value was observed, indicating that the compositions slightly deviated to BNdT tetragonal-rich phase. The change in crystal structure to be more tetragonal-rich may also contribute to the reduction in dielectric and piezoelectric performance of BNKT-BNdT ceramics similar to the reduction of both ϵ_r and d_{33} observed in previous work on BNKT-BZT system [6].

Figure 3 shows the temperature dependence of dielectric constant (ϵ_r) and dielectric loss ($\tan\delta$) as a function of BNdT concentration. Since it has been reported that BNT-based ceramics exhibited two dielectric anomalies corresponding to the maximum dielectric constant temperature (T_m : temperature at which dielectric constant reaches the maximum, T_m could be considered as the Curie point, T_c) and depolarization temperature (T_d : temperature

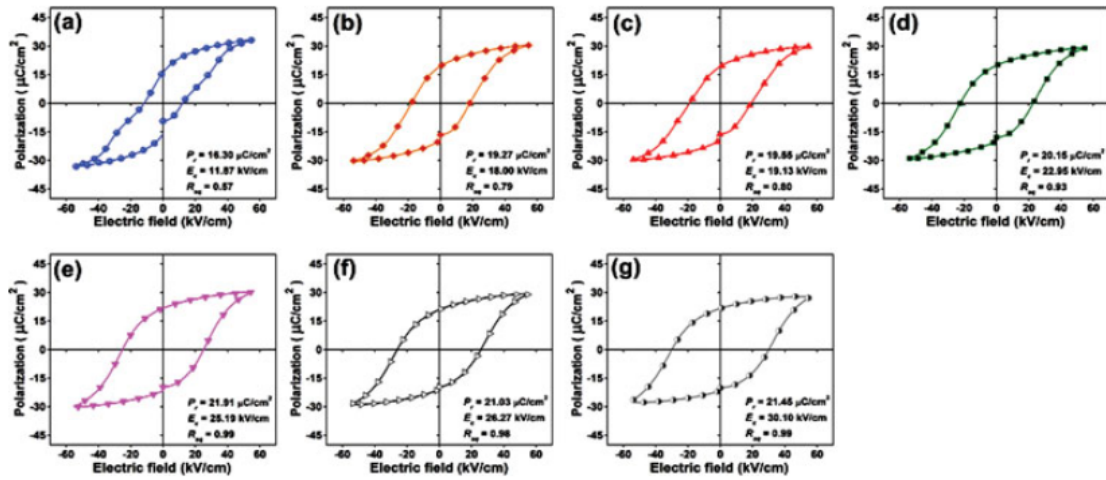


Figure 4. Plots of polarization and electric field of $(1-x)\text{BNKT}-x\text{BNdT}$ ceramics where (a) $x = 0.05$, (b) $x = 0.07$, (c) $x = 0.09$, (d) $x = 0.10$, (e) $x = 0.11$, (f) $x = 0.13$ and (g) $x = 0.15$. (Color figure available online.)

at which the phase transition from rhombohedral to tetragonal). The ε_r versus temperature curves of all samples were similar. Two transition temperatures of T_d and T_m were observed from a room temperature (25°C) to a higher temperature (500°C). From Table 1, the T_d and T_m of $\text{BNKT}-0.05\text{BNdT}$ ceramic were found to be 136°C and 320°C , respectively. Both T_d and T_m increased with increasing BNdT content, however, the T_m reached the maximum value of 328°C at $x = 0.11$. For further increasing in BNdT content, T_m started to decrease. The enlargement of unit cell size was thought to play an important role in this observed trend. Chen *et al.* [6] studied an addition of $\text{Ba}(\text{Zr}_{0.04}\text{Ti}_{0.96})\text{O}_3$ into $\text{Bi}_{0.5}(\text{Na}_{0.84}\text{K}_{0.16})_{0.5}\text{TiO}_3$ also found similar enlargement of unit cell and a decrease of T_m .

Room temperature measurement of polarization-electric field (P - E) hysteresis loop was performed on the samples in order to determine remanent polarization (P_r), coercive electric field (E_c) and loop squareness (R_{sq}). The samples were exposed to an external electric field of up to 55 kV/cm. It could be seen that the saturated and normal P - E hysteresis loops were observed for all samples. As seen from the hysteresis curves, BNdT had significant influence on loop shape as shown in Fig. 4. For more details, the values of P_r , E_c and R_{sq} are also listed in Table 1. The hysteresis loop of $\text{BNKT}-0.05\text{BNdT}$ exhibited a typical ferroelectric behavior having values of $P_r \sim 16.30 \mu\text{C}/\text{cm}^2$, $E_c \sim 11.87 \text{ kV}/\text{cm}$ and $R_{sq} \sim 0.57$. The ferroelectric performances increased with increasing of BNdT and reached the maximum values of $P_r = 21.91 \mu\text{C}/\text{cm}^2$ and $R_{sq} = 0.99$ at $x = 0.11$. Because of the MPB-like behavior, improved ferroelectric performances where P_r and R_{sq} were maximized could be achieved for $0.89\text{BNKT}-0.11\text{BNdT}$ sample. Further increasing in BNdT content, a slight decrease in P_r and R_{sq} were then observed while E_c gradually increased with increasing BNdT.

4. Conclusions

Lead-free piezoelectric ceramics $(1-x)\text{Bi}_{0.5}(\text{Na}_{0.8}\text{K}_{0.2})_{0.5}\text{TiO}_3-x(\text{Ba}_{0.98}\text{Nd}_{0.02})\text{TiO}_3$ or $(1-x)\text{BNKT}-x\text{BNdT}$ (when $x = 0.05-0.15$ mol fraction) were successfully synthesized by a conventional mixed oxide method. All compositions exhibited a single perovskite structure without detectable secondary phase and MPB region with coexisting rhombohedral and

tetragonal structures was found to occur at around $x = 0.11$. The sample at this composition showed an improved dielectric ($T_m = 328^\circ\text{C}$, $\epsilon_r = 1736$, $\tan\delta = 0.0714$), ferroelectric ($P_r = 21.91 \mu\text{C}/\text{cm}^2$, $R_{sq} = 0.99$) and piezoelectric properties ($d_{33} = 228 \text{ pC/N}$) compared to the other compositions.

Acknowledgments

This work is financially supported by the Thailand Research Fund (TRF) and the National Research University Project under Thailand's Office of the Higher Education Commission (OHEC). The Faculty of Science and the Graduate School, Chiang Mai University is also acknowledged. P. Jaita would like to acknowledge financial support from the TRF through the Royal Golden Jubilee Ph.D. Program.

References

1. L. Wang, J. H. Cho, Y. S. Sung, M. H. Kim, T. K. Song, S. S. Kim, and B. C. Choi, Dielectric and piezoelectric properties of lead-free $\text{BaTiO}_3\text{-Bi}(\text{Zn}_{0.5}\text{Ti}_{0.5})\text{O}_3$ and $(\text{Bi}_{0.5}\text{Na}_{0.5})\text{TiO}_3\text{-Bi}(\text{Zn}_{0.5}\text{Ti}_{0.5})\text{O}_3$ ceramics. *Ferroelectrics* **380**, 177–182 (2009).
2. A. Sasaki, T. Chiba, Y. Mamiya, and E. Otsuki, Dielectric and piezoelectric properties of $(\text{Bi}_{0.5}\text{Na}_{0.5})\text{TiO}_3\text{-(Bi}_{0.5}\text{K}_{0.5})\text{TiO}_3$ systems. *Jpn. J. Appl. Phys.* **38**, 5564–5567 (1999).
3. K. Yoshii, Y. Hiruma, H. Nagata, and T. Takenaka, Electrical properties and depolarization temperature of $(\text{Bi}_{1/2}\text{Na}_{1/2})\text{TiO}_3\text{-(Bi}_{1/2}\text{K}_{1/2})\text{TiO}_3$ lead-free piezoelectric ceramics. *Jpn J Appl Phys.* **45**, 4493–4496 (2006).
4. Y. Hiruma, H. Nagata, and T. Takenaka, Phase transition temperatures and piezoelectric properties of $(\text{Bi}_{1/2}\text{Na}_{1/2})\text{TiO}_3\text{-(Bi}_{1/2}\text{K}_{1/2})\text{TiO}_3\text{-BaTiO}_3$ lead-free piezoelectric ceramics. *Jpn J Appl Phys.* **45**, 7409–7412 (2006).
5. X. X. Wang, X. G. Tang, and H. L. W. Chan, Electromechanical and ferroelectric properties of $(\text{Bi}_{1/2}\text{Na}_{1/2})\text{TiO}_3\text{-(Bi}_{1/2}\text{K}_{1/2})\text{TiO}_3\text{-BaTiO}_3$ lead-free piezoelectric ceramics. *Appl Phys Lett.* **85**, 91–93 (2004).
6. Z. W. Chen and J. Q. Hu, Piezoelectric and dielectric properties of $\text{Bi}_{0.5}(\text{Na}_{0.84}\text{K}_{0.16})_{0.5}\text{TiO}_3\text{-Ba}(\text{Zr}_{0.04}\text{Ti}_{0.96})\text{O}_3$ lead free piezoelectric ceramics. *Adv Appl Ceram.* **107**, 222–226 (2008).
7. Z. Yao, H. Liu, Y. Liu, Z. Wu, Z. Shen, Y. G. Liu, and M. Cao, Structure and dielectric behavior of Nd-doped BaTiO_3 perovskites. *Mater Chem Phys.* **109**, 475–481 (2008).
8. Y. R. Zhang, J. F. Li, and B. P. Zhang, Enhancing electrical properties in NBT-KBT lead-free piezoelectric ceramics by optimizing sintering temperature. *J Am Ceram Soc.* **91**, 2716–2719 (2008).
9. H. E. Swanson and R. K. Fuyat, Standard X-ray diffraction powder patterns. *Natl Bur Stand Circ (U.S.)* **539**, 3, 44–45 (1954).
10. R. D. Shannon, Revised effective ionic radii and systematic studies of interatomic distances in halides and chalcogenides. *Acta Cryst.* **A32**, 751–767 (1976).



ELSEVIER

Contents lists available at ScienceDirect

Journal of Alloys and Compounds

journal homepage: www.elsevier.com/locate/jalcom

Enhancement in dielectric, ferroelectric, and electrostrictive properties of $\text{Pb}(\text{Mg}_{1/3}\text{Nb}_{2/3})_{0.9}\text{Ti}_{0.1}\text{O}_3$ ceramics by CuO addition



M. Promsawat^a, J.Y.Y. Wong^b, Z. Ren^b, H.N. Taylor^b, A. Watcharapasorn^{a,c}, Z.-G. Ye^b, S. Jiansirisomboon^{a,c,*}

^a Department of Physics and Materials Science, Faculty of Science, Chiang Mai University, 239 Huay Kaew Road, Muang, Chiang Mai, 50200, Thailand

^b Department of Chemistry and 4D LABS, Simon Fraser University, 8888 University Drive, Burnaby, British Columbia, V5A 1S6, Canada

^c Materials Science Research Center, Faculty of Science, Chiang Mai University, 239 Huay Kaew Road, Muang, Chiang Mai, 50200, Thailand

ARTICLE INFO

Article history:

Received 13 June 2013

Received in revised form 31 October 2013

Accepted 31 October 2013

Available online 9 November 2013

Keywords:

Ceramics

Ferroelectrics

Sintering

Microstructure

ABSTRACT

Effects of CuO on dielectric, ferroelectric and electrostrictive properties of $\text{Pb}(\text{Mg}_{1/3}\text{Nb}_{2/3})_{0.9}\text{Ti}_{0.1}\text{O}_3$ (PMNT) ceramics were studied. The PMNT/ x CuO (with $x = 0, 0.2, 0.4, 2.0$ and 4.0 mol.%) ceramics were prepared by using solid state reaction and sintering process. It was found that the pseudo-cubic lattice parameter, a , gradually increased while the angle α decreased with increasing CuO content. Maximum dielectric constant showed a decreasing trend with increasing CuO with an abrupt increase in value at $x = 2.0$ mol.%. The temperature of maximum dielectric constant and depolarization temperature tended to increase while the diffuseness of dielectric peak decreased with increasing CuO concentration. Remanent polarization and coercive field of pure PMNT sample were $\sim 1.8 \mu\text{C}/\text{cm}^2$ and $0.6 \text{ kV}/\text{cm}$, respectively, which were increased to $\sim 3.5 \mu\text{C}/\text{cm}^2$ and $1.8 \text{ kV}/\text{cm}$ when $x = 0.2$ mol.%. With $x > 0.2$ mol.%, coercive field gradually decreased with increasing CuO content while remanent polarization did not significantly change. With $x \leq 2.0$ mol.%, induced strain and electrostrictive coefficient tended to increase with increasing CuO content, with maximum values of 0.09% (at $10 \text{ kV}/\text{cm}$) and $19.90 \times 10^{-16} \text{ m}^2/\text{V}^2$, respectively, for the PMNT/2.0 mol.% CuO sample. An enhancement in polar order of PMNT ceramics due to an addition of CuO was observed.

© 2013 Elsevier B.V. All rights reserved.

1. Introduction

Complex perovskite solid solution compound of $\text{Pb}(\text{Mg}_{1/3}\text{Nb}_{2/3})_{0.9}\text{Ti}_{0.1}\text{O}_3$ (PMNT) is a well known relaxor ferroelectric material that shows good electrostrictive properties around room temperature. This makes PMNT suitable for applications such as electrostrictive actuators. The origin of its excellent properties has often been explained in terms of polar nano-regions (PNRs) or polar microdomains [1–3] which nucleated as the material was cooled down below Burns temperature (T_B). The size and volume of PNRs grew as the temperature was decreased further, leading to an increase in dielectric permittivity. However, with further decreasing the temperature, the dynamic of PNRs slowed down. This resulted in a decrease in dielectric permittivity and thereby creating the maximum dielectric permittivity and the temperature of dielectric maximum (T_{max}). The dynamic of PNRs was frozen when the temperature was decreased below the freezing temperature (T_f) [4]. At $T < T_f$, polar macrodomains could be induced by an application of

electric field, which led to the exhibition of piezoelectric response, i.e. polarization versus electric field (P - E) hysteresis loops and butterfly-like strain versus electric field (S - E) curves [5]. However, the induced polar macrodomains disappeared as the materials were heated above the depolarization temperature (T_d). Therefore, at T_d , a transition between an induced polar macrodomain and a polar microdomain was observed [6]. Interestingly, a large longitudinal induced strain and high electrostrictive coefficient (M) were observed around the temperature above and near T_d . As observed in the study of Hao et al., they found that an enhancement of strains in $\text{Bi}_{0.5}(\text{Na}_{0.80}\text{K}_{0.20})_{0.5}\text{TiO}_3$ -based materials around room temperature corresponded to the T_d near room temperature. This was due to the response of the coexisting polar macro- and microdomains [3,6,7].

Based on these recent studies on PMNT, it was expected that an electric field induced strain and electrostrictive coefficient of this compound could be enhanced by shifting T_d toward room temperature ($T_d \sim 0^\circ\text{C}$ [8]). Ionic substitution was found to contribute to a unit cell distortion, leading to an increase in T_d [2]. In a study by Hou et al., the substitution of Cu^{2+} ion for the ions located at octahedral site caused unit cell distortion due to asymmetric distribution of electrons of Cu^{2+} exhibiting a Jahn–Teller ion [9].

* Corresponding author at: Department of Physics and Materials Science, Faculty of Science, Chiang Mai University, 239 Huay Kaew Road, Muang, Chiang Mai, 50200, Thailand. Tel.: +66 53 941921x631; fax: +66 53 943445.

E-mail address: sukanda.jian@cmu.ac.th (S. Jiansirisomboon).

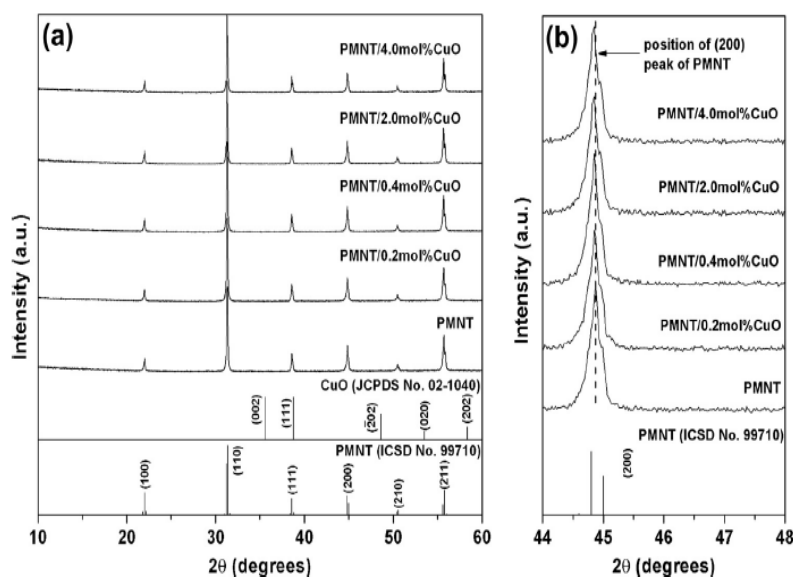


Fig. 1. (a) XRD patterns of the PMNT/xCuO ceramics sintered at 1150 °C. (b) Enlarged views of the (200) peaks at $2\theta \approx 45^\circ$.

Table 1
Lattice parameters and sintering results of the PMNT/xCuO ceramics.

CuO content x (mol.%)	Lattice parameter, a (Å)	$90 - \alpha$ (°)	Grain size (μm)	Bulk density (g/cm ³)
0	4.0373 ± 0.0002	0.012 ± 0.003	1.3 ± 0.1	7.87 ± 0.02
0.2	4.0387 ± 0.0002	0.015 ± 0.003	1.5 ± 0.1	7.88 ± 0.01
0.4	4.0386 ± 0.0001	0.016 ± 0.002	1.5 ± 0.1	7.90 ± 0.01
2.0	4.0394 ± 0.0002	0.021 ± 0.003	6.6 ± 0.7	7.83 ± 0.03
4.0	4.0385 ± 0.0001	0.023 ± 0.003	9.4 ± 0.7	7.73 ± 0.03

Note: α Represents the angle between the lattice parameters a of pseudo-cubic lattices.

Several other studies also employed CuO as a substituent in relaxor and electrostrictive ceramics. Beside its use as a sintering aid, CuO was found to affect dielectric, piezoelectric and ferroelectric properties of some piezoelectric and relaxor compounds. As examples, Fang et al. found that CuO caused an increase in dielectric permittivity and remanent polarization of 0.8PMN-0.2PT (80/20) ceramics [10]. Kang et al. found that CuO addition resulted in an improvement of electrostrictive coefficient (Q_{33}) of $\text{Bi}_{1/2}(\text{Na,K})_{1/2}\text{TiO}_3$ ceramics with Q_{33} of $0.023 \text{ m}^4 \text{ C}^{-2}$ [11]. In these studies, the sintering-aid effect of CuO seemed to play a large part in improving the materials' density, and therefore improved properties. In our previous study on PMNT (90/10), which possesses highest electrostrictive coefficient among PMNT compositions, its dielectric and electrostrictive properties were enhanced by ZnO modification with electrostrictive coefficient (M) of $12.94 \times 10^{-16} \text{ m}^2/\text{V}^2$ [12]. Therefore, this present study attempted to investigate the effect of CuO addition in PMNT (90/10) ceramic on its phase, crystal structure and microstructure, as well as to elucidate in details a relationship between these factors and measured dielectric, ferroelectric and electrostrictive properties.

2. Experimental details

$\text{Pb}(\text{Mg}_{1/3}\text{Nb}_{2/3})_{0.9}\text{Ti}_{0.1}\text{O}_3$ (PMNT) powder was prepared by using the columbite precursor method [13]. Different amounts ($x = 0, 0.2, 0.4, 2.0$ and $4.0 \text{ mol.}\%$) of spherical shaped CuO nano-particles (99%, Nanostructured & Amorphous Materials) with particle size in between ~ 30 and 50 nm were added into PMNT powder. Polyvinyl alcohol was added to the mixed powder as a binder and then pressed uniaxially into pellets using $\sim 5.5 \text{ MPa}$ pressure. Each pellet (10 mm in diameter, 2 mm in

thickness and the density of $\sim 4.84 \text{ g/cm}^3$) was sintered in a PMNT atmosphere at 1050°C for 2 h. Bulk density of the ceramics was determined by the Archimedes' method. Structure, phase and chemical composition were characterized using X-ray diffraction method (XRD, Model X-pert, Panalytical B.V., The Netherlands) with $\text{Cu K}\alpha$ radiation of 1.5405 \AA wavelength and energy dispersive X-ray technique (EDX, JSM-6335F, JEOL, Japan). Microstructure of the ceramics was observed using a scanning electron microscope (SEM, JEOL JSM-6335F, Japan). Average grain size was determined by employing a mean linear interception method on SEM micrographs. Temperature dependent dielectric constant (ϵ') and loss tangent ($\tan\delta$) of unpoled samples were measured at 1 kHz using a computer-controlled alpha dielectric analyzer (Novocontrol), in order to reveal the depolarization temperature (T_d), a sample was firstly poled at room temperature with an electric field of 20 kV/cm . While the sample was being poled, it was cooled down to -50°C . At -50°C , the applied field was removed and the temperature dependent dielectric constant of the poled sample was then measured upon heating. Polarization versus electric field of unpoled samples was measured using a ferroelectric testing instrument (Radiant Technologies RT66A). Strain versus electric field curves of unpoled samples were measured by using a Fotonics Sensor (MTI 2000, MTI Instruments) in conjunction with a computer controlled electrometer/voltage source (Keithley 2517A).

3. Results and discussion

3.1. Phase formation and microstructural analysis

XRD patterns of PMNT/xCuO ceramics are shown in Fig. 1(a), which were found to match the standard ICSD file no. 99710 of $\text{Pb}(\text{Mg}_{0.3}\text{Nb}_{0.6}\text{Ti}_{0.1})\text{O}_3$ with $Pm\bar{3}m$ cubic space group [14]. It could be seen from the enlarged patterns in Fig. 1(b) that the position of (200) peak at $2\theta \approx 45^\circ$ slightly shifted to lower angles with increasing CuO content. Based on the position of XRD peaks, the lattice parameter a and α (representing the angle between the lattice parameter a of pseudo-cubic lattice) were calculated and the results are given in Table 1. The pseudo-cubic parameter a of $\sim 4.0373 \text{ \AA}$ of pure PMNT ceramic gradually increased to 4.0394 \AA with increasing CuO content up to $2.0 \text{ mol.}\%$, which could be attributed to the substitution of the larger Cu^{2+} ion for smaller ions ($r_{\text{Cu}^{2+}} = 0.73 \text{ \AA}$, $r_{\text{Mg}^{2+}} = 0.72 \text{ \AA}$, $r_{\text{Nb}^{5+}} = 0.64 \text{ \AA}$ and $r_{\text{Ti}^{4+}} = 0.605 \text{ \AA}$ [15]) on the B-site of PMNT lattice. This was consistent with our previous study as reported in Ref. [16]. However, the lattice parameter a did not increase further with higher amount of CuO. This suggested that the solubility limit of CuO in PMNT was $2.0 \text{ mol.}\%$. The angle α was found to decrease with increasing CuO concentration. It was believed that the substitution of Cu^{2+} ion into the B-site of the perovskite structure of PMNT would lead to structural

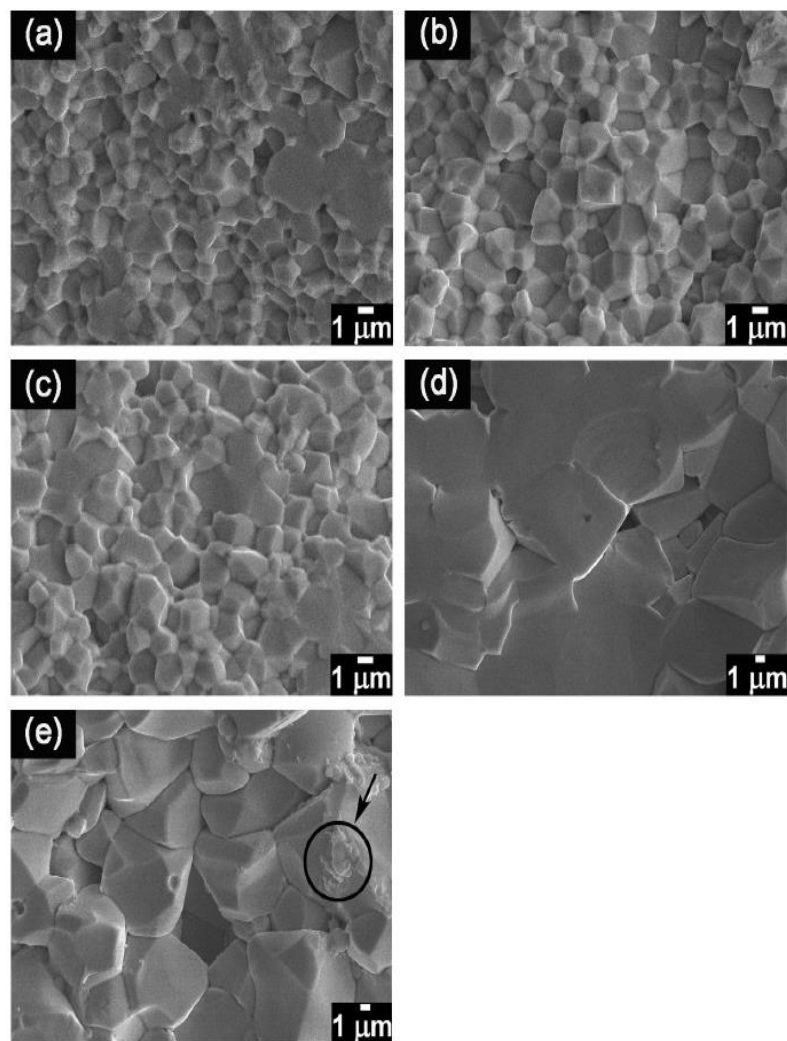


Fig. 2. SEM images of fractured surfaces of (a) pure PMNT ceramic and the ceramics added with (b) 0.2, (c) 0.4, (d) 2.0 and (e) 4.0 mol.% CuO. Circle indicates secondary phase.

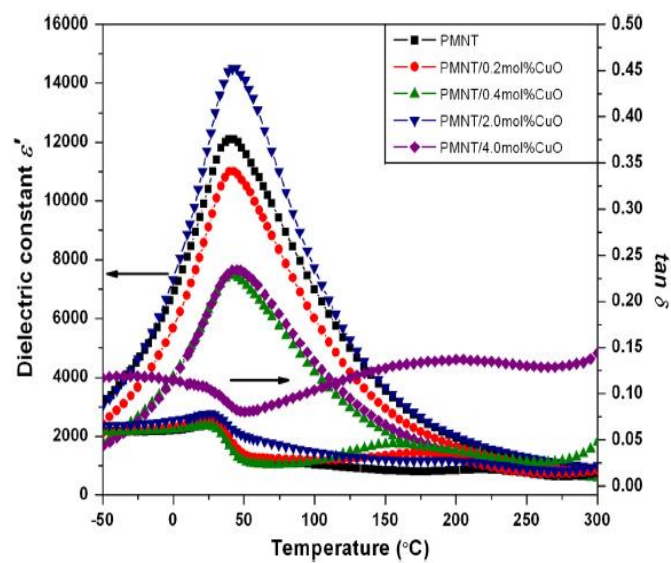


Fig. 3. Variation of dielectric constant (ϵ') and loss tangent ($\tan \delta$) of unpoled PMNT/xCuO ceramics as a function of temperature measured at 1 kHz.

Table 2
Dielectric properties of the PMNT/xCuO ceramics.

CuO content x (mol.%)	ϵ'_{\max}	$\tan \delta$	T_{\max} (°C)	δ (°C)	T_d (°C)
0	10,473	0.065	40	57	-3
0.2	9,079	0.073	41	51	0
0.4	6,300	0.065	41	53	2
2.0	11,897	0.078	43	48	5
4.0	6270	0.106	45	49	6

Note: ϵ'_{\max} and $\tan \delta$ represent dielectric constant and dielectric loss tangent values measured at the temperature of the maximum dielectric constant (T_{\max}) at 1 kHz. δ is diffuseness parameter and T_d represents depolarization temperature.

distortion because Cu^{2+} ion has an asymmetrical electronic configuration (d^9) under octahedral field, and hence the lattice would undergo Jahn–Teller distortion. This agreed with the previous result of Hou et al. [9].

Average grain sizes of the ceramics determined from SEM images, as shown in Fig. 2, are listed in Table 1. Compared to the PMNT/CuO ceramics sintered at 950 °C [16], the grain size of the PMNT/CuO ceramics sintered at 1050 °C apparently increased. This suggested that an increase in sintering temperature could enhance atomic diffusion and sinterability of the ceramics [17]. It was found that an average grain size of the ceramics tended to increase with

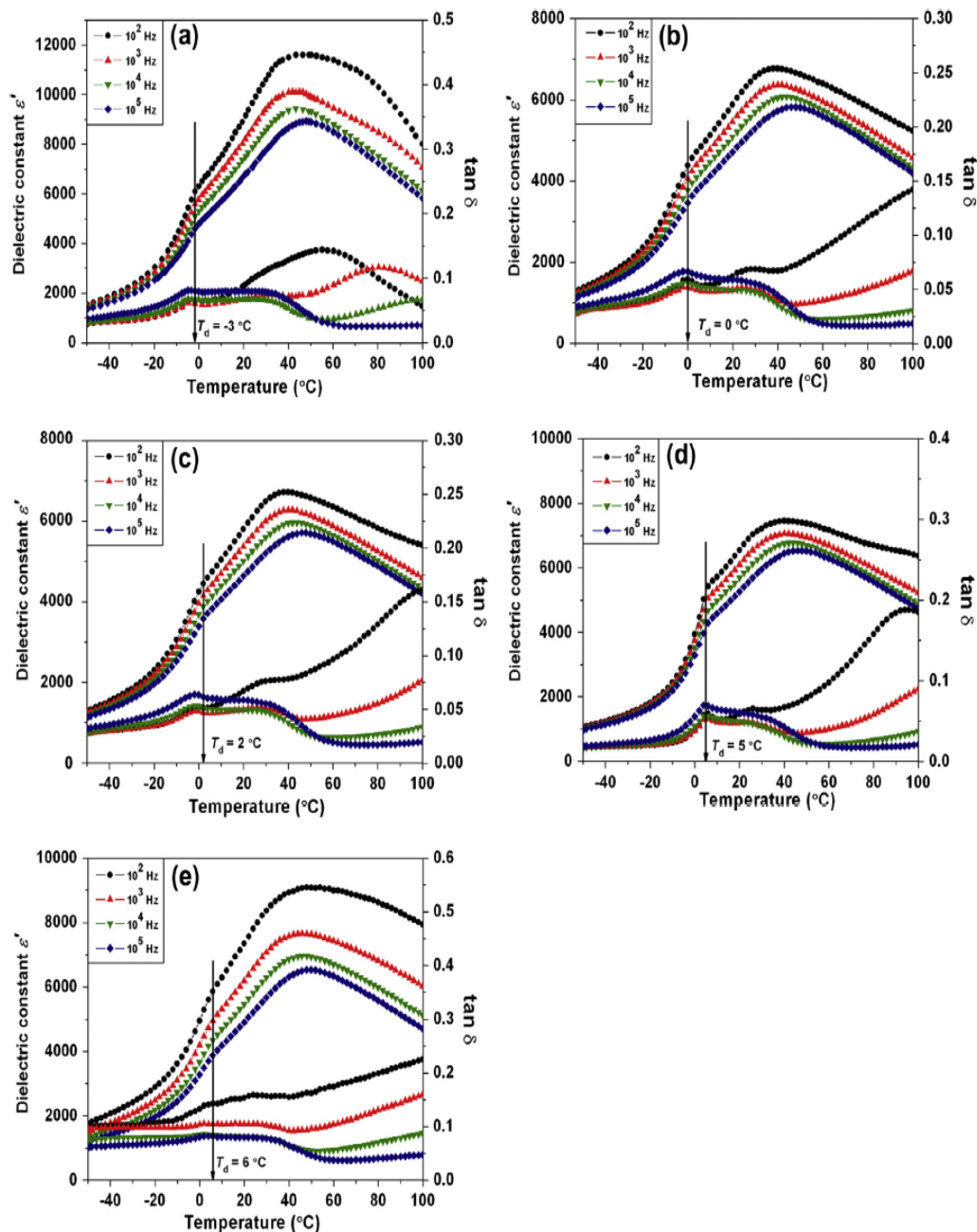


Fig. 4. The temperature dependent dielectric constant (ϵ') and loss tangent ($\tan \delta$) measured upon heating after poling of (a) pure PMNT ceramic and the ceramics added with (b) 0.2, (c) 0.4, (d) 2.0 and (e) 4.0 mol.% CuO. T_d represents depolarization temperature.

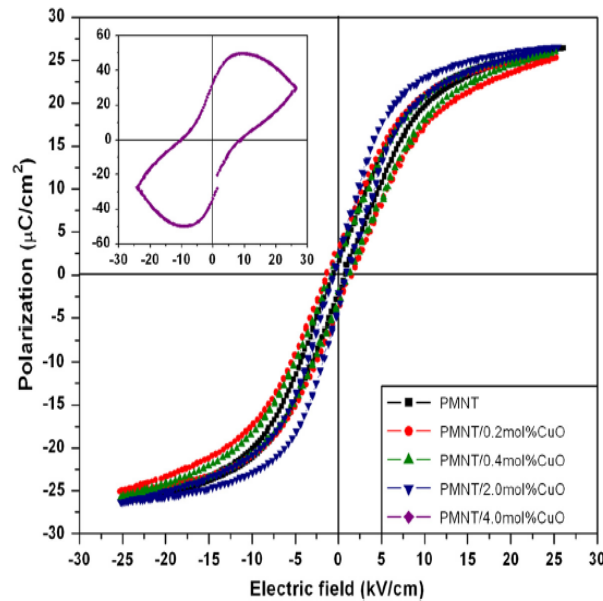


Fig. 5. *P*–*E* loops of unpoled PMNT/*x*CuO ceramics measured at room temperature and a frequency of 1 Hz.

increasing CuO content; the values were about 1.26, 1.52, 1.54, 6.60, and 9.38 μm for pure PMNT ceramic and the ceramics added with 0.2, 0.4, 2.0, and 4.0 mol.% CuO, respectively. Density of pure PMNT ceramic was $\sim 7.87 \text{ g/cm}^3$, which was consistent with the value of ~ 7.70 – 8.00 g/cm^3 in previous reports [18,19] and it gradually increased to $\sim 7.90 \text{ g/cm}^3$ with increasing CuO content up to 0.4 mol.%. It appeared that an addition of CuO enhanced grain growth and densification of PMNT ceramics. This could be attributed to the formation of low-melting point compound or solid solution induced by CuO doping, leading to the appearance of liquid phase at relatively low temperatures, enhancement of mass transport and improvement in a sintering capability of a reaction sintering process [20–22]. At $x > 0.4 \text{ mol.}\%$, the density decreased with increasing CuO concentration. It was probably attributed to an increase in an evaporation of raw component or re-emergence of gas pores, leading to a decrease in density of the ceramics [10]. A secondary phase was observed in the PMNT/4.0 mol.% CuO sample, which was indicated with a circle in Fig. 2(e). Chemical analysis by means of energy dispersive X-ray spectroscopy (EDX) revealed that the secondary phase was Pb-rich. This was believed to be related to the formation of liquid caused by PbO because it has a low melting point (888 $^\circ\text{C}$ [23]). However, an exact composition of this Pb-rich phase could not be determined reliably.

3.2. Dielectric properties

Temperature dependent dielectric constant (ϵ') and loss tangent ($\tan\delta$) of unpoled PMNT/*x*CuO samples measured at 1 kHz are shown in Fig. 3. Selected values of dielectric properties are listed in Table 2. Maximum dielectric constant (ϵ'_{max}) value of $\sim 10,000$ of pure PMNT ceramic decreased to $\sim 6,000$ as CuO content was increased to $x = 0.4 \text{ mol.}\%$, while $\tan\delta$ did not significantly change. ϵ'_{max} reached the maximum value of $\sim 12,000$ for the sample with 2.0 mol.% CuO. However, ϵ'_{max} was found to decrease and $\tan\delta$ increase when CuO content was increased to 4.0 mol.%. An increase in dielectric constant could be attributed to a significant increase in grain size of ceramics [24]. This was consistent with the previous work in which the grain size of the 0.8PMN–0.2PT ceramics increased with CuO doping, leading to an enhancement of ϵ'_{max}

[10]. The temperature of maximum dielectric constant (T_{max}) of PMNT/*x*CuO ceramics is given in Table 2. The result showed that T_{max} tended to increase with increasing CuO content. In comparison to CuO-doped 0.8PMN–0.2PT ceramics [10], T_{max} of PMNT/CuO ceramics in this study were lower than those of CuO-doped 0.8PMN–0.2PT ceramics. This was due to the fact that the PMNT/CuO ceramics had a lower degree of interaction strength between polar clusters [19].

In order to investigate effects of CuO on the diffuseness of dielectric peak, high temperature slope of dielectric curve of unpoled samples was fitted to a quadratic law introduced by Bokov and Ye [25,26] to describe dielectric permittivity of relaxors in general, i.e.

$$\epsilon_A/\epsilon = 1 + [(T - T_A)^2]/2\delta^2 \quad (1)$$

where T_A and ϵ_A represent the temperature and value at the peak of static conventional permittivity of relaxors, respectively, which are the values extrapolated from the quadratic law. δ (to be distinguished from the δ in $\tan\delta$) represents the diffuseness of dielectric peak. The values of δ are given in Table 2 and they tended to decrease with increasing CuO content.

Temperature dependent dielectric constant, $\epsilon'(T)$, of poled samples measured upon heating is shown in Fig. 4. Depolarization temperature (T_d), above which an induced macroscopic polarization is extinguished by thermal energy, was observed as an abrupt increase in ϵ' as indicated in Fig. 4. T_d value of pure PMNT ceramic

Table 3
Ferroelectric and electrostrictive properties of the PMNT/*x*CuO ceramics.

CuO content <i>x</i> (mol.%)	P_r ($\mu\text{C/cm}^2$)	E_c (kV/cm)	Strain (%)	M ($\times 10^{-16} \text{ m}^2/\text{V}^2$)
0	1.8	0.6	0.06	7.65
0.2	3.5	1.8	0.07	8.72
0.4	2.8	1.3	0.08	15.10
2.0	3.0	1.1	0.09	19.90
4.0	–	–	–	–

Note: Ferroelectric hysteresis loops and bipolar electrostrictive properties were measured at room temperature at 1 Hz. P_r and E_c represent remanent polarization and coercive field, respectively. Strain and M represent maximum induced strain (at 10 kV/cm) and electrostrictive coefficient, respectively.

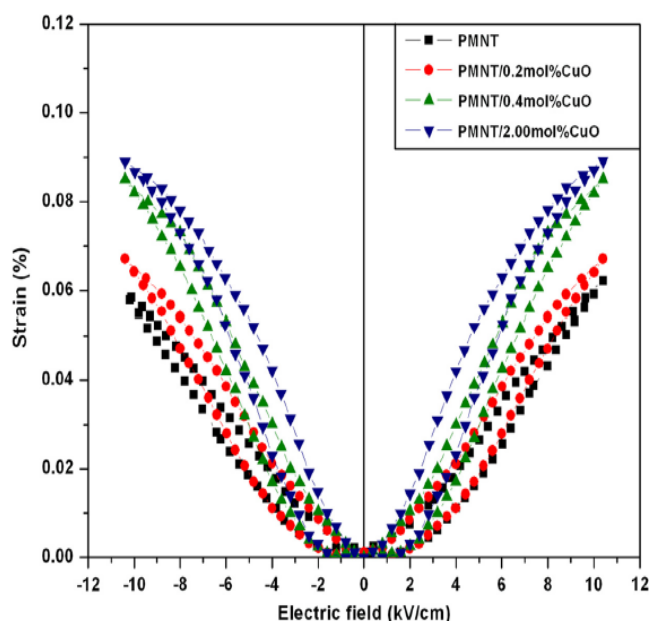


Fig. 6. *S*–*E* loops of unpoled PMNT/*x*CuO ceramics measured at room temperature and a frequency of 1 Hz.

was -3°C which increased to 0, 2, 5 and 6°C for 0.2, 0.4, 2.0 and 4.0 mol.% CuO-added samples, respectively. An increase in T_{max} , T_d and a decrease in δ were indicative of an increase in size of polar clusters and their interaction strength, which was believed to be caused by lattice distortion. Displacement of the ions located on B-site of PMNT lattice could be much easier due to an increase in lattice parameter a and a decrease in angle α , leading to an increased polar order and degree of ferroelectric order of the ceramics. It can also be seen from Fig. 4 that at temperatures lower than T_d , frequency dispersion of dielectric properties of PMNT ceramics was enhanced with 4.0 mol.% CuO addition. In all samples, at temperatures higher than T_d , the frequency dispersion of dielectric properties measured at low frequencies (10^2 – 10^3 Hz) was present. This was expected to be due to a response of charge defects [27].

3.3. Ferroelectric properties

Plots of polarization as a function of electric field (*P*–*E* curves) of unpoled PMNT/*x*CuO ceramics measured at room temperature and a frequency of 1 Hz are shown in Fig. 5. The selected values of ferroelectric properties, i.e., remanent polarization (P_r) and coercive field (E_c), are tabulated in Table 3. Compared to a typical $\text{Pb}(\text{Mg}_{1/3}\text{Nb}_{2/3})\text{O}_3$ (PMN) relaxor, which showed almost linear *P*–*E* curves [28,29], the PMNT/CuO ceramics showed the *P*–*E* loops with higher P_r and E_c . This was attributed to an increase in the interaction strength between polar clusters due to an effect of PbTiO_3 incorporation [19]. It could be confirmed by similarly higher P_r and E_c values of CuO-doped 0.8PMN–0.2PT ceramics [10]. It can be seen from the inset in Fig. 5 that the PMNT/4.0 mol.%CuO sample showed a lossy loop, which revealed that the sample was rather conductive. It was believed that Pb and oxygen vacancies were created due to a formation of Pb-rich phase and a substitution of Cu^{2+} ion for the ions that have higher valency (i.e., Nb^{5+} and Ti^{4+}), respectively. These Pb and oxygen vacancies acted as mobile charge carriers, causing an increase in leakage current and thus resulting in a lossy loop [27]. For pure PMNT ceramic, P_r and E_c values were $\sim 1.8 \mu\text{C}/\text{cm}^2$ and $\sim 0.6 \text{ kV}/\text{cm}$, respectively, which were increased to $\sim 3.5 \mu\text{C}/\text{cm}^2$ and $\sim 1.8 \text{ kV}/\text{cm}$, respectively, for the sample added with 0.2 mol.% CuO. It was believed to be due to an increase in polar order and degree of ferroelectric

order of the ceramics. With $x > 0.2$ mol.%, P_r did not increase further. However, E_c gradually decreased with increasing CuO content, which could be attributed to an increase in grain size of the ceramics [30–32]. From a previous study of CuO-doped 0.8PMN–0.2PT ceramics [10], the doping of CuO also resulted in an increase of P_r and a decrease of E_c of the ceramics in agreement with the result of our study.

3.4. Electrostrictive properties

Plots of strain as a function of electric field (*S*–*E* curves) of unpoled PMNT/*x*CuO ceramics measured at room temperature and a frequency of 1 Hz are shown in Fig. 6. Compared to the typical $\text{Pb}(\text{Mg}_{1/3}\text{Nb}_{2/3})\text{O}_3$ (PMN) electrostrictive material, which showed almost parabolic *S*–*E* curves [28,29] or linear *S*–*E*² relationship [31] for low field region ($< 2 \text{ kV}/\text{cm}$) which was in agreement with PMNT/CuO ceramics in this study. Since much higher electric field was used in this investigation, *P*–*E* behavior showed hysteresis loop with corresponding non-parabolic *S*–*E* (or non-linear *S*–*E*²) relationship. This was mainly due to an increase in the interaction strength between polar clusters [19]. Electrostrictive properties of the 4.0 mol.% CuO-doped PMNT sample could not be measured because it broke down when high electric field was applied. Maximum induced strain and electrostrictive coefficient (M) of pure PMNT sample were found to be 0.06% and $7.65 \times 10^{-16} \text{ m}^2/\text{V}^2$, respectively, as shown in Table 3. The values increased to 0.09% and $19.90 \times 10^{-16} \text{ m}^2/\text{V}^2$, respectively, at $x = 2.0$ mol.%. It was believed that a distortion of unit cell, an increase in density and grain size all contributed to an enhancement of electrostrictive properties of PMNT/*x*CuO ceramics.

4. Conclusions

CuO-modified ceramics, i.e. $0.9\text{Pb}(\text{Mg}_{1/3}\text{Nb}_{2/3})\text{O}_3$ – 0.1PbTiO_3 (PMNT/*x*CuO), with densities of ~ 7.73 – $7.90 \text{ g}/\text{cm}^3$, were prepared by a solid state reaction method. Lattice parameter of pseudo-cubic structure increased while the angle between lattice parameters decreased with increasing CuO content. Grain size of the ceramics increased with increasing CuO content. Maximum dielectric con-

stant of the ceramics decreased with increasing CuO content up to 0.4 mol.% but then abruptly increased to highest value with an addition of 2.0 mol.% CuO. Dielectric loss tangent did not significantly change with an addition of CuO up to 2.0 mol.% but it significantly increased in PMNT/4.0 mol.% CuO sample. Temperature of maximum dielectric constant and depolarization temperature increased while diffuseness parameters decreased with increasing CuO content. Remanent polarization and coercive field showed an increasing trend up to $x = 0.2$ mol.% CuO. For $x > 0.2$ mol.%, remanent polarization did not increase further while coercive field gradually decreased with increasing CuO content. Maximum induced strain and electrostrictive coefficient increased with increasing CuO concentration and reached maximum in PMNT/2.0 mol.% CuO sample. With an addition of CuO, polar order of PMNT ceramics was enhanced while relaxor behavior was reduced. The enhanced long-range polarization and the resulting properties were attributed to effects of lattice distortion by partial substitution of Cu^{2+} for the ions on B-site of PMNT lattice.

Acknowledgements

This work was supported by the Thailand Research Fund (TRF) and the National Research University Project under Thailand's Office of the Higher Education Commission (OHEC), the Faculty of Science and the Graduate School, Chiang Mai University. M.P. would also like to thank the financial support from the TRF through the Royal Golden Jubilee Ph.D. Program. The work at Simon Fraser University was supported by the U.S. Office of Naval Research (ONR, Grants No. N00014-11-1-0552 and N00014-12-1-1045) and the Natural Science and Engineering Research Council of Canada (NSERC).

References

- [1] A.S. Mischenko, Q. Zhang, R.W. Whatmore, J.F. Scott, N.D. Mathur, *Appl. Phys. Lett.* 89 (2006) 242912/1–3.
- [2] H. Cheng, W. Zhou, H. Du, F. Luo, D. Zhu, D. Jiang, B. Xu, *J. Alloys Comp.* 579 (2013) 192–197.
- [3] R.-H. Liang, W.-Z. Zhang, M. Gao, L. Wang, X.-L. Dong, *Ceram. Int.* 39 (2013) 563–569.
- [4] A.A. Bokov, Z.-G. Ye, *J. Mater. Sci.* 41 (2006) 31–52.
- [5] G. Du, R. Liang, J. Wang, L. Wang, W. Zhang, G. Wang, X. Dong, *Ceram. Int.* 39 (2013) 9299–9303.
- [6] J. Hao, W. Bai, W. Li, B. Shen, J. Zhai, *J. Appl. Phys.* 114 (2013) 044103/1–12.
- [7] F. Wang, C. Jin, Q. Yao, W. Shi, *J. Appl. Phys.* 114 (2013) 027004/1–5.
- [8] Z.-G. Ye, Y. Bing, J. Gao, A.A. Bokov, P. Stephens, B. Noheda, G. Shirane, *Phys. Rev. B* 67 (2003) 104104/1–8.
- [9] Y.D. Hou, M.K. Zhu, H. Wang, B. Wang, H. Yan, C.S. Tian, *Mater. Sci. Eng. B* 110 (2004) 27–31.
- [10] B. Fang, N. Jiang, C. Ding, Q. Du, *J. Ding Phys. Status Solidi A* 209 (2012) 254–261.
- [11] J.-K. Kang, D.-J. Heo, V.Q. Nguyen, H.-S. Han, J.-S. Lee, K.-K. Ahn, *J. Kor. Phys. Soc.* 61 (2012) 899–902.
- [12] M. Promsawat, A. Watcharaporn, H.N. Tailor, S. Jiansirisomboon, Z.-G. Ye, *J. Appl. Phys.* 113 (2013) 204101/1–6.
- [13] S.L. Swartz, T.R. Shrout, *Mater. Res. Bull.* 17 (1982) 1245–1250.
- [14] J.C. Bruno, A.A. Cavaleiro, M.A. Zaghe, M. Cilense, J.A. Varela, *Mater. Chem. Phys.* 84 (2004) 120–125.
- [15] R.D. Shannon, *J. Appl. Phys.* 73 (1993) 348–366.
- [16] M. Promsawat, A. Watcharaporn, S. Jiansirisomboon, *Ceram. Int.* 39 (2013) 569–573.
- [17] M. Promsawat, Y.Y. Jenny, A. Wong, S. Watcharaporn, Jiansirisomboon, *Mater. Chem. Phys.* 141 (2013) 549–552.
- [18] J.H. Chen, Y.C. Liou, *Ceram. Int.* 30 (2004) 157–162.
- [19] R. Wongmaneeerung, A. Rittidech, O. Khamman, R. Yimnirun, S. Ananta, *Ceram. Int.* 35 (2009) 125–129.
- [20] Y. Lee, J. Yoo, K. Lee, I. Kim, J. Song, Y.-W. Park, *J. Alloys Comp.* 506 (2010) 872–876.
- [21] B. Fang, C. Ding, J. Wu, Q. Du, *J. Ding Phys. Status Solidi A* 208 (2011) 1641–1645.
- [22] C.-L. Huang, K.-H. Chiang, *Mater. Res. Bull.* 39 (2004) 1701–1708.
- [23] S. Fushimi, T. Ikeda, *J. Am. Ceram. Soc.* 50 (1967) 129–132.
- [24] X.-G. Tang, H.L.-W. Chan, *J. Appl. Phys.* 97 (2005) 034109/1–6.
- [25] A.A. Bokov, Z.-G. Ye, *Solid State Commun.* 116 (2000) 105–108.
- [26] A.A. Bokov, Z.-G. Ye, *Phys. Rev. B* 74 (2006) 132102/1–4.
- [27] S.B. Majumder, D.C. Agrawal, Y.N. Mohapatra, R.S. Katiyar, *Integr. Ferroelectr.* 29 (2000) 63–74.
- [28] K. Uchino, S. Nomura, L.E. Cross, J. Jang, R.E. Newnham, *J. Appl. Phys.* 51 (1980) 1142–1145.
- [29] A. Hall, M. Allahverdi, E.K. Akdogan, A. Safari, *J. Electroceram.* 15 (2005) 143–150.
- [30] B.M. Jin, J. Kim, S.C. Kim, *Appl. Phys. A* 65 (1997) 53–56.
- [31] G.H. Haertling, *J. Am. Ceram. Soc.* 82 (1999) 797–818.
- [32] D. Shihua, S. Tianxiu, Y. Xiaojing, L. Guanghua, *Ferroelectrics* 402 (2010) 55–59.



Contents lists available at ScienceDirect

Journal of Alloys and Compounds

journal homepage: www.elsevier.com/locate/jalcom

Dielectric, ferroelectric and electric field-induced strain behavior of $\text{Ba}(\text{Ti}_{0.90}\text{Sn}_{0.10})\text{O}_3$ -modified $\text{Bi}_{0.5}(\text{Na}_{0.80}\text{K}_{0.20})_{0.5}\text{TiO}_3$ lead-free piezoelectrics

Pharatree Jaita^a, Anucha Watcharapasorn^{a,b}, David P. Cann^c, Sukanda Jiansirisomboon^{a,b,*}^a Department of Physics and Materials Science, Faculty of Science, Chiang Mai University, Chiang Mai 50200, Thailand^b Materials Science Research Center, Faculty of Science, Chiang Mai University, Chiang Mai 50200, Thailand^c Materials Science, School of Mechanical, Industrial and Manufacturing Engineering, Oregon State University, Corvallis, OR 97331, USA

ARTICLE INFO

Article history:

Received 21 October 2013

Received in revised form 6 January 2014

Accepted 25 January 2014

Available online 3 February 2014

Keywords:

Ceramics

Sintering

Piezoelectricity

X-ray diffraction

Strain

ABSTRACT

Lead-free piezoelectric ceramics of $(1-x)\text{Bi}_{0.5}(\text{Na}_{0.80}\text{K}_{0.20})_{0.5}\text{TiO}_3$ - $x\text{Ba}(\text{Ti}_{0.90}\text{Sn}_{0.10})\text{O}_3$ or $(1-x)\text{BNKT}$ - $x\text{BTS}$ (when $x = 0$ – 0.20 mol fraction) were investigated. Optimum sintering temperature was found to be 1125°C at which all compositions had relative densities 98–99% of their theoretical values. All compositions exhibited a single perovskite structure. The unit cell size expansion was observed as BTS content increased. A slight reduction of grain size was noticeable when small amount of BTS was added. The BNKT - 0.05BTS sample had a large electric field-induced strain (S_{max}) of 0.36% which corresponded to the normalized strain coefficient (d'_{33}) of 649 pm/V. The highest piezoelectric coefficient ($d_{33} = 215$ pC/N) with good dielectric ($\epsilon_r = 1721$, $\tan \delta = 0.0724$ and $T_c = 333^\circ\text{C}$) and ferroelectric properties ($P_r = 20.49$ $\mu\text{C}/\text{cm}^2$, $R_{90} = 0.87$) were obtained for BNKT - 0.10BTS sample, suggesting that this composition had a potential to be one of the promising lead-free piezoelectric candidates for further use in actual applications.

© 2014 Elsevier B.V. All rights reserved.

1. Introduction

At present, the most widely used piezoelectric materials are $\text{Pb}(\text{Zr}, \text{Ti})\text{O}_3$ -based ceramics because of their superior piezoelectric properties [1]. PZT with high dielectric and piezoelectric exists at the morphotropic phase boundary (MPB) between rhombohedral and tetragonal phases [2]. Therefore, MPB composition ceramics for piezoelectric transducer, sensor and resonator have been widely utilized due to their excellent piezoelectric effect [3–5]. However, devices made from these compounds pose some environmental concerns. Many manufacturers are currently being constrained to reduce and ultimately eliminate lead content in their devices [6]. Moreover, upcoming environmental regulations in Europe, parts of Asia, and US prohibit the use of lead-based materials because of their toxicity. For this reason, alternative lead-free piezoelectric systems analogous to PZT are urgently desired [7,8].

Compared to PZT-based piezoelectric ceramics, bismuth sodium potassium titanate, $\text{Bi}_{0.5}(\text{Na}_{1-x}\text{K}_x)_{0.5}\text{TiO}_3$ or BNKT is currently of interest as a candidate for lead-free piezoelectric applications

[9]. It has received considerable attention due to its excellent ferroelectric and piezoelectric properties near rhombohedral-tetragonal MPB region. Sasaki et al. [10] have already reported on BNKT solid solution. This system's MPB structure at $0.16 \leq x \leq 0.2$ showed relatively high piezoelectric coefficient with piezoelectric constant d_{33} of 151 pC/N and d_{31} of 46.9 pC/N. In order to further improve piezoelectric properties of BNKT ceramic, incorporation of various dopants and formation of solid solutions with other compounds such as SrTiO_3 [11], $\text{Ba}(\text{Zr}_{0.04}\text{Ti}_{0.96})\text{O}_3$ [12], MnCO_3 [13] and CeO_2 [14] have been intensively carried out.

Previously, barium stannate titanate, $\text{Ba}(\text{Ti}_{1-x}\text{Sn}_x)\text{O}_3$ or BTS, as well as doped- BaTiO_3 compounds were studied by Smolensky [15] as prototypes of ferroelectric material with diffused phase transition. BTS had a perovskite structure with ABO_3 formula. Replacing partially Ti^{4+} with Sn^{4+} was found to decrease Curie temperature (T_c) and improve dielectric behavior. The BTS ceramics may be used in various applications because the Curie temperature (T_c) can be widely shifted by changing Sn content. In 1996, $\text{Ba}(\text{Ti}_{1-x}\text{Sn}_x)\text{O}_3$ ceramics had been extensively studied by Yasuda et al. [16]. They reported that at $x > 0.10$, a change in phase transition from normal ferroelectric to relaxor was observed. In normal ferroelectric region ($x < 0.1$), the maximum dielectric constant at room temperature (ϵ_r) of 7500 and T_c of 60°C was found for $\text{Ba}(\text{Ti}_{0.9}\text{Sn}_{0.1})\text{O}_3$ sample. Later in 2011, Cai et al. [17] investigated

* Corresponding author at: Department of Physics and Materials Science, Faculty of Science, Chiang Mai University, Chiang Mai 50200, Thailand. Tel.: +66 53 941921x631; fax: +66 53 943445.

E-mail address: sukandajian@cmu.ac.th (S. Jiansirisomboon).

<http://dx.doi.org/10.1016/j.jallcom.2014.01.183>

0925-8388/© 2014 Elsevier B.V. All rights reserved.

phase, microstructure, dielectric and ferroelectric properties of $\text{Ba}(\text{Ti}_{1-x}\text{Sn}_x)\text{O}_3$ ceramics. They found that BTS ceramics had a tetragonal structure when $x = 0$ –0.10 but transformed to cubic at $x = 0.15$ –0.30. The incorporation of Sn^{4+} limited grain growth in BTS ceramics and T_c decreased with increasing amount of Sn. For ferroelectric measurement, an enhancement in the diffuseness of phase transition and coercive electric field (E_c) was observed when $x = 0.10$ –0.20 while the remanent polarization (P_r) decreased with increasing Sn content. The highest room temperature dielectric constant (ϵ_r) of 7000 and $2P_r$ of $1.4 \mu\text{C}/\text{cm}^2$ and $2E_c$ of $0.5 \text{ kV}/\text{cm}$ with lowest dielectric loss were obtained for $\text{Ba}(\text{Ti}_{0.9}\text{Sn}_{0.1})\text{O}_3$ sample. Singh et al. [18,19] also found the decreasing trend in electromechanical coupling factor (k_p) and unipolar strain as Sn content increased. An increasing trend in bulk density and piezoelectric charge constant (d_{33}) with increasing Sn content were also observed in these ceramics.

However, detailed investigation on the binary system of $\text{Bi}_{0.5}(\text{Na}_{0.80}\text{K}_{0.20})_{0.5}\text{TiO}_3$ – $\text{Ba}(\text{Ti}_{0.90}\text{Sn}_{0.10})\text{O}_3$ or BNKT–BTS compared with pure BNKT ceramic have not been done so far. This research thus aimed to fabricate the binary system of BNKT–BTS ceramics. The role of BTS concentration on density, phase evolution, microstructure, electrical properties (dielectric, ferroelectric and piezoelectric) and electric field-induced strain behavior of BNKT ceramic were investigated and discussed in details.

2. Experimental details

$\text{Bi}_{0.5}(\text{Na}_{0.80}\text{K}_{0.20})_{0.5}\text{TiO}_3$ or BNKT and $\text{Ba}(\text{Ti}_{0.90}\text{Sn}_{0.10})\text{O}_3$ or BTS powders were separately prepared by a conventional mixed oxide method. The analytical grade reagents of Bi_2O_3 (98%, Fluka), Na_2CO_3 (99.5%, Carlo Erba), TiO_2 (99%, Riedel-de Haën), K_2CO_3 (99%, Riedel-de Haën), BaCO_3 (98.5%, Fluka) and SnO_2 (99.9%, Sigma-Aldrich) were used as starting materials. All carbonate powders were firstly dried at 120°C for 24 h in order to remove the residual moisture. The raw materials of BNKT and BTS were stoichiometrically weighted, ball milled for 24 h in an ethanol solution and dried in an oven. Dried BNKT and BTS powders were separately calcined at 900°C and 1200°C for 2 h, respectively. BNKT and BTS calcined powders were then weighed, mixed and dried again to produce the mixed powders of $(1-x)\text{Bi}_{0.5}(\text{Na}_{0.80}\text{K}_{0.20})_{0.5}\text{TiO}_3$ – $x\text{Ba}(\text{Ti}_{0.90}\text{Sn}_{0.10})\text{O}_3$ or $(1-x)\text{BNKT}$ – $x\text{BTS}$ (when $x = 0, 0.05, 0.10, 0.15$ and 0.20 mol fraction). A few drops of 3 wt% polyvinyl alcohol (PVA) binders were then added to the mixed powders before being uniaxially pressed into 10 mm diameter discs. These pellets were covered with their own powders and then sintered at 1050 – 1175°C for 2 h with a heating/cooling rate of $5^\circ\text{C}/\text{min}$.

X-ray diffractometer (XRD-Phillip, X-pert) was used to identify phase of both powders and ceramics. Bulk density was measured in accordance with Archimedes' method. Theoretical densities of all samples were calculated based on the theoretical densities of BNKT ($5.84 \text{ g}/\text{cm}^3$) [20] and BT ($6.01 \text{ g}/\text{cm}^3$) [21]. Linear shrinkage of all samples was also measured. Scanning electron microscope (SEM, JEOL JSM-6335F) was used to determine microstructural features of the ceramics. Grain size was determined by a mean linear interception method. Before being subjected to electrical characterization, all samples were carefully polished to 1 mm thickness to obtain parallel scratch-free surface. Silver paste was fired onto two sides of each sample at 600°C for 15 min to form electrodes. Dielectric properties as a function of temperature (25 – 500°C) were carried out using 4192A LCR-meter connected to a high temperature furnace. A standard Sawyer-Tower circuit (Radiant Precision High Voltage Interface) was used to measure polarization–electric field (P – E) hysteresis loop. The AC electric field of $55 \text{ kV}/\text{cm}$ and a frequency of 1 Hz was applied to each sample. Remanent polarization (P_r), maximum polarization (P_{max}), coercive field (E_c), maximum electric field (E_{max}) and loop squareness (R_{sq}) values were determined from hysteresis loops. Prior to the measurement of piezoelectric properties, each sample was poled in silicone oil bath at 60°C under DC electric field of $5 \text{ kV}/\text{mm}$ for 15 min. Piezoelectric coefficient (d_{33}) was recorded from 1-day aged samples using d_{33} -meter (KCF technologies, S5865). Room temperature strain–electric field (S – E) were obtained using an optical displacement sensor (Fotonic Sensor, MTI-2100) combined with radiant ferroelectric system. The high electric field of $55 \text{ kV}/\text{cm}$ and frequency of 0.1 Hz was applied for each sample to determine the butterfly curve.

3. Results and discussion

After sintering the pellet-shaped samples at various temperatures (1050 – 1175°C), it was found that at 1175°C , doped samples containing 5–20 mol% BTS started to melt. Thus, these sintered

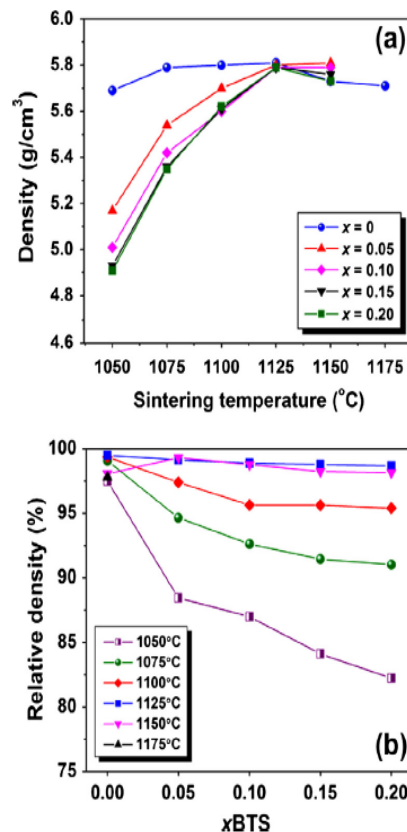


Fig. 1. (a) Plots of density as a function of sintering temperature and (b) plots of relative density as a function of composition of $(1-x)\text{BNKT}$ – $x\text{BTS}$ ceramics.

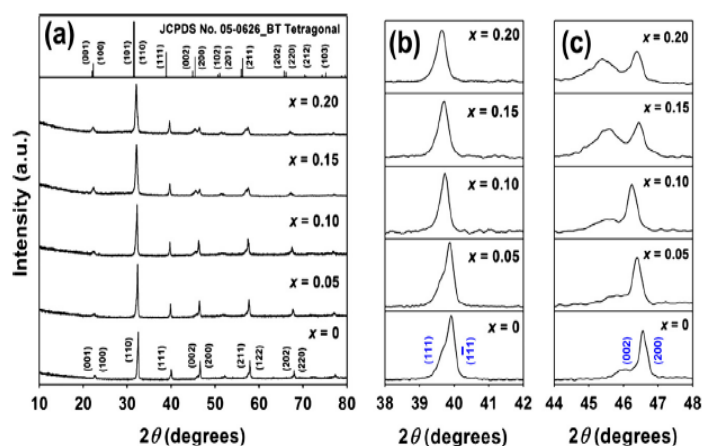
samples were excluded from further characterization. Fig. 1(a) shows density variation of $(1-x)\text{BNKT}$ – $x\text{BTS}$ ceramics plotted as a function of sintering temperature. The data clearly showed that variation of sintering temperature had significant influence on sample density. As the temperature was increased, the density of all samples rapidly increased, especially for doped samples, and reached their maximum values at 1125°C . Above this temperature, the high density values were maintained for doped samples while it started to drop for pure BNKT. The evaporation of volatile alkali metal oxides and partial melting at high temperature were likely the main causes for density reduction. Therefore, the optimum sintering temperature of BNKT–BTS system was found to be 1125°C at which all samples had densities ranging in between 5.79 and $5.81 \text{ g}/\text{cm}^3$, corresponding to 98–99% of their theoretical values. In addition, the variation of linear shrinkage with increasing sintering temperature showed similar trend to that of density value. The maximum linear shrinkage of 17–19% was also found at 1125°C . Plots of relative density as a function of composition of $(1-x)\text{BNKT}$ – $x\text{BTS}$ ceramics are shown in Fig. 1(b). Based on density data at the optimum sintering temperature of 1125°C , the data clearly showed that the variation of composition had no significant influence on sample density. The addition of BTS into BNKT ceramic caused a slight decrease in samples' relative density. This result was also correlated with linear shrinkage values as shown in Table 1. The linear shrinkage value slightly decreased with increasing BTS content. However, all sample achieved their maximum density values at this temperature and the values were rather similar (see Table 1). Thus, the samples sintered at 1125°C were selected for further characterization.

X-ray diffraction patterns of optimally sintered $(1-x)\text{BNKT}$ – $x\text{BTS}$ ceramics with $2\theta = 10$ – 80° are shown in Fig. 2(a). All studied

Table 1

Physical, microstructure and dielectric properties of $(1-x)\text{BNKT}-x\text{BTS}$ ceramics sintered at 1125 °C.

x	Density (g/cm^3)	Relative density (%)	Linear shrinkage (%)	c/a	Grain size (μm)	ϵ_r^a	$\tan\delta^a$	T_d^b (°C)	T_m^b (°C)
0	5.81 ± 0.01	99.48 ± 0.06	18.80 ± 0.01	1.0110	0.60 ± 0.09	1419	0.0479	179	320
0.05	5.80 ± 0.02	99.14 ± 0.09	18.16 ± 0.09	1.0122	0.40 ± 0.04	1600	0.0600	153	321
0.10	5.79 ± 0.04	98.88 ± 0.08	17.52 ± 0.02	1.0137	0.44 ± 0.04	1721	0.0724	159	333
0.15	5.79 ± 0.02	98.77 ± 0.09	17.03 ± 0.06	1.0176	0.57 ± 0.08	1482	0.0698	178	322
0.20	5.79 ± 0.01	98.66 ± 0.09	17.00 ± 0.03	1.0191	0.60 ± 0.09	1465	0.0723	181	295

^a Dielectric data obtained at room temperature and a frequency of 1 kHz.^b Dielectric data obtained at high temperature (25–500 °C) and a frequency of 10 kHz.Fig. 2. X-ray diffraction patterns of $(1-x)\text{BNKT}-x\text{BTS}$ ceramics sintered at 1125 °C where (a) $2\theta = 10\text{--}80^\circ$, (b) $2\theta = 38\text{--}42^\circ$ and (c) $2\theta = 44\text{--}48^\circ$.

compositions possessed a single phase of perovskite structure. No second phases or impurities could be detected, confirming that the starting reagents completely reacted to form the final compounds. This suggested that BTS had diffused into BNKT lattice to form complete solid solutions during sintering process [22]. The position of all peaks slightly shifted to lower 2θ angles in comparison with those of pure BNKT. This observation implied an expansion of lattice constant, resulting in an enlargement of unit cell size. It was expected that Ba^{2+} (1.42 Å) successfully substituted into A-site position [Bi^{3+} (1.17 Å), Na^+ (1.18 Å), K^+ (1.33 Å)] and Sn^{4+} (0.81 Å) successfully entered into B-site position [Ti^{4+} (0.74 Å)] to form BNKT-BTS solid solutions [23]. An increase of peak shift resulted in an increase of lattice energy and finally induced a phase transformation in order to stabilize the structure. Similar peak shifting behavior by partial substitution of Ba^{2+} for $[\text{Bi}_{0.5}(\text{Na}_{0.80}\text{K}_{0.20})]^{2+}$ and Zr^{4+} for Ti^{4+} was also observed in BNKT-BZT system studied by Chen and Hu [12]. They found (110) peak shifted to lower 2θ angles, indicating a consecutive increase in lattice constant with increasing BZT fraction. Lower X-ray scan speed in narrower ranges was performed particularly at $2\theta = 38\text{--}42^\circ$ and $2\theta = 44\text{--}48^\circ$ and the results are shown in Fig. 2(b) and (c), respectively. BNKT ceramic presented features of mixed rhombohedral–tetragonal symmetry but showed a domination of rhombohedral over tetragonal structure as evidenced by a slight splitting of (111)/(1 $\bar{1}\bar{1}$) rhombohedral peaks at $2\theta \sim 40^\circ$ [24,25]. This result was consistent with previous work on BNT-BKT ceramics reported by Sasaki et al. [10] who found a relatively broad MPB region in the range of $x = 0.16\text{--}0.20$ between rhombohedral BNT and tetragonal BKT phases. The mixed rhombohedral–tetragonal phases were maintained even when BTS was added into BNKT up to 10 mol%. At this composition, the peak at $2\theta \sim 46^\circ$ was slightly asymmetrical and featured with slightly splitting of (200)/(002) peaks. The separation of (002)/(200) peaks were significantly intensified with further increasing BTS up to 15–20 mol%. The (002) peak became

more dominant whereas (200) peak became weaker which indicated the crystal structure transformed to tetragonal-rich phase. This behavior became clearer after lattice parameter analysis which indicated an increase in tetragonality (c/a) value as shown in Table 1. This increasing trend in c/a value clearly indicated that the addition of BTS increased the lattice anisotropy of BNKT-BTS systems [26].

Typical surfaces of $(1-x)\text{BNKT}-x\text{BTS}$ ceramics sintered at 1125 °C are shown in Fig. 3. It can be seen that all samples were well sintered and dense with having relative density higher than 98% of their theoretical density. The regular grain shape and grain boundaries clearly occurred in all samples. Average grain size values of all samples are listed in Table 1. Grain sizes were measured and calculated based on a mean linear intercept method. This method was the quantitative measurement of grain size within dense uniform structures and it was best suited where the boundaries of each grain were relatively easy to determine. The determination of the linear intercept for each line on each image was taken along with overall average values. Based on the XRD results, BNKT showed mixed rhombohedral (major) and tetragonal (minor) phases and had a cubic-like shape grains with side length of around 0.60 μm . Addition of 5 mol% BTS caused small expansion of overall crystal structure with a reduction in grain size from 0.60 μm to around 0.40 μm . Noticeably, grains with sharp corners were still present. We believe that the observed grain morphology and slightly reduced grain size for this sample were due the solute drag effect of dissolved BTS [27,28] since diffusivity of solute atoms was normally different from those of host atoms. From 10 mol% and higher content of BTS, it seemed that tetragonal phase started to have more influence on grain morphology and grain size. Therefore, with further increasing BTS concentration, the grain size was slightly bigger with more equiaxed grain morphology.

Temperature dependence of dielectric constant (ϵ_r) and dielectric loss ($\tan\delta$) of all samples measured at various frequencies

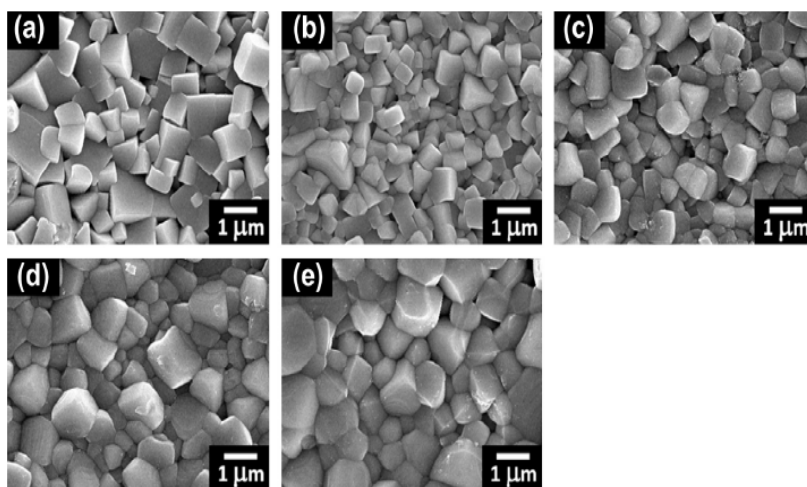


Fig. 3. SEM micrographs of $(1-x)\text{BNKT}-x\text{BTS}$ ceramics sintered at $1125\text{ }^{\circ}\text{C}$ where (a) $x=0$, (b) $x=0.05$, (c) $x=0.10$, (d) $x=0.15$ and (e) $x=0.20$.

are shown in Fig. 4. All specimens showed two transition points similar to other works on BNT-based ceramics which corresponded to the depolarization temperature (T_d) and maximum temperature (T_m) [10,24]. There was still a controversy in the interpretation of T_d but it was long believed to be the ferroelectric to antiferroelectric phase transition point on heating. However, T_d was recently interpreted as the nonergodic relaxor (NR) to ergodic relaxor (ER) phase transition point [29,30]. For some BNT-based piezoelectric ceramics, T_c was also frequently reported in the literature although, because of the relaxor behavior of these materials, the temperature of maximum dielectric constant, T_m , could not be considered as the Curie point since there was no structural phase transition involved and Curie–Weiss law did not apply above this temperature [20]. In some BNT-based systems, it was found that there was a weak polar intermediate phase of ergodic relaxor (ER), which occurred between T_d and T_m , and so called nonergodic relaxor (NR) phase below T_d [30]. Although the dielectric constant–temperature curves for BNKT–BTS system in this study were similar to those of BNT-based compounds [30], no polar nano-regions had been directly observed and no freezing temperature (T_f) and Burns temperature (T_B) had been found or calculated. Therefore, the discussion below still used the values of T_d and T_m only to indicate the transition points observed in the dielectric constant data and how they were affected by compositional changes. It can be seen that the ϵ_r increased with increasing temperature, jumped at T_d , reached a maximum value at T_m and then gradually decreased with further increasing the temperature. This feature intrinsically came from pure BNT, which was reported to have two diffuse structural phase transition at $\sim 200\text{ }^{\circ}\text{C}$ and $\sim 320\text{ }^{\circ}\text{C}$ [15]. From Fig 4(a), dielectric curves of pure BNKT ceramic exhibited broad T_d and T_m peaks. The addition of 5 mol% BTS slightly shifted T_d to lower temperature of $153\text{ }^{\circ}\text{C}$ while further increasing BTS up to 20 mol% shifted T_d to higher temperature of $181\text{ }^{\circ}\text{C}$ (see Table 1). The slight decrease in T_d value could be a consequence of ferroelectric order destabilization and may be associated with the possible presence of non-polar phase in this sample [24]. Similar behavior was observed in recent investigations of Zr-modified BNKT ceramics [5], where T_d decreased with increasing Zr content in BNKT ceramics, resulting in the stabilization of non-polar phase. However, T_m peak gradually broadened, suggesting that BTS induced a diffuse phase transition in BNKT–BTS system and attributed to disordering of A and/or B-site cation [31,32]. Based on dielectric data at a frequency of 10 kHz in Table 1, BNKT ceramic in this study had T_d and T_m of $179\text{ }^{\circ}\text{C}$ and $320\text{ }^{\circ}\text{C}$, respectively. Sasaki et al. [10] also found T_m

value of BNKT ceramic $\sim 317\text{ }^{\circ}\text{C}$. T_m increased to a maximum value of $333\text{ }^{\circ}\text{C}$ for BNKT–0.10BTS sample. With further increasing of BTS greater than 10 mol%, T_m started to slightly decrease and T_d of all ceramics varied in between 153 and $181\text{ }^{\circ}\text{C}$. The reported ionic radius of Ba^{2+} (1.42 \AA) was larger than that of Bi^{3+} (1.17 \AA), Na^{+} (1.18 \AA), K^{+} (1.33 \AA) and Sn^{4+} (0.81 \AA) was larger than Ti^{4+} (0.74 \AA) [23]. BNKT–BTS was a complex system having both A-site and B-site substitution. In this case, B-site was isovalent substitution with larger ion (i.e. Sn^{4+} replacing Ti^{4+}). B-site substitution alone could result in a decrease in T_c , an increased in room temperature dielectric constant and limited grain growth (as observed for Sn-doped BaTiO_3 [15–19]). However, the more complicated A-site substitution in which Ba^{2+} could substitute $\text{Na}^{+}/\text{K}^{+}$ as donor or Bi^{3+} as acceptor, also played a part in determining the overall effect on structural changes. It was expected that random site substitution should occur with possible existence of localized polar regions and domains. Hence, in our results, the direct effect of ionic site substitution and charge-compensation induced defects may be difficult to discern. It was more likely that the effect of structures, domains and domain wall motion largely contributed to observed piezoelectric, dielectric and ferroelectric properties. Similar effects from enlargement of unit cell size and phase transition on dielectric properties were observed in $(\text{Bi}_{0.5}\text{Na}_{0.5})\text{TiO}_3$ – $(\text{Ba}, \text{Sr})\text{TiO}_3$ system previously investigated by Lee et al. [33]. They found that Ba^{2+} (1.42 \AA) and Sr^{2+} (1.44 \AA) with larger ionic radii diffused into BNT lattice, i.e. Bi^{3+} (1.17 \AA) and Na^{+} (1.18 \AA), resulting in an enlargement of lattice parameters and consequently reducing the T_m value.

Fig. 5 shows polarization–electric field (P – E) hysteresis loops of $(1-x)\text{BNKT}-x\text{BTS}$ system obtained at room temperature ($25\text{ }^{\circ}\text{C}$). The samples were subjected to an external electric field of 55 kV/cm and a frequency of 1 Hz . Higher values of applied voltage caused the samples to undergo a dielectric breakdown. For more details, P_r , E_c and R_{sq} values are also listed in Table 2. The well saturated P – E hysteresis loops were observed for all samples. BNKT ceramic displayed a typical ferroelectric behaviour with square shape, indicating strong ferroelectric order. It had maximum values of $P_r = 30.48\text{ }\mu\text{C/cm}^2$, $E_c = 31.49\text{ kV/cm}$ and $R_{sq} = 1.12$, which were all in good agreement with those from the literature [9,34]. Addition of BTS had a significant influence on ferroelectric hysteresis loops. This caused the ceramics to show softer ferroelectric hysteresis behavior which corresponded to decreasing P_r and E_c values. When 5 mol% BTS was added into BNKT ceramic, the P_r and E_c values rapidly decreased. P_r drastically decreased from

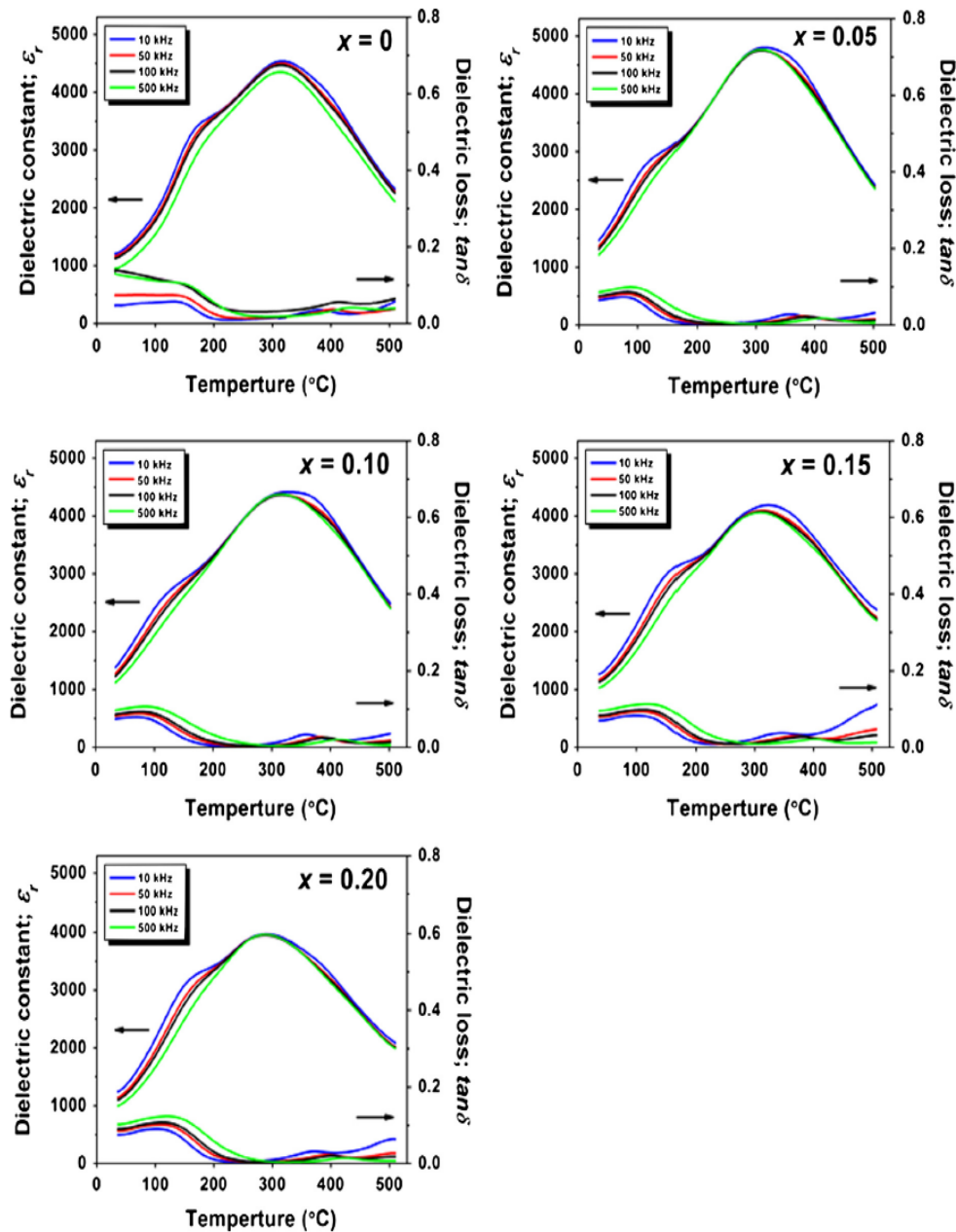


Fig. 4. Temperature dependence on dielectric constant (ϵ_r) and dielectric loss ($\tan\delta$) of $(1-x)\text{BNKT}-x\text{BTS}$ ceramics sintered at 1125°C measured at various frequencies.

$30.48 \mu\text{C}/\text{cm}^2$ to $12.80 \mu\text{C}/\text{cm}^2$ and E_c decreased from $31.49 \text{ kV}/\text{cm}$ to $10.90 \text{ kV}/\text{cm}$. It indicated that the ferroelectric order of BNKT was disturbed by chemical modification with BTS. As of current data and recent literature reviews related to relaxor-like behavior of non-lead piezoelectric compounds, the addition of 5 mol% BTS seemed to induce an existence of non-polar phase (region) and the formation of defect dipoles in parent BNKT ferroelectric material. The presence of defect dipoles generated internal bias field which resisted and counteracted the effect of external field, causing P - E hysteresis curve to become constricted [24,35]. This also corresponded to a significant decrease in both P_r and E_c values and resulted in a slight pinched-type loop with relatively small remanent polarization observed in this composition as shown in Fig. 5(b). Recently, Jo et al. [36] monitored the total volume change during the electric field-induced phase transition in $(\text{K}_{0.5}\text{Na}_{0.5})\text{-NbO}_3$ -modified $(\text{Bi}_{0.5}\text{Na}_{0.5})\text{TiO}_3$ - BaTiO_3 system. They proposed

that a pinch-type character in P - E loop originated from an existence of non-polar phase which could induce the destabilization of ferroelectric order and noticeable change from normal ferroelectric hysteresis loop to a pinch-type hysteresis shape. This behavior would be expected to cause significant enhancement of electric field-induced strain response in BNKT-0.05BTS sample. However, E_c and P_r values increased considerably with increasing BTS greater than 5 mol%. The hysteresis loops exhibited back to a typical square shape, indicating again a strong ferroelectric behavior. The addition of 10–20 mol% BTS showed rather similar values of P_r (20.49 – $20.88 \mu\text{C}/\text{cm}^2$) whereas R_{sq} were found to be in a range of 0.87 – 0.89 .

Temperature dependent polarization–electric field (P - E) hysteresis loops of $(1-x)\text{BNKT}-x\text{BTS}$ ceramics, measured at $55 \text{ kV}/\text{cm}$ and a frequency of 1 Hz , are shown in Fig. 6. All samples showed a typical ferroelectric shape consistent with other reports [9,37]

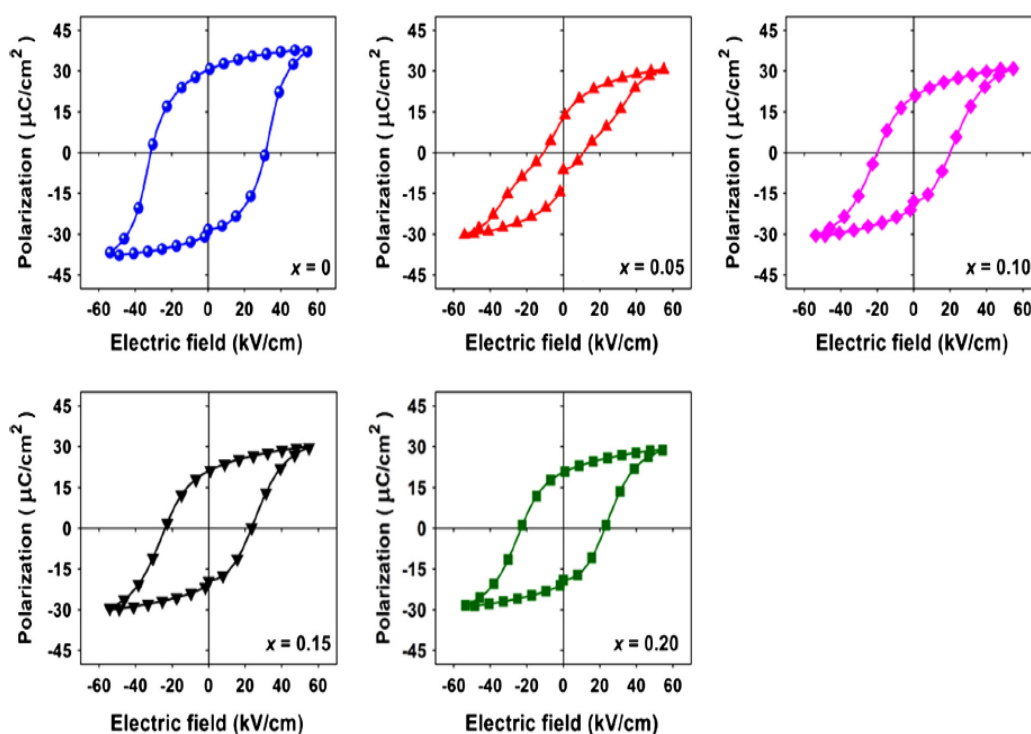


Fig. 5. Polarization–electric field (P – E) hysteresis loops of $(1-x)\text{BNKT}$ – $x\text{BTS}$ ceramics sintered at 1125°C , measured at 55 kV/cm and a frequency of 1 Hz .

Table 2

Ferroelectric and piezoelectric properties of $(1-x)\text{BNKT}$ – $x\text{BTS}$ ceramics sintered at 1125°C .

x	P_r^a ($\mu\text{C/cm}^2$)	E_c^a (kV/cm)	R_{90}^a	d_{33} (pC/N)	S_{max} (%)	S_{neg} (%)	d_{33}^* (pm/V)
0	30.48	31.49	1.12	178	0.23	−0.12	418
0.05	12.80	10.90	0.47	174	0.36	−0.02	649
0.10	20.49	19.92	0.87	215	0.25	−0.07	450
0.15	20.88	23.55	0.89	153	0.23	−0.07	409
0.20	20.53	23.09	0.89	137	0.21	−0.07	383

^a Ferroelectric data obtained at room temperature (25°C) and a frequency of 1 Hz .

and well-saturated P – E loops at room temperature (25°C). When the temperature increased to 50°C , the P_r and E_c values slightly decreased for all compositions but the hysteresis loops still maintained the square shape. With further increasing temperature to 100 – 125°C , the P_r , E_c and P_{max} values dramatically decreased. The narrower P – E loop was observed while the square loop disappeared. With increasing temperature up to 150°C , the P_r and E_c values further decreased close to zero and led to a narrower pinched-type P – E loop. The observation of pinched-type loop at high temperature may be due to the weakening of nonergodic relaxor (NR) state and enhancing ergodic relaxor (ER) state. The constricted or pinched-type P – E loop have previously been observed in BNT-based ceramics at high temperature [37]. The coexistence of nonergodic relaxor (NR) and ergodic relaxor (ER) states seemed to occur near 150°C which was close to the measurement of T_d value ~ 153 – 181°C as shown in Table 1. Similar to that observed in the ternary system of BNT–BKT–BT studied by Zhang et al. [38] who found an appearance of ER state near T_d . Many researchers considered an appearance of a pinched-type hysteresis loop near T_d to be nonergodic relaxor (NR) to ergodic relaxor (ER) phase transition which resulted in a large electric-field induced strain [29,30].

Fig. 7 displays the bipolar electric field-induced strain curves of $(1-x)\text{BNKT}$ – $x\text{BTS}$ ceramics measured at room temperature. The measurement was done under an electric field of 55 kV/cm and a

frequency of 0.1 Hz . The maximum strain (S_{max}), negative strain (S_{neg} , i.e. the difference between zero-field strain and the lowest strain and only visible in the bipolar cycle [38]), and normalized strain coefficient ($d_{33}^* = S_{\text{max}}/E_{\text{max}}$) are also listed in Table 2. The variation of S_{max} values with increasing BTS content showed a similar trend to that of d_{33} values. BNKT ceramic without any addition of BTS exhibited a typical butterfly-shaped strain loop with S_{max} of 0.23% and calculated d_{33}^* of 418 pm/V , indicating that the ferroelectric domain switching was involved at E_c where the largest S_{neg} of -0.12% was observed. On the contrary, BNKT– 0.05BTS sample exhibited drastic deviation from a typical ferroelectric behavior. This was evidenced by the drastic reduction of S_{neg} from -0.12% for pure BNKT to around -0.02% for BNKT– 0.05BTS sample. In addition, a pronounced enhancement in the maximum positive strain response, i.e. S_{max} of 0.36% , was observed. This could be related to the degree of an inducible ferroelectric order under an electric field becoming unstable at zero field due to the chemical modification with BTS. At a critical chemical modification level of $x = 0.05$ (BNKT– 0.05BTS sample), the onset of non-polar phase (region) and the formation of defect dipoles in parent ferroelectric material occurred. These defect dipoles which generated internal bias field, enhanced the short range interaction at the cost of ferroelectric long range order and reduced the correlation between initial ferroelectric domains which, as a consequence, tend to be randomized (i.e. increasing non- 180° domains) in the absence of

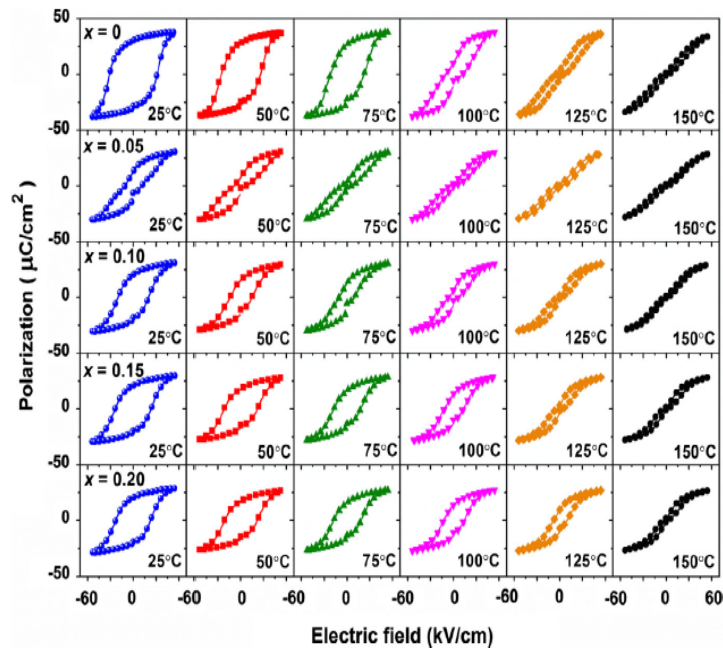


Fig. 6. Temperature dependent polarization–electric field (P – E) hysteresis loops of $(1-x)\text{BNKT}$ – xBTS ceramics sintered at 1125°C , measured at 55 kV/cm and a frequency of 1 Hz .

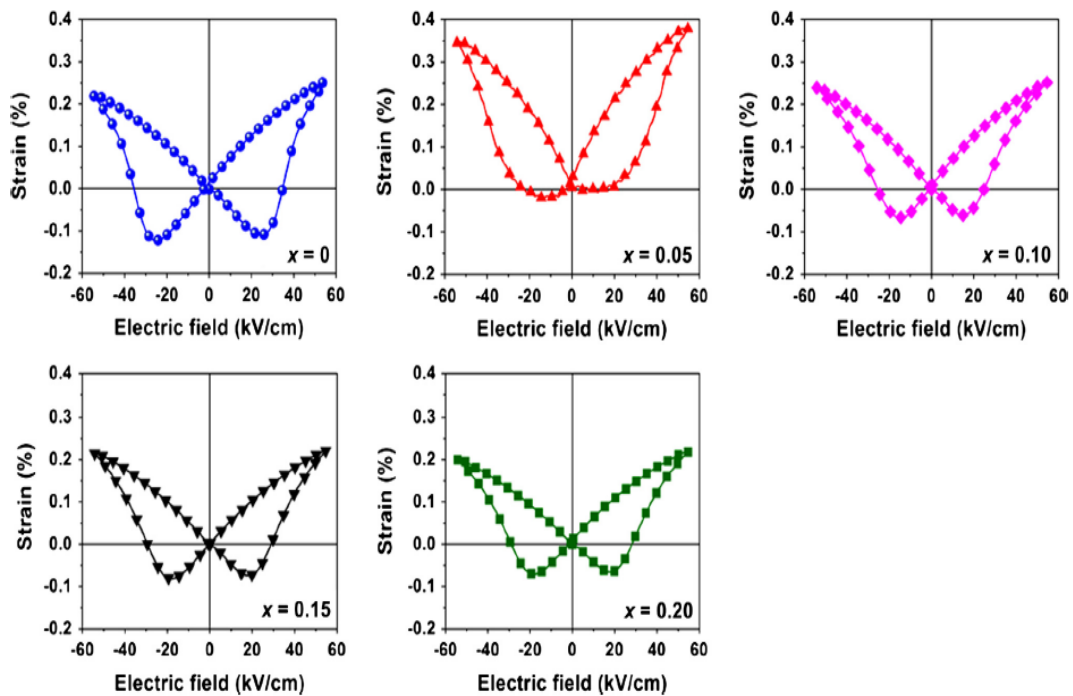


Fig. 7. Bipolar strain–electric field (S – E) of $(1-x)\text{BNKT}$ – xBTS ceramics sintered at 1125°C , measured at room temperature, under an electric field 55 kV/cm and a frequency of 0.1 Hz .

external electric field ($E = 0$). When an external electric field was applied, the non-polar phase (supposedly co-existing with ferroelectric region) could reversibly transform into ferroelectric phase, which was responsible for providing a restoring force for a large reversible domain switching, thus causing a high apparent strain (S_{max}) obtained in this composition [24,39]. This mechanism provided a general method to achieve a large electric field-induced strain similarly observed in other reports [25]. The above results

was correlated with a constriction of P – E hysteresis loop at this critical composition as shown in Fig. 5(b), a decrease of piezoelectric coefficient ($d_{33} \sim 174\text{ pC/N}$) and enhancement of converse piezoelectric effect with a large value of $d_{33}^* \sim 649\text{ pm/V}$ as shown in Table 2 [26]. Recently, Jo et al. [35,36] observed the working mechanism for the large strain response in KNN-modified BNT–BT system. They also proposed that the giant strain originated from the presence of a non-polar phase at zero electric field. Non polar

phase destabilized and randomized any electrically induced ferroelectric order, and caused an easy transition between non-polar and ferroelectric phases due to their comparable free energies. Thus, a high unipolar strain of 40.5% was observed in this system. It could be noted that the observed large strain seemed to exist only in a narrow compositional region where ferroelectric and non-polar phase order coexisted and had competitive free energy. Away from this narrow region, either the free energy of ferroelectric phase or a non-polar phase would dominate. Each of these phases alone could not deliver a strain as large as that measured from the compositions close to this region, at which the strain got contribution from both domain switching and electric field induced phase transition. If the composition was too far in a non-polar phase, an electric field required to induce the transition to ferroelectric phase might exceed the dielectric breakdown strength, impeding the development of large strain in the ceramics [40]. In this study, therefore with further increasing BTS content greater than 5 mol%, the presence of non-polar phase seemed to gradually decrease and eventually a normal butterfly-shaped strain loop was obtained again. It seemed that beyond narrow region of $x = 0.05$ of $(1-x)\text{BNKT}-x\text{BTS}$ system, non-polar phase disappeared while ferroelectric phase became dominant again which corresponded to an increase in P_r and E_c values (see Table 2). One possible explanation for this reversed ferroelectric behavior might be due to an increasing trend in tetragonality (c/a) value which clearly indicated that the addition of BTS greater than 10 mol% increased the lattice anisotropy of BNKT-BTS ceramics (i.e. rhombohedral phase decreased while tetragonal phase increased) [25,26]. The increasing trend in lattice anisotropy which showed slight distortion of XRD patterns was attributed to larger sized Ba^{2+} (1.42 Å) ion diffused into BNKT lattice to replace Bi^{3+} (1.17 Å), Na^+ (1.18 Å) and K^+ (1.33 Å), and Sn^{4+} (0.81 Å) replaced Ti^{4+} (0.74 Å) [23], resulting in the enlargement of lattice constant and lattice energy which induced a phase transformation in order to stabilize the structure [33]. The increasing trend in lattice anisotropy indicated the presence of ferroelectric order over non-polar regions. In addition, the decrease of non-polar phase at higher concentration of BTS likely suppressed reversed domain switching ability. Thus, the material in a single ferroelectric phase would be unable to deliver a strain as large as that previously obtained from the critical composition of $x = 0.05$ [40]. Therefore, a slight decrease in S_{max} and d_{33}^* values were observed at a higher concentration of BTS. The S_{max} and d_{33}^* values then dropped to a minimum value of 0.21% and 383 pm/V, respectively for BNKT-0.20BTS sample. S_{neg} also increased again to around -0.06 to -0.07% with increasing BTS content as expected.

The piezoelectric constant (d_{33}) of the optimally sintered ceramics are summarized in Table 2. The d_{33} values were found to be in a range of 137–215 pC/N. Pure BNKT ceramic had d_{33} of 178 pC/N which was close to the value reported earlier by Hiruma et al. [41]. The highest d_{33} value of 215 pC/N was observed for BNKT-0.10BTS sample. This value was higher than that observed earlier in $0.94\text{Bi}_{0.5}(\text{Na}_{0.84}\text{K}_{0.16})_{0.5}\text{TiO}_3-0.06\text{SrTiO}_3$ ceramic near MPB composition by Yoo et al. [11] who obtained d_{33} of 205 pC/N. With further increasing BTS greater than 10 mol%, a slight decrease in d_{33} was observed. The variation of piezoelectric behavior with increasing BTS content also showed similar trend to that of dielectric response. Based on room temperature dielectric constant (ϵ_r) and dielectric loss ($\tan\delta$) values in Table 1, pure BNKT ceramic had ϵ_r of 1419 with $\tan\delta$ of 0.0479. The ϵ_r increased to the highest value of 1721 for BNKT-0.10BTS sample. It was understood that the MPB-like compositions of this studied BNKT-BTS system with coexistence of rhombohedral and tetragonal structures at optimum relative fraction may be located near BNKT-0.10BTS composition. Thus, the optimal dielectric and piezoelectric properties would occur near this composition. The highest ϵ_r and d_{33} values

of BNKT-0.10BTS sample could be attributed to an increasing number of possible polarization directions because of the coexistence of more than one anisotropic crystal structure. The tetragonal phase has 6 different polarizations in the (100) direction for reorientation, while there are 8 different polarizations in (100) for rhombohedral phase. The large number of polarization directions cause enhanced crystallographic orientations under electric field, thus resulting in high polarization and piezoelectric properties [12,24]. Thus, BNKT-0.10BTS sample enabled the dipole moments to align efficiently with electric field, resulting in higher polarizability and an increase in both ϵ_r and d_{33} values [24]. However, the ϵ_r and d_{33} values then dropped to the minimum value of 1465 and 137 pC/N for BNKT-0.20BTS sample. Because of the crystal structure changed to tetragonal-rich phase of BTS, thus resulting in lower dielectric and piezoelectric response. This result was also similar to that observed previously by Lee et al. [33]. On the other hand, E_c values tended to increase and the relative density values tended to decrease with increasing BTS while P_r showed nearly the same values of 20.49–20.88 $\mu\text{C}/\text{cm}^2$. The higher E_c seemed to agree with the lower d_{33} values due to more difficulties in poling [2]. This also played a significant role in the reduction of dielectric and piezoelectric performance. However, the observed values of P_r may have some contribution from domain wall motion of tetragonal phase (with remaining rhombohedral phase) and interaction among them. This point will need further concrete proof of domain structure and possible presence of polar nano-regions.

4. Conclusions

Lead-free $(1-x)\text{Bi}_{0.5}(\text{Na}_{0.80}\text{K}_{0.20})_{0.5}\text{TiO}_3-x\text{Ba}(\text{Ti}_{0.90}\text{Sn}_{0.10})\text{O}_3$ or $(1-x)\text{BNKT}-x\text{BTS}$ piezoelectric ceramics with $x = 0-0.20$ mol fraction were successfully synthesized by a simple conventional mixed-oxide method. The maximum density was obtained for the ceramics sintered at 1125 °C. A pure perovskite structure was achieved for all studied composition range, suggesting the complete solid solutions between BTS and BNKT phases. The addition of BTS slightly affected grain size and shape of BNKT ceramic. A large electric field-induced strain of 0.36% corresponding to d_{33}^* of 649 pm/V were found in BNKT-0.05BTS sample. BNKT-0.10BTS sample was found to have relatively good piezoelectric ($d_{33} = 215$ pC/N), dielectric ($\epsilon_r = 1721$, $\tan\delta = 0.0724$ and $T_c = 333$ °C) and ferroelectric ($P_r = 20.49$ $\mu\text{C}/\text{cm}^2$, $R_{90} = 0.87$) properties. Moreover, ferroelectric hysteresis behavior also indicated that addition of BTS caused BNKT ceramic to become softer. Based on our results, it was suggested that BNKT-BTS ceramics have potential to be one of a promising lead-free piezoelectric candidate for piezoelectric applications.

Acknowledgements

This work is financially supported by the Thailand Research Fund (TRF) and the National Research University Project under Thailand's Office of the Higher Education Commission (OHEC). The Faculty of Science and the Graduate School, Chiang Mai University is also acknowledged. P. Jaita would like to acknowledge financial support from the TRF through the Royal Golden Jubilee Ph.D. Program.

References

- [1] P. Palei, P. Kumar, Solid State Sci. 14 (2012) 1338–1342.
- [2] B. Jaffe, W.R. Cook, H. Jaffe, Piezoelectric Ceramics, Academic Press, London, 1971.
- [3] S.H. Lee, J.H. Yoo, J. KIEEME. 11 (1998) 164–171.
- [4] S.K. Min, J.H. Yoo, J. KIEEME. 15 (2002) 671–677.
- [5] A. Hussain, C.W. Ahn, J.S. Lee, A. Ullah, I.W. Kim, Sens. Actuators A: Phys. 158 (2010) 84–89.

- [6] C. Xu, D. Lin, K.W. Kwok, *Solid State Sci.* 10 (2008) 934–940.
- [7] W. Li, Z. Xu, R. Chu, P. Fu, Y. Zhang, *Mater. Res. Bull.* 46 (2011) 871–874.
- [8] T.R. Shrout, S.J. Zhang, *J. Electroceram.* 19 (2007) 111–124.
- [9] Z. Yang, B. Liu, L. Wei, Y. Hou, *Mater. Res. Bull.* 43 (2008) 81–89.
- [10] A. Sasaki, T. Chiba, Y. Mamiya, E. Otsuki, *Jpn. J. Appl. Phys.* 38 (1999) 5564–5567.
- [11] J. Yoo, D. Oh, Y. Jeong, J. Hong, M. Jung, *Mater. Lett.* 58 (2004) 3831–3835.
- [12] Z.W. Chen, J.Q. Hu, *Adv. Appl. Ceram.* 107 (2008) 222–226.
- [13] X.P. Jiang, L.Z. Li, M. Zeng, H.L.W. Chan, *Mater. Lett.* 60 (2006) 1786–1790.
- [14] S. Supriya, S. Kalainathan, S. Swaroop, *Int. J. Chem. Technol. Res.* 3 (2011) 488–494.
- [15] G.A. Smolensky, *J. Phys. Soc. Jpn. (Suppl.)* 28 (1970) 26–37.
- [16] N. Yasuda, H. Ohwa, S. Asano, *Jpn. J. Appl. Phys.* 35 (1996) 5099–5103.
- [17] W. Cai, Y. Fan, J. Gao, C. Fu, X. Deng, *J. Mater. Sci.: Mater. Electron.* 22 (2011) 265–272.
- [18] K.C. Singh, A.K. Nath, R. Laishram, O.P. Thakur, *J. Alloys Comp.* 509 (2011) 2597–2601.
- [19] K.C. Singh, C. Jiten, *J. Mater. Sci.: Mater. Electron.* 24 (2013) 4247–4252.
- [20] Y.R. Zhang, J.F. Li, B.P. Zhang, *J. Am. Ceram. Soc.* 91 (8) (2008) 2716–2719.
- [21] H.E. Swanson, R.K. Fuyat, *Natl. Bur. Stand. Circ. (U.S.)* 539 (3) (1954) 44–45.
- [22] C. Peng, J.F. Li, W. Gong, *Mater. Lett.* 59 (2005) 1576–1580.
- [23] R.D. Shannon, *Acta Cryst.* A32 (1976) 751–767.
- [24] A. Hussain, A. Zaman, Y. Iqbal, M.H. Kim, *J. Alloys Comp.* 574 (2013) 320–324.
- [25] A. Ullah, C.W. Ahn, A. Hussain, S.Y. Lee, J.S. Kim, I.W. Kim, *J. Alloys Comp.* 509 (2011) 3148–3154.
- [26] A. Ullah, C.W. Ahn, S.Y. Lee, J.S. Kim, I.W. Kim, *Ceram. Int.* 38S (2012) S363–S368.
- [27] Y.M. Chiang, D.P. Birnie, W.D. Kingery, *Physical Ceramics: Principles for Ceramics Science and Engineering*, John Wiley & Sons Inc., New York, 1997.
- [28] S.H. Yoon, S.H. Kwon, K.H. Hur, *J. Appl. Phys.* 109 (2011). 084117–8.
- [29] W. Jo, S. Schaab, E. Sapper, L.A. Schmitt, H.J. Kleebe, A.J. Bell, J. Rödel, *J. Appl. Phys.* 110 (2011). 074106–9.
- [30] E.M. Anton, W. Jo, D. Damjanovic, J. Rödel, *J. Appl. Phys.* 110 (2011) 094108.
- [31] G. Fan, W. Lu, X. Wang, F. Liang, J. Xiao, *J. Phys. D: Appl. Phys.* 41 (2008) 035403–035406.
- [32] D. Lin, K.W. Kwok, H.L.W. Chan, *Solid State Ionics* 178 (2008) 1930–1937.
- [33] W.C. Lee, C.Y. Huang, L.K. Tsao, Y.C. Wu, *J. Alloys Comp.* 492 (2010) 307–312.
- [34] X.X. Wang, S.H. Choy, X.G. Tang, H.L.W. Chan, *J. Appl. Phys.* 97 (2005) 104101–104104.
- [35] W. Jo, R. Dittmer, M. Acosta, J. Zang, C. Groh, E. Sapper, K. Wang, J. Rödel, *J. Electroceram.* 29 (2012) 71–93.
- [36] W. Jo, T. Granzow, E. Aulbach, J. Rödel, D. Damjanovic, *J. Appl. Phys.* 105 (2009) 094102–094105.
- [37] B. Wang, L. Luo, F. Ni, P. Du, W. Li, H. Chen, *J. Alloys Comp.* 526 (2012) 79–84.
- [38] S.T. Zhang, B. Yang, W. Cao, *Acta Mater.* 60 (2012) 469–475.
- [39] X. Ren, *Nat. Mater.* 3 (2004) 91–94.
- [40] S.T. Zhang, A.B. Kouna, E. Aulbach, T. Granzow, W. Jo, H.J. Kleebe, J. Rödel, *J. Appl. Phys.* 103 (2008). 034107–8.
- [41] Y. Hiruma, K. Yoshii, H. Nagata, T. Takenaka, *J. Appl. Phys.* 103 (2008). 084121–7.

Polarization Fatigue in Ferroelectric $\text{Pb}(\text{Zr}_{0.52}\text{Ti}_{0.48})\text{O}_3\text{-SrBi}_2\text{Nb}_2\text{O}_9$ Ceramics

Orapim Namsar,¹ Soodkhet Pojprapai,^{2,3} Anucha Watcharapasorn,^{1,4} and Sukanda Jiansirisomboon^{1,4,*}

¹Department of Physics and Materials Science, Faculty of Science, Chiang Mai University,
Chiang Mai 50200, Thailand

²School of Ceramic Engineering, Suranaree University of Technology, Nakhon Ratchasima 30000, Thailand

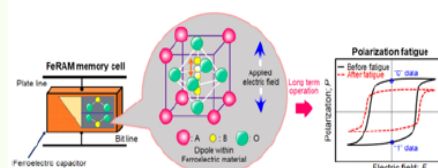
³Smart and Innovative Energy Research Unit, Suranaree University of Technology,
Nakhon Ratchasima 30000, Thailand

⁴Materials Science Research Center, Faculty of Science, Chiang Mai University,
Chiang Mai 50200, Thailand

(received date: 14 November 2014 / accepted date: 23 February 2015 / published date: 10 September 2015)

Ferroelectric fatigue induced by cyclic electric loading of the $(1-x)\text{PZT-xSBN}$ ceramics ($0.1 \leq x \leq 0.3$) have been investigated in comparison with pure PZT and SBN ceramics. The results showed that pure PZT ceramic possessed severe polarization fatigue after long bipolar switching pulses. This was mainly attributed to the appearance of microstructural damage at the near-electrode regions. Whereas, pure SBN ceramic exhibited no fatigue at least up to 1×10^6 switching cycles. The fatigue-free behavior of SBN ceramics was due primarily to weak domain wall pinning. PZT-SBN ceramics showed less polarization fatigue up to 1×10^6 switching cycles than pure PZT. This could be attributed to their low oxygen vacancy concentration. Therefore, this new ceramic PZT-SBN system seems to be an alternative material for replacing PZT in ferroelectric memory applications.

Keywords: fatigue, ferroelectric, dielectric, PZT, SBN



1. INTRODUCTION

Polarization switching in ferroelectrics has been considered for a number of potential applications; i.e. actuators and non-volatile random access memories. One critical limitation on the performance of these applications is the polarization fatigue associated with repeated electrical cycling. To overcome the fatigue problem in these applications, a new ferroelectric material with high fatigue endurance is thus required. It is commonly known that a popular ferroelectric material for ferroelectric applications is $\text{Pb}(\text{Zr}_{0.52}\text{Ti}_{0.48})\text{O}_3$ (PZT). PZT exhibits high remanent polarization and small coercive field.^[1,2] However, it is very prone to electrical fatigue degradation.^[3] On the contrary, the bismuth layered structure compounds such as $\text{SrBi}_2\text{Nb}_2\text{O}_9$ (SBN) has become

attractive candidates for these ferroelectric applications (especially in memory application) because of its excellent fatigue endurance.^[4] Nevertheless, SBN has only limited applications due to its low polarization value and high coercive field.^[5,6] In order to solve the problem associated with PZT and SBN, therefore, the new ceramic of PZT-SBN system is investigated here. Also, polarization fatigue endurance of $(1-x)\text{PZT-xSBN}$ ($0.1 \leq x \leq 0.3$) ceramics was analyzed in comparison with pure PZT and SBN ceramics. It is expected that the PZT-SBN ceramic may provide improved ferroelectric properties such as large remnant polarization, a small coercive field and excellent fatigue endurance, which are the advantage properties for non-volatile random access memory applications.

2. EXPERIMENTAL PROCEDURE

The ceramics with formula $(1-x)\text{Pb}(\text{Zr}_{0.52}\text{Ti}_{0.48})\text{O}_3\text{-}$

*Corresponding author: sukanda.jian@cmu.ac.th
©KIM and Springer

$x\text{SrBi}_2\text{Nb}_2\text{O}_9$ or $(1-x)\text{PZT}-x\text{SBN}$ were prepared by a conventional solid-state mixed-oxide reaction. First, pure PZT and SBN powders were synthesized separately from high purity raw materials of PbO , TiO_2 , ZrO_2 , SrCO_3 , Bi_2O_3 and Nb_2O_5 . The starting powders were weighed, ball-milled in ethanol for 24 h and dried at 120°C . The mixed powders were calcined at 800°C for 2 h for PZT and at 950°C for 3 h for SBN powders. The calcined PZT and SBN powders were then weighed, mixed by ball-milling and dried to produce a powder mixture of $(1-x)\text{PZT}-x\text{SBN}$, where $x = 0, 0.1, 0.3$ and 1.0 weight fraction. Each mixture was pressed into pellets with 3 wt. % polyvinyl alcohol added as a binder. The pellets were sintered at 1050°C in air for 3 h. In order to avoid compositional deviation from PbO and Bi_2O_3 volatilization during sintering process, the green pallets were covered with their own powders.

The crystalline structure was analyzed by using x-ray diffraction analysis (Phillips Model X-pert). Before fatigue testing, the ceramic samples were ground and polished by SiC papers. Then, silver paste was fired on both sides of the polished samples at 600°C for 10 min as the electrodes. For fatigue characteristic, the samples were subjected to bipolar electric field of ~ 2 times the coercive field ($\sim 2E_c$) with the frequency fixed at 50 Hz up to 1×10^6 switching cycles. This fatigue test was examined through a conventional Sawyer-Tower circuit.^[7] During bipolar electric cycling, the samples were put in a sample holder and immersed in silicone oil to prevent flashovers and mounted into a fixture connected to a high-voltage AC amplifier (Trek 610D) with the input sinusoidal signal (50 Hz) from a function generator (GAG-809). Polarization hysteresis (P - E) loops were recorded after a certain number of switching cycles with a measurement frequency of 50 Hz by a digital oscilloscope (HP 54645A). The dielectric properties of unfatigued and fatigued samples were also studied by an LCR meter (Hewlett-Packard 4194A) at 100 kHz. To investigate the damage at the near-electrode regions as a result of fatigue process, a scanning electron microscope (SEM, JEOL JSM-5910LV) was used to observe the fracture surfaces of unfatigued and fatigued samples.

3. RESULTS AND DISCUSSION

Figure 1(a) shows x-ray diffraction (XRD) patterns for pure PZT, $(1-x)\text{PZT}-x\text{SBN}$ ($0.1 \leq x \leq 0.3$) and pure SBN. The pattern of pure PZT ceramic showed mainly a tetragonal symmetry. Whereas, pure SBN ceramic was identified as a single phase bismuth layered structure having orthorhombic symmetry without significant preferred orientation. For the PZT-SBN ceramics, it was found that the crystalline phases of the samples were indexed to be a tetragonal PZT phase which coexisted with a new multinary phase. This new multinary compound in the PZT-SBN ceramics matched the

standard JCPDS diffraction data file no. 74-0660 of $\text{Pb}_2(\text{Nb}_{1.33}\text{Ti}_{0.66})\text{O}_{6.66}$ (PNT) phase which had a cubic symmetry. The formation of PNT phase suggested that the chemical reaction between PZT and SBN phases during sintering process was occurred. With careful observation, it can be seen that the diffraction peaks of PZT phase in the PZT-SBN ceramics shifted towards a higher angle and the diffraction peak around 2θ of $43 - 46^\circ$ was found to split, as shown in Fig. 1(b). In addition, the XRD peaks of PZT phase in these ceramics were broader than those of pure PZT ceramic. These observations suggested that the PZT phase in these ceramics was PZT-based solid solution. More importantly, it was noteworthy that the original SBN phase was not found in the PZT-SBN ceramics. There were two processes that account for the disappearance of SBN phases. Firstly, some

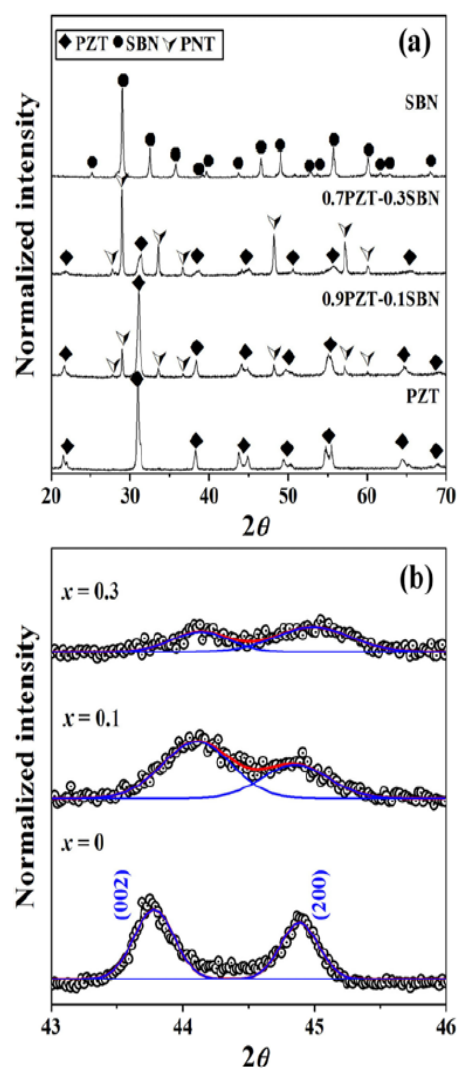


Fig. 1. (a) XRD patterns of pure PZT, $(1-x)\text{PZT}-x\text{SBN}$ ($0.1 \leq x \leq 0.3$) and pure SBN ceramics (b) tetragonal splitting of the 43-46 degrees peaks of PZT phase.

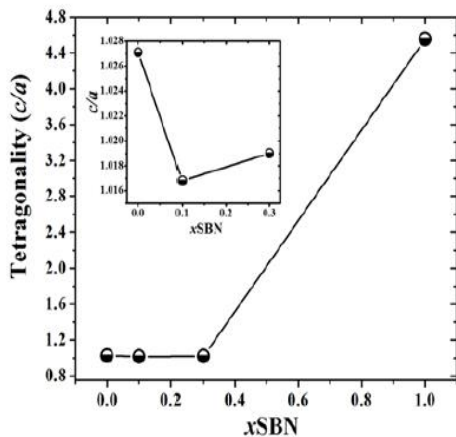


Fig. 2. The tetragonality (c/a) of $(1-x)\text{PZT}-x\text{SBN}$ ceramics as a function of SBN content.

SBN phase reacted with some PZT phase to form a new multinary compound such PNT during sintering process. The other process was the dissolution of SBN into PZT matrix phase to form the PZT-based solid solutions.

This process was supported by the change of the tetragonality (c/a) of PZT phase in PZT-SBN ceramics as

shown in Fig. 2. It was found that the c/a decreased rapidly after 0.1SBN incorporation. However, further increase the content of SBN to $x=0.3$ slightly increased c/a . This reduction of c/a demonstrated that the crystal structure of PZT phase in PZT-SBN ceramics transforms from tetragonal to cubic. Based on the x-ray results, the phase transformation in PZT-SBN ceramics was expected to influence their fatigue performance.

The P - E loops of the PZT, PZT-SBN and SBN ceramics for three different bipolar cycle numbers (1 cycle, 1×10^5 and 1×10^6 cycles) are provided in Fig. 3. The remanent polarization and coercive field values before and after fatigue test are also listed in Table 1. When considering the shape and size of P - E loops for all unfatigued samples, it was noteworthy that the hysteresis loop of pure PZT ceramic showed the square shaped with high remanent polarization and low coercive field, which was a typical hysteresis loop of PZT ceramic.^[8] Whereas, pure SBN ceramic showed large degree of hysteresis loop opening with large coercive field but small remanent polarization. This suggested that the PZT domains were relatively easier to switch than those of the SBN domains under the applied electric field, which reflected as lower coercive field value in Table 1. For PZT-

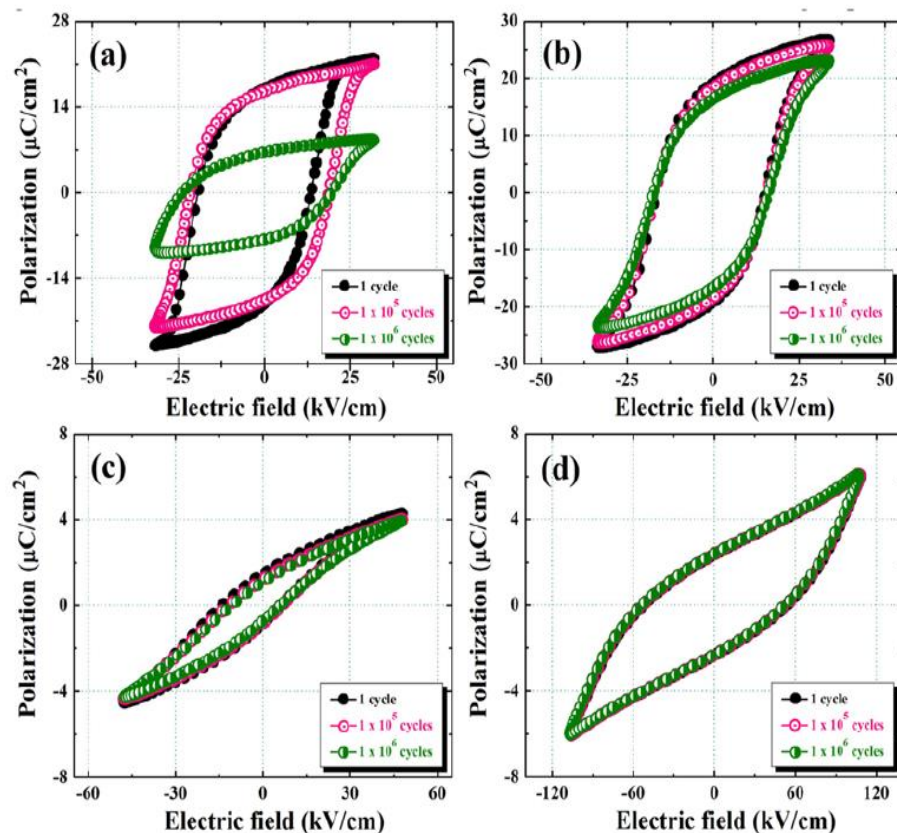


Fig. 3. Polarization loops of $(1-x)\text{PZT}-x\text{SBN}$ ceramics at 1 , 1×10^5 and 1×10^6 bipolar cycles, when (a) $x=0$ (PZT), (b) $x=0.1$, (c) $x=0.3$ and (d) $x=1.0$ (SBN).

SBN ceramics, there was a trade-off between the ferroelectric properties of both perovskite PZT and bismuth layered SBN. Namely, the PZT-SBN ceramics had a higher remanent polarization than that of pure PZT ceramic and smaller coercive field than that of pure SBN ceramic. After the application of bipolar electric cycling, the results showed that bipolar cycling led to a strong degradation of the polarization hysteresis loop of pure PZT ceramic, as shown in Fig. 3(a). On the other hand, the hysteresis loop of pure SBN ceramic showed no apparent change of both the remanent polarization and coercive field after electric cycling process (Fig. 3(d)). In the case of $(1-x)\text{PZT}-x\text{SBN}$ ceramics ($0.1 \leq x \leq 0.3$), a small decrease of the remanent polarization was observed after fatigue measurement (Fig. 3(b-c)). In order to compare the fatigue rate from different samples, the normalized remanent polarization and coercive field as a function of switching cycles were investigated (as shown in Fig. 4(a-b)). The inset in Fig. 4(a) and (b) represents the change of remanent polarization ($2P_r$) and coercive field ($2E_c$) with accumulative switching cycles, respectively. As can be seen from Fig. 4(a), the normalized remanent polarization of pure PZT ceramics increased slightly after 1×10^3 cycles and then began to decrease after 5×10^4 cycles. Finally, it dropped to 59% of the initial values after 10^6 switching cycles. An important mechanism responsible for an increased remanent polarization at 1×10^3 to 5×10^4 cycles was the 'wake-up' process.^[9-11] This wake up process could be effected by the locked localized space charges present at the ferroelectric bulks/electrode interfaces. In general, lead and oxygen vacancy defects are formed due to PbO evaporation during sintering.^[12] As the mobility of lead vacancies is lower than that of oxygen vacancies, the oxygen vacancies can move more easily under the application of electric field during fatigue proceeds. The positively-charged oxygen vacancies are driven towards to domain

walls, grain boundaries and/or PZT/electrode interfaces because of the relatively lower potential energies at these sites. They are then captured by space charge. These defect charges obstruct the reorientation of domains and hence limit the reversible domain numbers. Nevertheless, they are easily removed by the repeated domain switching cycles. Thereby, the normalized remanent polarization of PZT ceramic increased at this stage. After 1×10^5 switching cycles, a strong loss of the switchable polarization was caused by the field screening effect.^[13] By this field screening effect, the effective field reached the undamaged regions of PZT sample was significantly decreased because of the voltage dropped across the cracks in the damaged layer. Consequently, the field in some regions was too small to switch domains, resulting in a loss of polarization (Fig. 4(a)). But, other regions were unaffected, increasing the coercive field. The next paragraph will discuss the reasons for the increase in the coercive field after fatigue process.

Figure 4(b) displays the variation of the normalized coercive field as a function of switching cycles for PZT ceramic. It was observed that there were three different rates present in the normalized coercive field. The normalized coercive field changed slowly before 1×10^3 cycles, rapidly increased after approximately $1 \times 10^3 - 5 \times 10^4$ cycles, and then it decreased slightly after 5×10^5 switching cycles. For the bipolar fatigue properties in ferroelectric materials, especially in PZT, the domain wall pinning and microstructural damage are the main mechanisms attributed to polarization degradation. The change in the coercive field can be used to qualitatively determine the electrical fatigue mechanism as proposed by Jiang *et al.*^[14] Namely, the electrical fatigue is dominated by domain wall pinning if the coercive field remains nearly constant. When the coercive field increase sharply with increasing switching cycles, the mechanical degradation (i.e. crack) become dominant in the fatigue

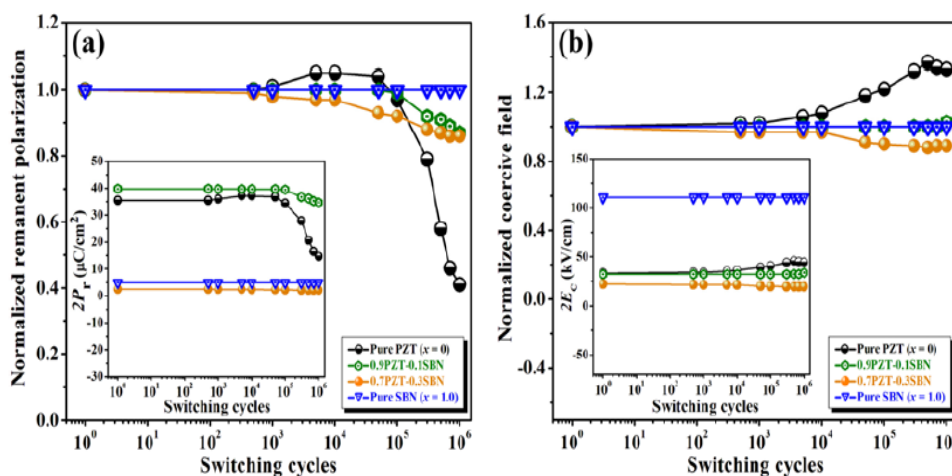


Fig. 4. (a) The normalized polarization as a function of switching cycles and (b) the normalized coercive field as a function of switching cycles of $(1-x)\text{PZT}-x\text{SBN}$ ceramics.

mechanism. Our experiments showed that the electrical fatigue process was occurred by both domain wall pinning (at 1 to 1×10^3 switching cycles) and microstructural damage cracking (after 1×10^3 switching cycles). In the region dominated by the domain wall pinning mechanism (up to 1×10^3 switching cycles), the normalized coercive field showed a small increase in 8% compared to its unfatigued value. Whereas in the region dominated by the microstructural damage cracking mechanism (after 1×10^3 switching cycles), the normalized coercive field showed an increase in 33% from its unfatigued value. This suggested that the mechanical degradation (i.e. crack) contributed more significantly to the polarization fatigue of PZT ceramic as compared to the domain wall pinning mechanism. Nevertheless, a slight reduction of the normalized coercive field at the end of fatigue process (after 5×10^5 switching cycles) indicated a decrease in the influence of cracking due to the saturation of crack growth. In order to confirm that the polarization switching fatigue of PZT was controlled by cracking mechanism, the fracture surfaces in regions close to the electrode of unfatigued and fatigued samples of PZT ceramic were investigated, as shown in Fig. 5(a-b). The result provided that the fracture surface of unfatigued and fatigued samples of PZT ceramic showed a strong change in the microstructure close to the electrodes. The unfatigued sample in Fig. 5(a) showed a typical fracture surface of PZT with mainly transgranular fracture mode. For fatigued PZT sample, the damaged layer was formed at underneath the electrode regions with thickness of approximately 15 nm, while the microstructure in the bulk ceramic remained unchanged (Fig. 5(b)). The original of this damaged layer was due to mechanical stresses during the repeated domain switching.^[13] The repeated switching of the domains in PZT

ceramic under the large applied alternating field generated large mechanical stress and led to the formation of micro-cracking along grain boundaries. This was in accordance with literatures on several PZT-related systems.^[13-20] The field screening concept can be used to explain the relationship between the damaged near electrode regions and the electrical fatigue behavior.^[13] Since the difference in dielectric constant between the damaged layer and the bulk, the applied electric field would be screened and prevented from reaching the bulk. This indicated that the electric field amplitude in the bulk was significantly reduced.^[13,19] The lower effective field in the bulk was not strong enough to complete the domains switching and consequent decreased of the remanent polarization of PZT ceramic as depicted in Fig. 4(a). In addition, these domains required the higher external field for domain switching which was reflected by the observed increase the coercive field in fatigue measurement as shown in Fig. 4(b).

As the small amount of 0.1SBN was incorporated to PZT, the fatigue started after 1×10^5 cycles and the normalized remanent polarization dropped to 13% of the initial values after 1×10^6 cycles with no apparent change in the normalized coercive field (Fig. 4(a-b)). This ceramic showed much improvement in fatigue endurance compared to pure PZT ceramic. The high fatigue endurance of this ceramic was controlled by the weak domain wall pinning mechanism as a result of donor-like substitution. It is well recognized that the poor fatigue properties in perovskite PZT mainly come from oxygen vacancy accumulation near-electrode regions^[21] and domain wall pinning by oxygen vacancy planes.^[22-24] In this ceramic, Bi^{3+} and Nb^{5+} ions (from SBN) could be considered as a donor dopants for PZT lattice. As the charge compensation, the cation vacancies in Pb-sites were created in perovskite

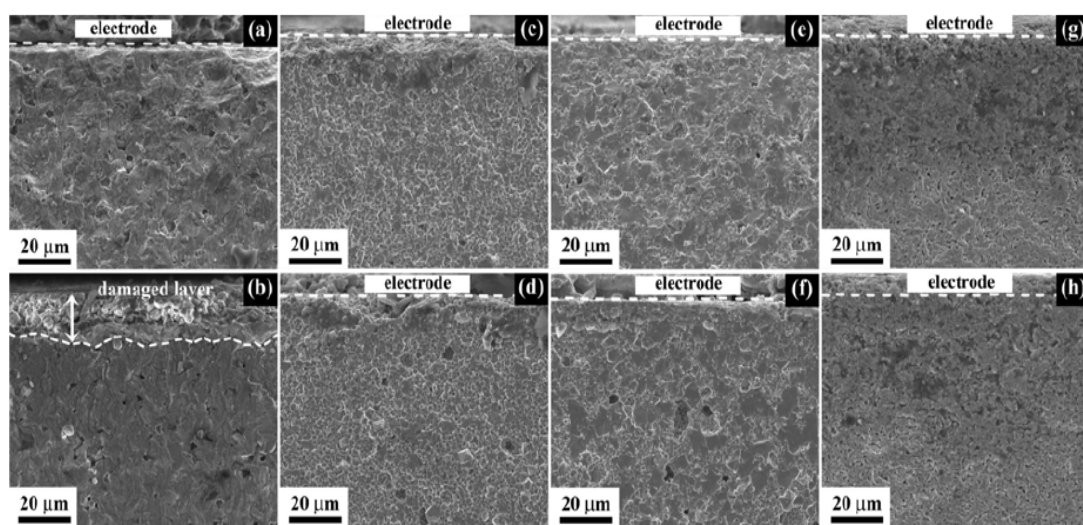


Fig. 5. Fracture cross sections of unfatigued (above) and fatigued samples (below) for $(1-x)\text{PZT}_x\text{SBN}$ ceramics, where (a-b) $x = 0$ (PZT), (c-d) $x = 0.1$, (e-f) $x = 0.3$ and (g-h) $x = 1.0$ (SBN), respectively.

PZT structure while the oxygen vacancy concentration was greatly reduced. The suppression in the concentration of oxygen vacancies resulted in the decrease the possibility of their accumulation at the ceramic bulk-electrode interface or the pinning of the domain walls or grain boundaries during the repeated switching cycles. This led to the high stability of domain switching process, and thereby high fatigue resistance was observed.

When the amount of SBN was increased to $x = 0.3$, the normalized remanent polarization started to decrease after 1×10^3 cycles and reduced by about 15% of the initial value at 1×10^6 cycles (Fig. 4(a)). It should be noted that this ceramic showed a lower degree of degradation in the normalized polarization when compared to pure PZT ceramic, although the value of the remanent polarization ($2P_r$) was lower than that of pure PZT ceramic (see Fig. 4(a) and Table 1). The enhancement in fatigue endurance can be understood on the basis of the observed behavior of the tetragonality (c/a) as provided in Fig. 2. It is generally accepted that one of factors leading to ferroelectric fatigue is the internal (residual) stress.^[25-27] Internal stress can suddenly induce microcracking if cycle loading is applied to the ferroelectric materials.^[20,28] Also, internal stresses are reported to have a significant role on domain switching behavior as they affect the spatial distribution of the stored elastic energy.^[29] Namely, if the stress level is high enough, it is expected that the switching of domains is completely suppressed. The magnitude of the internal stress is dependent on the transformation strain owing to ferroelectric domain switching, which in turn is related to the crystal distortion in term of tetragonality ratio, c/a .^[30] Okazaki^[31] reported that internal stress is proportional to the ratio of c/a . In this regard, from Fig. 2, the c/a value of 0.9PZT-0.3SBN was smaller than that of pure PZT ceramic, implying that the internal stress concentration involved in domain switching process should be quite small. Therefore, less reduction of polarization was observed for this ceramic. For the variation of the normalized coercive field as a function of switching cycles for this sample, as provided in Fig. 4(b), it can be seen that the normalized coercive field was stable up to approximately 1×10^4 cycles and then began to decrease after 1×10^4 cycles. Finally, it reduced slightly to 11% of the unfatigued values after 1×10^6 switching cycles. The decrease in the normalized coercive field for this ceramic suggested that the increased mobility of some domains as a result of the applied electric cycling.^[28,32]

Compared to pure PZT and PZT-SBN, pure SBN ceramic showed excellent fatigue endurance up to 1×10^6 switching cycles with no significant change in the normalized coercive field. The fatigue free behavior of SBN ceramic was based on the weak domain wall pinning effect of oxygen vacancies.^[33,34] Oxygen vacancy was once believed to be a major contribution to electric fatigue in normal perovskite

ferroelectric materials.^[17] In the case of bismuth layered perovskite $\text{SrBi}_2\text{Nb}_2\text{O}_9$ (SBN), the lattice structure consists of perovskite building (SrNb_2O_7) blocks separated by bismuth oxide (Bi_2O_3) layers (Fig. 6). Oxygen vacancies are preferably formed in Bi_2O_3 layers due to the volatility of Bi_2O_3 . Nevertheless, the efficiency of pinning at domain boundaries of oxygen vacancies created in Bi_2O_3 layers was low.^[34] The degree of domain wall pinning effect due to oxygen vacancy near the domain walls during the fatigue process became much less pronounced, hence preventing the fatigue behavior. According to fatigue measurements, the field screening effect caused a strong reduction of ferroelectric properties of PZT ceramics (i.e. decreased in the remanent polarization and increased in the coercive field, see Fig. 4 and Table 1). This result was supported by the appearance of the near electrode cracking in fatigued PZT sample after electric cycling process (Fig. 5(b)), as discussed above. In the case of the PZT-SBN and pure SBN ceramics, the greater fatigue resistance was explained by the low number of pinned domain walls. To confirm this hypothesis, the fracture surfaces of unfatigued and fatigued samples for these ceramics were compared with pure PZT ceramic. The microstructures visible in SEM images, displayed in Fig. 5(c-h), for the 0.9PZT-0.1SBN, 0.7PZT-0.3SBN and pure SBN ceramics showed no significant difference between the fracture surfaces of the unfatigued and fatigued samples. There was no mechanical damage cracking layer noticeable in the near electrode regions. These observation suggested that polarization fatigue behavior of these ceramics was not influenced by the microstructure cracking mechanism. It again confirmed the finding that the weak domain wall pinning mechanism was responsible for the high fatigue resistance in bipolar electric cycling for the $(1-x)\text{PZT}-x\text{SBN}$ ($0.1 \leq x \leq 0.3$) and SBN ceramics. The low number of pinned domains caused less

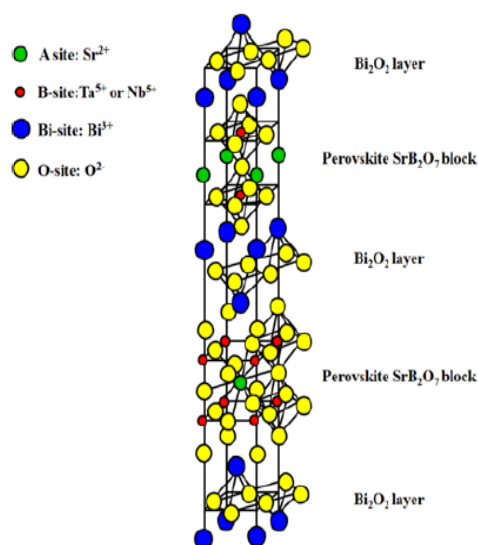


Fig. 6. Schematic of the lattice structure of $\text{SrBi}_2\text{B}_2\text{O}_9$.^[4]

residual ferroelastic stress,^[35,36] resulting in the reduction of the probability of crack propagation. Less cracks led to less field screening effect and hence greater fatigue resistance for these ceramics.

As mentioned previously, the interaction between defects and ferroelectric domain walls (domain wall pinning) was one of the main polarization fatigue mechanisms under bipolar electric cycling of ferroelectric materials. A ferroelectric fatigue model based on pinning effect had been purposed by Brennan.^[37] The domain wall pinning effect leads to the reduction of the polarization as the logarithm of the number of polarization reversals. This model can be defined as:

$$2P_r(N) = 2P_r(0) - B \ln N \quad (1)$$

where $P_r(N)$ is the remanent polarization at N switching cycles, $P_r(0)$ is the initial unfatigued remanent polarization and B is a rate factor.

As seen in Fig. 7, the fitting curves based on the Brennan's model showed a strong correlation with the experimental fatigue data. The decay rate factor (B) from different samples was calculated from fitting of these curves. The decay rate factor sharply decreased with increasing SBN concentration until nearly zero in pure SBN ceramic, as shown in Fig. 8. This implies that the effect of domain wall pinning was lessened in these ceramics. This result substantiated the previously hypothesis that the high fatigue resistance in (1-

x)PZT- x SBN ($0.1 \leq x \leq 0.3$) and pure SBN came from the weak domain wall pinning.

Room temperature dielectric constant (ϵ_r) before and after electrical fatigue test of (1- x)PZT- x SBN ceramics are listed in Table 1. As shown in Table 1, the dielectric constant of both unfatigued and fatigued samples grew sharply when the addition of 0.1SBN was added to PZT. High dielectric constant for this ceramic was dominantly related to effect of donor-like substitution. In this sample, Nb^{5+} and Bi^{3+} from SBN was substituted for $(\text{Zr/Ti})^{4+}$ and Pb^{2+} sites in PZT structure, respectively. These substitutions would induce A-site cation vacancies in perovskite PZT,^[12] which resulted in a rapid reduction in the positively-charged oxygen vacancy concentration. As oxygen vacancy can inhibit the polarization switching by pinning domain walls in ferroelectric materials, the domain switching ability is largely controlled by oxygen vacancy concentration. Therefore, within this ceramic, a rapid decrease in oxygen vacancy concentration due to donor-like ionic substitutions led to the reduction of the pinning effect on the domain walls. This in turn increased the ease of domain movement, resulting in an increase of the dielectric constant. However, the dielectric constant suddenly decreased when the amount of SBN was increased to $x = 0.3$. This degradation in dielectric constant was caused by an increase in non-ferroelectric cubic PNT phase, as observed in x-ray diffraction analysis (Fig. 1).

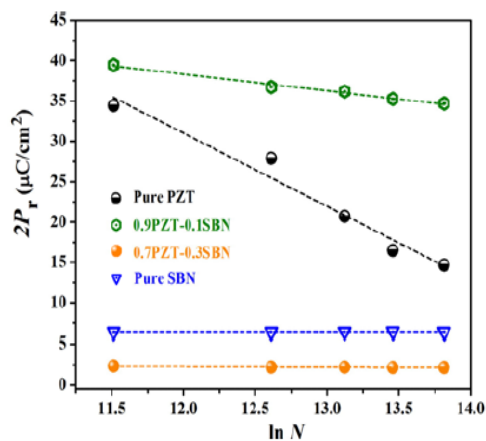


Fig. 7. The change of the remanent polarization ($2P_r$) of (1- x)PZT- x SBN ceramics with cumulative switching cycles ($\ln N$). The dashed lines are fitting curves calculated by Eq. (1).

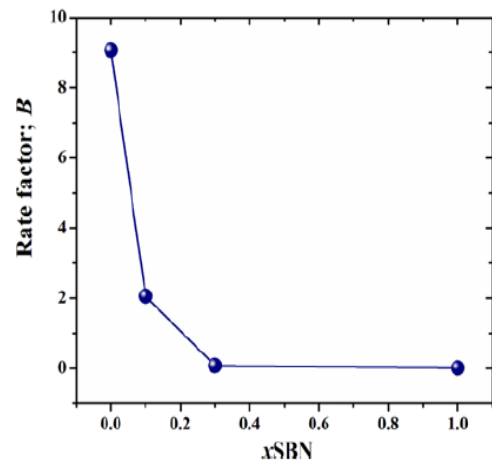


Fig. 8. The absolute values of B for (1- x)PZT- x SBN ceramics with x SBN addition.

Table 1. Dielectric and ferroelectric properties of (1- x)PZT- x SBN ceramics measured before and after fatigued tests.

x	ϵ_r			$2P_r$ ($\mu\text{C}/\text{cm}^2$)			$2E_c$ (kV/cm)		
	before	after	% of decrease	before	after	% of decrease	before	after	% of change
0 (PZT)	922.17	302.79	67	35.48	14.65	59	33.45	44.38	increased by 33%
0.1SBN	1629.67	1571.39	4	39.78	34.71	13	32.33	34.41	increased by 6%
0.3SBN	639.51	583.12	9	2.5	2.13	15	22.25	19.72	decreased by 11%
1.0 (SBN)	143.10	142.68	0.3	4.9	4.9	0	110.67	110.66	0%

After considering the dielectric constant of fatigued samples, however, it was observed that the PZT ceramic showed much reduction in dielectric (dropped by 67% of the initial value). The strong degradation of dielectric constant was predominately attributed to the grains deterioration. This was supported by the occurrence of the cracks in the near-electrode regions as shown in Fig. 5(b). It is well known that the dielectric constant are caused by the movement of the ferroelectric domain wall.^[38-40] In this ceramic, some grains were deteriorated due to ferroelectric fatigue process, leading to reduction of the ability of domain wall movement in the grains. Hence, a strong reduction in dielectric constant was observed. For the PZT-SBN and pure SBN ceramics, there was a smaller decrease in the dielectric constant. This phenomenon was mainly due to low pinned domains during bipolar electric cycling. The low number of locked domain walls led to easy domain wall movement which in turn resulted in small loss of dielectric constant after fatigue process. For dielectric measurements, bipolar electric cycling did not significantly lead to a degradation of the dielectric constant of the PZT-SBN and SBN ceramic, suggesting that these ceramic had high stability of domain switching than those of PZT ceramic. This research therefore demonstrated that the PZT-SBN showed an improvement of fatigue endurance in PZT ceramic after incorporation of the layered perovskite SBN.

4. CONCLUSIONS

Ferroelectric fatigue due to repeated domain switching plays an important role for the performance of ferroelectric applications, especially in memory devices. Perovskite PZT with high remanent polarization and bi-layered compound SBN with fatigue-free characteristic are both popular materials for memory devices. To combine these two advantages, the new ceramic PZT-SBN system was fabricated. Also, polarization fatigue under bipolar electric field cycling was investigated for the PZT, PZT-SBN and SBN ceramics. The fatigue tests demonstrated that the perovskite PZT showed a strong degradation of the remanent polarization and increase the coercive field. Microcracking layer was formed in near electrode regions after bipolar fatigue, which contributed significantly to the degradation of the ferroelectric properties of PZT. Whereas, the bismuth layered structure SBN ceramic exhibited no obvious reduction of switchable polarization at 1×10^6 cycles. The fatigue-free behavior of SBN was mainly attributed to the weak domain wall pinning. The fatigue resistance of PZT ceramic was much improved after small amount of 0.1SBN incorporation. The improvement in fatigue endurance of this ceramic was mainly owing to the low content of oxygen vacancies in bulk ceramic and less pinning effect to ferroelectric domain walls. For the 0.7PZT-0.3SBN ceramics, the ferroelectric showed small remanent

polarization and high fatigue endurance when compared to pure PZT ceramic. Small internal stress was a primary cause for the less reduction of remanent polarization for this ceramic. The dielectric measurement showed small deterioration in dielectric constant in PZT-SBN and pure SBN ceramics after 1×10^6 polarization reverse cycles. As the results, the 0.9PZT-0.1SBN ceramic is a new promising ferroelectric material for memory devices because of its high $2P_r$, low $2E_c$ and good fatigue performance.

ACKNOWLEDGEMENTS

This work is financially supported by the Thailand Research Fund (TRF) (Grant no. RSA5780032) and the National Research University Project under Thailand's Office of the Higher Education Commission (OHEC). The Faculty of Science and the Graduate School, Chiang Mai University is also acknowledged. ON would like to acknowledge financial support from the TRF through the Royal Golden Jubilee Ph.D. Program.

REFERENCES

1. R. Dat, D. J. Lichtenwalner, O. Auciello, and A. I. Kingon, *Appl. Phys. Lett.* **64**, 2673 (1999).
2. T. Mihara, H. Yoshimori, H. Watanbe, and C. A. Paz de Araujo, *Jpn. J. Appl. Phys.* **34**, 5233 (1995).
3. D. H. Bao, N. Wakiya, K. Shinozaki, and N. Mizutani, *J. Phys. D: Appl. Phys.* **35**, L1 (2002).
4. C. A. Paz De Araujo, J. D. Cuchiaro, L. D. McMillan, M. C. Scott, and J. F. Scott, *Nature* **374**, 627 (1995).
5. K. Kato, *Jpn. J. Appl. Phys.* **37**, 5178 (1998).
6. J. Qiu, G.-Z. Liu, M. He, H.-S. Gu, and T.-S. Zhou, *Physica B* **400**, 134 (2007).
7. C. B. Sawyer and C. H. Tower, *Phys. Rev.* **35**, 269 (1930).
8. G. H. Haertling, *J. Am. Ceram. Soc.* **82**, 797 (1999).
9. S. Okamura, S. Miyata, Y. Mizutani, T. Nishida, and T. Shiosaki, *Jpn. J. Appl. Phys.* **38**, 5364 (1999).
10. S. Okamura, M. Takaoka, T. Nishida, and T. Shiosaki, *Jpn. J. Appl. Phys.* **39**, 5481 (2000).
11. S. Okamura, N. Abe, Y. Otani, and T. Shiosaki, *Integrated Ferroelectr.* **52**, 127 (2003).
12. R. B. Atkin and R. M. Fulrath, *J. Am. Ceram. Soc.* **54**, 26 (1971).
13. N. Balke, H. Kungl, T. Granzow, D. C. Lupascu, M. J. Hoffmann, and J. Rödel, *J. Am. Ceram. Soc.* **90**, 3869 (2007).
14. Q. Y. Jiang, E. C. Subbarao, and L. E. Cross, *Acta. Metall. Mater.* **42**, 3687 (1994).
15. H.-T. Chung, B.-C. Shin, and H.-G. Kim, *J. Am. Ceram. Soc.* **72**, 327 (1989).
16. A. Furuta and K. Uchino, *J. Am. Ceram. Soc.* **76**, 1615 (1993).
17. E. C. Subbarao, V. Srikanth, W. Cao, and L. E. Cross, *Ferroelectrics* **145**, 271 (1993).

18. J. Nuffer, D. C. Lupascu, and J. Rödel, *J. Eur. Ceram. Soc.* **21**, 1421 (2001).
19. J. Nuffer, D. C. Lupascu, A. Glazounov, H. J. Kleebe, and J. Rödel, *J. Eur. Ceram. Soc.* **22**, 2133 (2002).
20. D. Fang, B. Liu, and C. T. Sun, *J. Am. Ceram. Soc.* **87**, 840 (2004).
21. J. F. Scott, C. A. Araujo, B. M. Melnick, I. D. McMillan, and R. Zuleeg, *J. Appl. Phys.* **70**, 382 (1991).
22. A. Gruverman, O. Auciello, and H. Tokumoto, *Appl. Phys. Lett.* **69**, 3191 (1996).
23. E. L. Colla, S. Hong, D. V. Taylor, A. K. Tagantsev, N. Setter, and K. No, *Appl. Phys. Lett.* **72**, 2763 (1998).
24. C. H. Park and D. J. Chadi, *Phys. Rev. B* **57**, R13961 (1998).
25. Q. Y. Jiang, E. C. Subbarao, and L. E. Cross, *J. Appl. Phys.* **75**, 7433 (1994).
26. K. Khachatryan, *J. Appl. Phys.* **7**, 6449 (1995).
27. D. Wang, Y. Fotinich, and G. P. Carman, *J. Appl. Phys.* **83**, 5342 (1998).
28. J. Nuffer, D. C. Lupascu, and J. Rödel, *Acta. Mater.* **48**, 3783 (2000).
29. C. S. Lynch, *Acta. Mater.* **44**, 4137 (1996).
30. D. A. Hall, T. Mori, T. P. Comyn, E. Ringgaard, and J. P. Wright, *J. Appl. Phys.* **114**, 024103 (2013).
31. K. Okazaki, *J. Am. Ceram. Soc.* **63**, 1150 (1983).
32. W. L. Warren, B. A. Tuttle, and D. Dimos, *Appl. Phys. Lett.* **67**, 1426 (1995).
33. H. N. Al-Shareef, D. Dimos, T. J. Boyle, W. L. Warren, and B. A. Tuttle, *Appl. Phys. Lett.* **68**, 690 (1996).
34. B. H. Park, B. S. Kang, S. D. Bu, T. W. Noh, J. Lee, H.-D. Kim, and T. H. Kim, *J. Korean Phys. Soc.* **35**, S1306 (1999).
35. S. Pojprapai, J. L. Jones, A. J. Studer, J. Russell, N. Valanoor, and M. Hoffman, *Acta Mater.* **56**, 1577 (2008).
36. S. Pojprapai, J. Russell, H. Manc, J. L. Jones, J. E. Daniels, and M. Hoffman, *Acta Mater.* **57**, 3932 (2009).
37. C. Brennan, *Ferroelectrics* **150**, 199 (1993).
38. W. D. Wei, Z. D. Qing, Y. Jie, Z. Q. Liang, L. H. Mei, W. Z. Ying, and C. M. Sheng, *Chin. Phys. Soc.* **18**, 2596 (2009).
39. J. O. Gentner, P. Gerthsen, N. A. Schmidt, and R. E. Send, *J. Appl. Phys.* **49**, 4485 (1978).
40. E. L. Colla, D. V. Taylor, A. K. Tagantsev, and N. Setter, *Appl. Phys. Lett.* **72**, 2478 (1998).

Large Electric Field-Induced Strain and Piezoelectric Responses of Lead-Free $\text{Bi}_{0.5}(\text{Na}_{0.80}\text{K}_{0.20})_{0.5}\text{TiO}_3\text{-Ba}(\text{Ti}_{0.90}\text{Sn}_{0.10})\text{O}_3$ Ceramics Near Morphotropic Phase Boundary

Pharatree Jaita,¹ Anucha Watcharapasorn,^{1,2} Nitish Kumar,³ David P. Cann,³ and Sukanda Jiansirisomboon^{4,*}

¹Department of Physics and Materials Science, Faculty of Science, Chiang Mai University, Chiang Mai 50200, Thailand

²Materials Science Research Center, Faculty of Science, Chiang Mai University, Chiang Mai 50200, Thailand

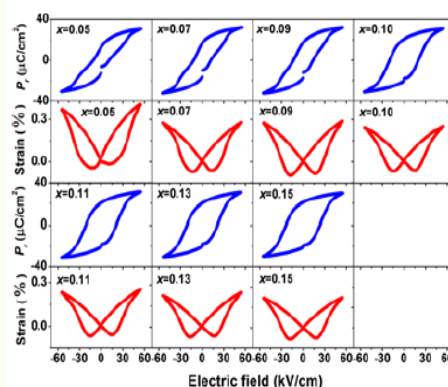
³Materials Science, School of Mechanical, Industrial and Manufacturing Engineering, Oregon State University, Corvallis, OR 97331, USA

⁴School of Ceramic Engineering, Suranaree University of Technology, Nakhon Ratchasima, 30000, Thailand

(received date: 14 November 2014 / accepted date: 23 February 2015 / published date: 10 September 2015)

Lead-free piezoelectric ceramics with compositions belonging to family of compositions $(1-x)\text{Bi}_{0.5}(\text{Na}_{0.80}\text{K}_{0.20})_{0.5}\text{TiO}_3\text{-}x\text{Ba}(\text{Ti}_{0.90}\text{Sn}_{0.10})\text{O}_3$ or $(1-x)\text{BNKT-}x\text{BTS}$ (when $x = 0.05 - 0.15$ mol fraction) near the morphotropic phase boundary (MPB) were fabricated by a conventional mixed oxide method. Sintered samples had relative densities greater than 98% of their theoretical values. X-ray diffraction data revealed that the MPB region consisted of coexisting rhombohedral and tetragonal phases in the BNKT-BTS system was identified over the entire compositional range. A large electric field-induced strain (S_{max}) of 0.36% and a normalized strain coefficient (d_{33}^*) of 649 pm/V were observed in the BNKT-0.05BTS sample. The sample close to the MPB composition (BNKT-0.11BTS) exhibited the maximum dielectric constant ($\epsilon_r = 1770$), temperature of maximum permittivity ($T_m = 333^\circ\text{C}$) and low-field piezoelectric coefficient ($d_{33} = 227$ pC/N), along with reasonable ferroelectric properties ($P_r = 20.6$ mC/cm², $R_{90} = 0.88$) and strain properties ($d_{33}^* = 445$ pm/V and $S_{\text{max}} = 0.24\%$).

Keywords: electric field-induced strain, piezoelectric, dielectric, ferroelectric, lead free



1. INTRODUCTION

PZT-based ceramics have been the dominant piezoelectric material for a half century. They are widely used in various applications such as actuators, sensors and ultrasonic transducers.^[1] The compositions near the morphotropic phase boundary (MPB) in PZT-based ceramics have attracted great attention because of their excellent electromechanical

properties.^[2] However, with the potential for regulations (RoHS/WEEE) that may restrict the use of hazardous substances in electronic devices, intensive efforts have been devoted to search for lead-free piezoelectric materials to serve as a substitute for PZT-based ceramics. In searching for high-performance lead-free piezoelectric ceramics, the MPB between two end members with different crystal structures has been one of the main strategies.

Within the MPB region, maximum polarization values are attainable which leads to enhanced electrical properties.^[2] Much attention has been paid to BNT-based solid solutions^[3-7]

*Corresponding author: sukanda.jian@cmu.ac.th
©KIM and Springer

because of their outstanding dielectric, ferroelectric and piezoelectric properties at compositions near the MPB. Generally the MPB region of the binary system is constrained to a very narrow range. For BNT-BKT or $\text{Bi}_{0.5}(\text{Na}_{1-x}\text{K}_x)\text{TiO}_3$ system, the MPB region was found over the range of $x = 0.16 - 0.20$. The $\text{Bi}_{0.5}(\text{Na}_{0.80}\text{K}_{0.20})_{0.5}\text{TiO}_3$ composition near the MPB possesses excellent ferroelectric ($P_r = 38 \mu\text{C}/\text{cm}^2$) and piezoelectric properties ($d_{33} = 167 \text{ pC}/\text{N}$, $d_{31} = 46.9 \text{ pC}/\text{N}$, $S_{\text{max}} = 0.19\%$, $d'_{33} = 240 \text{ pV}/\text{m}$ and $k_{33} = 0.56$).^[3,4] In addition, BNKT ceramics at the MPB have been modified by ionic substitution on the A and/or B-site in order to improve the dielectric and piezoelectric properties; for examples, BiAlO_3 -modified $\text{Bi}_{0.5}(\text{Na}_{0.80}\text{K}_{0.20})_{0.5}\text{TiO}_3$,^[5] $\text{Bi}_{0.5}(\text{Na}_{0.78}\text{K}_{0.22})_{0.5}\text{TiO}_3$ - $(\text{Bi}_{0.5}\text{La}_{0.5})\text{AlO}_3$,^[6] $\text{Bi}_{0.5}(\text{Na}_{0.84}\text{K}_{0.16})_{0.5}\text{TiO}_3$ - $\text{Ba}(\text{Zr}_{0.04}\text{Ti}_{0.96})\text{O}_3$ ^[7] and $\text{Bi}_{0.5}(\text{Na}_{0.80}\text{K}_{0.20})_{0.5}\text{TiO}_3$ - $(\text{Ba}_{0.7}\text{Sr}_{0.3})\text{TiO}_3$.^[8] All of these systems have demonstrated improvements in piezoelectric properties and facile poling. Our preliminary research has also indicated that $\text{Ba}(\text{Ti}_{0.90}\text{Sn}_{0.10})\text{O}_3$ was an effective additive for improving the piezoelectric properties of $\text{Bi}_{0.5}(\text{Na}_{0.80}\text{K}_{0.20})_{0.5}\text{TiO}_3$. The results showed that the BNKT-0.10BST composition exhibited an optimum low-field piezoelectric coefficient (d_{33}) of $215 \text{ pC}/\text{N}$.^[9]

However, in this work, $\text{Ba}(\text{Ti}_{0.90}\text{Sn}_{0.10})\text{O}_3$ was added to $\text{Bi}_{0.5}(\text{Na}_{0.80}\text{K}_{0.20})_{0.5}\text{TiO}_3$ ceramics to form solid solution of $(1-x)\text{Bi}_{0.5}(\text{Na}_{0.80}\text{K}_{0.20})_{0.5}\text{TiO}_3$ - $x\text{Ba}(\text{Ti}_{0.90}\text{Sn}_{0.10})\text{O}_3$ or $(1-x)\text{BNKT}$ - $x\text{BTS}$. This work is focused on the narrow MPB region $x = 0.05 - 0.15$ mol fraction. Further study in detail for MPB region of this system is necessary. The insight on composition dependent electrical properties would be beneficial to confirm the composition with the maximum piezoelectric responses. A systematic investigation on the electrical properties of refined compositions within the MPB region may also be helpful for further optimizing and understanding their functional properties and ultimately highlighting the most appropriate material for piezoelectric applications.

Moreover, to the best of our knowledge, there are currently no reports on the binary system of $\text{Bi}_{0.5}(\text{Na}_{0.80}\text{K}_{0.20})_{0.5}\text{TiO}_3$ - $\text{Ba}(\text{Ti}_{0.90}\text{Sn}_{0.10})\text{O}_3$ or BNKT-BTS to date. For $\text{Ba}(\text{Ti}_{0.90}\text{Sn}_{0.10})\text{O}_3$, it has been used in various applications such as capacitor, actuator and microwave phase shifter because of its high permittivity (~ 7500) and bias field sensitivity. It was expected that these new lead-free piezoelectric $(1-x)\text{BNKT}$ - $x\text{BTS}$ ceramics near the MPB composition would show superior electrical properties compared to the unmodified and previously modified BNKT ceramics.

2. EXPERIMENTAL PROCEDURE

A conventional mixed-oxide technique was used to synthesize $\text{Bi}_{0.5}(\text{Na}_{0.80}\text{K}_{0.20})_{0.5}\text{TiO}_3$ or BNKT and $\text{Ba}(\text{Ti}_{0.90}\text{Sn}_{0.10})\text{O}_3$ or BTS powders. Regent-grade powders of Bi_2O_3 (98%, Fluka), Na_2CO_3 (99.5%, Carlo Erba), TiO_2 (99%, Riedel-de Haën), K_2CO_3 (99%, Riedel-de Haën), BaCO_3 (98.5%,

Fluka) and SnO_2 (99.9%, Sigma-Aldrich) were used as the starting raw materials. All carbonate powders were first dried at 120°C for 24 h to remove any moisture. The raw materials of BNKT and BTS were stoichiometrically weight and mixed by ball milling in 99.9% ethanol for 24 h and the slurry was dried using an oven. Dried BNKT and BTS powders were separately calcined in a closed Al_2O_3 crucible at 900°C and 1200°C for 2 h, respectively. Both calcined powders were then weighed and mixed in order to produce an appropriate stoichiometry for the compositions $(1-x)\text{BNKT}$ - $x\text{BTS}$ with $x = 0.05, 0.07, 0.09, 0.10, 0.11, 0.13$ and 0.15 mol fraction. After drying and sieving, the powders were granulated by adding a few drops of 3 wt. % PVA as a binder and then pressed into disks with 10 mm in diameter and about 1.3 mm in thickness. The pellets were then preheated in air at 500°C for 1 h to remove organic binder and then sintered at 1125°C for 2 h dwell time with a heating/cooling rate of $5^\circ\text{C}/\text{min}$.

An x-ray diffractometer (XRD-Phillip, X-pert) was used to identify phase of powder and sintered ceramics in $2\theta = 20 - 70^\circ$. Bulk densities of all ceramics was determined using the Archimedes' method. The relative density of all samples was calculated based on the theoretical densities of BNKT ($5.84 \text{ g}/\text{cm}^3$)^[10] and BT ($6.01 \text{ g}/\text{cm}^3$).^[11] The surface morphologies of the sintered ceramics was observed using a field-emission scanning electron microscope (FE-SEM, JEOL JSM-6335F). The grain size of each sample was determined by a mean linear interception method from the SEM micrographs.

For electrical measurements, all samples were polished to 1 mm thickness and high temperature silver paste was fired on both sides at 700°C for 15 min to form the electrodes. Temperature dependence of the dielectric properties was measured using a 4284A LCR-meter over a temperature range of $25 - 500^\circ\text{C}$ at a frequency of 10 kHz. A ferroelectric test system based on Radiant Technology was used to measure the polarization-electric field (P - E) hysteresis behavior. An AC electric field of $55 \text{ kV}/\text{cm}$ at a frequency of 1 Hz was utilized in the hysteresis measurement. Electro-mechanical strain measurements were taken with the Radiant Technology ferroelectric system in conjunction with MTI Instruments 2100 Fotonic Sensor. Again, an electric field of $55 \text{ kV}/\text{cm}$ at a frequency of 0.1 Hz was utilized to determine the butterfly curve or bipolar strain-electric field (S - E) curve. The samples were poled in silicone oil at 60°C under DC electric field of $5.5 \text{ kV}/\text{mm}$ for 15 min. The low-field piezoelectric coefficient (d_{33}) was measured after aging for at least 24 h using d_{33} -meter (KCF technologies, S5865).

3. RESULTS AND DISCUSSION

After sintering the pellet-shaped samples at 1125°C for 2 h dwell time with a heating/cooling rate of $5^\circ\text{C}/\text{min}$, it was

Table 1. Physical, microstructure and electrical properties of (1-x)BNKT-xBTS ceramics.

x	Relative density (%)	Grain size (μm)	T_d ($^{\circ}\text{C}$)	T_m ($^{\circ}\text{C}$)	P_r^a ($\mu\text{C}/\text{cm}^2$)	E_c^a (kV/cm)	ϵ_r	d_{33} (pC/N)	S_{max} (%)	S_{neg} (%)	d'_{33} (pm/V)
0.05	99.14 ± 0.39	0.40 ± 0.04	153	321	12.80	10.90	1600	174	0.36	-0.02	649
0.07	99.08 ± 0.11	0.40 ± 0.03	154	328	16.47	11.75	1654	185	0.28	-0.06	505
0.09	98.93 ± 0.21	0.40 ± 0.05	155	331	17.22	13.40	1699	203	0.28	-0.08	508
0.10	98.88 ± 0.68	0.44 ± 0.04	159	333	20.49	19.92	1721	215	0.25	-0.07	450
0.11	98.83 ± 0.01	0.46 ± 0.08	168	333	20.60	21.05	1770	227	0.24	-0.07	445
0.13	98.80 ± 0.01	0.56 ± 0.08	171	323	20.27	21.28	1683	178	0.23	-0.07	440
0.15	98.77 ± 0.39	0.57 ± 0.08	178	322	20.88	23.55	1482	153	0.23	-0.07	409

^aFerroelectric data obtained at room temperature (25°C) and a frequency of 1 Hz.

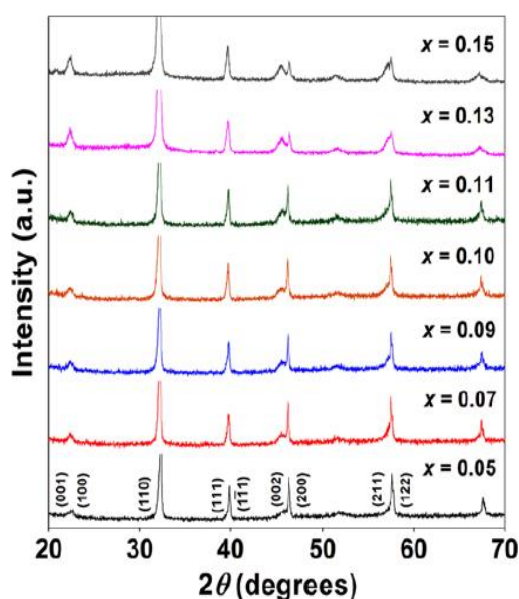


Fig. 1. X-ray diffraction patterns of (1-x)BNKT-xBTS ceramics sintered at 1125°C for 2 h with $2\theta = 20 - 70^{\circ}$.

found that high relative densities of 98 - 99% were obtained for all compositions and bulk density values exhibited a narrow range from 5.77 - 5.82 g/cm³ (Table 1). Based on the relative density values in Table 1, the data clearly show that the addition of BTS into BNKT ceramic caused a slight decrease in samples' relative density.

X-ray diffraction data on the sintered ceramics are shown in Fig. 1. All compositions exhibited a single perovskite phase at room temperature without any secondary phases within the detection limits of XRD. A series of stable solid solutions were formed between BNKT and BTS, confirming that the starting reagents reacted completely. With increasing BTS content, the diffraction peaks shifted to lower 2θ angles indicating an increase in the unit cell size. The magnitudes of the shifts were increased proportional to the concentration of BTS in the sample. This is expected because the ionic radius

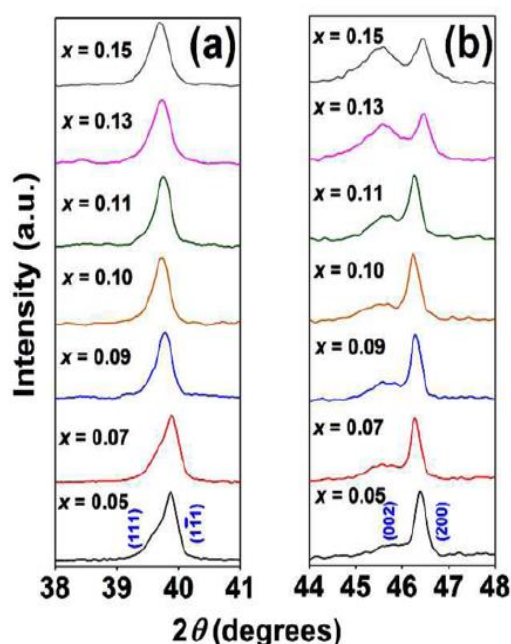


Fig. 2. X-ray diffraction patterns of (1-x)BNKT-xBTS ceramics sintered at 1125°C for 2 h where (a) $2\theta = 38 - 41^{\circ}$ and (b) $2\theta = 44 - 48^{\circ}$.

of Ba²⁺ (1.42 Å) is significantly larger than that of Bi³⁺ (1.17 Å), Na⁺ (1.18 Å), K⁺ (1.33 Å) and the B-cation Sn⁴⁺ (0.81 Å) is larger than Ti⁴⁺ (0.74 Å).^[12]

A detailed view of the XRD data in Figs. 2(a) and (b) suggests that the MPB region consists of coexisting rhombohedral and tetragonal phases over the entire compositional range. The composition BNKT-0.05BTS is likely a mixture of rhombohedral and tetragonal phases but with a higher volume fraction of rhombohedral phase over tetragonal phase. This is clearly seen by a noticeable splitting of (111)/(11̄1) peaks at $2\theta \sim 40^{\circ}$.^[13] With an increase in the BTS mole content, the splitting in the (111)/(11̄1) peaks decreases and the peak shape becomes nearly symmetric for compositions near $x = 0.15$. The compositional trend in the splitting in the

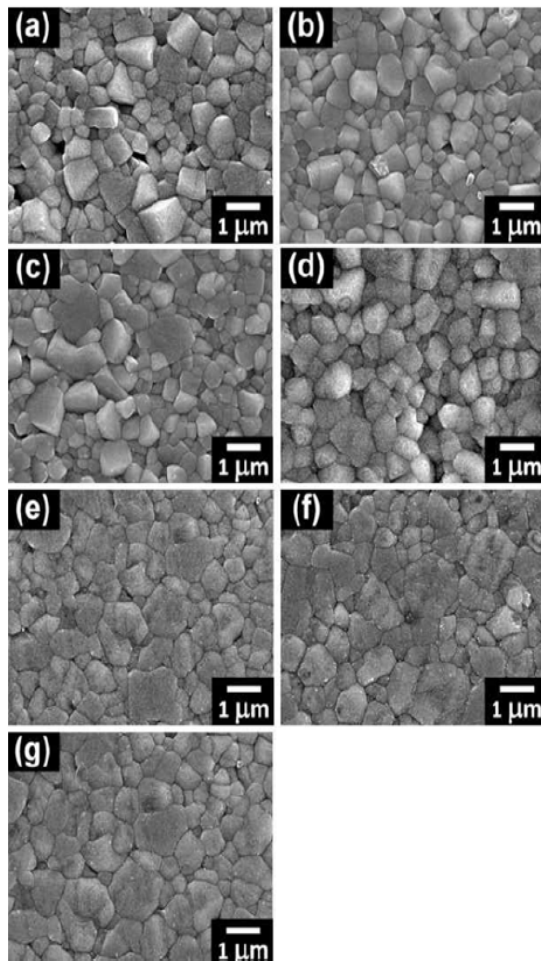


Fig. 3. Thermally etched surfaces of (1-x)BNKT-xBTS ceramics sintered at 1125°C for 2 h where (a) $x = 0.05$, (b) $x = 0.07$, (c) $x = 0.09$, (d) $x = 0.10$, (e) $x = 0.11$, (f) $x = 0.13$ and (g) $x = 0.15$.

(002)/(200) peaks is more complex. With an increase in BTS content, the splitting becomes more apparent however the peak shape is not clearly attributable to a doublet peak as expected for a single tetragonal phase. In fact, the integrated intensity of the (002) peak becomes comparable to the (002)/(200) peak. This could suggest texturing in the microstructure or the presence of multiple phases. Nonetheless, the addition of BTS would be expected to enhance the tetragonal distortions^[6] and the splitting of the (002)/(200) peaks does increase as shown in Fig. 2(b).

SEM micrographs of polished and thermally etched surfaces of BNKT-BTS ceramics are shown in Fig. 3. SEM observation confirmed that all samples were considerably dense with well-developed microstructure and granular morphology which were correlated with high relative densities of 98 - 99%. The average grain size values of all compositions was found to range from 0.40 - 0.57 μm (Table 1). The addition of 5 - 11 mol. % BTS into BNKT had no

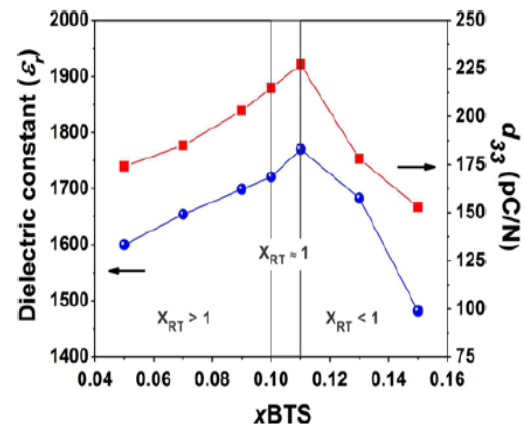


Fig. 4. Plot of room temperature dielectric constant (ϵ_r) and low-field piezoelectric coefficient (d_{33}) as a function of BTS content. $X_{RT} = f_{\text{Rhombohedral}}/f_{\text{Tetragonal}}$, where f = the fraction of rhombohedral and tetragonal phases.

significant influence on grain size and the values were similar (0.40 - 0.46 μm). However, average grain size values tended to slightly increase to around 0.56 - 0.57 μm with further increasing of BTS up to 13 - 15 mol. % and somewhat coarse grains formed near these compositions.

A plot of the room temperature dielectric constant (ϵ_r) and low-field piezoelectric coefficient (d_{33}) as a function of BTS content is shown in Fig. 4. The ϵ_r initially increased with increasing BTS content and reached a maximum value of 1770 for the BNKT-0.11BTS composition. It should be noted that the ϵ_r value for the BNKT-0.11BTS sample in this work were much higher than the value observed by Chen *et al.* ($\epsilon_r \sim 949$) for the BNKT-0.06BZT system near the MPB composition.^[7] With further increase in BTS content above $x = 0.11$, ϵ_r decreased to a minimum value of 1482. In addition, the piezoelectric behavior showed similar trend with increasing BTS content to that of the dielectric properties. The low-field d_{33} value increased from 174 pC/N for the BNKT-0.05BTS composition to a maximum value of 227 pC/N for the BNKT-0.11BTS composition. At higher BTS content, the d_{33} value was found to decrease to a minimum value of 153 pC/N. It can be seen that the dielectric and low-field piezoelectric properties exhibited a strong compositional and phase dependence within the MPB region of the BNKT-BTS system. While the XRD data was not conclusive in determining the coexistence of rhombohedral and tetragonal phases, this behavior suggests that an exist at approximately 11 mol. % BTS due to the enhanced dielectric and piezoelectric activity.^[14] This results is consistent with the finding of Lee *et al.*^[15] where the crystal structure changed from a rhombohedral-rich phase to a tetragonal-rich phase for BST content at 6 mol. % in the $(\text{Bi}_{0.5}\text{Na}_{0.5})\text{TiO}_3$ - $(\text{Ba}_{0.7}\text{Sr}_{0.3})\text{TiO}_3$ system, with a similar enhancement in dielectric and piezoelectric response.

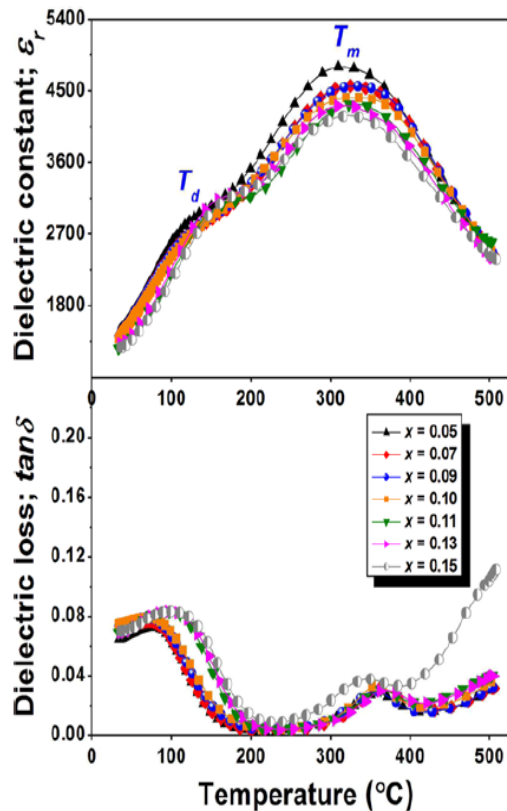


Fig. 5. Temperature dependence on dielectric constant (ϵ_r) and dielectric loss ($\tan\delta$) of $(1-x)\text{BNKT}-xB\text{TST}$ ceramics, measured at a frequency of 10 kHz.

Figure 5 shows temperature dependence of the dielectric constant (ϵ_r) and dielectric loss ($\tan\delta$) for $(1-x)\text{BNKT}-xB\text{TST}$ ceramics measured at a frequency of 10 kHz. Two dielectric anomalies, designated as T_d and T_m , were observed in the dielectric spectra of all BNKT-BTS compositions, which corroborates with the previously obtained dielectric behavior of BNT and other BNT-based ceramics.^[3-7,10,14] The depolarization temperature (T_d), corresponds to the relaxor transition from an ergodic to a non-ergodic state. The temperature at which ϵ_r reached a maximum value (T_m) corresponds to a diffuse transition. It's generally accepted that there is no phase transition across T_m in relaxors. It's a consequence of size distribution of polar nano regions, which also gives rise to frequency dependence.^[16] The dielectric spectra of all BNKT-BTS ceramics exhibited broad T_d and T_m peaks which could be attributed to compositional fluctuations occurring at A and/or B-site cations and resulting in disorder and change in the perovskite unit cell.^[17,18] This behavior suggested that BTS induced a diffuse phase transition in the BNKT-BTS system. Diffuse phase transitions have commonly been observed in other BNT-based ceramic systems in which either the A-site or B-site is occupied by at least two different cations.^[18] Both T_d and T_m values increased with increasing BTS content. The T_m reached a maximum value of 333°C for the composition close to the MPB with $x = 0.10 - 0.11$. With further increasing BTS content up to 13 - 15 mol. %, a slight decrease in T_m values was observed. Chen *et al.*^[7] who studied the addition $\text{Ba}(\text{Zr}_{0.04}\text{Ti}_{0.96})\text{O}_3$ into $\text{Bi}_{0.5}(\text{Na}_{0.84}\text{K}_{0.16})_{0.5}\text{TiO}_3$ ceramics also found similar an

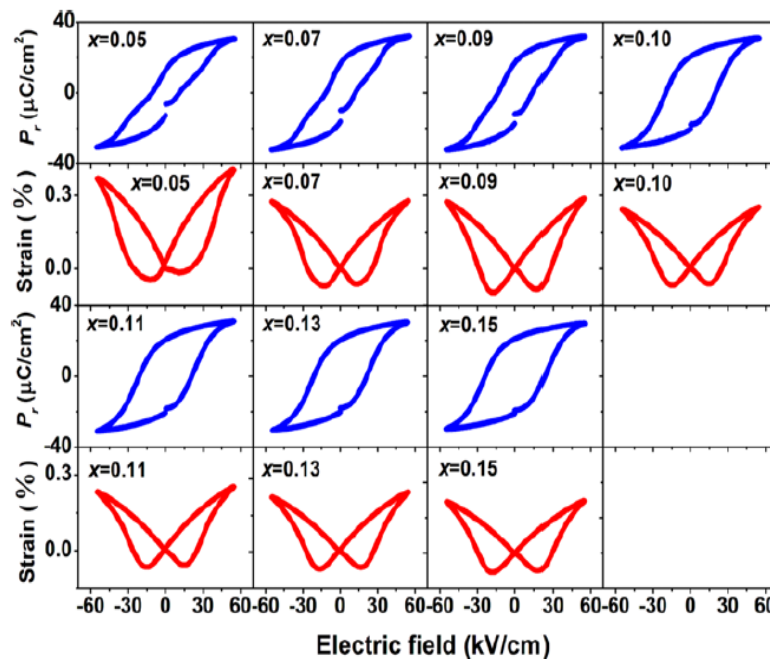


Fig. 6. Polarization-electric field (P - E) hysteresis loops and bipolar strain-electric field (S - E) of $(1-x)\text{BNKT}-xB\text{TST}$ ceramics, measured at room temperature, under an electric field of 55 kV/cm where $x = 0.05 - 0.15$.

enlargement of unit cell and then decreasing T_m value. In contrast to T_m , T_d value was found to increase with BTS concentration up to maximum amount used in this study. This indicates that ionic substitution with BTS stabilized ferroelectric ordering. This is also related to the large tetragonal splitting seen in the XRD data (Fig. 2).

Figure 6 shows polarization-electric field (P - E) hysteresis data for $(1-x)\text{BNKT}-x\text{BTS}$ system compositions obtained at room temperature (25°C). The P_r and E_c values determined from the data, were listed in Table 1. All samples showed well saturated P - E loops at room temperature. It is clear from Fig. 6 that BTS had a noticeable influence on the hysteresis behavior. Bipolar strain-electric field (S - E) curves of $(1-x)\text{BNKT}-x\text{BTS}$ ceramics measured at room temperature under a maximum electric field of 55 kV/cm and a frequency of 0.1 Hz are also shown in Fig. 6. The maximum strain (S_{max}), negative strain (S_{neg} , i.e. the difference between zero-field strain and the lowest strain^[19]), and normalized strain coefficient ($d_{33}^* = S_{max}/E_{max}$) are also listed in Table 1. A large strain of 0.36% and d_{33}^* of 649 pm/V were obtained for BNKT-0.05BTS composition. The d_{33}^* value of this BNKT-0.05BTS studied was much higher than these reported for other polycrystalline lead-free systems.^[5,19,20] The emergence of such large strain was accompanied by a significant reduction in S_{neg} of -0.02%. Giant strain and behavior of bipolar S - E loops were similarly found in many recent works on BNT-based ceramics.^[5,7,18-24] With further increasing BTS content up to 7 - 15 mol. %, the bipolar S - E loops exhibited back to normal butterfly-like strain loops. An increase in S_{neg} to around -0.06 to -0.08% was observed. This corresponded to an increase in P_r from 12.80 $\mu\text{C}/\text{cm}^2$ to around 20 - 21 $\mu\text{C}/\text{cm}^2$ with increasing E_c value (Table 1). Correspondingly, a slight decrease in S_{max} and d_{33}^* values were observed at higher concentrations of BTS. The addition of 15 mol. % BTS was found to decrease S_{max} and d_{33}^* to the minimum values of 0.23% and 409 pm/V, respectively.

All the above characteristics are typical of BNT-based ceramics. In the ceramic system studied in this work, in essence BTS was added to an MPB 80BNT-20BKT or $\text{Bi}_{0.5}(\text{Na}_{0.80}\text{K}_{0.20})_{0.5}\text{TiO}_3$ composition. As has been reported earlier, BTS is a stable ferroelectric ceramic with a Curie temperature of ~60°C.^[25] As Sn replaces Ti in BTS, the Curie temperature goes down and above 20% substitution level, it starts to exhibit relaxor behavior.^[25] Therefore, the BTS in this study (which has 10% Ti substituted by Sn) should be expected to have ferroelectric ordering at room temperature. Therefore, addition of more BTS to the solid solution should impart more ferroelectric characteristics to the P - E and S - E curves like similar ceramic systems e.g. BNT-BKT-BT and others.^[4,26] As was seen earlier, this was supported by the XRD data (Fig. 1 and Fig. 2) as well where the (200) peak splitting enhanced as the amount of BTS content increased. With increase in the content of stable

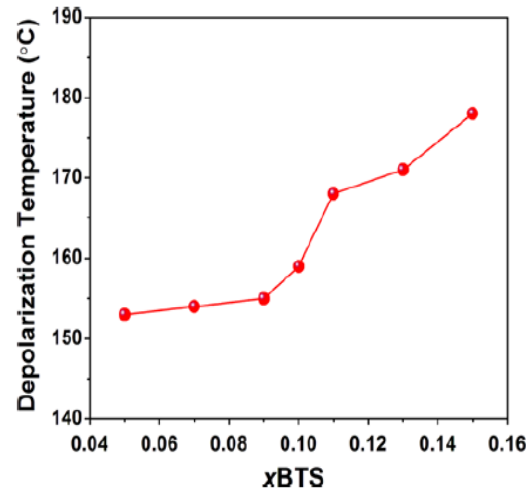


Fig. 7. Plots of depolarization temperature as a function of BTS content.

ferroelectric end-member in the solid solution, an increase in domain stability should be expected. This could be seen in Fig. 6, where the polarization curves transitioned from pinched to more ferroelectric-like behavior as the amount of BTS increased in the solid solution. A similar characteristic was observed in S - E curves as well where negative strain increased with BTS content. These suggested that the compositions transitioned from ergodic behavior where domains are unstable in absence of electric field, to a non-ergodic relaxor behavior where domains are stable even in absence of electric field after a relaxor to ferroelectric transformation has occurred on application of high-enough electric fields. It was reflected in the P_r and E_c values as well as listed in Table 1. A non-ergodic composition is in general expected to have higher E_c and P_r values. An increase in domain stability was also supported by increase in depolarization temperature with BTS content (Fig. 7 and Table 1), where it could be seen that T_d increased from 153°C to 178°C as BTS content increased from 5 to 15 mol. % in the solid solution. This indicated that the compositions with more BTS were more non-ergodic at room temperature and thus had higher domain stability. A decrease in d_{33}^* with BTS content could be attributed to increase in tetragonality in polycrystalline ceramics, where constraints put by grain boundaries makes it more difficult for domains to move as the tetragonal behavior increases.

Figure 8 shows the evolution of polarization loops for various compositions with temperature. It supported the argument presented above regarding the stability of domains and non-ergodic to ergodic transition as well. In general, a pinched P - E behavior indicates the onset of ergodic behavior. It could be seen in Fig. 8 that for 5% BTS composition, the loop was pinched at a temperature as low as 50°C. On the other hand, for 15% BTS composition, the pinched-loop

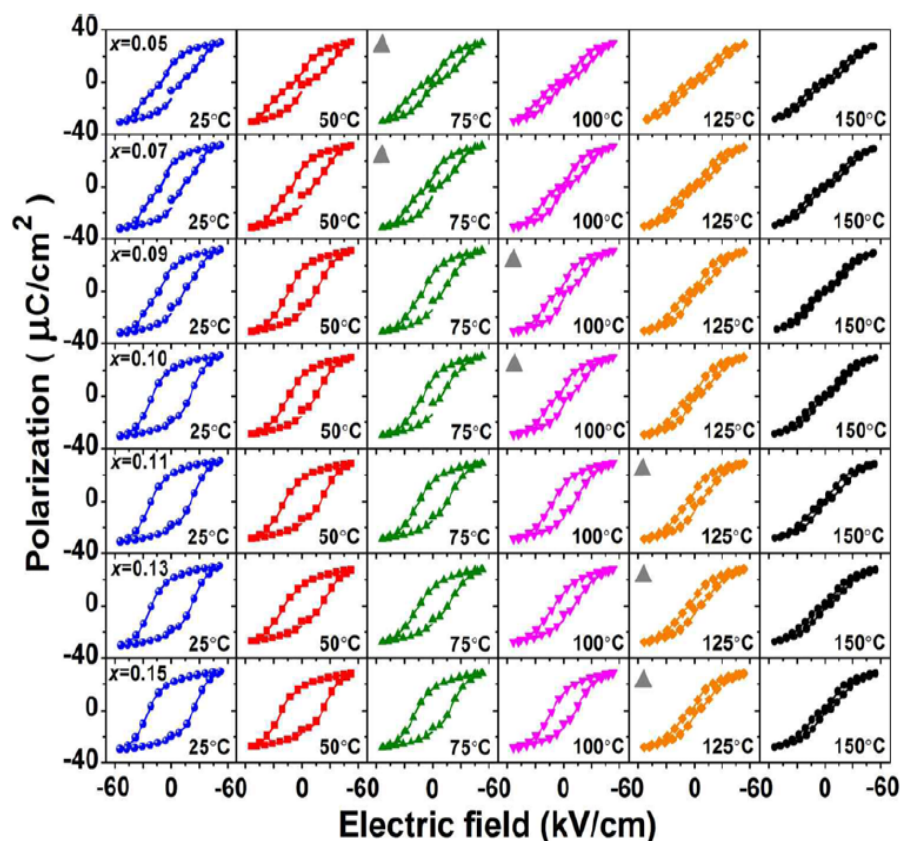


Fig. 8. Temperature dependent on polarization-electric field (P - E) hysteresis loops of $(1-x)\text{BNKT-xBTS}$ ceramics, measured under an electric field of 55 kV/cm and a frequency of 1 Hz; where \blacktriangle = indicates approximate onset temperature of the relaxor transition from a non-ergodic to ergodic state for each composition.

behavior was not evident even at 100°C. It clearly suggested that non-ergodic to ergodic relaxor transition was pushed to higher temperatures as the BTS content increased. It was consistent with Fig. 7, where depolarization temperature determined from temperature dependence of permittivity increased as the amount of BTS increased in the solid solution.

4. CONCLUSIONS

The $(1-x)\text{Bi}_{0.5}(\text{Na}_{0.80}\text{K}_{0.20})_{0.5}\text{TiO}_3\text{-xBa}(\text{Ti}_{0.90}\text{Sn}_{0.10})\text{O}_3$ or $(1-x)\text{BNKT-xBTS}$ (when $x = 0.05 - 0.15$ mol fraction) ceramics within the MPB region were successfully synthesized by a conventional mixed oxide method. In this MPB region, varying fraction of rhombohedral and tetragonal ferroelectric phases of this system was found throughout the whole composition range with tetragonal phase becoming dominant at higher BTS content. The sample near the region (*i.e.* $x = 0.10 - 0.11$) showed an improvement of electrical properties compared to that of other compositions. The relative amount of rhombohedral and tetragonal structure as well as lattice

expansion caused the non-ergodic to ergodic transition temperature to be higher with increasing BTS content. In this study, it seemed that the optimum composition ($x = 0.10 - 0.11$) was obtained when nearly equal fraction of rhombohedral and tetragonal phases was present in the system at which the temperature of maximum permittivity ($T_m = 333^\circ\text{C}$) and relatively good dielectric ($\epsilon_r = 1770$, $\tan\delta = 0.0746$), ferroelectric ($P_r = 20.60 \mu\text{C}/\text{cm}^2$) and piezoelectric properties ($d_{33} = 227 \text{ pC/N}$, $d_{33}^* = 445 \text{ pm/V}$ and $S_{\text{max}} = 0.24\%$) were obtained.

ACKNOWLEDGEMENTS

This work is financially supported by the Thailand Research Fund (TRF) (Grant no. RSA5780032). The Faculty of Science and the Graduate School, Chiang Mai University, Materials Science, School of Mechanical, Industrial and Manufacturing Engineering, Oregon State University, USA are also acknowledged. P. Jaita would like to acknowledge financial support from the TRF through the Royal Golden Jubilee Ph.D. Program.

REFERENCES

1. S. H. Lee, H. J. Kim, and Y. H. Lee, *Electron. Mater. Lett.* **8**, 289 (2012).
2. T. Takenaka, H. Nagata, Y. Hiruma, Y. Yoshii, and K. Matumoto, *J. Electroceram.* **19**, 259 (2007).
3. A. Sasaki, T. Chiba, Y. Mamiya, and E. Otsuki, *Jpn. J. Appl. Phys.* **38**, 5564 (1999).
4. K. Yoshii, Y. Hiruma, H. Nagata, and T. Takenaka, *Jpn. J. Appl. Phys.* **45**, 4493 (2006).
5. A. Ullah, C. W. Ahn, A. Hussain, I. W. Kim, H. I. Hwang, and N. K. Cho, *Solid State Commun.* **150**, 1145 (2010).
6. A. Ullah, C. W. Ahn, S. Y. Lee, J. S. Kim, and I. W. Kim, *Ceram. Int.* **38S**, S363 (2012).
7. Z. W. Chen and J. Q. Hu, *Adv. Appl. Ceram.* **107**, 222 (2008).
8. P. Jaita, A. Watcharapasorn, and S. Jiansirisomboon, *Electron. Mater. Lett.* **9**, 437 (2013).
9. P. Jaita, A. Watcharapasorn, D. P. Cann, and S. Jiansirisomboon, *J. Alloy Compd.* **596**, 98 (2014).
10. Y. R. Zhang, J. F. Li, and B. P. Zhang, *J. Am. Ceram. Soc.* **91**, 2716 (2008).
11. H. E. Swanson and R. K. Fuyat, *Natl. Bur. Stand. Circ. (U.S.)* **539**, 3, 44 (1954).
12. R. D. Shannon, *Acta Cryst.* **A32**, 751 (1976).
13. Y. J. Dai, X. W. Zhang, and K. P. Chen, *Int. J. Appl. Ceram. Technol.* **8**, 423 (2011).
14. W. Zhao and R. Zuo, *Ceram. Int.* **39**, 9121 (2013).
15. W. C. Lee, C. Y. Huang, L. K. Tsao, and Y. C. Wu, *J. Alloy Compd.* **492**, 307 (2010).
16. G. A. Smolenskii, V. A. Isupov, A. I. Agranovskaya, and N. N. Krainik, *Sov. Phys. Solid State.* **2**, 2651 (1961).
17. D. Lin, K. W. Kwok, and H. L. W. Chan, *Solid State Ionics* **178**, 1930 (2008).
18. G. Fan, W. Lu, X. Wang, F. Liang, and J. Xiao, *J. Phys. D: Appl. Phys.* **41**, 035403 (2008).
19. S. T. Zhang, B. Yang, and W. Cao, *Acta Mater.* **60**, 469 (2012).
20. B. Wang, L. Luo, F. Ni, P. Du, W. Li, and H. Chen, *J. Alloy Compd.* **526**, 79 (2012).
21. A. Hussain, A. Zaman, Y. Iqbal, and M. H. Kim, *J. Alloy Compd.* **574**, 320 (2013).
22. W. Jo, R. Dittmer, M. Acosta, J. Zang, C. Groh, E. Sapper, K. Wang, and J. Rödel, *J. Electroceram.* **29**, 71 (2012).
23. J. Li, F. Wang, C. M. Leung, S. W. Or, Y. Tang, X. Chen, T. Wang, X. Qin, and W. Shi, *J. Mater. Sci.* **46**, 5702 (2011).
24. W. Jo, T. Granzow, E. Aulbach, J. Rodel, and D. Damjanovic, *J. Appl. Phys.* **105**, 094102 (2009).
25. X. Wang and B. Li, *Solid State Commun.* **149**, 537 (2009).
26. T. Takenaka, H. Nagata, and Y. Hiruma, *Jpn. J. Appl. Phys.* **47**, 3787 (2008).

Dielectric, Polarization and Strain Response of Enhanced Complex Ceramics: The Study through $\text{Pb}(\text{Zr}_{0.52}\text{Ti}_{0.48})\text{O}_3\text{-SrBi}_2\text{Ta}_2\text{O}_9$

ORAPIM NAMSAR,¹ ANUCHA WATCHARAPASORN,^{1,2}
 MARK HOFFMAN,³ JULIA GLAUM,³ AND SUKANDA
 JIANSIRISOMBOON^{4,*}

¹Department of Physics and Materials Science, Faculty of Science, Chiang Mai University, Chiang Mai 50200, Thailand

²Materials Science Research Center, Faculty of Science, Chiang Mai University, Chiang Mai 50200, Thailand

³School of Materials Science and Engineering, University of New South Wales, NSW 2052, Australia

⁴School of Ceramic Engineering, Suranaree University of Technology, Nakhon Ratchasima 30000, Thailand

Electrical properties of the (1-x)PZT-xSBT ceramics (0.1 ≤ x ≤ 0.3) were investigated in comparison with pure PZT and SBT ceramics. It was found that the dielectric constant increased with small addition of SBT (x = 0.1) into PZT. The hysteresis loop measurement demonstrated that the PZT-SBT ceramics showed larger remanent polarization than pure PZT and less coercive field than pure SBT ceramic. Strain behavior showed a symmetric butterfly curve in the compositions with 0 ≤ x ≤ 0.3 but the low strain obtained was found in pure SBT. This research suggested that 0.9PZT-0.1SBT ceramic is a promising material to be further utilized in ferroelectric memory devices.

Keywords Dielectric properties; ferroelectric properties; piezoelectric properties; PZT-SBT

Introduction

$\text{Pb}(\text{Zr}_{0.52}\text{Ti}_{0.48})\text{O}_3$ or PZT is an important material used in many ferroelectric applications (actuators, capacitors and non-volatile random access memories) because of its excellent dielectric, ferroelectric and piezoelectric properties [1]. Nonetheless, one of the problems with PZT is its low fatigue resistance [2] which is a disadvantage for ferroelectric devices. Layer-type bismuth compound of $\text{SrBi}_2\text{Ta}_2\text{O}_9$ is considered as an alternative ferroelectric material which has come to play an important role in many ferroelectric devices due to its fatigue-free properties [3]. But, SBT still has several drawbacks such as small remanent

Received October 26, 2014; in final form January 19, 2015.

*Corresponding author. E-mail: sukanda.jian@cmu.ac.th

Color versions of one or more figures in this article can be found online at www.tandfonline.com/gfer.

[247]/79

polarization, high coercive field, low dielectric constant and poor piezoelectric properties [4–5].

Previous researchers have attempted to combine the advantages of PZT and SBT together in the form of multilayer-structured films. In 2008, Zhang *et al.* [6] studied ferroelectric properties of bilayer structured $\text{Pb}(\text{Zr}_{0.52}\text{Ti}_{0.48})\text{O}_3/\text{SrBi}_2\text{Ta}_2\text{O}_9$ (PZT/ SBT) thin films. They reported that the films exhibited larger remanent polarization than pure SBT and better fatigue resistance than pure PZT. Park *et al.* [7] studied ferroelectric properties of four different PZT/SBT multilayer films, i.e. 4-PZT, PZT/ 2-SBT/PZT, SBT/2-PZT/SBT, and 4-SBT. They reported that the sandwiched structure of SBT/2-PZT/SBT exhibited higher remanent polarization value, which was comparable to that of 4-PZT multilayer films and much higher than that of pure 4-SBT multilayer film. Moreover, the films with SBT layers in contact with Pt electrodes showed improved fatigue behavior compared to the films with PZT layers at the top and bottom. These results suggested that the combination of PZT and SBT might lead to better ferroelectric materials. However, fundamental research on the combination of these two important ferroelectric materials in a form of polycrystalline ceramic is quite scarce. Recently, Namsar *et al.* [8] studied the ferroelectric properties $(1-x)\text{PZT}-x\text{SBT}$ ceramics (when $x = 0, 0.1, 0.3$ and 0.5) at a low electric field (~ 25 kV/cm). The results showed that the ferroelectric properties of PZT were improved after incorporation of a small amount of SBT ($0.1 \leq x \leq 0.3$) (i.e. increased remanent polarization and decreased coercive field). But so far, the dielectric, piezoelectric as well as the saturated ferroelectric hysteresis loops for these ceramics have not been studied. Therefore, the present study aims to further investigate the important electrical characteristics (i.e. dielectric, polarization and strain response) of the $(1-x)\text{PZT}-x\text{SBT}$ ($0.1 \leq x \leq 0.3$) ceramics, in comparison with pure PZT and SBT ceramics.

Experimental Procedures

The starting powders of $(1-x)\text{Pb}(\text{Zr}_{0.52}\text{Ti}_{0.48})\text{O}_3-x\text{SrBi}_2\text{Ta}_2\text{O}_9$ or $(1-x)\text{PZT}-x\text{SBT}$ with $x = 0, 0.1, 0.3$ and 1.0 weight fraction, were prepared using raw materials of PbO (99%, Riedel-de Haën), ZrO_2 (99%, Riedel-de Haën), TiO_2 (99%, Riedel-de Haën), SrCO_3 (98%, Aldrich), Bi_2O_3 (99.9%, Aldrich) and Ta_2O_5 (99%, Aldrich). The starting powders were weighed, ball-milled in ethanol for 24 h and dried. After that, the mixed powders were calcined at 800°C for 2 h for PZT and at 950°C for 3 h for SBT powders. The calcined PZT and SBT powders were then weighed with different weight fraction of SBT, mixed by ball-milling and dried to produce a powder mixture of $(1-x)\text{PZT}-x\text{SBT}$. Each powder was pressed into disc-shaped pellets with the size of 10 mm in diameter and 1.50 mm in thickness. In order to avoid compositional deviation from PbO and Bi_2O_3 volatilization during sintering, the pellets were covered with their own powders and sintered at 1200°C for 3 h.

The crystal structure and phase evolution of the nominal $(1-x)\text{PZT}-x\text{SBT}$ ceramics were identified by an X-ray diffractometer (XRD, Phillip Model X-pert). Microstructural investigation of the ceramics was observed using a scanning electron microscope (SEM, JEOL JSM-6335F). The average grain size in the samples was determined using the Image J program. The polarization - electric field (P - E) and strain - electric field (S - E) loops were characterized at a frequency of 50 Hz using an aixACCT TF2000HS analyzer equipped with a laser interferometer. The dielectric constant and loss at room temperature were analyzed by LCR Hitester (Agilent, E4980A) with a frequency of 1 kHz. In

addition, the LCR Hitester (Hioki 3532–50) connected to a high-temperature furnace was used to measure the high temperature dielectric properties.

Results and Discussion

The phase formation behavior of the sintered XRD patterns for pure PZT, $(1-x)\text{PZT-xSBT}$ ($0.1 \leq x \leq 0.3$) and pure SBT ceramics was determined using X-ray diffraction as shown in Figure 1(a). For the ceramics with $0 \leq x \leq 0.3$, the experimental results on the phase evolution have been discussed extensively in earlier publications [8]. However, some additional phase characteristics for these ceramics are further discussed here. For pure PZT ceramic, a tetragonal perovskite structure with a cell volume (V) of $\sim 67.15 \text{ \AA}^3$ and tetragonality (c/a) of ~ 1.017 was observed. The dominant tetragonal structure was confirmed by the splitting of $(112)_T$ and $(211)_T$ peaks at $2\theta \sim 54\text{--}56.5^\circ$ as shown in Figure 1(b). On the other hand, the SBT ceramic showed a single-phase orthorhombic bismuth-layered perovskite structure with a large cell volume, high tetragonality (c/a) and low orthorhombic distortion (b/a). Addition of 0.1 SBT into PZT caused a slight shift of the PZT peaks to higher diffraction angles. The diffraction peak around 2θ of $54\text{--}56.5^\circ$ was also found to split as shown in Figure 1(b). In addition, a small amount of a new multinary phase was also observed in this sample. The new multinary phase was $\text{Pb}_{1.2}\text{Ti}_{0.4}\text{Ta}_{1.6}\text{O}_6$ (PTT). As the amount of SBT was increased to $x = 0.3$, the intensity of the PZT peaks decreased rapidly while the intensity of the PTT peaks increased markedly. The PZT peaks continuously shifted toward higher angles. In addition, the diffraction peak around 2θ of $54\text{--}56.5^\circ$ was found to transform from two peaks of $(112)_T$ and $(211)_T$ of tetragonal phase, into only single peak of $(121)_R$ (rhombohedral phase) (Figure 1(b)). With careful observation, it can be seen that the XRD peaks of PZT phase in these ceramics ($0.1 \leq x \leq 0.3$) were broader than those of pure PZT ceramic. This suggested that the PZT

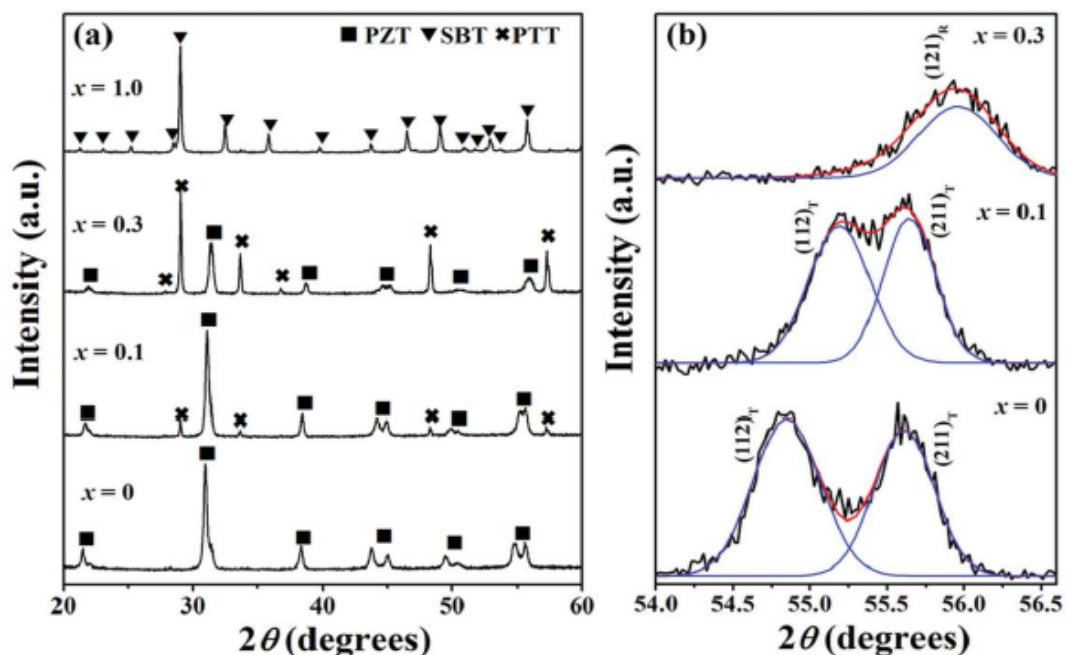


Figure 1. (a) X-ray diffraction patterns of $(1-x)\text{PZT-xSBT}$ ceramics and (b) comparison of $(112)_T$, $(121)_R$ and $(211)_T$ peaks reflections for the ceramics with $0 \leq x \leq 0.3$.

phase in these ceramics was PZT-based solid solution. More importantly, it was noteworthy that the original SBT phase was not present in the ceramics with $0.1 \leq x \leq 0.3$. There were two processes that account for the disappearance of SBT phases. The first process was the dissolution of SBT into PZT matrix phase to form the PZT-based solid solutions. This process was confirmed by the reduction in unit cell volume (V) and tetragonality (c/a) of PZT phase as listed in Table 1. The decrease of the unit cell volume and tetragonality resulting from SBT addition was attributed to the occupation of smaller Sr^{2+} (1.18 Å [9]) and Bi^{3+} (1.03 Å [9]) ions at the Pb^{2+} (1.19 Å [9]) sites, and Ta^{5+} (0.64 Å [9]) into Zr^{4+} (0.78 Å)/ Ti^{4+} (0.605 Å [9]) sites of perovskite PZT lattice. Secondly, some SBT phase reacted with some PZT phase to form a new multinary compound i.e. PTT during sintering process. As in the XRD results, the addition of SBT into PZT caused a significant change in phase transformation of $(1-x)\text{PZT}-x\text{SBT}$ ceramics which in turn was expected to influence their electrical properties.

The fracture surfaces for pure PZT, PZT-SBT and pure SBT ceramics were also examined by SEM, as seen in Figure 2. Pure PZT ceramic had equiaxed grains with mainly transgranular fracture mode, as provided in Figure 2(a). Whereas, the SBT ceramic was composed of plate-like grains with mainly intergranular fracture mode (Figure 2(d)). For the samples with $0.1 \leq x \leq 0.3$, the ceramics were composed of both equiaxed grains of PZT and irregularly-shaped grains of PTT. The PZT phase in these samples showed mainly an intergranular fracture mode (as labeled by open circle), which implied the enhancement of grain strength after SBT incorporation. Whereas, the mainly transgranular fracture mode was observed in PTT phase. From these observations, the addition of SBT caused the transformation of the fracture mode from mainly transgranular in pure PZT ceramic to the mixed-mode between intergranular and transgranular in the PZT-SBT ceramics. This phenomenon might be due to the heterogeneous microstructure and different orientation between the PZT and PTT grains. Moreover, the PZT-SBT ceramics showed dense structures. The increase in the densification of these samples could be attributed to a donor-like substitution effect. It is well known that the densification mechanism of the perovskite PZT is controlled by the concentration of A-site vacancies [10]. In our samples, the Bi and Ta additives from SBT are proposed to substitute into the A- and B-site of perovskite PZT possibly leading to the creation of Pb (A-site) vacancies to maintain electroneutrality, which in turn would enhance the diffusion rate and promote densification of the ceramics. Considering the grain size (see Table 2), it was found that the addition of SBT ($0.1 \leq x \leq 0.3$) led to the reduction in grain size of PZT matrix phase. This indicated that the grain growth of PZT matrix was effectively limited by adding SBT. The decrease in grain size in these ceramics could be also described by donor-like substitution. As mentioned previously, Pb-site vacancies were believed to

Table 1
The crystal structural parameters of pure PZT, PZT-SBT and pure SBT ceramics

Composition	PZT phase		PTT phase	SBT phase		
	$V (\text{\AA}^3)$	c/a	$V (\text{\AA}^3)$	$V (\text{\AA}^3)$	b/a	c/a
PZT	67.154	1.017	—	—	—	—
0.9PZT-0.1SBT	66.504	1.007	1209.50	—	—	—
0.7PZT-0.3SBT	65.337	1.005	1204.30	—	—	—
SBT	—	—	—	767.57	1.002	4.5545

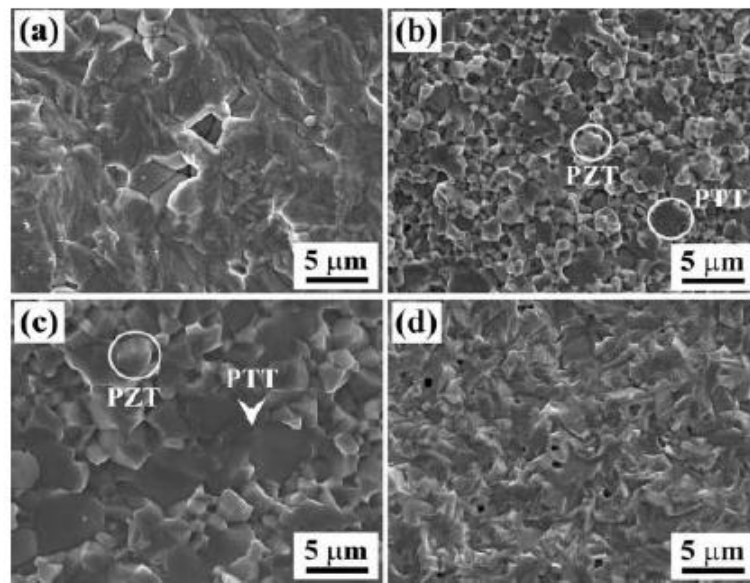


Figure 2. Fracture surfaces of $(1-x)PZT-xSBT$ ceramics, where (a) pure PZT, (b) 0.9PZT-0.1SBT, (c) 0.7PZT-0.3SBT and (d) pure SBT.

create in the PZT structure by the donor ions (Bi^{3+} , Ta^{5+}) of SBT. These vacancies existed along grain boundaries which was thermodynamically more stable. This pinned the grain boundaries and limited grain growth, resulting in relatively small grains [11–12]. Based on these results, the addition of SBT could modify the microstructures of PZT-SBT ceramics.

The room temperature dielectric constant (ϵ_r) and loss ($\tan \delta$) measured at 1 kHz are listed in Table 3. It was found that the perovskite PZT and layered perovskite SBT ceramics exhibited quite different dielectric behavior. Namely, pure PZT ceramic had high dielectric constant and loss whereas pure SBT possessed low dielectric constant and loss. When a small amount of 0.1SBT was added into PZT, the dielectric constant and loss increased significantly. This result was mainly due to smaller grain size of ferroelectric PZT matrix phase. In the sample with smaller grain size, clamping of domain walls at the grain boundaries from its neighbors caused the relative increase in domain density

Table 2
Average grain size of pure PZT, PZT-SBT and pure SBT ceramics

Composition	Average grain size (μm)			
	PZT grains	PTT grains	SBT grains	
			Thickness	Length
PZT	2.72 ± 0.13^a	—	—	—
0.9PZT-0.1SBT	1.73 ± 0.07	2.83 ± 0.12	—	—
0.7PZT-0.3SBT	1.84 ± 0.09	3.63 ± 0.38	—	—
SBT	—	—	0.76 ± 0.05^a	2.15 ± 0.11^a

^aThe grain sizes were measured from the thermally etched surface.

Table 3
Dielectric, ferroelectric and piezoelectric properties of pure PZT, PZT-SBT and pure SBT ceramics

x	Room temp. dielectric props.		High temp. dielectric props.		T_c	Ferroelectric props.		Piezoelectric props.	
	ϵ_r	$\tan \delta$	ϵ_r	$\tan \delta$		$2P_r$ ($\mu\text{C}/\text{cm}^2$)	$2E_c$ (kV/mm)	S_{\max} (%)	d_{33}^* (pm/V)
0	996.72	0.006	19432.39	3.901	387	27.33	3.05	0.16	350.93
0.1	1636.48	0.016	19605.94	0.254	239	38.82	3.80	0.14	350.72
0.3	1005.74	0.031	1569.83	0.060	120	6.52	2.72	0.03	58.49
1.0	117.99	0.007	804.82	1.242	320	2.21	5.46	0.02	—

[13]. Higher domain density also allowed a larger amount of wall movement [14–15], which in turn resulted in larger dielectric constant and loss observed in the small-grained sample. With an increase in the nominal SBT content to $x = 0.3$, the dielectric constant decreased but the dielectric loss increased sharply. This result seemed to be attributed to an increase in the non-piezoelectric cubic PTT phase in the ceramics as observed in X-ray diffraction patterns. Our results shown here were in good agreement with the reduction in dielectric properties of Pb-based ceramics due to the presence of a non-ferroelectric cubic phase [16–17].

The dielectric properties versus temperature behavior of PZT-SBT ceramic was then analyzed and compared to pure PZT and pure SBT ceramics, as shown in Figure 3. The variation of the Curie temperature (T_c) and dielectric data are listed in Table 3. It was found that pure PZT ceramic showed a high dielectric constant and loss with a single phase transition at T_c of $\sim 387^\circ\text{C}$. However, pure SBT ceramic exhibited a small dielectric constant (~ 805), low dielectric loss (1.242) and high T_c ($\sim 320^\circ\text{C}$). After the small amount of 0.1 SBT was incorporated into PZT, the dielectric constant did not change significantly, while dielectric loss and T_c decreased. Further increase in the addition of SBT to $x = 0.3$ SBT caused a large drop of the dielectric constant, dielectric loss and T_c . The reduction in dielectric constant in this ceramic was mainly due to the occurrence of cubic PTT phase. Considering T_c , the decrease in T_c as a result of the addition of SBT

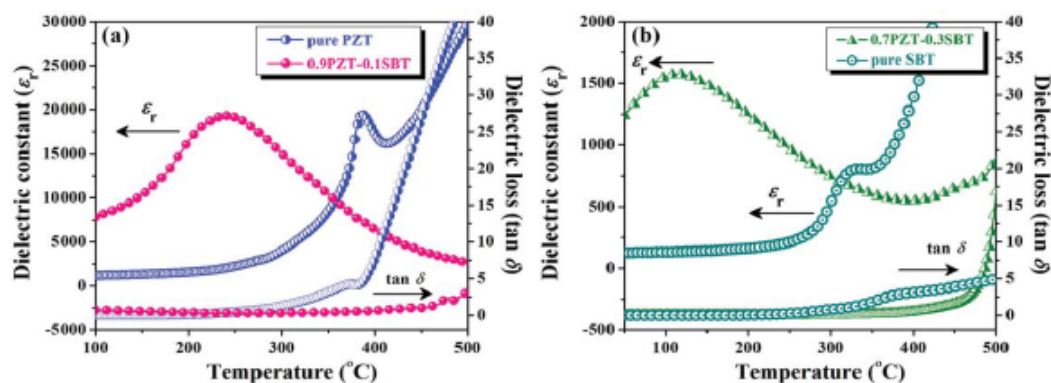


Figure 3. Temperature dependences of dielectric constant (ϵ_r) and loss ($\tan \delta$) for $(1-x)\text{PZT}-x\text{SBT}$ ceramics, when (a) $x = 0 - 0.1$ and (b) $x = 0.3$ and 1.0 .

($0.1 \leq x \leq 0.3$) could be explained by their tetragonality (c/a). Since tetragonality (or tetragonal strain) is the internal strain in the lattice of ferroelectrics, this parameter can be used to determine amount of internal strain [18]. The lower value of tetragonality suggested that less thermal energy is required for phase transition. Therefore, the reduction in T_c was observed in the PZT-SBT ceramics ($0.1 \leq x \leq 0.3$). In addition, a broadened dielectric peak was observed in PZT-SBT ($0.1 \leq x \leq 0.3$) ceramics (Figure 3), which is in contrast to the sharp transition commonly observed in PZT ceramics. Since the ceramics with $0.1 \leq x \leq 0.3$ exhibited a mixture of two phases –the PZT-based solid solution and the PTT-based solid solution–, the compositional inhomogeneity of these ceramics might be the main cause for the broadening of the dielectric peak. The observed reduction in the dielectric loss with SBT concentration may be related to donor-like behavior. For insulating ceramics, a combination of space charge polarization and domain wall relaxation is a dominant cause of dielectric loss [19–20]. The presence of defects such as oxygen vacancies which act as space charge and contribute to the electrical polarization of perovskite materials, can thus be related to the dielectric loss. However, in these ceramics, the suppression of oxygen vacancy concentration due to the donor-like ceramics led to small dielectric loss.

The polarization-electric field (P - E) hysteresis loops of $(1-x)$ PZT- x SBT ceramics are shown in Figure 4. The corresponding remanent polarization ($2P_r$) and coercive field ($2E_c$) for the studied ceramics are given in Table 3. From Figure 4, pure PZT ceramic showed well-developed and symmetric hysteresis loops with larger remanent polarization and smaller coercive field than those of pure SBT ceramic. This was due to the fact that the ferroelectric domains of PZT are relatively easy to switch compared to SBT domains [21]. Namely, the PZT showed larger displacements of ions than those of the SBT upon the application of an electric field. For the composition with $x = 0.1$ SBT, the remanent polarization was found to be $38.82 \mu C/cm^2$ which was higher than that of the PZT ceramic, while the coercive field did not change significantly. The increase in remanent polarization was mainly attributed to

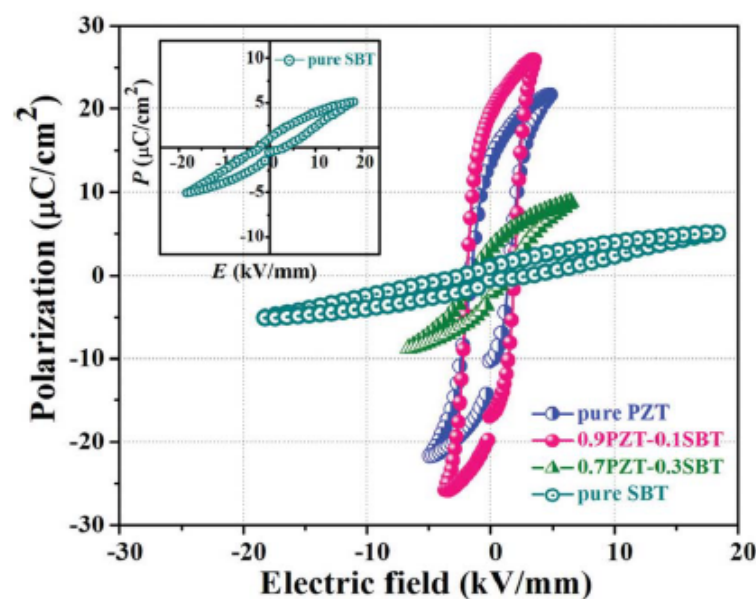


Figure 4. Electric field induced polarization response for pure PZT, PZT-SBT and pure SBT ceramics.

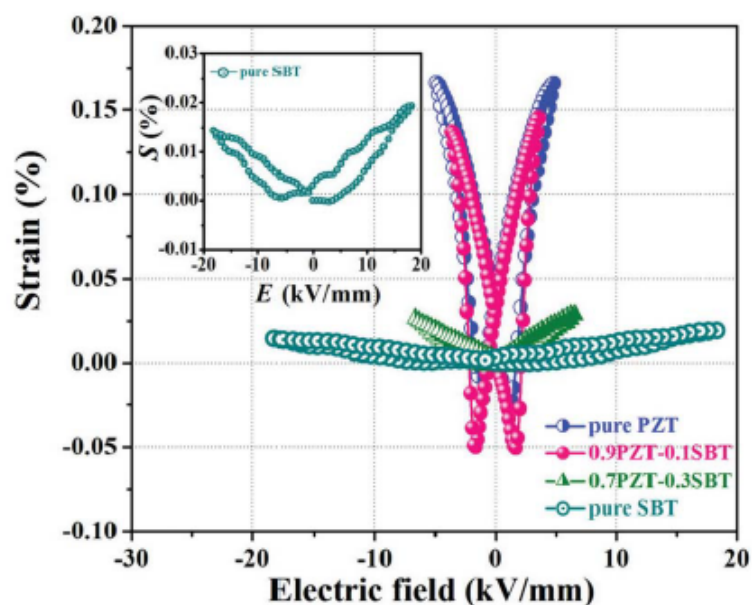


Figure 5. S - E loops of pure PZT, PZT-SBT and pure SBT ceramics.

donor doped behavior. In this sample, donor doping of Bi^{3+} and Ta^{5+} ions from SBT would be expected to create A-site vacancy into PZT lattice and reduce the oxygen vacancy concentration for charge compensation. The suppression of oxygen vacancies led to a rapid decrease of domain wall pinning and hence enhanced domain reorientation. Thus, the measured remanent polarization was increased. When the content of SBT was increased to $x = 0.3$, a very slim polarization loop with small remanent polarization and coercive field was observed. This was due to an increased amount of cubic PTT phase, as observed in XRD and microstructural studies. As materials with cubic symmetry (centro-symmetric) do not possess polar properties [22], PTT is a non-ferroelectric material. Therefore, this phase could obstruct the polarization switching process of the ferroelectric PZT phase, which led to a reduction in the remanent polarization of this sample. Ferroelectric measurements suggested that the presence of cubic PTT phase led to a strong degradation in the ferroelectric properties of PZT-SBT system.

Figure 5 displays the plots of bipolar strain (S) versus electric field (E) for $(1-x)$ PZT- x SBT ceramics. Values of longitudinal piezoelectric constant (d_{33}^*) determined from the slope of the S - E plot [23] are listed in Table 3. Pure PZT ceramic exhibited a symmetric butterfly curve with a larger maximum strain (S_{max}) than that of pure SBT ceramic, as can be seen in Figure 5. As a small amount of 0.1SBT was added to PZT, the sample could maintain piezoelectric properties of pure PZT ceramic with the maximum strain of $\sim 0.14\%$ at an external electric field of 3.5 kV/mm and d_{33}^* of 350 pm/V. An addition of $x = 0.3$ SBT into PZT led to a very slim butterfly loop with a markedly decreasing strain and d_{33}^* . This result was mainly because of the increasing amount of non-piezoelectric PTT phase. In this research, therefore, it was observed that 0.9PZT-0.1SBT ceramics exhibited better electrical properties (i.e. dielectric and ferroelectric piezoelectric) than pure PZT ceramic. Nonetheless, the strain behavior of the sample was similar to pure PZT ceramic.

Conclusions

Ceramics with formula $(1-x)PZT-xSBT$ were prepared by a conventional mixed oxide method. The small addition of SBT ($0.1 \leq x \leq 0.3$) into PZT ceramic resulted in a distorted tetragonal crystal structure toward rhombohedral and pseudocubic, causing observed reduction of T_c . Electrical measurements indicated that the small addition of 0.1SBT into PZT resulted in an increase of the dielectric constant and remanent polarization. This could be attributed to the process of incorporation of donor dopants like Bi^{3+} and Ti^{5+} (from SBT) in the perovskite PZT lattice. Further increase in the content of SBT severely decreased electrical properties of the ceramics due to the presence of the non-piezoelectric secondary phase in this PZT-SBT system. Based on our results, the electrical properties (i.e. dielectric and ferroelectric) of 0.9PZT-0.1SBT ceramic could be improved further for ferroelectric memory applications.

Funding

This work is financially supported by the Thailand Research Fund (TRF) under Grant No. RSA5780032, Chiang Mai University and the Australian Research Council under Grant No. DP0988182. JG acknowledges support from DE120102644. ON would like to acknowledge financial support from the TRF through the Royal Golden Jubilee Ph.D. Program.

References

1. B. Jaffe, W. R. Cook and H. Jaffe, *Piezoelectric Ceramics*. London: Academic Press; (1971).
2. N. Balke, H. Kungl, T. Granzow, D. C. Lupascu, M. J. Hoffmann and J. Rödel, Bipolar fatigue caused by field screening in $Pb(Zr,Ti)O_3$ ceramics. *J Am Ceram Soc.* **90**, 3869–3874 (2007).
3. C. A. Paz de Arujo, J. C. Cuchiaro, L. D. McMillan, M. C. Scott and J. F. Scott, Fatigue-free ferroelectric capacitors with platinum electrodes. *Nature*. **374**, 627–629 (1995).
4. I. Coondoo, A. K. Jha and S. K. Agarwal, Structural, dielectric and electrical studies in tungsten doped $SrBi_2Ta_2O_9$ ferroelectric ceramics. *Ceram Inter.* **33**, 41–47 (2007).
5. I. Coondoo, S. K. Agarwal and A. K. Jha, Ferroelectric and piezoelectric properties of tungsten substituted $SrBi_2Ta_2O_9$ ferroelectric ceramics. *Mater Res Bull.* **44**, 1288–1292 (2009).
6. W. Q. Zhang, A. D. Li, Q. Y. Shao, Y. D. Xia, D. Wu, Z. G. Liu and N. B. Ming, Ferroelectric properties of bilayer structured $Pb(Zr_{0.52}Ti_{0.48})O_3/SrBi_2Ta_2O_9$ (PZT/SBT) thin films on $Pt/TiO_2/SiO_2/Si$ substrates. *Appl Surf Sci.* **254**, 1583–1586 (2008).
7. H. H. Park, H. H. Park, T. S. Kim and R. H. Hill, Electric and ferroelectric properties of PZT/SBT multilayer films prepared by photochemical metal-organic deposition. *Sensors and Actuat B.* **130**, 696–700 (2008).
8. O. Namsar, A. Watcharapasorn, M. Hoffman, J. Glaum and S. Jiansirisomboon, Improvement of ferroelectric properties of PZT ceramics by SBT addition. *Ferroelectrics*, **451**, 22–29 (2013).
9. R. D. Shannon, Revised effective ionic radii and systematic studies of interatomic distances in halides and chalcogenides. *Acta Cryst A.* **32**, 751–767 (1976).
10. M. Hammer and M. J. Hoffmann, Sintering Model for mixed-oxide-derived lead zirconate titanate ceramics. *J Am Ceram Soc.* **81**, 3277–3284 (1998).
11. G. V. Lewis, R. A. Catlow and REW Casselton, PTCT effect in $BaTiO_3$. *J Am Ceram Soc.* **68**, 555–558 (1985).
12. P. G. Lucuta, F. L. Constantinescu and D. Barb, Structural dependence on sintering temperature of lead zirconate-titanate solid solutions. *J. Am. Ceram. Soc.* **68**, 533–537 (1985).
13. R. Herbiet, U. Robels, H. Dederichs and G. Arlt, Domain wall and volume contributions to material properties of PZT ceramics. *Ferroelectrics*. **98**, 107–121 (1989).

14. G. Arlt, D. Hennings and G. de With, Dielectric properties of fine grained barium titanate ceramics. *J Appl Phys.* **58**, 1619–1625 (1985).
15. T. Hoshina, Size effect of barium titanate: fine particles and ceramics. *J. Ceram. Soc. Jpn.* **121**, 156–161 (2013).
16. S. L. Swartz, T. R. Shrout, W. A. Schulze and L. E. Cross, Dielectric properties of lead–magnesium niobate ceramics. *J Am Ceram Soc.* **67**, 311–315 (1984).
17. A. L. Costa, C. Galassi, G. Fabbri, E. Roncari and C. Capiati, Pyrochlore phase and microstructure development in lead magnesium niobate materials. *J Euro Ceram Soc.* **21**, 1165–1170 (2001).
18. I. Coondoo, A. K. Jha, S. K. Agarwal, N. C. Soni, Phase transition and electrical studies of wolframium doped $\text{SrBi}_2\text{Ta}_2\text{O}_9$ ferroelectric ceramics. *J Electroceram.* **16**, 393–398 (2006).
19. I. S. Zheludev, Physics of Crystalline Dielectrics, Electrical Properties. New York: Plenum; (1971).
20. Y. Wu, C. Nguyen, S. Seraji, M. J. Forbess, S. J. Limmer, T. Chou and G. Cao, Processing and properties of strontium bismuth vanadate niobate ferroelectrics. *J Am Ceram Soc.* **84**, 2882–2888 (2001).
21. R. R. Das, S. B. Majumder and R. S. Katiyar, Comparison of the electrical characteristics of PZT and SBT thin films. *Integr Ferroelectr.* **42**, 323–334 (2002).
22. G. H. Haertling, Ferroelectric ceramics: history and technology. *J Am Ceram Soc.* **82**, 797–818 (1999).
23. S. Mahajan, O. P. Thakur, C. Prakash, Effect of sintering temperature on structural and piezoelectric properties of PNN-PZT ceramics. *Defence Sci J.* **57**, 23–28 (2007).

Phase Development and Dielectric, Ferroelectric and Piezoelectric Properties of $\text{Pb}(\text{Mg}_{1/3}\text{Nb}_{2/3})_{0.9}\text{Ti}_{0.1}\text{O}_3\text{-Bi}_{0.5}(\text{Na}_{0.74}\text{K}_{0.26})_{0.5}\text{TiO}_3$ Ceramics

METHEE PROMSAWAT,^{1,2} MUKRAWEE SRIYOD,¹
 ZENGHUI LIU,³ WEI REN,³ ANUCHA WATCHARAPASORN,^{1,2}
 ZUO-GUANG YE,^{3,4} AND SUKANDA JIANSIRISOMBOON^{1,2,*}

¹Department of Physics and Materials Science, Faculty of Science, Chiang Mai University, 239 Huay Kaew Road, Muang, Chiang Mai, 50200, Thailand

²Materials Science Research Center, Faculty of Science, Chiang Mai University, 239 Huay Kaew Road, Muang, Chiang Mai, 50200, Thailand

³Electronic Materials Research Laboratory, Key Laboratory of the Ministry of Education & International Center for Dielectric Research, Xi'an Jiaotong University, Xi'an, Shaanxi, 710049, P.R. China

⁴Department of Chemistry and 4D LABS, Simon Fraser University, 8888 University Drive, Burnaby, British Columbia, V5A 1S6, Canada

In this work, the relationships between phase development and the properties of a new relaxor based ferroelectric $(1-x)\text{Pb}(\text{Mg}_{1/3}\text{Nb}_{2/3})_{0.9}\text{Ti}_{0.1}\text{O}_3\text{-}x\text{Bi}_{0.5}(\text{Na}_{0.74}\text{K}_{0.26})_{0.5}\text{TiO}_3$ ceramics (when $x = 0.0, 0.1, 0.3, 0.5, 0.7, 0.9$ and 1.0 mole fraction) was studied. The pseudo-cubic structure was observed in the ceramics with $x \leq 0.7$ mole fraction. The rhombohedral and tetragonal phases were found to coexist when x increased to 0.9 , which transformed into the single tetragonal phase when x increased to 1.0 . The dielectric constant measured at room temperature decreased with increasing x . The remnant polarization and piezoelectric constant of the ceramics significantly increased when x increased to 0.9 and 1.0 .

Keywords PMNT-BNKT; phase; dielectric; ferroelectric; piezoelectric

1. Introduction

Complex perovskite relaxor-based ferroelectrics are the well-known materials that show excellent dielectric, ferroelectric and piezoelectric properties, which are suitable for electronic device applications such as multilayer capacitors, ferroelectric random access memories, and electromechanical transducers [1–5]. $\text{Pb}(\text{Mg}_{1/3}\text{Nb}_{2/3})_{0.9}\text{Ti}_{0.1}\text{O}_3$ (PMNT) is a relaxor material that exhibits excellent dielectric and electrostrictive properties [6, 7]. Because of these excellent properties, the relationships between the crystal structures and physical properties have been widely investigated [8–11].

Received October 26, 2014; in final form February 15, 2015

*Corresponding author. E-mail: sukanda.jian@cmu.ac.th

Color versions of one or more of the figures in the article can be found online at www.tandfonline.com/gfer.

As reported in the previous studies, the incorporations of Pb-free ferroelectrics such as BaTiO₃ (BT) and (Bi_{0.5}Na_{0.5})TiO₃ (BNT) can improve the phase stability and electrical properties of lead-based relaxor ferroelectrics [12–17]. In the present study, Bi_{0.5}(Na_{0.74}K_{0.26})_{0.5}TiO₃ (BNKT) compound, which is a Pb-free ferroelectric material showing good electromechanical properties [18–20], was incorporated into the PMNT material to form a new solid-solution system of PMNT-BNKT. It was believed that the ferroelectric ordering of PMNT materials will be enhanced with the BNKT substitution. Moreover, the morphotropic phase boundary (MPB) compositions could be found with optimum BNKT contents, which makes the materials with excellent dielectric and piezoelectric properties. Therefore, in this study, the relationships between phase development, microstructure and electrical properties were investigated and discussed in terms of the BNKT content in the PMNT-BNKT solid solution.

2. Experimental Procedure

Pb(Mg_{0.33}Nb_{0.67})_{0.9}Ti_{0.1}O₃ (PMNT) and Bi_{0.5}(Na_{0.74}K_{0.26})_{0.5}TiO₃ (BNKT) powders were separately prepared by a conventional mixed-oxide method. Different amounts of BNKT were mixed with the PMNT powders to prepare the (1-*x*)PMNT-*x*BNKT powders (when *x* = 0.0, 0.1, 0.3, 0.5, 0.7, 0.9 and 1.0 mole fraction). Polyvinyl alcohol was added into the mixed powder as a binder which was then uniaxially pressed into a pellet by a pressure of 57 MPa. The green bodies (with 10 mm in diameter, 2 mm in thickness and a raw density about 4.84 g/cm³) were sintered in a PMNT-BNKT atmosphere at 1125°C for 2 hrs. The densities of the sintered ceramics were determined by the Archimedes' method. The phase formations were characterized using X-ray diffraction (XRD, X-pert, Panalytical B.V., The Netherlands) with CuK_α radiation of 1.5405 Å wavelength. The microstructures of as-sintered surfaces were observed by a scanning electron microscope (SEM, JEOL JSM-6335F, Japan). The average grain sizes were determined by employing a mean linear interception method on a SEM micrograph. The temperature dependences of dielectric properties were measured using a computer-controlled alpha dielectric analyzer (Novocontrol). The polarization versus electric field curves were displayed by a modified Sawyer-Tower circuit. The sample was poled at room temperature with the application of a DC electric field of 40 kV/cm. The piezoelectric coefficients (*d*₃₃) were measured using a *d*₃₃ meter (ZJ-6B, China).

3. Results and Discussion

The XRD patterns of the (1-*x*)PMNT-*x*BNKT ceramics are shown in Fig. 1(a). No impurity phase was observed in the patterns. The XRD pattern of the pure PMNT ceramic matched the standard inorganic crystal structure database (ICSD) file No. 99710 of Pb(Mg_{0.3}Nb_{0.6}Ti_{0.1})O₃ with the pseudo-cubic space group of *Pm* $\bar{3}$ *m* [21]. The enlarged patterns of the peaks at $2\theta = 44\text{--}48^\circ$ are shown in Fig. 1(b). The (200)_C peak of a pseudo-cubic lattice of the pure PMNT ceramic was shifted to higher angles when *x* increased up to 0.7 mole fraction. This indicates a decrease in the pseudo-cubic lattice parameters of PMNT materials with the BNKT substitution, as shown Table 1. The peak split into three peaks when *x* increased to 0.9 mole fraction, which is believed to be due to the formation of the morphotropic phase boundary (MPB), at which the rhombohedral and tetragonal phases coexisted. The split peaks were fitted into the Gaussian's function. The fitted peaks located on the left and right-hand sides correspond to the (002)_T and (200)_T planes, respectively, of the tetragonal phase, while the middle peak is from the (020)_R plane of

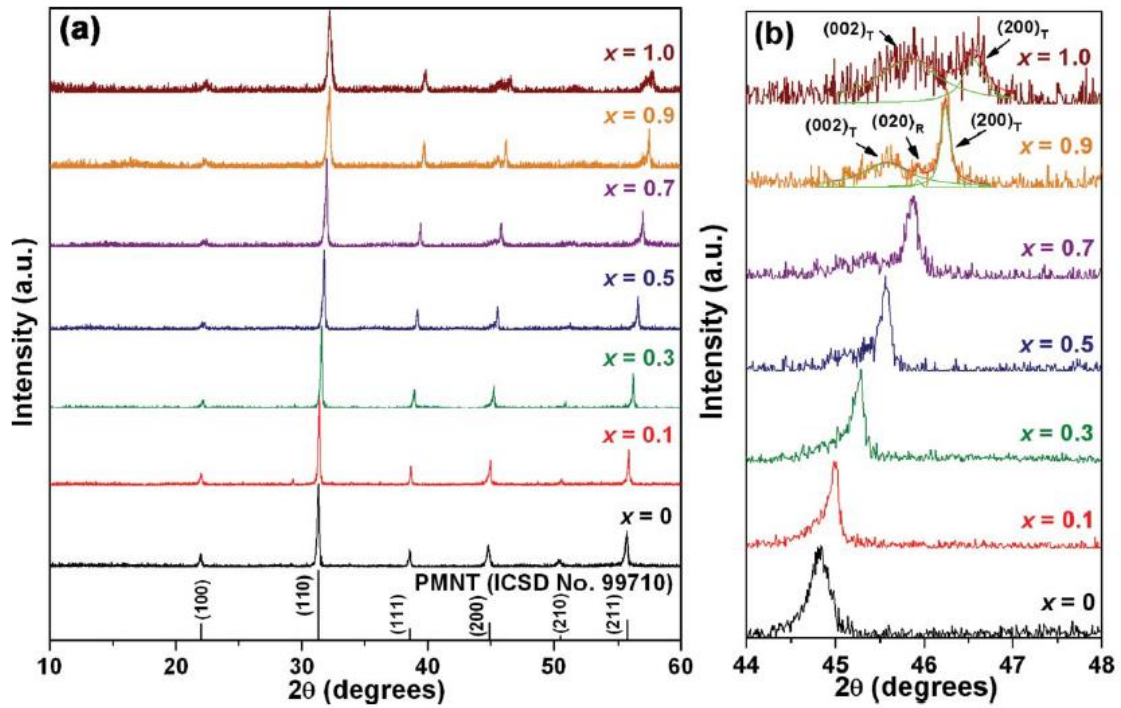


Figure 1. (a) XRD patterns of the (1-*x*)PMNT-*x*BNKT ceramics. (b) Enlarged views of the patterns at $2\theta = 44\text{--}48^\circ$.

the rhombohedral phase. However, the (020)_R peak disappeared when *x* increased to 1.0 mole fraction. This indicates that the pure BNKT ceramic has a single phase of tetragonal structure. This is consistent with the previous result studied by Otonicar *et al.* that the BNKT material exhibited the single tetragonal phase [19]. These observed results can be attributed to the substitutions of complex $[Bi_{0.5}(Na_{0.74}K_{0.26})_{0.5}]^{2+}$ ions for the Pb^{2+} ions located on the A-site of the PMNT lattices ($r_{Pb^{2+}} = 1.49 \text{ \AA}$, $r_{Mg^{2+}} = 0.72 \text{ \AA}$, $r_{Nb^{5+}} = 0.64 \text{ \AA}$, $r_{Ti^{4+}} = 0.605 \text{ \AA}$, $r_{Bi^{3+}} = 1.17 \text{ \AA}$, $r_{Na^{+}} = 1.39 \text{ \AA}$ and $r_{K^{+}} = 1.64 \text{ \AA}$ [22]), resulting in the unit cell distortion and the formation of MPB [16].

Table 1

Lattice parameters, relative densities and grain sizes of the (1-*x*)PMNT-*x*BNKT ceramics

BNKT content, <i>x</i> , (mole fraction)	Lattice parameter (Å)			Relative density (%)	Grain size (μm)
	<i>a</i> _R	<i>a</i> _T	<i>c</i> _T		
0.0	4.0394	—	—	97.12 ± 0.02	4.29 ± 0.33
0.1	4.0250	—	—	96.69 ± 0.01	4.14 ± 0.17
0.3	4.0005	—	—	96.88 ± 0.01	3.22 ± 0.21
0.5	3.9777	—	—	97.08 ± 0.01	1.69 ± 0.06
0.7	3.9515	—	—	97.40 ± 0.01	1.65 ± 0.04
0.9	3.9466	3.9212	3.9769	98.38 ± 0.01	1.33 ± 0.04
1.0	-	3.8963	3.9556	99.07 ± 0.03	0.95 ± 0.03

Note: Lattice parameter *a* of rhombohedral structure is represented by *a*_R. Lattice parameters *a* and *c* of tetragonal structure are represented by *a*_T and *c*_T, respectively.

The PMNT-BNKT ceramics with a relative density of about 97 %, as shown in Table 1, were obtained by a solid-state sintering process. The SEM images of as-sintered surfaces of the ceramics with $x = 0.0, 0.3, 0.7$ and 1.0 mole fraction are shown in Fig. 2 (a), (b), (c) and (d), respectively. Irregularly-shaped grains were observed in the pure PMNT ceramic while more homogenous grains were observed in the ceramic with $x = 0.3$. Cubic-like grains were observed in the ceramics with $x = 0.7$ and 1.0 . The average grain sizes were determined and the results are given in Table 1. The grain size of the PMNT ceramic was reduced by the BNKT substitution. For the BNKT-substituted samples, the grain size tends to decrease with increasing x . The observed cubic-like and small grains were attributed to the characteristic morphology of the BNKT ceramics which usually exhibit smaller and more cubic-like grains compared with the PMNT ceramics sintered at the same temperature [7, 19].

The temperature dependences of the dielectric constant (ϵ_r) and dielectric loss ($\tan\delta$) of the ceramics with $x = 0.0, 0.3, 0.7$ and 1.0 , measured at the frequencies ranging from 10^2 to 10^6 Hz, are shown in Fig. 3(a), (b), (c) and (d), respectively. Typical characteristics of relaxors, i.e. a decrease in the maximum dielectric constant ($\epsilon_{r\text{-max}}$) and an increase in the temperature of $\epsilon_{r\text{-max}}$ (T_{max}) with increasing frequency, were observed in the ceramics with $x = 0.0$ and 0.3 . A dielectric shoulder was observed in the $\epsilon_r(T)$ curves of the ceramics with $x = 0.0$ and 0.3 at the temperatures of 100 and 0°C , respectively. These shoulders are attributed to the responses of charge defects, i.e. cation and oxygen vacancies created during the sintering process. This is consistent with the previous result observed by Zhong *et al.* [23, 24]. For the ceramics with $x = 0.0$ and 0.3 , the dielectric

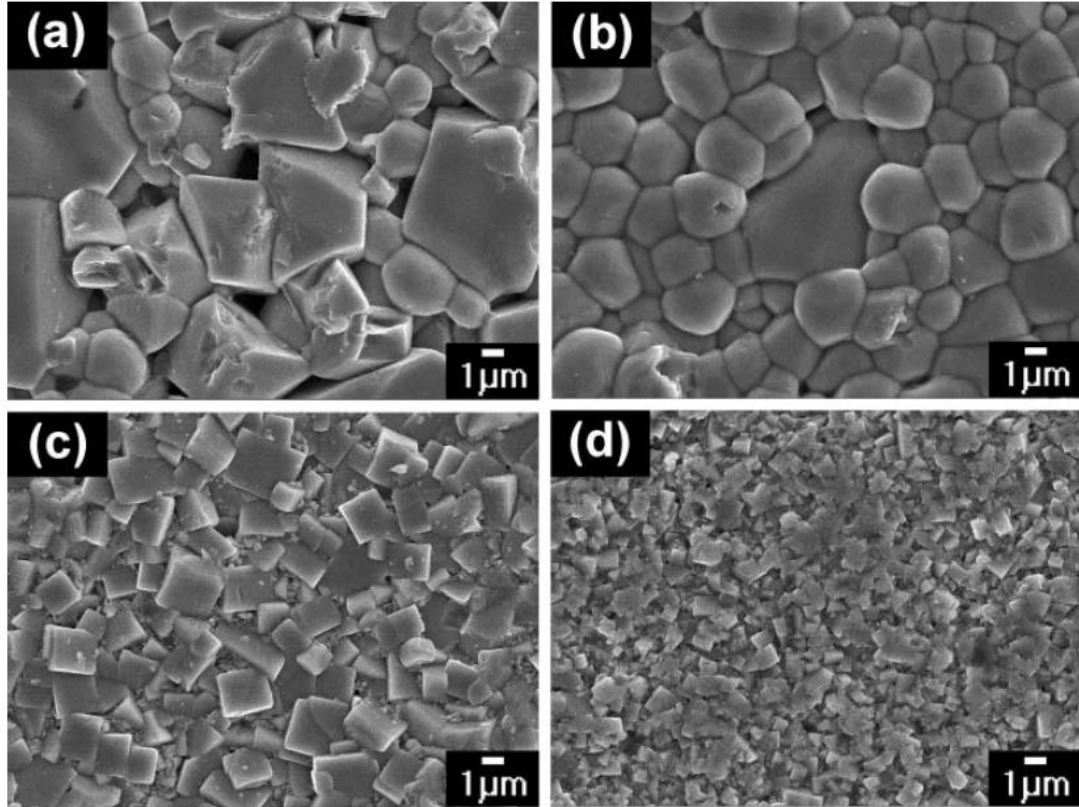


Figure 2. SEM micrographs of as-sintered surfaces of the pure PMNT ceramics (a) and the ceramics substituted with 0.3 (b), 0.7 (c) and 1.0 (d) mole fraction of BNKT, respectively.

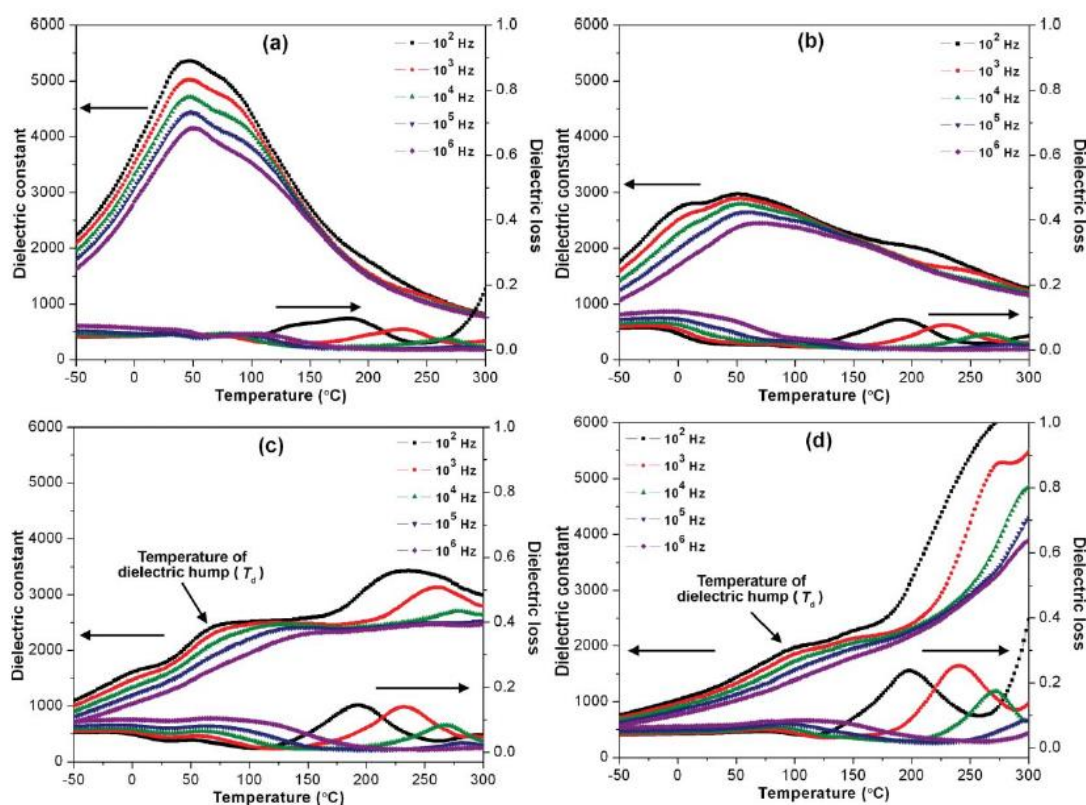


Figure 3. Temperature dependences of the dielectric constant and dielectric loss of the (1-x)PMNT-xBNKT ceramics measured at various frequencies.

constant above T_{max} decreased with increasing temperature. Interestingly, for the ceramic with $x = 0.7$, the dielectric constant became temperature independent at frequencies above 10^5 Hz, when the temperature was above the temperature of dielectric hump (T_d), as shown in Fig. 3(c). In contrast, for the pure BNKT ceramic, at $T > T_d$, the dielectric

Table 2

Dielectric, ferroelectric and piezoelectric properties of the (1-x)PMNT-xBNKT ceramics

BNKT content, x , (mole fraction)	ϵ_r	$\tan\delta$	T_{max} (°C)	P_r ($\mu C/cm^2$)	E_C (kV/cm)	d_{33} (pC/N)
0.0	5050	0.05	45	8.5	2.0	28
0.1	3300	0.02	23	2.5	1.5	16
0.3	2900	0.02	52	1.5	2.0	15
0.5	2450	0.01	94	2.0	3.0	15
0.7	2500	0.02	105	3.5	4.0	17
0.9	2250	0.05	133*	14.5	12.0	165
1.0	2150	0.03	150*	13.0	11.0	155

Note: ϵ_r , $\tan\delta$ and T_{max} are dielectric constant, dielectric loss and the temperature of maximum dielectric constant, respectively, measured at 25°C at the frequency of 1 kHz. The temperatures remarked by * are the temperatures at the dielectric hump (T_d). P_r and E_C are the remnant polarization and coercive field, respectively. Piezoelectric constant (d_{33}) was measured after the ceramics were poled at an applied field of 40 kV/cm.

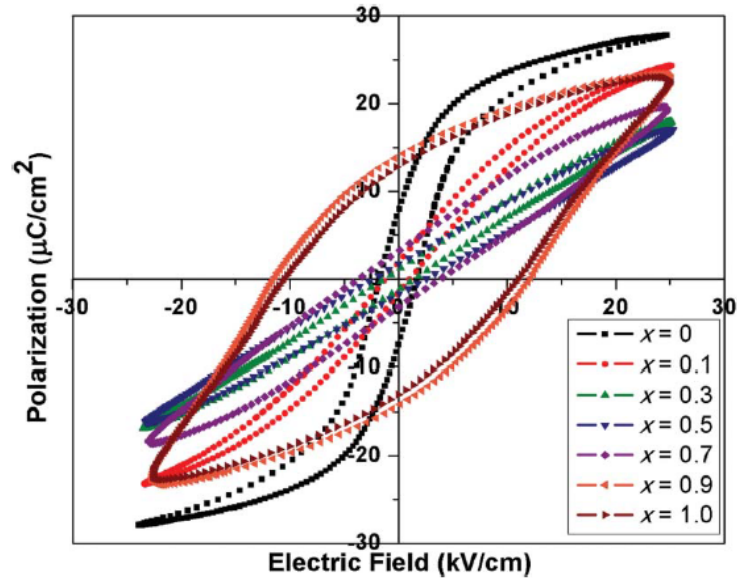


Figure 4. P - E curves of the $(1-x)$ PMNT- x BNKT ceramics measured at the room temperature at the frequency of 25 Hz.

constant increased further with increasing temperature, which is the characteristic dielectric behavior of the BNKT materials [25, 26]. The ϵ_r and $\tan\delta$ values of the ceramics measured at room temperature (25°C) at the frequency of 1 kHz are listed in Table 2. The ϵ_r values decreased with increasing x while the values of $\tan\delta$ did not change significantly. The increase in x resulted in the increases in both T_{max} and T_d .

Polarization-electric field (P - E) curves of the ceramics are shown in Fig. 4. The P - E curves of the ceramics with $x \leq 0.7$ appeared as the slim loops with a low remanent polarization (P_r) and a low coercive field (E_C), which is characteristic of relaxor ferroelectric behavior. However, P - E curves opened up when x increased to 0.9 and 1.0, resulting in the abrupt increases in P_r and E_C , as shown in Table 2. The values of piezoelectric constant (d_{33}) are given in Table 2. d_{33} showed a similar trend as P_r with composition x ; it abruptly increased when x increased to 0.9 and 1.0. These variations were believed to be caused by the distortion of pseudo-cubic lattice and the formation of MPB [27–29].

4. Conclusions

Complex perovskite relaxor-based ferroelectric $(1-x)$ PMNT- x BNKT ceramics were successfully prepared by a solid state sintering process. With increasing x up to 0.7 mole fraction, the pseudo-cubic lattice parameters decreased. A morphotropic phase boundary was found to exist at the composition of $x = 0.9$. The crystal structure changed into a single tetragonal phase when x increased from 0.9 to 1.0. Small and cubic-like grains were observed in the ceramics of high BNKT concentration. Typical characteristics of relaxor ferroelectrics were observed in the ceramics with $x \leq 0.3$ while the behavior of normal ferroelectrics was observed in the ceramics with $x \geq 0.9$. Interestingly, when the composition approached the MPB with x increasing to 0.9 and 1.0, the values of P_r , E_C and d_{33} suddenly increased due to the beneficial effects of the MPB. These MPB-enhanced properties make the $(1-x)$ PMNT- x BNKT ceramics promising materials for electromechanical applications.

Funding

This work was supported by Chiang Mai University and the Thailand Research Fund (TRF, Grant No. RSA5780032). This work was partly supported by the United States Office of Naval Research (ONR, Grant No. N00014-12-1-1045) and the Natural Science and Engineering Research Council of Canada (NSERC). The work performed at XJTU was supported by the Natural Science Foundation of China (Grant Nos. 50728201 and 90923001), the International Science & Technology Cooperation Program of China (Grant No. 2011DFA51880), the “111 Project” of China (Grant No. B14040).

References

1. A. A. Bokov and Z. G. Ye, Recent progress in relaxor ferroelectrics with perovskite structure. *J Mater Sci.* **41**, 31–52 (2006).
2. V. V. Shvartsman, A. L. Kholkin, I. P. Raevski, S. I. Raevskaya, F. I. Savenko, and A. S. Emelyanov, Macroscopic and local piezoelectric properties of $Pb(Mg_{1/3}Nb_{2/3})O_3$ - $PbTiO_3$ single crystals exhibiting giant piezoelectric response. *J Appl Phys.* **113**, 187208/1–4 (2013).
3. S. Xu, G. Poirier, and N. Yao, PMN-PT nanowires with a very high piezoelectric constant. *Nano Lett.* **12**, 2238–2242 (2012).
4. Y. Cheng, Y. Yang, Y. Wang, and H. Meng, Study on $Pb(Mg_{1/3}Ta_{2/3})O_3$ - $Pb(Mn_{1/3}Sb_{2/3})O_3$ - $Pb(Zr_xTi_{1-x})O_3$ high power piezoelectric ceramics near the morphotropic phase boundary. *J Alloys Compd.* **508**, 364–369 (2010).
5. Z. G. Ye, High-performance piezoelectric single crystals of complex perovskite solid solutions. *Mater Res Soc Bull.* **34**, 277–283 (2009).
6. X. Zhu, E. Defay, G. L. Rhun, M. Aid, Y. Xu, Q. Zhang, Y. Xiao, H. Gao, D. Liang, J. Zhu, J. Zhu, and D. Xiao, High permittivity $0.9Pb(Mg_{1/3}Nb_{2/3})O_3$ - $0.1PbTiO_3$ relaxor thin films for high-value, wide-temperature capacitor applications. *J Appl Phys.* **112**, 054105/1–5 (2012).
7. M. Promsawat, J. Y. Y. Wong, Z. Ren, H. N. Taylor, A. Watcharapasorn, Z. G. Ye, and S. Jiansirisomboon, Enhancement in dielectric, ferroelectric, and electrostrictive properties of $Pb(Mg_{1/3}Nb_{2/3})_{0.9}Ti_{0.1}O_3$ ceramics by CuO addition. *J Alloys Compd.* **587**, 618–624 (2014).
8. N. Triamnak, M. Unruan, S. Ananta, and R. Yimnirun, Effects of uniaxial stress on dielectric properties of $0.9PMN$ - $0.1PT$ ceramics. *J Electroceram.* **21**, 819–822 (2008).
9. R. Skulski, P. Wawrzala, and M. Plonska, The dipole moments in $0.9PMN$ - $0.1PT$ ceramic samples. *Physica B.* **349**, 316–321 (2004).
10. J. H. Ko, D. H. Kim, S. Tsukada, S. Kojima, A. A. Bokov, and Z. G. Ye, Crossover in the mechanism of ferroelectric phase transition of $Pb[(Mg_{1/3}Nb_{2/3})_{1-x}Ti_x]O_3$ single crystals studied by Brillouin light scattering. *Phys Rev B.* **82**, 104110/1–7 (2010).
11. X. Wen, C. Feng, L. Chen, and S. Huang, Effect of order-disordered nano-domains on the dielectric and electrical properties of PMNT ceramics. *J Alloys Compd.* **422**, 244–248 (2006).
12. U. Syamaprasad, A. R. S. Nair, M. S. Sarma, P. Guruswamy, P. S. Mukherjee, A. D. Damodaran, L. Krishnamurthy, and M. Achuthan, Multilayer capacitor ceramics in the PMN-PT-BT system: effect of MgO and $4PbO \cdot B_2O_3$ additions. *J Mater Sci.* **8**, 199–205 (1997).
13. L. Huang, J. Zeng, W. Ruan, W. Zhao, K. Zhao, and G. Li, Fabrication and dielectric properties of transparent PZN-BT ceramic. *Ceram Int.* **39**, S171–S174 (2013).
14. F. Xia and X. Yao, Piezoelectric and dielectric properties of PZN-BT-PZT solid solutions. *J Mater Sci.* **34**, 3341–3343 (1999).
15. W. Z. Zhu and M. Yan, Effect of Mn-doping on the morphotropic phase boundary of PZN-BT-PT system. *J Mater Sci Lett.* **20**, 1527–1529 (2001).
16. N. Jaitanong, W. C. Vittayakorn, and A. Chaipanich, Phase development and dielectric responses in PMN-BNT ceramics. *Ceram Int.* **36**, 1479–1483 (2010).
17. P. Jaita, A. Watcharapasorn, and S. Jiansirisomboon, Effects BNT compound incorporated on structure and electrical properties of PZT ceramic. *Curr Appl Phys.* **11**, S77–S81 (2011).

18. X. X. Wang, X. G. Tang, and H. L. W. Chan, Electromechanical and ferroelectric properties of $(\text{Bi}_{1/2}\text{Nb}_{1/2})\text{TiO}_3$ - $(\text{Bi}_{1/2}\text{K}_{1/2})\text{TiO}_3$ - BaTiO_3 lead-free piezoelectric ceramics. *Appl Phys Lett.* **85**, 91–93 (2004).
19. M. Otonicar, S. D. Skapin, M. Spreitzer, and D. Suvorov, Compositional range and electric properties of the morphotropic phase boundary in the $\text{Na}_{0.5}\text{Bi}_{0.5}\text{TiO}_3$ - $\text{K}_{0.5}\text{Bi}_{0.5}\text{TiO}_3$ system. *J Eur Ceram Soc.* **30**, 971–979 (2010).
20. H. Nagata, M. Yoshida, Y. Makiuchi, and T. Takenaka, Large piezoelectric constant and high curie temperature of lead-free piezoelectric ceramic ternary system based on bismuth sodium titanate-bismuth potassium titanate-barium titanate near the morphotropic phase boundary. *Jpn J Appl Phys.* **42**, 7401–7403 (2003).
21. J. C. Bruno, A. A. Cavaleiro, M. A. Zaghe, M. Cilense, and J. A. Varela, Structural effects of Li and K additives on the columbite precursor and 0.9PMN-0.1PT powders. *Mater Chem Phys.* **84**, 120–125 (2004).
22. R. D. Shannon, Dielectric polarizabilities of ions in oxides and fluorides. *J Appl Phys.* **73**, 348–366 (1993).
23. N. Zhong, X. L. Dong, D. Sun, P. H. Xiang, H. Du, Electrical properties of $\text{Pb}(\text{Mg}_{1/3}\text{Nb}_{2/3})\text{O}_3$ - PbTiO_3 ceramics modified with WO_3 . *Mater Res Bull.* **39**, 175–184 (2004).
24. N. Zhong, P. H. Xiang, D. Z. Sun, and X. L. Dong, Effect of rare earth additives on the microstructure and dielectric properties of $0.67\text{Pb}(\text{Mg}_{1/3}\text{Nb}_{2/3})\text{O}_3$ - 0.33PbTiO_3 ceramics. *Mater Sci Eng B.* **116**, 140–145 (2005).
25. Z. Yang, B. Liu, L. Wei, and Y. Hou, Structure and electrical properties of $(1-x)\text{Bi}_{0.5}\text{Na}_{0.5}\text{TiO}_3$ - $x\text{Bi}_{0.5}\text{K}_{0.5}\text{TiO}_3$ ceramics near morphotropic phase boundary. *Mater Res Bull.* **43**, 81–89 (2008).
26. V. D. N. Tran, T. H. Dinh, H. S. Han, W. Jo, and J. S. Lee, Lead-free $\text{Bi}_{1/2}(\text{Na}_{0.82}\text{K}_{0.18})_{1/2}\text{TiO}_3$ relaxor ferroelectrics with temperature insensitive electrostrictive coefficient. *Ceram Int.* **39**, S119–S124 (2013).
27. O. Bidault, M. Licheron, E. Husson, G. Calvarin, and A. Morell, Experimental evidence for spontaneous relaxor to ferroelectric phase transition in $\text{Pb}(\text{Mg}_{1/3}\text{Nb}_{2/3})\text{O}_3$ -10%Ti. *Solid State Commun.* **98**, 765–769 (1996).
28. M. Promsawat, A. Watcharapasorn, H. N. Taylor, S. Jiansirisomboon, and Z. G. Ye, Enhanced dielectric, ferroelectric, and electrostrictive properties of $\text{Pb}(\text{Mg}_{1/3}\text{Nb}_{2/3})_{0.9}\text{Ti}_{0.1}\text{O}_3$ ceramics by ZnO modification. *J Appl Phys.* **113**, 204101/1–6 (2013).
29. G. H. Haertling, Ferroelectric ceramics: history and technology. *J Am Ceram Soc.* **82**, 797–818 (1999).

X-ray Photoelectron Spectroscopy Analysis and Electrical Properties of $\text{Bi}_{0.5}(\text{Na}_{0.80}\text{K}_{0.20})_{0.5}\text{TiO}_3\text{-LiNbO}_3$ Lead-Free Piezoelectrics

PIMPILAI WANNASUT,¹ PHARATREE JAITA,¹
 ANUCHA WATCHARAPASORN,^{1,3} AND
 SUKANDA JIANSIRISOMBOON^{4,*}

¹Department of Physics and Materials Science, Faculty of Science, Chiang Mai University, Chiang Mai 50200, Thailand

²Research and Development Institute, Rajamangala University of Technology 10 Lanna (RMUTL), Chiang Mai 50220, Thailand

³Materials Science Research Center, Faculty of Science, Chiang Mai University, Chiang Mai 50200, Thailand

⁴School of Ceramic Engineering, Suranaree University of Technology, Nakhon Ratchasima 30000, Thailand

Lead-free piezoelectric ceramics with formula of $(1-x)\text{Bi}_{0.5}(\text{Na}_{0.80}\text{K}_{0.20})_{0.5}\text{TiO}_3\text{-xLiNbO}_3$ or $(1-x)\text{BNKT-xLN}$ (when $x = 0, 0.005, 0.010, 0.015$ and 0.020 mol fraction) were produced by a solid-state mixed oxide method. The ceramics with density ranging $5.38 - 5.68 \text{ g/cm}^3$ were obtained by sintering at 1100°C . X-ray diffraction pattern showed that $(1-x)\text{BNKT-xLN}$ ceramics exhibited pure perovskite structure. X-ray photoelectron spectroscopy analysis was used to identify of chemical composition, chemical state and binding energy of ionic species in the ceramics. Dielectric, ferroelectric and piezoelectric properties of all ceramics were investigated and found to be optimized at the composition of $x = 0.005$.

Keywords Lead-free piezoelectrics; X-ray diffraction; X-ray photoelectron spectroscopy; electrical properties

1. Introduction

Piezoelectric ceramics have been widely used in various industries such as automotives, electronics and medical equipment. Lead-based piezoelectric ceramics especially $\text{Pb}(\text{Zr}, \text{Ti})\text{O}_3$ or PZT has dominated for piezoelectric applications. However, lead is considered to be toxic and causes environmental problems [1-2]. Thus, the development of lead-free piezoelectric ceramics is expected as an alternative to PZT-based materials. Bismuth sodium potassium titanate, $\text{Bi}_{0.5}(\text{Na}_{1-x}\text{K}_x)_{0.5}\text{TiO}_3$ or BNKT have been known as one of the consideration due to interesting compounds for replacing lead-based piezoelectric ceramics. It has received a significant to its excellent piezoelectric and ferroelectric

Received October 26, 2014; in final form February 15, 2015.

*Corresponding author. E-mail: sukanda.jian@cmu.ac.th

Color versions of one or more figures in this article can be found online at www.tandfonline.com/gfer.

[466]/118

properties near rhombohedral-tetragonal morphotropic phase boundary (MPB). Sasaki *et al.* [3] have reported that a solid solution of $\text{Bi}_{0.5}(\text{Na}_{1-x}\text{K}_x)_{0.5}\text{TiO}_3$ or BNT-BKT represented the development in piezoelectric properties in MPB region at $0.16 \leq x \leq 0.20$. The highest of $P_r = 19.9 \mu\text{C}/\text{cm}^2$, $\epsilon_r = 1000$ and $d_{31} = 46.9 \text{ pC/N}$ values were found at BNT-0.20BKT composition. For future piezoelectric improvement of BNKT ceramic, investigations in terms of various dopants and formation of solid solutions with other compounds such as Li_2CO_3 [4], MnCO_3 [5], LiSbO_3 [6] and LiNbO_3 [7] were carried out.

LiNbO_3 or LN had a perovskite structure with ABO_3 formula. It is a ferroelectric material for an optic and electronic device applications, such as electro-optical, piezoelectric and nonlinear optical devices [8]. Chen *et al.* [4] reported that a solid solution of $[\text{Bi}_{0.5}(\text{Na}_{0.82-x}\text{K}_{0.18}\text{Li}_x)_{0.5}]\text{TiO}_3$ system could increase piezoelectric properties. Then, Zhou *et al.* [7] have reported that a solid solution of $(1-x-y)\text{Bi}_{0.5}\text{Na}_{0.5}\text{TiO}_3-x\text{Bi}_{0.5}\text{K}_{0.5}\text{TiO}_3-y\text{LiNbO}_3$ showed an improvement in electrical properties. The highest d_{33} value of 195 pC/N was obtained at the composition of $x = 0.01$. Moreover, Mahboob *et al.* presented an X-ray photoelectron spectroscopy (XPS) study on $(\text{Na}_{0.5-x}\text{K}_x\text{Bi}_{0.5-x}\text{Nd}_x)\text{TiO}_3$ ceramics. XPS spectra illustrated that the binding energy of Ti 2p and Bi 4f corresponding to only one chemical state, Ti^{+4} and Bi^{+3} . For XPS spectra of O 1s showed extra peaks which combined those of adsorbed oxygen and oxygen vacancy [9].

In this study, attempt to combine both $\text{Bi}_{0.5}(\text{Na}_{0.80}\text{K}_{0.20})_{0.5}\text{TiO}_3$ and LiNbO_3 compounds was then carried out. In this research, LiNbO_3 was employed as an additive for $\text{Bi}_{0.5}(\text{Na}_{0.80}\text{K}_{0.20})\text{TiO}_3$ ceramic to form $(1-x)\text{Bi}_{0.5}(\text{Na}_{0.80}\text{K}_{0.20})_{0.5}\text{TiO}_3-x\text{LiNbO}_3$ or $(1-x)\text{BNKT-xLN}$ (when $x = 0, 0.005, 0.0100, 0.015$ and 0.020 mol fraction). This work thus aims to study X-ray photoelectron spectroscopy and electrical properties of $\text{Bi}_{0.5}(\text{Na}_{0.80}\text{K}_{0.20})_{0.5}\text{TiO}_3\text{-LiNbO}_3$ lead-free piezoelectric ceramics.

2. Experimental

The starting materials for preparation of $\text{Bi}_{0.5}(\text{Na}_{0.80}\text{K}_{0.20})\text{TiO}_3$ or BNKT and LiNbO_3 or LN powder were Bi_2O_3 (98%, Fiuka), Na_2CO_3 (99.5%, Carlo Erba), TiO_2 (99%, Riedel-de Haën), K_2CO_3 (99%, Riedel-de Haën), Li_2CO_3 (99.0%, Sigma-Aldrich) and Nb_2O_5 (99.0%, Sigma-Aldrich). All powders were prepared by a conventional mixed oxide method. All carbonate powders (Na_2CO_3 , K_2CO_3 , Li_2CO_3) were firstly dried at 120°C for 24 h order to remove the residual moistures. All powders were weighed and mixed to produce the mixed powders of $(1-x)\text{BNKT-xLN}$ (when $x = 0, 0.005, 0.010, 0.015$ and 0.020 mol fraction), ball milled for 24 h in an ethanol solution (99.99%) and dried in an oven. The mixed powders were calcined at 850°C for 2 h with a heating/cooling rate of $5^\circ\text{C}/\text{min}$. The mixed powders were ball milled again in an ethanol solution (99.99%) for 15 h and were then characterized by XRD analysis. Afterward, a few drops of 3 wt% polyvinyl alcohol (PVA) binders were added to the mixed powders before being uniaxial pressed into 15 mm diameter discs. The pellet were then sintered at $1025 - 1125^\circ\text{C}$ for 2 h with a heating/cooling rate of $5^\circ\text{C}/\text{min}$ for all BNKT-LN ceramics.

X-ray diffractometer (XRD-Phillip, X-pert) was used to identify phase of both powders and ceramics. Bulk density was measured in accordance with Archimedes' method. Linear shrinkage of all samples was also measured. The highest density samples were selected for further characterizations.

The chemical composition, chemical state and binding energy of sample surface was investigated by X-ray photoelectron spectrometer (XPS; AXIS Ultra ^{DLD}, Kratos analytical, Manchester UK). The base pressure in XPS analysis chamber was about 5×10^{-9} torr. The samples were excited with X-ray hybrid mode $700 \times 300 \mu\text{m}$ spot area

with a monochromatic Al $K_{\alpha 1, 2}$ radiation at 1.4 keV. X-ray anode was run at 15 kV, 10 mA 150 W. The photoelectrons were detected with a hemispherical analyzer positioned at an angle of 90° with respect to the normal to the sample surface. NIST XPS Database was used as reference in this work. Scanning electron microscope (SEM, JEOL JSM-6335F) was used to determine microstructural features of the ceramics. Grain size was determined by a mean linear interception method.

For electrical characterization, room temperature dielectric constant and dielectric loss of (1-x)BNKT-xLN system were measured at a frequency of 1 kHz by 4263B LCR-meter. Polarization-electric field (P - E) hysteresis loops were measured at room temperature (25°C) using a Sawyer-Tower Circuit at a frequency of 25 Hz. Remanent polarization (P_r), maximum polarization (P_{max}), coercive field (E_c), maximum coercive field (E_{max}), and loop squareness (R_{sq}) values were determined from the hysteresis loops. For piezoelectric properties, all samples were poled in silicone oil bath at 55°C under DC electric field of 3 kV/mm for 15 min. Piezoelectric coefficient (d_{33}) was recorded from 1-day aged samples using d_{33} meter (KCF technologies, S5865)

3. Results and Discussion

X-ray diffraction patterns of (1-x)BNKT-xLN mixed powders at $2\theta = 20 - 80^\circ$ are shown in Figure 1. The peaks of XRD show perovskite structure without any secondary phase. Figure 2(a) shows density variation of (1-x)BNKT-xLN ceramics plotted as a function of the sintering temperature. The densities increase with increasing sintering temperature. The optimum sintering temperature is found at 1100°C for all BNKT-LN ceramics. The densities then drop at higher sintering temperature of 1125°C . The density values are obtained in a range of 5.38 - 5.68 g/cm³ which corresponds to 93 - 99% of their theoretical values. In addition, the variation of linear shrinkage with increasing sintering temperature shows similar trend to that of density value as shown in Figure 2(b). The maximum linear shrinkage of 21 - 22% is observed for pure BNKT-LN ceramics sintered at 1100°C (see Table 1). Thus, the samples sintered at 1100°C for BNKT-LN ceramics are selected for further characterization.

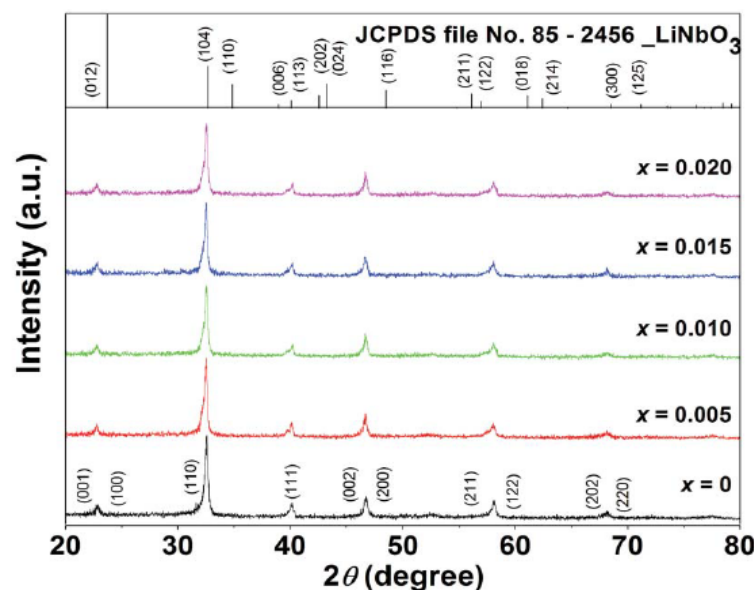


Figure 1. X-ray diffraction patterns of (1-x)BNKT-xLN mixed powders with $2\theta = 20-80^\circ$.

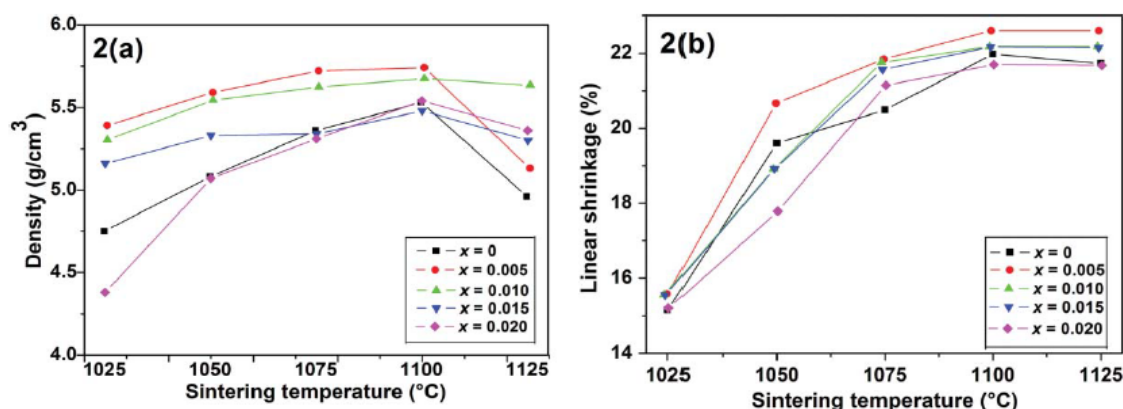


Figure 2. (a) Plots of density as a function of sintering temperature of $(1-x)\text{BNKT-xLN}$ ceramics, (b) Plots of linear shrinkage as a function of sintering temperature $(1-x)\text{BNKT-xLN}$ ceramics.

X-ray diffraction patterns of $(1-x)\text{BNKT-xLN}$ ceramics at $2\theta = 20 - 80^\circ$ are shown in Figure 3(a). All compositions exhibit a pure perovskite structure without any secondary phase. This confirms that the starting reagents completely reacted to form the final compounds. This suggests that LN has diffused into BNKT lattice to form complete solid solutions during the sintering process. The solubility limit of LN in BNKT lattice is believed to be more than 0.02 mol fraction because no trace of secondary phases are observed in XRD patterns. BNKT ceramics shows features of mixed rhombohedral-tetragonal symmetry but shows a domination of rhombohedral over tetragonal structure. This result is also correlated with that reported by Sasaki *et al.* [3]. Addition of LN into BNKT indicates a dominating rhombohedral phase, corresponding to a decrease in the tetragonality (c/a) as shown in Table 1. This believe Li^+ ions (1.06 Å) diffuse to A-site Bi^{3+} (1.17 Å), Na^+ (1.18 Å) and K^+ (1.33 Å) positions while Nb^{5+} ions (0.64 Å) diffuse into B-site of Ti^{4+} positions (0.61 Å) [10].

XPS analysis was carried out to obtain some information about the chemical composition, binding energy and chemical state of ionic species in $(1-x)\text{BNKT-xLN}$ ceramics. The chemical information are found for five elements, including Na, O, Ti, K and Bi. However, Li is not detected when LN was added into BNKT. This may be due to the small concentration of Li in the sample and/or Li loss from the surface of sample. XPS spectra of Bi 4f, Na 1s, K 2p, Ti 2p, Nb 3d and O 1s are shown in Figure 4. Na shows highest binding energy values of 1068 eV (BNKT) - 1070 eV(BNKT-LN) illustrating of

Table 1

Physical properties and microstructure of $(1-x)\text{BNKT-xLN}$ ceramics sintered at 1100°C

x	Density (g/cm^3)	Relative density (%)	Linear shrinkage (%)	Grain range (μm)	Average grain size (μm)	c/a
0	5.53 ± 0.03	94.56	21.98	0.97 - 1.02	1.04 ± 0.01	1.0247
0.005	5.68 ± 0.01	99.10	22.58	0.62 - 0.89	0.72 ± 0.02	1.0164
0.010	5.62 ± 0.04	96.88	22.18	0.73 - 0.92	0.88 ± 0.05	1.0163
0.015	5.48 ± 0.05	95.70	22.09	0.76 - 0.98	0.90 ± 0.03	1.0160
0.020	5.38 ± 0.03	93.57	21.73	0.85 - 0.98	0.95 ± 0.03	1.0122

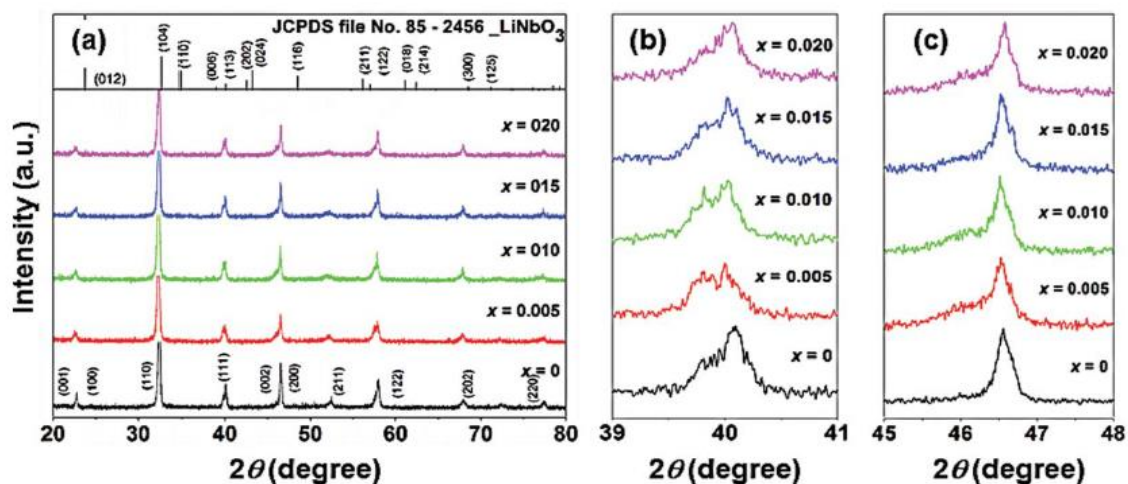


Figure 3. X-ray diffraction patterns of the optimal $(1-x)\text{BNKT}-x\text{LN}$ sintered ceramics where (a) $2\theta = 20\text{--}80^\circ$, (b) $2\theta = 39\text{--}41^\circ$ and (c) $2\theta = 45\text{--}48^\circ$.

the Na^{1+} ion in the perovskite lattice in agreement with the values reported earlier by Mahboob *et al* [9]. The small shift in binding energy in LN-doped BNKT seems to indicate a slight change in chemical environment of Na^{1+} ion. The XPS spectrum of K 2p representing the K^{1+} ion in the perovskite lattice also indicates a small shift from ~ 295 eV in BNKT to lower binding energy in LN-doped BNKT. Hence, it seems that local defects such as vacancies near Na^{1+} and K^{1+} sites can play some roles in observed peak shift. The Bi 4f shows two binding energies at approximately 159.500 and 164.445 eV for all compositions. The spectral line of higher and lower binding energy indicates Bi 4f_{7/2} and Bi 4f_{5/2}, respectively [9]. The spin-orbit splitting between the lower and higher binding energy peak is around 4.945 eV. The Ti 2p peaks indicate mainly

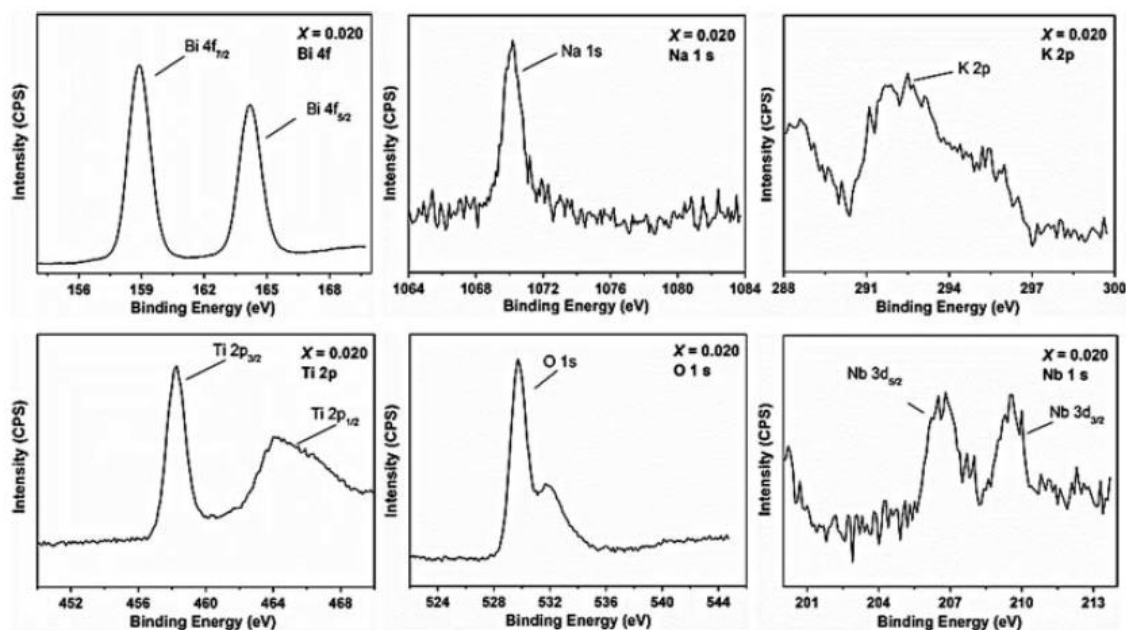


Figure 4. XPS spectra of $(1-x)\text{BNKT}-x\text{LN}$ ceramics with $x = 0.020$.

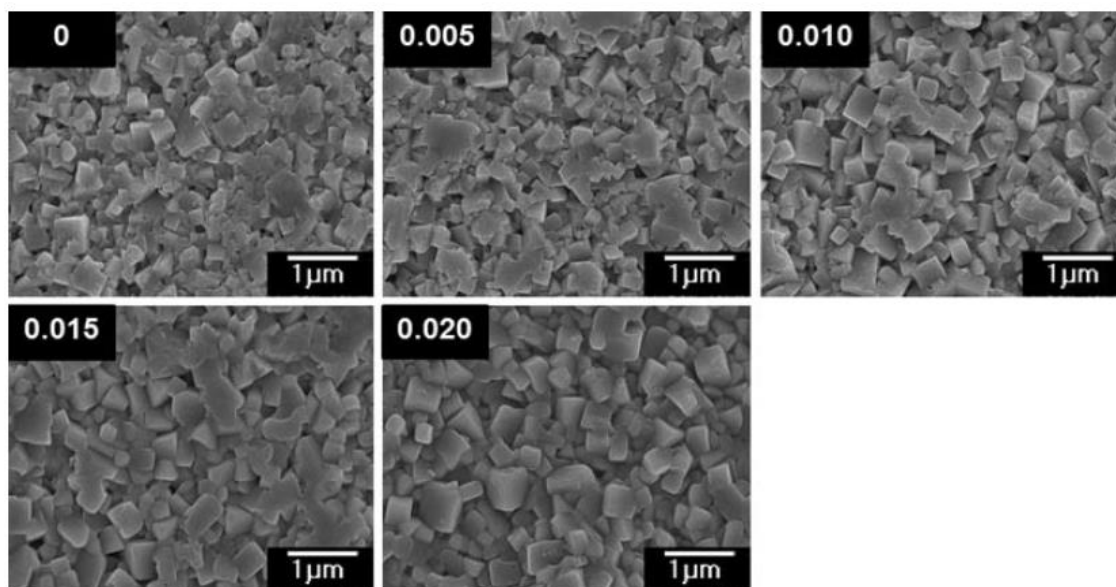


Figure 5. SEM micrographs of as-sintered surface of the optimal (1-x)BNKT-xLN sintered ceramics.

Ti^{4+} ion existing inside the material. The higher binding energy belongs to the spectral line $Ti\ 2p_{3/2}$ and lower binding energy $Ti\ 2p_{1/2}$ [9]. The spin-orbit splitting between the lower and higher is 5.703 eV. For LN-doped BNKT samples, Nb 3d doublet peaks show binding energies around 206.950 and 209.851 eV. The lower binding energy indicates Nb $3d_{5/2}$ spectral line and higher binding energy Nb $3d_{3/2}$. The energy position, binding energy and full width at half maximum value of all samples are shown in Table 3. It should be noted that, for Nb $3d_{5/2}$, the binding energy values for both undoped and LN-doped sample are close to the standard value of 206.2 eV (from NIST database of NbO_2 with six fold coordinated oxygen surrounding Nb ion). This suggests that Nb most likely

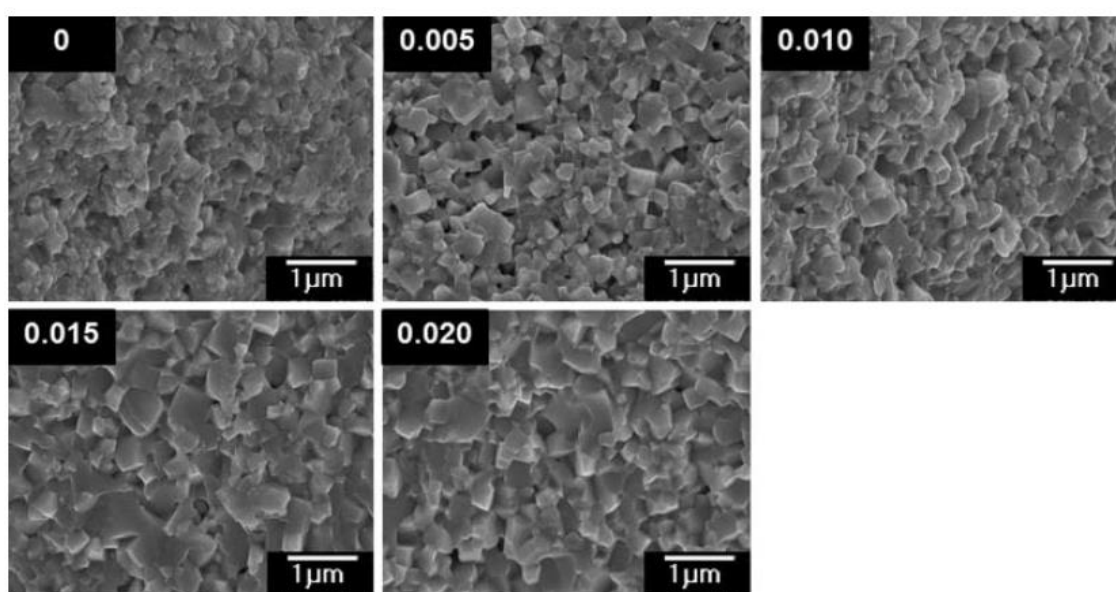


Figure 6. SEM micrographs of fracture surface of the optimal (1-x)BNKT-xLN sintered ceramics.

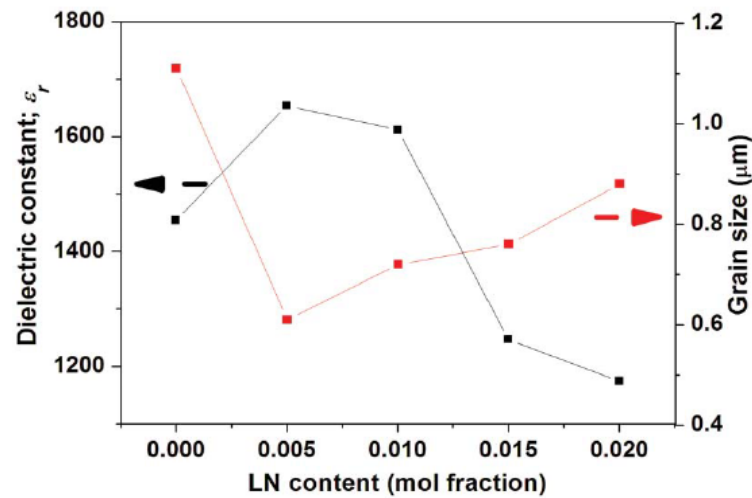


Figure 7. Plots of dielectric constant (ϵ_r) and grain size as a function of LiNbO_3 content.

substitutes Ti site in BNKT lattice. The slightly higher values of Nb $3d_{5/2}$ in this study are possibly due to the presence of majority Nb^{5+} rather than Nb^{4+} ion in these perovskite lattice.

SEM micrographs of as-sintered surface of $(1-x)\text{BNKT}-x\text{LN}$ ceramics are shown in Figure 5. Grain range values of all samples are listed in Table 1. It can be seen that all samples are dense and well sintered with high density value. The cubic-like grain shape occurs in all BNKT-LN samples. Pure BNKT ceramic represents a formation of a cubic-like shape with side length of around $0.97 - 1.02 \mu\text{m}$. The addition of LN does not obviously change the grain shape. The formation of cubic-like shape is still observed for all amount of added LN content. The addition a small amount of LN ($x = 0.005$) into BNKT ceramic inhibits grain growth and grain size increases with increasing LN content. We believe that a reduction of grain size for these samples is due to a solute drag effect of the

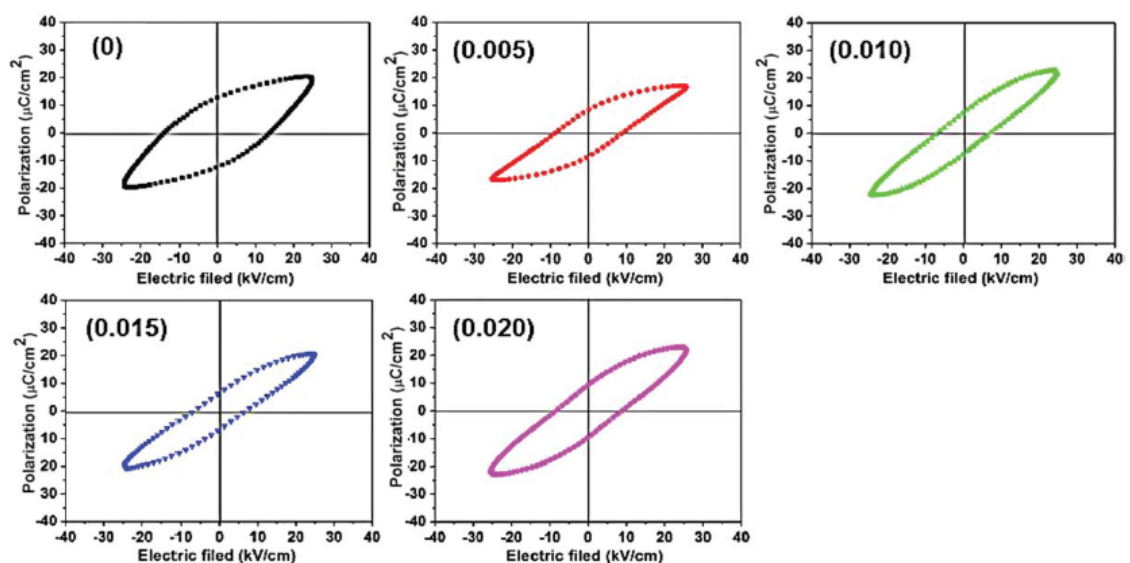


Figure 8. Polarization-electric field (P - E) hysteresis loop of the optimal $(1-x)\text{BNKT}-x\text{LN}$ sintered ceramics.

Table 2
Chemical state, chemical composition, binding energy (B.E.) and full width at half maximum values (FWHM) of (1-x)BNKT-xLN ceramics sintered at 1100°C

	$x = 0$				$x = 0.005$				$x = 0.010$				$x = 0.015$				$x = 0.020$			
Composition	B.E. (eV)	FWHM (eV)	B.E. (eV)	FWHM (eV)	B.E. (eV)	FWHM (eV)	B.E. (eV)	FWHM (eV)	B.E. (eV)	FWHM (eV)	B.E. (eV)	FWHM (eV)	B.E. (eV)	FWHM (eV)	B.E. (eV)	FWHM (eV)	B.E. (eV)	FWHM (eV)	B.E. (eV)	FWHM (eV)
Bi 4f _{7/2}	159.500	1.449	159.108	0.998	159.194	0.985	158.620	0.938	158.864	1.159										
Bi 4f _{5/2}	164.806	1.449	164.445	1.044	164.495	0.985	163.927	0.971	164.214	1.182										
Na 1s	1068.778	1.479	1071.044	1.1412	1070.957	1.199	1070	1.119	1070.154	1.211										
K 2p	295.872	1.502	293.100	1.508	295.252	1.502	293.100	1.803	292.100	1.509										
Ti 2p _{3/2}	458.017	1.206	458.334	1.116	458.232	1.078	458.511	1.116	458.280	1.206										
Ti 2p _{1/2}	463.720	2.167	464.105	2.233	463.935	1.890	464.349	2.036	466.217	2.2925										
O 1s	529.335	1.214	529.863	1.214	529.685	1.130	530.200	1.214	529.746	1.214										
Nb 3d _{5/2}	-	-	206.496	1.055	206.950	1.170	206.496	1.055	206.673	1.170										
Nb 3d _{3/2}	-	-	209.232	1.077	209.581	1.170	209.323	1.077	209.465	0.996										

[473]/125

Table 3
Electrical properties of (1-*x*)BNKT-*x*LN ceramics sintered at 1100°C

<i>x</i>	ϵ_r	$\tan\delta$	P_r ($\mu\text{C}/\text{cm}^2$)	E_c (kV/cm)	P_r/P_{\max}	E_c/E_{\max}	R_{sq}	d_{33} (pC/N)
0	1454	0.0643	13.66	13.11	0.71	0.52	0.72	139
0.005	1654	0.0632	10.39	9.48	0.67	0.38	0.77	162
0.010	1611	0.0646	9.41	6.00	0.38	0.24	0.24	145
0.015	1246	0.0649	9.40	5.37	0.39	0.25	0.25	119
0.020	1174	0.0656	8.94	5.21	0.42	0.21	0.21	101

dissolved LN [11]. Since the solute diffusion near grain boundary region is usually slower than the intrinsic diffusion of host atoms across the boundary plane, this becomes a rate-limiting factor and therefore effectively slows the grain boundary movement. LN may aggregate on a very small scale at grain boundaries which results in inhibition of grain growth and grain boundary movement during the sintering process. This seems to be the main mechanism governing the observe microstructure [12]. However, grain size increase to 0.88 - 0.95 μm with increasing LN concentration ($x = 0.010 - 0.020$). Increasing LN content in BNKT may induce charge defects such as vacancies due to requirement of charge balance and this may provide some ease an atomic diffusion, hence slightly increasing grain growth rate. Fractured surface of (1-*x*)BNKT-*x*LN ceramics indicates a switch of intergranular to transgranular fracture mode when LN content is increased as can be seen from the typical fracture surface morphologies shown in Figure 6.

Room temperature dielectric constant (ϵ_r) and dielectric loss ($\tan\delta$) values of (1-*x*)BNKT-*x*LN system measured at a frequency of 1 kHz are shown in Figure 7 and the values are also listed in Table 3. It can see that the addition of small amount of LN into BNKT ceramic can significantly improve dielectric properties. Pure BNKT ceramic has ϵ_r of 1454 which is close to the value reported earlier by Jaita *et al.* [13]. The ϵ_r increases with increasing LN content up to $x = 0.010$. The maximum room temperature dielectric constant of 1654 is obtained for BNKT-0.005LN sample. This result is attributed to the relatively high density and linear shrinkage of the sample. Since the grain shape and size of all samples are similar, these should not have significant effect on dielectric constant. Addition of small amount of LN (i.e. up to 0.010) seems to show dominant donor-doping effect and this is another factor that can induce high dielectric constant values. Above $x = 0.010$, the dielectric constant started to decrease below that of undoped BNKT sample. This may be the result of induced charge defects acting against donor-doped behavior. The dielectric loss of all sample were more or less the same, indicating that conductive loss or changes in domain wall motion due to LN doping are negligible. Figure 8 shows polarization-electric field (*P-E*) hysteresis loop of (1-*x*)BNKT-*x*LN system. *P-E* hysteresis loop of BNKT-LN shows typical ferroelectric shape at room temperature. The P_r and E_c slightly decrease with increasing LN content. The piezoelectric constant (d_{33}) of the (1-*x*)BNKT-*x*LN ceramics are summarized in table 3. Pure BNKT ceramic has d_{33} of 139 pC/N. The highest $d_{33} = 162$ pC/N value is obtained at the composition of $x = 0.005$ as shown in Table 2. The addition of small amount of LN ($x = 0.005$) shows improvement of d_{33} properties. It seems that BNKT-0.005LN possesses optimum electrical properties due to the effect of local polarization from donor-doped behavior and high sample density.

4. Conclusions

Lead-free piezoelectric ceramics of $(1-x)Bi_{0.5}(Na_{0.80}K_{0.20})_{0.5}TiO_3-xLiNbO_3$ (when $x = 0, 0.005, 0.010, 0.015$ and 0.020 mol fraction) were successfully prepared by conventional mixed oxide method. X-ray diffraction patterns represented a single perovskite structure without any secondary phase. The dominance of rhombohedral phase became more apparent with increasing LN concentration. The X-ray photoelectron spectroscopy showed chemical state of Bi 4f, Na 1s, K 2p, Ti 2p, Nb 3d and O 1s, which suggested the Ti B-site substitution by Nb. The addition of LN into BNKT had very small effect on grain size and shape. The addition of small amount of LN up to $x = 0.010$ enhanced dielectric and piezoelectric properties of BNKT ceramic. The highest dielectric constant measured at room temperature was 1654 for the composition of $x = 0.005$. The highest d_{33} of 162 pC/N value was also obtained at the composition of $x = 0.005$. The P_r and E_c decreased with increasing LN content. These observed behavior was thought to be caused by the changes in local polarization due to donor-like doing rather than the effect of domain wall movement.

Funding

This work is financially supported by Suranaree University of Technology, Thailand and the Thailand Research Fund (TRF).

References

1. S. H. Lee, S. D. Baek, H. J. Kim, S. G. Lee, and Y. H. Lee, Ferroelectric and piezoelectric properties of lead-free $0.98(Na_{0.5}K_{0.5})NbO_3-0.02Ba(Zr_{0.52}Ti_{0.48})O_3$ ceramics with various sintering temperature. *Electron.Mater.Lett.* **8**, 147–150 (2012).
2. S. H. Lee, S. J. Kim, S. G. Lee, J. H. Koh, S. D. Baek, and Y. H. Lee, Electrical properties of lead-free $0.98(Na_{0.5}K_{0.5}Li_x)NbO_3-0.02Ba(Zr_{0.52}Ti_{0.48})O_3$ ceramics. *Electron. Mater.Lett.* **8**, 43–45 (2012).
3. A. Sasaki, T. Chiba, Y. Mamiya, and E. Otsuki, Dielectric and piezoelectric properties of $(Bi_{0.5}Na_{0.5})TiO_3-(Bi_{0.5}K_{0.5})TiO_3$ systems. *Jpn. J. Appl. Phys.* **38**, 5564–5567 (1999).
4. P. Y. Chen, C. Y. Chou, T. Y. Tseng, and H. D. Chen, Impedance spectroscopic study on Li-doped BNKT piezoelectric ceramics. *Ferroelectrics.* **380**, 100–104 (2009).
5. X. P. Jiang, L. Z. Li, M. Zang, and H. L. W. Chan, Dielectric properties of Mn-doped $(Na_{0.8}K_{0.2})_{0.5}Bi_{0.5}TiO_3$. *Ceramics. Mater. Lett.* **60**, 1786–1790 (2006).
6. A. Hussain, A Zaman, Y. Iqbal, and M. H. Kim, Dielectric, ferroelectric and field induce strain properties of Nb-modified Pb-free $0.99Bi_{0.5}(Na_{0.82}K_{0.18})_{0.5}TiO_3-LiSbO_3$ ceramics. *J. Alloys Compd.* **574**, 320–324 (2013).
7. C. Zhou, X. Liu, W. Li, and C. Yuan, Microstructure and electrical properties of $(Bi_{0.5}Na_{0.5})TiO_3-(Bi_{0.5}K_{0.5})TiO_3-LiNbO_3$ system. *J. Appl. Phys.* **70**, 541–545 (2009).
8. H. Du, F. Tang, D. Liu, D. Zhu, W. Zhou, and S. Qu, The microstructure and ferroelectric ceramic. *Mater. Sci. Eng.* **136**, 165–169 (2007).
9. S. Mahboob, G. Prasad, C. C. Chou, and G. S. Kumar, Electrical and X-ray photoelectron spectroscopy study on $(Na_{0.5-x}K_xBi_{0.5-x}Nd_x)TiO_3$ ceramics. *Ferroelectrics.* **445**, 161–171 (2013).
10. Y. R. Zhang, J. F. Li, and B. P. Zhang, Enhancing electrical properties in NBT-KBT lead-free piezoelectric ceramics by optimizing sintering temperature. *J. Am. Ceram. Soc.* **91**, 2716–2719 (2008).
11. Y. M. Chiang, D. P. Birnie III, and W. D. Kingery, *Physical Ceramics: Principles for ceramics science and engineering*. John Wiley & Son Ltd, New York, 1997.

12. A. J. Moulson and J. M. Herbert, *Electroceramics*, 2nd Edn., John Wiley & Sons Ltd, New York, 2003.
13. P. Jaita, A. Watcharapasorn, and S. Jiansirisoomboon, Dielectric, ferroelectric and Electric field-induced strain behavior of $\text{Ba}(\text{Ti}_{0.90}\text{Sn}_{0.10})\text{O}_3$ modified $\text{Bi}_{0.5}(\text{Na}_{0.80}\text{K}_{0.20})_{0.5}\text{TiO}_3$ lead-free piezoelectrics. *J. Alloys Compd.* **596**, 98–106 (2014).



Enhanced Dielectric and Ferroelectric Properties of $\text{Pb}(\text{Mg}_{1/3}\text{Nb}_{2/3})_{0.65}\text{Ti}_{0.35}\text{O}_3$ Ceramics by ZnO Modification

Methee Promsawat,^{‡,§} Anucha Watcharapasorn,^{‡,§} Zuo-Guang Ye,[†] and Sukanda Jiansirisomboon^{‡,§,†}

[‡]Faculty of Science, Department of Physics and Materials Science, Chiang Mai University, Muang, Chiang Mai 50200, Thailand

[§]Faculty of Science, Materials Science Research Center, Chiang Mai University, Muang, Chiang Mai 50200, Thailand

[†]Department of Chemistry and 4D LABS, Simon Fraser University, Burnaby, British Columbia V5A 1S6, Canada

Phase formation, microstructures, dielectric, and ferroelectric properties of ZnO-modified $\text{Pb}(\text{Mg}_{1/3}\text{Nb}_{2/3})_{0.65}\text{Ti}_{0.35}\text{O}_3$ (PMNT)/ $x\text{ZnO}$, where $x = 0, 0.4, 2.0, 4.0$, and 11.0 mol% ceramics were studied. A coexistence of rhombohedral and tetragonal ferroelectric phases was observed at room temperature in all samples. The ceramics with the relative densities of 93%–95% were prepared. The modification by ZnO led to an increase in grain sizes of PMNT ceramics. The maximum dielectric constant of the pure PMNT ceramic was increased with $x = 0.4$ – 4.0 mol% ZnO doping, with the highest value being observed in the 2.0 mol% sample. Both the temperature at which the transition between rhombohedral and tetragonal ferroelectric phases took place (T_{R-T}) and the Curie temperature of the ceramics tended to increase with increasing x . The ferroelectric properties were enhanced with increased remanent polarization and $P(E)$ loop squareness in the compositions with $x = 0.4$ – 4.0 mol%. However, the ferroelectric properties were attenuated with $x = 11.0$ mol%.

I. Introduction

COMPLEX perovskite solid solution, $\text{Pb}(\text{Mg}_{1/3}\text{Nb}_{2/3})_{1-x}\text{Ti}_x\text{O}_3$, is a well-known relaxor-based ferroelectric material that exhibits excellent piezo-/ferroelectric properties, which make it promising for applications as electronic devices.^{1–3} The materials show extremely high piezoelectric properties at a composition lying in the morphotropic phase boundary (MPB) with PT content of 30–35 mol% ($x = 0.30$ – 0.35),^{2,4,5} at which rhombohedral, tetragonal, and monoclinic ferroelectric phases coexist. However, this system suffers from a low temperature (T_{R-T}) at which the rhombohedral phase in the MPB region transforms into a tetragonal phase. This restricts the operating temperature range of the piezoceramics.⁶ Therefore, the phase transition temperatures of the ceramics should be increased to maintain their excellent properties in a wide temperature range for applications.

ZnO has been widely used as a sintering aid for dielectric and piezoelectric ceramics.^{7–10} As demonstrated previously, the addition of ZnO could promote the formation of a liquid phase which expedited mass transfer during a sintering process, resulting in an enhancement of density, grain size as well as electrical properties of ceramics.^{11,12} Moreover, ZnO was also used as a substituent for both lead-based solid solution ferroelectric ceramics, that is, $\text{Pb}(\text{Mg}_{1/3}\text{Nb}_{2/3})_{0.9}\text{Ti}_{0.1}\text{O}_3$,¹³ $\text{Pb}(\text{Mg}_{1/2}\text{W}_{1/2})\text{O}_3$ – $\text{Pb}(\text{Ni}_{1/3}\text{Nb}_{2/3})\text{O}_3$ – PbTiO_3 – PbZrO_3 ,⁷

$\text{Pb}(\text{Zr}_{0.55}\text{Ti}_{0.45})\text{O}_3$ – $\text{Pb}(\text{Zn}_{1/3}\text{Nb}_{2/3})\text{O}_3$,¹⁴ and $\text{Pb}(\text{Mn}_{1/3}\text{Nb}_{2/3})\text{O}_3$ – $\text{Pb}(\text{Zr}_{0.52}\text{Ti}_{0.48})\text{O}_3$,¹⁵ and lead-free ferroelectric ceramics, that is, $\text{Bi}_{0.5}\text{Na}_{0.5}\text{TiO}_3$,^{16,17} and $(\text{Na}_{0.5}\text{K}_{0.5})\text{NbO}_3$.¹⁸ These results suggested that Zn^{2+} ion could substitute a cation located on B-site lattice of the perovskite ceramics, which could in turn change the phase transition temperature and improve the electrical property of those ceramics. Moreover, the Zn^{2+} substitution could enhance the perovskite phase stabilization of the ternary solid solution $\text{PbMg}_{1/3}\text{Nb}_{2/3}\text{O}_3$ – $\text{PbZn}_{1/3}\text{Nb}_{2/3}\text{O}_3$ – PbTiO_3 .^{19–21} These advantages make ZnO interesting to be used as a substituent for the $\text{Pb}(\text{Mg}_{1/3}\text{Nb}_{2/3})_{0.65}\text{Ti}_{0.35}\text{O}_3$ (PMNT) ceramics, which are the materials at the MPB composition that have been widely studied.^{22–26} It is believed that the use of nanosized ZnO particles which have a high specific (reactive) surface area can further improve the efficiency of a sintering process. To the best of our knowledge, the effects of ZnO modification on the properties of the PMNT ceramics have not been reported yet. Therefore, in this study, ZnO is selected as a substituent for the PMNT ceramics to modify their electrical properties. The effects of ZnO modification on the phase formation, density, microstructure, dielectric, and ferroelectric properties of the PMNT ceramics have been investigated and discussed.

II. Experimental Procedure

$\text{Pb}(\text{Mg}_{1/3}\text{Nb}_{2/3})_{0.65}\text{Ti}_{0.35}\text{O}_3$ (PMNT) powders were prepared by the columbite precursor method.²⁷ Different amounts of spherically shaped ZnO nanoparticles (99.5%; Nanostructured & Amorphous Materials, Houston, TX) with a particle size of 20 nm were added into PMNT powders to obtain PMNT/ $x\text{ZnO}$ (where $x = 0, 0.4, 2.0, 4.0$, and 11.0 mol%) powders. Polyvinyl alcohol was added to the mixed powders as a binder and then uniaxially pressed into pellets by a pressure of ~5.0 MPa. Each pellet (10 mm in diameter, 2 mm in thickness, and a raw density of ~4.84 g/cm³) was sintered in a PMNT atmosphere at 1240°C for 2 h. Bulk densities of the ceramics were determined by the Archimedes method. Phase formation and chemical compositions were characterized using X-ray diffraction method (XRD; Rapid Axis, Rigaku, Tokyo, Japan) with CuK_α radiation of 1.5405 Å wavelength and an energy-dispersive X-ray technique (EDX; Dual Beam Strata 235, FEI, Hillsboro, OR), respectively. Microstructures of the ceramics were imaged using a scanning electron microscope (SEM; Dual Beam Strata 235, FEI). Average grain sizes were determined from the SEM micrographs. For dielectric measurements, the samples were firstly poled by the application of an electric field of 20 kV/cm. While the sample was being poled, it was cooled down to 0°C, at which the applied field was removed and the temperature dependence of dielectric properties (dielectric constant and dielectric loss) was then measured upon heating by a computer-controlled alpha dielectric analyzer (Novocontrol,

X. M. Chen—contributing editor

Manuscript No. 35429. Received August 6, 2014; approved November 10, 2014.
[†]Author to whom correspondence should be addressed. e-mail: sukanda.jian@cmu.ac.th

Montabaur, Germany). The polarization versus electric field relations were measured using a ferroelectric testing instrument (Radiant Technologies RT66A, Albuquerque, NM).

III. Results and Discussion

(1) Phase Formation

The XRD patterns of the PMNT/*x*ZnO ceramics are shown in Fig. 1(a), which were found to match the standard inorganic crystal structure database (ICSD) file No. 157487 of $\text{Pb}(\text{Mg}_{1/3}\text{Nb}_{2/3})_{0.65}\text{Ti}_{0.35}\text{O}_3$ with tetragonal *P4mm* space group.²⁸ No secondary phase was observed on the patterns. Enlarged patterns of peaks at $2\theta \approx 45^\circ$ are shown in Fig. 1(b). The patterns were fitted with multiple Lorentz's peaks which are indicated as green peaks in Fig. 1(b). It can be seen from the fitted peaks that the rhombohedral and tetragonal phases coexisted in the samples. From the positions of the fitted peaks, the rhombohedral and tetragonal lattice parameters were determined as given in Table I. The rhombohedral lattice parameter *a* (*a_R*), tetragonal lattice parameter *a* and *c* (*a_T* and *c_T*) of the pure PMNT sample decreased with 0.4 mol% ZnO modification. The *a_R* tended to increase with further increasing ZnO content up to 11.0 mol%. The *a_T* tended to increase with increasing ZnO content up to 4.0 mol% and then slightly decreased with further increasing ZnO content to 11.0 mol%. The *c_T* increased with 2.0 mol% ZnO incorporation. However, it did not increase further with higher ZnO contents. The calculated tetragonality (*c/a*) of the ceramics is given in Table I. It was found that the *c/a* of PMNT ceramics were increased with the ZnO modifications. The results suggest that ZnO modification results in the distortion and expansion of the perovskite unit cell of PMNT ceramics. This is attributed to the effects of the substitution of Zn^{2+} ion for an ion located on the B site of PMNT lattices. Based on the crystal chemistry requirements (the tolerance factor), for the stability of the perovskite structure, A site has to be a large cation (i.e., Pb^{2+}) whereas B site requires a relatively smaller cation (i.e., Mg^{2+} , Nb^{5+} , and Ti^{4+}). From the ionic radius of the ions located on the PMNT lattices, $r_{\text{Pb}^{2+}} = 1.49 \text{ \AA}$, $r_{\text{Mg}^{2+}} = 0.72 \text{ \AA}$, $r_{\text{Nb}^{5+}} = 0.64 \text{ \AA}$, $r_{\text{Ti}^{4+}} = 0.605 \text{ \AA}$, and $r_{\text{Zn}^{2+}} = 0.74 \text{ \AA}$,²⁹ it is clear that Zn^{2+} ion can only substitute a cation on the B-site PMNT lattices. Moreover, as the ionic radius of Zn^{2+} ion is similar to that of the Mg^{2+} ion,

Table I. Lattice Parameters and Tetragonality of the PMNT/*x*ZnO Ceramics

ZnO content, <i>x</i> (mol%)	Lattice parameters			Tetragonality; <i>c/a</i>
	<i>a_R</i> (Å)	<i>a_T</i> (Å)	<i>c_T</i> (Å)	
0	4.003	3.998	4.028	1.008
0.4	4.003	3.983	4.024	1.009
2.0	4.005	3.987	4.032	1.011
4.0	4.006	3.990	4.030	1.010
11.0	4.009	3.989	4.032	1.011

a_R represents the rhombohedral lattice parameter *a*. *a_T* and *c_T* are the tetragonal lattice parameters *a* and *c*, respectively.

it is possible that the Zn^{2+} ion substituted for the Mg^{2+} ion. This is consistent with the previous results observed in the PMN-PZN-PT,^{19–21} PZT-PMS-PZN,¹¹ PZN-PZT,¹⁴ PZNT,³⁰ PZT-PMN,³¹ PZT-PFW-PMN,³² and PZN-PT-BT³³ ceramics modified with ZnO. These results show that Zn^{2+} ion can substitute an ion located on the B site of perovskite lattices of similar ionic radius, leading to an increase in ceramic's lattice parameters.

(2) Density and Microstructure

The relative densities of the PMNT/*x*ZnO ceramics are given in Table II. The relative densities of the ceramics were decreased with *x* > 2.0 mol%. The average grain sizes of the ceramics were determined from SEM micrographs and the results are listed in Table II. The grain sizes of PMNT ceramics were found to increase with ZnO modifications. Moreover, the grain sizes tended to increase with increasing ZnO content. The increase in the grain size of the ZnO-modified ceramics is believed to arise from the effect of the formation of a liquid phase which promotes mass transport during a sintering process, expediting grain growth rates of the ceramics.^{27,34} A secondary phase was found to be presented at grain boundaries of the ceramics modified with *x* = 4.0 and 11.0 mol%, as indicated by the arrows in Figs. 2(d) and (e), respectively. Based on a chemical analysis by mean of energy-dispersive X-ray spectroscopy (EDX), this secondary phase was found to be Mg-rich as shown in Fig. 3(a). Moreover, the observed Zn in the secondary phase indicates that

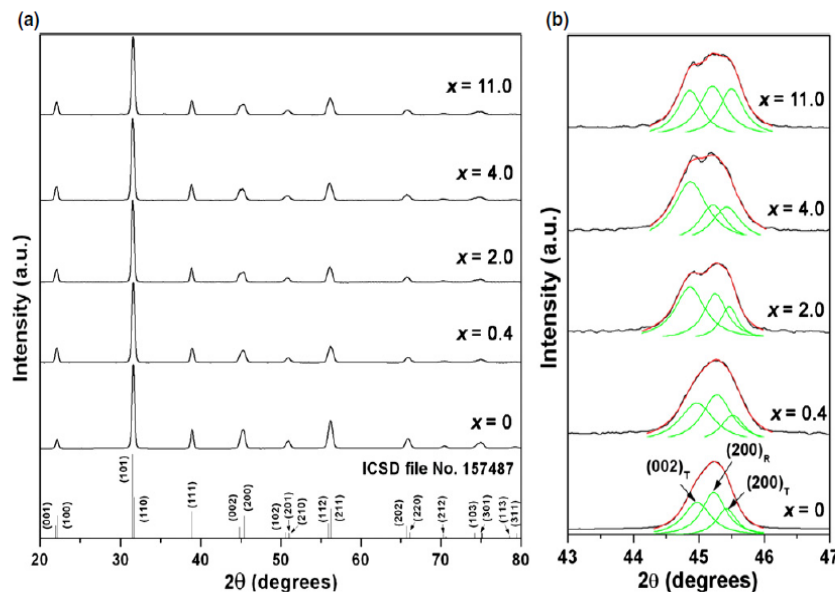


Fig. 1. (a) XRD patterns the PMNT/*x*ZnO ceramics. (b) Enlarged view and deconvolution of the peaks at $2\theta \approx 45^\circ$.

Table II. Relative Density, Grain Size, and Dielectric Properties of the PMNT/*x*ZnO Ceramics

ZnO content, <i>x</i> (mol%)	Relative density (%)	Grain size (μm)	ϵ_r	$\tan\delta$	T_{R-T} ($^{\circ}\text{C}$)	T_{max} ($^{\circ}\text{C}$)	γ
0	95.3 ± 0.1	2.1	15 250	0.11	50	165	1.78
0.4	95.6 ± 0.1	3.0	25 250	0.25	60	168	1.76
2.0	94.6 ± 0.1	5.6	29 000	0.10	56	172	1.68
4.0	92.5 ± 0.1	6.5	21 500	0.16	62	173	1.59
11.0	88.7 ± 0.1	10.6	15 250	0.14	89	190	1.56

ϵ_r and $\tan\delta$ are the dielectric constant and loss tangent, respectively, which were measured at the temperature of maximum dielectric constant (T_{max}) at the frequency of 1 kHz. T_{R-T} represents the temperature of the rhombohedral–tetragonal phase transition. The degree of diffuseness is denoted as γ .

ZnO could not completely dissolve in PMNT when its content is >2.0 mol%. This suggests that the solubility limit of ZnO in PMNT is 2.0 mol%. Moreover, it is believed that the Mg-rich phase was formed from the substitution of Zn^{2+} ion for Mg^{2+} ion, which is consistent with the XRD result. Figure 3(b) shows the EDX result of the secondary phase distributed along the grain boundaries of the PMNT/11.0 mol%ZnO

sample. The secondary phase contained high concentrations of Pb, Zn, and Ti (38.75, 14.19, and 11.44 wt%, respectively) and low contents of Nb and Mg (8.56 and 5.50 wt%) elements. This Pb-rich phase could be a liquid phase, which facilitated the diffusion and mass transport and thereby enhanced the grain growth of the ceramics during the sintering process, since PbO has a low melting point (888°C^{35}).

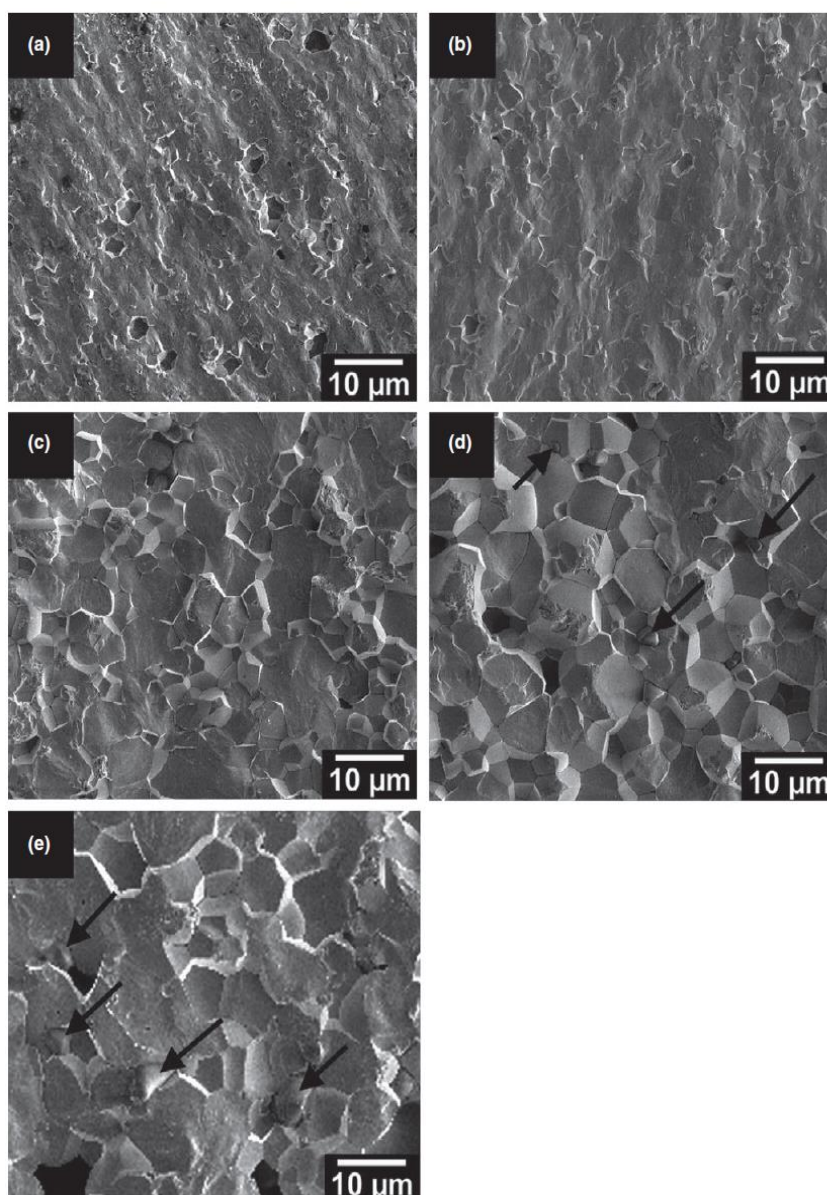


Fig. 2. SEM micrographs of fractured surfaces of the pure PMNT ceramic (a) and the ceramics modified with 0.4 (b), 2.0 (c), 4.0 (d), and 11.0 mol% ZnO (e). The arrows indicated a secondary phase.

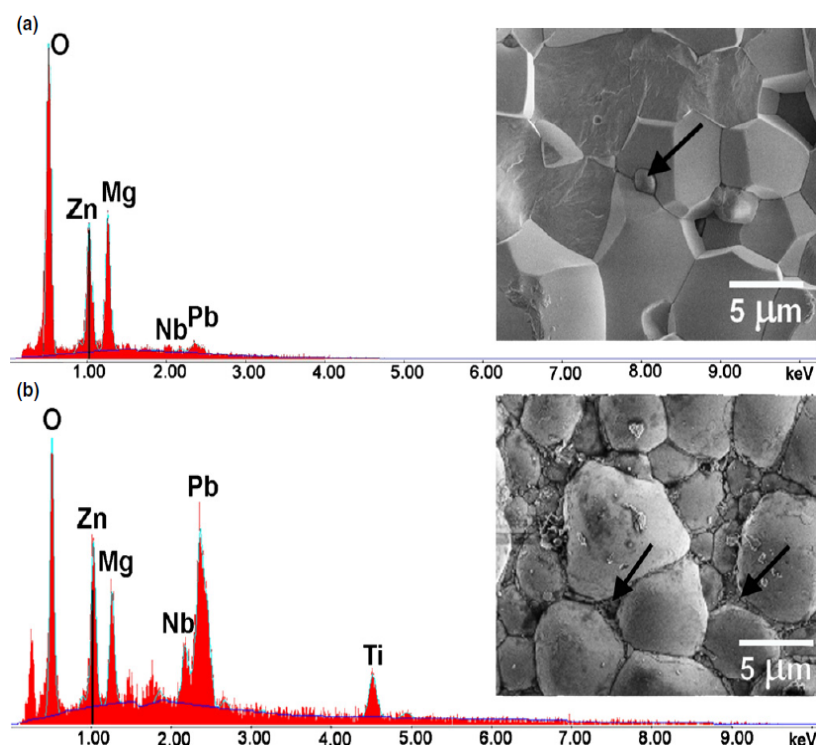


Fig. 3. EDX results of the secondary phases indicated by arrows in the ceramics modified with 4.0 (a) and 11.0 (b) mol% ZnO.

(3) Dielectric Properties

The temperature dependences of the dielectric constant and dielectric loss tangent measured at the frequency ranged from 10^1 to 10^5 Hz of the PMNT/ x ZnO ceramics are shown in Fig. 4. A sharp dielectric peak, characteristic of normal ferroelectrics, at the Curie temperature was observed in the pure PMNT ceramic and the ceramics with $x = 0.4$ – 4.0 mol%. In contrast, the 11.0 mol% ZnO-modified ceramic showed a dielectric peak with a shoulder at a lower temperature. The appearance of the dielectric shoulder is believed to be due to the responses of charge defects, that is, the cation and oxygen vacancies, created due to the formations of the Mg-rich and Pb-rich phases. This is consistent with previous works.^{36,37} Selected dielectric properties, that is, dielectric constant (ϵ') and dielectric loss tangent ($\tan\delta$) measured at the temperature of the maximum dielectric constant (T_{\max}) at a frequency of 1 kHz, are given in Table II. The results showed that the ϵ' of the pure PMNT ceramic was enhanced with $x = 0.4$ – 4.0 mol % and then decreased when x increased to 11.0 mol%. The $\tan\delta$ of the pure PMNT ceramic did not significantly change with $x = 2.0$ and 11.0 mol%. However, $\tan\delta$ significantly increased with $x = 0.4$ and 4.0 mol%. The enhancement in dielectric properties, that is, an increase in ϵ' and a decrease in $\tan\delta$, is attributed to the effects of an increase in grain size of the ceramics. The grain boundaries, which are usually nonpolar regions, are reduced with an increased grain size, resulting in an increase in dielectric constant and a decrease in loss tangent. This is consistent with the previous result observed in Ref. [38]. The degradation of dielectric properties, that is, a decrease in dielectric constant and an increase in dielectric loss, could result from the effects of the significant decrease in the density of the ceramics. The temperature of the rhombohedral-tetragonal ferroelectric phase transition, which was denoted as T_{R-T} , was determined as the temperature at which the first derivative of the $\epsilon'(T)$ curve is suddenly changed. The T_{R-T} values of the ceramics are given in Table II. The temperatures (T_{\max}) of maximum dielectric constant are also given in Table II. It can be seen from the results that the T_{R-T} and T_{\max} of PMNT ceramics were increased with the ZnO modifica-

tions, and they tended to increase with increasing ZnO content. The increases in T_{R-T} and T_{\max} can be attributed to the increases in the rhombohedral lattice parameters and tetragonality, respectively. It is believed that an increase in lattice parameter can contribute to the increase in the B-site ions displacements. This results in an increase in the degree and interaction strength of ferroelectric polarizations, leading to the increment of the phase transition temperatures.³⁹ This is consistent with the previous results which demonstrated that the rhombohedral-tetragonal and tetragonal-cubic phase transition temperatures increased with the increases in the rhombohedral and tetragonal lattice parameters, respectively.^{32,40}

To determine the degree of dielectric diffuseness, or the degree of relaxor behavior, of the ceramics, the dielectric constant values at the temperature range higher than T_{\max} were fitted to a modified Curie-Weiss relationship⁴¹:

$$\frac{1}{\epsilon_r} - \frac{1}{\epsilon_{\max}} = \frac{(T - T_{\max})^\gamma}{C} \quad (1)$$

where ϵ_{\max} is the maximum dielectric constant, ϵ_r is the dielectric constant at temperature T , T_{\max} is the temperature of the dielectric peak, C is the Curie constant, and γ is the degree of diffuseness, taking the value between 1 (for a normal ferroelectric) and 2 (for an ideal relaxor ferroelectric). The result indicated that the γ of PMNT ceramics was attenuated with the ZnO modifications, which the γ decreasing with increased ZnO content, as shown in Table II. The decrease in γ observed in the ceramics modified with $x \leq 2.0$ mol% is believed to be caused by the increase in the tetragonality. This is in agreement with the previous result that an increase in tetragonality could result in a decrease in γ of ceramics.³¹ For the ceramics with $x > 2.0$ mol%, the reduction in γ is attributed to the substitution of Zn^{2+} ion for the Mg^{2+} ion located on the B site of PMNT lattices. Compared with Mg^{2+} ion, Zn^{2+} ion possesses a $3d^{10}$ electronic configuration, which favors covalent bonding with $2p^6$ electrons of an oxygen ion when it occupies the octahedral site of the perovskite structure. This makes Zn^{2+} ion more

ferroelectrically active than Mg^{2+} ion. This can be attested by the fact that solid solution $\text{Pb}(\text{Zn}_{1/3}\text{Nb}_{2/3})\text{O}_3\text{-PbTiO}_3$ (PZN-PT) exhibits a higher degree of ferroelectric ordering and a lower degree of relaxor behavior than $\text{Pb}(\text{Mg}_{1/3}\text{Nb}_{2/3})\text{O}_3\text{-PbTiO}_3$ (PMN-PT) solid solution system at the same (low) PT concentrations.^{5,42,43}

(4) Ferroelectric Properties

The polarization–electric field, P – E , curves of the PMNT/ $x\text{ZnO}$ ceramics were measured at the room temperature at the frequency of 1 Hz. P – E hysteresis loops with a high remanent polarization and a high coercive field, which

are characteristic of normal ferroelectric materials, were displayed in all samples. The ferroelectric property parameters, i.e., the remanent polarization (P_r) and the coercive field (E_c), of the ceramics are given in Table III. Because of their temperature and field dependences, the ferroelectric parameters were thus normalized in the forms of P_r/P_{max} and E_c/E_{max} ^{44,45} and were plotted as a function of ZnO content, as shown in Fig. 5. Furthermore, the ferroelectric characteristics can be assessed with the hysteresis loop squareness (R_{sq}), which was calculated from the empirical expression $R_{\text{sq}} = (P_r/P_{\text{max}}) + (P_{1.1E_c}/P_r)$, where P_{max} is the maximum polarization obtained at a finite field strength below dielectric breakdown and $P_{1.1E_c}$ is the polarization at the field of

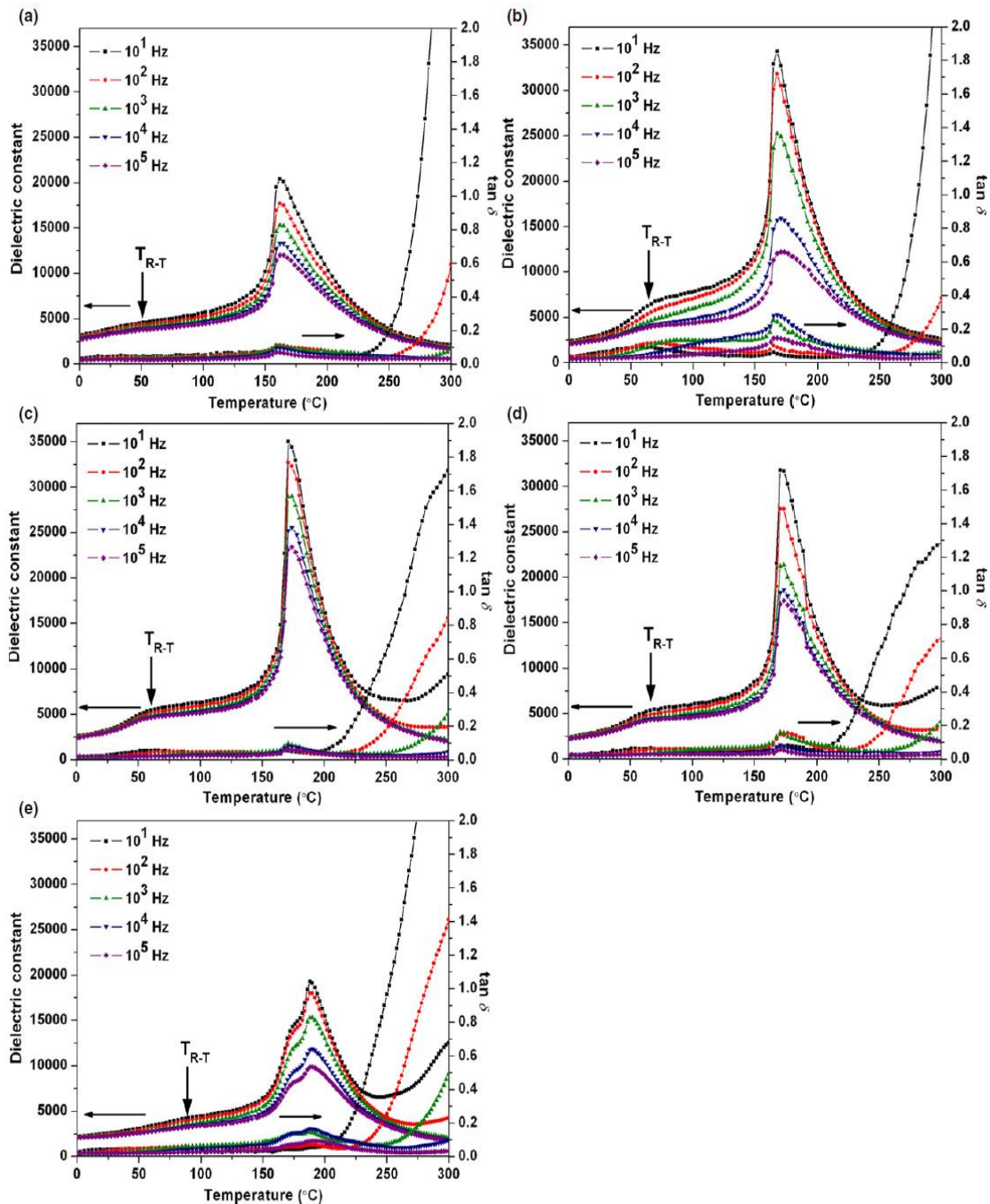


Fig. 4. Temperature dependences of the dielectric constant and loss tangent of the pure PMNT ceramic (a) and the ceramics modified with 0.4 (b), 2.0 (c), 4.0 (d), and 11.0 mol% ZnO (e). $T_{\text{R-T}}$ indicates the rhombohedral–tetragonal phase transition temperature.

Table III. Ferroelectric Property Parameters of the PMNT/ x ZnO Ceramics

ZnO content, x (mol%)	P_r ($\mu\text{C}/\text{cm}^2$)	E_C (kV/cm)	R_{sq}
0	25.9 ± 0.3	7.0 ± 0.3	0.97 ± 0.01
0.4	31.0 ± 0.1	6.6 ± 0.1	1.20 ± 0.01
2.0	29.6 ± 0.1	6.6 ± 0.1	1.38 ± 0.01
4.0	28.6 ± 0.2	6.7 ± 0.2	1.38 ± 0.01
11.0	22.1 ± 0.1	7.0 ± 0.1	0.96 ± 0.01

P_r and P_{max} are the polarization at zero field and a maximum field, respectively. E_C and E_{max} are the electric field at the polarization equals to zero and a maximum applied field, respectively. R_{sq} is the hysteresis loop squareness.

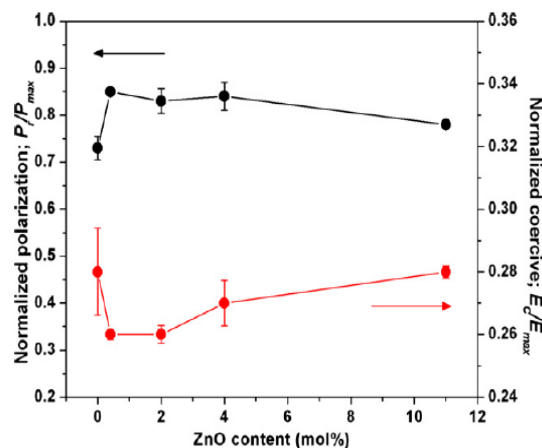


Fig. 5. Plots of the normalized polarization (P_r/P_{max}) and coercive field (E_C/E_{max}) as a function of ZnO content of the PMNT/ x ZnO ceramics.

$1.1E_C$. For an ideal square loop, R_{sq} is equal to 2.00. Moreover, the squareness can be used to measure not only the deviation in the polarization axis but also that in the electric field axis.⁴⁶ The R_{sq} values of the ceramics are listed in Table III. It can be seen from the results that ferroelectric properties of the PMNT ceramics were enhanced, i.e., the increases in P_r , P_r/P_{max} , and R_{sq} , and the decreases in E_C , E_C/E_{max} , and R_{sq} , with 0.4–4.0 mol% ZnO modifications. However, they slightly decreased when ZnO content increased to 11.0 mol%. The improvement of the ferroelectric properties of the ceramics was attributed to the effects of the increase in size of the ceramics' grains. As grain boundaries, which are nonpolar regions, are decreased with increasing grain size, the reorientations of polarizations are enhanced, leading to a better loop squareness. This also results in the increase in the P_r of the ceramics.³⁹ However, the slight decrease in P_r and increase in the E_C observed in the PMNT/11.0 mol% ZnO sample are believed to be caused by the increase in the ceramic's porosity. Moreover, it is believed that charge defects, that is, cation and oxygen vacancies, can exhibit as space charges which inhibit the polarization switching under a high applied field amplitude, resulting in a decrease in P_r and an increase in E_C of the ceramics.⁴⁷

IV. Conclusions

ZnO-modified $\text{Pb}(\text{Mg}_{1/3}\text{Nb}_{2/3})_{0.65}\text{Ti}_{0.35}\text{O}_3$ (PMNT) ceramics of complex perovskite structure with relative densities 93%–95% were successfully prepared by solid-state reaction and sintering method. The XRD patterns measured at room temperature showed the coexistence of the rhombohedral and tetragonal ferroelectric phases, which is a characteristic of PMNT solid solution system at the MPB composition. A dis-

tortion of the perovskite unit cell and an increase in lattice parameters, and tetragonality of the PMNT ceramics were observed by ZnO modifications. The average grain sizes of the ceramics tended to increase with increasing ZnO content. The dielectric constant measured at T_{max} of the pure PMNT ceramic was enhanced with 0.4–4.0 mol% ZnO modification. T_{R-T} and T_{max} of the ceramics tended to increase while the degree of diffuseness decreased with increasing ZnO content. The enhancement of ferroelectric properties, i.e., the increases in P_r and R_{sq} , and the decrease in E_C , was observed when 0.4–4.0 mol% ZnO was incorporated. From all the results, it can be seen that the optimum ZnO content is 2.0 mol%, which makes the ceramics with good dielectric and ferroelectric properties. The PMNT ceramic modified with 2.0 mol% ZnO is a promising material for applications as multilayer capacitors, electromechanical transducers, and nonvolatile ferroelectric random access memories.

Acknowledgments

This work was supported by the Thailand Research Fund (TRF) and the National Research University Project under Thailand's Office of the Higher Education Commission (OHEC), the Faculty of Science and the Graduate School, Chiang Mai University. The work at Simon Fraser University was supported by the U.S. Office of Naval Research (Grant #N00014-12-1-1045) and the Natural Science and Engineering Research Council of Canada (NSERC).

References

- L. E. Cross, "Ferroelectric Materials for Electromechanical Transducer Applications," *Mater. Chem. Phys.*, **43** [10] 8–115 (1996).
- M. Alguero, A. Moure, L. Pardo, J. Hole, and M. Kosec, "Processing by Mechanochemical Synthesis and Properties of Piezoelectric $\text{Pb}(\text{Mg}_{1/3}\text{Nb}_{2/3})\text{O}_3$ - PbTiO_3 with Different Compositions," *Acta Mater.*, **54**, 501–11 (2006).
- P. Moetakef and Z. A. Nemat, "Synthesis of Pyrochlore Free PMN-PZT Ceramics via a Seeding Method," *Sens. Actuators, A*, **141**, 463–70 (2008).
- O. Noblanc, P. Gaucher, and G. Calvarin, "Structural and Dielectric Studies of $\text{Pb}(\text{Mg}_{1/3}\text{Nb}_{2/3})\text{O}_3$ - PbTiO_3 Ferroelectric Solid Solutions Around the Morphotropic Boundary," *J. Appl. Phys.*, **79**, 4291, 7pp (1996).
- B. Noheda, D. E. Cox, G. Shirane, J. Gao, and Z.-G. Ye, "Phase Diagram of the Ferroelectric Relaxor $(1-x)\text{PbMg}_{1/3}\text{Nb}_{2/3}1-x\text{PbTiO}_3$," *Phys. Rev. B*, **66**, 054104, 7pp (2002).
- X. B. Hu, J. Y. Wang, L. L. Ma, X. G. Xu, H. S. Luo, P. P. Zhu, and Y. L. Tian, "Domain Structures and Phase Transitions of PMNT Single Crystals," *J. Cryst. Growth*, **275**, e1703–6 (2005).
- J. Y. Ha, J. W. Choi, C. Y. Kang, D. J. Choi, H. J. Kim, and S. J. Yoon, "Effects of ZnO on Piezoelectric Properties of 0.01PMW-0.41PNN-0.35PT-0.23PZ Ceramics," *Mater. Chem. Phys.*, **90**, 396–400 (2005).
- C. W. Ahn, H. C. Song, and S. Nahm, "Effect of ZnO and CuO on the Sintering Temperature and Piezoelectric Properties of a Hard Piezoelectric Ceramic," *J. Am. Ceram. Soc.*, **89**, 921–5 (2006).
- M. S. Yoon, Y. M. Kim, S. Y. Kwon, T. W. Hong, Y. G. Lee, S. L. Ryu, H. J. Kim, and S. C. Ur, "Effects of ZnO on the Piezoelectric Properties of $\text{Pb}(\text{Mn}_{1/3}\text{Sb}_{2/3})\text{O}_3$ - $\text{Pb}(\text{Zr,Ti})\text{O}_3$ Ceramics," *J. Electroceram.*, **18**, 73–5 (2007).
- M. F. Rubio, J. J. Romero, M. G. Navarro-Rojero, and J. F. Fernandez, "Effect of ZnO on the Structure, Microstructure and Electrical Properties of KNN-Modified Piezoceramics," *J. Eur. Ceram. Soc.*, **29**, 3045–52 (2009).
- H. Li, Z. Yang, L. Wei, and Y. Chang, "Effect of ZnO Addition on the Sintering and Electrical Properties of (Mn,W)-Doped PZT-PMS-PZN Ceramics," *Mater. Res. Bull.*, **44**, 638–43 (2009).
- H. T. Li, B. P. Zhang, M. Cui, W. G. Yang, N. Ma, and J. F. Li, "Microstructure, Crystalline Phase, and Electrical Properties of ZnO-Added $\text{Li}_{0.04}(\text{Nb}_{0.535}\text{K}_{0.48})_{0.94}\text{NbO}_3$ Ceramics," *Curr. Appl. Phys.*, **11**, S184–8 (2011).
- M. Promsawat, A. Watcharaporn, H. N. Tailor, S. Jiansirisomboon, and Z.-G. Ye, "Enhanced Dielectric, Ferroelectric, and Electrostrictive Properties of $\text{Pb}(\text{Mg}_{1/3}\text{Nb}_{2/3})_{0.9}\text{Ti}_{0.1}\text{O}_3$ Ceramics by ZnO Modification," *J. Appl. Phys.*, **113**, 204101–6 (2013).
- X. Zeng, A. Ding, X. S. Zheng, and T. Liu, "Effects of Excess ZnO Addition on La-Doped PZN-PZT Ceramics Prepared by Hot Pressing," *Ceram. Int.*, **33**, 883–5 (2007).
- C. C. Tsai, S. Y. Chu, C. S. Hong, and S. F. Chen, "Effects of ZnO on the Dielectric, Conductive and Piezoelectric Properties of Low-Temperature-Sintered PMN-PZT Based Hard Piezoelectric Ceramics," *J. Eur. Ceram. Soc.*, **31**, 2013–22 (2011).
- C. C. Lee, T. K. Lee, and J. H. Jan, "Piezoelectric Properties and Microstructures of Zn-Doped $\text{Bi}_{0.5}\text{Na}_{0.5}\text{TiO}_3$ Ceramics," *J. Eur. Ceram. Soc.*, **31**, 3145–52 (2011).
- K. Kumari, A. Prasad, and K. Prasad, "Structural and Dielectric Properties of ZnO Added $(\text{Na}_{1/2}\text{Bi}_{1/2})\text{TiO}_3$ Ceramics," *J. Mater. Sci. Technol.*, **27**, 213–7 (2011).
- I. Y. Kang, I. T. Seo, Y. J. Cha, J. H. Choi, S. Nahm, T. H. Sung, and J. H. Paik, "Low Temperature Sintering of ZnO and MnO_2 -Added $(\text{Na}_{0.5}\text{K}_{0.5})\text{NbO}_3$ Ceramics," *J. Eur. Ceram. Soc.*, **32**, 2381–7 (2012).

- ¹⁹H. M. Jang, K.-M. Lee, and M.-H. Lee, "Stabilization of Perovskite Phase and Dielectric Properties of $\text{Pb}(\text{Zn,Mg})_{1/3}\text{Nb}_{2/3}\text{O}_3\text{-PbTiO}_3$ Ceramics Prepared by Excess Constituent Oxides," *J. Mater. Res.*, **9**, 2634–44 (1994).
- ²⁰P. Escure, E. Lattard, M. Lejeune, and J. F. Baumard, "Stability of the Perovskite Phase in PMN-PZN-PT Ceramics," *J. Mater. Sci.*, **31**, 3937–43 (1996).
- ²¹K. Singh and S. Band, "A Comparative Study on the Processing, Dielectric and Electrical Properties of PMN Based Solid Solutions," *Bull. Mater. Sci.*, **20**, 265–77 (1997).
- ²²Y. H. Chen, K. Uchino, and D. Viehland, "Substituent Effects in 0.65Pb($\text{Mg}_{1/3}\text{Nb}_{2/3}$) O_3 -0.35PbTiO₃ Piezoelectric Ceramics," *J. Electroceram.*, **6**, 13–9 (2001).
- ²³K. R. Han, J. W. Jeong, C. S. Kim, and Y. S. Kwon, "Low-Temperature Fabrication of 0.65PMN-0.35PT by a Mixed Oxide Method," *Mater. Lett.*, **60**, 3596–600 (2006).
- ²⁴J. Liao, X. P. Jiang, G. S. Xu, H. S. Luo, and Q. R. Yin, "Investigation on the Effect of the Annealing Process on the Domain Structure of 0.65Pb($\text{Mg}_{1/3}\text{Nb}_{2/3}$) O_3 -0.35PbTiO₃ Single Crystal Using Scanning Electron Acoustic Microscopy," *Mater. Charact.*, **44**, 453–7 (2000).
- ²⁵S. Sen, S. K. Mishra, S. S. Palit, S. K. Das, and A. Tarafdar, "Impedance Analysis of 0.65Pb($\text{Mg}_{1/3}\text{Nb}_{2/3}$) O_3 -0.35PbTiO₃ Ceramic," *J. Alloys. Compd.*, **453**, 395–400 (2008).
- ²⁶Z. Xia, L. Wang, W. Yan, Q. Li, and Y. Zhang, "Comparative Investigation of Structure and Dielectric Properties of Pb($\text{Mg}_{1/3}\text{Nb}_{2/3}$) O_3 -PbTiO₃ (65/35) and 10% PbZrO₃-Doped Pb($\text{Mg}_{1/3}\text{Nb}_{2/3}$) O_3 -PbTiO₃ (65/35) Ceramics Prepared by a Modified Precursor Method," *Mater. Res. Bull.*, **42**, 1715–22 (2007).
- ²⁷S. L. Swartz and T. R. Shrout, "Fabrication of Perovskite Lead Magnesium Niobate," *Mater. Res. Bull.*, **17**, 1245–50 (1982).
- ²⁸E. B. Araujo, R. N. Reis, C. A. Guarany, C. T. Meneses, J. M. Sasaki, A. G. Souza Fiho, and J. Mendes Fiho, "Synthesis of Slightly (111)-Oriented 0.65(Pb $\text{Mg}_{0.333}\text{Nb}_{0.667}$) O_3 -0.35(PbTiO₃) Ceramic Prepared From Fine Powders," *Mater. Chem. Phys.*, **104**, 40–3 (2007).
- ²⁹R. D. Shannon, "Revised Effective Ionic-Radii and Systematic Studies of Interatomic Distances in Halides and Chalcogenides," *Acta. Crystallogr.*, **32**, 751–67 (1976).
- ³⁰K. Harada, S. Shimanuki, T. Kobayashi, Y. Yamashita, and S. Saitoh, "Growth of High-Quality Pb($\text{Zn}_{1/3}\text{Nb}_{2/3}$) $\text{O}_{0.91}\text{Ti}_{0.09}$) O_3 Single Crystals by Excess ZnO Addition," *J. Am. Ceram. Soc.*, **85**, 145–9 (2002).
- ³¹C. C. Tsai, C. S. Hong, C. C. Shih, and S. Y. Chu, "Electrical Properties and Temperature Behavior of ZnO-Doped PZT-PMN Modified Piezoelectric Ceramics and Their Applications on Therapeutic Transducers," *J. Alloys Compd.*, **511**, 54–62 (2012).
- ³²X. Chao, Z. Yang, X. Huang, D. Ma, and J. Zeng, "Electrical Characteristics and Low-Temperature Sintering of BiFeO₃-Modified Pb(Zr,Ti)O₃-Pb($\text{Fe}_{2/3}\text{W}_{1/3}$) O_3 -Pb($\text{Mn}_{1/3}\text{Nb}_{2/3}$) O_3 Ceramics with ZnO Addition," *Curr. Appl. Phys.*, **9**, 1283–7 (2009).
- ³³M. Bonyani, A. Mirzaee, A. Barzegar, and M. R. Saeri, "Effect of Nano ZnO Addition on Microstructure and Dielectric Properties of Pb($\text{Zn}_{1/3}\text{Nb}_{2/3}$) O_3 -PbTiO₃-BaTiO₃ (PZN-PT-BT) Relaxor Ferroelectric," *Micro Nano Lett.*, **7**, 762–5 (2012).
- ³⁴B. Fang, C. Ding, J. Wu, Q. Du, and J. Ding, "Effects of Dopants on the Synthesis of Pb($\text{Mg}_{1/3}\text{Nb}_{2/3}$) O_3 -PbTiO₃ Ceramics by the Reaction-Sintering Method," *Phys. Status Solidi A*, **208**, 1641–5 (2011).
- ³⁵S. Fushimi and T. Ikeda, "Phase Equilibrium in the System PbO-TiO₂-ZrO₂," *J. Am. Ceram. Soc.*, **50**, 129–32 (1967).
- ³⁶N. Zhong, X. L. Dong, D. Sun, P. H. Xiang, and H. Du, "Electrical Properties of Pb($\text{Mg}_{1/3}\text{Nb}_{2/3}$) O_3 -PbTiO₃ Ceramics Modified with WO₃," *Mater. Res. Bull.*, **39**, 175–84 (2004).
- ³⁷N. Zhong, P. H. Xiang, D. Z. Sun, and X. L. Dong, "Effect of Rare Earth Additives on the Microstructure and Dielectric Properties of 0.67Pb($\text{Mg}_{1/3}\text{Nb}_{2/3}$) O_3 -0.33PbTiO₃ Ceramics," *Mater. Sci. Eng., B*, **116**, 140–5 (2005).
- ³⁸X. G. Tang and H. L. W. Chan, "Effect of Grain Size on the Electrical Properties of (Ba,Ca)(Zr,Ti)O₃ Relaxor Ferroelectric Ceramics," *J. Appl. Phys.*, **97**, 034109, 6pp (2005).
- ³⁹G. H. Haertling, "Ferroelectric Ceramics: History and Technology," *J. Am. Ceram. Soc.*, **82**, 797–818 (1999).
- ⁴⁰M. Otonicar, S. D. Skapin, M. Spreitzer, and D. Suvorov, "Compositional Range and Electrical Properties of the Morphotropic Phase Boundary in the Na_{0.5}Bi_{0.5}TiO₃-K_{0.5}Bi_{0.5}TiO₃ System," *J. Eur. Ceram. Soc.*, **30**, 971–9 (2010).
- ⁴¹K. Uchino and S. Nomura, "Critical Exponents of the Dielectric Constants in Diffused-Phase-Transition Crystals," *Ferroelectr. Lett.*, **44**, 55–61 (1982).
- ⁴²D. La-Orauttapong, B. Noheda, Z.-G. Ye, P. M. Gehring, J. Toulouse, D. E. Cox, and G. Shirane, "Phase Diagram of the Relaxor Ferroelectric (1-x)Pb($\text{Zn}_{1/3}\text{Nb}_{2/3}$) O_3 -xPbTiO₃," *Phys. Rev. B*, **65**, 144101, 7pp (2002).
- ⁴³A. A. Bokov and Z.-G. Ye, "Dielectric Relaxation in Relaxor Ferroelectrics," *J. Adv. Dielectrics*, **2**, 1241010, 24pp (2012).
- ⁴⁴A. I. Burkhanov, A. V. Shilnikov, A. V. Sopit, and A. G. Luchaninov, "Dielectric and Electromechanical Properties of (1-x)PMN-xPZT Ferroelectric Ceramics," *Phys. Solid State*, **42**, 936–43 (2000).
- ⁴⁵V. Koval, C. Alemany, J. Briancin, H. Brunckova, and K. Saksil, "Effect of PMN Modification on Structure and Electric Response of xPMN-(1-x)PZT Ceramic Systems," *J. Eur. Ceram. Soc.*, **23**, 1157–66 (2003).
- ⁴⁶G. H. Haertling and W. J. Zimmer, "Analysis of hot-Pressing Parameters for Lead Zirconate-Lead Titanate Ceramics Containing Two Atom Percent Bismuth," *Am. Ceram. Soc. Bull.*, **45**, 1084–9 (1966).
- ⁴⁷K. Okazaki and K. Nagata, "Effects of Grain Size and Porosity on Electrical and Optical Properties of PLZT Ceramics," *J. Am. Ceram. Soc.*, **56**, 82–6 (1973). □

Electrical properties of ternary system $\text{Bi}_{0.5}(\text{Na}_{0.80}\text{K}_{0.20})_{0.5}\text{TiO}_3$ - 0.005LiNbO_3 - BaTiO_3 lead-free piezoelectric ceramics

Pimpilai Wannasut^a, Pharatree Jaita^a, Anucha Watcharapasorn^{a,b},
and Sukanda Jiansirisomboon^c

^aDepartment of Physics and Materials Science, Faculty of Science, Chiang Mai University, Chiang Mai, Thailand; ^bMaterials Science Research Center, Faculty of Science, Chiang Mai University, Chiang Mai, Thailand; ^cSchool of Ceramic Engineering, Suranaree University of Technology, Nakhon Ratchasima, Thailand

ABSTRACT

Ternary system of lead-free piezoelectric ceramics with the formula of $(1-x-y)\text{Bi}_{0.5}(\text{Na}_{0.80}\text{K}_{0.20})_{0.5}\text{TiO}_3$ - $x\text{LiNbO}_3$ - $y\text{BaTiO}_3$ or $(1-x-y)\text{BNKT}$ - $x\text{LN}$ - $y\text{BT}$ ($x = 0.005$ and $y = 0, 0.01, 0.02, 0.03, 0.04, 0.05, 0.06$ and 0.07 mol fraction) were sintered at the temperature of 1125°C for 2 h. All samples have the density ranging of $5.59 - 5.73 \text{ g/cm}^3$. X-ray diffraction pattern exhibited a single perovskite structure without any secondary phase. Scanning electron micrographs indicated a cubic-like grain shape occurred for all compositions with side length of $0.49 - 0.77 \mu\text{m}$. At a composition BNKT - 0.005LN - 0.04BT showed the highest piezoelectric coefficient ($d_{33} = 198 \text{ pC/N}$) with good dielectric ($\epsilon_r = 1775$, $\tan\delta = 0.0534$) and ferroelectric properties ($P_r = 17.36 \mu\text{C/cm}^2$, $R_{sq} = 1.67$).

ARTICLE HISTORY

Received 28 November 2015
Accepted 28 March 2016


KEYWORDS

Ternary system; lead-free piezoelectrics; X-ray diffraction

Introduction

Piezoelectric ceramics have been widely used in various industries such as automobiles, electronics and medical industries. Dominate piezoelectric ceramic is lead zirconate titanate compound or PZT. However, lead (PbO) is considered to be toxic and causes an environmental problem [1]. Therefore, lead-free piezoelectric ceramics have attracted because of their outstanding advantages as environmental friendly materials [2]. $\text{Bi}_{0.5}(\text{Na}_{1-x}\text{K}_x)_{0.5}\text{TiO}_3$ or BNKT have been known as one of interesting lead-free piezoelectric ceramics. Sasaki et al. [3] have reported that a solid solution of BNKT show improved piezoelectric properties in morphotopic phase boundary (MPB) region at $0.16 \leq x \leq 0.20$ and the composition of $x = 0.20$ showed $P_r = 19.9 \mu\text{C/cm}^2$, $\epsilon_r = 1000$ and $d_{33} = 46.9 \text{ pC/N}$.

Among LiNbO_3 or LN had perovskite structure with ABO_3 formula and very important ferroelectric material for applications in optics and electronics, such as electro-optical, piezoelectric and nonlinear optical devices [4]. In 2007, Du et al. [5] have reported that a solid solution of $(1-x)\text{K}_{0.5}\text{Na}_{0.5}\text{NbO}_3$ - $x\text{LiNbO}_3$ showed an

CONTACT Sukanda Jiansirisomboon  sukanda.jian@cmu.ac.th

Color versions of one or more of the figures in the article can be found online at www.tandfonline.com/ginf.

© 2016 Taylor & Francis Group, LLC

improvement in electrical properties. Recently, Hao et al. [6] studied the binary system of $(1-x)\text{Bi}_{0.5}(\text{Na}_{0.8}\text{K}_{0.2})_{0.5}\text{TiO}_3-x\text{LiNbO}_3$. At composition of $x = 0.025$ showed the highest $d_{33} = 475$ pm/V.

BaTiO_3 is a prototypical ferroelectric material with a characteristic tetragonal distortion of the perovskite structure [7]. In 2014, Acharya et al. [8] study in ferroelectric and piezoelectric properties of lead-free $\text{Bi}_{0.5}\text{Na}_{0.5}\text{TiO}_3\text{-Bi}_{0.5}\text{K}_{0.5}\text{TiO}_3\text{-BaTiO}_3$ thin film. The composition of 0.884BNT-0.08BKT-0.036BT showed the best electrical properties with a dielectric constant (638), remnant polarization ($27 \mu\text{C}/\text{cm}^2$), and effective piezoelectric constant (79 pC/N).

The past of my research study in $(1-x)\text{Bi}_{0.5}(\text{Na}_{0.80}\text{K}_{0.20})_{0.5}\text{TiO}_3-x\text{LiNbO}_3$ system was found to be optimized dielectric, ferroelectric and piezoelectric properties at the composition of $x = 0.005$. This research aims to study the microstructure and electrical properties of the ternary system $(1-x-y)\text{Bi}_{0.5}(\text{Na}_{0.8}\text{K}_{0.20})\text{TiO}_3-x\text{LiNbO}_3-y\text{BaTiO}_3$ or $(1-x-y)\text{BNKT-xLN-yBT}$ ceramics (when $x = 0.005$ and $y = 0, 0.01, 0.02, 0.03, 0.04, 0.05, 0.06$ and 0.07 mol fraction)

Experimental

Conventional mixed-oxide and sintering method was used to prepare of $(1-x-y)\text{BNKT-xLN-yBT}$ ceramics (when $x = 0.005$ and $y = 0, 0.01, 0.02, 0.03, 0.04, 0.05, 0.06$ and 0.07 mol fraction). Starting materials are Bi_2O_3 , Na_2O_3 , TiO_2 , K_2CO_3 , Li_2CO_3 , Nb_2O_3 and BaCO_3 . All starting materials were stoichiometrically weighted with composition of $(1-x-y)\text{BNKT-xLN-yBT}$, ball milled for 24 h in an ethanol solution (99.99%) and dried in an oven. Then, dried powders was calcined at 900°C for 2 h. After that, a few drops of 3 wt% polyvinyl alcohol (PVA) binders to the mixed powders before being uniaxial pressed into 15 mm diameter discs. After that the green body were sintered at 1025 to 1125°C for 2 h with a heating and cooling rate of $5^\circ\text{C} / \text{min}$.

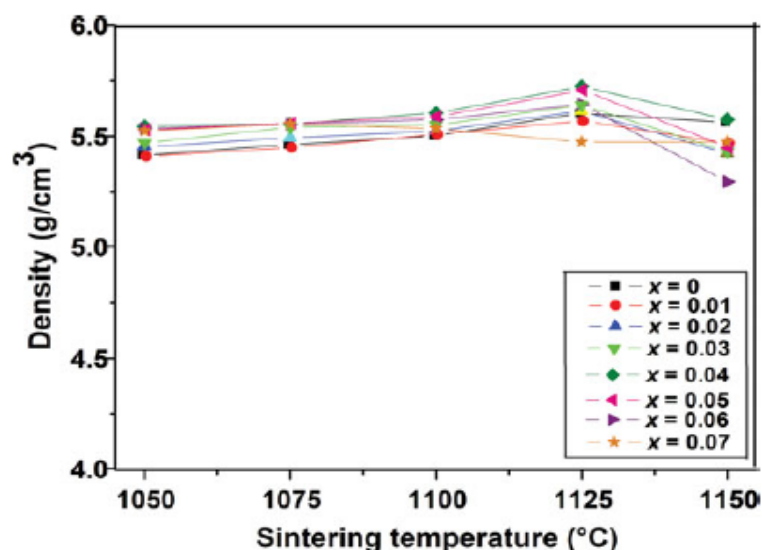
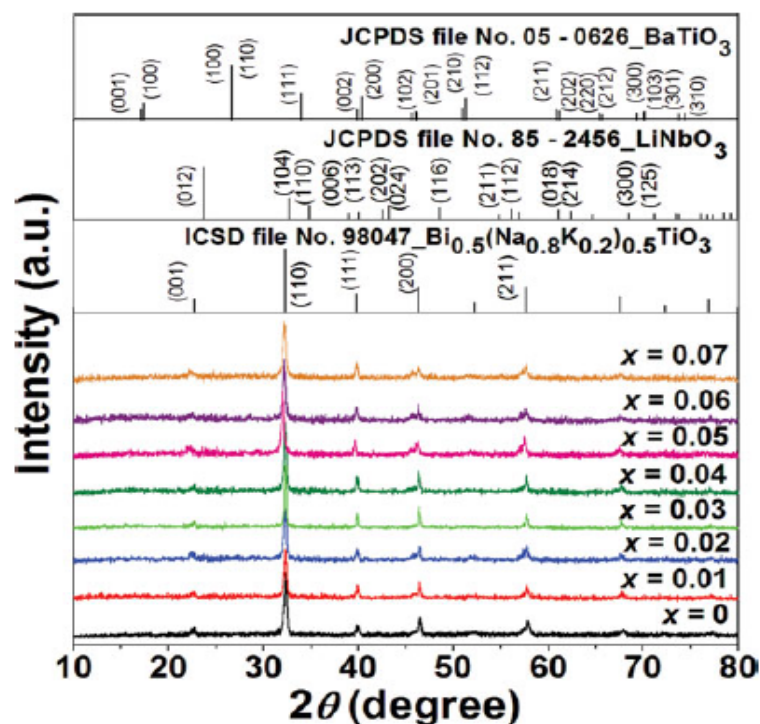


Figure 1. Plots of density as a function of sintering temperature of BNKT-LN-BT ceramics.

Table 1. Physical and electrical properties of the BNKT-LN-BT sintered ceramics.

x	Density (g/cm ³)	Linear shrinkage (%)	Average grain size (μ m)	ϵ_r	$\tan\delta$	P_r (μ C/cm ²)	E_c (kV/cm)	R_{sq}	d_{33} (pC/N)
0	5.59 \pm 0.03	20.76 \pm 0.03	1.05 \pm 0.04	1360	0.0564	24.87	11.90	1.42	142
0.01	5.58 \pm 0.06	21.75 \pm 0.02	0.83 \pm 0.04	1420	0.0555	20.04	6.19	1.22	153
0.02	5.63 \pm 0.03	21.80 \pm 0.04	0.59 \pm 0.02	1456	0.0683	26.60	8.38	1.55	169
0.03	5.64 \pm 0.04	21.92 \pm 0.05	0.53 \pm 0.04	1579	0.0454	20.43	6.45	1.21	172
0.04	5.73 \pm 0.02	21.95 \pm 0.03	0.49 \pm 0.07	1775	0.0534	37.47	11.47	1.78	198
0.05	5.72 \pm 0.03	21.40 \pm 0.06	0.54 \pm 0.02	1663	0.0544	29.93	11.52	1.67	162
0.06	5.65 \pm 0.07	21.02 \pm 0.05	0.65 \pm 0.04	1564	0.0777	32.74	11.15	1.46	159
0.07	5.48 \pm 0.01	20.81 \pm 0.04	0.70 \pm 0.08	1355	0.0654	16.53	10.52	1.65	138

X-ray diffractometer (XRD-Rigaku, MiniFlex II) was used to determine the phase of both powders and ceramics. Bulk density was measured by Archimedes' method. Linear shrinkage of all samples was also measured. Scanning electron microscope (SEM, JEOL JSM-6335F) was used to identify microstructural features of the ceramics. Grain size was determined by a mean linear interception method. This method was the quantitative measurement of grain size within densely uniform structures and it was best suited where the boundaries of each grain were relatively easy to determine. For electrical characterization, all samples were polished to 1 mm thickness to obtained parallel scratch-free surface. Silver paste was painted onto both surface for form electrodes. The 4263B LCR-meter was used to measured dielectric properties. The Sawyer-Tow Circuit was used to determined ferroelectric properties. For piezoelectric properties, all samples were pole in silicone oil bath at 55°C under DC electric field of 4 kV/mm for 15 min. Piezoelectric coefficient (d_{33}) was recorded from 1 day aged samples using d_{33} meter (KCF technologies, S5865).

**Figure 2.** X-ray diffraction patterns of BNKT-LN-BT sintered ceramics at $2\theta = 10 - 80$.

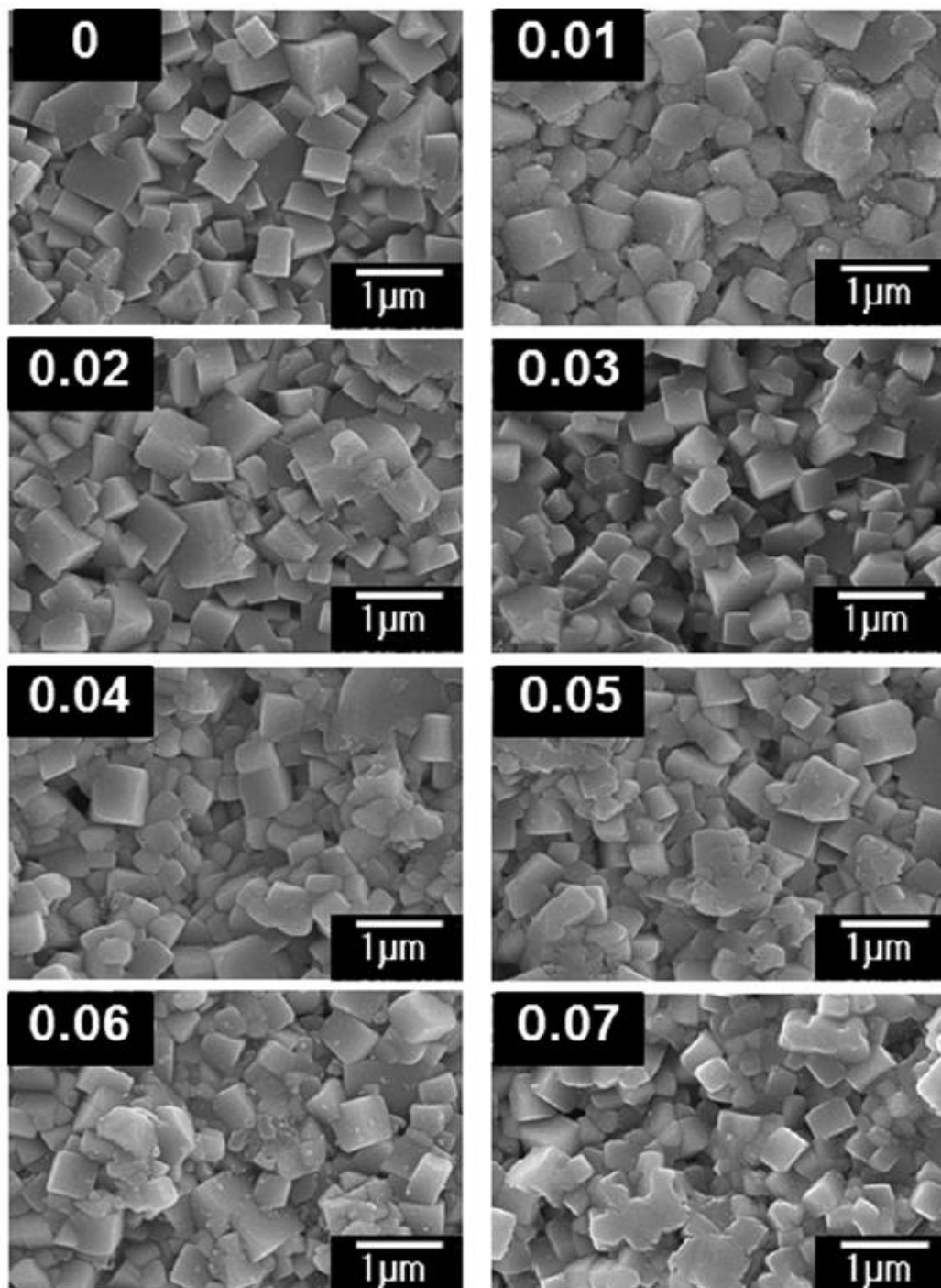


Figure 3. SEM micrographs of as-sintered surface of BNKT-LN-BT sintered ceramics.

Results and discussion

The density values of $(1-x-y)\text{BNKT}-x\text{LN}-y\text{BT}$ were obtained between 5.58–5.73 g/cm³. The optimum sintering temperature was found to be 1125°C for all BNKT-LN-BT ceramics. The densities were then dropped at higher sintering temperature of greater than 1125°C as showed in Figure 1. The linear shrinkage increasing with increased sintering temperature and showed similar trend of density. The

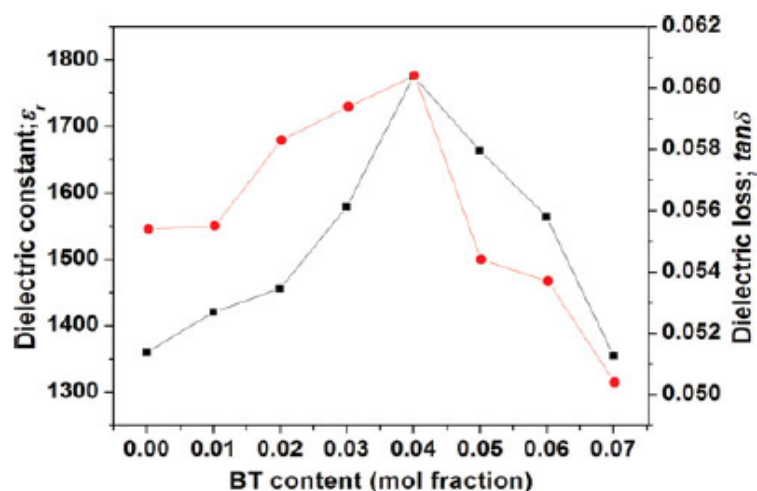


Figure 4. Plots of room temperature dielectric constant (ϵ_r) and dielectric loss ($\tan\delta$) values as a function of BT content measured at a frequency of 1 kHz.

highest linear shrinkage of 20 - 22% was observed for BNKT-LN-BT ceramics sintered at 1125°C (see Table 1). So, the samples sintered at 1125°C were selected for further characterization. Figure 2 shown X-ray diffraction patterns of BNKT-LN-BT ceramics with $2\theta = 10 - 80^\circ$. All compositions indicated a pure perovskite structure and no detectable secondary phase. This confirmed that the starting reagents completely reacted to form the final compounds. This suggested that LN and BT had diffused into BNKT lattice to form complete solid solutions during the sintering process. BNKT ceramics showed features of mixed rhombohedral-tetragonal symmetry. However, rhombohedral showed over tetragonal structure. This result similar to reported by Sasaki et al. [3]. We believed Li^+ ions (1.06 Å) and Ba^{2+} (1.42 Å) was diffuse to A-site Bi^{3+} (1.17 Å), Na^+ (1.18 Å) and K^+ (1.33 Å) positions [9] while Nb^{5+} ions (0.64 Å) diffused into B-site of Ti^{4+} positions (0.61 Å) [10]. SEM image of as-sintered surface of BNKT-LN-BT ceramics are shown in Figure 3. This confirmed that all ceramics were of high density sintered at 1125°C. The average grain size values of all samples are listed in Table 1. The cubic-like grain shape represent in all BNKT-LN-BT samples. So, the addition of BT in to BNKT-LN did not evidently change in grain shape. However, the addition of BT into BNKT-0.005LN slightly inhibited grain growth. We believe that a reduction of grain size BNKT-LN were due to a solute drag effect of the dissolved BT [9].

Plots of room temperature dielectric constant (ϵ_r) and dielectric loss ($\tan\delta$) values as a function of BT content measured at a frequency of 1 kHz are shown in Figure 4 and the values are also summarized in Table 1. This measured ϵ_r at low frequency (1 kHz) may be due to the active represent of all type of polarization *i.e.* ionic, orientation, electronic and space charge polarization [11]. The ϵ_r of BNKT-0.005LN ceramic had ϵ_r of 1360 with $\tan\delta$ values of 0.0564. The ϵ_r starting increased with increasing BT content. The BNKT-LN-0.04BT sample indicated a maximum room temperature dielectric constant of 1775. This result was attributed to a reduction of grain size in this composition which played an important role in raising dielectric constant value. While grain size decreased, domains became smaller and had large

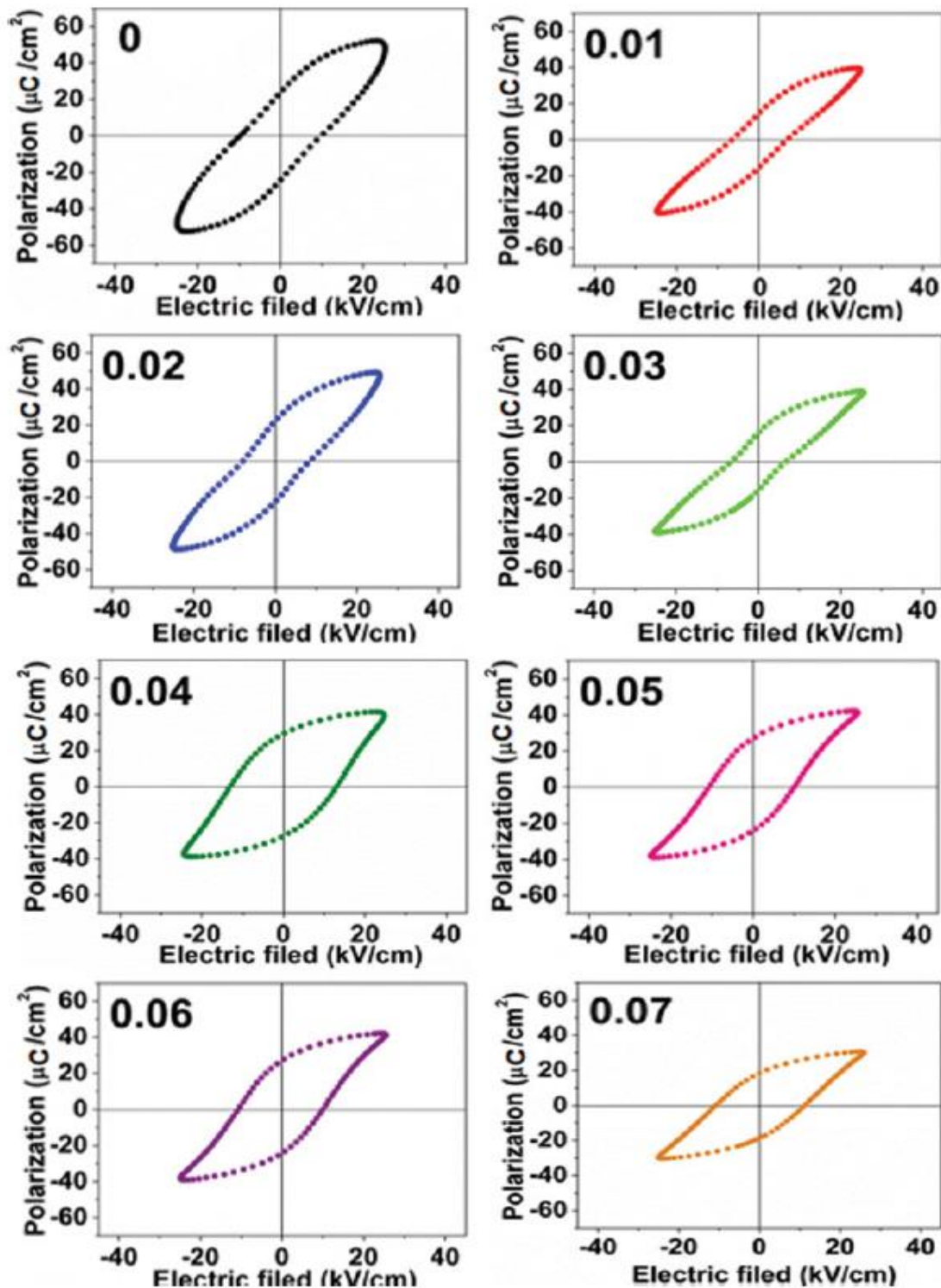


Figure 5. Polarization-electric field (P - E) hysteresis loop of the BNKT-LN-BT sintered ceramics.

unrelieved stress that increased internal stress in the domain accompanied by an increase in permittivity [12]. At a composition of BNKT-0.005LN-0.05BT illustrate initially ϵ_r value decreased. This result was also relation with slowly increasing of grain size as shown in Figure 3. The large grains caused internal stresses within the grain could be reduced by formation of appropriate arrangement of 90° domains

mechanism [9]. Polarization-electric field (P - E) hysteresis loop of BNKT-LN-BT are showed in Figure 5. The P - E hysteresis loop of BNKT-LN showed typical ferroelectric shape at room temperature. It can be seen the P_r value trend increasing with BT content and showed the maximum of $P_r = 37.47 \mu\text{C}/\text{cm}^2$ at BNKT-LN-0.04BT sample. Whereat, P_r started decreased at $y \geq 0.05$. However, E_c has trend decreased with increasing BT content. The decreased of P_r and E_c values caused in a slight pinched-type loop with relation small remanent polarization. The effect like to that observed in many BNT-based ceramics i.e. $(\text{Bi}_{0.5}\text{Na}_{0.5})\text{TiO}_3$ - SrTiO_3 [13], and $(\text{Bi}_{0.5}\text{Na}_{0.5})\text{TiO}_3$ - KNbO_3 [14] ceramics. The piezoelectric constant (d_{33}) of the BNKT-LN-BT ceramics are listed in table 1. Pure BNKT ceramic had d_{33} of 142 pC/N. The highest $d_{33} = 198 \text{ pC}/\text{N}$ value was obtained at the BNKT-LN-0.04BT. The addition of BT showed improvement of d_{33} properties. It can be seen the addition of BT showed increasing of d_{33} value compared with BNKT-LN sample.

Conclusions

Ternary Lead-Free of $(1-x-y)\text{Bi}_{0.5}(\text{Na}_{0.80}\text{K}_{0.20})_{0.5}\text{TiO}_3-x\text{LiNbO}_3-y\text{BaTiO}_3$ ceramics (when $x = 0.005$ and $y = 0.01, 0.02, 0.03, 0.04, 0.05, 0.06$ and 0.07 mol fraction) were successfully synthesis by conventional mixed oxide and sintering method. X-ray diffraction patterns presence a single perovskite structure and cannot detect impurity phase. The addition of BT in BNKT-LN can be improving dielectric, ferroelectric and piezoelectric properties of ceramics. The maximum ϵ_r of 1775, $P_r = 37.47 \mu\text{C}/\text{cm}^2$, $E_c = 11.47 \text{ kV}/\text{cm}$, $R_{sq} = 1.78$ and $d_{33} = 198 \text{ pC}/\text{N}$ were obtained for BNKT-0.005LN-0.04BT sample.

Funding

This research is financially supported by the Thailand Research Fund (TRF) and School of Ceramic Engineering, Suranaree University of Technology, Nakhon Ratchasima.

References

1. D. Bao, N. Wakiya, K. Shinozaki, and N. Mizutani, Ferroelectric properties of sandwich structured $(\text{Bi}, \text{La})_4\text{Ti}_3\text{O}_{12}/\text{Pb}(\text{Zr}, \text{Ti})\text{O}_3/(\text{Bi}, \text{La})_4\text{Ti}_3\text{O}_{12}$ thin films on $\text{Pt}/\text{Ti}/\text{SiO}_2/\text{Si}$ substrates. *J. Appl. Phys.* **35**, L1-L5 (2002).
2. T. Takenaka, K. Maruyama, and K. Sakata, $(\text{Bi}_{1/2}\text{Na}_{1/2})\text{TiO}_3$ - BaTiO_3 system for lead-free piezoelectric ceramics. *Jpn. J. Appl. Phys.* **30**, 2236-2239 (1991).
3. A. Sasaki, T. Chiba, Y. Mamiya, and E. Otsuki, Dielectric and piezoelectric properties of $(\text{Bi}_{0.5}\text{Na}_{0.5})\text{TiO}_3$ - $(\text{Bi}_{0.5}\text{K}_{0.5})\text{TiO}_3$ systems. *Jpn. J. Appl. Phys.* **38**, 5564-5567 (1999).
4. N.S. Prasad, K.B.R. Varma, Y. Takahashi, Y. Benino, T. Fujiwara, and T. Komatsu, Evolution of ferroelectric LiNbO_3 phase in a reactive glass matrix (LiBO_2 - Nb_2O_5). *J. Solid State Chem.* **173**, 1455-1465 (2003).
5. H. Du, F. Tang, D. Liu, D. Zhu, and S. Qu, The microstructure and ferroelectric properties of $(\text{K}_{0.5}\text{Na}_{0.5})\text{NbO}_3$ - LiNbO_3 lead-free piezoelectric ceramic. *Mater. Sci. Eng.* **136**, 165-169 (2007).

6. J. Hao, W. Bai, W. Li, B. Shen, and J. Zhai, Phase transition, relaxor behavior and large strain response in LiNbO_3 modified $\text{Bi}_{0.5}(\text{Na}_{0.80}\text{K}_{0.20})_{0.5}\text{TiO}_3$ lead free piezoceramics. *J. Appl. Phys.* **114**, 044103 (2013).
7. R. Wahl, D. Vogtenhuer, and G. Kresse, SrTiO_3 and BaTiO_3 revisited using the projector augmented wavemethod Performance of hybrid and semilocal functionals. *Phys. Rev.* **78**, 104–116 (2008).
8. SK Acharya, TM Kim, J.H. Hyung, B.G. Ahn, and S.K. Lee, Ferroelectric and piezoelectric properties of lead-free $\text{Bi}_{0.5}\text{Na}_{0.5}\text{TiO}_3$ - $\text{Bi}_{0.5}\text{K}_{0.5}\text{TiO}_3$ - BaTiO_3 -thin films near the morphotropic phase boundary. *J. Alloys Compd.* **586**, 549–554 (2014).
9. R.D. Shannon, Revised effective ionic radii and systematic studies of interatomic distances in halides and chalcogenides. *Acta Cryst.* **32**, 751–767 (1976).
10. Y.R. Zhang, J.F. Li, and B.P. Zhang, Enhancing electrical properties in NBT-KBT lead-free piezoelectric ceramics by optimizing sintering Temperature. *J. Am. Ceram. Soc.* **91**, 2716–2719 (2008).
11. A. Hussain, A. Zaman, Y. Iqbal, and M.H. Kim, Dielectric, Ferroelectric and field induced strain properties of Nb-modified Pb-free $0.99\text{Bi}_{0.5}(\text{Na}_{0.82}\text{K}_{0.18})_{0.5}\text{TiO}_3$ - 0.01LiSbO_3 ceramics. *J. Alloys. Compd.* **574**, 320–324 (2013).
12. P. Jaita, and S. Jiansirisomboon, Dielectric, ferroelectric and electric field-induced strain behavior of $\text{Ba}(\text{Ti}_{0.90}\text{Sn}_{0.10})\text{O}_3$ modified $\text{Bi}_{0.5}(\text{Na}_{0.80}\text{K}_{0.20})_{0.5}\text{TiO}_3$ lead-free piezoelectrics. *J. Alloys Compd.* **596**, 98–106 (2014).
13. Y. Hiruma, Y.O. Imai, Y Watanabe, and T. Takenaka, Large electrostrain near the phase transition temperature of $(\text{Bi}_{0.5}\text{Na}_{0.5})\text{TiO}_3$ - SrTiO_3 ferroelectric ceramics. *Appl. Phys. Lett.* **92**, 262904 (2008).
14. G. Fan, W. Lu, and X. Wang, Phase transition behavior and electromechanical properties of $(\text{Na}_{1/2}\text{Bi}_{1/2})\text{TiO}_3$ - KNbO_3 lead-free piezoelectric ceramics. *J. Appl. Phys.* **41**, 035403–035406 (2008).



Dielectric properties, electric-field-induced polarization and strain behavior of Lead Zirconate Titanate-Strontium bismuth Niobate ceramics

Orapim Namsar¹ · Anucha Watcharapasorn^{1,2} · Mark Hoffman³ · Julia Glaum³ · Sukanda Jiansirisomboon⁴

Received: 12 June 2014 / Accepted: 21 March 2016 / Published online: 13 April 2016
© Springer Science+Business Media New York 2016

Abstract The dielectric properties and electric-field-induced polarization and strain behavior of $(1-x)\text{PZT}-x\text{SBN}$ (x ranged from 0 to 1.0 weight fraction) ceramics prepared by a conventional mixed-oxide method were investigated. The dielectric properties indicated that the dielectric constant of PZT could be enhanced with small addition of SBN ($x = 0.1$). From the polarization hysteresis loop measurements, it was found that the ferroelectric properties of nominal PZT-SBN ceramics changed strongly from the normal ferroelectric in PZT-rich ceramics to the paraelectric character in SBN-rich compositions. The strain hysteresis loops of nominal PZT-SBN under bipolar electric field loading suggested that the butterfly curve was observed in some compositions ($0 \leq x \leq 0.3$ and pure SBN ceramic). This research clearly showed the significance of SBN in controlling the electrical properties of nominal PZT-SBN ceramics.

Keywords Perovskite · Bismuth layered structures · Dielectric properties · Ferroelectricity · Strain

1 Introduction

Ferroelectric materials have attracted considerable attention because of their possible uses in electronic devices such as nonvolatile random access memories (NVRAM), capacitors and actuators [1]. Isotropic perovskite structure and bismuth layered structure compounds are the two most important materials employed in these applications. Perovskite-structure compounds such as $\text{Pb}(\text{Zr}_{0.52}\text{Ti}_{0.48})\text{O}_3$ (PZT) show excellent ferroelectric properties with large remanent polarization and small coercive field [2] but they exhibit a rather poor fatigue resistance [3]. The bismuth layered perovskite compounds i.e. $\text{SrBi}_2\text{Nb}_2\text{O}_9$ (SBN) and $\text{SrBi}_2\text{Ta}_2\text{O}_9$ (SBT) exhibit excellent fatigue characteristics as compared to those of PZT [4]. However, the major problems of these bismuth layered perovskite ferroelectrics include small remanent polarization and high processing temperature [5]. Therefore, many research groups have attempted to combine the superior ferroelectric properties of PZT and fatigue-free properties of SBT in a form of multilayer thin films [6, 7]. Many previous works reported that the binary film systems had better ferroelectric and dielectric properties over those of pure PZT thin films. However, fundamental research on a combination of PZT and bismuth layered compounds in a form of bulk ceramic is quite scarce. Therefore, this research aims to fabricate new ceramic systems based on PZT-SBN. A series of ceramics with formula $(1-x)\text{PZT}-x\text{SBN}$ (when $x = 0, 0.1, 0.3, 0.5, 0.7, 0.9$ and 1.0 weight fraction) were prepared. The ceramics were characterized particularly in terms of phase evolution and its relationship to strain behavior, dielectric and ferroelectric properties.

2 Experimental

The conventional solid state reaction method was employed to prepare the ceramics with formula $(1-x)\text{Pb}(\text{Zr}_{0.52}\text{Ti}_{0.48})\text{O}_3-$

✉ Sukanda Jiansirisomboon
sukanda.jian@cmu.ac.th

¹ Department of Physics and Materials Science, Faculty of Science, Chiang Mai University, Chiang Mai 50200, Thailand

² Materials Science Research Center, Faculty of Science, Chiang Mai University, Chiang Mai 50200, Thailand

³ School of Materials Science and Engineering, University of New South Wales, Sydney, NSW 2052, Australia

⁴ School of Ceramic Engineering, Suranaree University of Technology, Nakhon Ratchasima 30000, Thailand

$x\text{SrBi}_2\text{Nb}_2\text{O}_9$ or $(1-x)\text{PZT}-x\text{SBN}$ where $x = 0, 0.1, 0.3, 0.5, 0.7, 0.9$ and 1.0 weight fraction. PZT and SBN were synthesized separately. The raw materials of PbO (99 %, Riedel-de Haën), ZrO_2 (99 %, Riedel-de Haën), TiO_2 (99 %, Riedel-de Haën) were weighed according to $\text{Pb}(\text{Zr}_{0.52}\text{Ti}_{0.48})\text{O}_3$ composition. The mixture of raw materials was ball milled in alcohol for 24 h using zirconia balls. After that, the powder mixture was calcined at 800°C for 2 h to form the perovskite PZT. SBN was similarly prepared from mixed SrCO_3 (98 %, Aldrich), Bi_2O_3 (99.9 %, Aldrich) and Nb_2O_5 (99.9 %, Aldrich) powders which were reacted at a calcination temperature of 950°C for 3 h. Then, the PZT and SBN powders with different relative weight fraction were wet mixed for 24 h in a plastic jar with zirconia balls and ethanol. The dried powders were pressed into pellets with 10 mm in diameter. The green pellets were then placed in a sealed alumina crucible. These pellets were covered with powder having the same composition to avoid compositional deviation from PbO and Bi_2O_3 volatilization during sintering at 1050°C for 3 h with a heating/cooling rate of $5^\circ\text{C}/\text{min}$. The amount of excess powder was about 5 g per crucible.

Phase characterization of $(1-x)\text{PZT}-x\text{SBN}$ ceramics was carried out using X-ray diffractometry (XRD, Phillip Model X-pert). The polarization-electric field (P - E) and strain-electric field (S - E) loops were measured at a frequency of 50 Hz using an aixACCT TF2000HS analyzer equipped with a laser interferometer. Dielectric properties were measured at room temperature with a measurement frequency of 1 kHz using the LCR Hitester (Agilent, E4980A).

3 Results and discussion

X-ray diffraction patterns of $(1-x)\text{PZT}-x\text{SBN}$ ceramics after sintering at 1050°C for 3 h are shown in Fig. 1(a). The XRD pattern of the PZT sample was identified as a single-phase pattern with a perovskite structure having tetragonal symmetry while the SBN ceramic was found to be a bismuth layered structure with an orthorhombic symmetry. The addition of 0.1SBN into PZT caused a shift of the PZT peaks to higher angles while a newly formed phase started to appear. X-ray peak matching procedure indicated that this new phase was found to have a pattern very similar to the standard data of the $\text{Pb}_2(\text{Nb}_{1.33}\text{Ti}_{0.66})\text{O}_{6.66}$ (PNT) whose structure is cubic with space group $\text{Fd}\bar{3}m$ (JCPDS file no. 74-0660). Similar results have been observed by Yang et al. [8] in the $\text{PZT}-\text{Bi}_4\text{Ti}_3\text{O}_{12}$ system. They found that the new stable phase of composition $\text{PbBi}_4\text{Ti}_4\text{O}_{15}$ coexisted with the PZT matrix phase. This confirmed that a chemical reaction and dissolution between the perovskite PZT and bismuth layered SBN occurred during the sintering process. During the dissolution process, it was expected based on ionic size that Sr^{2+} ($r_{\text{Sr}^{2+}} = 1.18 \text{ \AA}$) or Bi^{3+} ($r_{\text{Bi}^{3+}} = 1.03 \text{ \AA}$) substituted for Pb^{2+} ($r_{\text{Pb}^{2+}} = 1.19 \text{ \AA}$), and

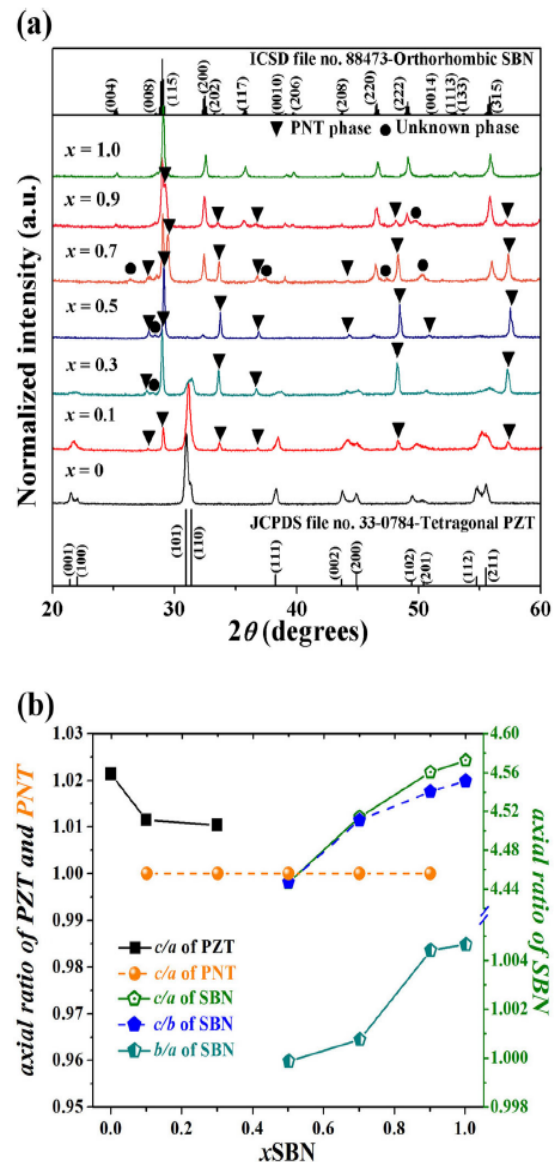


Fig. 1 (a) X-ray diffraction patterns of $(1-x)\text{PZT}-x\text{SBN}$ ceramics (b) Axial ratio of $(1-x)\text{PZT}-x\text{SBN}$ ceramics

Nb^{5+} ($r_{\text{Nb}^{5+}} = 0.64 \text{ \AA}$) ion substituted for Ti^{4+} ($r_{\text{Ti}^{4+}} = 0.605 \text{ \AA}$) or Zr^{4+} ($r_{\text{Zr}^{4+}} = 0.72 \text{ \AA}$) [9] in PZT. This ionic substitution resulted in a shift of all PZT diffraction peaks towards higher angles. For $x = 0.3$, the intensity of the PNT peaks increased rapidly while the intensity of the PZT peaks sharply decreased. For the composition $x = 0.5$, the pattern indicates that peaks of PNT became the major phase with the appearing SBN as a minor phase while the peaks of the PZT phase completely disappeared. An increase in SBN content from $x = 0.7$ and 0.9 led to a gradual reduction of PNT peak intensity and the shift of SBN peaks to lower angles with a continuous increase in intensity. This peak shift implied the expansion of the unit cell of the SBN phase. With careful

phase characterization, it was shown that some extra peaks of unknown phase were also present in the composition range of $0.3 \leq x \leq 0.9$, which were indicated by black circles in Fig. 1(a). Furthermore, as shown in Fig. 1(b), it was observed that the variation of axial ratio of PZT, PNT and SBN phases in nominal PZT-SBN ceramics showed a strong reduction in c/a after the incorporation of a small amount of SBN ($0.1 \leq x \leq 0.3$) compared to PZT without SBN addition. This implied that the ions from SBN dissolved into the PZT phase creating the shift in the XRD peaks mentioned previously. On the other hand, the addition of PZT into SBN (in the compositions with SBN-rich phase ($0.5 \leq x \leq 0.9$)) led to a continuous reduction of an axial ratio (c/a , c/b and b/a) of SBN, suggesting that ions from the PZT phase substituted in the SBN lattice. Based on the X-ray results, it should be noted that peak shift and the change of axial ratio was observed for the compositional range of $0.1 \leq x \leq 0.9$, implying that all phases present were solid solutions.

Figure 2 displays the variation of phase content of PZT, PNT and SBN in the nominal PZT-SBN ceramics as a function of SBN concentration. Five regions can be distinguished from the phase evolution behaviour in this ceramic system. Phase field I and V represented PZT-based (PZT(s.s.)) and SBN-based (SBN (s.s.)) solid solutions. Two composite regions (II and IV) were also present. Region II ($0.1 \leq x \leq 0.3$) indicated composite ceramics between PZT(s.s.) and PNT phases. It was found that the amount of PZT(s.s.) decreased while that of PNT increased with increasing SBN content up to $x = 0.3$. This suggested that the PZT rapidly dissolved into SBN to form PNT phase. For further addition of SBN up to $x = 0.5$ (region III in Fig. 2), PNT phase became the dominating phase. However, the phase content of PNT could not be determined due to the small number of compositions investigated in this study. In addition, a small amount of 17 wt% SBN was also contained in this region. However, it was noted that

there was no PZT phase in this region. This result demonstrated that a certain amount of PZT preferred to dissolve into SBN structure to form the PNT phase. Furthermore, it can also be said that the SBN phase was a more stable phase than that PZT phase in region III. The region IV ($0.5 \leq x \leq 0.9$) was composed of SBN(s.s.) and PNT phases. In this region, the concentration of SBN phase suddenly increased with increasing SBN addition, whereas the PNT content rapidly decreased. This phase field vs. SBN content plot roughly represented the room temperature stable phase diagram of the nominal PZT-SBN system. It should be noted that the existence of the PNT phase covered a very wide range of compositions ($0.1 \leq x \leq 0.9$), suggesting the stability of this phase as well as the limited solubility of PZT in SBN and vice versa.

SEM micrographs and grain size of the nominal PZT-SBN samples are shown in Fig. 3(a, b), respectively. The shapes and sizes of pure PZT and SBN grains were quite different. As can be seen from Fig. 3(a), the pure PZT ceramic ($x = 0$) had equiaxed grains while the pure SBN ceramic ($x = 1.0$) contained plate shaped grains. For the sample with $0.1 \leq x \leq 0.3$, the ceramic consisted of both equiaxed grains of PZT and irregularly shaped grains of PNT. As the SBN content was increased up to $x = 0.9$, there were two component phases with different shapes and sizes of PNT and SBN in the ceramics. The amount of plate-shaped grains increased gradually while irregularly shaped grains decreased. The variation of grain size for all ceramics are shown in Fig. 3(b). It was interesting to note that the PNT phase formed in this system led to the reduction of the size of the equiaxed grains compared to pure PZT. However, there was little change when compared to pure SBN ceramic. The second PNT particles could inhibit grain boundary migration and limit grain growth in the ceramics. It has also been reported that the presence of a secondary phase can reduce grain sizes of PZT-based ceramics [10].

The room temperature dielectric properties measured at 1 kHz are listed in Table 1. In the case of pure PZT and SBN ceramics, the dielectric constant (ϵ_r) values were ~ 1040 and ~ 175 while the dielectric loss ($\tan \delta$) values were ~ 0.004 and ~ 0.018 , respectively. Starting from pure PZT, the addition of $x = 0.1$ SBN caused a sudden increase in the dielectric constant and loss. The smaller grain size of the ferroelectric PZT matrix phase was partly the main contributor to the improved dielectric behavior in this composition due to its greater domain density [11]. Higher domain density also allowed a larger amount of wall movement, thus causing larger dielectric constant and loss observed in the small-grained sample. In addition, the donor-like substitution also played a role in an increase of dielectric constant and loss. Namely, donor-like substitution behavior in which Bi^{3+} substituting for Pb^{2+} and Nb^{5+} for Ti^{4+} or Zr^{4+} . The Bi^{3+} and Nb^{5+} ions from SBN provided extra electrons which could counteract the natural p -type conductivity of PZT ceramic and raise the electrical resistivity [1]. The sample was likely to be charge

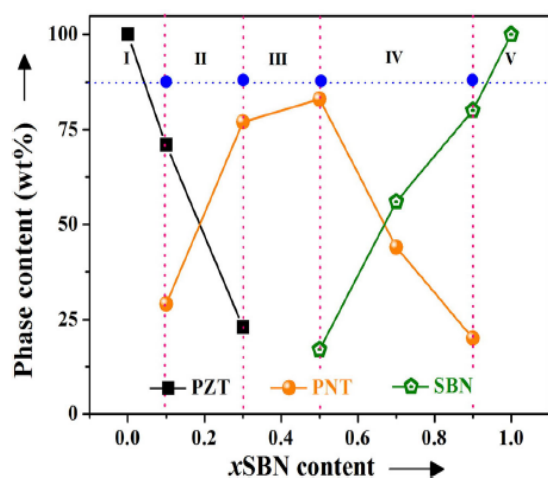
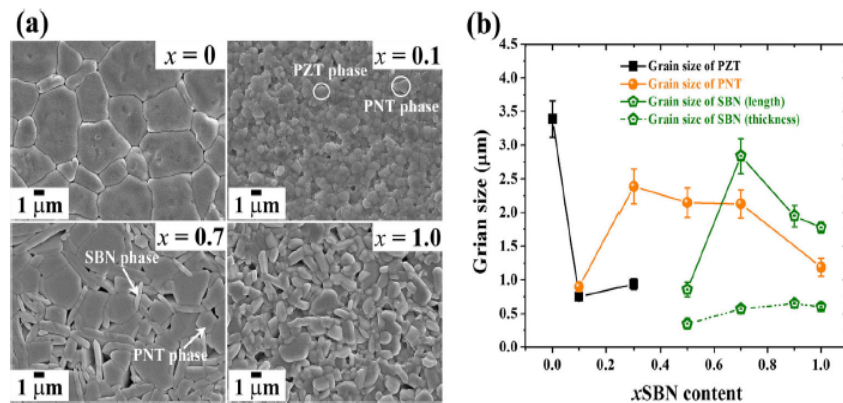


Fig. 2 The relationship between phase field and SBN content in PZT ceramic

Fig. 3 (a) SEM images of (1- x)PZT- x SBN ceramics (b) Grain size of nominal (1- x)PZT- x SBN ceramics



compensated by the formation of cation vacancies such as Pb^{2+} and Ti^{4+} and the released ions then formed the PNT phase observed. On the other hand, the concentration of oxygen vacancies also got significantly reduced [12, 13]. Typically, oxygen vacancies are believed to be a major contributor to domain wall pinning [14]. The reduction of oxygen vacancies led to an enhancement in domain reorientation [15, 16], resulting in high dielectric constant and loss [1]. An increase in SBN content up to $x = 0.7$ caused the dielectric constant and loss of the ceramics to suddenly decrease. This result was attributed to the presence of the non-piezoelectric cubic PNT phase and possibly also to a small amount of some unknown phases, as observed in the X-ray diffraction study. For the composition with $x = 0.9$ SBN, the dielectric constant and loss slightly increased. This composition was basically a PZT-doped SBN-based solid solution. However, the small increase in dielectric constant and nearly the same value of dielectric loss compared to pure SBN was not sufficient to indicate with certainty the defect types present in the material. This was made more difficult by the presence of a small amount of PNT secondary phase in this sample.

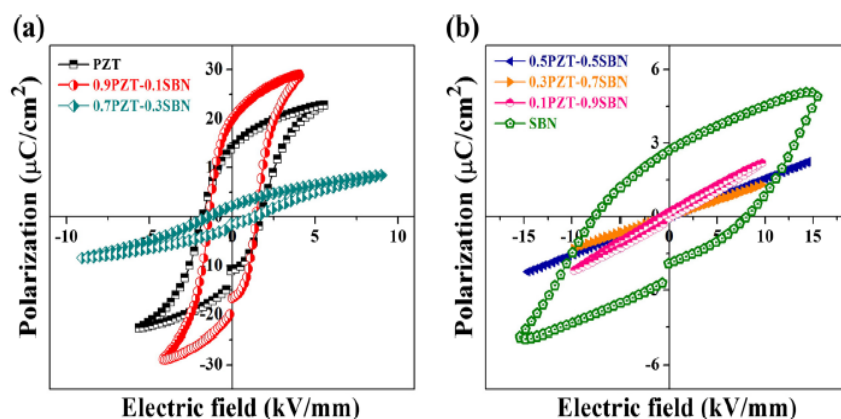
The polarization-electric field (P - E) loops of nominal (1- x)PZT- x SBN ceramics are shown in Fig. 4. Some ferroelectric parameters extracted from these loops are listed in Table 1. From Fig. 4(a, b), pure PZT ceramic showed larger remanent polarization ($2P_r$) and smaller coercive field ($2E_c$) than pure

SBN ceramic. Addition of $x = 0.1$ SBN into the PZT matrix phase led to an increase of the remanent polarization and decrease of the coercive field. This ceramic composition can be a promising material for ferroelectric memory applications due to its high remanent polarization and low coercive field. The increase in the remanent polarization and reduction in the coercive field of the sample was attributed to the effect of donor-like substitution. In this sample, donor dopants (i.e. Bi and Nb from SBN) induced Pb and Ti vacancies in the PZT matrix for charge compensation, and simultaneously reduced the oxygen vacancy content [12, 13]. The reduced oxygen vacancy concentration then contributed to the increase in mobility of domain walls by lowering the stability of domain structure against external electrical field [17], causing the increase of the remanent polarization and reduction of the coercive field. Moreover, the low content of cubic PNT phase also played a role in improving the ferroelectric properties of this composition. For sample with $x = 0.3$ SBN, a very slim polarization loop with small remanent polarization and coercive field was present. This was due to an increased amount of cubic PNT phase. Since the cubic PNT phase in the ceramic exhibited non-piezoelectric characteristics, it could obstruct the polarization process of the ferroelectric PZT phase, leading to a reduction of the remanent polarization of this sample. When more SBN ($0.5 \leq x \leq 0.9$) was added to PZT, the P - E loops showed an obvious linear polarization behavior, which

Table 1 Dielectric, ferroelectric and piezoelectric properties of (1- x)PZT- x SBN ceramics

x	Dielectric props.		Ferroelectric props.		Piezoelectric props.		
	ε_r	$\tan\delta$	$2P_r$ ($\mu\text{C}/\text{cm}^2$)	$2E_c$ (kV/mm)	S_{max} (%)	E_{max} (kV/mm)	d_{33}^* (pm/V)
0	1040.20	0.0043	28.37	3.52	0.17	5.54	320.58
0.1	1799.31	0.0280	39.94	2.86	0.13	4.09	335.18
0.3	761.53	0.0233	4.62	2.82	0.02	8.98	30.12
0.5	165.98	0.0091	-	-	-	-	-
0.7	136.97	0.0031	-	-	-	-	-
0.9	182.40	0.0175	-	-	-	-	-
1.0	174.69	0.0182	5.30	15.73	-	-	-

Fig. 4 P - E loops of $(1-x)$ PZT- x SBN ceramics, when (a) $x = 0$ –0.3 and (b) $x = 0.5$ –1.0

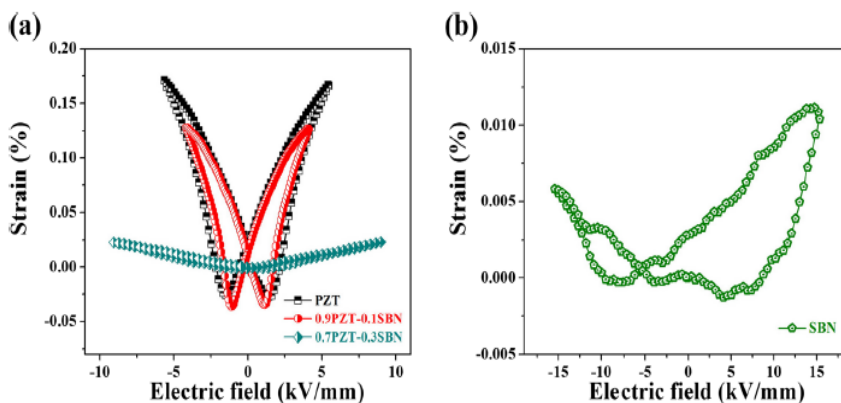


is a characteristic of paraelectric materials [18]. It should be noted that the 0.1PZT-0.9SBN composition also had poor hysteresis loop although this sample was a SBN-rich phase. In this case, the material seemed to exhibit a p -type behavior due to that lower valent Pb^{2+} , Zr^{4+} , Ti^{4+} ions substituted into the SBN structure. This led to the formation of oxygen vacancies from charge compensation process. It was expected that the major carrier in this system was holes, implying that this material was a p -type semiconductor. The presence of oxygen vacancies obstructed domain reorientation by pinning them, producing a poor hysteresis loop. Over a large compositional range, the presence of the cubic PNT phase obviously led to degradation of the ferroelectric properties of the nominal PZT-SBN system.

The relationships between the field-induced strain (S) and the applied external electric field (E) for nominal $(1-x)$ PZT- x SBN ceramics are shown in Fig. 5. The values of the longitudinal piezoelectric constant (d_{33}^*) determined from the slope of strain versus electric field plot [19] are listed in Table 1. From Fig 5(a), the pure PZT ceramic showed a typical butterfly curve with high strain and d_{33}^* values of $\sim 0.17\%$ and ~ 320 pm/V, respectively. On the other hand, the pure SBN ceramic showed asymmetric strain loop with very low maximum strain, as shown in Fig 5(b). When a small amount of

0.1SBN was added to PZT, the sample could deliver a field-induced strain of $\sim 0.13\%$ with at an external electric field of ~ 4 kV/mm, which was comparable to the strain of undoped PZT. Moreover, the maximum d_{33}^* value was also achieved for this sample (see Table 1). It is well known that the materials for piezoelectric applications are required to possess properties such as high d_{33}^* at low applied electric field [20]. From these results, the piezoelectric properties seemed to be optimized for the 0.9PZT-0.1SBN composition. The donor-doped behavior contributed to the improved piezoelectric properties of this sample. The substitution of Sr^{2+} , Bi^{3+} and Nb^{5+} ions into the PZT introduced the A-site vacancies and also significantly reduced oxygen vacancy concentration. The switching of domains upon electric field application is one of the major mechanisms contributing to the strain response [21, 22]. As mentioned previously, ferroelectric domain walls can be pinned by oxygen vacancies [13]. In this sample, therefore, a decrease in oxygen vacancy concentration resulted in an improvement in ferroelectric domain switching, leading to an increase in strain and corresponding d_{33}^* response. Further increasing SBN content to $x = 0.3$ resulted in a slim butterfly loop with a markedly decreased strain and d_{33}^* . Degradation of the piezoelectric properties in this composition was mainly due to the increased amount of non-ferroelectric

Fig. 5 S - E loops of $(1-x)$ PZT- x SBN ceramics when (a) $x = 0$ –0.3 and (b) $x = 1.0$ (Pure SBN ceramic)



PNT phase. For higher concentration of SBN ($0.5 \leq x \leq 0.9$), no S - E loops could be obtained as the strain values were too low and close to the detection limit of the instrument. In addition, the loss of strain response for these ceramics could be caused by the effect of PNT and other unknown phases. These phases might suppress ferroelectric domain switching, causing the loss of strain responses. Therefore, they were not included in Fig. 5. The observed hysteresis loops indicated that these ceramic compositions were neither ferroelectric materials nor exhibited piezoelectric properties. Again, the presence of the non-piezoelectric cubic PNT phase played a major role in the development of the electrical properties of this new material system.

4 Conclusion

$(1-x)\text{Pb}(\text{Zr}_{0.52}\text{Ti}_{0.48})\text{O}_3$ - $x\text{SrBi}_2\text{Nb}_2\text{O}_9$ ceramics were successfully prepared by a solid-state mixed-oxide method. The pure PZT ceramic showed mainly tetragonal phase. Addition of small amounts ($0.1 \leq x \leq 0.3$) of SBN into PZT resulted in a tetragonal lattice distortion of the PZT-based solid solution as well as the appearance of a cubic-structured PNT phase. With an increase in the content of SBN, the orthorhombic SBN and the cubic PNT phase were both present in the XRD patterns. This observation suggested that suitable content of added SBN ($x = 0.1$) into nominal PZT-SBN ceramics could improve the electrical properties over those of pure PZT and SBN ceramics. Further increasing SBN content ($x \geq 0.3$) resulted in poor dielectric, ferroelectric and piezoelectric properties. The observed non-piezoelectric secondary phase indicated the high tendency of reaction between PZT and SBN and its presence strongly affected the electrical properties of this material system.

Acknowledgments This work is financially supported by the Thailand Research Fund (TRF) and the National Research University Project under Thailand's Office of the Higher Education Commission (OHEC) and the Australian Research Council under Grant No. DP0988182. JG

acknowledges support from Australian Research Council under Grant No. DE120102644. The Faculty of Science and the Graduate School, Chiang Mai University is also acknowledged. ON would like to acknowledge financial support from the TRF through the Royal Golden Jubilee Ph.D. Program.

References

1. G. H. Haertling, J. Am. Ceram. Soc. **82**, 797 (1999)
2. K. Miura, Appl. Phys. Lett. **80**, 2967 (2002)
3. D. H. Bao, N. Wakiya, K. Shinozaki, N. Mizutani, J. Phys. D: Appl. Phys. **35**, L1 (2002)
4. K. Amanuma, T. Hase, Y. Miyasaka, Appl. Phys. Lett. **66**, 211 (1995)
5. K. Kato, Jpn. J. Appl. Phys. **37**, 5178 (1998)
6. W. Q. Zhang, A. D. Li, Q. Y. Shao, Y. D. Xia, D. Wu, Z. G. Liu, N. B. Ming, Appl. Surf. Sci. **254**, 1583 (2008)
7. H. H. Park, H. H. Park, T. S. Kim, R. H. Hill, Sensors and Actuators **B130**, 696 (2008)
8. J. S. Yang, X. M. Chen, T. Aizawa, M. Kuwabara, Solid State Ionics **108**, 117 (1998)
9. R. D. Shannon, Acta Cryst **A32**, 751 (1976)
10. S.-J. Yoon, J.-W. Choi, J.-Y. Choi, D. Wan, Q. Li, Y. Yang, J. Korean Phys. Soc. **57**, 863 (2010)
11. G. Arlt, D. Hennings, G. De With, J. Appl. Phys. **58**, 1619 (1985)
12. K. B. Lee, H. S. Lee, S. K. Cho, J. Korean Phys. Soc. **31**(3), 532 (1997)
13. M. Pereira, A. G. Peixoto, M. J. M. Gomes, J. Eur. Ceram. Soc. **21**, 1353 (2001)
14. W. L. Warren, D. Dimos, B. A. Tuttle, G. E. Pike, H. N. Al-Shareef, Integ. Ferro. **16**, 77 (1997)
15. W. Zhu, I. Fujii, W. Ren, S.T.-McKinstry, J. Am. Ceram. Soc. **95**, 2906 (2012)
16. G. H. Haertling, C. E. Land, J. Am. Ceram. Soc. **54**, 1 (1971)
17. Q. M. Zhang, J. Zhao, K. Uchino, J. Zheng, J. Mater. Res. **12**, 34 (1997)
18. W. Jo, R. Dittmer, M. Acosta, J. Zang, C. Groh, E. Sapper, K. Wang, J. Rödel, J. Electroceram. **29**, 71 (2012)
19. S. Mahajan, O. P. Thakur, C. Prakash, Defence Sci. J. **57**, 23 (2007)
20. S.-T. Zhang, A. B. Kounga, E. Aulbach, H. Ehrenberg, J. Rödel, Appl. Phys. Lett. **91**, 112906 (2007)
21. W. Jo, J. Rödel, Appl. Phys. Lett. **99**, 042901 (2011)
22. Y. Hiruma, H. Nagata, T. Takenaka, Jpn. J. Appl. Phys. **48**, 09KC08 (2009)

Comparative study of properties of BCZT ceramics prepared from conventional and sol-gel auto combustion powders

Piyaporn Jaimeewong^a, Methee Promsawat^b, Anucha Watcharapasorn^c, and Sukanda Jiansirisomboon^d

^aDepartment of Physics and Materials Science, Faculty of Science, Chiang Mai University, Chiang Mai, Thailand; ^bDepartment of Materials Science and Technology, Faculty of Science, Prince of Songkla University, Songkhla, Thailand; ^cMaterials Science Research Center, Faculty of Science, Chiang Mai University, Chiang Mai, Thailand; ^dSchool of Ceramic Engineering, Suranaree University of Technology, Nakhon Ratchasima, Thailand

ABSTRACT

This work studies properties of $\text{Ba}_{0.85}\text{Ca}_{0.15}\text{Ti}_{0.9}\text{Zr}_{0.1}\text{O}_3$ (BCZT) ceramics prepared from the BCZT powders synthesized by conventional mixed oxide (so called M) and sol-gel auto combustion (so called A) methods. The M and A powders were calcined at 1200 and 900°C, respectively. Different amounts (0, 50 and 100 wt%) of A powder were added into M powder then sintered at 1450°C for 2 h. Grain size and dielectric constant (ϵ_r) tended to decrease with A powder content. The highest ϵ_r value of 5342 but slimmest was observed in the ceramic with 100 wt% A powder addition.

ARTICLE HISTORY

Received 28 November 2015
Accepted 28 March 2016

KEYWORDS

Lead free; piezoelectric; BCZT; mixed oxide; sol-gel auto combustion

1. Introduction

Nowadays, electroceramics are used in many applications such as sensors, actuators and piezoelectric devices. Lead zirconate titanate (PZT) is a piezoelectric material that shows high piezoelectric performance suitable for using in piezoelectric applications. However, PbO evaporated during high temperature processes is a toxic compound for human and environment. The European Union (EU) have the rule to restrict the use of heavy metals such as lead (Pb), cadmium (Cd), chromium (Cr), mercury (Hg), tin (Sn) and other heavy metals [1–2]. From these reasons, lead-free piezoelectric materials and their properties are developed to use for piezoelectric applications instead PZT. They include barium titanate (BaTiO_3 : BT), bismuth sodium titanate ($\text{Bi}_{0.5}\text{Na}_{0.5}\text{TiO}_3$: BNT), bismuth potassium titanate ($\text{Bi}_{0.5}\text{K}_{0.5}\text{TiO}_3$: BKT) and potassium sodium niobate (KNaNbO_3 : KNN). However, lead-free materials still have low piezoelectric properties as compared to PZT material. In 2009, Liu and Ren [3] prepared a lead-free perovskite $\text{Ba}_{0.85}\text{Ca}_{0.15}\text{Zr}_{0.1}\text{Ti}_{0.9}\text{TiO}_3$ (BCZT) material. It showed higher piezoelectric coefficient than PZT (d_{33} of PZT = 500–600 pC/N while d_{33} of BCZT \sim 620 pC/N). For BCZT ceramics, the coexistence of

CONTACT Sukanda Jiansirisomboon  sukanda.jian@sut.ac.th  School of Ceramic Engineering, Suranaree University of Technology, Nakhon Ratchasima 3000, Thailand.

Color versions of one or more of the figures in the article can be found online at www.tandfonline.com/ginf.

© 2016 Taylor & Francis Group, LLC

tetragonal (T), cubic (C) and rhombohedral (R) phases was observed at the morphotropic phase boundary (MPB) [3]. Nevertheless, disadvantages of the BCZT materials are high calcination and sintering temperatures, i.e. > 1300 and 1500°C , respectively [4]. Therefore, the reduction of the processing temperatures is the first aim of this work. The wet chemical processes, i.e. sol-gel, hydrothermal, pechini and sol-gel auto combustion methods, have been used to prepare BCZT powders [5]. Very few studies have reported about BCZT powder synthesized by the sol-gel auto combustion method [6].

In this work, the sol-gel auto combustion method was selected to synthesize BCZT powders. With using this method, homogeneous, stoichiometric and small size powders, which could help in increasing reactive surface area and reducing calcination temperature, were believed to be obtained. Furthermore, base on our knowledge, effects of BCZT powder sizes on properties of BCZT ceramics have not yet been studied. Therefore, in this study, BCZT ceramics were prepared from the BCZT powders synthesized by the sol-gel auto combustion (A) and the conventional mixed oxide (M) methods. The M powder was mixed with different contents of the A powder, which were 0, 50 and 100 wt%. The ceramics were characterized in terms of chemical composition, microstructure, phase, density, and dielectric and ferroelectric properties. The relations between A powder content and the properties of the ceramics were studied and discussed.

2. Experiments

$\text{Ba}_{0.85}\text{Ca}_{0.15}\text{Zr}_{0.1}\text{Ti}_{0.9}\text{TiO}_3$ (BCZT) powders were firstly prepared via conventional mixed oxide (M) and sol-gel auto combustion (A) methods. For the M method, barium carbonate (BaCO_3 , 99.0%, Sigma Aldrich), calcium carbonate (CaCO_3 , 99.5%, Sigma Aldrich), zirconium (IV) oxide (ZrO_2 , 98.5%, Riedel-de Haën) and titanium (IV) oxide (TiO_2 , 99.0%, Sigma Aldrich) powders were used as the starting precursors. The stoichiometric amounts of the starting powders were mixed by ball-milling for 24 hrs in ethanol medium. The slurries were dried at 120°C for 24 hrs. The dried powders were calcined at 1200°C for 2 hrs with a heating/cooling rate of $5^{\circ}\text{C}/\text{min}$. For the A method, barium nitrate ($\text{Ba}(\text{NO}_3)_2$, 99.0%, Himedia), calcium nitrate tetrahydrate ($\text{Ca}(\text{NO}_3)_2 \cdot 4\text{H}_2\text{O}$, 99.0%, Sigma Aldrich), zirconium (IV) oxynitrate hydrate ($\text{Zr}(\text{NO}_3)_4 \cdot 3\text{H}_2\text{O}$, 99.0%, Sigma Aldrich), titanium (IV) butoxide ($(\text{C}_4\text{H}_9\text{O})_4\text{Ti}$, 97.0%, Sigma Aldrich) and citric acid ($\text{C}_6\text{H}_8\text{O}_7$, 99.5%, Sigma Aldrich) powders were used as the starting materials. The predetermined amounts of the starting powders were mixed with citric acid, with the ratio of the mixed powder to the citric acid fixed as 1:1, and then dissolved in deionized (DI) water. The solution was stirred under the temperature of 70°C until it became transparent. The NH_4OH was gradually added into the solution to adjust pH value of the solution equal to 7. The solution was heated at 120°C for 4 hrs and, eventually, the solution became black powder (burnt powder). The burnt powder was calcined at 900°C for 2 hrs with a heating/cooling rate of $5^{\circ}\text{C}/\text{min}$. Different amounts, which were 0, 50 and 100 wt%, of the A powder were mixed with the M powder by ball-milling for

24 hrs in an ethanol medium. The mixtures were dried at 120°C for 24 hrs. The dried powders were mixed with 3 wt% polyvinyl alcohol (PVA) as a binder and pressed under 1 ton pressure for 15 seconds to form a pellet shape. The green bodies were sintered at 1450°C for 2 hrs with a heating/cooling rate of 5°C/min.

Phase formation of the calcined powders and the ceramics was characterized by X-ray diffraction technique (X' Pert Phillips) with $\text{CuK}\alpha$ radiation of 1.54178 Å wavelength at 2θ range of 20–80°. Densities of the ceramics were determined by Archimedes' method (ASTM C 378–88). Microstructure was observed by a scanning electron microscope (SEM, JEOL JSM-6335F). Grain size was determined by a linear intercept method from SEM images. The parallel surfaces of each sample were sequentially polished using 400, 600, 800 grit SiC paper. The samples were annealed at 500°C for 5 hrs to remove residual stress due to the polishing process. Conductive electrodes were made on the polished surfaces using a colloidal silver paste. Ferroelectric and dielectric properties were measured by a modified Sawyer-Tower circuit and LCR meter (Agilent 2638B), respectively.

3. Results and discussion

The XRD patterns of the M and A powders showed mainly perovskite structure and small amount of secondary phase [3,6] while the other ceramics showed pure perovskite phase without any unwanted phase as illustrated in Fig. 1(a). The secondary phase presented in the M and A powders was believed to be created from incomplete reaction of starting precursors. The enlarged views of the diffraction peaks at $2\theta \approx 45^\circ$, 56° and 66° are shown in Fig. 1(b), (c) and (d), respectively. The peak at $2\theta \approx 45^\circ$ was fitted into two peaks corresponding to (002) and (200) planes for the left and right-hand side peaks, respectively. This could be the reflection of a tetragonal structure. The peak at $2\theta \approx 66^\circ$ was split into (202) and (220) planes for the left and right-hand side peaks, respectively. This was also the reflection of the tetragonal phase. The splitting of the peaks at $2\theta \approx 45^\circ$ and 66° of a tetragonal structure could be confirmed with the ICSD file No. 01-076-0744 of BaTiO_3 compound with

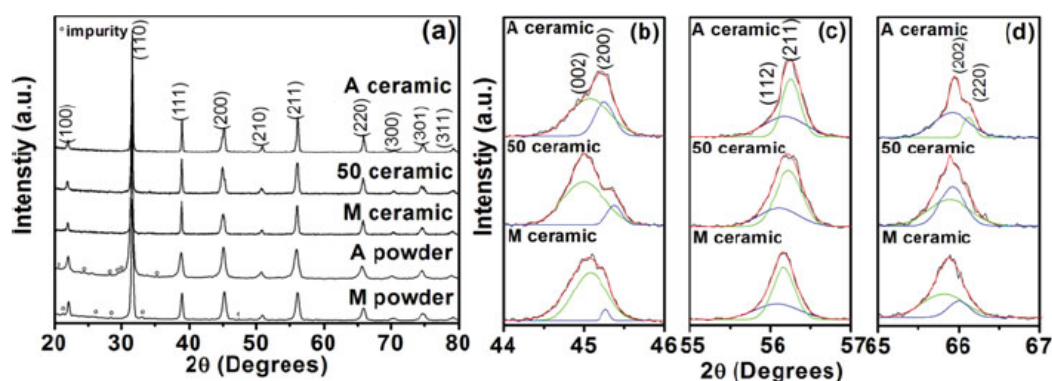


Figure 1. (a) XRD patterns of BCZT powders and ceramics. The enlarged views of the peaks at $2\theta \approx$ (b) 45° , (c) 56° and (d) 66° . The ceramics with M:A ratios of 100:0, 50:50 and 0:100 are represented by M, 50 and A ceramics, respectively.

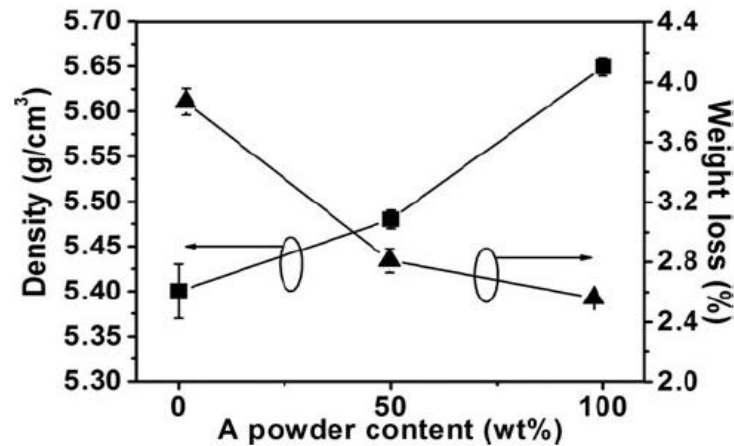


Figure 2. Plots of density and weight loss as a function of ceramics composition of BCZT ceramics.

a tetragonal phase. The peak at $2\theta \approx 56$ was fitted into (112) and (211) planes, which were located on the left and the right hand sides, respectively. The splitting of this diffraction peak could be the reflection of a rhombohedral structure. This was consistent with the peak splitting at $2\theta \approx 56^\circ$ as observed in BaTiO_3 compound (ICDS file No. 01-085-1797). The result agreed with the results observed in the previous studies in Ref. 2, 3, 6 and 7.

The plots of density and weight loss as a function of A powder content of BCZT ceramics are shown in Fig. 2. The density tended to increase while weight loss decreased with increasing A powder content. The maximum density of 5.65 g/cm^3 ($> 97\%$ of the theoretical density), which was higher than that of the BCZT ceramics prepared from sol-gel powders [6]. As shown in Fig. 3(a) and (b), the M and A powders had the particle sizes in the ranges of $0.15\text{--}3.0 \text{ }\mu\text{m}$ and $20\text{--}30 \text{ nm}$, respectively. It was believed that added smaller size A powders could fill the gaps between the larger size M powder. This could result in increases in a degree of the packing and a

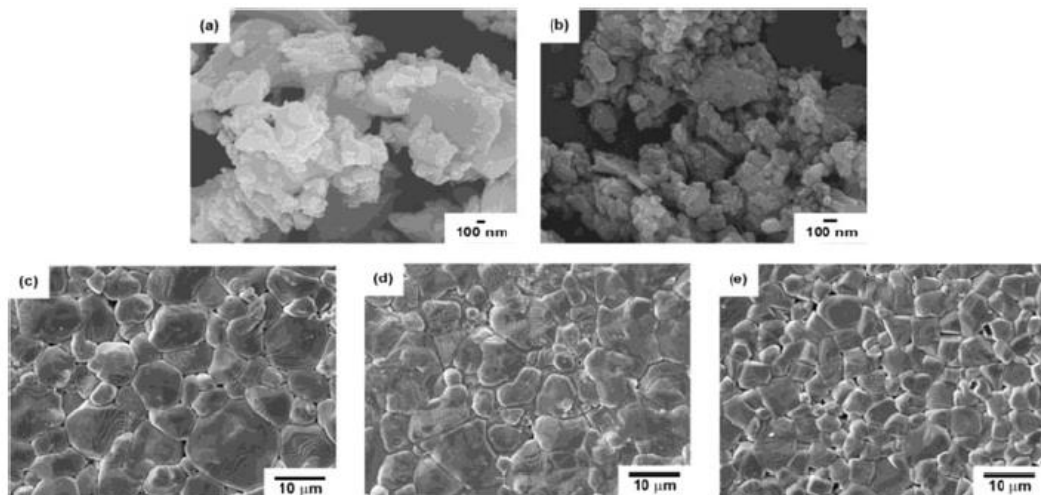


Figure 3. SEM micrographs of (a) M and (b) A powders and as-sintered surfaces of (c) 100:0, (d) 50:50 and (e) 0:100 ceramics.

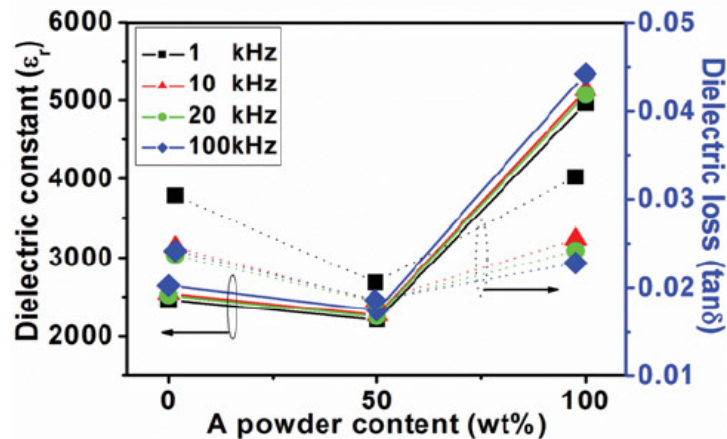


Figure 4. Plots of dielectric constants and dielectric losses measured at various frequencies as a function of ceramics' composition of BCZT ceramics.

reaction surface area of the mixed powders which led to the enhancement of densification during the sintering process. It can be seen from Fig. 3(a) and (b) that the A powder was more homogeneous and agglomerated than the M powder. Microstructures of as-sintered surfaces of all samples are shown Fig. 3(c)–(e). A coexistence of equiaxial and irregular shaped grains was observed in all ceramics. Grain size tended to decrease with increasing A powder content. The average grain sizes of the ceramics with 0, 50 and 100 wt% A powder were 8.8, 5.3 and 3.4 μm , respectively. The degree of homogeneity of grain size distribution increased with increasing A powder content. This was likely due to the characteristic of A powders, which had smaller grain and more homogenous grain size distribution, which was more dominated at higher A powder content. It was found from the density and the grain size results that the small size powder had a more significant role on densification and grain growth processes.

The plots of dielectric constants (ϵ_r) and dielectric loss ($\tan\delta$) measured at room temperature and at different frequencies as a function of A powder content are illustrated in Fig. 4. The ϵ_r and $\tan\delta$ of the M ceramic slightly decreased with 50 wt% A powder incorporation. However, they significantly increased as A powder content increased to 100 wt%. The increase in ϵ_r could be caused by decreasing of grain size as described in Devonshire's phenomenological theory [9–10]. Moreover, it was believed that the increase in density contributed to the enhancement of ϵ_r [11]. A high ϵ_r at a low frequency could be caused by the response of space charge polarization created due to the formation of lattice vacancies, i.e. cation or oxygen vacancies. However, space charge polarizations were restricted as frequency increased which caused a decrease in ϵ_r [9]. Polarization-electric field (P - E) hysteresis loops measured at a frequency of 25 Hz of the BCZT ceramics are shown in Fig. 5. For all ceramics, P - E curves were found to be a slim loop [13]. The remnant polarization (P_r) and coercive field (E_c) of the M ceramic increased with 50 wt% A powder incorporation. The P_r and E_c values observed in this study were consistent with the previous result observed by Wang *et al.* [3]. However, the values

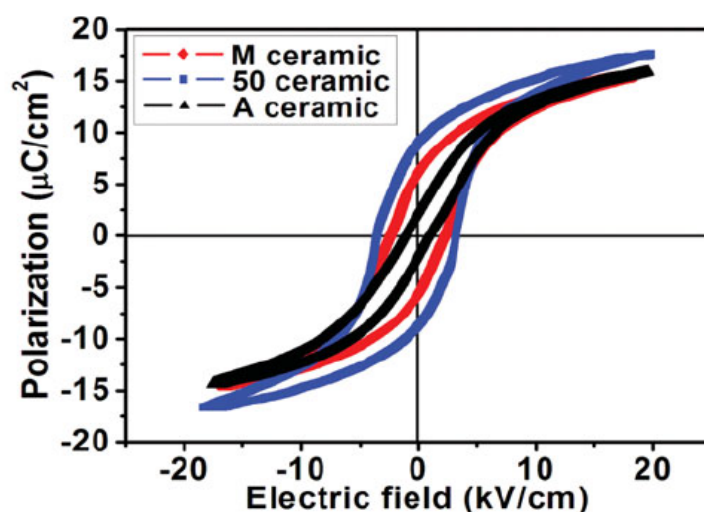


Figure 5. P - E hysteresis loops measured at the frequency of 25 Hz of BCZT ceramics.

Table 1. Dielectric and ferroelectric properties of BCZT ceramics.

Sample (M:A)	ϵ_r at 1 kHz and 30°C	$\tan\delta$ at 1 kHz and 30°C	Remnant polarization; P_r ($\mu\text{C}/\text{cm}^2$)	Coercive field; E_c (kV/cm)
100:0	2643	0.0304	7.38 ± 0.33	2.32 ± 0.07
50:50	3865	0.0206	9.40 ± 0.14	3.40 ± 0.19
0:100	5342	0.0255	1.95 ± 0.57	1.04 ± 0.29

decreased as the A powder content increased to 100%, as shown in Table 1. The results were seemed to in agreement with Hao's work, considering the three ranges of grain sizes. Firstly, the ceramics with the grain size in the range of 0.4–5 μm presented an increased P_r . Secondly, for the ceramics with the grain size $\sim 5 \mu\text{m}$, they showed the P_r closed to 9 $\mu\text{C}/\text{cm}^2$. Thirdly, the ceramics with the grain size of 6–10 μm , P_r exhibited lower than 8 $\mu\text{C}/\text{cm}^2$ [13]. In addition, the ferroelectric properties were consistent with the dielectric displacement-electric field (D - E) hysteresis loop based on the Avrami model reported by Orihara [15]. For the model, a formula, $f = f_0[1 - \exp(-G_a d^3/kT)]$, where f is ferroelectrics properties, d is a grain size and G_a is a constant and expression of the grain isotropy energy density, was proposed. From the formula, it was revealed that ferroelectric properties were proportional to grain size due to polarization and ferroelectricity increased with increasing grain size [13, 15]. This supported the observed result that smaller grain ceramic possessed lower ferroelectric properties.

4. Conclusion

BCZT ceramics were obtained by solid state sintering at 1450°C for 2 hrs. The A powders had smaller size than the M powders. The XRD patterns of all samples showed coexisting of rhombohedral and tetragonal phases. Density tended to increase while grain size decreased with increasing A powder content. The ϵ_r and

$\tan\delta$ of the M ceramic decreased while P_r and E_c increased with 50 wt% A powder incorporation. However, as A powder content increased to 100 wt%, the dielectric properties increased while the ferroelectric properties decreased. Among these ceramics, the ceramic incorporated with 50 wt% A powder exhibited good ferroelectric properties with had P_r and E_c of $9.40 \mu\text{C}/\text{cm}^2$ and $3.40 \text{ kV}/\text{cm}$, respectively.

Funding

This work was financially supported by the Thailand Research Fund (TRF) (Grant no. RSA5780032) and the National Research University Project under Thailand's Office of the Higher Education Commission (OHEC). The Faculty of Science and the Graduate School, Chiang Mai University is also acknowledged. PJ would like to acknowledge financial support from the TRF through the The 50th Anniversary Chiang Mai University Fund for Ph.D. Program (PHD/018/2556) and the National Research University (NRU) Project for Chiang Mai University (CMU).

References

1. Directive 2011/65/EU of the european parliament and of the council on the restriction of the use of certain hazardous substances in electrical and electronic equipment. *Off J Eur union*. 174(88)–174(110) (2011).
2. W. F. Liu, and X. B. Ren, Large piezoelectric effect in pb-free ceramics. *Phy Rev Lett*. **103**, 257602(1)–257602(4) (2009).
3. P. Wang, Y. X. Li, and Y. Q. Lu, Enhanced piezoelectric properties of $(\text{Ba}_{0.85}\text{Ca}_{0.15})(\text{Ti}_{0.9}\text{Zr}_{0.1})\text{O}_3$ lead-free ceramics by optimizing calcination and sintering temperature. *J Eur Ceram Soc*. **31**, 2005–2012 (2011).
4. K. C. Patil, M. S. Hegde, T. Rattan, and S. T. Aruna, *Chemistry of Nanocrystalline Oxide Materials Combustion Synthesis, Properties and Applications*. Singapore: World Scientific Publishing Co. Pte. Ltd.; (2008).
5. G. K. Sahoo, and R. Mazumder, Low temperature synthesis of $\text{Ba}(\text{Zr}_{0.2}\text{Ti}_{0.8})\text{O}_3$ - $0.5(\text{Ba}_{0.7}\text{Ca}_{0.3})\text{TiO}_3$ nanopowders by solution based auto combustion method. *J Mater Sci: Mater Electron*. **25**, 3515–3519 (2014).
6. J. P. Praveen, T. Karthik, A. R. James, E. Chandrakala, S. Asthana, and D. Das, Effect of poling process on piezoelectric properties of sol–gel derived. *J Eur Ceram Soc*. **35**, 1785–1798 (2015).
7. M. C. Ehmke, S. N. Ehrlich, J. E. Blendell, and K. J. Bowman, Phase coexistence and ferroelastic texture in high strain $(1-x)\text{Ba}(\text{Zr}_{0.2}\text{Ti}_{0.8})\text{O}_3$ - $x(\text{Ba}_{0.7}\text{Ca}_{0.3})\text{TiO}_3$ piezoceramics. *J Appl Phys*. **111**, 124110(1)–124110(7) (2012).
8. I. D. Coondoo, N. R. Panwar, H. V. Amorin, M. G. Alguero, and A. L. Kholkin, Synthesis and characterization of lead-free $0.5\text{Ba}(\text{Zr}_{0.2}\text{Ti}_{0.8})\text{O}_3$ - $0.5(\text{Ba}_{0.7}\text{Ca}_{0.3})\text{TiO}_3$ ceramic. *J Appl Phys*. **113**, 214107(1)–214107(6) (2013).
9. A. J. Moulson, and J. M. Herbert, *Electroceramics* 2nd editions Chichester, England: John Wiley and Sons; (2003).
10. H. T. Kim, and Y. H. Han, Sintering of nanocrystalline BaTiO_3 . *Ceram Int*. **30**(7), 1719–1723 (2004).
11. L. Guo, H. Luo, J. Gao, L. Guo, and J. Yang, Microwave hydrothermal synthesis of barium titanate powders. *Mat Lett*. **60**, 3011–3014 (2006).
12. A. C. Nigrawal, and N. V. Chand, Electrical and dynamic mechanical analysis of nano alumina addition on polyvinyl alcohol (PVA) composites. *Progress in Nanotechnology and Nanomaterials*, **2**, 25–33 (2013).

13. J. G. Hao, W. F. Bai, W. Li, and J. W. Zhai, Correlation between the microstructure and electrical properties in high-performance $(\text{Ba}_{0.85}\text{Ca}_{0.15})(\text{Zr}_{0.1}\text{Ti}_{0.9})\text{O}_3$ lead-free piezoelectric ceramics. *J Am Ceram Soc.* **95**, 1998–2006 (2012).
14. U. R. Intatha, P. P. Parjansri, K. P. Pengpat, G. W. Rujijanagul, T. W. Tunkasiri, and S. K. Eitssayeam, Phase formation, dielectric and ferroelectric properties of Mn, Al doped BCZT ceramics by molten salt method. *Int Ferroelectrics*, **139**, 83–91 (2012).
15. L. E. Cross, *Ferroelectric Ceramics: Tailoring Properties for Specific Applications: Ferroelectric Ceramics*, Edited by N. Setter, E. L. Colla. Basel: Birkhauser Verlag; (1993).



Contents lists available at ScienceDirect

Ceramics International

journal homepage: www.elsevier.com/locate/ceramint

Effects of frequency on electrical fatigue behavior of ZnO-modified $\text{Pb}(\text{Mg}_{1/3}\text{Nb}_{2/3})_{0.65}\text{Ti}_{0.35}\text{O}_3$ ceramics



Methee Promsawat^{a,*}, Napatporn Promsawat^b, Jenny W. Wong^c, Zhenhua Luo^d,
Soodkhet Pojprapai^e, Sukanda Jiansirisomboon^e

^a Department of Materials Science and Technology, Faculty of Science, Prince of Songkla University, Hat Yai, Songkhla 90112, Thailand

^b Synchrotron Light Research Institute, Muang, Nakhon Ratchasima 30000, Thailand

^c Department of Chemistry and 4D LABS, Simon Fraser University, Burnaby, British Columbia, Canada, V5A 1S6

^d School of Water, Energy and Environment, Cranfield University, Cranfield MK43 0AL, UK

^e School of Ceramic Engineering, Suranaree University of Technology, Muang, Nakhon Ratchasima 30000, Thailand

ARTICLE INFO

Keywords:

Fatigue
Ferroelectricity
Microstructure
Piezoelectricity

ABSTRACT

This work aims to study the effects of frequency on the electrical fatigue behavior of ZnO-modified $\text{Pb}(\text{Mg}_{1/3}\text{Nb}_{2/3})_{0.65}\text{Ti}_{0.35}\text{O}_3$ (PMNT) ceramics. Changes in microstructures, ferroelectric and piezoelectric properties of the ceramics at bipolar electrical fatigue frequencies of 5, 10, 50 and 100 Hz were observed. The thickness of damaged surface of the ceramics decreased with increasing frequency. The degradation of properties of the ceramics fatigued at low frequency was greater than those fatigued at high frequency. The degradation by electrical fatigue at lower frequencies, 5 and 10 Hz, could be caused by the effects of both field screening and domain pinning, while at higher frequencies the fatigue was mainly a result of the field screening effect. The fatigue properties of ZnO-modified PMNT ceramics was compared to Pb-based and Pb-free ferroelectric ceramics. It was found that the fatigue endurance of ZnO-modified PMNT ceramic was greater than that of hard PZT ceramic but less than that of Pb-free ferroelectric ceramic.

1. Introduction

Complex perovskite solid solution $\text{Pb}(\text{Mg}_{1/3}\text{Nb}_{2/3})_{0.65}\text{Ti}_{0.35}\text{O}_3$ (PMNT) is a well-known relaxor-based ferroelectric material that shows excellent electromechanical properties [1,2]. PMNT's extremely high piezoelectric constant and remnant polarization make it a promising material for applications such as piezoelectric actuators, piezoelectric energy harvesters and ferroelectric-based random access memories (Fe-RAMs) [3,4]. In actual applications, these devices will be under repeating electrical loading cycles, which may cause degradation in properties called electrical fatigue.

A decade ago, a large number of researchers investigated the electrical fatigue behavior of the well-known lead-based piezoelectric material, $\text{Pb}(\text{Zr,Ti})\text{O}_3$ (PZT), as well as its damage mechanisms due to electrical fatigue [5–8]. It was believed that the electrical fatigue of piezoelectric ceramics was attributed to domain pinning, and microcracks arising from large incompatible stress between grains and resultant damages [9,10]. Many publications have reported the observation of microcracks in fatigued bulk ferroelectrics [11,12], however, it was unclear whether these microcracks were a consequence of

fatigue or a main cause of fatigue. A comprehensive review article on the fatigue of ferroelectric materials was written by Glaum and Hoffman [13]. Recently, there were reports on electrical fatigue behaviors in terms of ferroelectric properties in PMNT and its related materials under a bipolar electric field, in particular in $(1-x)\text{Pb}(\text{Mg}_{1/3}\text{Nb}_{2/3})\text{O}_3$ - $x\text{PbTiO}_3$ [(1-x)PMN-xPT] materials with compositions lying in the morphotropic phase boundary ($x = 0.30$ – 0.35) [14,15]. Although there were studies on the effects of experimental parameters such as fatigue loading amplitude on fatigue behaviors of PMN-PT materials [14,16], the frequency effect, which is a significant factor contributing to electrical fatigue degradation, has not yet been well understood. It was reported that fatigue degradation rate increased at lowering fatigue frequency [17]. Majumder et al. found that polarization fatigue degradation was proportional to N/f^2 , where N and f represented cycle number and fatigue frequency, respectively [18]. Moreover, Grossmann et al. proposed that frequency had an effect on fatigue loss only in the case of incomplete domain switching [19].

In our previous work, it was found that 0.4 mol% ZnO-modified PMNT ceramics with density of 7.7 g/cm^3 (a relative density of 96%) and grain size of $3 \mu\text{m}$ have improved ferroelectric and piezoelectric

* Corresponding author.

E-mail address: m.promsawat@hotmail.com (M. Promsawat).

<http://dx.doi.org/10.1016/j.ceramint.2017.07.052>

Received 29 March 2017; Received in revised form 6 July 2017; Accepted 7 July 2017
Available online 08 July 2017

0272-8842/ © 2017 Elsevier Ltd and Techna Group S.r.l. All rights reserved.

properties [20]. Therefore, 0.4 mol% ZnO-modified PMNT ceramic will be further investigated in this work, in terms of the effects of electrical frequency on the fatigue behavior. Moreover, fatigue behavior of this ceramic system will be compared to Pb-based and Pb-free ferroelectric ceramics [21–24].

2. Experimental procedure

Pb(Mg_{1/3}Nb_{2/3})_{0.65}Ti_{0.35}O₃ (PMNT) powders were prepared by using PbO, MgO, Nb₂O₅ and TiO₂ powders as precursors. MgNb₂O₆ powders were firstly synthesized and then mixed with predetermined amounts of PbO and TiO₂ powders. The mixed powders were calcined at 850 °C for 2 h. PMNT powders were mixed with 0.4 mol% ZnO powders and then uniaxially pressed into pellets under ~ 5.5 MPa pressure. The pellets were sintered at 1240 °C for 2 h. The ZnO-modified PMNT ceramics with an average relative density of 96% were then obtained. All ceramic samples were cut and polished using 1200 grit SiC paper to a sample dimension of 1.5 × 3.5 × 3.0 mm³. The 3.5 × 3.0 mm² surface of each sample was polished using 5.0, 1.0 and 0.05 μm alumina powders, sequentially, for a mirror-like surface. All the polished samples were annealed at 500 °C for 5 h to remove any residual stress due to the polishing process. Electrode was painted on the 3.5 × 1.5 mm² surfaces using a colloidal silver paste (DT1402, Heraeus, USA). The silver-painted samples were cured at 650 °C for 15 min to decompose the organic solvent and increase the bonding strength between the electrode and the sample surfaces. Electrical fatigue tests were performed at frequencies of 5, 10, 50 and 100 Hz. For each fatigue test, a sample was submerged in silicon oil and mounted into a fixture connected to a high voltage supplier (20/20 C, Trek, USA). A bipolar sinusoidal electric field with amplitude ± 2 times of the coercive field (equivalent to ± 14 kV/cm) was applied across the electroded surfaces of the sample for up to 10⁶ cycles. At each fatigue frequency, polarization-electric field (*P-E*) curves at different cycle numbers (*N*) were recorded at its cycling frequency by a Sawyer-Tower circuit. For each *P-E* loop, remnant polarization (*P_r*) and coercive field (*E_c*) values were extracted. In order to determine the contribution of domain pinning (reversible) and field screening (irreversible) effects on the fatigue behavior of each frequency ceramic, *P-E* loops at different states; (I) before fatigue test, (II) at 10⁶ cycles fatigue test, (III) after removing damaged surfaces and (IV) after annealing at 500 °C for 2 h, were recorded. In order to determine the fatigue degradation of piezoelectric properties, percent strain-electric field (%*Strain-E*) curves at different *N* up to 10⁵ cycles were recorded by a strain sensor (ZX-TDS01T, OMRON, Japan) in conjunction with the high voltage supplier. For all the fatigue tests, the %*Strain-E* curves were measured at a frequency of 50 mHz due to the limitation of the sensor. The % *S_{total}*, which was the difference between the maximum and the minimum %*Strain*, of each %*Strain-E* curve was determined. The piezoelectric constant (*d₃₃*^{*}) was determined by the slope of a displacement-voltage curve at zero field (the result was not shown here). In the case of an asymmetric loop, *d₃₃*^{*} was averaged from both the positive and negative slopes at zero field. Microstructures of the mirror-like surface for the sample at each frequency were observed via a scanning electron microscope (SEM, JSM-6335F, JEOL, Japan). Moreover, the surface damage in a sample fatigued at 50 Hz, i.e. change of thickness in the damaged layer, was also investigated.

3. Results and discussion

3.1. Microstructures of electrically fatigued ZnO-modified PMNT ceramics

SEM images on the microstructures of the mirror-like surfaces of the samples electrically fatigued at different frequencies for 10⁶ cycles are shown in Fig. 1. Microstructural damages of the surfaces caused by electrical fatigue were observed in all the samples. The observed

surface damages are consistent with the results in the previous study [5]. It was also found that electrical fatigue had more pronounced effect on the damage of the surfaces perpendicular to the direction of the applied electric field. This is consistent with a previous observed result in Ref. [25]. Besides the damage of the surface underneath the electrode, fatigue induced cracks in the bulk region of the mirror-like surface were observed for the samples fatigued at 5 and 10 Hz, as shown in Fig. 2. The enlarged views of cracks in both the samples (5 and 10 Hz), as shown in Fig. 2(a) and (b), indicated an intergranular fracture mode. It was also observed that the number and size of cracks in a sample fatigued at a lower frequency were greater than those at a higher frequency. Thickness of damaged layer and size of cracks, represented by *L_D* and *L_C*, respectively, of ceramics were found to be decreasing with increasing frequency. *L_D* values of the samples fatigued at 5, 10, 50 and 100 Hz were equal to 165 ± 7, 121 ± 5, 98 ± 4 and 66 ± 4 μm, respectively. *L_C* values of the samples fatigued at 5 and 10 Hz were about 45 ± 2 and 19 ± 1 μm, respectively. We believe that the initiation and propagation of cracks are the cause of fatigue degradation in ferroelectric and piezoelectric properties of the ZnO-modified PMNT ceramics. This will be discussed in the next sections.

3.2. Ferroelectric/piezoelectric properties of electrically fatigued ZnO-modified PMNT ceramics

Polarization-electric field (*P-E*) curves at different *N* at frequencies of 5, 10, 50 and 100 Hz were measured. To obtain the same ferroelectric response as fatigue test, the frequency of the *P-E* loop measurement was the same as the fatigue frequency. Ferroelectric property parameters, i.e. remnant polarization (*P_r*) and coercive field (*E_c*), measured at different *N* were normalized to those measured before fatigue test. Plots of normalized *P_r* and normalized *E_c* as a function of *N* are shown in Fig. 3(a) and (b), respectively. At *N* ≤ 10³ cycles, normalized *P_r* and *E_c* of all samples did not change with the cycle number. However, the normalized *P_r* tended to decrease with further increase of *N* up to 10⁶ cycles. The normalized *E_c* increased with increasing *N* up to 10⁵ cycles and then decreased with further increasing of *N* up to 10⁶ cycles. However, for samples fatigued at 5 and 10 Hz, the normalized *E_c* did not decrease further when *N* ≥ 4 × 10⁵ cycles. As observed in previous works, the electrical fatigue degradation was attributed by field screening caused by surface damages and domain pinning [9,26,27], which will be described in the next parts.

In order to determine causes of the fatigue degradations of the ceramics, *P-E* loops at different states; (I) at the beginning of fatigue test, (II) after fatigue testing for 10⁶ cycles, (III) after removing the damaged layers and (IV) after annealing at 500 °C for 2 h, were measured. The result is shown in Fig. 4. For all frequencies samples, the *P-E* loops measured at state II were more restricted, at which the *P_r* values were much lower than those measured at state I. At State III, *P-E* loops of samples fatigued at 50 and 100 Hz were completely recovered after removing the damaged layers. However, *P-E* loops of samples fatigued at 5 and 10 Hz did not recover completely using the same technique. At State IV after the thermal annealing, the *P-E* loop of the sample fatigued at 10 Hz was completely recovered while that of the sample fatigued at 5 Hz was only partly recovered. The incomplete recovering of the *P-E* loop of the sample fatigued at 5 Hz was due to fatigue induced cracks. Although the sample fatigued at 10 Hz had cracks, nevertheless, the cracks were lesser and smaller. Hence, the *P-E* loops of the 10 Hz sample were less difficult to be recovered by layer removal and thermal annealing.

Moreover, in order to determine a relationship between the damaged layer and the change of ferroelectric properties, cycle number dependences of an average damaged layers' thickness, *P_r* and *E_c* of the sample fatigued at 50 Hz were observed, as shown in Fig. 5. At *N* ≤ 10⁵ cycles, an increased thickness of damaged layer resulted in a decrease in *P_r* and an increase in *E_c*. At *N* > 10⁵ cycles, the thickness of damaged layer only increased very slightly. At this cycle number range,

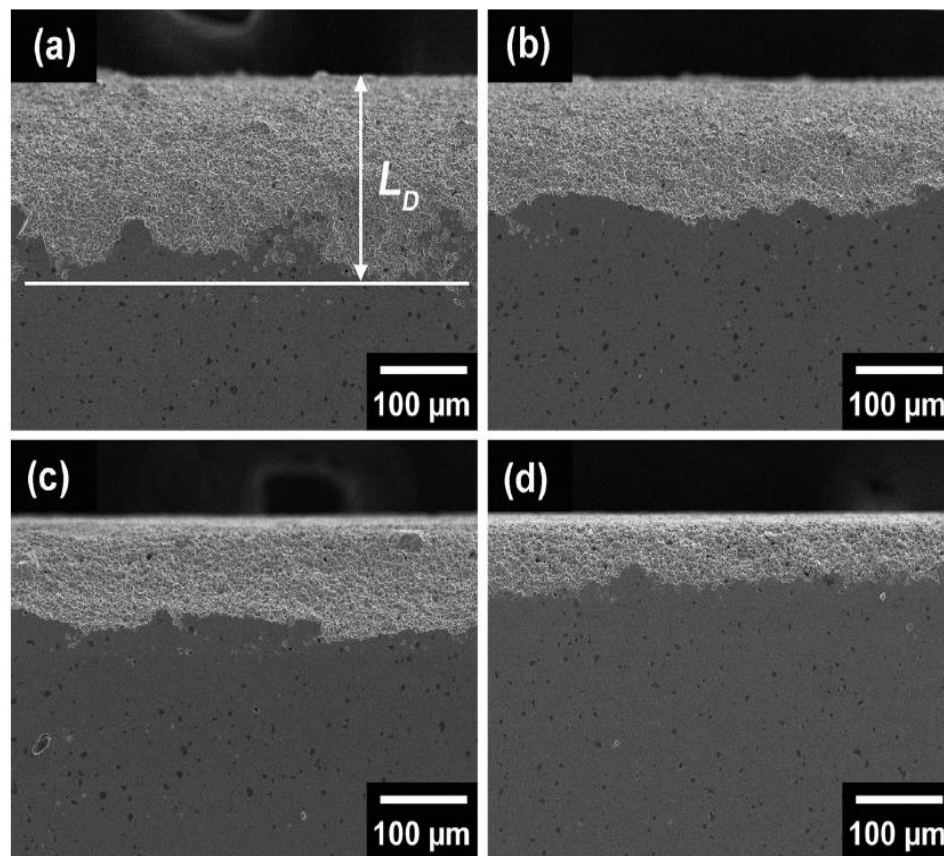


Fig. 1. SEM images of surfaces near an electrode layer of samples fatigued at (a) 5, (b) 10, (c) 50 and (d) 100 Hz for 10^6 cycles. Damaged layer thickness is denoted as L_D .

P_r continued to decrease while E_c started decreasing with increasing N to 10^6 cycles.

Fatigue induced degradation cycle number of ferroelectric properties, i.e. a cycle number at which a degradation rate of normalized P_r is maximum, was determined and given in Table 1. Degradation cycle number increased with increasing frequency. This implied faster initiations of fatigue degradations in samples fatigued at lower frequency. The %changes of the properties after 10^5 cycles of fatigue tests compared to those at the beginning of the tests were determined and given in Table 1. The magnitude of the degradation of ferroelectric properties tended to decrease with increasing frequency. It indicated that the severity of fatigue degradation of ferroelectric properties in the ceramics decreased with increasing fatigue frequency.

3.3. Electric field-induced strain of electrically fatigued ZnO-modified PMNT bulk samples

Strain versus electric field (S - E) butterfly-loops of samples fatigued at 5, 10, 50 and 100 Hz were measured at different N cycles up to 10^5 cycles, as shown in Fig. 6. For all frequencies samples, their S - E loops fatigued for 10^5 cycles were asymmetric, illustrating incomplete domain switching. For each frequency sample, a total strain ($\%S_{total}$) was determined by a difference between maximum ($\%S_{max}$) and minimum ($\%S_{min}$) strains. Moreover, d_{33}^* value was determined by a slope at zero voltage in a displacement versus voltage curve (the result is not shown here). A d_{33}^* value measured before fatigue was equal to 1700 p.m./V. For each frequency sample, $\%S_{total}$ and d_{33}^* values measured after 10^5 cycles were compared to those measured at the beginning of the test. Plots of changes in $\%S_{total}$ and d_{33}^* as a function of frequency are shown in Fig. 7(a). As frequency increased, the changes in $\%S_{total}$ and d_{33}^* decreased.

Percentages of changes in P_r and E_c after 10^6 cycles of samples fatigued at 10 Hz were compared to lead-based and lead-free ferroelectrics as shown in Table 2. The changes in ferroelectric properties of ZnO-modified PMNT ceramics were greater than those of La-doped $\text{Pb}(\text{Mg}_{1/3}\text{Nb}_{2/3})\text{O}_3$ (PMN) ceramics [9]. The change in P_r of the ceramics was not significantly different from that of 0.675 $\text{Pb}(\text{Mg}_{1/3}\text{Nb}_{2/3})\text{O}_3$ -0.325 PbTiO_3 (0.675PMN-0.325PT) ceramic [15], but the change in E_c was much lower. Moreover, a fatigue endurance of the ceramics in our work were greater than that of commercial PZT ceramics [28]. On the other hand, comparing to lead-free materials, i.e. 0.025 $\text{Bi}(\text{Mg}_{1/2}\text{Ti}_{1/2})\text{O}_3$ -0.40($\text{Bi}_{1/2}\text{K}_{1/2}$) TiO_3 -0.575($\text{Bi}_{1/2}\text{Na}_{1/2}$) TiO_3 (2.5BMT-40BKT-57.5BNT) [24], SrTiO_3 -modified $\text{Bi}_{0.5}\text{Na}_{0.5}\text{TiO}_3$ - BaTiO_3 (ST-modified BNT-BT) [29] and CaZrO_3 -modified ($\text{K}_{0.49}\text{Na}_{0.49}\text{Li}_{0.02}$)($\text{Ta}_{0.2}\text{Nb}_{0.8}$) O_3 (CZr-modified KNN) [30], ZnO-modified PMNT ceramics showed a greater magnitude of the changes in ferroelectric properties. This indicated that the fatigue endurance of ZnO-modified PMNT ceramics was lower than that of lead-free materials.

3.4. Discussion

During an application of cycling electric field, some domain walls did not move following a change of the field's direction. This might be attributed to a hindering of microscopic defects within grains which reduce the mobility of domain walls [31], causing the formation of internal stresses. Surface damages could be originated at these points when stress intensities reached the mechanical fracture toughness (K_{IC}) of the materials [32,33]. In the case of low cycling frequencies, domains experienced a longer time under local electric field in a single cycle, which promoted domain wall movements. As a result, greater stress intensities were produced, enhancing degree of surface damages.

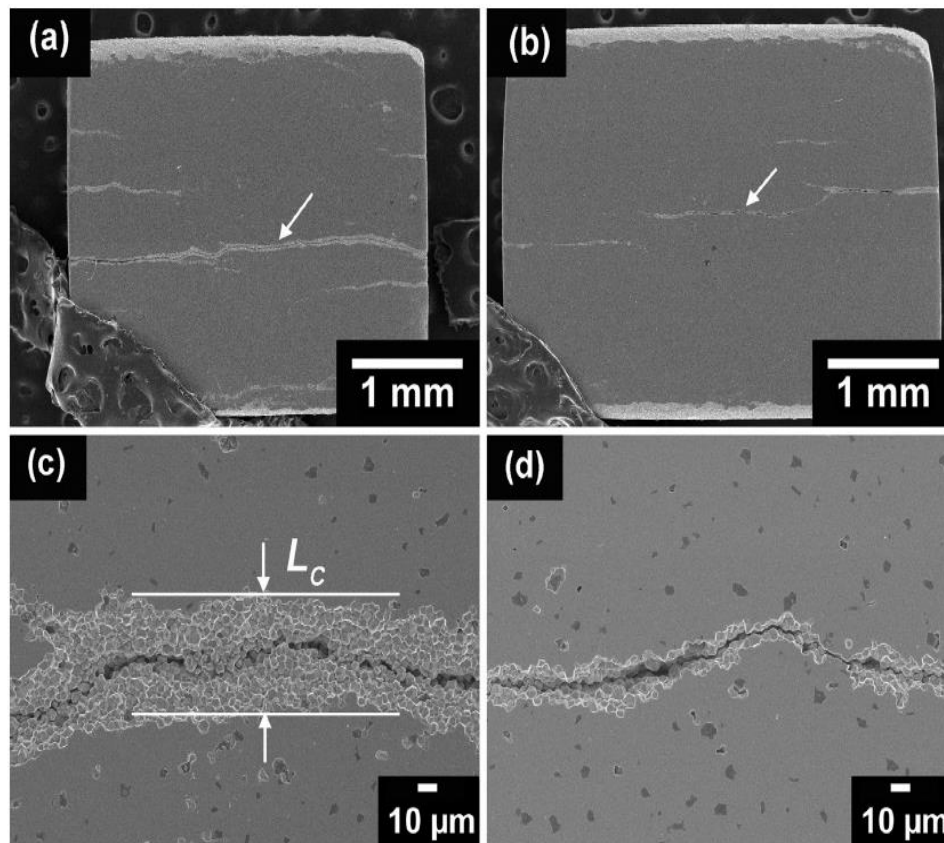


Fig. 2. SEM images of mirror-like surfaces of samples fatigued for 10^6 cycles at (a) 5 and (b) 10 Hz. Electric field induced-cracks are indicated by the arrows. Enlarged views of a crack observed in samples fatigued at 5 and 10 Hz are shown in (c) and (d), respectively. Crack width is denoted as L_c .

It was confirmed by the higher value of P_r of the P - E loops measured at lower frequencies, which was indicative of greater domain wall movements, as shown in Fig. 7(b). For samples fatigued at 5 and 10 Hz, due to the large local stresses with high intensities were produced, fatigue induced cracks were produced as a result.

From Fig. 4, the fatigue observed in the samples fatigued at 50 and 100 Hz was mainly attributed to the surface damages (the irreversible process), since their P - E loops were able to recover after removing the damaged layers. The recovery of P - E loops by removal of damaged layers was incomplete for the samples fatigued at 5 and 10 Hz. This

indicated that the degradation of ferroelectric properties due to the fatigue at 5 and 10 Hz was also attributed to the domain pinning effect (the reversible process). Under electric field at low cycling frequency, charged defects such as oxygen vacancies could move to local interfaces, i.e. domain walls, and obstructed domains from switching, resulting in the degradation of ferroelectric properties [34]. When thermally annealed, the P - E loop of the sample fatigued at 10 Hz was completely recovered. However, the P - E loop of the sample fatigued at 5 Hz only improved slightly after the sample was thermally annealed. This could be caused by the presence of the large sized cracks formed

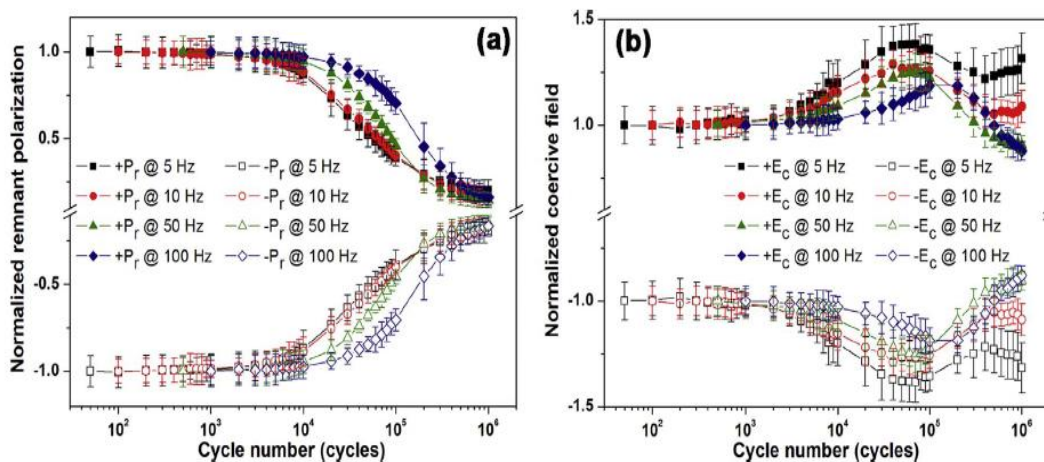


Fig. 3. Plots of (a) normalized remnant polarization and (b) normalized coercive field as a function of cyclic number of the samples under bipolar electric fields with an amplitude of ± 14 kV/cm at frequencies of 5, 10, 50 and 100 Hz.

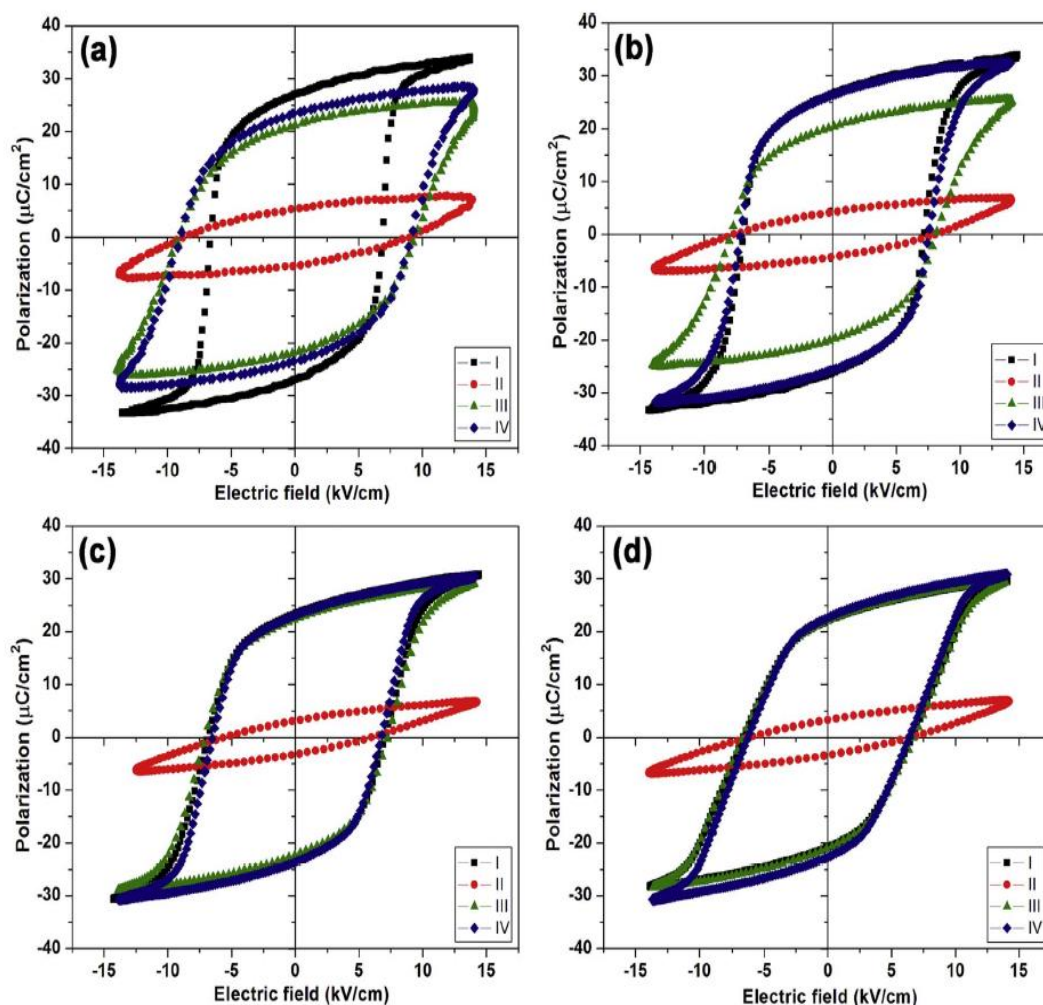


Fig. 4. P - E loops measured (I) before fatigue test, (II) at 10^5 cycles fatigue test, (III) after removing the damaged layers and (IV) after annealing at $500\text{ }^{\circ}\text{C}$ for 2 h of the samples fatigued at (a) 5, (b) 10, (c) 50 and (d) 100 Hz.

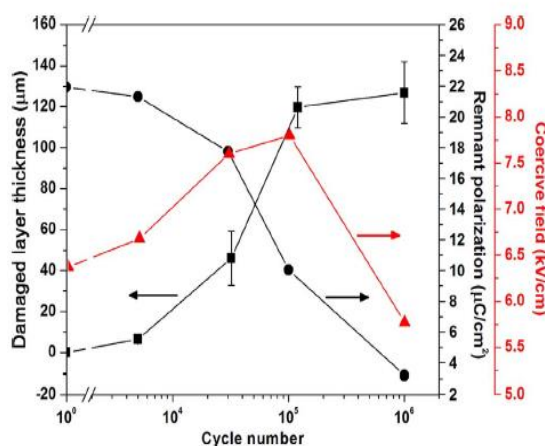


Fig. 5. Plots of damaged layer thickness, remnant polarization and coercive field as a function of cycle number of ZnO-modified PMNT ceramic fatigued at 50 Hz.

by the fatigue. From above discussion, greater microstructural damages, i.e. the damage of the electrode surfaces and the fatigue induced cracks, were resulted under lower cycling frequency, contributing to the larger degradation of ferroelectric and piezoelectric properties, i.e. the decrease in P_r , $\%S_{\text{total}}$ and d_{33}^* , and the increase in

Table 1
Electrical fatigue behaviors of ferroelectric properties after fatigue testing for 10^5 cycles at different frequencies of ZnO-modified PMNT ceramics.

Frequency (Hz)	N (cycles)	% change in normalized P_r	% change in normalized E_c
5	30,000	-61	+36
10	63,000	-60	+26
50	86,000	-54	+22
100	140,000	-29	+19

Note: N represents the cycle number at which the normalized P_r decreases.

E_c of the materials.

As shown in Fig. 5, at $N \leq 10^5$ cycles, the drop of P_r with decreasing E_c was attributed to the formation of damaged layers that had low ferroelectricity and dielectric properties, i.e. a low P_r , a high E_c and a low dielectric constant [35]. It should be noted that at this range of cycle number the screened electric field from field screening effect was still higher than the E_c of the material, thus promoting a complete domain switching. At $N > 10^5$ cycles, although the thickness of the damaged layer only increased slightly, it was believed that microcracks could be formed by fatigue at such large cycle numbers. Therefore, at $N > 10^5$ cycles, the applied field was screened by both the damaged layers and the microcracks. This caused the decrease in the amplitude of the field acting on the undamaged layer. The field amplitude could be lower

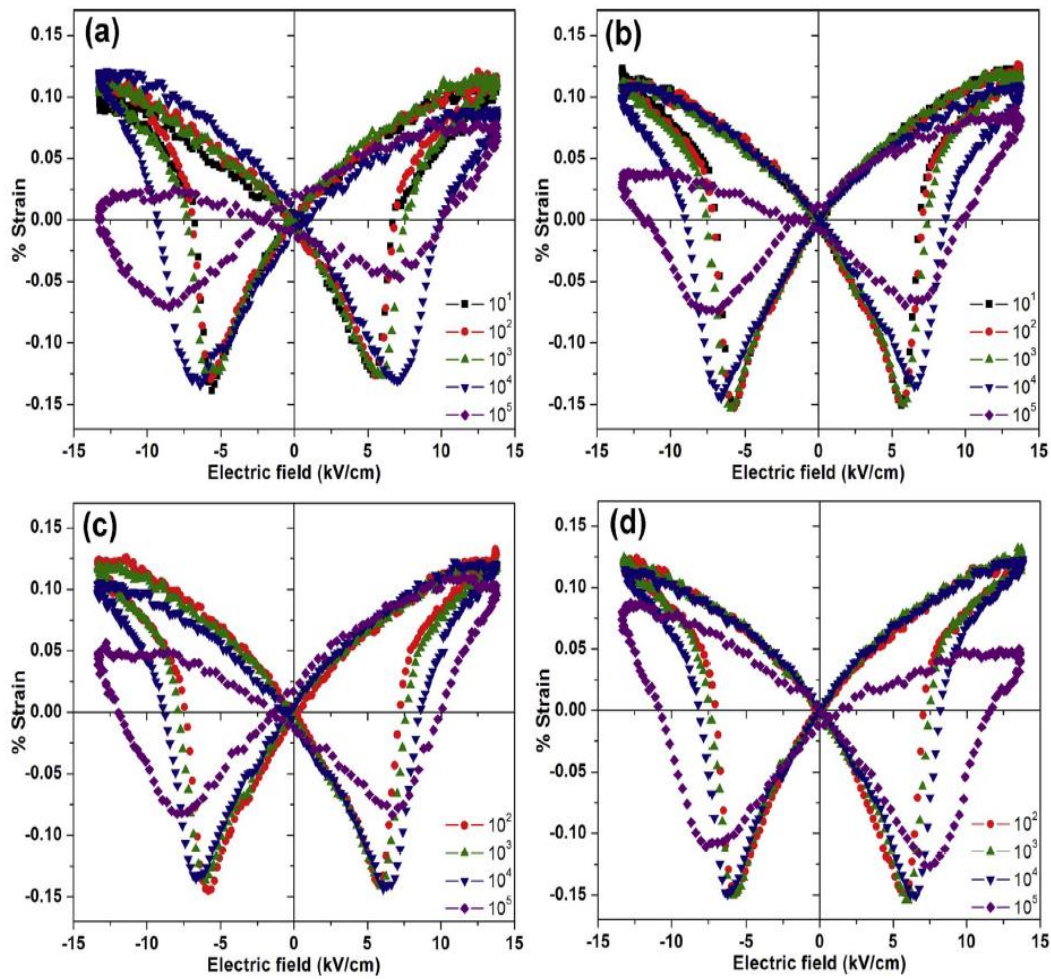


Fig. 6. %Strain versus electric field loops measured at different cycle numbers of the samples fatigued at (a) 5, (b) 10, (c) 50 and (d) 100 Hz.

than the E_c of the material. An application of the electric field with such amplitude resulted in incomplete switching of the domains in the undamaged layer, thereby leading to the lowered P_r of the ceramic. Moreover, the incomplete switching of the domains also resulted in the lowered interaction strength between the domains. Subsequently, the

material required a lower amplitude of the field used for switching its domains, resulting in the decrease in E_c of the ceramic.

It was proposed by Lou that the factors influenced on the fatigue behaviors of ferroelectric ceramics include: (i) type of electrode material, (ii) quality of material-electrode interface, (iii) crystal struc-

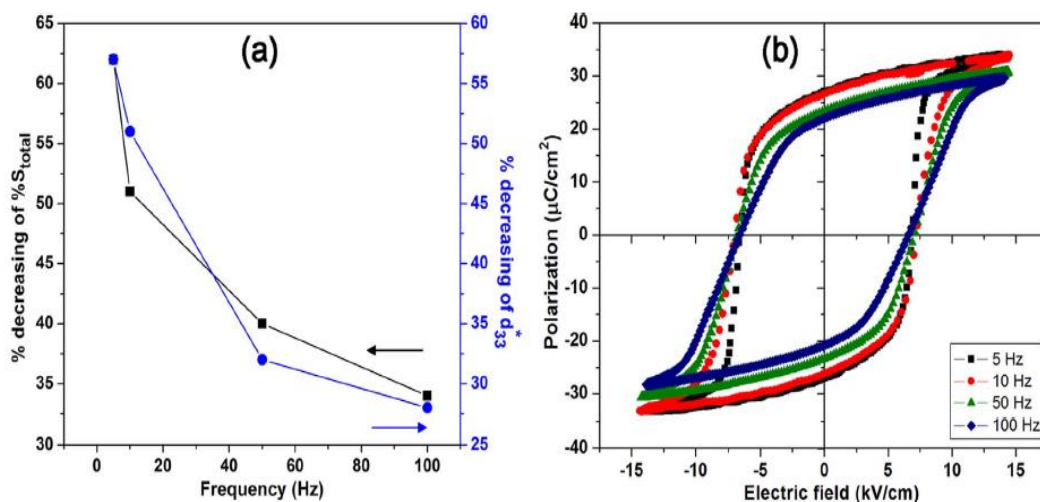


Fig. 7. (a) Plots of percent decrease in $\%S_{total}$ and d_{33}^* as a function of fatigue frequencies and (b) P - E loops measured at frequencies of 5, 10, 50 and 100 Hz of an unfatigued sample.

Table 2

Percent changes in remnant polarization and coercive field of ZnO-modified PMNT ceramics compared with those of lead-based and lead-free ferroelectric ceramics available in the literature.

Material	Cycling frequency, field ^a	Cycle numbers	% change in P_r	% change in E_c	Refs.
ZnO-modified PMNT	10 Hz, $2E_c$	10^6	–83	+9	This work
1%La-doped PMN	–	10^6	–1	0	[9]
0.675PMN-0.325PT	10 Hz, $3E_c$	10^6	–72	+82	[15]
PZT	10 Hz, $2E_c$	5×10^5	–63	+49	[28]
2.5BMT-40BKT-57.5BNT	10 Hz, $3.3E_c$	10^6	–1	–2	[24]
ST-modified BNT-BT	10 Hz, $2E_c$	10^6	–1	–23	[29]
CZr-modified KNN	50 Hz, $2E_c$	10^6	–6	–4	[30]

^a The maximum electric field is in multiples of the coercive field.

ture of material, (iv) crystal microstructure including composition, grain size and porosity, (v) doping with other elements, (vi) processing conditions used in fabrication of material and (vii) direction of property measurement in respect to fatigue cycling direction [36]. From the comparison in Table 2, different fatigue behaviors of ZnO-modified PMNT ceramics and the PZT ceramic could be caused by their difference in crystal structure. The PZT ceramic has a tetragonal phase (K350, Piezo Technologies, Indianapolis, IN, USA) while the ZnO-modified PMNT ceramic has a combination of monoclinic and tetragonal phases [20]. For PMN-based materials, a greater fatigue degradation could be caused by the higher degree of tetragonality. This was supported by an observed result investigated by Jiang et al., where the fatigue degradations of materials with a rhombohedral symmetry were much lower than those of materials with tetragonal or orthorhombic symmetries [9]. The excellent fatigue endurance of lead-free ceramics could be due to a low concentration of intrinsic defects such as cation and anion vacancies [23], an increase in ergodicity and a lack of induced tetragonality during fatigue cycles [37]. From the comparison, the fatigue resistance of the ZnO-modified PMNT ceramic was slightly greater than that of a soft PZT ceramic, but poorer than that of the lead-free piezoelectric ceramics. Therefore, for the applications such as actuators and FRAMs, the fatigue endurance of ZnO-modified PMNT need to be further improved, which required further investigation.

4. Conclusions

Electrical fatigue tests on ZnO-modified $\text{Pb}(\text{Mg}_{1/3}\text{Nb}_{2/3})_{0.65}\text{Ti}_{0.35}\text{O}_3$ ceramics at frequencies of 5, 10, 50 and 100 Hz were studied. Surface damages underneath the electrodes were observed in all samples, while electrical fatigue induced cracks in the bulk were only observed in the samples fatigued at 5 and 10 Hz. Thickness of the damaged layers and size of the cracks decreased with increasing frequency. Fatigue degradations in samples at lower frequencies were initiated faster than those at higher frequencies. The changes of P_r , E_c , %Strain and d_{33}^* decreased with increasing frequency. Local fatigue induced strain by the applied electric fields was reduced with an increase in frequency. This contributed to the lowering degree of fatigue induced surface damages and, consequently, less degradations of properties. Fatigue behaviors of the samples at low frequency could be caused by both reversible (domain pinning effect) and irreversible (surfaces damage) processes. At high frequency, the irreversible process had more pronounced effect on the fatigue behaviors. The fatigue endurance of ZnO-modified PMNT ceramic was slightly greater than that of a PZT ceramic but poorer than that of monolithic PMN and lead-free piezoelectric ceramics. Therefore, further development is needed on the crystal structure and microstructure of ZnO-modified PMNT in order to use it for actuator and FERAM applications.

Acknowledgements

This research was supported by Natural Rubber Innovation Research Institute, Prince of Songkla University (Grant No.

SCI601093S). SJ would like to thank the Thailand Research Fund (TRF, Grant no. RSA5780032). SP and ZL would like to acknowledge the Royal Academy of Engineering (UK) and Office for Higher Education (Thailand) Coordination's Industry Academia Partnership Programme (IAPPT2/100000).

References

- [1] M. Alguero, A. Moure, J. Pardo, J. Holc, M. Kosec, Processing by mechano synthesis and properties of piezoelectric $\text{Pb}(\text{Mg}_{1/3}\text{Nb}_{2/3})\text{O}_3$ - PbTiO_3 with different compositions, *Acta Mater.* 54 (2006) 501–511.
- [2] Z.-G. Ye, High-performance piezoelectric single crystals of complex perovskite solid solutions, *Mater. Res. Bull.* 34 (2009) 277–283.
- [3] Y. Chen, K.H. Lam, D. Zhou, W.F. Cheng, J.Y. Dai, H.S. Luo, H.L.W. Chan, High frequency PMN-PT single crystal focusing transducer fabricated by a mechanical dimpling technique, *Ultrasonics* 53 (2013) 345–349.
- [4] G.-T. Hwang, H. Park, J.-H. Lee, S. Oh, K.-I. Park, M. Byun, H. Park, G. Ahn, C.K. Jeong, K. No, H.-S. Kwon, S.-G. Lee, B. Joung, K.J. Lee, Self-powered cardiac pacemaker enabled by flexible single crystalline PMN-PT piezoelectric energy harvester, *Adv. Mater.* 26 (2014) 4880–4887.
- [5] N. Balke, H. Kungl, T. Granzow, D.C. Lupascu, M.J. Hoffmann, J. Rödel, Bipolar fatigue caused by field screening in $\text{Pb}(\text{Zr,Ti})\text{O}_3$ ceramics, *J. Am. Ceram. Soc.* 90 (2007) 3869–3874.
- [6] J. Glaum, T. Granzow, J. Rödel, Evaluation of domain wall motion in bipolar fatigued lead-zirconate-titanate: a study on reversible and irreversible contributions, *J. Appl. Phys.* 107 (2010) 104119/1–6.
- [7] F.W. Zeng, H. Wang, H. Lin, Fatigue and failure response of lead zirconate titanate multilayer actuator under unipolar high-field electric cycling fatigue, *J. Appl. Phys.* 114 (2013) 024101/1–9.
- [8] D.A. Hall, T. Mori, T.P. Conyn, E. Ringgaard, J.P. Wright, Residual stress relief due to fatigue in tetragonal lead zirconate titanate ceramics, *J. Appl. Phys.* 114 (2013) 024101/1–9.
- [9] Q.Y. Jiang, E.C. Subbarao, L.E. Cross, Effect of composition and temperature on electric fatigue of La-doped lead zirconate titanate ceramics, *J. Appl. Phys.* 75 (1994) 7433–7443.
- [10] L. Jin, F. Li, S. Zhang, Decoding the fingerprint of ferroelectric loops: comprehension of the material properties and structures, *J. Am. Ceram. Soc.* 97 (2014) 1–27.
- [11] J. Nuffer, D.C. Lupascu, J. Rödel, Microcrack clouds in fatigued electrostrictive 9.5/65/35 PLZT, *J. Eur. Ceram. Soc.* 21 (2001) 1421–1423.
- [12] J. Nuffer, D.C. Lupascu, A. Glazounov, H.J. Kleebe, J. Rödel, Microstructural modifications of ferroelectric lead zirconate titanate ceramics due to bipolar electric fatigue, *J. Eur. Ceram. Soc.* 22 (2002) 2133–2142.
- [13] J. Glaum, M. Hoffman, Electric fatigue of lead-free piezoelectric materials, *J. Am. Ceram. Soc.* 97 (2014) 665–680.
- [14] D. Lin, Z. Li, Z.-Y. Cheng, Z. Xu, X. Yao, Electric-field-induced polarization fatigue of [001]-oriented $\text{Pb}(\text{Mg}_{1/3}\text{Nb}_{2/3})\text{O}_3$ -0.32 PbTiO_3 single crystals, *Solid State Commun.* 151 (2011) 1188–1191.
- [15] Y. Yan, Y. Zhou, S. Gupta, S. Priya, Fatigue mechanism of textured $\text{Pb}(\text{Mg}_{1/3}\text{Nb}_{2/3})\text{O}_3$ - PbTiO_3 ceramics, *Appl. Phys. Lett.* 103 (2013) 082906/1–5.
- [16] E.A. McLaughlin, T. Liu, C.S. Lynch, Relaxor ferroelectric PMN-32%PT crystals under stress and electric field loading: i-32 mode measurements, *Acta Mater.* 52 (2004) 3849–3857.
- [17] K. Lee, B.R. Rhee, C. Lee, Characteristics of ferroelectric $\text{Pb}(\text{Zr,Ti})\text{O}_3$ thin films having Pt/PtO₂ electrode barriers, *Appl. Phys. Lett.* 79 (2001) 821–823.
- [18] S.B. Majumder, Y.N. Mohapatra, D.C. Agrawal, Fatigue resistance in lead zirconate titanate thin ferroelectric films: effect of cerium doping and frequency dependence, *Appl. Phys. Lett.* 70 (1997) 138–140.
- [19] M. Grossmann, D. Bolten, O. Lohse, U. Boettger, R. Waser, S. Tiedke, Correlation between switching and fatigue in $\text{PbZr}_{0.3}\text{Ti}_{0.7}\text{O}_3$ thin films, *Appl. Phys. Lett.* 77 (2000) 1894–1896.
- [20] M. Promsawat, A. Watcharaprasorn, Z.-G. Ye, S. Jansirisomboon, Enhanced dielectric and ferroelectric properties of $\text{Pb}(\text{Mg}_{1/3}\text{Nb}_{2/3})_{0.65}\text{Ti}_{0.35}\text{O}_3$ ceramics by ZnO modification, *J. Am. Ceram. Soc.* 98 (2015) 848–854.
- [21] S. Pojprapai, J. Russell, H. Man, J.L. Jones, J.E. Daniels, M. Hoffman, Frequency effects on fatigue crack growth and crack tip domain-switching behavior in a lead

- zirconate titanate ceramic, *Acta Mater.* 57 (2009) 3932–3940.
- [22] Z. Luo, J. Glaum, T. Granzow, W. Jo, R. Dittmer, M. Hoffman, J. Rödel, Bipolar and unipolar fatigue of ferroelectric BNT-based lead-free piezoceramics, *J. Am. Ceram. Soc.* 94 (2011) 529–535.
- [23] E.A. Patterson, D.P. Cann, Bipolar piezoelectric fatigue of $\text{Bi}(\text{Zn}_{0.5}\text{Ti}_{0.5})\text{O}_3$ - $(\text{Bi}_{0.5}\text{K}_{0.5})\text{TiO}_3$ - $(\text{Bi}_{0.5}\text{Na}_{0.5})\text{TiO}_3$ Pb-free ceramics, *Appl. Phys. Lett.* 101 (2012) (042905/1–6).
- [24] N. Kumar, D.P. Cann, Electromechanical strain and bipolar fatigue in $\text{Bi}(\text{Mg}_{1/2}\text{Ti}_{1/2})\text{O}_3$ - $(\text{Bi}_{1/2}\text{K}_{1/2})\text{TiO}_3$ - $(\text{Bi}_{1/2}\text{Na}_{1/2})\text{TiO}_3$ ceramics, *J. Appl. Phys.* 114 (2013) (054102/1–6).
- [25] D.N. Fang, Y.H. Zhang, G.Z. Mao, Electric-field-induced fatigue crack growth in ferroelectric ceramics, *Theor. Appl. Fract. Mech.* 54 (2010) 98–104.
- [26] C. Brennan, Model of ferroelectric fatigue due to defect/domain interactions, *Ferroelectrics* 150 (1993) 199–208.
- [27] J. Glaum, T. Granzow, L.A. Schmitt, H.J. Kleebe, J. Rödel, Temperature and driving field dependence of fatigue processes in PZT bulk ceramics, *Acta Mater.* 59 (2011) 6083–6092.
- [28] Z. Luo, S. Pojprapai, J. Glaum, M. Hoffman, Electrical fatigue-induced cracking in lead zirconate titanate piezoelectric ceramic and its influence quantitatively analyzed by refatigue method, *J. Am. Ceram. Soc.* 95 (2012) 2593–2600.
- [29] C. Tian, F. Wang, X. Ye, Y. Xie, T. Wang, Y. Tang, D. Sun, W. Shi, Bipolar fatigue-resistant behavior in ternary $\text{Bi}_{0.5}\text{Na}_{0.5}\text{TiO}_3$ - BaTiO_3 - SrTiO_3 solid solutions, *Scr. Mater.* 83 (2014) 25–28.
- [30] F.-Z. Yao, E.A. Patterson, K. Wang, W. Jo, J. Rödel, J.-F. Li, Enhanced bipolar fatigue resistance in CaZrO_3 -modified $(\text{K},\text{Na})\text{NbO}_3$ lead-free piezoceramics, *Appl. Phys. Lett.* 104 (2014) (242912/1–5).
- [31] D. Lupascu, J. Rödel, Fatigue in bulk lead zirconate titanate actuator materials, *Adv. Eng. Mater.* 7 (2005) 882–898.
- [32] Q.Y. Jiang, E.C. Subbarao, L.E. Cross, Grain size dependence of electric fatigue behavior of hot pressed PLZT ferroelectric ceramics, *Acta Metall. Mater.* 42 (1994) 3687–3694.
- [33] J. Shieh, J.E. Huber, N.A. Fleck, Fatigue crack growth in ferroelectrics under electrical loading, *J. Eur. Ceram. Soc.* 26 (2006) 95–109.
- [34] Y.A. Genenko, J. Glaum, M.J. Hoffmann, K. Albe, Mechanisms of aging and fatigue in ferroelectrics, *Mater. Sci. Eng. B* 192 (2015) 52–82.
- [35] W. Li, R.M. McMeeking, C.M. Landis, On the crack face boundary conditions in electromechanical fracture and an experimental protocol for determining energy release rates, *Eur. J. Mech. A Solids* 27 (2008) 285–301.
- [36] X.J. Lou, Polarization fatigue in ferroelectric thin films and related materials, *J. Appl. Phys.* 105 (2009) (024101/1–24).
- [37] N. Kumar, T.Y. Ansell, D.P. Cann, Role of point defects in bipolar fatigue behavior of $\text{Bi}(\text{Mg}_{1/2}\text{Ti}_{1/2})\text{O}_3$ modified $(\text{Bi}_{1/2}\text{K}_{1/2})\text{TiO}_3$ - $(\text{Bi}_{1/2}\text{Na}_{1/2})\text{TiO}_3$ relaxor ceramics, *J. Appl. Phys.* 115 (2014) (154104/1–9).

ภาคผนวก 2
ผลงานที่นำเสนอในประชุมวิชาการระดับชาติ



การประชุมวิชาการวิทยาศาสตร์และเทคโนโลยี
แห่งประเทศไทย ครั้งที่ 41 (วทท 41)

THE 41st CONGRESS ON SCIENCE AND TECHNOLOGY
OF THAILAND (STT41)

ประตูสู่อาเซียนด้วยวิทยาศาสตร์และเทคโนโลยี
"Gateway to ASEAN with Science and Technology"



Scientific Sessions Program Book

November 6-8, 2015

Suranaree University of Technology
Nakhon Ratchasima, Thailand

Organized by:
The Science Society of Thailand under the Patronage of His Majesty the King
Suranaree University of Technology, Nakhon Ratchasima, Thailand
<http://www.scisoc.or.th/stt41>

Surface morphology of the films were examined using atomic force microscopy and scanning electron microscopy. The chemical structures of the films were characterized by Raman spectroscopy. Furthermore, Wetting property of the films was characterized using a water contact angle measurement and optical property was examined by UV-vis spectrophotometry. The results have shown that the surface roughness and anatase/rutile phase transformation of the annealed TiO₂ films increased with increasing of the treatment time. Moreover, the optical property and wettability of the as-deposited and the annealed films will be reported and discussed. (abstract only)

D_D0005: IMPROVEMENT OF FERROELECTRIC AND PIEZOELECTRIC PROPERTIES OF Pb(Mg_{1/3}Nb_{2/3})_{0.65}Ti_{0.35}O₃ CERAMICS BY ZnO MODIFICATION

Methee Promsawat,¹ Anucha Watcharapasorn,¹ Soodkhet Pojprapai,² Zuo-Guang Ye,³ Sukanda Jiansirisomboon^{2,*}

¹Department of Physics and Materials Science, Faculty of Science, Chiang Mai University, Chiang Mai 50200, Thailand

²School of Ceramic Engineering, Suranaree University of Technology, Nakhon Ratchasima 30000, Thailand

³Department of Chemistry and 4D LABS, Simon Fraser University, Burnaby, British Columbia V5A 1S6, Canada

*e-mail: sukanda.jian@cmu.ac.th

Abstract: In this work, Pb(Mg_{1/3}Nb_{2/3})_{0.65}Ti_{0.35}O₃ (PMNT) ceramics modified with ZnO were prepared via a mixed oxide and sintering technique. Different contents of ZnO were incorporated into PMNT to form PMNT/xZnO ceramics, where $x = 0, 0.4, 2.0, 4.0$ and 10.0 mol%. The ceramics were characterized in terms of ferroelectric and piezoelectric properties. The results show that the remnant polarization (P_r) of the monolithic PMNT ceramic increases while the coercive field (E_c) slightly decreases with 0.4-4.0 mol% ZnO incorporations. However, P_r decreases while E_c increases as the ZnO content increases to 10.0 mol%. The unipolar piezoelectric constant (d_{33}^*) and the electric field-induced strain of the PMNT ceramic are improved with 0.4-2.0 mol% ZnO modifications. They decrease with further increasing ZnO content. The quasi-static piezoelectric constant (d_{33}) and the electromechanical coupling factor (k_p) of the PMNT ceramic are enhanced with an incorporation of 0.4 mol% ZnO. They tend to decrease with increasing ZnO content above 2.0 mol%. The enhancement of the properties is attributed to increasing of the densities and grain sizes of the 0.4-4.0 mol% ZnO-modified ceramics. For the higher ZnO content ceramics, the decrease in density and the observation of a secondary phase are believed to be contributed to the degradation of the ceramics' properties. It is found that the optimum ZnO content is 0.4 mol% which makes the ceramic showing good properties and promising for high performance piezoelectric actuators. (abstract only)

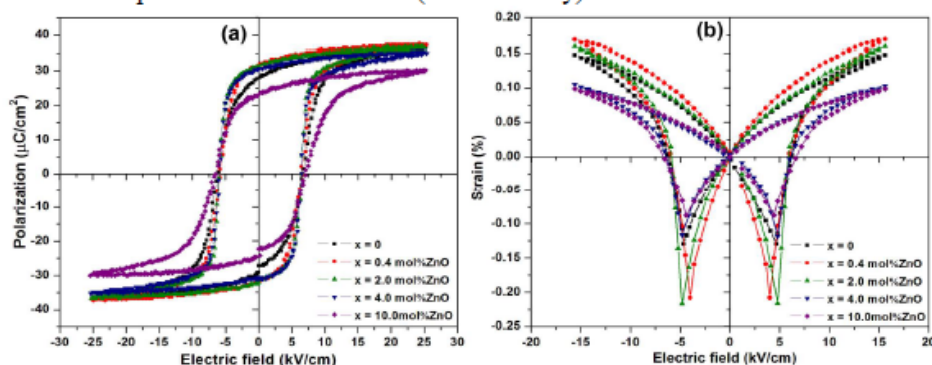


Figure 1. (a) Polarization-electric field curves measured at 1 Hz and (b) strain-electric field curves measured at 50 mHz of PMNT/xZnO ceramics

break of PVAM-g-BDO were found at 7:3 PVAM: BDO and its value was 253% and 700%, respectively. Moreover, the maximum tensile strength of PVAM-g-BDO was observed at 9:1 PVAM:BDO. Finally, the PVAM-g-BDO was used a polymer matrix for the encapsulation of capsaicin. Results showed that the rate of the capsaicin release from polymer matrix in water medium increase as a function of water immersion time and capsaicin content. After its use, it was easily degraded in nature soil. (abstract only)

D_D0003: PIEZOELECTRIC PERFORMANCE OF LEAD-FREE

$(1-x-y)\text{Bi}_{0.5}(\text{Na}_{0.80}\text{K}_{0.20})_{0.5}\text{TiO}_3-0.005\text{LiNbO}_3-y\text{BaTiO}_3$ TERNARY SYSTEM

Pimpilai Wannasut,¹ Pharatree Jaita,¹ Anucha Watcharapasorn,^{1,2} Sukanda Jiansirisomboon^{3,*}

¹Department of Physics and Materials Science, Faculty of Science, Chiang Mai University, Chiang Mai 50200, Thailand

²Materials Science Research Center, Faculty of Science, Chiang Mai University, Chiang Mai 50200, Thailand

³School of Ceramic Engineering, Suranaree University of Technology, Nakhon Ratchasima, 30000, Thailand

*e-mail: sukanda.jian@cmu.ac.th

Abstract: The ternary system of $(1-x-y)\text{Bi}_{0.5}(\text{Na}_{0.80}\text{K}_{0.20})_{0.5}\text{TiO}_3-x\text{LiNbO}_3-y\text{BaTiO}_3$ or $(1-x-y)\text{BNKT}-x\text{LN}-y\text{BT}$ lead free piezoelectric (when $x = 0.005$, $y = 0, 0.01, 0.02, 0.03, 0.04, 0.05, 0.06$ and 0.07 mol fraction) have been prepared by conventional and sintering at 1125°C for 2h. The relative density of all sample higher than 97% of their theoretical values. X-ray diffraction pattern showed a single perovskite structure without any secondary phase and showed the mixed rhombohedral and tetragonal phase. Fracture surface of BNKT-0.005LN-BT indicated switch from mixed inter-granular fracture to mainly transgranular fracture. The maximum electrical field-induced strain behavior ($S_{\text{max}} = 0.25\%$, $S_{\text{neg}} = -0.09\%$, $d_{33}^* = 833$ pm/V) was observed for BNKT-0.005LN-0.04BT ceramics. (abstract only)

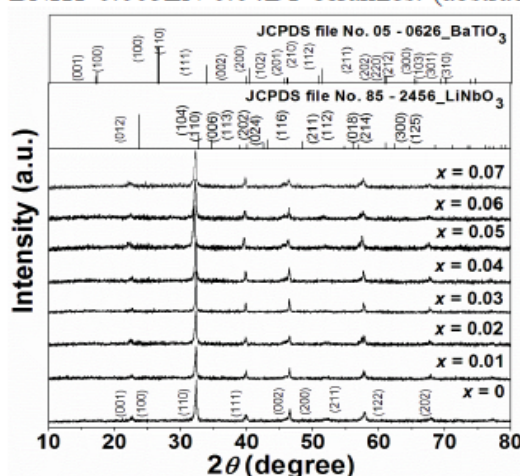


Figure 1. X-ray diffraction pattern of $(1-x-y)\text{BNKT}-x\text{LN}-y\text{BT}$ ceramics

D_D0004: EFFECT OF HOT AIR BLOW HEAT TREATMENT ON PROPERTIES OF TiO_2 FILMS PREPARED BY SPARKING PROCESS

Arisara Panthawan,¹ Wiradej Thongsuwan,^{1,2} Pisith Singjai^{1,2,*}

¹Materials Science Research Center, Department of Physics and Materials Science, Faculty of Science, Chiang Mai University, Chiang Mai 50200, Thailand

²Nanomaterials Research Laboratory, Department of Physics and Materials Science, Faculty of Science, Chiang Mai University, Chiang Mai 50200, Thailand

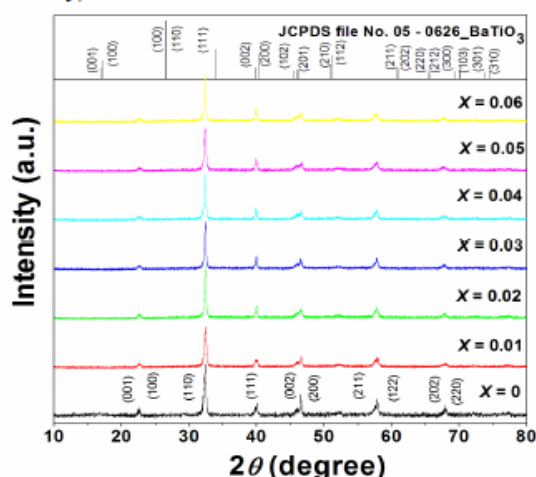
*e-mail: pisith.s@cmu.ac.th

Abstract: The study was conducted to find out the effect of hot air blow heat treatment of TiO_2 films. TiO_2 films were prepared by a sparking process on glass substrate. The films were annealed using a simple and low cost hot air blow at different periods (1-60 min).

D_D0001: PREPARATION AND CHARACTERIZATION OF LEAD-FREE **$\text{Bi}_{0.5}(\text{Na}_{0.80}\text{K}_{0.20})_{0.5}\text{TiO}_3-(\text{Ba}_{0.7}\text{Sr}_{0.3})\text{TiO}_3$ PIEZOELECTRIC CERAMICS**Suphakarn Faichaekhammun,¹ Pimpilai Wannasut,¹ Pharatree Jaita,¹ Methee Promsawat,¹Anucha Watcharapasorn,^{1,2} Sukanda Jiansirisomboon^{3,*}¹Department of Physics and Materials Science, Faculty of Science, Chiang Mai University, Chiang Mai 50200, Thailand²Materials Science Research Center, Faculty of Science, Chiang Mai University, Chiang Mai 50200, Thailand³School of Ceramic Engineering, Suranaree University of Technology, Nakhon Ratchasima 30000, Thailand

*e-mail: sukanda.jian@cmu.ac.th

Abstract: The binary system of $(1-x)\text{Bi}_{0.5}(\text{Na}_{0.8}\text{K}_{0.2})_{0.5}\text{TiO}_3-(\text{Ba}_{0.7}\text{Sr}_{0.3})\text{TiO}_3$ or $(1-x)\text{BNKT}-x\text{BST}$ lead-free piezoelectric ceramics with $x = 0, 0.01, 0.02, 0.03, 0.04, 0.05$ and 0.06 mol fraction were synthesized by a solid state reaction method and sintered at 1125°C for 2 h. The effects of BST content on the phase equilibria, the dielectric, ferroelectric and piezoelectric responses were systematically investigated. All BNKT-BST samples had relative density greater than 98% of their theoretical values. X-ray diffraction pattern showed a single perovskite structure with a mixed rhombohedral and tetragonal phase. SEM micrograph of all samples showed a cubic liked grain shape. The maximum dielectric constant at room temperature (ϵ_r) of 1411 was obtained for BNKT-0.01BST sample. The addition of BST was also found to improve the ferroelectric and piezoelectric properties of BNKT ceramic. (abstract only)

Figure 1. X-ray diffraction pattern of $(1-x)\text{BNKT}-x\text{BST}$ ceramics**D_D0002: PREPARATION AND PHYSICAL PROPERTIES OF MALEATED POLY(VINYL ALCOHOL) GRAFTED WITH 1,4-BUTANE DIOL**Sa-Ad Riyajan,^{1,*} Suhaila Bunlangok²¹Department of Chemistry, Faculty of Science and Technology, Thammasat University, Pathumthani 12120, Thailand²Department of Materials Science and Technology, Faculty of Science, Prince of Songkla University, Songkhla 90110, Thailand

*e-mail: saadriyajan@hotmail.com

Abstract: Nowadays, hydrogels are widely used in many fields such as biosensor, engineering tissue and agriculture due to their high swelling behavior in water and softness. The objective of this work was to study the preparation and physical properties of maleated poly(vinyl alcohol) (PVA)-g-butanediol (BDO) (PVAM-g-BDO) by using $\text{K}_2\text{S}_2\text{O}_8$ as an initiator. The swelling behavior of the PVAM-g-BDO was increased with increasing BDO content. After incorporation of the BDO into of the PVAM, the glass transition temperature of the PVAM decreased observed by DMTA. The highest swelling ratio and elongation at



The 10th Annual Siam Physics Congress 2015

On the Occasion of the 60th Birthday Anniversary Celebration of
Her Royal Highness Princess Maha Chakri Sirindhorn



The Centennial Celebration of General Relativity Theory
and 80 Years of Thai Physics Graduate

20-22 May 2015
Sofitel Krabi Phokeethra Golf and Spa Resort,
Krabi, Thailand



- MNA-29 Effects of Zn Substituted on the Structure of Hydroxyapatite Synthesized from Waste Chicken Eggshells
PAIKAEW, Chutharat
- MNA-30 Strongly Enhanced Dielectric Response and Dielectric Relaxation in BaTiO_3 /poly(vinylidene fluoride) Nanocomposites
SILAKAEW, Kanyapak
- MNA-31 Thermal and Electrical Properties of P_2O_5 - CaO - Na_2O Glass Containing $\text{Ba}_{0.6}\text{Sr}_{0.4}\text{TiO}_3$
INTAWIN, Pratthana
- MNA-32 Crystallization and Dielectric Properties of Nd^{3+} Doped Ferroelectric Glass-Ceramics in the Na_2O - BaO - Nb_2O_5 - SiO_2 System
BOONSONG, Paitoon
- MNA-33 Giant Dielectric Properties and Electrical Response Grain Boundary of $\text{Na}_{1/3}\text{Ca}_{1/3}\text{La}_{1/3}\text{Cu}_3\text{Ti}_4\text{O}_{12}$ Ceramics
SAENGVONG, Pariwat
- MNA-34 Effect of Annealing Temperature on the Magnetic Properties of Fe Doped SrTiO_3 Nanoparticles
WANNASEN, Likkhasit
- MNA-35 Synchrotron X-ray Absorption Spectroscopy Study of Local Structure in Hydroxyapatite Doped by Strontium
BOOTCHANONT, Atipong
- MNA-36 Preparation and dielectric properties of poly (vinylidene fluoride hexafluoropropylene) fibers
NAWAKA, Kanokwan
- MNA-37 Influence of LiSbO_3 on Microstructure and Electrical Properties of $\text{Bi}_{0.5}(\text{Na}_{0.90}\text{K}_{0.20})_{0.5}\text{TiO}_3$ Ceramics
WANNASUT, Pimpilai
- MNA-38 Synthesis of Gold Nanorods with Different Aspect Ratios for Sensing Applications
NGERNPIMAI, Sawinee
- MNA-39 Characterization and Magnetic Properties of Fe-doped MgO Nanoparticles
PHOKHA, Sumalin
- MNA-40 Effects of Substrate Materials on Optical Behavior of $\text{ZnO}:\text{Al}$ Film Prepared by RF-sputtering
KHEANWONG, Jantree
- MNA-41 Fabrication of Electrospun LiFePO_4 /Carbon Composite Fibers as a Cathode Material for Lithium-ion Batteries
HONGTONG, Rattiya
- MNA-42 Effect of Annealing in Reducing Atmosphere on Dielectric Properties of $\text{CaCu}_3\text{Ti}_4\text{O}_{12}$ / CaTiO_3 Composites
NACHAITHONG, Theeranuch

Influence of LiSbO_3 on Microstructure and Electrical Properties of $\text{Bi}_{0.5}(\text{Na}_{0.80}\text{K}_{0.20})_{0.5}\text{TiO}_3$ Ceramics

Thursday, 21 May 2015 13:00 (210)

This research studied the effect of LiSbO_3 on microstructure and electrical properties of lead-free $\text{Bi}_{0.5}(\text{Na}_{0.80}\text{K}_{0.20})_{0.5}\text{TiO}_3$ ceramics with the composition belonging to $\text{Bi}_{0.5}(\text{Na}_{0.80}\text{K}_{0.20})_{0.5}\text{TiO}_3\text{-LiSbO}_3$ or $(1-x)\text{BNKT-xLS}$ (when $x = 0, 0.005, 0.010, 0.015, 0.020$ mol fraction). The BNKT-LS ceramics were prepared by a conventional mixed oxide method and sintered at 1100°C for 2h. X-ray diffraction pattern of all compositions exhibited a single perovskite structure without impurity phase. Scanning electron microscopy (SEM) was used to determine the microstructure of ceramics. Pure BNKT ceramic promoted a formation of cubic-like shape grains with an average grain size of 0.25 ± 0.05 μm . With increasing LS concentration, average grain size value gradually increased and showed the maximum value of 0.34 ± 0.10 μm at $x = 0.02$. The addition of LS into BNKT ceramic did not obviously change grain morphology, however, it caused fracture surface to switch from mixed inter-transgranular fracture for pure BNKT to mainly transgranular fracture for LS-added samples. A large room temperature dielectric constant of 1367 and dielectric loss of 0.0435 were observed for BNKT-0.015LS sample.

Summary

Primary author(s) : Ms. WANNASUT, Pimpilai (Department of Physics and Materials Science, Faculty of Science, Chiang Mai University, Chiang Mai, THAILAND 50200)

Co-author(s) : Prof. WATCHARAPASORN, Anucha (Department of Physics and Materials Science, Faculty of Science, Chiang Mai University, Chiang Mai, THAILAND 50200); Dr. JAITA, Pharatree (Department of Physics and Materials Science, Faculty of Science, Chiang Mai University, Chiang Mai, THAILAND 50200); Prof. JIANSIRI-SOMBOON, Sukanda (Department of Physics and Materials Science, Faculty of Science, Chiang Mai University, Chiang Mai, THAILAND 50200)

Presenter(s) : Ms. WANNASUT, Pimpilai (Department of Physics and Materials Science, Faculty of Science, Chiang Mai University, Chiang Mai, THAILAND 50200)

Session Classification : Poster-3

Track Classification : Material Physics, Nanoscale Physics and Nanotechnology



- MNA-43 Synthesis and Electrochemical Properties of SnO_2 Nanostructures via a Hydrothermal Method for Li-ion Batteries
BUEKEAW, sunisa
- MNA-44 Characteristics of AZO/Ag/AZO Tri-layer Film by RF-sputtering
KHUMMANEE, Yuttapichai
- MNA-45 Nano-materials from Rice Husks for Lithium Ion Battery Applications
CHAIKAWANG, Chirapan
- MNA-46 Fabrication of $\text{CsSn}_{1-x}\text{F}_x$ Doped with ZnO for Photogenerated Holes in Solid-state Dye-sensitized Solar Cells
ARDCHONGTHONG, Pornpanarat
- MNA-47 Characterization and Analyzation of Chitosan from Paphia Undulate Shell
SIRIPROM, Wichian
- MNA-48 Synthesis Thermoelectric Material Mg_2Si by Quartz Tube Vacuum Furnace from Starting Mg Powder and SiO_2 Rice Husk
KHOWJALERN, Phonlakit
- MNA-49 Fabrication and mechanical properties of doped-hydroxyapatite composite
TP, Likit
- MNA-50 WS_2 Nanoparticles and Multiwalled Carbon Nanotubes Counter Electrode for Dye-sensitized Solar Cells
KAEWPHAISAN, Ladavan
- MNA-51 New Dye Sensitizers from Anthraquinone Derivatives for Application in Dye-Sensitized Solar Cells: a DFT Study
TONTAPHA, Sarawut
- MNA-52 Comparative Study of Effects of Metal Oxides Modifications on Properties of $\text{Pb}(\text{Mg}_{1/3}\text{Nb}_{2/3}\text{O}_{9-0.1-x})\text{Ti}_x\text{O}_3$ Ceramics
PROMSAWAT, Methee
- MNA-53 The Study of Spin Seebeck Effect on Iron Alloy
SUksAWAT, Champ
- MNA-54 Study of Thermoelectric Structure Prepared by Hydrothermal Method
KAMONPHA, Phitsamai
- MNA-55 Enhancing the Cycling Stability of SnO_2 Hollow Spheres for a Li-ion Battery Anode by Titanium Dioxide Coating
KAEWMALA, Songyoot
- MNA-56 Simulation and Design High-temperature Microwave Furnace for Thermoelectric Material Synthesis
BOONTHUM, Direk
- MNA-57 Phase Transition of $\text{LiMn}_{0.85}\text{Cr}_{0.15}\text{PO}_4$ Cathode Material by In-Situ Time-Resolved XANES
PONGHA, Sarawut

Comparative study of effects of metal oxides modifications on properties of $\text{Pb}(\text{Mg}_{1/3}\text{Nb}_{2/3})_{0.9}\text{Ti}_{0.1}\text{O}_3$ ceramics

*(Methee Promsawat) Department of Physics and Materials Science, Faculty of Science, Chiang Mai University, Chiang Mai, THAILAND 50200.
Materials Science Research Center, Faculty of Science, Chiang Mai University, Chiang Mai, THAILAND 50200.*

(Napatporn Petnoi) School of Electrical Engineering, Suranaree University of Technology, Nakhon Ratchasima, THAILAND 30000.

(Anucha Watcharapasorn) Department of Physics and Materials Science, Faculty of Science, Chiang Mai University, Chiang Mai, THAILAND 50200.

Materials Science Research Center, Faculty of Science, Chiang Mai University, Chiang Mai, THAILAND 50200.

*(Sukanda Jiansirisomboon) Department of Physics and Materials Science, Faculty of Science, Chiang Mai University, Chiang Mai, THAILAND 50200.
Materials Science Research Center, Faculty of Science, Chiang Mai University, Chiang Mai, THAILAND 50200.*

Abstract

This work studies effects of metal oxides (MO ; $\text{M} = \text{Zn}^{2+}$, Cu^{2+} and Ni^{2+}) modifications on phase, microstructure, dielectric, ferroelectric and electrostrictive properties of $\text{Pb}(\text{Mg}_{1/3}\text{Nb}_{2/3})_{0.9}\text{Ti}_{0.1}\text{O}_3$ (PMNT) ceramics. Different contents of MO (2 and 4 mol%) were modified into PMNT ceramics. The ceramics with the density about 7.80 g/cm^3 were prepared. XRD pattern and lattice parameters of the PMNT ceramic did not change with the MO modifications. An average grain size of the PMNT ceramic increased with the ZnO and NiO modifications. The grain size was extremely enlarged with the CuO modification. A maximum dielectric constant ($\epsilon_{r,\max}$) of the PMNT ceramic was enhanced with 2 mol% ZnO and 2 mol% CuO modifications while 2 mol% NiO modification resulted to a reduction of the $\epsilon_{r,\max}$. A temperature of $\epsilon_{r,\max}$ (T_{\max}) of the PMNT ceramic shifted toward a higher temperature with 2 mol% ZnO modification. T_{\max} decreased with 2 mol% CuO and 2 mol% NiO modifications. Polarization-electric field curves of the ceramics were well developed with a higher remnant polarization (P_r) with 4 mol% ZnO modification while they were slimmer with a lower P_r with the NiO modification. A maximum strain and an electrostrictive coefficient of the PMNT ceramic were enhanced with 2 mol% ZnO and 2 mol% CuO modifications.

Keywords: PMNT; Dielectric; Ferroelectric; Electrostrictive

Proceedings of the

MST31 2014

Annual Conference



**The 31st Annual Conference
of the Microscopy Society of Thailand**

**29-31 January 2014
Nakhonratchasima, Thailand**



Poster Presentation

Microstructure and Electrical Properties of Lead-Free $\text{Bi}_{0.5}(\text{Na}_{0.80}\text{K}_{0.20})_{0.5}\text{TiO}_3\text{-LiNbO}_3$ Ceramics

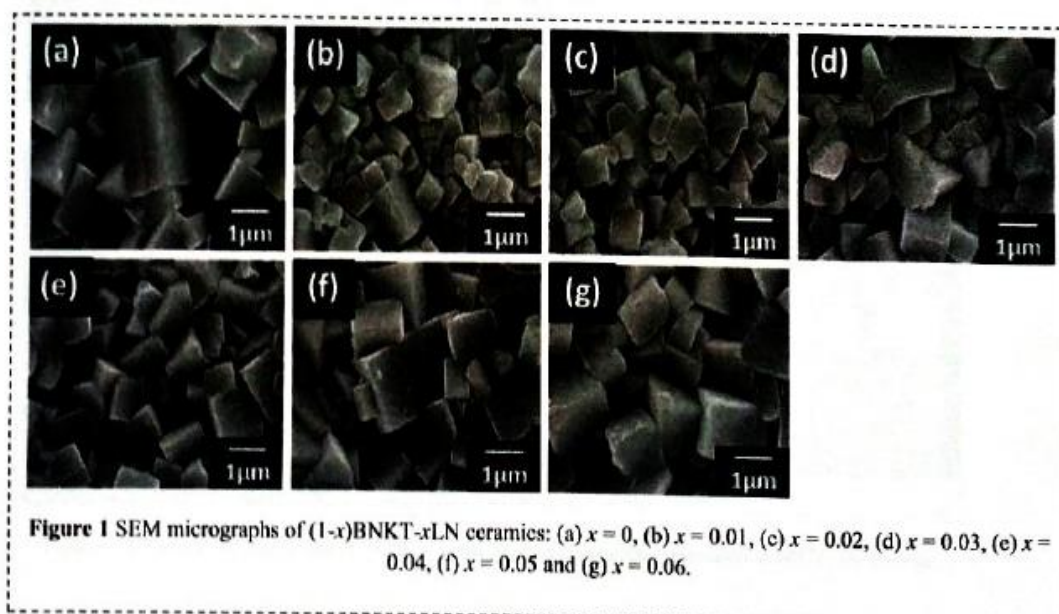
Pimpilai Wannasut¹, Pharatree Jaita¹, Anucha Watcharapasorn^{1,2}, Sukanda Jiansirisomboon^{1,2*}¹Department of Physics and Materials Science, Faculty of Science, Chiang Mai University, Chiang Mai 50200, Thailand²Materials Science Research Center, Faculty of Science, Chiang Mai University, Chiang Mai 50200, Thailand*Corresponding author, e-mail: sukanda.jian@cmu.ac.th

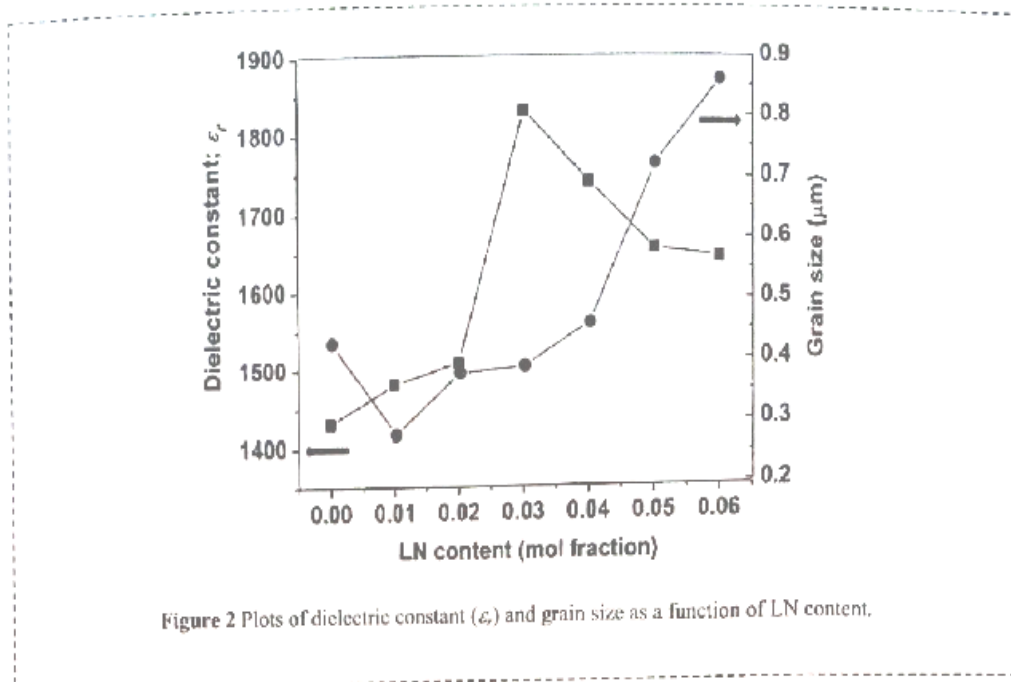
Abstract

Lead-free piezoelectric ceramics formula $(1-x)\text{Bi}_{0.5}(\text{Na}_{0.80}\text{K}_{0.20})_{0.5}\text{TiO}_3\text{-}x\text{LiNbO}_3$ or $(1-x)\text{BNKT-}x\text{LN}$ system (when $x = 0, 0.01, 0.02, 0.03, 0.04, 0.05$ and 0.06 mol fraction) were fabricated by a solid-state mixed oxide and sintering method. The effect of LN content on physical properties, phase, microstructure and electrical properties was investigated. X-ray diffraction pattern showed that all compositions exhibited pure perovskite structure without any secondary phase. The addition of a small amount of LN ($x = 0.01 - 0.02$) into BNKT inhibited grain growth. While grain size value increased with increasing LN concentration ($x = 0.03 - 0.06$). Scanning electron micrographs indicated a switch of fracture behavior from intergranular to transgranular fracture mode when LN content was increased. The addition of LN also improved dielectric property of BNKT ceramic. The maximum dielectric constant measured at room temperature was 1830 for BNKT-0.03LN sample.

References

1. A. Sasaki, T. Chiba, Y. Mamiya, E. Otsuki, Dielectric and piezoelectric properties of $(\text{Bi}_{0.5}\text{Na}_{0.5})\text{TiO}_3\text{-(Bi}_{0.5}\text{K}_{0.5})\text{TiO}_3$ systems, *Jpn. J. Appl. Phys.* 38, 5564-5567 (1999).
2. P. Jaita, A. Watcharapasorn, S. Jiansirisomboon, Investigation of a new lead-free $\text{Bi}_{0.5}(\text{Na}_{0.40}\text{K}_{0.10})\text{TiO}_3\text{-(Ba}_{0.7}\text{Sr}_{0.3})\text{TiO}_3$ piezoelectric ceramics, *Nanoscale. Res. Lett.* 7:24, 3-6 (2012).
3. Y.M. Chiang, D.P. Birnie, III, W.D. Kingery, *Physical Ceramics*, first ed., John Wiley & Son Ltd., New York, 1997.
4. C.A. Randall, N. Kim, J.P. Kucera, W.J. Cao, T.R. Shrout, Intrinsic and extrinsic size effects in fine-grained morphotropic-phase-boundary lead zirconate titanate ceramics, *J. Am. Ceram. Soc.*, 81, 677-688 (1998).





137

Microstructure and Dielectric Properties of (1-x)Pb(Mg_{1/3}Nb_{2/3})_{0.9}Ti_{0.1}O₃-xBi_{0.5}(Na_{0.74}K_{0.26})_{0.5}TiO₃ Ferroelectric Ceramics

Mukrawee Sriyod¹, Methee Promsawat¹, Anucha Watcharapasorn^{1,2} and Sukanda Jiansirisomboon^{1,2*}

¹ Department of Physics and Materials Science, Faculty of Science, Chiang Mai University, Chiang Mai 50200, Thailand

² Materials Science Research Center, Faculty of Science, Chiang Mai University, Chiang Mai 50200, Thailand

*Corresponding author, e-mail: sukanda.jian@cmu.ac.th

Abstract

This research was conducted to study a preparation of (1-x)Pb(Mg_{1/3}Nb_{2/3})_{0.9}Ti_{0.1}O₃-xBi_{0.5}(Na_{0.74}K_{0.26})_{0.5}TiO₃ or (1-x)PMNT-xBNKT (where x = 0, 0.1, 0.3, 0.5, 0.7, 0.9 and 1.0 mole fraction) ceramics by a solid state reaction and sintering method. The ceramics sintered at 1125°C for 2 h were characterized in terms of phase, density, microstructure and dielectric properties. The density of ceramics tended to decrease with increasing BNKT content. Based on X-ray diffraction (XRD) patterns, no secondary phase was observed in the patterns. Tetragonality of the ceramics was increased with increasing x. A mixed mode of inter-/transgranular fracture was observed in the ceramics with x = 0.1-0.4 and 0.6-1.0 mole fraction. A purely transgranular fracture was observed in the ceramic with x = 0.5 mole fraction. Grain size of the ceramics tended to decrease with increasing BNKT content. Dielectric constant measured around room temperature at a frequency of 1 kHz of pure PMNT ceramic was about 7000. It significantly decreased to ~3000 with x = 0.3 and then slightly decreased to ~2000 with x = 1.0. Dielectric loss value of ~0.12 for pure PMNT ceramic decreased to 0.05 with x = 0.3 and then slightly increased to ~0.07 with x = 0.5. It did not significantly change with a further increase in BNKT content. It seemed therefore that addition of BNKT helped reduce dielectric loss low frequency field.

References

1. S. Ananta, N. W. Thomas, Relationships between sintering conditions, microstructure and dielectric properties of lead magnesium niobate, J. Eur. Ceram. Soc. 19, 629–635 (1999).
2. R. Wongmaneeerung, R. Yimnirun, S. Ananta, Synthesis and electrical properties of Pb(Mg_{1/3}Nb_{2/3})O₃-PbTiO₃ ceramics, Curr. Appl Phys. 9, 268–273 (2009).
3. M. Promsawat, A. Watcharapasorn, H. N. Tailor, S. Jiansirisomboon, Z.-G. Ye, Enhanced dielectric, ferroelectric, and electrostrictive properties of Pb(Mg_{1/3}Nb_{2/3})_{0.9}Ti_{0.1}O₃ ceramics by ZnO modification, J. Appl. Phys. 113, 204101/1–6 (2013).
4. M. Otonicar, S.D. Skapin, M. Spreitzer, D. Suvorov, Compositional range and electrical properties of the morphotropic phase boundary in the Na_{0.5}Bi_{0.5}TiO₃-K_{0.5}Bi_{0.5}TiO₃ system, J. Eur. Ceram. Soc. 30, 971–979 (2010).
5. Y. Li, W. Chen, J. Zhou, Q. Xu, H. Sun, M. Liao, Dielectric and ferroelectric properties of lead-free Na_{0.5}Bi_{0.5}TiO₃-K_{0.5}Bi_{0.5}TiO₃ ferroelectric ceramics, Ceram. Int. 31, 139–142 (2005).

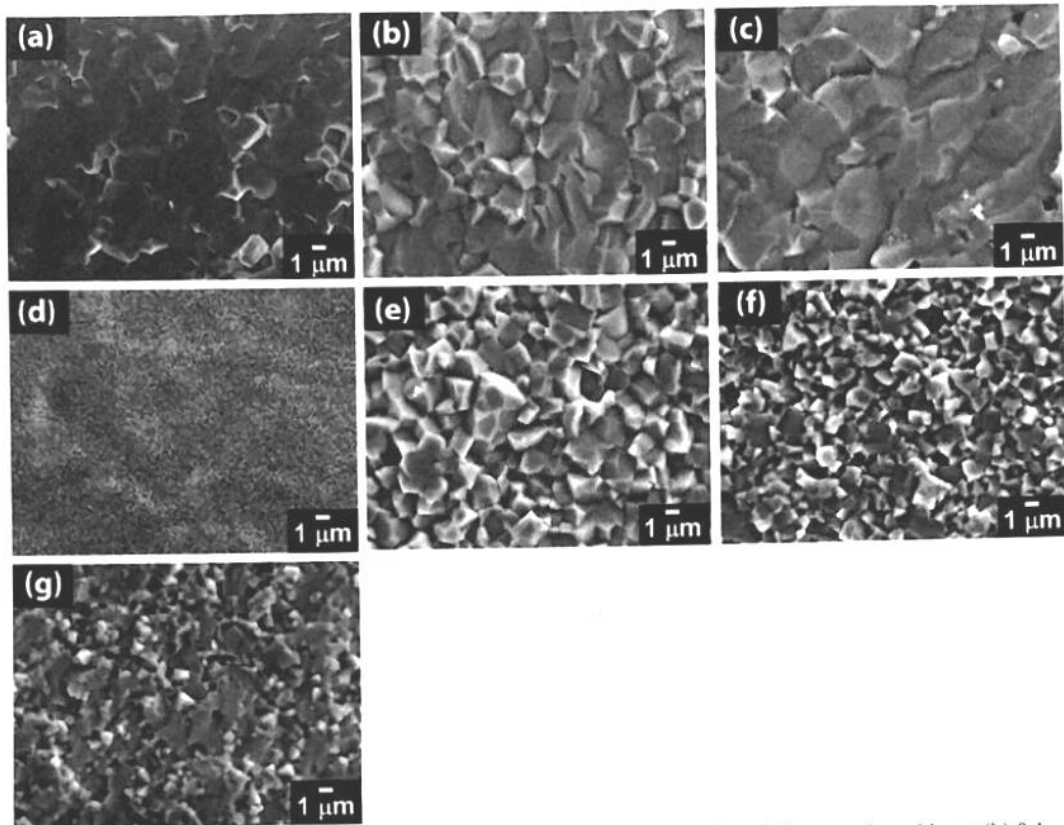


Figure 1 SEM micrographs of fractured surfaces of (a) pure PMNT ceramic and the ceramics with $x =$ (b) 0.1, (c) 0.3, (d) 0.5, (e) 0.7, (f) 0.9 and (g) 1.0 mole fraction of BNKT.

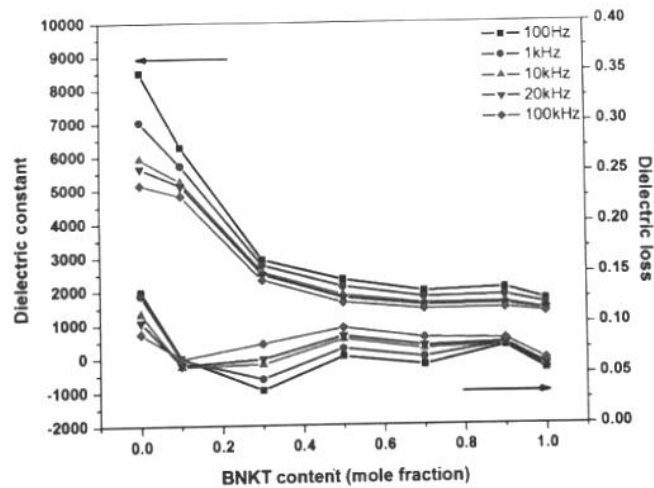


Figure 2 Plots of dielectric constant and dielectric loss measured at room temperature at various frequencies as a function of BNKT content of $(1-x)\text{PMNT}-x\text{BNKT}$ ceramics.

ภาคผนวก 3
ผลงานที่นำเสนอในประชุมวิชาการระดับนานาชาติ



NEWS & NOTICE

- 8 Things to Know about ENGE 2014 Before You Go! 2014-10-31
- Final Program (Printed Ver.) of Enge 2014 has been announced! 2014-10-14
- Program Schedule of Enge 2014 has been announced! 2014-09-22
- Acceptance Notification announced via E-mail! 2014-07-31

IMPORTANT DATES

- Submission of Abstracts : ~~May 31, 2014~~ June 30, 2014
- Notification of Abstract Acceptance : ~~June 30, 2014~~ July 31, 2014
- Author/Pre-Registration : ~~August 31, 2014~~ September 12, 2014
- Hotel Reservation : September 30, 2014
- Submission of Manuscript : November 15, 2014

PROMOTIONAL VIDEO



TOUR



Hosted by



Sponsored by



Supported by



ENGE 2014

ENGE2014 Secretariat
KIM (The Korean Institute of Metals and Materials)
Business No.: 110-82-04081 | President: Changho Lee
80h M., Seocho-dae-ro 36-gil 35, Seocho-gu, Seoul 137-881, Korea
Tel: 432-2-668-8871 E-mail: secretary@enge2014.org



Materials and Process for BEOL and 3D Integration (MB)

Nov. 18, 2014 (Tue.)

MBP-2 (Materials and Process for BEOL and 3D Integration 2)

Ramada Ballroom Lobby

08:00-09:00 & 16:00-18:00

- MBP-2-1224 Effect of Pd(P) Layer on Reflow Reaction of Submicron Au/Pd(P)/Ni(P) Surface Finish with Sn-Ag-(Cu) Solders**
Yu Ri Chae, Joo Youl Huh
Korea University
- MBP-2-1620 Effects of Leveler Concentration in High Aspect Ratio via Filling in 3D SiP**
Se-Hyun Jang, Jae-Ho Lee
Hongik University
- MBP-2-1967 Development of Chip-on-flex Bonding using Sn-based Bumps and Non-conductive Adhesive**
Sun-Chul Kim, Kyoung-Moo Harr, Young-Min Kim, Myung-Hwan Hong, Ji-Hyun Lee, Young-Ho Kim
Hanyang University
- MBP-2-2598 Failure Mechanism of Power Semiconductor under Intermittent Operating Condition**
SungSoon Choi, WooYoung Lee, KwanHun Lee
Korea Electronics Technology Institute
- MBP-2-2631 Effects of Alternative Voltage on the Electrochemical Migration and Corrosion Behaviors of Sn and Sn-Cu Intermetallic Compound**
JongSoo Kim, MiSeok Park, HyukSang Kwon
Korea Advanced Institute of Science and Technology
- MBP-2-2872 Packaging-Completed Flexible Electronic Device using Flip-Chip Bonding Technology**
Do Hyun Kim, Keon Jae Lee
Korea Advanced Institute of Science and Technology

Sensors and Oxide Semiconductor (MD)

Nov. 18, 2014 (Tue.)

MDP (Sensors and Oxide Semiconductor)

Ramada Ballroom Lobby

08:00-09:00 & 16:00-18:00

- MDP-0141 Room Temperature Oxygen Sensing Properties of Multiple Networked Nb₂O₅ Nanorod Sensors Functionalized with Au Nanoparticle**
Sunghoon Park, Soohyun Kim, Sangbo Park, Chongmu Lee
Inha University
- MDP-0273 Large Electric Field-Induced Strain and Piezoelectric Responses of Lead-Free Bi_{0.5}(Na_{0.80}K_{0.20})_{0.5}TiO₃-Ba(Ti_{0.90}Sn_{0.10})O₃ Ceramics near Morphotropic Phase Boundary**
Pharatree Jaita¹, Anucha Watcharapasom¹, David P. Cann², Sukanda Jiansirisomboon¹
¹Chiang Mai University, ²Oregon State University
- MDP-0304 Room Temperature Acetone Sensing Properties of WO₃ Nanorod Sensors Decorated with Pt-Au Bimetallic Nanoparticles**
Sunghoon Park, Soohyun Kim, Sangbo Park, Chongmu Lee
Inha University
- MDP-0357 Photo-thermally Induced Current Switching in Vanadium-dioxide-based Devices using CO₂ Laser Pumping**
Jihoon Kim, Yong Wook Lee
Pukyong National University
- MDP-0769 Effects of Electrode in Oxide Semiconductor Gas Sensors**
Sung Pil Lee
Kyungnam University
- MDP-0792 Synthesis, Characterization and for Optoelectronic Application of Green Precursor based Lead Sulfide (PbS) Colloidal Quantum Dots**
M.V. Bharathi¹, Kaustab Ghosh¹, Y. Suneel Kumar¹, F. Nawaz Khan², Eun Hyuk Chung², Euh Duck Jeong²
¹VIT University, ²Korea Basic Science Institute
- MDP-0801 Influence of Annealing Temperature on the Microstructural and Electrical Characteristics of Sol-**

Large Electric Field-Induced Strain and Piezoelectric Responses of Lead-Free $\text{Bi}_{0.5}(\text{Na}_{0.80}\text{K}_{0.20})_{0.5}\text{TiO}_3\text{-Ba}(\text{Ti}_{0.90}\text{Sn}_{0.10})\text{O}_3$ Ceramics near Morphotropic Phase Boundary

Pharatree Jaita¹, Anucha Watcharapasorn^{1,2}, David P. Cann³ and Sukanda Jiansirisomboon^{1,2*}

¹Department of Physics and Materials Science, Faculty of Science, Chiang Mai University, Chiang Mai 50200, Thailand

²Materials Science Research Center, Faculty of Science, Chiang Mai University, Chiang Mai 50200, Thailand

³Materials Science, School of Mechanical, Industrial and Manufacturing Engineering, Oregon State University, Corvallis, OR 97331, USA

*Corresponding author. Tel: +66-53-94-1921 ext 631; Fax: +66-53-94-3445

E-mail address: sukanda.jian@cmu.ac.th (S. Jiansirisomboon)

Lead-free piezoelectric ceramics with compositions belonging to family of compositions $(1-x)\text{Bi}_{0.5}(\text{Na}_{0.80}\text{K}_{0.20})_{0.5}\text{TiO}_3\text{-}x\text{Ba}(\text{Ti}_{0.90}\text{Sn}_{0.10})\text{O}_3$ or $(1-x)\text{BNKT-xBTS}$ (when $x = 0.05 - 0.15$ mol fraction) near a morphotropic phase boundary (MPB) were fabricated by a conventional mixed oxide method. Sintered samples had relative densities greater than 98% of their theoretical values. X-ray diffraction patterns revealed that the MPB region consisted of coexisting rhombohedral and tetragonal phases in the BNKT-BTS system was identified over the entire compositional range. A large electric field-induced strain (S_{max}) of 0.36% and a normalized strain coefficient (d_{33}^*) of 649 pm/V were observed in the BNKT-0.05BTS sample. The sample close to the MPB composition (BNKT-0.11BTS) exhibited the maximum dielectric constant ($\epsilon_r = 1770$), Curie temperature ($T_c = 333^\circ\text{C}$) and low-field piezoelectric coefficient ($d_{33} = 227$ pC/N), and reasonable ferroelectric properties ($P_r = 20.6$ $\mu\text{C}/\text{cm}^2$, $R_{sq} = 0.88$) and strain properties ($d_{33}^* = 445$ pm/V and $S_{\text{max}} = 0.24$ %) were observed.

Keywords: Lead free piezoelectric, Dielectric, Ferroelectric, Electric field-induced strain

Poster Presentation

Materials and Processes for Logic and Memory Devices (MA)

Nov. 17, 2014 (Mon.)

MAP (Materials and Processes for Logic and Memory Devices)

Ramada Ballroom Lobby

08:00-09:00 & 17:45-19:00

- MAP-0353 Low-power Switching of Phase Change Memory Ring Arrays formed by using Self-assembled Block Copolymer Nanostructures**
Woon Ik Park^{1,2}, Jong Min Kim¹, Jae Won Jeong¹, Jaesuk Choi¹, Kwang Ho Kim², Yeon Sik Jung¹
¹Korea Advanced Institute of Science and Technology, ²Global Frontier Project Team
- MAP-0723 Polarization Fatigue in Ferroelectric PZT-SBN Ceramics**
Orapim Namsar¹, Anucha Watcharapasorn¹, Soodkhet Pojprapai², Sukanda Jiansirisomboon¹
¹Chiang Mai University, ²Suranaree University of Technology
- MAP-0909 Analysis of Electronic Structure & Internal Photoemission at Interfaces in Metal-Insulator-Metal and Metal-Oxide-Semiconductor**
Sang Yeon Lee, Jin Seo Kim, Hyung Tak Seo
Ajou University
- MAP-1350 Fabrication of MnO Resistive Switching Random Access Memory (ReRAM) using Layer-by-layer (LbL) Process**
Chiyong Lee¹, Myeonggi Kim¹, Jaegab Lee¹, Jinhan Cho²
¹Kookmin University, ²Korea University
- MAP-1390 Dielectric Properties of Strontium Carbonate doped Barium Iron Tantalum Ceramics**
Lalita Tawee, Gobwute Rujjanagul
Chiangmai University
- MAP-1400 Preparation and Dielectric Properties of (Sr_{1-x}Ba_x)Fe_{0.5}Nb_{0.5}O₃ ; (x=0.0, 0.1 and 0.2) Ceramics**
Thanatop Phatungthane, Gobwute Rujjanagul
Chiangmai University
- MAP-1883 Charge Trap Memory Devices using Atomic Layer Depositions of Silicon Oxide and Silicon Nitride**
Yong-Ho Noh, Jae-Min Park, Byeol Han, Jong-Wan Jung, Won-Jun Lee
Sejong University
- MAP-2033 The Effect of Bi-doping on the Phase Change Properties of In₃SbTe₂**
Minho Choi¹, Yong Tae Kim², Jinho Ahn¹
¹Hanyang University, ²Korea Institute of Science and Technology
- MAP-2068 Wide Voltage Operation for Resistive Switching in Metal/HfO₂/Metal Resistors**
Yong Chan Jung, Sejong Seong, Taehoon Lee, In-Sung Park, Jinho Ahn
Hanyang University
- MAP-2244 Two-step Growth of High-quality InP Epitaxial Layers on GaAs (001) by Metal Organic Chemical Vapor Deposition**
Young Dae Cho^{1,2}, In-Geun Lee^{1,2}, In-Hye Choi², Chan-Soo Shin², Kyung-Ho Park², Won-Kyu Park², Hyuk-Min Kwon³, Dae-Hyun Kim³, Dae-Hong Ko¹
¹Yonsei University, ²Korea Advanced Nano Fab Center, ³SEMATECH
- MAP-2465 Effects of Magnetic Domain Walls on the Anisotropic Magnetoresistance in Permalloy Nanowires**
Chunhee Nam
Hannam University
- MAP-2654 Carrier Transport Mechanism of Metal Contact on Amorphous Hafnium Indium Zinc Oxides**
Seongjun Kim, Youngun Gil, Hyunsoo Kim
Chonbuk National University
- MAP-2706 The Effects of High Pressure Annealing on the Tunneling Field Effect Transistor (TFET)**
Donghwan Lim¹, Woosuk Jung¹, Sung Kwan Lim², Yong Hun Kim², Uk Jin Jung², Byoung Hun Lee², Changhwan Choi¹
¹Hanyang University, ²Gwangju Institute of Science and Technology
- MAP-2788 Engineering of Magnetic Properties of MgO/ CoFeB/ Nonmagnetic Layers for Magnetic Tunnel Junctions**

Polarization Fatigue in Ferroelectric PZT-SBN Ceramics

Orapim Namsar^{1, 2}, Anucha Watcharapasorn^{1, 2}, Soodkhet Pojprapai³,
Sukanda Jiansirisomboon^{1, 2 *}

¹*Department of Physics and Materials Science, Faculty of Science, Chiang Mai University, Chiang Mai, 50200, Thailand*

²*Materials Science Research Center, Faculty of Science, Chiang Mai University, Chiang Mai, 50200, Thailand*

³*School of Ceramic Engineering, Suranaree University of Technology, Nakhon Ratchasima, 30000, Thailand*

**Corresponding author. Tel: +66-53-94-1921 ext 631; Fax: +66-53-94-3445*

E-mail address: sukanda.jian@cmu.ac.th (S. Jiansirisomboon)

Ferroelectric materials are widely applied in electronic devices. Many of these applications require materials with superior ferroelectric properties. Both lead zirconate titanate (PZT) and strontium bismuth niobate (SBN) play a dominant role in these applications. PZT shows excellent ferroelectric properties with large remanent polarization (P_r) and a small coercive field (E_c). However, one of the problems with PZT is its low fatigue resistance. On the other hand, SBN compositions exhibit excellent fatigue endurance. Nonetheless, its ferroelectric properties are not favorable. Therefore, this study aims to combine the fatigue-free properties of SBN and the superior ferroelectric properties of PZT. The ceramic samples of compound $(1-x)\text{PZT}-x\text{SBN}$ with $x = 0 - 1.0$ weight fraction were prepared by a solid-state mixed oxide method. Electrical fatigue behavior of $(1-x)\text{PZT}-x\text{SBN}$ ceramics was then characterized. It was found that pure PZT ceramic had severe polarization fatigue. This was mainly attributed to the occurrence of the macroscopic cracks at the near-electrode regions. On the contrary, pure SBN ceramic exhibited excellent fatigue resistance, which was attributed primarily to weak domain walls pinning. The fatigue endurance of PZT ceramic was improved with small addition of SBN ($0.1 \leq x \leq 0.3$). This demonstrated that the ceramics had a high stability during the repeated domain switching due to their low oxygen vacancy concentration. Therefore, the results suggested that this new ceramic PZT-SBN system seems to be an alternative material for replacing PZT in ferroelectric memory applications.

Keywords: Fatigue, Perovskite structure, Bi-layered structure, Ferroelectric

9th Asian Meeting on Ferroelectricity
Asian Meeting on Electroceramics
AMF-AMEC-2014

October 26-30, 2014, Shanghai, China Shanghai International Convention Center

Program and Abstracts Book

Organizer Shanghai Institute of Ceramics
Chinese Academy of Sciences



Co-Organizers Nanjing University



Tongji University



AMF-AMEC-2014

p001-A011

Influences of Milling Method and Calcination Condition on Phase Formation and Particle Size of BaTiO₃ Nanopowders**Laongnuan Srisombat**^{1,*}, Jeeranan Nonkumwong¹, Phomsawat Baipaywad², Supon Ananta²¹Department of Chemistry, Faculty of Science, Chiang Mai University, Chiang Mai 50200 Thailand²Department of Physics and Materials Science, Faculty of Science, Chiang Mai University, Chiang Mai 50200 Thailand

email address: slaongnuan@yahoo.com*

Barium titanate, BaTiO₃, is one of the classic perovskite ferroelectric materials which have been investigated extensively as a potential candidate for electroceramic components such as multilayer capacitors, transducer and actuator applications [1]. It is well documented that the mixed oxide technique is probably one of the most fundamental, practical routine methods which has been used, developed and modified in both scientific research and industrial mass production for many years [2]. In general, BaTiO₃ powders synthesized by a mixed oxide method have spatial fluctuations in their compositions. The extent of the fluctuation depends on the characteristics of the starting precursors as well as on the processing history. In this work, BaTiO₃ nanopowders have been prepared by a solid-state reaction. Both conventional ball-and rapid vibro-milling have been investigated as milling methods, with the formation of the BaTiO₃ phase investigated as a function of calcinations by DTA and XRD. The particle size distribution of the calcined powders was determined by laser diffraction technique, while morphology, crystal structure and phase composition were determined via a combination of SEM, TEM and EDX techniques. The type of milling method together with the designed calcination condition was found to show a considerable effect on the phase and morphology evolution of the calcined BaTiO₃ powders. It is seen that optimization of calcination conditions can lead to a pure perovskite phase of BaTiO₃ nanopowders in both milling methods. However, the formation temperature and soaking time for such nanopowders were lower with the rapid vibro-milling technique.

Keywords: Barium titanate, Nanopowders, Solid-state reaction, Milling, Calcination

References:

1. A. J. Moulson and J. M. Herbert, *Electroceramics*, 2nd ed., Wiley, Chichester, 2003.
2. R. Wongmaneeerung, W. Chaisan, O. Khamman, R. Yimnirun, S. Ananta, *Ceramics International*, 2008, 34: 813-817.

p002-A012

Effects of Gold Nanoparticle Additives on Microstructure and Electrical Properties of Ferroelectric BaTiO₃ Ceramics**Jeeranan Nonkumwong**^{1,*}, Laongnuan Srisombat¹, Naratip Vittayakorn², Supon Ananta³¹Department of Chemistry, Faculty of Science, Chiang Mai University, Chiang Mai 50200 Thailand²Department of Chemistry, Faculty of Science, King Mongkut's Institute of Technology Ladkrabang, Bangkok 10520 Thailand³Department of Physics and Materials Science, Faculty of Science, Chiang Mai University, Chiang Mai 50200 Thailand

email address: jeeranan.bees@gmail.com*

As is well known, almost all useful barium titanate (BaTiO₃; BT) ceramics, which have been regarded as one of the significant perovskite ferroelectrics in electroceramic industries due to their excellent dielectric, ferroelectric and piezoelectric characteristics, are modified either chemically or physically to tailor their key properties for specific utilizations [1]. One approach of modification is adding small amount of various metal oxides additives which is believed to create some disturbance on the Ba/Ti ratio, resulting in a great influence on the sintering behavior, microstructure and electrical properties of the ceramics [2]. In this work, the effect of gold nanoparticles on microstructure and electrical properties of BT-based ceramics was examined via a combination of XRD, XPS, SEM, EDX, dielectric and ferroelectric measurement techniques. It is seen that the adding of gold nanoparticles can effectively suppress the grain growth of BT ceramics. Dense microstructures could be obtained by sintering at lower temperature in comparison with the unmodified BT case. It was also observed that dielectric constant and ferroelectric hysteresis loop of gold modified BT ceramics is strongly dependent on the grain size.

Keywords: Barium titanate, Gold nanoparticle, Additive, Microstructure, Electrical properties

References:

1. A. J. Moulson and J. M. Herbert, *Electroceramics: Materials, Properties, Applications*, John Wiley & Sons Ltd., Chichester, 2003.
2. L. Srisombat, S. Ananta, B. Singhana, T. Randall Lee, R. Yimnirun, *Ceramics International*, 2013, 39: S591-S594.

p003-A014

Phase Development, and Dielectric, Ferroelectric and Piezoelectric Responses in Pb(Mg_{1/3}Nb_{2/3})_{0.9}Ti_{0.1}O₃-Bi_{0.5}(Na_{0.74}K_{0.26})_{0.5}TiO₃ Ceramics**Methee Promsawat**^{1,2,3}, Mukrawee Sriyod¹, Zenghui Liu⁴, Anucha Watcharapasorn^{1,2}, Wei Ren⁴, Zuo-Guang Ye³, Sukanda Jiansirisomboon^{1,2,*}¹Department of Physics and Materials Science, Faculty of Science, Chiang Mai University, 239 Huay Kaew Road, Muang, Chiang Mai, 50200, Thailand

email address:

m.promsawat@hotmail.com (M. Promsawat)

mukrawee.203@hotmail.com (M. Sriyod)

anucha@stanfordalumni.org (A. Watcharapasorn)

sukanda.jian@cmu.ac.th (S. Jiansirisomboon)

²Materials Science Research Center, Faculty of Science,

Chiang Mai University, 239 Huay Kaew Road, Muang, Chiang Mai, 50200, Thailand

³Department of Chemistry and 4D LABS, Simon Fraser University, 8888 University Drive, Burnaby, British Columbia, V5A 1S6, Canada

email address: zye@sfu.ca (Z.-G. Ye)

⁴Electronic Materials Research Laboratory, Key Laboratory of the Ministry of Education & International Center for Dielectric Research, Xi'an Jiaotong University, Xi'an, Shaanxi, 710049, P.R. China

email address: zenghuiliu@126.com (Z. Liu)

email address: wren@mail.xtju.edu.cn (W. Ren)

This work studied properties of $(1-x)\text{Pb}(\text{Mg}_{1/3}\text{Nb}_{2/3})_{0.9}\text{Ti}_{0.1}\text{O}_3$ - $x\text{Bi}_{0.5}(\text{Na}_{0.74}\text{K}_{0.26})_{0.5}\text{TiO}_3$ or $(1-x)\text{PMNT}$ - $x\text{BNKT}$ ceramics. It was found that lattice parameter, grain size and dielectric constant of the ceramics tended to decrease while tetragonality increased with increasing x . Typical characteristics of relaxor ferroelectrics were found in the ceramics with $x = 0$ - 0.5 mole fraction, while the characteristic of normal ferroelectrics when $x > 0.7$ mole fraction, at which a piezoelectric constant (d_{33}) was found to be about 160 pC/N.

Keywords: Phase development, Microstructure, Dielectric, Ferroelectric, Piezoelectric

References:

1. M. Otonicar, S.D. Skapin, M. Spreitzer and D. Suvorov, Journal of the European Ceramic Society, 2010, 30: 971-979.
2. N. Jaitanong, W.C. Vittayakorn and A. Chaipanich, Ceramics International, 2010, 36: 1479-1483.

p004-A017

Crystallographic Structure and Ferroelectricity of $(\text{A}_x\text{La}_{1-x})_2\text{Ti}_2\text{O}_7$ (A= Sm and Eu) solid solutions

Chen Chen¹, Haixue Yan^{1,2}, Mike Reece^{1,2}

¹School of Engineering and Materials Science, Queen Mary University of London, London E1 4NS, UK

²Nanoforce Technology Ltd, London E1 4NS, UK

The $\text{A}_2\text{B}_2\text{O}_7$ compounds, like $\text{La}_2\text{Ti}_2\text{O}_7$ and $\text{Sr}_2\text{Nb}_2\text{O}_7$, are the best candidates for high temperature ($> 1000^\circ\text{C}$) piezoelectrics because of their super-high Curie points ($> 1300^\circ\text{C}$) and good thermal stability. The structure and properties of $(\text{A}_x\text{La}_{1-x})_2\text{Ti}_2\text{O}_7$ (A = Sm and Eu) solid solutions were investigated. The crystallographic structure of the solid solutions was studied using X-ray diffraction and Raman spectroscopy. The solubility limits of Eu and Sm in $(\text{A}_x\text{La}_{1-x})_2\text{Ti}_2\text{O}_7$ were found to be greater than $x = 0.5$ and $x = 0.8$, respectively. The X-ray and Raman data suggest that the solid solutions have a monoclinic perovskite-like layered structure, like the pure $\text{La}_2\text{Ti}_2\text{O}_7$, when x is less than the solubility limit. When x is above the solubility limit the materials are biphasic, consisting of $(\text{A}_x\text{La}_{1-x})_2\text{Ti}_2\text{O}_7$ perovskite-like layered structured and pure $\text{Sm}_2\text{Ti}_2\text{O}_7$ pyrochlore structured phases. The effect of A-site substitution on the properties of $\text{La}_2\text{Ti}_2\text{O}_7$ was investigated by measuring the dielectric permittivity and loss at different frequencies and temperatures. The highest piezoelectric constant d_{33} is 2.8

pC/N for $(\text{Sm}_{0.1}\text{La}_{0.9})\text{Ti}_2\text{O}_7$.

Keywords: $\text{La}_2\text{Ti}_2\text{O}_7$; $\text{Eu}_2\text{Ti}_2\text{O}_7$; $\text{Sm}_2\text{Ti}_2\text{O}_7$; perovskite layered structure; high Curie point.

p005-A040

Effect of CeO_2 Additive on dielectric and ferroelectric properties of $0.85(\text{Na}_{0.5}\text{Bi}_{0.5})\text{TiO}_3$ - $0.12(\text{K}_{0.5}\text{Bi}_{0.5})\text{TiO}_3$ - 0.03BaTiO_3 ceramics

Mouteng Yao, Yongping Pu*, Qian Jin, Hanyu Zheng, Yaru Wang

School of Materials Science and Engineering, Shaanxi University of Science and Technology, Xi'an, 710021, People's Republic of China

229516747@qq.com

$0.85(\text{Na}_{0.5}\text{Bi}_{0.5})\text{TiO}_3$ - $0.12(\text{K}_{0.5}\text{Bi}_{0.5})\text{TiO}_3$ - 0.03BaTiO_3 + $x\text{wt}\%\text{CeO}_2$ ($x=0, 0.2, 0.4, 0.6, 0.8, 1.0$) lead-free ceramics were prepared by a conventional mixed-oxide method. The effects of CeO_2 content on the phase structure, surface morphologies, dielectric and ferroelectric properties were investigated. The X-ray diffraction patterns show that a single phase structure is obtained for all samples. The SEM images show that all samples were dense and grain size distribute inhomogeneous. Temperature dependence of dielectric constant curves show that dielectric constant increased with the increase of CeO_2 content and reached maximum value ($\epsilon_r=5788$) at temperature T_m for $x=0.4$ doped, but the temperature T_m decreased with the increase of CeO_2 content. The P - E hysteresis loops show that remnant polarization and coercive field increased with the increase of CeO_2 content and reached maximum value ($P_r=27.3\mu\text{C}/\text{cm}^2$, $E_c=27\text{kV}/\text{cm}$) for $x=0.4$ doped, which is similar to dielectric constant.

Keywords: $(\text{Na}_{0.5}\text{Bi}_{0.5})\text{TiO}_3$; $(\text{K}_{0.5}\text{Bi}_{0.5})\text{TiO}_3$; BaTiO_3 ; dielectric; ferroelectric

References:

1. Min Chen, Qing Xu, Bok Hee Kim, Byeong Kuk Ahn, Wen Chen, Effect of CeO_2 addition on structure and electrical properties of $(\text{Na}_{0.5}\text{Bi}_{0.5})_{0.93}\text{Ba}_{0.07}\text{TiO}_3$ ceramics prepared by citric method, Materials Research Bulletin, 2008, 43 (6): 1420-1430.
2. Xiaoxing Wang, Helen Lai-Wa Chan, Chung-loong Choy, Piezoelectric and dielectric properties of CeO_2 -added $(\text{Na}_{0.5}\text{Bi}_{0.5})_{0.94}\text{Ba}_{0.06}\text{TiO}_3$ lead-free ceramics, Solid State Communications, 2003, 125 (7-8): 395-399.
3. Laijun Liu, Huiqing Fan, Shanming Ke, Xiuli Chen, Effect of sintering temperature on the structure and properties of cerium-doped $0.94(\text{Na}_{0.5}\text{Bi}_{0.5})\text{TiO}_3$ - 0.06BaTiO_3 piezoelectric ceramics, Journal of Alloys and Compounds, 2008, 458 (1-2): 504-508.

p006-A050

Giant Dielectric Behavior and Complex Impedance of Cu^{2+} Doped $\text{Ba}_{0.9}\text{Ca}_{0.1}\text{Ti}_{0.9}\text{Zr}_{0.1}\text{O}_3$ Ceramics Prepared by Hydrothermal Method

Zixiong Sun¹, Yongping Pu¹

AMF-AMEC-2014

USA

*Corresponding author's email: jeong@pusan.ac.kr

Oxygen-deficient $\text{BaTiO}_{3-\delta}$ exhibits an insulator-metal transition with increasing δ . We performed neutron total scattering measurements to study structural evolution across an insulator-metal transition in $\text{BaTiO}_{3-\delta}$ [1]. Despite its significant impact on resistivity, slight oxygen reduction ($\delta = 0.09$) caused only a small disturbance on the local doublet splitting of Ti-O bond. This finding implies that local polarization is well preserved under marginal electric conduction. In the highly oxygen-deficient metallic state ($\delta = 0.25$), however, doublet splitting of the Ti-O bond became smeared. The smearing of the local Ti-O doublet found using pair distribution function (PDF) analysis is complemented by long-range structural analysis and demonstrates that the metallic conduction in the highly oxygen-reduced $\text{BaTiO}_{3-\delta}$ is due to the appearance of non-ferroelectric cubic lattice.

Keywords: ferroelectrics, oxygen vacancy, local structure, PDF analysis

Reference:

1. I.-K. Jeong *et al.*, Phys. Rev. B **84**, 064125 (2011)

p049-A556

Dielectric, Polarization and Strain Response of Enhanced Complex Ceramics: The Study Through $\text{Pb}(\text{Zr}_{0.52}\text{Ti}_{0.48})\text{O}_3\text{-SrBi}_2\text{Ta}_2\text{O}_9$

Orapim Namsar¹, Anucha Watcharapasorn^{1, 2}, Mark Hoffman³, Julia Glaum³,

Sukanda Jiansirisomboon^{1, 2, *}

¹Department of Physics and Materials Science, Faculty of Science, Chiang Mai University, Chiang Mai, 50200, Thailand

aorapim_nam@hotmail.com (O. Namsar)

²Materials Science Research Center, Faculty of Science, Chiang Mai University, Chiang Mai, 50200, Thailand

anucha@stanfordalumni.org (A. Watcharapasorn),

*sukanda.jian@cmu.ac.th (S. Jiansirisomboon)

³School of Materials Science and Engineering, University of New South Wales, New South Wales, Sydney, 2052, Australia

mark.hoffman@unsw.edu.au (M. Hoffman),

j.glaum@unsw.edu.au (J. Glaum)

Ferroelectric materials are used in many applications such as actuators, sensors as well as non-volatile random access memories. Many of these applications require high performance materials with good electrical properties (i.e. dielectric, ferroelectric and piezoelectric properties). $\text{Pb}(\text{Zr}_{0.52}\text{Ti}_{0.48})\text{O}_3$ (PZT) has been widely used in these applications due to its excellent electric properties [1]. Nevertheless, a serious problem of PZT is poor fatigue endurance [2]. Another alternative ferroelectric material which overcomes such problem is the bismuth layered structure $\text{SrBi}_2\text{Ta}_2\text{O}_9$ (SBT). SBT exhibits good ferroelectric properties along with higher fatigue endurance [2]. However, the major problems of SBT are

small remanent polarization, high coercive field, low dielectric and poor piezoelectric properties [3]. Therefore, this research aims to combine the advantages of PZT and SBT in form of a ceramic system. The electrical properties of a series of new complex structured ceramics with formula $(1-x)\text{PZT}-x\text{SBT}$ with $x = 0-1.0$ weight fraction were characterized. Measurement of dielectric response indicated an increase in dielectric constant with small addition of SBT ($x = 0.1$) into PZT. Further increase in the SBT fraction caused the dielectric constant to rapidly decrease. The polarization hysteresis loop measurement demonstrated that the ferroelectric properties changed from normal ferroelectric behavior in PZT-rich ceramics to paraelectric behavior in SBT-rich ceramics. Strain behavior showed a symmetric butterfly curve in the compositions with $0 \leq x \leq 0.3$, but the strain obtained was found to rapidly decrease with increasing SBT content. This research suggested that the optimum electrical properties can be obtained for 0.9PZT-0.1SBT ceramic. Such ceramic is a promising material to be further utilized in ferroelectric memory devices.

Keywords: Dielectric properties, Ferroelectric properties, Piezoelectric properties

References:

1. G. H. Haertling, *Journal of the American Ceramic Society*, 1999, **82**(4): 797-818.
2. W. Zhang, A. D. Li, Q. -Y. Shao, Y. -D. Xia, D. Wu, Z. -G. Liu and N. -B. Ming, *Applied Surface Science*, 2008, **254**: 1583-1586.
3. H. Amorin, M. E. V. Costa, A. L. Kholkin and J. L. Baptista, *Journal of the European Ceramic Society*, 2004, **24**: 1535-1539.

p050-A573

Transparent $(\text{K}_{0.5}\text{Na}_{0.5})\text{NbO}_3$ -based lead-free transparent ferroelectric ceramics

Hongliang Du¹, Shaobo Qu¹, Xiaoxia Tian¹, Jiafu Wang¹, Binke Wang¹, Xiaoyong Wei², Zhuo Xu²,

¹Science College, Air Force Engineering University Xi'an 710051, P. R. China

duhongliang@126.com

²Electronic Materials Research Laboratory, Key Laboratory of Educational Ministry, Xi'an Jiaotong University, Xi'an 710049, China

Highly transparent lead-free ferroelectric transparent ceramics of $(\text{K}_{0.5}\text{Na}_{0.5})\text{NbO}_3$ were fabricated by press-less sintering without atmosphere protection. The ceramics showed the optical transparency as high as 60-70% in the visible and near-infrared regions, which is close to the optical transparency of the famous $(\text{Pb}, \text{La})(\text{Zr}, \text{Ti})\text{O}_3$ (PLZT) ceramics. However, compared with the conventional PLZT ceramics, the $(\text{K}_{0.5}\text{Na}_{0.5})\text{NbO}_3$ ceramics have three advantages: (1) the material does not contain lead, it is environment friendly from the viewpoint of sustainable development, (2) the simple fabrication conditions and the low cost during the preparation, do not need to use hot-pressure sintering, ultrafine powder synthesis and atmosphere protection, (3) relatively high Curie temperature (240 °C) than PLZT

AMF-AMEC-2014

References:

1. J. Dou, L. Navarrete, R. Schad, P. Padmini, R. K. Pandey, H. Guo, and A. Gupta, *J. Appl. Phys.*, 2008, **103**, 07D117
2. Hajime Hojo, Koji Fujita, Katsuhisa Tanaka, and Kazuyuki Hirao, *Appl. Phys. Lett.*, 2006, **89**, 082509.

F. F. Lange, *Science*, 1996, **273**, 903-909.

p091-A753

A study on ferrite materials by selective laser sintering for 3D printing applications

LEE Wen-Hsi

In our works, to develop an inductor by 3D printing, the sintering of ferrite materials was studied by selective laser sintering. Effect of particle size of ferrite powder, laser power and soaking time on microstructure is investigated. The phase and microstructure of ferrite are respectively examined by XRD and SEM. A dense and homogenous microstructure of ferrite has been successfully achieved based on 30μm and 170mj laser power. The promising microstructure would be reflected to performance of inductor and the result would be valid to fabricate an inductor by 3D printing instead of conventional pressing and sintering processes.

p092-A070

X-ray photoelectron spectroscopy analysis and electrical properties of $\text{Bi}_{0.5}(\text{Na}_{0.80}\text{K}_{0.20})_{0.5}\text{TiO}_3\text{-LiNbO}_3$ lead-free piezoelectrics

Pimpilai Wannasut¹, Pharatree Jaita¹, Anucha Watcharapasorn^{1,2}, Sukanda Jiansirisomboon^{1,2*}

¹ Department of Physics and Materials Science, Faculty of Science, Chiang Mai University, Chiang Mai 50200, Thailand

E-mail address: Pimpilai.mats@gmail.com (P. Wannasut), pharatree@gmail.com (P. Jaita), anucha@stanfordalumni.org (A. Watcharapasorn), sukanda.jian@cmu.ac.th (S. Jiansirisomboon)

² Materials Science Research Center, Faculty of Science, Chiang Mai University, Chiang Mai 50200, Thailand

Lead-free piezoelectric ceramics with formula of $\text{Bi}_{0.5}(\text{Na}_{0.80}\text{K}_{0.20})_{0.5}\text{TiO}_3\text{-xLiNbO}_3$ or $(1\text{-x})\text{BNKT-xLN}$ (when $x = 0, 0.005, 0.010, 0.015$ and 0.020 mol fraction) were fabricated by solid-state mixed oxide and sintering method. The ceramics with density of 5.7 g/cm^3 were obtained by a sintering temperature at 1100°C . X-ray diffraction pattern showed that the $(1\text{-x})\text{BNKT-xLN}$ ceramics exhibited pure perovskite structure. X-ray photoelectron spectroscopy analysis was performed to investigate the influence of LN content on homogeneity of chemical composition and binding energy of atoms in the ceramics. Dielectric, ferroelectric and piezoelectric properties of the ceramics were investigated and found to be maximized at $x = 0.005$ mol fraction.

Keywords: lead-free piezoelectrics, X-ray diffraction,

X-ray photoelectron spectroscopy

References:

1. C. Zhou, X. Liu, W. Li, C. Yuan, *J. Phys. Chem. Solids*, 2009, **70**: 541-545
2. P. Jaita, A. Watcharapasorn, S. Jiansirisomboon, *Electron. Mater. Lett.*, 2013, **9**: 437-440

p093-A087

Balance Large d_{33} and High T_c in New Potassium Sodium Niobate Lead-free Ceramics

Cheng Xiaojing, Xiao Dingquan, Zhu Jianguo, and Wu Jiagang*

Department of Materials Science, Sichuan University, Chengdu 610064, P. R. China

* wujiagang0208@163.com

The lead-based piezoceramics possess admirable properties with the sacrifice of human health, and then lead-free ceramics recently attract more attention because of environmental friendliness and good electrical properties. In this work, the doping with Li^+ is used to mediate the T_c and d_{33} of $(\text{K},\text{Na})\text{NbO}_3$ -based ceramics, and the new system consisting of $0.96\text{K}_{0.45}\text{Na}_{0.55}\text{Nb}_{0.96}\text{Sb}_{0.04}\text{O}_3\text{-}0.04\text{Bi}_{0.5}(\text{Na}_{1-x}\text{Li}_x)_{0.5}\text{ZrO}_3$ is studied in detail. The ceramics endure a phase transition from rhombohedral-tetragonal phase boundary to tetragonal phase as the Li^+ increases. With the increase of Li contents, the d_{33} drops gradually, while T_c increases. In addition, the good thermal stability of piezoelectric properties is shown in all ceramics. $T_c=247\sim 275^\circ\text{C}$ and $d_{33}=296\sim 410 \text{ pC/N}$ could be attained, which is dependent on Li^+ content. We believe that the doping with Li^+ could well mediate the T_c and d_{33} of potassium sodium niobate ceramics.

Keyword: Lead-free piezoelectric, Large d_{33} , High T_c , Good thermal stability

References:

1. Xiaojing Cheng, Jiagang Wu, Xiaopeng Wang, Binyu Zhang, Jianguo Zhu, Dingquan Xiao, Xiangjian Wang, and Xiaojie Lou, *APPLIED PHYSICS LETTERS*, 2013, **103**, 052906.
2. Xiaojing Cheng, Jiagang Wu, Xiaojie Lou, Xiangjian Wang, Xiaopeng Wang, Dingquan Xiao, and Jianguo Zhu, *ACS Applied Materials & Interfaces*, 2014, **6**(2): 750-756.

p094-A088

Modified strain and piezoelectricity of $(\text{K},\text{Na})(\text{Nb},\text{Sb})\text{O}_3\text{-Bi}_{0.5}\text{Na}_{0.5}\text{SnO}_3$ lead-free ceramics

Ting Zheng, Dingquan Xiao, Jianguo Zhu, and Jiagang Wu*

Department of Materials Science, Sichuan University, Chengdu 610064, P.R. China

*msewujg@scu.edu.cn and wujiagang0208@163.com

In this work, new $(1\text{-x})\text{K}_{0.48}\text{Na}_{0.52}\text{Nb}_{0.96}\text{Sb}_{0.04}\text{O}_3\text{-}$



ISAF-ISIF-PFM 2015

IEEE International Symposium on Applications of Ferroelectric (ISAF),
International Symposium on Integrated Functionalities (ISIF),
Piezoresponse Force Microscopy Workshop (PFM)

24-27 MAY 2015, SINGAPORE



87	A-0423	Dielectric Properties of Samarium Bismuth Ferrite Ceramic	Edita PALAIMIENE ¹ , Jan MACUTKEVIC ¹ , Dzmitry KARPINSKY ² , Andrei L. KHOLKIN ² , Juras BANYIS ¹ ¹ Vilnius University, Lithuania, ² University of Aveiro, Portugal
88	A-0429	Effects of Different Ratios of Potassium to Sodium on the Structure and Properties of (K _x Na _{1-x})NbO ₃ Ceramics	Dongsheng ZHANG, Zheng ZHANG Xi'an Jiaotong University, China
89	A-0430	Generating Characteristics of a Hump Shaped Piezoelectric Energy Harvester	Byeong Ha LEE, Seong Su JEONG, Seong Kyu CHEON, Yong Woo HA, Tae Gone PARK Changwon National University, South Korea
90	A-0432	Design of an Ultrasonic Linear Motor Which has Simple Plate Type Stator	Seong Kyu CHEON, Seong Su JEONG, Byeong Ha LEE, Myong Ho KIM, Tae Gone PARK Changwon National University, South Korea
91	A-0433	Computational of Localized Magnetic Flux Inside LSMO Based Structure	Mahmoud AL AHMAD United Arab Emirates University, United Arab Emirates
92	A-0434	Extraction of Piezoelectric Constant Using Force-Capacitance Dependency	Mahmoud AL AHMAD United Arab Emirates University, United Arab Emirates
93	A-0435	The Ferroelectric and Antiferroelectric Properties of HfO ₂ /ZrO ₂ Nanolaminate Systems	Min Hyuk PARK, Han Joon KIM, Yu Jin KIM, Young Hwan LEE, Taehwan MOON, Keum Do KIM, Cheol Seong HWANG Seoul National University, South Korea
94	A-0436	Piezoelectric d33 Based Generator Power Estimations	Mahmoud AL AHMAD United Arab Emirates University, United Arab Emirates
95	A-0438	High Temperature Coefficient of Resistance Based on Ferroelectric Polymer Tunnel Junction	Xiaolin ZHAO ¹ , Yang LIU ² , Jianlu WANG ¹ , Bobo TIAN ¹ , Bolu LIU ¹ , Xudong WANG ¹ , Hai HUANG ¹ , Tie LIN ¹ , Shuo SUN ¹ , Yuhong ZOU ¹ , Li HAN ¹ , Hong SHEN ¹ , Jinglan SUN ¹ , Xiangjian MENG ¹ , Junhao CHU ¹ ¹ Shanghai Institute of Technical Physics, Chinese Academy of Sciences, China, ² CNRS-Ecole Centrale Paris, France
96	A-0442	Effect of Frequency on Bipolar Electrical Fatigue Behavior of ZnO-Modified Lead Magnesium Niobate Titanate Ceramics	M. PROMSAWAT ¹ , N. PETNOI ² , S. POJPRAPA ² , Sukanda JIANSIRISOMBOON ¹ ¹ Chiang Mai University, Thailand, ² Suranaree University of Technology, Thailand
97	A-0444	Comparison of Actuator Performance in Lead-Based and Lead-Free Piezoelectric Cymbals	Piyalak NGERNCHUKLIN ¹ , Chutima EAMCHOTCHAWALIT ¹ , Ahmad SAFARI ² ¹ Thailand Institute of Scientific and Technological Research, Thailand, ² Rutgers University, United States
98	A-0460	Anatomy of Vertical Heteroepitaxial Interfaces Reveals the Memristive Mechanism in Nb ₂ O ₅ -NaNbO ₃ Thin Films	Linglong LI, Lu LU, yaodong YANG Xi'an Jiaotong University, China
99	A-0462	Polar Discontinuities and Piezoelectric Properties of Honeycomb Lattices	Md NOOR-A-ALAM, Hye Jung KIM, Young-Han SHIN University of Ulsan, South Korea
100	A-0469	Acoustic Anomalies of Ferroelectric Ba _{0.79} Sr _{0.21} TiO ₃ Single Crystals Studied by Brillouin Spectroscopy	Sunhyub SHIN ¹ , Jae-Hyeon KO ¹ , Choong Jae WON ² , Nam Jung HUR ² , Young Ho KO ³ , Kwang Joo KIM ³ ¹ Hallym University, South Korea, ² Inha University, South Korea, ³ Agency for Defense Development, South Korea
101	A-0471	Effect of Dopant/BaTiO ₃ Weight Ratio on the Dielectric Temperature Behavior of Ni BaTiO ₃ - High Capacitance MLCC	S.N SEOK, D.S SHIN, M.K KIM, Jung Rag YOON Samwha Capacitor. Co. Ltd, South Korea
102	A-0494	Domain Structure Investigation in Sr-Doped Potassium Sodium Niobate Lead-Free Piezoelectric Ceramics	Jitka HREŠČAK ¹ , Julian WALKER ¹ , Goran DRAZIC ² , Denis ALIKIN ³ , Anton TURIGIN ³ , Tadej ROJAC ¹ , Barbara MALIC ¹ , Vladimir SHUR ³ , Andrei L. KHOLKIN ⁴ , Andreja BENCAN ¹ ¹ Jožef Stefan Institute, Slovenia, ² National Institute of Chemistry, Slovenia, ³ Ural Federal University, Russian Federation, ⁴ University of Aveiro, Portugal
103	A-0495	Frequency and Temperature Dependences of Electrical Properties of Lead-free (Na _{0.53} K _{0.47})(Nb _{1-x} Ta _x)O ₃ Piezoelectric Ceramics	Jin Soo KIM, A. HUSSAIN, T. K. SONG, W. J. KIM, H. S. LEE, M. H. KIM Changwon National University, South Korea

Effect of Frequency on Bipolar Electrical Fatigue Behavior of ZnO-Modified Lead Magnesium Niobate Titanate Ceramics

M. Promsawat^{1,2*}, N. Petnoi³, S. Pojprapai³, and S. Jiansirisomboon^{1,2*}

¹Department of Physics and Materials Science, Faculty of Science, Chiang Mai University, 239 Huay Kaew Road, Muang, Chiang Mai, 50200, Thailand

²Materials Science Research Center, Faculty of Science, Chiang Mai University, 239 Huay Kaew Road, Muang, Chiang Mai, 50200, Thailand

³School of Electrical Engineering, Suranaree University of Technology, 111 University Avenue, Muang, Nakhon Ratchasima, 30000, Thailand

*e-mail: sukanda.jian@cmu.ac.th

This work was conducted to investigate the effect of frequency on bipolar electrical fatigue behavior of $\text{Pb}(\text{Mg}_{1/3}\text{Nb}_{2/3})_{0.65}\text{Ti}_{0.35}\text{O}_3$ (PMNT) ceramics modified with 0.4 mol% ZnO. The ceramics sintered at 1240 °C for 2 h with a bulk density of 7.6 g/cm³ were subjected to apply bipolar electric field at frequencies of 1, 10, 50 and 100 Hz up to 10⁶ cycles. The number of a cycle at which the remanent polarization, which is taken from the polarization-electric field hysteresis loop, abruptly decreases increased with increasing frequency. The percentage of the degradation of the remanent polarization after 10⁶ cycles decreased with increasing frequency. The number of a cycle at which the coercive field abruptly increases increased with increasing frequency. The percentage of the increasing of the coercive field after 10⁴ cycles decreased with increasing frequency. Moreover, the surface area damaged due to an electrical fatigue test at a lower frequency was larger than that at a higher frequency. When compared to PZT, the commercial material for piezo-and ferroelectric applications, the electrical fatigue behavior of the ZnO modified-PMNT materials seemed to be better than that of PZT materials. This could make the ZnO modified-PMNT as an alternative material for ferroelectric actuator and Fe-RAM applications.

- A-0265 **Dielectric Properties of Oriented BaTiO₃-Bi(Mg_{1/2}Ti_{1/2})O₃ Thin Films Fabricated by Chemical Solution Deposition**
 Shota MOKI^{1*}, Junichi KIMURA², Hiroshi FUNAKUBO², Hiroshi UCHIDA¹
¹Sophia University, Japan, ²Tokyo Institute of Technology, Japan
- A-0268 **Properties of 0.74BiNaTiO₃-0.06SrTiO₃/ Bi_{0.5}(Na_{0.8}K_{0.2})_{0.5}TiO₃ Ceramic Composite**
 Soon-Jong JEONG^{1*}, M. S. KIM¹, S. M. JANG¹, I. S. KIM¹, S. J. SONG¹, M. SALEEM^{1,2}
¹Korea Electrotechnology Research Institute, South Korea, ²University of Science and Technology, South Korea
- A-0275 **Effect of Potassium Content on the Dielectric and Electrical Properties of Sodium Potassium Niobate Ceramics**
 Suman KUMARI¹, Seema SHARMA¹, Dhananjay K. SHARMA^{2*}, Andrei L. KHOLKIN²
¹A.N. College, India, ²University of Aveiro, Portugal
- A-0280 **Carrier Density Control of 2-Dimensional Electron Gas at a-Al₂O₃/SrTiO₃ Interface by ALD Using O₃ Treatment**
 Taehwan MOON^{1*}, Min Hyuk PARK¹, Yu Jin KIM¹, Han Joon KIM¹, Keum Do KIM¹, Young Hwan LEE¹, Sang Woon LEE², Cheol Seong HWANG¹
¹Seoul National University, South Korea, ²Ajou University, South Korea
- A-0281 **Direct Measurements of Electrocaloric Effect in Lead-Free (1-x)Ba(Zr_{0.2}Ti_{0.8})O₃-x(Ba_{0.7}Ca_{0.3})TiO₃ Ceramics**
 Mehmet SANLI^{1*}, Vladimir SHVARTSMAN^{1*}, Matias ACOSTA², Doru C. LUPASCU¹
¹University Duisburg-Essen, Germany, ²Technische Universität Darmstadt, Germany
- A-0286 **Anisotropy of Deformation of a Precision Actuator Based on Single Crystalline Bidomain Lithium Niobate**
 Ilya KUBASOV^{1*}, Sergey KSENICH, Dmitry KISELEV, Alexander BYKOV, Roman ZHUKOV, Anastasiya CHERNYKH, Alexandr TEMIROV, Nikita TIMUSHKIN, Mikhail MALINKOVICH
 National University of Science and Technology "MISIS", Russian Federation
- A-0290 **Computed Phase Diagram and Temperature-Dependent Properties of the Ba(Zr_{0.2}Ti_{0.8})O₃-x(Ba_{0.7}Ca_{0.3})TiO₃ Lead-Free Piezoceramic**
 Matias ACOSTA¹, Nasser KHAKPASH², Takumi SOMEYA³, Nikola NOVAK¹, Wook JO², Hajime NAGATA³, George A. ROSSETTI¹, Jürgen RÖDEL^{1*}
¹Technische Universität Darmstadt, Germany, ²University of Connecticut, United States, ³Tokyo University of Science, Japan
- A-0294 **Microstructure and Electrical Properties of Ternary Lead-Free Bi_{0.5}(Na_{0.80}K_{0.20})_{0.5}TiO₃-0.005LiNbO₃-BaTiO₃ Piezoelectric Ceramics**
 Pimpilai WANNASUT^{1*}, Pharatree JAITA², Anucha WATCHARAPASORN¹, Sukanda JIANSIRISOMBOON¹
¹Chiang Mai University, Thailand, ²Rajamangala University of Technology Lanna (RMUTL), Thailand
- A-0295 **Magnetocaloric and Electrocaloric Effect in Geometrically Frustrated CaBaCo₄O₇**
 C. DHANASEKHAR^{1*}, A.K DAS, A. VENIMADHAV
 Indian Institute of Technology, Kharagpur, India
- A-0296 **Effect of Cobalt Substitution on the Structural, Electrical and Magnetic Properties of BaTiO₃ Ceramics**
 Alka RANI^{1*}, Jayant KOLTE, Prakash GOPALAN
 Indian Institute of Technology Bombay, India
- A-0298 **Fabrication of Tetragonal Pb(Zr,Ti)O₃ Nanorods by Focused Ion Beam and Characterization of the Domain Structure**
 Daisuke ITO^{1*}, Tomoaki YAMADA¹, Osami SAKATA^{2,3}, Junki KUROISHI⁴, Takahiro NAMAZU⁴, Takahisa SHIRAI³, Takao SHIMIZU³, Hiroshi FUNAKUBO³, Masahito YOSHINO¹, Takanori NAGASAKI¹
¹Nagoya University, Japan, ²National Institute for Materials Science, Japan, ³Tokyo Institute of Technology, Japan, ⁴University of Hyogo, Japan
- A-0310 **Ferroelectric Properties of Stress-Modulated PbTiO₃ Thick Films on the Different Substrates Fabricated by Aerosol Deposition**
 Jungkeun LEE^{1*}, Soobin KANG¹, Ji-Ho LIM¹, Hwee-Jong KIM¹, Jungho RYU², Daeyong JEONG¹
¹Inha University, South Korea, ²Korea Institute of Materials Science (KIMS), South Korea

Microstructure and Electrical Properties of Ternary Lead-Free $\text{Bi}_{0.5}(\text{Na}_{0.80}\text{K}_{0.20})_{0.5}\text{TiO}_3\text{-}0.005\text{LiNbO}_3\text{-BaTiO}_3$ Piezoelectric Ceramics

Pimpilai Wannasut¹, Pharatree Jaita², Anucha Watcharapasorn^{1,3},

Sukanda Jiansirisomboon^{1,3*}

¹Department of Physics and Materials Science, Faculty of Science,

Chiang Mai University, Chiang Mai 50200, Thailand

²Research and Development Institute, Rajamangala University of Technology Lanna (RMUTL), Chiang

Mai, 50220 Thailand

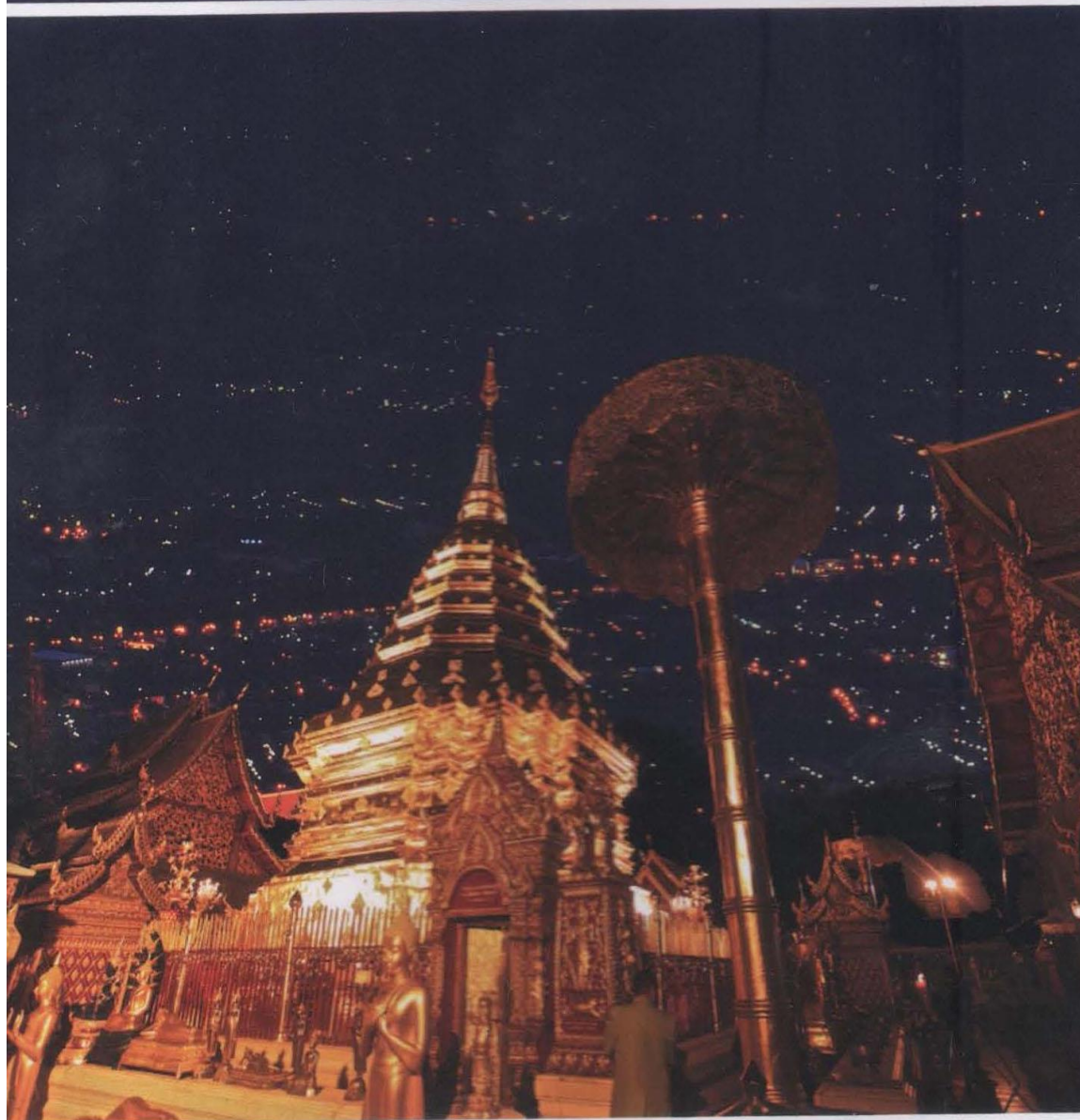
³Materials Science Research Center, Faculty of Science, Chiang Mai University,

Chiang Mai 50200, Thailand

*Corresponding author, e-mail: sukanda.jian@cmu.ac.th

Lead-free piezoelectric ceramics with the formula of $(1-x-y)\text{Bi}_{0.5}(\text{Na}_{0.80}\text{K}_{0.20})_{0.5}\text{TiO}_3\text{-}x\text{LiNbO}_3\text{-}y\text{BaTiO}_3$ or $(1-x-y)\text{BNKT-xLN-yBT}$ ternary system, when $x = 0.005$ and $y = 0, 0.01, 0.02, 0.03, 0.04, 0.05, 0.06$ and 0.07 mol fraction, were fabricated by a conventional mixed oxide method and sintered at the temperature of 1125°C for 2 h. All ceramics were focused in terms of phase, microstructure, dielectric, ferroelectric and piezoelectric properties. All samples have the density ranging of $5.59 - 5.73 \text{ g/cm}^3$. X-ray diffraction pattern exhibited a single perovskite structure without any secondary phase. Scanning electron micrographs indicated a cubic-like grain shape occurred for all compositions with side length of $0.49 - 0.77 \mu\text{m}$. The addition amount of BT with ($y = 0.04$) into BNKT-0.005LN inhibited grain growth. However, grain size value increased with increasing BT concentration ($y = 0.05 - 0.07$). The highest piezoelectric coefficient ($d_{33} = 198 \text{ pC/N}$) with good dielectric ($\epsilon_r = 1775$, $\tan\delta = 0.0534$) and ferroelectric properties ($P_r = 17.36 \mu\text{C/cm}^2$, $R_{sq} = 1.67$) were obtained for the BNKT-0.005LN-0.04BT sample.

**ABSTRACTS AND PROCEEDINGS OF
THE 10TH INTERNATIONAL CONFERENCE ON
THE PHYSICAL PROPERTIES AND APPLICATION
OF ADVANCED MATERIALS**



**17-21 NOVEMBER 2015
CHIANG MAI, THAILAND**

Electrical Properties of Ternary System $\text{Bi}_{0.5}(\text{Na}_{0.80}\text{K}_{0.20})_{0.5}\text{TiO}_3\text{-}0.005\text{LiNbO}_3\text{-BaTiO}_3$ Lead-Free Piezoelectric Ceramics

Pimpilai Wannasut¹, Pharatree Jaita¹, Anucha Watcharapasorn^{1,2}, Sukanda Jiansirisomboon^{1,3*}

¹ *Department of Physics and Materials Science, Faculty of Science, Chiang Mai University,
Chiang Mai 50200, Thailand*

² *Materials Science Research Center, Faculty of Science, Chiang Mai University,
Chiang Mai 50200, Thailand*

³ *School of Ceramic Engineering, Suranaree University of Technology,
Nakhon Ratchasima, 30000, Thailand*

Tel: +66-5394-3367, Fax: +66-5394-3445, *E-mail: Sukanda.jian@cmu.ac.th

Abstract

Ternary system of lead-free piezoelectric ceramics with the formula of $(1-x-y)\text{Bi}_{0.5}(\text{Na}_{0.80}\text{K}_{0.20})_{0.5}\text{TiO}_3\text{-}x\text{LiNbO}_3\text{-}y\text{BaTiO}_3$ or $(1-x-y)\text{BNKT-}x\text{LN-}y\text{BT}$ ($x = 0.005$ and $y = 0, 0.01, 0.02, 0.03, 0.04, 0.05, 0.06$ and 0.07 mol fraction) were synthesized using a conventional solid-state reaction method and sintered at the temperature of 1125°C for 2 h. All samples were studied in terms of phase, dielectric, ferroelectric and piezoelectric properties. All samples have the density ranging of $5.59 - 5.73 \text{ g/cm}^3$. X-ray diffraction pattern exhibited a single perovskite structure without any secondary phase. Scanning electron micrographs indicated a cubic-like grain shape occurred for all compositions with side length of $0.49 - 0.77 \mu\text{m}$. At a composition $\text{BNKT-}0.005\text{LN-}0.04\text{BT}$ showed the highest piezoelectric coefficient ($d_{33} = 198 \text{ pC/N}$) with good dielectric ($\epsilon_r = 1775$, $\tan\delta = 0.0534$) and ferroelectric properties ($P_r = 17.36 \mu\text{C/cm}^2$, $R_{90} = 1.67$).

Keywords: Ternary system, Lead-free piezoelectrics, X-ray diffraction,

Comparative Study of Properties of BCZT Ceramics Prepared from Conventional and Sol-Gel Auto Combustion Method

P. Jaimeewong¹, M. Promsawat¹, A. Watcharapasorn^{1,2}, S. Jiansirisomboon^{3*}

¹*Department of Physics and Materials Science, Faculty of Science, Chiang Mai University,
Chiang Mai 50200, Thailand*

²*Materials Science Research Center, Faculty of Science, Chiang Mai University,
Chiang Mai 50200, Thailand*

³*School of Ceramic Engineering, Suranaree University of Technology,
Nakhon Ratchasima 3000, Thailand*

*Tel: +66-5394-3367, Fax: +66-5394-3445, *E-mail:sukandajian@cmu.ac.th*

Abstract

This work studies properties of Pb-free complex perovskite $\text{Ba}_{0.85}\text{Ca}_{0.15}\text{Ti}_{0.9}\text{Zr}_{0.1}\text{O}_3$ (BCZT) ceramics prepared from the BCZT powders synthesized from conventional mixed oxide (M) and sol-gel auto combustion (S) methods. M and S powders were calcined at 1200 and 900°C, respectively. M powder was mixed with S powder with weight percentage ratios of 100:0, 50:50 and 0:100, and were then ground by ball milling for 24 hrs using ethanol as a medium. The powders were dried and pressed to form a pellet shape by hydraulic pressing. Green bodies were sintered at 1450°C for 2 hrs. The ceramics were characterized in terms of microstructure, phase, density, dielectric and ferroelectric properties by a scanning electron microscope (SEM), X-ray diffractometer (XRD), Archimedes's method, LCR meter and Sawyer-Tower circuit, respectively. It was found that density of the ceramics tended to increase with increasing S powder content. XRD patterns showed the coexistence of rhombohedral and tetragonal phases. Grain size of the obtained ceramics tended to decreasing of S powder. For all samples, dielectric constant (ϵ) measured at room temperature was frequency dependent, at which ϵ decreased with increasing frequency. The ϵ tended to increase with increasing S content. The highest ϵ was 5342, which was observed in the ceramic at a weight percentage ratio of 0:100. The P - E loops of the ceramics were measured at room temperature under a bipolar applied field of ± 20 kV/cm with a frequency of 25 Hz. Slim P - E loops were observed in all ceramics.

Keywords: Lead-free, Piezoelectric, BCZT, Mixed-oxide, Sol-gel auto combustion

SMMIB-19

The 19th International Conference on Surface Modification
of Materials by Ion Beams

ABSTRACTS



<http://www.smmib2015.org/>



ENDORSED
MEETINGS

November 22-27, 2015
The Empress Hotel, Chiang Mai, Thailand



ID : BP2

Influence of pH values on properties of BCZT nanopowders synthesized via sol-gel auto combustion method

Piyaporn Jaimeewong¹⁾, Methee Promsawat¹⁾, Anucha Watcharapasorn^{1,2)}
and Sukanda Jainsirisomboon^{1,2)*}

¹⁾Department of Physics and Materials Science, Faculty of Science, Chiang Mai University,
Chiang Mai 50200, Thailand,

²⁾Materials Science Research Center, Faculty of Science, Chiang Mai University, Chiang Mai 50200,
Thailand

Barium calcium titanate ($\text{Ba}_{0.85}\text{Ca}_{0.15}\text{Zr}_{0.1}\text{Ti}_{0.9}\text{O}_3$; BCZT) is one of the most widely studied piezoelectric materials due to its highest piezoelectric coefficient among lead free systems, which was about 637-650 pC/N [1-3]. There was a few number of works studying on the synthesis of BCZT nanopowders from a wet chemical method. In this paper, the BCZT nanopowders were fabricated by the auto combustion method with controlling pH values.

In the BCZT nanopowder synthesis, variation of pH values, i.e. 5, 7 and 9 were controlled by NH_4OH content and fixed ratio of metal and citric acid as 1:1. The burnt powder was calcined at 900°C for 2 h and was then characterized in terms of chemical bonding, crystal structure and morphology using Raman, FTIR spectroscopy, XRD and TEM techniques. Increase of pH value did not affected particle size but increased tetragonality of the powder. Raman spectrum peaks of as burnt powders showed an amorphous phase which was confirmed by XRD result. The calcined powders showed a broad peak at $\sim 562\text{ cm}^{-1}$ relating to the stretching vibration of Ti-O and Zr-O bonds in perovskite structure. Crystallite sizes, which were calculated by using Sherrer's equation, were in a range of 20-40 nm. TEM result showed that the burnt synthesized at pH = 5 and 9 were non-crystalline while burnt powder at pH = 7 and the calcined powders were polycrystalline.

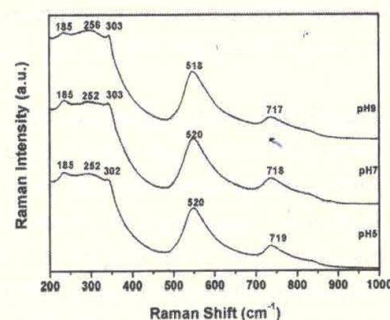


Fig. 1 Raman spectra of BCZT powders with different pH values.

References:

- 1) Wenfeng L., Xiaobing R., Phys. Rev. Lett., 103, 257602(1)-257602(4) (2009)
- 2) Wang P., Li Y., Lu Y., J. Eur. Ceram. Soc., 31, 2005-2012 (2011)
- 3) Paul Praveen J., Karthik T., James A.R., Chandrakala E., Asthana S., Das D., J. Eur. Ceram. Soc., 35, 1785-1798 (2015)
- 4) Hayashi H., Nakamura T., Ebina T., J. Phys. Chem. Solids., 74, 957-962 (2013)

Keywords: Nano powders, BCZT, Sol-gel auto combustion, pH values, Raman spectrum

Corresponding author*: sukanda.jian@cmu.ac.th